

Advances in
APPLIED MECHANICS

VOLUME 41

Edited by
Hassan Aref
Erik van der Giessen



Advances in Applied Mechanics

Volume 41

This page intentionally left blank

ADVANCES IN

APPLIED MECHANICS

Edited by

Hassan Aref

VIRGINIA TECH COLLEGE OF ENGINEERING
BLACKSBURG, VA, USA

Erik van der Giessen

UNIVERSITY OF GRONINGEN
GRONINGEN, THE NETHERLANDS

VOLUME 41



ELSEVIER

Amsterdam • Boston • Heidelberg • London • New York • Oxford

Paris • San Diego • San Francisco • Singapore • Sydney • Tokyo

Academic Press is an imprint of Elsevier



Academic Press is an imprint of Elsevier
84 Theobald's Road, London WC1X 8RR, UK
Radarweg 29, PO Box 211, 1000 AE Amsterdam, The Netherlands
The Boulevard, Langford Lane, Kidlington, Oxford OX5 1GB, UK
30 Corporate Drive, Suite 400, Burlington, MA 01803, USA
525 B Street, Suite 1900, San Diego, CA 92101-4495, USA

First edition 2007

Copyright © 2007 Elsevier Inc. All rights reserved

No part of this publication may be reproduced, stored in a retrieval system
or transmitted in any form or by any means electronic, mechanical, photocopying,
recording or otherwise without the prior written permission of the publisher

Permissions may be sought directly from Elsevier's Science & Technology Rights
Department in Oxford, UK: phone (+44) (0) 1865 843830; fax (+44) (0) 1865 853333;
email: permissions@elsevier.com. Alternatively you can submit your request online by
visiting the Elsevier web site at <http://elsevier.com/locate/permissions>, and selecting
Obtaining permission to use Elsevier material

Notice

No responsibility is assumed by the publisher for any injury and/or damage to persons or
property as a matter of products liability, negligence or otherwise, or from any use or
operation of any methods, products, instructions or ideas contained in the material
herein. Because of rapid advances in the medical sciences, in particular, independent
verification of diagnoses and drug dosages should be made

ISBN-13:978-0-12-002057-7

ISBN-10:0-12-002057-2

ISSN:0065-2156

For information on all Academic Press publications
visit our website at books.elsevier.com

Printed and bound in USA

06 07 08 09 10 10 9 8 7 6 5 4 3 2 1

Working together to grow
libraries in developing countries

www.elsevier.com | www.bookaid.org | www.sabre.org

ELSEVIER BOOK AID International Sabre Foundation

Contents

PREFACE	vii
-------------------	-----

Streamline Topology: Patterns in Fluid Flows and their Bifurcations

Morten Brøns

Abstract	1
I. Introduction	1
II. Basic Concepts	4
III. Bifurcation of Flows Away from Boundaries	9
IV. Flow Near a Wall	20
V. Flow Near a Wall with Mirror Symmetry	27
VI. Axisymmetric Flows and Application to Vortex Breakdown	32
VII. Conclusions and Outlook	38
References	40

Electrospinning of Nanofibers from Polymer Solutions and Melts

D.H. Reneker, A.L. Yarin, E. Zussman and H. Xu

Abstract	44
I. Introduction and Background	45
II. Various Methods of Producing Nanofibers	46
III. Electrospinning of Nanofibers	46
IV. Taylor Cone and Jetting from Liquid Droplets in Electrospinning of Nanofibers	47
V. Bending Instability of Electrically Charged Liquid Jets of Polymer Solutions in Electrospinning	73
VI. Scientific and Technological Challenges in Producing Nanofibers with Desirable Characteristics and Properties	146
VII. Characterization Methods and Tools for Studying the Nanofiber Properties	156

VIII. Development and Applications of Several Specific Types of Nanofibers	172
Acknowledgment	184
References	184

A Bibliography of Vortex Dynamics 1858–1956*Vyacheslav V. Meleshko and Hassan Aref*

1. Introduction	197
2. Case studies	209
3. Conclusion	244
Acknowledgements	245
References	245

Field-Assisted Self-Assembly of Superparamagnetic Nanoparticles for Biomedical, MEMS and BioMEMS Applications*Ranjan Ganguly and Ishwar K. Puri*

I. Practical Significance of Ferrofluids and Magnetic Microspheres	294
II. Field-Induced Ferrofluid Aggregation	300
III. Thermomechanical Ferrofluid Applications	319
IV. BioMEMS and Biomedical Applications of Magnetic Microspheres	322
V. Closing Remarks	330
References	331

SUBJECT INDEX	337
-------------------------	-----

COLOR PLATE SECTION	
---------------------	--

Preface

It has long been recognized that major developments in the fields of fluid and solid mechanics are scattered throughout an array of technical journals, often making it difficult to find what the real advances are, especially for a researcher new to the field or an individual interested in discovering the state-of-the-art in connection with applications. Since its first publication in 1948 the *Advances in Applied Mechanics* book series has drawn together timely, significant advances in various topics in applied mechanics. *Advances in Applied Mechanics* aims to provide authoritative review articles on topics in the mechanical sciences, primarily of interest to scientists and engineers working in the various branches of mechanics, but also of interest to the many who use the results of investigations in mechanics in various application areas such as aerospace, chemical, civil, environmental, mechanical and nuclear engineering.

Authors are encouraged to write at such a level and in such a style that a graduate student looking for a research area or a worker in another area of mechanics could use the article to quickly reach the frontlines of the topic reviewed. As such, articles will often be more didactic than may be common in many reviews these days. *Advances in Applied Mechanics* does not set a page limit on articles or volumes, and some volumes will be published with a few longer articles, others with several shorter articles. A successful article will speak authoritatively to readers and will become a treasured point of reference. We believe such articles will have considerable impact and will promote our science.

Volume 41 in the series contains articles on topological fluid mechanics, electrospinning, vortex dynamics and self-assembly.

Hassan Aref
Erik van der Giessen

This page intentionally left blank

Streamline Topology: Patterns in Fluid Flows and their Bifurcations

MORTEN BRØNS

Department of Mathematics, Technical University of Denmark, Denmark

Abstract	1
I. Introduction	1
II. Basic Concepts	4
III. Bifurcation of Flows Away from Boundaries	9
IV. Flow Near a Wall	20
V. Flow Near a Wall with Mirror Symmetry	27
VI. Axisymmetric Flows and Application to Vortex Breakdown	32
VII. Conclusions and Outlook	38
References	40

Abstract

Using dynamical systems theory, we consider structures such as vortices and separation in the streamline patterns of fluid flows. Bifurcation of patterns under variation of external parameters is studied using simplifying normal form transformations. Flows away from boundaries, flows close to fixed walls, and axisymmetric flows are analyzed in detail. We show how to apply the ideas from the theory to analyze numerical simulations of the vortex breakdown in a closed cylindrical container.

I. Introduction

A starting point in any analysis of a fluid mechanics problem is invariably a determination of the overall flow structure. Is the flow turbulent or laminar? Is the flow separated or attached to solid boundaries? Are there vortical structures and recirculating zones in the flow? Answers to questions such as these are needed to understand the physics of the flow and to obtain important parameters such as lift and drag, pressure and load distributions,

and transfer rates of heat and mass. Thus, even if the final goal of treating a fluid mechanics problem is a *quantitative* one, a basic *qualitative* understanding of the structures in the flow is necessary.

As an illustration, consider the flow around a simple bluff body, a circular cylinder. The flow is characterized by a Reynolds number

$$\text{Re} = \frac{Ud}{v}, \quad (1.1)$$

where U is the velocity of the incoming flow, d the cylinder diameter, and v the kinematic viscosity of the fluid. For low values of Re , the flow follows the cylinder surface, but at a certain $\text{Re}_0 \approx 5$ the flow separates, and two counter-rotating vortices are created behind the cylinder (see Fig. 1.1). A *bifurcation* in the streamline pattern takes place at Re_0 .

The flows shown in Fig. 1.1 are steady. The figure shows the streamlines, which are the curves that are everywhere tangent to the velocity field $\mathbf{v}(\mathbf{x})$. That is, the curves $\mathbf{x}(t)$ which fulfill the differential equation

$$\frac{d\mathbf{x}(t)}{dt} = \mathbf{v}(\mathbf{x}(t)). \quad (1.2)$$

The analysis of a streamline pattern commences by locating the *critical points* \mathbf{x}_0 where $\mathbf{v}(\mathbf{x}_0) = 0$. In Fig. 1.1(a), there are no critical points in the fluid away from the cylindrical surface, while in Fig. 1.1(b) three such points exist. Two of these are located in the centers of the vortices and are hence denoted *centers*. The streamlines close to the centers are closed, and the motion of fluid particles is a rotation around the centers. The third critical point is of *saddle* type and is located further downstream on the axis of symmetry. Saddle points are characterized by the existence of two streamlines which approach the point – *the stable separatrices* – and two

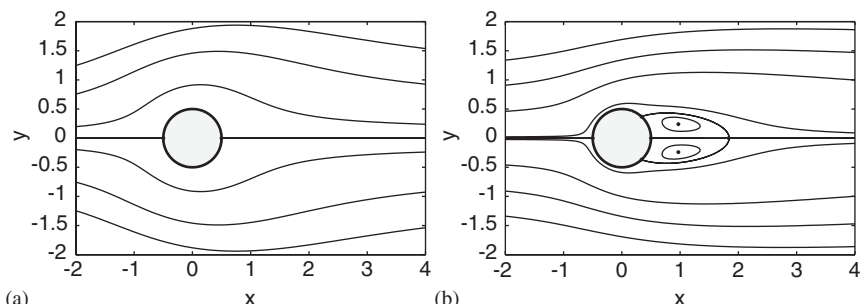


FIG. 1.1. Numerical simulations of the flow from left to right around a circular cylinder. (a) $\text{Re} = 1.54$. (b) $\text{Re} = 26$. Reproduced from Bisgaard (2005).

streamlines which emanate from it – *the unstable separatrices*. All other streamlines in a neighborhood come close to the saddle along a stable separatrix and leave again along an unstable separatrix.

Owing to the no-slip boundary condition, all points on the cylindrical surface are critical points. However, it appears that there are saddle-like points on the surface which divide the flow. In Fig. 1.1(a) there is a *point of attachment* on the upstream side of the cylinder and a corresponding *point of separation* on the downstream side. In Fig. 1.1(b), there are two additional points of separation on the cylinder. The stable separatrices of the in-flow saddle coincide with the unstable separatrices of the separation points. The unstable separatrices of the in-flow saddle lie on the line of symmetry. One meets the cylinder in a point of attachment, the other goes away downstream.

It appears that when the critical points, the points of separation and attachment and the separatrices are located, a complete qualitative description of the streamline pattern is obtained. Together they form a *skeleton* of the streamline pattern. Separatrices divide the flow into regions of different kinds of motion. Inside the region formed by the cylinder and the separatrices of the in-flow saddle, all streamlines are closed. Outside, the streamlines go from the upstream to the downstream. In fluid mechanics, separatrices are commonly known as *dividing streamlines*.

In the above analysis, we have focused on the *topology* of the flow pattern and how it bifurcates under variation of a control parameter, the Reynolds number Re . It is the purpose of the present paper to give an introduction to the mathematical methods that can be used to analyze such bifurcations systematically. We will construct bifurcation diagrams which represent possible changes that can occur when certain well-defined degeneracy conditions are met. An important tool is *normal form transformations* which allow a considerable simplification of the velocity fields. The technique is a cornerstone in the theory of dynamical systems. For a general introduction see e.g. [Chow et al. \(1994\)](#) and [Wiggins \(1990\)](#). The analysis will be *local*, and will be based on power series expansions of the velocity field in a neighborhood of a given point in the fluid. For simplicity, we will only consider patterns in 2D flows.

The idea of obtaining a qualitative insight in fluid flows by analyzing the streamlines of Eq. (1.2), and in particular the critical points, is an old one. Early ideas on separation are proposed by [Legendre \(1956\)](#), recently reviewed in by [Déler \(2001\)](#), [Oswatitsch \(1958\)](#), [Davey \(1961\)](#), [Dean \(1950\)](#), and [Lighthill \(1963\)](#). Review papers by [Tobak and Peake \(1982\)](#) and [Perry and Chong \(1987\)](#) provide useful overviews. In his thesis, [Bakker \(1991\)](#) was the first to use bifurcation theory to systematically describe changes of patterns. Here, we present some further developments of Bakker's approach

based on Brøns (1994, 1999), Brøns and Hartnack (1999), Brøns et al. (1999, 2001), and Hartnack (1999a, 1999b) including an application to a specific flow, vortex breakdown in a confined geometry.

II. Basic Concepts

The fundamental law of mechanics, Newton's second law, is a second-order differential equation. Thus, to determine the motion of a particle, two integrations must be performed. In fluid mechanics, the first integration is performed by solving the Euler equations for inviscid flows, the Navier–Stokes equations for viscous flows, or more complex equations for non-Newtonian fluids for the velocity field $\mathbf{v}(\mathbf{x}, t)$. With this, one further integration can be performed to obtain the motion of a fluid particle. We are concerned with the second step only, and assume that an *incompressible* velocity field is given, be it determined experimentally, numerically, or theoretically.

From a time-dependent velocity field, several families of curves can be defined. The *streamlines* are the instantaneous integral curves of the velocity field. At a given time instant t_0 they are the solution curves to the system of ordinary differential equations

$$\frac{d\mathbf{x}}{dt} = \mathbf{v}(\mathbf{x}, t_0). \quad (2.1)$$

The *pathlines* are the curves fluid particles follow in time. These are the same paths massless tracer particles will follow, and they are found by solving

$$\frac{d\mathbf{x}}{dt} = \mathbf{v}(\mathbf{x}, t). \quad (2.2)$$

Finally, *streaklines* are curves connecting particles that have passed through a common point \mathbf{x}_0 . If dye is continuously fed into the flow at \mathbf{x}_0 , the dye will form a streakline. If the solution to Eq. (2.2) which fulfills the initial condition $\mathbf{x}(t_0) = \mathbf{x}_0$ is denoted $\mathbf{x}(t; t_0)$, the streakline at time t is the curve

$$t_0 \rightarrow \mathbf{x}(t; t_0), t_0 \in [t_s, t], \quad (2.3)$$

where t_s is the time the experiment (or dye release) is started.

If the flow is steady, all three families of curves coincide. In general, there is no simple connection between the curves. We will be concerned with the structure of the streamlines.

We are interested in the qualitative structure of streamline patterns, and must first define what it means that two streamline patterns are qualitatively alike. Here the concept of topological equivalence is useful:

Definition 1. Two velocity fields \mathbf{v} and \mathbf{v}' are topologically equivalent if there exists a continuous, bijective map h , whose inverse is also continuous, that maps the streamlines of \mathbf{v} onto the streamlines of \mathbf{v}' such that the sense of time is preserved. If h is defined in a subset of the flow domain only, \mathbf{v} and \mathbf{v}' are locally topologically equivalent.

Think of the streamlines of \mathbf{v} being printed on a sheet of rubber. If the rubber sheet can be stretched and compressed (but not torn apart) such that the streamline pattern of \mathbf{v}' appears, the two velocity fields are topologically equivalent. In particular, the number of critical points are the same. As we are concerned with the local structure of flows, we will, in general, consider local topological equivalence only.

Having defined what we mean by topologically equivalent patterns, we can introduce a concept of robustness of fluid patterns with respect to perturbations or imperfections. Perturbations may be generated by a change of the geometry of the flow domain, of the boundary conditions, the constitutive equations for the fluid (Newtonian/Non-Newtonian), the physical effects included in the model, and so on. The question is whether a perturbation of this kind will result in a qualitative change in the pattern or not. The following definition captures the idea of robustness.

Definition 2. A velocity field $\mathbf{v}(\mathbf{x})$ is structurally stable if all perturbations $\mathbf{v}(\mathbf{x}) + \mathbf{v}'(\mathbf{x})$ are topologically equivalent to $\mathbf{v}(\mathbf{x})$, as long as \mathbf{v}' is sufficiently small. A velocity field which is not structurally stable is structurally unstable. A velocity field $\mathbf{v}(\mathbf{x})$ is locally structurally stable at \mathbf{x}_0 if $\mathbf{v}(\mathbf{x}) + \mathbf{v}'(\mathbf{x})$ is locally topologically equivalent to $\mathbf{v}(\mathbf{x})$ at \mathbf{x}_0 .

The definition requires a concept of a velocity field being “sufficiently small”. There are subtle mathematical issues in setting this up rigorously, based on introducing a norm on the space of velocity fields with appropriate smoothness. In the present paper, we will consider Taylor expansions of velocity fields, and consider cases where low-order terms determine the streamline topology. Hence, we will essentially operate on polynomial velocity fields, and here a norm is easily obtained: A polynomial velocity field is small if the coefficients are small.

Structural stability and instability can be demonstrated in a simple way. Consider the flow generated by n identical rollers placed in the vertices of a regular n -gon, n even. Consecutive rollers rotate in opposite directions with the same angular velocity and drive a viscous flow. If $n = 4$, Fig. 2.1(a), the flow is organized around a stagnation point of saddle type. We will show later that a saddle point is structurally stable, so a perturbation, e.g. a small

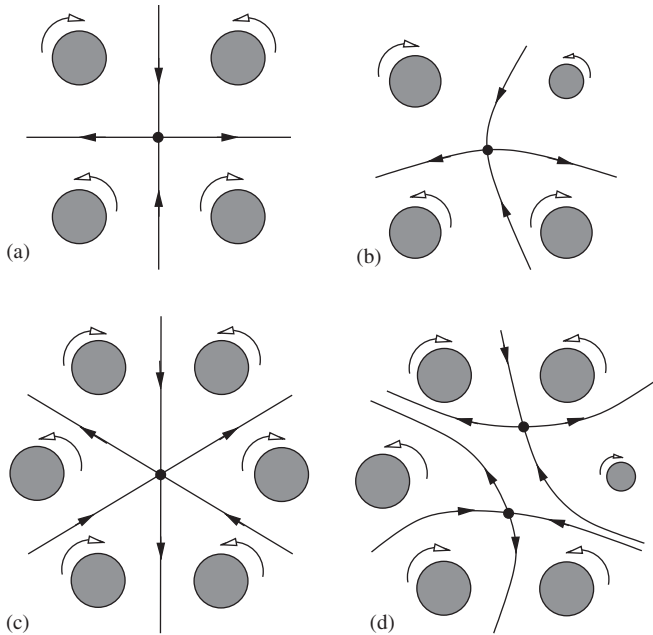


FIG. 2.1. (a) Four mill roll. (b) Perturbed four mill roll. (c) Six mill roll. (d) Perturbed six mill roll.

displacement or a change of size of a roller, will not change the flow qualitatively, Fig. 2.1(b). For $n = 6$, Fig. 2.1(c), the geometry does not allow a regular saddle. The critical point is known as a *topological saddle with six hyperbolic sectors*, and it is structurally unstable. A perturbation will give rise to a qualitatively different flow pattern, for example as in Fig. 2.1(d), where an alleyway of fluid through the center is created.

Special constraints will influence the structural stability of a given velocity field. The smaller the set of allowed perturbations, the easier it is for the field to be structurally stable. This is important when symmetry is considered. A velocity field may be structurally stable with respect to perturbations obeying a symmetry, but unstable if more general perturbations are also taken into account.

It is important to distinguish structural stability from traditional hydrodynamical stability. Several situations are of interest, the simplest being the following. Consider a steady solution $\mathbf{v}_0(\mathbf{x})$ to the Navier–Stokes equations, and consider the temporal development of a perturbation $\mathbf{v}(\mathbf{x}, t)$ which at time $t = 0$ is $\mathbf{v}_0(\mathbf{x}) + \mathbf{v}'(\mathbf{x})$. If $\mathbf{v}(\mathbf{x}, t)$ stays close to $\mathbf{v}_0(\mathbf{x})$ for $t > 0$ so long as \mathbf{v}' is sufficiently small, \mathbf{v} is hydrodynamically stable. If further $\mathbf{v}(\mathbf{x}, t) \rightarrow \mathbf{v}_0(\mathbf{x})$ for $t \rightarrow \infty$, the steady field is asymptotically stable.

There is no immediate connection between the structural stability and the dynamic stability of a velocity field. This is illustrated by the flow around a circular cylinder. There is no dynamic instability associated with the topological transition at Re_0 . There is a unique asymptotically stable steady velocity field for Re up to about 48, where the steady flow loses stability in a Hopf bifurcation and stable periodic solutions are created.

The Flow Box Theorem gives an important description of almost all points in a flow.

Theorem 1. *Let \mathbf{x}_0 be a regular point for the velocity field \mathbf{v} , that is, a point where $\mathbf{v}(\mathbf{x}_0) \neq 0$. Then there exists a neighborhood of \mathbf{x}_0 where \mathbf{v} is topologically equivalent to the constant velocity field $(1, 0)$.*

For a proof see e.g. [Abraham et al. \(1983\)](#). If a velocity field with a regular point is perturbed slightly, the regularity of the point will persist. Hence, an immediate consequence of the Flow Box Theorem is

Theorem 2. *Regular points are locally structurally stable.*

We are interested in changes in the flow pattern, and hence must look for the structurally unstable fields. From the above it follows that we must look for the critical points (see [Fig. 2.2](#)).

The ideas and concepts discussed hitherto hold in any dimensions. From now on we consider two-dimensional flows only.

Incompressibility of the fluid imposes a special structure of the streamlines. The velocity field is divergence free, $\nabla \cdot \mathbf{v} = 0$, and it follows that a stream function $\psi(x, y)$ exists such that

$$u = \frac{\partial \psi}{\partial y}, \quad v = \frac{\partial \psi}{\partial x}, \quad (2.4)$$

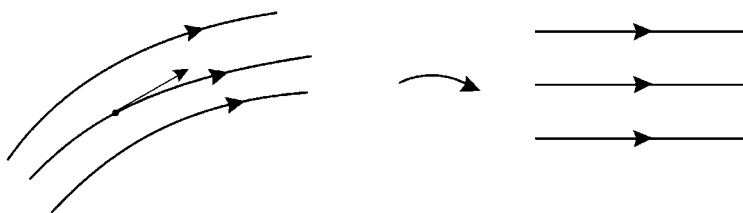


FIG. 2.2. The flow box theorem. Close to a regular critical point the streamline topology is trivial.

where $\mathbf{v} = (u, v)$. The differential equations (2.1) for the streamlines now become

$$\frac{dx}{dt} = \frac{\partial \psi}{\partial y}, \quad \frac{dy}{dt} = -\frac{\partial \psi}{\partial x}, \quad (2.5)$$

which is a Hamiltonian system with Hamiltonian ψ . This means that ψ is constant along the streamlines,

$$\frac{d\psi}{dt} = \frac{\partial \psi}{\partial x} \frac{dx}{dt} + \frac{\partial \psi}{\partial y} \frac{dy}{dt} = \frac{\partial \psi}{\partial x} \frac{\partial \psi}{\partial y} + \frac{\partial \psi}{\partial y} \left(-\frac{\partial \psi}{\partial x} \right) = 0. \quad (2.6)$$

Hence, the streamlines lie on the iso-curves of ψ .

We consider an expansion of ψ in a Taylor series at the origin,

$$\psi = \sum_{n,m=0}^{\infty} a_{n,m} x^n y^m, \quad (2.7)$$

and the differential equations (2.5) for the streamlines are then

$$\begin{pmatrix} dx/dt \\ dy/dt \end{pmatrix} = \begin{pmatrix} a_{0,1} \\ -a_{1,0} \end{pmatrix} + \begin{pmatrix} a_{1,1} & 2a_{0,2} \\ -2a_{2,0} & -a_{1,1} \end{pmatrix} \begin{pmatrix} x \\ y \end{pmatrix} + \mathcal{O}(2), \quad (2.8)$$

where $\mathcal{O}(2)$ denotes terms of order $(x,y)^2$.

If $a_{1,0} = a_{0,1} = 0$, the origin is a critical point. The eigenvalues of the linearization of (2.8), obtained by dropping the $\mathcal{O}(2)$ term, are $\lambda = \pm \sqrt{4a_{2,0}a_{0,2} - a_{1,1}^2}$. If the linearization is regular, there is either a pair of real eigenvalues of opposite sign or a pair of purely imaginary eigenvalues. In the first case, the linearized system has a saddle point at the origin, in the latter case a center. The separatrices for the saddle approach the critical point along the eigendirections. The stable separatrices are tangent to the eigendirection of the negative eigenvalue, the unstable separatrices are tangent to the eigendirection of the positive eigenvalue. If ψ takes the value K at a saddle, the separatrices can be found by solving $\psi(x,y) = K$.

Standard theory for Hamiltonian systems, see e.g. Grimshaw (1991) and Wiggins (1990), shows that this behavior persists if higher order terms are included. Furthermore, it is not difficult to see that a general small perturbation of ψ will only make the critical point move slightly, keeping its type. Hence,

Theorem 3. *Non-degenerate critical points are locally structurally stable.*

Hence to locate bifurcation we must seek *degenerate critical points* where the Jacobian matrix in Eq. (2.8) is singular. In such points, the higher order

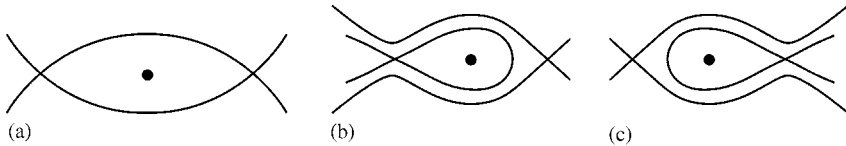


FIG. 2.3. (a) A heteroclinic connection. (b, c) Typical perturbations of a heteroclinic cycle.

terms $\mathcal{O}(2)$ which were dropped in the linearization become decisive. We analyze degenerate critical points in the next section, and conclude here by pointing out global configurations which are structurally unstable, namely *heteroclinic connections*. If an unstable separatrix of one saddle point is identical to a stable separatrix of another saddle point, this streamline is denoted a *heteroclinic streamline*. The typical situation where the two saddles are connected in a heteroclinic loop is shown in Fig. 2.3. This configuration requires that ψ takes the same value at both saddles. A small perturbation will preserve the saddle structure near the critical points, but arbitrarily small perturbations may move the saddles away from the same level of ψ and destroy the cycle.

III. Bifurcation of Flows Away from Boundaries

We now turn to the analysis of degenerate critical points for the stream function (2.7). If $a_{1,0} = a_{0,1} = 0$, the origin is a critical point. If the determinant of the Jacobian $4a_{2,0}a_{0,2} - a_{1,1}^2$ is zero, the critical point is degenerate, and zero is an eigenvalue of the Jacobian with algebraic multiplicity 2. Two sub-cases arise. The geometric multiplicity of the eigenvalue is one or it is two, and the Jacobian is the zero matrix. We consider the first case, a *simple linear degeneracy*. Without loss of generality, we assume that the coordinate system is chosen such that the Jacobian is in Jordan normal form

$$J_0 = \begin{pmatrix} 0 & 2a_{0,2} \\ 0 & 0 \end{pmatrix}. \quad (3.1)$$

Thus, we consider the *degeneracy conditions*

$$a_{1,0} = a_{0,1} = 0 = a_{1,1} = a_{2,0} = 0, \quad (3.2)$$

and the non-degeneracy condition

$$a_{0,2} \neq 0. \quad (3.3)$$

To analyze the role of the cubic terms of ψ (quadratic in the velocity field), we first perform a coordinate transformation to simplify ψ as much as possible. We define a *near-identity quadratic transformation* by

$$\begin{aligned} x &= \xi + r_{2,0}\xi^2 + r_{1,1}\xi\eta + r_{0,2}\eta^2, \\ y &= \eta + s_{2,0}\xi^2 + s_{1,1}\xi\eta + s_{0,2}\eta^2. \end{aligned} \quad (3.4)$$

The Jacobian determinant of the mapping is 1 at the origin, and it follows from the Inverse Function Theorem that it is invertible in a neighborhood of the origin and hence defines a local coordinate transformation. The inverse transformation can be found as a power series,

$$\begin{aligned} \xi &= x + \bar{r}_{2,0}x^2 + \bar{r}_{1,1}xy + \bar{r}_{0,2}y^2 + \dots, \\ \eta &= y + \bar{s}_{2,0}x^2 + \bar{s}_{1,1}xy + \bar{s}_{0,2}y^2 + \dots, \end{aligned} \quad (3.5)$$

by inserting (3.5) in (3.4) and equating terms of the same order. We are free to choose $r_{n,m}$ and $s_{n,m}$, and will do so to make the transformed ψ as simple as possible.

With the transformation (3.4) inserted in the stream function (2.7) we obtain

$$\begin{aligned} \psi &= a_{0,2}\eta^2 + a_{3,0}\xi^3 \\ &\quad + (2a_{0,2}s_{2,0} + a_{2,1})\xi^2\eta \\ &\quad + (2a_{0,2}s_{1,1} + a_{1,2})\xi\eta^2 \\ &\quad + (2a_{0,2}s_{0,2} + a_{0,3})\eta^3 + \mathcal{O}(4). \end{aligned} \quad (3.6)$$

By choosing

$$s_{2,0} = -\frac{a_{2,1}}{2a_{0,2}}, \quad s_{1,1} = -\frac{a_{1,2}}{2a_{0,2}}, \quad s_{0,2} = -\frac{a_{0,3}}{2a_{0,2}}, \quad (3.7)$$

we remove three third-order terms of ψ and get

$$\psi = a_{0,2}\eta^2 + a_{3,0}\xi^3 + \mathcal{O}(4). \quad (3.8)$$

Note, that the coefficients $r_{n,m}$ in (3.4) do not appear in the transformed stream function (3.6). Hence we may set them all to zero. Alternatively, as in Brøns and Hartnack (1999), they can be chosen to make the transformation *canonical*, which in 2D is equivalent to being area-preserving. Canonical transformations are commonly used in Hamiltonian dynamics, but as we are only interested in the shape of the streamlines, and not the temporal details of the motion of the fluid particles, any transformation will do.

If $a_{3,0} = 0$, no cubic terms are left, and we must proceed to fourth order terms in ψ to resolve the behavior close to the critical point. Renaming the coordinates back to x, y the transformed stream function (3.8) can be written as

$$\psi = a_{0,2}y^2 + \tilde{a}_{4,0}x^4 + \tilde{a}_{3,1}x^3y + \tilde{a}_{2,2}x^2y^2 + \tilde{a}_{0,4}y^4 + \mathcal{O}(5) \quad (3.9)$$

with

$$\begin{aligned} \tilde{a}_{4,0} &= a_{4,0} - \frac{a_{2,1}^2}{4a_{0,2}}, \\ \tilde{a}_{3,1} &= a_{3,1} - \frac{a_{1,2}a_{2,1}}{a_{0,2}}, \\ \tilde{a}_{2,2} &= a_{2,2} + \frac{6a_{2,1}a_{0,3} - 3a_{1,2}^2}{4a_{0,2}}, \\ \tilde{a}_{1,3} &= a_{1,3} - 2\frac{a_{1,2}a_{0,3}}{a_{0,2}}, \\ \tilde{a}_{0,4} &= a_{0,4} - \frac{5a_{0,3}^2}{4a_{0,2}}, \end{aligned} \quad (3.10)$$

where the influence of the quadratic transformation on the fourth-order terms presents itself. With a cubic near-identity transformation

$$\begin{aligned} x &= \xi + r_{3,0}\xi^3 + r_{2,1}\xi^2\eta + r_{1,2}\xi\eta^2 + r_{0,3}\eta^3, \\ y &= \eta + s_{3,0}\xi^3 + s_{2,1}\xi^2\eta + s_{1,2}\xi\eta^2 + s_{0,3}\eta^3, \end{aligned} \quad (3.11)$$

we obtain

$$\begin{aligned} \psi &= a_{0,2}\eta^2 + \tilde{a}_{4,0}\xi^4 \\ &\quad + (2a_{0,2}s_{3,0} + \tilde{a}_{3,1})\xi^3\eta + (2a_{0,2}s_{2,1} + \tilde{a}_{2,2})\xi^2\eta^2 \\ &\quad + (2a_{0,2}s_{1,2} + \tilde{a}_{1,3})\xi\eta^3 + (2a_{0,2}s_{0,3} + \tilde{a}_{0,4})\eta^4 + \mathcal{O}(5). \end{aligned} \quad (3.12)$$

Again, the $r_{n,m}$ do not appear, so we set them to zero. By choosing

$$s_{3,0} = -\frac{\tilde{a}_{3,1}}{2a_{2,0}}, \quad s_{2,1} = -\frac{\tilde{a}_{2,2}}{2a_{2,0}}, \quad s_{1,2} = -\frac{\tilde{a}_{1,3}}{2a_{2,0}}, \quad s_{0,3} = -\frac{\tilde{a}_{0,4}}{2a_{2,0}}, \quad (3.13)$$

we get

$$\psi = a_{0,2}\eta^2 + \tilde{a}_{4,0}\xi^4 + \mathcal{O}(5). \quad (3.14)$$

If $\tilde{a}_{4,0} = 0$ all fourth-order terms are zero, and fifth-order terms must be taken into account. To simplify these terms, a fourth-order near-identity

transformation is employed. And so on, to any finite order. In each stage, the decisive coefficient is

$$\begin{aligned} \tilde{a}_{N,0} &= a_{N,0} + \text{a non-linear combination} \\ &\quad \text{of } a_{n,m} \text{'s of lower order than } N, \end{aligned} \quad (3.15)$$

and $\tilde{a}_{3,0} = a_{3,0}$. The general case is summarized in the following

Theorem 4. *Let the origin be a degenerate critical point for the stream function ψ given in (2.7) such that $a_{1,0} = a_{0,1} = a_{1,1} = a_{2,0} = 0$, but $a_{0,2} \neq 0$. If $\tilde{a}_{n,0} = 0$ for $n < N$ and $\tilde{a}_{N,0} \neq 0$ there is a change of coordinates which brings ψ into the normal form*

$$\psi = a_{0,2}y^2 + \tilde{a}_{N,0}x^N + \mathcal{O}(N+1), \quad (3.16)$$

where $\tilde{a}_{N,0} = a_{N,0} + \text{a non-linear combination of } a_{n,m} \text{'s of lower order than } N$.

The normal form (3.16) strongly simplifies the analysis. Disregarding the \mathcal{O} -term to get the *truncated normal form*, we see that there are separatrices approaching the critical point which has $\psi = 0$ of the form

$$y = \pm \sqrt{-\frac{\tilde{a}_{N,0}}{a_{0,2}}} x^N. \quad (3.17)$$

If N is odd, this gives rise to two separatrices meeting in a *cusp*. If N is even, two subcases occur. If $\tilde{a}_{N,0}/a_{0,2} > 0$, the critical point is a local extremum for ψ . No separatrices exist and the critical point is a *degenerate center*. If $\tilde{a}_{N,0}/a_{0,2} < 0$, we obtain four separatrices which meet in a *topological saddle*. See Fig. 3.1.

We are not only interested in the streamline pattern at the exact degeneracy given by (3.2), but also want to study the dynamics when the degeneracy conditions are not exactly fulfilled. To this end, we consider the degenerate parameters as small parameters,

$$\varepsilon_1 = a_{1,0}, \varepsilon_2 = a_{0,1}, \varepsilon_3 = a_{2,0}, \varepsilon_4 = a_{1,1}, \quad (3.18)$$

and assume the non-degeneracy conditions $a_{0,2} \neq 0, a_{3,0} \neq 0$.

To simplify the stream function under these conditions, we extend the quadratic transformation to include terms which are quadratic in both the coordinates and the parameters. Anticipating that only a transformation in y is needed as before we let $x = \xi$ and

$$\begin{aligned} y &= \eta + s_{2,0}\xi^2 + s_{1,1}\xi\eta + s_{0,2}\eta^2 \\ &\quad + (s_{1,0,1}\varepsilon_1 + s_{1,0,2}\varepsilon_2 + s_{1,0,3}\varepsilon_3 + s_{1,0,4}\varepsilon_4)\xi \\ &\quad + (s_{0,1,1}\varepsilon_1 + s_{0,1,2}\varepsilon_2 + s_{0,1,3}\varepsilon_3 + s_{0,1,4}\varepsilon_4)\eta. \end{aligned} \quad (3.19)$$

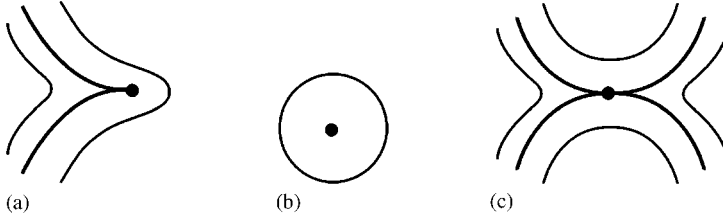


FIG. 3.1. Degenerate critical points obtained from the normal form (3.16). (a) Cusp. (b) Degenerate center. (c) Topological saddle.

Inserting this in (2.7) yields a long expression which we omit here. When all the $\varepsilon_k = 0$, the stream function reduces to the degenerate case, and hence we again make the choice (3.7). With this, most of the terms in (3.19) depending on the ε_k introduce new terms in ψ not present originally, and we set the corresponding $s_{n,m,k} = 0$. But three terms can be removed by a non-trivial choice, namely

$$\begin{aligned} & \left(2a_{2,0}s_{1,0,2} - \frac{a_{1,2}}{2a_{0,2}} \right) \xi \eta \varepsilon_2, (1 + 2a_{0,2}s_{1,0,3}) \xi \eta \varepsilon_3, \\ & \left(2a_{0,2}s_{0,1,2} - \frac{a_{0,3}}{2a_{0,2}} \right) \eta^2 \varepsilon_2. \end{aligned} \quad (3.20)$$

These terms are removed by choosing

$$s_{1,0,2} = \frac{a_{1,2}}{4a_{0,2}^2}, s_{1,0,3} = -\frac{1}{2a_{0,2}}, s_{0,1,2} = \frac{a_{0,3}}{4a_{0,2}^2} \quad (3.21)$$

With this, we obtain

$$\psi = \mu_1 \xi + \mu_2 \eta + \mu_3 \xi^2 + a_{0,2} \eta^2 + a_{3,0} \xi^3 + \mathcal{O}(4) \quad (3.22)$$

where $\mathcal{O}(4)$ are terms of fourth order in coordinates and parameters and

$$\begin{aligned} \mu_1 &= \varepsilon_1 + \frac{a_{1,2}}{4a_{0,2}^2} \varepsilon_2^2 - \frac{1}{2a_{0,2}} \varepsilon_2 \varepsilon_3, \\ \mu_2 &= \varepsilon_2 + \frac{a_{0,3}}{4a_{0,2}^2} \varepsilon_2^2, \mu_3 = \varepsilon_4 - \frac{a_{2,1}}{2a_{0,2}} \varepsilon_2, \end{aligned} \quad (3.23)$$

are new small parameters. Note, that the number of small parameters are reduced from four to three. The procedure can be continued to any order in the ε_k by adding terms of higher order in the ε_k in transformation (3.19). A formal proof can be made with the use of the Implicit Function Theorem.

Further simplification can be obtained by a translation of the origin, since it is always possible to remove the term of the next-highest degree in a univariate polynomial in this way. In Bakker (1991), this is denoted *the movement principle*. With the transformation $\xi \rightarrow \xi + \xi_0$, $\eta \rightarrow \eta + \eta_0$ we can remove the ξ^2 and η term in (3.22) by choosing

$$\xi_0 = -\frac{\mu_2}{2a_{0,2}} \quad \eta_0 = -\frac{\mu_3}{3a_{3,0}}, \quad (3.24)$$

and we find

$$\psi = \left(\mu_1 + \frac{\mu_3^2}{3a_{3,0}} \right) \xi + a_{0,2} \eta^2 + a_{3,0} \xi^3 + \mathcal{O}(4). \quad (3.25)$$

Here a constant term introduced by the transformation has been omitted, as we are only interested in the level curves of ψ . Two more small parameters have been removed.

Finally, we scale ψ by dividing by $2a_{0,2}$ and scale ξ by

$$\xi \rightarrow \left(\frac{2a_{0,2}}{3a_{3,0}} \right)^{1/3} \xi \quad (3.26)$$

to obtain

$$\psi = c_1 \xi + \frac{1}{2} \eta^2 + \frac{1}{3} \xi^3 + \mathcal{O}(4) \quad (3.27)$$

with

$$c_1 = \left(12a_{0,2}a_{3,0}^2 \right)^{-1/3} \left(\mu_1 + \frac{\mu_3^2}{3a_{3,0}} \right). \quad (3.28)$$

If $a_{3,0}$ is also small, we need to include terms of fourth order in ψ , and use a near-identity transformation of order four to make the initial transformations. The latter transformations can be performed if $\tilde{a}_{0,4}$ defined in (3.10) is non-zero. In general, one obtains

Theorem 5. *Let $a_{1,0}$, $a_{0,1}$, $a_{2,0}$, $a_{1,1}$, and $\tilde{a}_{n,0}$ for $n < N-1$ be small parameters, and assume the non-degeneracy conditions $a_{0,2} \neq 0$ and $\tilde{a}_{N,0} \neq 0$. Then there is a coordinate transformation that brings ψ into the normal form*

$$\begin{aligned} \psi &= \frac{\sigma}{2} y^2 + f(x) + \mathcal{O}(N+1), \\ f(x) &= \sum_{n=1}^N c_n x^n, c_{N-1} = 0, c_N = \frac{1}{N}, \end{aligned} \quad (3.29)$$

where

$$\sigma = \begin{cases} -1 & \text{for } N \text{ even and } a_{0,2}/\tilde{a}_{N,0} < 0, \\ +1 & \text{for } N \text{ even and } a_{0,2}/\tilde{a}_{N,0} > 0 \text{ or } N \text{ odd,} \end{cases} \quad (3.30)$$

and c_1, \dots, c_{N-2} are small parameters.

The two subcases arise from the generalization of (3.26). For N even, only the root of the absolute value exists, and the transformation is

$$\xi \rightarrow \left| \frac{2a_{0,2}}{N\tilde{a}_{N,0}} \right|^{1/N} \xi. \quad (3.31)$$

In the case $a_{0,2}/\tilde{a}_{N,0} < 0$, the resulting coefficient of ξ^N is $-1/N$. Then ψ is replaced by $-\psi$, and the form (3.29) results with $\sigma = -1$.

We now analyze the *truncated normal forms* obtained by dropping the $\mathcal{O}(N+1)$ term in (3.29) so ψ reduces to a polynomial.

Before analyzing specific cases, some general observations can be made. The reduced normal form is even in y , and all streamline patterns will have reflectional symmetry in the x -axis. Critical points fulfill

$$\frac{\partial \psi}{\partial x} = f'(x) = 0, \quad \frac{\partial \psi}{\partial y} = \sigma y = 0. \quad (3.32)$$

Hence, they are all situated on the x -axis and there are at most $N-1$ of them. The Jacobian at a critical point is

$$\begin{pmatrix} 0 & \sigma \\ -f''(x) & 0 \end{pmatrix}, \quad (3.33)$$

and we see that it is a center if $\sigma f''(x) > 0$ and a saddle if $\sigma f''(x) < 0$. If $f''(x) = 0$, the critical point is degenerate.

Bifurcation will also occur when two saddle points are connected by a heteroclinic streamline. If the two points are $(x_1, 0)$ and $(x_2, 0)$, the condition for this to happen is

$$\begin{aligned} f(x_1) &= f(x_2), \quad f'(x_1) = f'(x_2) = 0, \\ f''(x_1) &< 0, \quad f''(x_2) < 0. \end{aligned} \quad (3.34)$$

The first condition says that the stream function has the same value at the two critical points, the second that they indeed are critical points, and the inequalities say that the critical points are saddles.

For $N = 3$ we have

$$f(x) = c_1 x + \frac{1}{3} x^3. \quad (3.35)$$

and $\sigma = +1$. The critical points fulfill

$$f'(x) = c_1 + x^2 = 0, \quad (3.36)$$

that is, there are solutions $x = \pm\sqrt{-c_1}$ if $c_1 \leq 0$. At these solutions, $f''(x) = \pm 2\sqrt{-c_1}$ showing that one is a saddle and one is a center which coalesce and disappear for $c_1 = 0$. The bifurcation diagram is shown in Fig. 3.2. The bifurcation has been denoted a *cusp bifurcation*.

For $N = 4$ we have

$$f(x) = c_1 x + c_2 x^2 + \frac{1}{4} x^4, \quad (3.37)$$

leading to the bifurcation conditions

$$f'(x) = c_1 + 2c_2 x + x^3 = 0, \quad f''(x) = 2c_2 + 3x^2 = 0. \quad (3.38)$$

Solving the latter equation for $x = \pm\sqrt{-2c_2/3}$ and inserting in the first equation yields the bifurcation curve

$$27c_1^2 + 32c_2^3 = 0. \quad (3.39)$$

For parameter values along this curve, a degenerate critical point exists in the flow. One finds easily that $f''' \neq 0$ here, hence the critical point is a cusp. It is also easy to see that there are three critical points when $27c_1^2 + 32c_2^3 > 0$, two of which are centers and one is a saddle if $\sigma = -1$ and vice versa if $\sigma = +1$. When $27c_1^2 + 32c_2^3 < 0$ there is one critical point which is a center if $\sigma = +1$ and a saddle if $\sigma = -1$.

When $\sigma = -1$, there can be two saddles, and hence a possibility for structurally unstable heteroclinic connections. After a little algebra, one finds that the conditions (3.34) are fulfilled when $c_1 = 0, c_2 < 0$, which then is

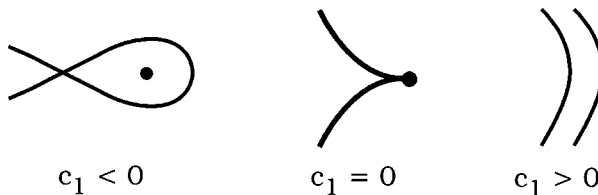


FIG. 3.2. Bifurcation in the normal form of order 3.

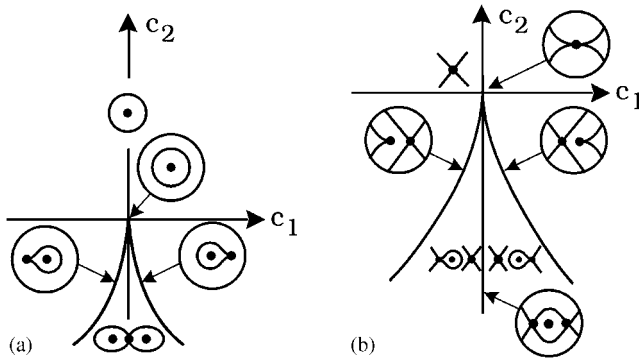


FIG. 3.3. Bifurcation diagrams for normal form of order 4. (a) $\sigma = +1$. (b) $\sigma = -1$.

yet a bifurcation curve. The findings are summarized in the bifurcation diagrams in Fig. 3.3.

For $N = 5$ we consider

$$\psi = \frac{1}{2}y^2 + c_1x + c_2x^2 + c_3x^3 + \frac{1}{5}x^5. \quad (3.40)$$

Local bifurcation occurs when

$$f'(x) = c_1 + 2c_2x + 3c_3x^2 + x^4 = 0, \quad f''(x) = 2c_2 + 6c_3x + 4x^3 = 0. \quad (3.41)$$

From the second equation we find

$$c_2 = -x(3c_3 + 2x^2), \quad (3.42)$$

and inserting this in the first equation of (3.41), one obtains

$$-\frac{1}{3}c_1 + c_3x^2 + x^4 = 0. \quad (3.43)$$

This is a quadratic equation in x^2 , and it will be convenient to use the discriminant D of this equation as a parameter instead of c_1 ,

$$D = c_3^2 + \frac{4}{3}c_1. \quad (3.44)$$

When $D \geq 0$, the solutions of (3.43) are

$$x^2 = -\frac{c_3}{2} \pm \frac{1}{2}\sqrt{D}. \quad (3.45)$$

Inserting this into (3.42) and squaring yields the condition for bifurcation

$$c_2^2 = \frac{1}{2} \left(-c_3 \pm \sqrt{D} \right) \left(2c_3 \pm \sqrt{D} \right)^2. \quad (3.46)$$

Heteroclinic streamlines occur when conditions (3.34) are fulfilled. Eliminating x_1, x_2 from the two equations yields after some algebra

$$27D^3 - 198D^2c_3^2 + 483c_3^4D + 54c_3c_2^2D - 392c_3^6 - 142c_2^2c_3^3 + 9c_2^4 = 0. \quad (3.47)$$

As the inequalities in (3.34) must also be fulfilled, only a part of the set defined by (3.47) will represent bifurcation points.

The parameter space (c_2, c_3, D) is three-dimensional. On the basis of the above, we can construct slices of the space for fixed values of D . For $D = 0$ bifurcation occurs at the cusp-shaped curve

$$c_2^2 = -2c_3^3 \quad (3.48)$$

as shown in Fig. 3.4(b). For $D > 0$, (3.46) gives rise to two curves as shown in Fig. 3.4(c), and additionally the heteroclinic bifurcation curve (3.47) appears. For $D < 0$ there is no bifurcation, so all streamline patterns are topologically equivalent. It is not difficult to verify that in this case there are two critical points.

The analysis of the truncated normal form (3.29) can in principle be continued to any order N , resulting in more and more complex interactions of critical points and heteroclinic streamlines. We have performed an analysis of the truncated normal form, where terms beyond the lowest order of non-degenerate terms are disregarded. A complete analysis should include a proof of this step being allowed, or, more precisely, that the truncated normal form is topologically equivalent to the full normal form. We have skipped this step which is tedious, and in some cases very technically demanding, see e.g. Chow et al. (1994). A rule of thumb for the truncated normal form being complete is that the streamline patterns are structurally stable away from the bifurcation sets obtained. This is the case for the examples considered here, but in Section VII we will see a 3D case where this is not the case.

There is some useful notation from singularity theory (Golubitsky and Schaeffer, 1985) associated with the type of analysis just performed. Let $\psi_0(x, y)$ be a given stream function, and let $\psi(x, y; \mathbf{p})$ where $\mathbf{p} \in \mathbb{R}^k$ be a k -parameter family of stream functions. If $\psi(x, y, \mathbf{0}) = \psi_0(x, y)$, ψ is denoted an *unfolding* of ψ_0 . If ψ captures all possible perturbations of ψ_0 , that is, if for all sufficiently small perturbations ψ' , there is a \mathbf{p} such that $\psi_0(x, y) + \psi'(x, y)$ is topologically equivalent to $\psi(x, y, \mathbf{p})$ the unfolding is called *versal*. Among

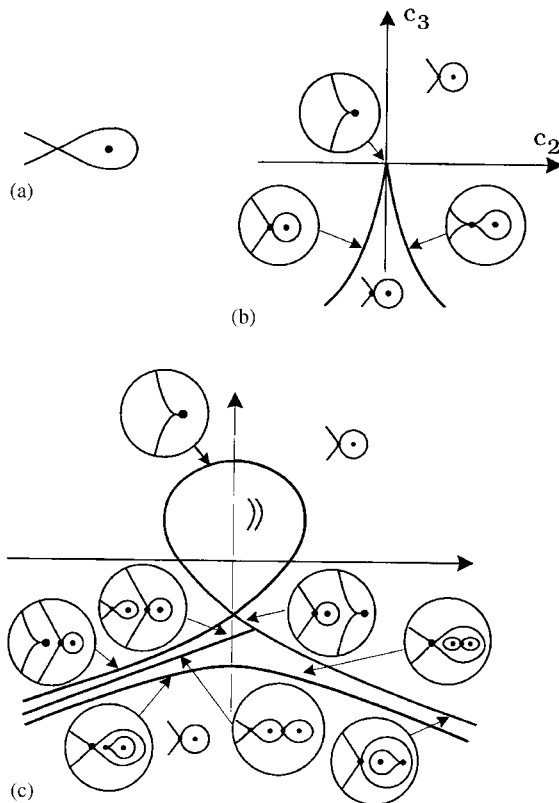


FIG. 3.4. Bifurcation diagram for the normal form of order 5. (a) $D < 0$. (b) $D = 0$, and (c) $D > 0$.

all possible versal unfoldings of ψ_0 those with the lowest possible dimension k of the parameter vector are *miniversal*. This dimension is the *codimension* of ψ_0 . If ψ is structurally stable, the codimension is zero: Since $\psi_0 + \psi'$ is topologically equivalent to ψ_0 for ψ' sufficiently small, the zero-parameter family ψ_0 itself is a miniversal unfolding. In the context of local behavior, as is our concern here, we can talk about the codimension of a critical point. The bifurcation analysis, summarized in Theorem 5, shows that the codimension of the normal form stream function (3.16) for the degenerate critical point of order N is $N-2$. The higher the codimension k of a critical point, the more unlikely it is to find in a flow. It will require k special conditions to be fulfilled simultaneously, and one will only expect it to be observed in problems with k independent parameters.

We conclude the present section with some remarks about the physical interpretation of the coefficients $a_{n,m}$. Obviously, the two first-order coefficients are directly related to the velocity components at the origin,

$$a_{1,0} = -v(0,0), \quad a_{0,1} = u(0,0). \quad (3.49)$$

Higher-order coefficients are related to derivatives of (u,v) , which again can be related to the viscous stress tensor at the origin. We have

$$\tau_{xx} = -\tau_{yy} = 2\mu \frac{\partial u}{\partial x} = 2\mu a_{1,1}, \quad \tau_{xy} = \tau_{yx} = \mu \left(\frac{\partial u}{\partial y} + \frac{\partial v}{\partial x} \right) = 2\mu(a_{0,2} - a_{2,0}). \quad (3.50)$$

By differentiation one can obtain relations between derivatives of the stress tensor and the higher-order coefficients. However, as the important parameters for bifurcation are not the $a_{n,m}$ themselves, but complicated algebraic combinations in the $\tilde{a}_{N,0}$ and the normal form coefficients c_n , it seems that it is very difficult to connect the presence of degenerate critical points and bifurcation curves with a direct physical interpretation.

IV. Flow Near a Wall

We now turn to incompressible flow close to a fixed wall, where the no-slip boundary condition applies. For simplicity, we consider the wall to be flat and choose a coordinate system such that the wall is the line $y = 0$, and the fluid is in the region $y \geq 0$ (see Fig. 3.5). The following analysis can easily be extended to a curved wall, see Hartnack (1999a).

The boundary conditions impose constraints on the stream function. As

$$v(x, 0) = -\frac{\partial \psi}{\partial x}(x, 0) = 0, \quad (4.1)$$

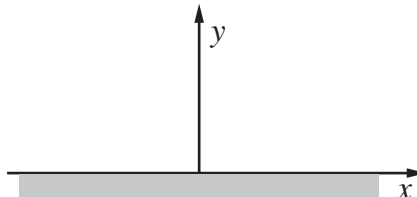


FIG. 3.5. Coordinate system for the flow close to a no-slip wall.

it follows that $\psi(x,0)$ is a constant which we choose to be zero and hence by Taylor's theorem that y is a factor in ψ ,

$$\psi = y\tilde{\psi}. \quad (4.2)$$

Now,

$$u(x,0) = \frac{\partial \psi}{\partial y}(x,0) = \tilde{\psi}(x,0) = 0, \quad (4.3)$$

so y is also a factor in $\tilde{\psi}$ whence y^2 is a factor in ψ ,

$$\psi = y\tilde{\psi} = y^2\hat{\psi}. \quad (4.4)$$

The differential equations for the streamlines (2.5) are then

$$\frac{dx}{dt} = \frac{\partial \psi}{\partial y} = y \left(2\hat{\psi} + y \frac{\partial \hat{\psi}}{\partial y} \right), \quad \frac{dy}{dt} = -\frac{\partial \psi}{\partial x} = -y^2 \frac{\partial \hat{\psi}}{\partial x}. \quad (4.5)$$

The differential equations (4.5) have y as a common factor on the right-hand sides. If a new time variable $s = ty$ is introduced, we get

$$\begin{aligned} \frac{dx}{ds} &= \frac{dx}{dt} \frac{dt}{ds} = \frac{dx}{dt} \frac{1}{y} = 2\hat{\psi} + y \frac{\partial \hat{\psi}}{\partial y}, \\ \frac{dy}{ds} &= \frac{dy}{dt} \frac{dt}{ds} = \frac{dy}{dt} \frac{1}{y} = -y \frac{\partial \hat{\psi}}{\partial x}, \end{aligned} \quad (4.6)$$

and the common factor is removed. The scaling is valid for $y > 0$. It does not change the streamlines, but it does change the speed with which the fluid particles move along the streamlines. This is, however, of no concern for the topology. Even if the transformation is not defined for $y = 0$, (4.6) is well-defined for all y . The streamlines cannot leave the wall, as $dy/dt = 0$ when $y = 0$. In contrast to the original system (4.5) where all points on the wall are critical points, the transformed system has critical points at the wall only where $\hat{\psi}(x,0) = 0$. Thus, the transformed system is identical to the original one except for some artificial streamlines on the wall.

The critical points on the wall for Eq. (4.6) are denoted *no-slip critical points*. They include points of attachment and separation as discussed in Section 1 and they have a simple physical meaning. The vorticity ω is given by

$$\omega = \frac{\partial v}{\partial x} - \frac{\partial u}{\partial y} = -\Delta\psi = -\left(y^2 \frac{\partial^2 \hat{\psi}}{\partial x^2} + 2\hat{\psi} + 4y \frac{\partial \hat{\psi}}{\partial y} + y^2 \frac{\partial^2 \hat{\psi}}{\partial y^2} \right). \quad (4.7)$$

Thus, the no-slip critical points are the points on the wall with zero vorticity. Also, as the wall stress is given by

$$\tau_w(x, 0) = \mu \frac{\partial u}{\partial y}(x, 0) = 2\mu \hat{\psi}(x, 0), \quad (4.8)$$

we see that no-slip critical points are also the points where the wall stress vanishes.

To study flow patterns near no-slip critical points, we will expand ψ in a Taylor series at a point on the wall which we take to be the origin. We let

$$\psi = y^2 \hat{\psi} = y^2 \sum_{n,m=0}^{\infty} a_{n,m+2} x^n y^m, \quad (4.9)$$

and (4.6) becomes

$$\begin{pmatrix} dx/dt \\ dy/dt \end{pmatrix} = \begin{pmatrix} 2a_{0,2} \\ 0 \end{pmatrix} + \begin{pmatrix} 2a_{1,2} & 3a_{0,3} \\ 0 & -a_{1,2} \end{pmatrix} \begin{pmatrix} x \\ y \end{pmatrix} + \mathcal{O}(2). \quad (4.10)$$

Thus, the origin is a no-slip critical point if $a_{0,2} = 0$. If $a_{1,2} \neq 0$, The eigenvalues of the linearization are of opposite signs, $2a_{1,2}$ and $-a_{1,2}$, and the point is a saddle. The separatrices corresponding to the eigenvalue $2a_{1,2}$ lie on the wall, one of the separatrices corresponding to the eigenvalue $-a_{1,2}$ go into the fluid. If $a_{1,2} > 0$, the point is a point of attachment, if $a_{1,2} < 0$ it is a point of separation (see Fig. 4.1).

If $a_{1,2} = 0$, the critical point is degenerate, and the streamline pattern depends on higher order terms of ψ . We consider the case where $a_{0,3} \neq 0$, a simple linear degeneracy. We try to simplify quadratic terms of Eq. (4.10) by a near-identity quadratic transformation of the form

$$x = \xi, y = \eta + s_{1,1}\xi\eta + s_{0,2}\eta^2. \quad (4.11)$$

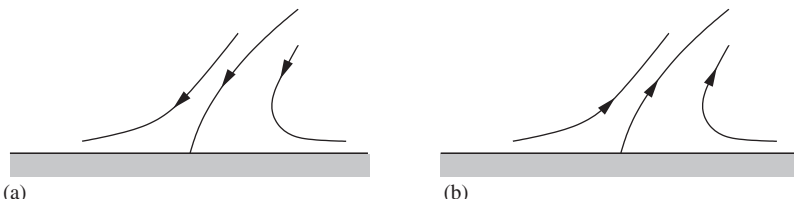


FIG. 4.1. Non-degenerate no-slip critical points. (a) Attachment. (b) Separation.

Note that we have changed the transformation from the previous choice Eq. (3.4) to map the wall $y = 0$ into the line $\eta = 0$. With this, the stream function becomes

$$\psi = \eta^2(a_{0,3}\eta + a_{2,2}\xi^2 + (3s_{1,1}a_{0,3} + a_{1,3})\xi\eta + (3s_{0,2}a_{0,3} + a_{0,4})\eta^2 + \mathcal{O}(3)). \quad (4.12)$$

If we choose

$$s_{1,1} = -\frac{a_{1,3}}{3a_{0,3}}, \quad s_{0,2} = -\frac{a_{0,4}}{3a_{0,3}}, \quad (4.13)$$

we get

$$\psi = \eta^2(a_{0,3}\eta + a_{2,2}\xi^2 + \mathcal{O}(3)). \quad (4.14)$$

If $a_{2,2} = 0$, we must proceed to higher order as in the in-flow case. We omit the details, as the procedure closely follows Section III, and only state the result.

Theorem 6. *Let the origin be a degenerate no-slip critical point such that $a_{n,2} = 0$ for $n < N$ and $a_{N,2} \neq 0$, $a_{0,3} \neq 0$. Then there is a change of coordinates which brings ψ into the normal form*

$$\psi = y^2(a_{0,3}y + a_{N,2}x^N + \mathcal{O}(N+1)). \quad (4.15)$$

Note that in contrast to the in-flow case, Theorem 4, the degeneracy conditions are related directly to the $a_{n,2}$.

The analysis of the truncated normal form from Theorem 6 is straightforward. Separatrices from the origin going into the fluid fulfill

$$\eta = -\frac{a_{N,2}}{a_{0,3}}\xi^N. \quad (4.16)$$

If N is odd, this represents a single separatrix. If N is even and $a_{N,2}/a_{0,3} < 0$, the curve (4.16) lies entirely below the wall, and does not represent a separatrix in the fluid domain. If $a_{N,2}/a_{0,3} > 0$, there are two separatrices in the fluid. The results are summarized in Fig. 4.2.

To study the bifurcation of flow patterns when the degeneracy conditions are not fulfilled exactly, we proceed as in Section III and set

$$\varepsilon_1 = a_{0,2}, \quad \varepsilon_2 = a_{1,2}, \quad (4.17)$$

and apply a near-identity transformation of the form

$$x = \xi, \quad y = \eta + s_{1,1}\xi\eta + s_{0,2}\eta^2 + (s_{0,1,1}\varepsilon_1 + s_{0,1,2}\varepsilon_2)\eta, \quad (4.18)$$

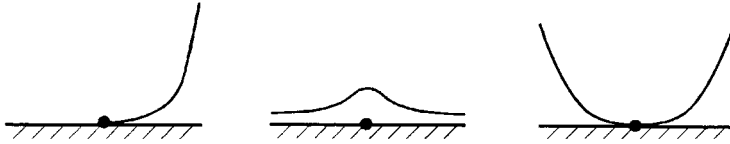


FIG. 4.2. Degenerate no-slip critical points. (a) N odd. (b) N even and $a_{N,2}/a_{0,3} < 0$. (c) N even and $a_{N,2}/a_{0,3} > 0$.

where we also include terms which are quadratic in the small parameters, and which again preserves the wall. With the choice Eq. (4.13), the stream function is

$$\begin{aligned} \psi = \eta^2 & \left(\varepsilon_1 + 2s_{0,1,1} \varepsilon_1^2 + 2s_{0,1,2} \varepsilon_1 \varepsilon_2 - \left(\frac{2a_{1,3}}{3a_{0,3}} \varepsilon_1 - \varepsilon_2 \right) \xi \right. \\ & + \left(a_{0,3} + \left(3a_{0,3}s_{0,1,1} - \frac{2a_{0,4}}{3a_{0,3}} \right) \varepsilon_1 + 3a_{0,3}s_{0,1,2} \varepsilon_2 \right) \eta \\ & \left. + a_{2,2} \xi^2 + \mathcal{O}(3) \right), \end{aligned} \quad (4.19)$$

and we can remove the ε -dependence in the η^3 term by

$$s_{0,1,1} = \frac{2a_{0,4}}{9a_{0,3}^2}, \quad s_{0,1,2} = 0. \quad (4.20)$$

This gives

$$\psi = \eta^2 \left(\varepsilon_1 + \frac{4a_{0,4}}{9a_{0,3}^2} \varepsilon_1^2 - \left(\frac{2a_{1,3}}{3a_{0,3}} \varepsilon_1 - \varepsilon_2 \right) \xi + a_{0,3} \eta + a_{2,2} \xi^2 + \mathcal{O}(3) \right). \quad (4.21)$$

If also $a_{2,2} \neq 0$, further simplification can be obtained. A translation $\xi \rightarrow \xi + \xi_0$ along the wall can remove the term of the next-highest order. With

$$\xi_0 = \frac{a_{1,3}}{3a_{0,3} a_{2,2}} \varepsilon_1 - \frac{1}{2a_{2,2}} \varepsilon_2 \quad (4.22)$$

we get

$$\psi = \eta^2 (\mu + a_{0,3} \eta + a_{2,2} \xi^2 + \mathcal{O}(3)), \quad (4.23)$$

and μ is a complicated non-linear combination of $\varepsilon_1, \varepsilon_2$ which we omit here. Finally, we scale ψ by dividing with $a_{0,3}$ and scale ξ by the substitution

$$\xi \rightarrow \sqrt{\left| \frac{a_{0,3}}{2a_{2,2}} \right|} \xi. \quad (4.24)$$

Multiplying by $\sigma = \text{sign}(a_{2,2}/a_{0,3})$ then yields

$$\psi = \eta^2 \left(\sigma \eta + c_0 + \frac{1}{2} \xi^2 + \mathcal{O}(3) \right), \quad (4.25)$$

where c_0 is a small parameter and

$$\sigma = \begin{cases} +1 & \text{for } a_{2,2}/a_{0,3} > 0, \\ -1 & \text{for } a_{2,2}/a_{0,3} < 0. \end{cases} \quad (4.26)$$

If $a_{2,2}$ is also a small parameter, we must proceed to higher orders until some non-degeneracy condition holds. The general result is

Theorem 7. *Let $a_{0,2}, a_{1,2}, a_{2,2}, \dots, a_{N-3,2}$ be small parameters, and assume the non-degeneracy conditions $a_{0,3} \neq 0, a_{N-2,2} \neq 0$. Then there is a coordinate change which brings the stream function (4.8) into the form*

$$\psi = y^2(\sigma y + f(x) + \mathcal{O}(N-1)), \quad f(x) = \sum_{n=0}^{N-2} c_n x^n, \quad c_{N-3} = 0, \quad c_{N-2} = \frac{1}{N-2}, \quad (4.27)$$

where

$$\sigma = \begin{cases} +1 & \text{for } a_{N-2,2}/a_{0,3} > 0 \text{ or } N \text{ odd,} \\ -1 & \text{for } a_{N-2,2}/a_{0,3} < 0, \end{cases} \quad (4.28)$$

and c_0, \dots, c_{N-4} are small parameters.

The two subcases (4.28) stem from the generalization of the scaling (4.24) which is

$$\xi \rightarrow \left| \frac{a_{0,3}}{(N-2)a_{N-2,2}} \right|^{1/(N-2)} \xi. \quad (4.29)$$

Truncation of the \mathcal{O} -term in the normal form (4.27) gives, after scaling with a factor y , the differential equations for the streamlines

$$\frac{dx}{dt} = 3\sigma y + 2f(x), \quad \frac{dy}{dt} = -yf'(x), \quad (4.30)$$

with Jacobian

$$\mathbf{J} = \begin{pmatrix} 2f'(x) & 3\sigma \\ -yf''(x) & -f'(x) \end{pmatrix}. \quad (4.31)$$

No-slip critical points satisfy

$$y = 0, \quad f(x) = 0, \quad (4.32)$$

so there are at most $N-2$ of them. They are degenerate when $|\mathbf{J}| = 0$, which occurs for $f'(x) = 0$. In-flow critical points satisfy

$$f'(x) = 0, \quad y = -\frac{2}{3}\sigma f(x). \quad (4.33)$$

Their type is determined from the Jacobian. One finds $|\mathbf{J}| = -2f(x)f''(x)$, bifurcation of in-flow critical points happen when $f''(x) = 0$.

Structurally unstable heteroclinic connections may occur for in-flow critical points, but heteroclinic connections between in-flow critical points and no-slip critical points are not possible. This follows from the fact that at an in-flow critical point we have

$$\psi(x, y) = \psi(x, -2/3\sigma f(x)) = -\frac{1}{2}\sigma y^3 \neq 0, \quad (4.34)$$

while $\psi = 0$ on the wall. In particular, the creation of the vortices behind the circular cylinder as shown in Fig. 1.1 cannot be covered by the normal form (4.27). We return to this matter in Section V.

For $N = 4$, we have $f(x) = c_0 + x^2/2$, so the no-slip critical points are $(x, y) = (\pm\sqrt{-2c_0}, 0)$ which exist for $c_0 \leq 0$. The single in-flow critical point is $(0, -2/3\sigma c_0)$ which is a center for $c_0 < 0$ and a saddle for $c_0 > 0$. For $c_0 < 0$ and $\sigma = +1$ the two no-slip saddles have a heteroclinic connection given by $y = -x^2/2 - c_0$. Note that in contrast to heteroclinic connections between in-flow critical points, this is structurally stable. A small perturbation of ψ which respects the no-slip boundary condition may move a no-slip saddle along the wall, but not away from it, preserving that $\psi = 0$. Bifurcation diagrams are shown in Fig. 4.3.

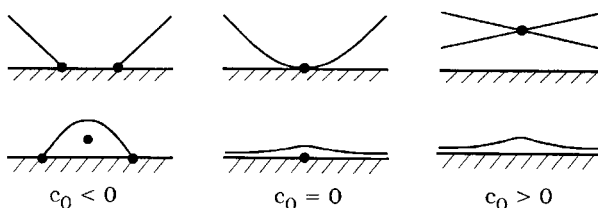


FIG. 4.3. Bifurcation diagrams for the fourth order normal form. Top row: $\sigma = +1$. Bottom row: $\sigma = -1$.

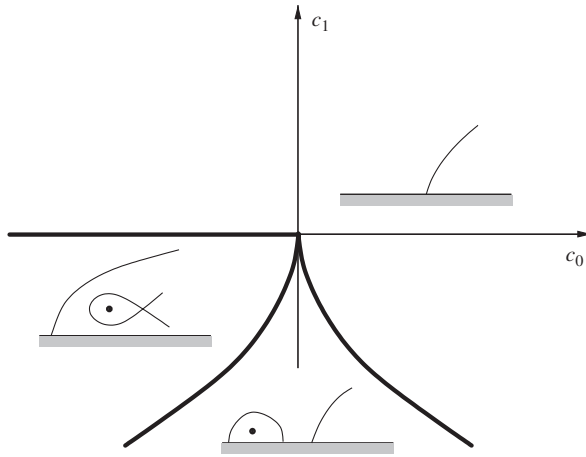


FIG. 4.4. Bifurcation diagram for the fifth order normal form.

For $N = 5$, we have $f(x) = c_0 + c_1x + x^3/3$. Bifurcation of no-slip critical points occurs when $f(x) = f'(x) = 0$. Eliminating x , we find the bifurcation curve

$$c_1^3 = -\frac{9}{4}c_0^2. \quad (4.35)$$

In-flow critical points exist for $c_0 \leq 0$ according to (4.33). Bifurcation occurs when $f'(x) = f''(x) = 0$, from which one finds $c_1 = 0$. The bifurcation diagram is shown in Fig. 4.4.

For $N = 6$, we have $f(x) = c_0 + c_1x + c_2x^2 + x^4/4$. Eliminating c_1 from the bifurcation conditions $f(x) = f'(x) = 0$ gives

$$c_0 - c_2x^2 - \frac{3}{4}x^4 = 0. \quad (4.36)$$

It is convenient to use the discriminant of this equation as a parameter rather than c_0 ,

$$D = c_2^2 + 3c_0. \quad (4.37)$$

We do not give the details of the bifurcation analysis here, but show the result in Figs. 4.5 and 4.6.

V. Flow Near a Wall with Mirror Symmetry

The flow around a circular cylinder shown in Fig. 1.1 possesses mirror symmetry both before and after the creation of the trailing vortices. If we

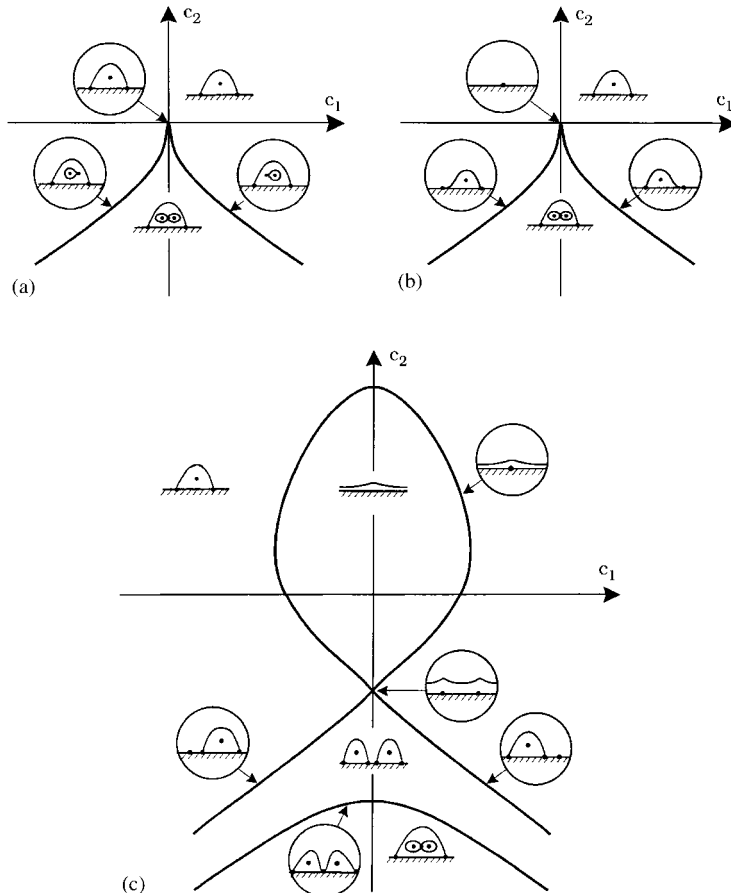


FIG. 4.5. Bifurcation diagram for the normal form of order 6 for $\sigma = +1$. (a) $D < 0$. (b) $D = 0$. (c) $D > 0$.

introduce a coordinate system based at the cylinder surface at the aft point of symmetry, see Fig. 5.1, we have the symmetry conditions

$$u(-x, y) = -u(x, y), \quad v(-x, y) = v(x, y), \quad (5.1)$$

i.e. u is an odd function of x , and v is an even function of x . These conditions are fulfilled if the stream function is odd in x ,

$$\psi(-x, y) = -\psi(x, y). \quad (5.2)$$

In the Taylor expansion (4.9), we then have all coefficients with an even first index are zero,

$$a_{2n,m} = 0 \quad \text{for all } n, m, \quad (5.3)$$

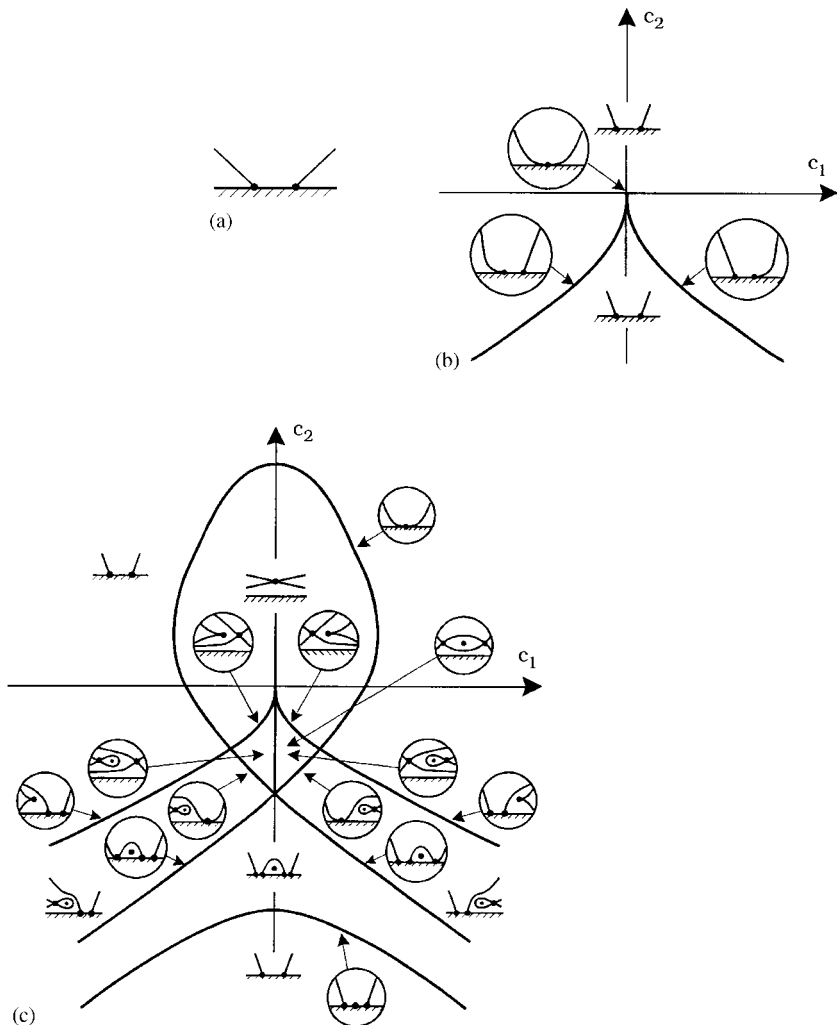


FIG. 4.6. Bifurcation diagram for the normal form of order 6 for $\sigma = -1$. (a) $D < 0$. (b) $D = 0$. (c) $D > 0$.

and the differential equations (4.10) become

$$\begin{pmatrix} dx/dt \\ dy/dt \end{pmatrix} = \begin{pmatrix} 2a_{1,2} & 0 \\ 0 & -a_{1,2} \end{pmatrix} \begin{pmatrix} x \\ y \end{pmatrix} + \mathcal{O}(2). \quad (5.4)$$

Hence, the origin is always a no-slip critical point, and if $a_{1,2} \neq 0$, it is a regular saddle. If $a_{1,2} = 0$, we have a non-simple degeneracy, since the Jacobian is the zero matrix. To analyze this, we make a normal form by a near-identity transformation (4.11), but choose $s_{1,1} = 0$ in advance. This

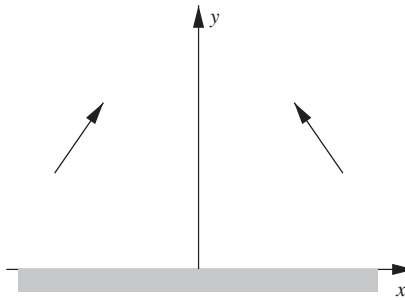
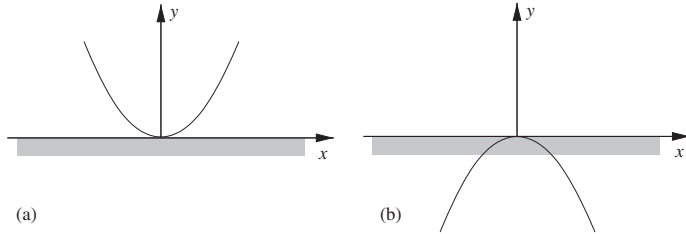


FIG. 5.1. Coordinate system for symmetric flow.

FIG. 5.2. Degenerate symmetric critical point. (a) $K < 0$. (b) $K > 0$.

makes the transformation odd in x , and hence the symmetry of ψ is preserved. The transformed stream function becomes

$$\psi = \xi \eta^2 (a_{1,3} \eta + a_{3,2} \xi^2 + (3s_{0,2} a_{1,3} + a_{1,4}) \eta^2 + \mathcal{O}(3)). \quad (5.5)$$

If $a_{1,3} \neq 0$, we can choose

$$s_{0,2} = -\frac{a_{1,4}}{3a_{1,3}}, \quad (5.6)$$

and obtain

$$\psi = \xi \eta^2 (a_{1,3} \eta + a_{3,2} \xi^2 + \mathcal{O}(3)). \quad (5.7)$$

For the truncated normal form, there are separatrices from the origin along

$$\xi = 0, \quad \eta = 0, \quad \eta = -K \xi^2 \quad \text{where } K = \frac{a_{3,2}}{a_{1,3}}, \quad (5.8)$$

which are all different if $K \neq 0$. The quadratic separatrix is in the flow domain $y > 0$ if $K < 0$ and outside the domain if $K > 0$ (see Fig. 5.2).

Perturbing the degeneracy but still keeping the symmetry, we now consider $a_{1,2} = \varepsilon$ a small parameter. We try to obtain a simplification by a transformation

$$x = \xi + r_{1,1}\xi\eta, \quad y = \eta + s_{0,2}\eta^2. \quad (5.9)$$

This is the most general quadratic near-identity transformation which preserves the wall and is odd in ξ . We obtain

$$\psi = \xi\eta^2(\varepsilon + (a_{1,3} + \varepsilon(r_{1,1} + 2s_{0,2}))\eta + ((3s_{0,2} + r_{1,1})a_{1,3} + a_{1,4})\eta^2 + \mathcal{O}(3)). \quad (5.10)$$

With

$$r_{1,1} = \frac{2a_{1,4}}{a_{1,3}}, \quad s_{0,2} = -\frac{a_{1,4}}{a_{1,3}}, \quad (5.11)$$

and after division by $a_{1,3}$ we get the normal form

$$\psi = \xi\eta^2(c + \eta + K\xi^2 + \mathcal{O}(3)), \quad c = \frac{\varepsilon}{K}. \quad (5.12)$$

One easily finds that the truncated normal form has two in-flow critical points at

$$(\xi, \eta) = \left(\pm \sqrt{-\frac{c}{K}}, -\frac{4}{K}c \right), \quad (5.13)$$

which are centers, and a saddle at $(\xi, \eta) = (0, -c)$. Furthermore, there are separatrices of the form

$$\xi = 0, \quad \eta = 0, \quad \eta = -K\xi^2 - c. \quad (5.14)$$

Thus, for $K > 0$, one obtains the streamline pattern in [Fig. 1.1\(a\)](#) for $c > 0$ and [Fig. 1.1\(b\)](#) for $c < 0$. Hence, the creation of trailing vortices as it occurs in the flow around a circular cylinder is the simplest bifurcation which can possibly happen in a flow with symmetry conditions (5.1). If the symmetry conditions are broken, by deforming the cylinder or changing the boundary conditions away from the body, symmetry-breaking terms must be included in the stream function, and a much more complicated bifurcation scenario occurs, see [Bakker \(1991\)](#) and [Brøns et al. \(2006\)](#). In this analysis, we have assumed that the cylinder wall is straight. The analysis can be extended to a curved wall, and it can be shown ([Brøns et al., 2006](#)) that no qualitative changes in the streamline topology or bifurcations arise.

VI. Axisymmetric Flows and Application to Vortex Breakdown

Consider a 3D flow described in cylindrical coordinates (r, θ, z) with corresponding velocity components (U, V, W) . The flow is *axisymmetric* if the velocity field only depends on r, z and not on the angle θ . This symmetry allows a reduction to a 2D description. Assuming incompressibility, the equation of continuity is

$$\frac{1}{r} \frac{\partial}{\partial r} (rU) + \frac{\partial W}{\partial z} = 0. \quad (6.1)$$

Introducing a new radial variable

$$\rho = \frac{1}{2}r^2, \quad (6.2)$$

and a corresponding velocity

$$u = \frac{d\rho}{dt} = r \frac{dr}{dt} = rU, \quad (6.3)$$

Eq. (6.1) can be rewritten, with $w = W$,

$$\frac{\partial u}{\partial \rho} + \frac{\partial w}{\partial z} = 0. \quad (6.4)$$

This is the standard equation of continuity for incompressible 2D flows with Cartesian coordinates (ρ, z) and velocity components (u, w) . Hence, there exists a stream function $\psi(\rho, z)$ such that

$$u = \frac{\partial \psi}{\partial z}, \quad w = -\frac{\partial \psi}{\partial \rho}, \quad (6.5)$$

or, in original variables,

$$U = \frac{1}{r} \frac{\partial \psi}{\partial z}, \quad W = -\frac{1}{r} \frac{\partial \psi}{\partial \rho}. \quad (6.6)$$

In the new variables, we get the following equations for the streamlines:

$$\frac{d\rho}{dt} = \frac{\partial \psi}{\partial z}, \quad \frac{dz}{dt} = -\frac{\partial \psi}{\partial \rho}, \quad \frac{d\theta}{dt} = \frac{1}{r}v. \quad (6.7)$$

The two first equations can be solved independently, and constitute a system of the same kind as we have considered hitherto. The streamlines which lie on the level curves of ψ are, however, not streamlines for the full system (6.7). These level curves are intersections of stream surfaces with a meridional plane $\theta = \text{constant}$. Individual streamlines wind around the axis

on the stream surfaces, with a θ -dependence given by the last equation of (6.7). Here we develop the theory for patterns in a meridional plane defined by the iso-curves of ψ .

The axisymmetry requires that the axis is a streamline, i.e.

$$u = \frac{\partial \psi}{\partial z} = 0 \text{ for } \rho = 0, \quad (6.8)$$

and it follows, cf. (4.1), that we can assume that ρ is a factor in ψ ,

$$\psi = \psi(z, \rho) = \rho \tilde{\psi}(z, \rho). \quad (6.9)$$

Hence, we consider the expansion

$$\psi = \rho \tilde{\psi} = \rho \sum_{n,m=0}^{\infty} a_{n,m+1} z^n \rho^m, \quad (6.10)$$

and proceed in the analysis as for the near-wall flow in Section IV. Only minor modifications are needed, and we obtain the following normal form theorem.

Theorem 8. *Let $a_{0,1}, a_{1,1}, a_{2,1}, \dots, a_{N-2,1}$ be small parameters, and assume the non-degeneracy conditions $a_{0,2} \neq 0$, $a_{N-1,1} \neq 0$. Then there is a coordinate change which brings the stream function (6.8) into the form*

$$\psi = \rho(\sigma\rho + f(z) + \mathcal{O}(N-1)), \quad f(z) = \sum_{n=0}^{N-1} c_n z^n, \quad c_{N-2} = 0, \quad c_{N-1} = \frac{1}{N-1}, \quad (6.11)$$

where

$$\sigma = \begin{cases} +1 & \text{for } a_{N-1,1}/a_{0,2} > 0 \text{ or } N \text{ odd,} \\ -1 & \text{for } a_{N-1,1}/a_{0,2} < 0, \end{cases} \quad (6.12)$$

and c_0, \dots, c_{N-3} are small parameters.

Furthermore, the bifurcation diagrams for the normal form (6.11) are identical to the ones obtained in Section IV in Figs. 4.3, 4.4, 4.5, and 4.6. For the streamline patterns, the wall must be replaced by the axis, and the coordinate y orthogonal to the axis corresponds to ρ .

The simplest bifurcation, which for the near-wall flow is the creation of a recirculation zone as in the top row of Fig. 4.3 must here be interpreted as the creation of a secondary flow structure on a main vortex. The full 3D flow is obtained by rotating the pictures around the axis. Hence, this bifurcation is the creation of a closed bubble-shaped region of fluid. This is the well-known

phenomenon of *vortex breakdown of bubble type*. It has been extensively studied experimentally and computationally for the flow in a closed cylindrical container, where the main vortex is created by rotating one or both end covers. The system parameters are

$$\text{Re} = \frac{\Omega_1 R^2}{\nu}, \quad h = \frac{H}{R}, \quad \gamma = \frac{\Omega_2}{\Omega_1}, \quad (6.13)$$

where Ω_1, Ω_2 are the angular velocities of the bottom and the top cover respectively, R, H the radius and height of the cylinder, respectively, and ν the viscosity of the fluid. Depending on these parameters, one or more recirculating zones can occur and merge as shown in Fig. 6.1. Some key papers on this flow and its bifurcation behavior are Brown and Lopez (1990), Escudier (1984), Lopez (1990), and Lopez and Perry (1992). Here we consider the steady domain for low Re only. For higher values of Re the flow becomes oscillatory through a loss of hydrodynamic stability. We will show how the ideas and results from the topological analysis can be used to efficiently generate bifurcation diagrams from numerical simulations, summarizing key results from Brøns and Bisgaard (2004, 2006), Brøns et al. (1999, 2001).

We use numerical simulations produced from a finite difference code (Daube, 1991; Daube and Sorensen, 1989; Sorensen and Loc, 1989). For fixed values of the system parameters, we obtain the axial velocity at the axis, $w(z,0)$. An example is shown in Fig. 6.2. Obviously, points where $w(z,0) = 0$ are critical points, and hence the creation or merging of bubbles – the bifurcations in Fig. 4.3 – can be monitored by keeping track of creation or disappearance of zeroes of $w(z,0)$. This can conveniently be done by finding the local extremal values of $w(z,0)$ as functions of the system parameters, e.g. $p_1 = p_1(\text{Re}, h, \gamma)$ as

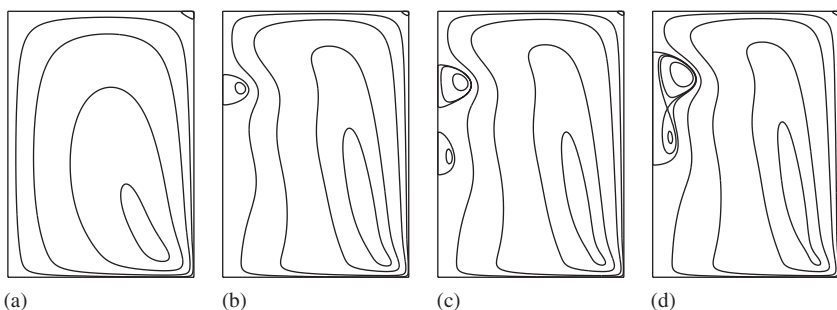


FIG. 6.1. Typical topologies of iso-curves of ψ in a meridional (r,z) plane for different combinations of the parameters (6.13). The line to the left is the cylinder axis.

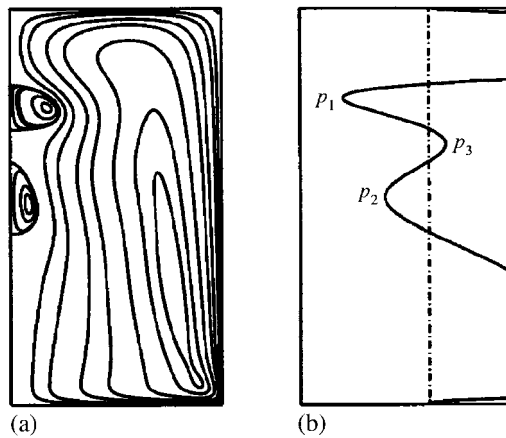


FIG. 6.2. (a) Iso-line of ψ showing two breakdown bubbles. (b) Corresponding graph of $w(z,0)$ Reproduced from Brøns et al. (1999) with permission from Cambridge University Press.

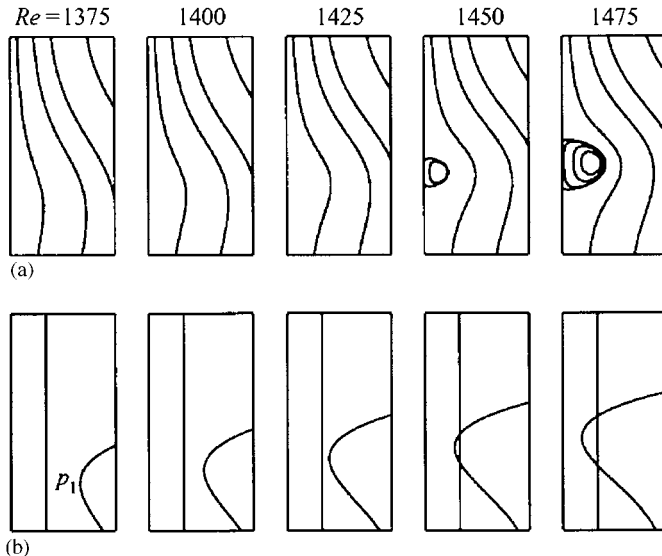


FIG. 6.3. (a) Sequence of iso-curves of ψ during a bubble creation. (b) Corresponding development of $w(z,0)$. Reproduced from Brøns et al. (1999) with permission from Cambridge University Press.

shown in Figs. 6.2 and 6.3, and then solving the bifurcation equation $p_k(\text{Re}, h, \gamma) = 0$ for each of the extrema p_k . For a fixed value of γ , this will result in one or more bifurcation curves in the (h, Re) plane. On the basis of numerical

simulations on a grid in the (h, Re) plane, the bifurcation equations are easily solved numerically, although some care must be taken as the number of extrema may vary with the parameters. See Bisgaard (2005), Brøns and Bisgaard (2006) for a practical implementation.

For $\gamma = 0$, we obtain the bifurcation diagram in Fig. 6.4. For low values of Re and h , there are no breakdown zones, and the topology is as in Fig. 6.1A. Crossing the outermost bifurcation curve, a recirculating zone is created, and the topology changes to type B. The next bifurcation curve marks the creation of yet a recirculating zone to type C, and at the third bifurcation curve the two bubbles merge and create one large zone with an inner structure, type D. The two first bifurcations are of the type in the top row of Fig. 4.3, the latter as in the bottom row.

When γ is increased, the two innermost bifurcation curves move closer. At $\gamma_0 \approx 0.009$, Fig. 6.5, the curves touch tangentially. For $\gamma > \gamma_0$, the bifurcation diagram has changed qualitatively to the form in Fig. 6.5.

This sequence of bifurcation diagrams can be explained as follows. In the regime we consider, there is a unique steady flow which depends smoothly on the physical parameters Re, h, γ . Suppose that when the parameters take

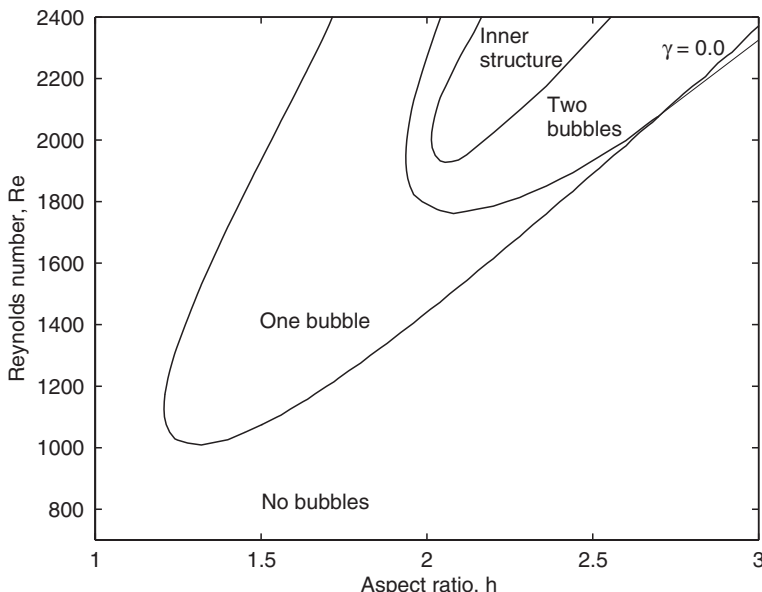


FIG. 6.4. Bifurcation diagram for $\gamma = 0$.

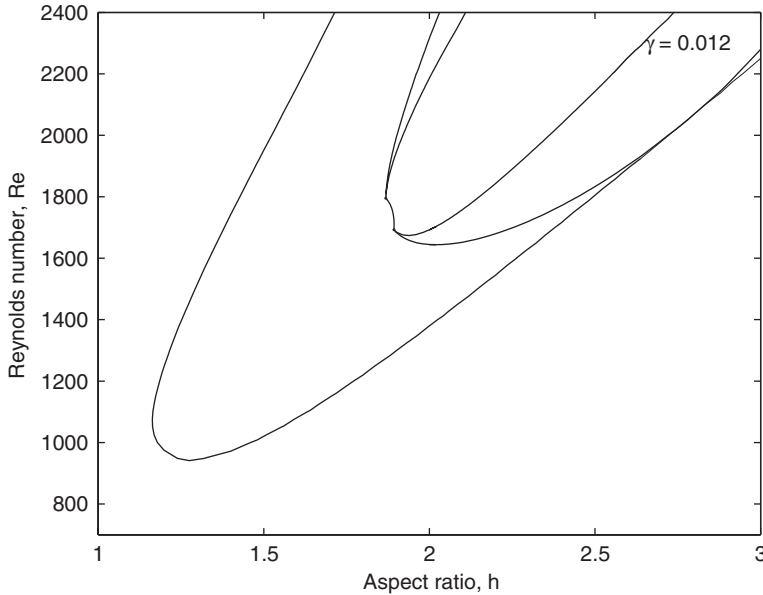


FIG. 6.5. Bifurcation diagram for $\gamma = 0.012$.

the values $\text{Re}^*, h^*, \gamma^*$ a codimension 2 degenerate critical point exist, that is, there is a z^* such that

$$\frac{\partial \psi}{\partial z}(z^*, 0) = \frac{\partial^2 \psi}{\partial z \partial \rho}(z^*, 0) = 0 \text{ and } \frac{\partial^2 \psi}{\partial \rho^2}(z^*, 0) \neq 0. \quad (6.14)$$

Then the flow topology for nearby parameter values is determined by the normal form coefficients c_0, c_1 and the bifurcation diagram in Fig. 4.3. The normal form coefficients are smooth functions of the $a_{n,m}$ in the expansion of ψ , and hence of the physical parameters, $c_0 = c_0(\text{Re}, h, \gamma)$, $c_1 = c_1(\text{Re}, h, \gamma)$. Now, assume a quadratic degeneracy in these relations,

$$\frac{\partial c_0}{\partial h}(\text{Re}^*, h^*, \gamma^*) = 0, \quad \frac{\partial^2 c_0}{\partial h^2}(\text{Re}^*, h^*, \gamma^*) \neq 0. \quad (6.15)$$

Rather than analyzing the general case, we consider a generic example,

$$c_0 = -(\text{Re} - \text{Re}^*) - (\gamma - \gamma^*) + h^2, \quad c_1 = -(\text{Re} - \text{Re}^*). \quad (6.16)$$

For a fixed γ , this can be understood as mapping the physical (h, Re) parameter plane into the mathematical (c_0, c_1) parameter plane by folding it along $h = 0$. The fold line maps into the line $c_1 = c_0 + (\gamma - \gamma^*)$, which is transversal to all the bifurcation curves at the origin.

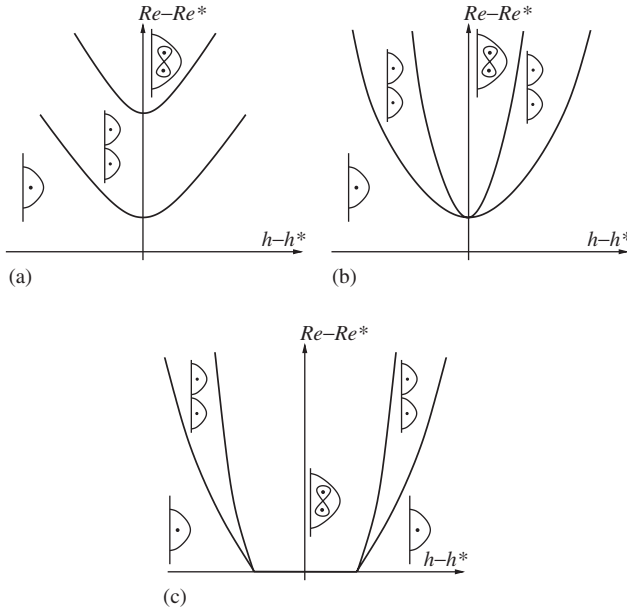


FIG. 6.6. Bifurcation diagrams for the folded mapping of the physical parameters (6.16) into the mathematical parameter space. (a) $\gamma < \gamma^*$. (b) $\gamma = \gamma^*$. (c) $\gamma > \gamma^*$.

Codimension 2 critical points occur when $c_0 = c_1 = 0$, that is, when $Re = Re^*$, $h = \pm\sqrt{\gamma - \gamma^*}$, so two such points exist when $\gamma > \gamma^*$. From this, the bifurcation diagram is easily obtained, as shown in Fig. 6.6, in agreement with the sequence of diagrams obtained numerically in Figs. 6.4 and 6.5.

Thus, in steady flows, multi-parameter bifurcation phenomena may be obtained by combining degenerate critical points with degeneracies in the relation between the physical parameters and the normal form parameters, where the present case is only an example.

We have only considered bifurcations in the vortex breakdown problem for very low values of γ . The flow is surprisingly sensitive, and further bifurcations occur as γ is increased (see Brøns and Bisgaard, 2006; Brøns and Hartnack, 1999; Brøns et al., 2001).

VII. Conclusions and Outlook

The topological analysis we have performed is of a very general nature. We have only assumed incompressibility of the fluid, and very simple boundary conditions. The results do not depend on the constitutive properties of the fluid,

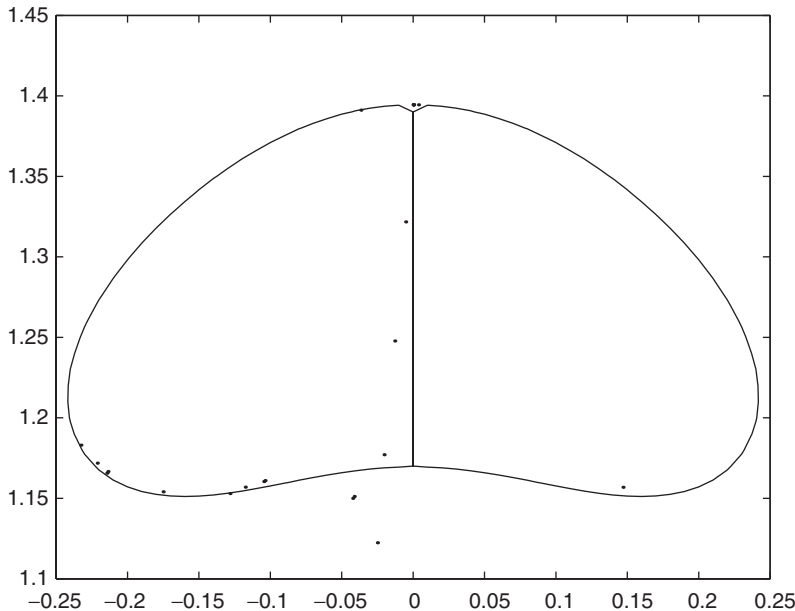


FIG. 7.1. Particle traces in vortex breakdown perturbed asymmetrically, closely resembling experimental results from Spohn (1998). The full curve is the bubble shape obtained from an axisymmetric simulation. Reproduced from Brøns (2001).

and will be valid for both Newtonian and non-Newtonian fluids. An interesting question is, whether all patterns and bifurcation can occur in *steady* flows. If the Taylor expansion of the stream function is inserted in the steady Navier–Stokes equations, further connections between the expansion coefficients are obtained, and these could impose limitations on the normal forms. For the unfoldings of simple degenerate points, it is shown in Brøns and Hartnack (1999) and Hartnack (1999a) that these extra conditions do not change the bifurcation diagrams, while certain non-simple degenerate critical points on the wall are incompatible with the steady Navier–Stokes equations. Whether this distinguishes Newtonian fluids from non-Newtonian fluids is unknown.

In the present paper, we have focused on patterns in 2D flows. Clearly, the analysis can be extended to 3D flows. In Chong et al. (1990), a classification of non-degenerate 3D critical points is obtained. One can proceed with normal form computations to obtain unfoldings of degenerate critical points as in the present paper, but one quickly encounters the fact that 3D flows allow chaotic particle paths. This is clearly illustrated by the vortex breakdown phenomenon (Hartnack et al., 2000). Considering this as a full 3D

flow, the creation of a recirculating zone is associated with a degenerate critical point with a Jacobian

$$\begin{pmatrix} 0 & -\omega & 0 \\ \omega & 0 & 0 \\ 0 & 0 & 0 \end{pmatrix}, \quad (7.1)$$

with eigenvalues 0 and $\pm i\omega$, the latter corresponding to the swirling motion around the cylinder axis. Proceeding with near-identity transformations, it turns out that all asymmetric terms can be removed to any finite order, and hence that any asymmetry can be pushed into the \mathcal{O} -terms. Thus, the effects of asymmetry cannot be studied from the truncated normal form, and we have the situation that the truncated normal form is not a versal unfolding.

This shows that the axisymmetric flow will be sensitive to asymmetric perturbations, in the sense that even the slightest asymmetry can induce particle paths which are not topologically equivalent with the axisymmetric case. This is illustrated in Fig. 7.1. Rather than a closed recirculating zone, one obtains an open bubble with in- and outflow, and complicated particle paths. High-resolution visualization experiments (Spohn et al., 1998) confirm this picture.

The bifurcation theory for 3D flow patterns is still in its infancy. Further developments may shed important light on the early phases of the transition from laminar to turbulent flow.

References

Abraham, R., Marsden, J. E., and Ratiu, T. (1983). *Manifolds, Tensor Analysis, and Applications*. Addison-Wesley, Reading, MA.

Bakker, P. G. (1991). *Bifurcations in Flow Patterns*. Kluwer Academic Publishers, Dordrecht.

Bisgaard, A. V. (2005). *Structures and Bifurcations in Fluid Flows with Applications to Vortex Breakdown and Wakes*. PhD thesis, Department of Mathematics, Technical University of Denmark.

Brøns, M. (1994). Topological fluid dynamics of interfacial flows. *Phys. Fluids* **6**(8), 2730–2737.

Brøns, M. (1999). Topological fluid mechanics of axisymmetric flows. In *Simulation and Identification of Organized Structures in Flows* (J. N., Sørensen, E. J., Hopfinger, and N., Aubry, eds.), pp. 213–222. Kluwer, Dordrecht.

Brøns, M. (2001). Streamline patterns and their bifurcations using methods from dynamical systems. In *An Introduction to the Geometry and Topology of Fluid Flows* (R. L., Ricca, Ed.), pp. 167–182. Kluwer, Dordrecht.

Brøns, M., and Bisgaard, A. (2004). Bifurcation of vortex breakdown patterns. In *Proceedings of the 2004 International Conference on Computational & Experimental Engineering & Sciences* (S. N., Atluri, and A. J. B., Tadeu, eds.), pp. 988–993. Tech Science Press, GA, USA.

Brøns, M., and Bisgaard, A. V. (2006). *Bifurcation of Vortex Breakdown Patterns in a Circular Cylinder with Two Rotating Covers*. To appear in *J. Fluid Mech.*

Brøns, M., and Hartnack, J. N. (1999). Streamline topologies near simple degenerate critical points in two-dimensional flow away from boundaries. *Phys. Fluids* **11**(2), 314–324.

Brøns, M., Niss, K., Jakobsen, B., Voigt, L. K., Bisgaard, A. V., & Petersen, R. (2006). *Streamline Topology Vorticity Patterns in the Near-Wake of a Circular Cylinder at Low Reynolds Numbers*. In Preparation.

Brøns, M., Voigt, L. K., and Sørensen, J. N. (1999). Streamline topology of steady axisymmetric vortex breakdown in a cylinder with co- and counter-rotating end-covers. *J. Fluid Mech.* **401**, 275–292.

Brøns, M., Voigt, L. K., and Sørensen, J. N. (2001). Topology of vortex breakdown bubbles in a cylinder with rotating bottom and free surface. *J. Fluid Mech.* **428**, 133–148.

Brown, G. L., and Lopez, J. M. (1990). Axisymmetric vortex breakdown part 2. Physical mechanisms. *J. Fluid Mech.* **221**, 553–576.

Chong, M. S., Perry, A. E., and Cantwell, B. J. (1990). A general classification of three-dimensional flow fields. *Phys. Fluids* **A2**(5), 765–777.

Chow, S. -N., Li, C., and Wang, D. (1994). *Normal Forms and Bifurcation of Planar Vector Fields*. Cambridge University Press, Cambridge.

Daube, O. (1991). Numerical simulations of axisymmetric vortex breakdown in a closed cylinder. In: *Vortex Dynamics and Vortex Methods*, volume 28 of *Lectures in Applied Mathematics* (C. R. Anderson and C. Greengard, editors), pp. 131–152, American Mathematical Society, Providence, RI.

Daube, O., and Sørensen, J. N. (1989). Simulation numerique de l'écoulement periodique axisymmetrique dans une cavite cylindrique. *Com. Rendus Acad. Sci. Sér.* **308**(2), 463–469.

Davey, A. (1961). Boundary-layer flow at a saddle point of attachment. *J. Fluid Mech.* **10**, 593–610.

Dean, W. R. (1950). Note on the motion of liquid near a position of separation. *Proc. Cambridge Philos. Soc.* **46**, 293–306.

Délery, J. (2001). Robert Legendre and Henri Werlé: Toward the elucidation of three-dimensional separation. *Ann. Rev. Fluid Mech.* **33**, 129–154.

Escudier, M. P. (1984). Observations of the flow produced in a cylindrical container by a rotating endwall. *Exp. Fluids* **2**, 189–196.

Golubitsky, M., and Schaeffer, D. G. (1985). *Singularities and Groups in Bifurcation Theory I*, Volume 51 of *Applied Mathematical Sciences*. Springer, New York.

Grimshaw, R. (1991). *Nonlinear Ordinary Differential Equations*. CRC Press, Boca Raton, FL.

Hartnack, J. N. (1999a). Streamline topologies near a fixed wall using normal forms. *Acta Mech.* **136**(1–2), 55–75.

Hartnack, J. N. (1999b). *Structural Changes in Incompressible Flow Patterns*. PhD thesis, Department of Mathematics, Technical University of Denmark.

Hartnack, J. N., Brøns, M., and Spohn, A. (2000). The role of asymmetric perturbations in steady vortex breakdown bubbles. DCAMM Report 628, Technical University of Denmark.

Legendre, R. (1956). Séparation de l'écoulement laminaire tridimensionnel. *La recherche aérospatiale* **54**, 3–8.

Lighthill, M. J. (1963). Attachment and separation in three-dimensional flow. In *Laminar Boundary Layers* (L. Rosenhead, Ed.), p. 72. Clarendon Press, Oxford.

Lopez, J. M. (1990). Axisymmetric vortex breakdown part 1. Confined swirling flow. *J. Fluid Mech.* **221**, 533–552.

Lopez, J. M., and Perry, A. D. (1992). Axisymmetric vortex breakdown part 3. Onset of periodic flow and chaotic advection. *J. Fluid Mech.* **234**, 449–471.

Oswatitsch, K. (1958). Die Ablösungsbedingung von Grenzschichten. In *IUTAM Symposium on Boundary Layer Research* (H., Görtler, Ed.), pp. 357–364. Springer, Berlin.

Perry, A. E., and Chong, M. S. (1987). A description of eddying motions and flow patterns using critical-point concepts. *Ann. Rev. Fluid Mech.* **19**, 125–155.

Sørensen, J. N., and Loc, T. P. (1989). High-order axisymmetric Navier-Stokes code: description and evaluation of boundary conditions. *Int. J. Numerical Methods in Fluids* **9**, 1517–1537.

Spohn, A., Mory, M., and Hopfinger, E. J. (1998). Experiments on vortex breakdown in a confined flow generated by a rotating disc. *J. Fluid Mech.* **370**, 73–99.

Tobak, M., and Peake, D. J. (1982). Topology of three-dimensional separated flows. *Ann. Rev. Fluid Mech.* **14**, 61–85.

Wiggins, S. (1990). *Introduction to Applied Nonlinear Dynamical Systems and Chaos*. Springer, New York.

Electrospinning of Nanofibers from Polymer Solutions and Melts

D.H. RENEKER^a, A.L. YARIN^{b,c}, E. ZUSSMAN^b and
H. XU^{a,d}

^a*Department of Polymer Science. The University of Akron, Akron, Ohio 44325-3909, USA*

^b*Faculty of Mechanical Engineering, Technion – Israel Institute of Technology, Haifa 32000, ISRAEL*

^c*Department of Mechanical and Industrial Engineering, University of Illinois at Chicago, Chicago 60607-7022, USA*

^d*The Procter & Gamble Company, Winton Hill Business Center, 6280 Center Hill Ave, Cincinnati, Ohio 45224, USA*

Abstract	44
I. Introduction and Background	45
II. Various Methods of Producing Nanofibers	46
III. Electrospinning of Nanofibers	46
IV. Taylor Cone and Jetting from Liquid Droplets in Electrospinning of Nanofibers	47
A. Taylor Cone as a Self-Similar Solution	48
B. Non-Self-Similar Solutions for Hyperboloidal Liquid Bodies	51
C. Failure of the Self-Similarity Assumption for Hyperboloidal Solutions	58
D. Experimental Results and Comparison with Theory	61
E. Transient Shapes and Jet Initiation	68
F. Summary	73
V. Bending Instability of Electrically Charged Liquid Jets of Polymer Solutions in Electrospinning	73
A. Experimental Set-Up for Electrospinning	74
B. Experimental Observations	79
C. Viscoelastic Model of a Rectilinear Electrified Jet	103
D. Bending Instability of Electrified Jets	107
E. Localized Approximation	109
F. Continuous Quasi-One-Dimensional Equations of the Dynamics of Electrified Liquid Jets	112
G. Discretized Three-Dimensional Equations of the Dynamics of the Electrospun Jets	115

H. Evaporation and Solidification	119
I. Growth Rate and Wavelength of Small Bending Perturbations of an Electrified Liquid Column.	122
J. Non-linear Dynamics of Bending Electrospun Jets	124
K. Multiple-Jet Electrospinning	139
L. Concluding Remarks	144
VI. Scientific and Technological Challenges in Producing Nanofibers with Desirable Characteristics and Properties	146
VII. Characterization Methods and Tools for Studying the Nanofiber Properties	156
VIII. Development and Applications of Several Specific Types of Nanofibers	172
A. Biofunctional (Bioactive) Nanofibers for Scaffolds in Tissue Engineering Applications and for Drug Delivery and Wound Dressing	172
B. Conducting Nanofibers: Displays, Lighting Devices, Optical Sensors, Thermovoltaic Applications	179
C. Protective Clothing, Chemical and Biosensors and Smart Fabrics	181
Acknowledgment	184
References	184

Abstract

A straightforward, cheap and unique method to produce novel fibers with a diameter in the range of 100 nm and even less is related to electrospinning. For this goal, polymer solutions, liquid crystals, suspensions of solid particles and emulsions, are electrospun in the electric field of about 1 kV/cm. The electric force results in an electrically charged jet of polymer solution flowing out from a pendant or sessile droplet. After the jet flows away from the droplet in a nearly straight line, it bends into a complex path and other changes in shape occur, during which electrical forces stretch and thin it by very large ratios. After the solvent evaporates, birefringent nanofibers are left. Nanofibers of ordinary, conducting and photosensitive polymers were electrospun. The present review deals with the mechanism and electrohydrodynamic modeling of the instabilities and related processes resulting in electrospinning of nanofibers. Also some applications are discussed. In particular, a unique electrostatic field-assisted assembly technique was developed with the aim to position and align individual conducting and light-emitting nanofibers in arrays and ropes. These structures are of potential interest in the development of novel polymer-based light-emitting diodes (LED), diodes, transistors, photonic crystals and flexible photocells. Some other applications discussed include micro-aerodynamic decelerators and tiny flying objects based on permeable nanofiber mats (smart dust), nanofiber-based filters, protective clothing, biomedical applications including wound dressings, drug delivery systems based on nanotubes, the design of

solar sails, light sails and mirrors for use in space, the application of pesticides to plants, structural elements in artificial organs, reinforced composites, as well as nanofibers reinforced by carbon nanotubes.

I. Introduction and Background

The preparation of organic and inorganic materials of semiconductor systems, which are functionalized via a structuring process taking place on the submicrometer scale – nanotechnology – is currently an area of intense activities both in fundamental and applied science on an international scale. Depending on the application, one has in mind three-dimensional systems (photonic band gap materials), two-dimensional systems (quantum well structures) or one-dimensional systems (quantum wires, nanocables). Semi-ordered or disordered (non-woven) systems are of interest for such applications as filter media, fiber-reinforced plastics, solar and light sails and mirrors in space, application of pesticides to plants, biomedical applications (tissue engineering scaffolds, bandages, drug release systems), protective clothing aimed for biological and chemical protection and fibers loaded with catalysts and chemical indicators. For a broad range of applications one-dimensional systems, i.e. nanofibers and hollow nanofibers (nanotubes) are of fundamental importance (Whitesides et al., 1991; Ozin, 1992; Schnur, 1993; Martin, 1994; Edelman, 1999).

The reduction of the diameter into the nanometer range gives rise to a set of favorable properties including the increase of the surface-to-volume ratio, variations in the wetting behavior, modifications of the release rate or a strong decrease of the concentration of structural defects on the fiber surface which will enhance the strength of the fibers.

For a great number of other types of applications, one is interested in tubular structures, i.e. hollow nanofibers, nanotubes and porous systems with narrow channels (Iijima, 1991; Ghadiri et al., 1994; Martin, 1995; Evans et al., 1996). Such systems are of interest among others for drug delivery systems, separation and transport applications, for micro-reactors and for catalysts, for microelectronic and optical applications (nanocables, light guiding, tubes for the near-field microscopy). Such tubular objects can be used to impose confinement effects on chemical, optical and electronic properties, or they can be used as templates for the growth of fiber-shaped systems, for the creation of artificial viruses or as a protein- or DNA-storage medium.

Various approaches leading to thin compact fibers and hollow fibers have been described in the above-mentioned works. Yet these approaches are either limited to fiber dimensions well above 1 μm or they are limited to

specific materials. The extrusion of hollow fibers or compact fibers from the melt or solution is an example for the first case and the preparation of carbon nanotubes (CNTs) is an example for the second case. Our main topic in the present review is the mechanics and physics of the electrospinning process allowing for the preparation of such nanoscaled objects for a broad range of different polymer materials and on a technical scale.

II. Various Methods of Producing Nanofibers

Nanofibers can be obtained by a number of methods: via air-blast atomization of mesophase pitch, via assembling from individual CNT molecules (Tseng and Ellenbogen, 2001), via pulling of non-polymer molecules by an atomic force microscope (AFM) tip (Ondarcuhu and Joachim, 1998), via depositing materials on linear templates or using whiskers of the semiconductor which spontaneously grow out of gold particles placed in the reactor chamber (Cobden, 2001). InP (indium phosphide) nanowires were prepared by laser-assisted catalytic growth (Duan *et al.*, 2001), molybdenum nanowires were electrodeposited (Zach *et al.*, 2000). Step-by-step application of organic molecules and metal ions on predetermined patterns (Hatzor and Weiss, 2001) and DNA-templated assembly (Braun *et al.*, 1998; Mbainyo *et al.*, 2001) were also proposed as possible routes toward nanofibers and nanowires.

While air-blast atomization of mesophase pitch allows for a fast generation of a significant and even a huge amount of non-woven nanofibers in a more or less uncontrollable manner, the other methods listed above allow for a rather good process control. However, all of them yield significantly short nanofibers and nanowires with the lengths of the order of several microns. They are also not very flexible with respect to material choice.

Electrospinning of nanofibers, nanowires and nanotubes represents a very flexible method, which allows for manufacturing of long nanofibers (of the order of 10 cm) and a relatively easy route for their assembly and manipulation. The number of polymers that were electrospun to make nanofibers and nanotubes exceeds 100. These include both organic and silicon-based polymers. Electrospinning is considered in detail in the following sections.

III. Electrospinning of Nanofibers

Electrospinning is a straightforward and cost-effective method to produce novel fibers with diameters in the range of from less than 3 nm to over 1 μm , which overlaps contemporary textile fiber technology. Electrified jets of

polymer solutions and melts were investigated as routes to the manufacture of polymer nanofibers (Baumgarten, 1971; Larrondo and Manley, 1981a–c; Reneker and Chun, 1996). Since 1934, when a U.S. patent on electrospinning was issued to Formhals (1934), over 30 U.S. patents have been issued. Nanofibers of polymers were electrospun by creating an electrically charged jet of polymer solution at a pendant or sessile droplet. In the electrospinning process a pendant drop of fluid (a polymer solution) becomes unstable under the action of the electric field, and a jet is issued from its tip. An electric potential difference, which is of the order of 10 kV, is established between the surface of the liquid drop (or pipette, which is in contact with it) and the collector/ground. After the jet flowed away from the droplet in a nearly straight line, it bent into a complex path and other changes in shape occurred, during which electrical forces stretched and thinned it by very large ratios. After the solvent evaporated birefringent nanofibers were left. The above scenario is characteristic of the experiments conducted by a number of groups with very minor variations (Baumgarten, 1971; Doshi and Reneker, 1995; Jaeger et al., 1996; Reneker and Chun, 1996; Fang and Reneker, 1997; Fong et al., 1999; Fong and Reneker, 1999; Reneker et al., 2000; Theron et al., 2001; Yarin et al., 2001a). Templates for manufacturing nanotubes are also electrospun by the same method (Bognitzki et al., 2000, 2001; Caruso et al., 2001). The existing reviews of electrospinning mostly deal with the material science aspects of the process and applications of the as-spun nanofibers (Fong and Reneker, 2000; Frenot and Chronakis, 2003; Huang et al., 2003; Dzenis, 2004; Li and Xia, 2004b; Ramakrishna et al., 2005; Subbiah et al., 2005).

IV. Taylor Cone and Jetting from Liquid Droplets in Electrospinning of Nanofibers

Sessile and pendant droplets of polymer solutions acquire stable shapes when they are electrically charged by applying an electrical potential difference between the droplet and a flat plate, if the potential is not too high. These stable shapes result only from equilibrium of the electric forces and surface tension in the cases of inviscid, Newtonian and viscoelastic liquids. It is widely assumed that when the critical potential φ_{0*} has been reached and any further increase will destroy the equilibrium, the liquid body acquires a conical shape referred to as the Taylor cone (Taylor, 1964), having a half angle of 49.3°. In the present section following Yarin et al. (2001b) and Reznik et al. (2004), we show that the Taylor cone corresponds essentially to a specific self-similar solution, whereas non-self-solutions exist which do not tend towards the Taylor cone. Thus, the Taylor cone does not represent a unique critical shape: another shape exists

which is not self-similar. The experiments demonstrate that the half angles observed are much closer to the new shape. In this section, a theory of stable and transient shapes of droplets affected by an electric field is exposed and compared with data acquired in the experimental work on electrospinning of nanofibers from polymer solutions.

Consider a droplet positioned inside a capacitor. As the strength of the electric field E increases, the droplet becomes more and more prolate until no shape is stable beyond some critical value E^* . This resembles the behavior recorded in the seminal work of [Taylor \(1964\)](#) for droplets subjected to a higher and higher potential Φ_0 : they elongate to some extent, but then suddenly tend to a cone-like shape. The boundary between the stable electrified droplets and those with a jet flowing from the tip lies somewhere near the critical value of the potential (or the field strength). Taylor calculated the half angle at the tip of an infinite cone arising from an infinite liquid body. In Section IV.A, we calculate the half angle by a different method which brings out the self-similar nature of the Taylor cone, and states the assumptions involved in its calculation. Then, in Section IV.B, we consider a family of non-self-similar solutions for the hyperbolical shapes of electrified liquid bodies in equilibrium with their own electric field due to surface tension forces. In Section IV.C, we show that these solutions do not tend to the self-similar solution corresponding to the family of the Taylor cone, and represent an alternative to the Taylor cone. Thus, we conclude that another shape, one tending towards a sharper cone than that of Taylor, can precede the stability loss and the onset of jetting. In Section IV.D, experimental results are presented and compared with the theory. These results confirm the theoretical predictions of Section IV.C. In Section IV.E, numerical simulations of stable and transient droplet shapes (the latter resulting in jetting) are discussed and compared to the experimental data.

A. TAYLOR CONE AS A SELF-SIMILAR SOLUTION

All the liquids we deal with throughout Section IV are considered to be perfect ionic conductors. The reason that the assumption of a perfect conductor is valid in the present case is in the following. The characteristic charge relaxation time $\tau_C = \varepsilon/(4\pi\sigma_e)$, where ε is the dielectric permeability and σ_e is the electric conductivity. Note that in the present review all the equations that contain terms that depend on the electric field are expressed in Gaussian (CGS) units, and the values of all the parameters are given in CGS units. This is especially convenient and customary in cases where both electrostatics and fluid mechanics are involved. The values of the electric potential, the electric field strength and the electric current and conductivity

are also converted into SI units for convenience. The plausible values of the parameters for the polymer solutions used in electrospinning and for many other leaky dielectric fluids are $\epsilon \approx 40$ and $\sigma_e = 9 \times 10^2 - 9 \times 10^6 \text{ s}^{-1}$, which is $10^{-7} - 10^{-3} \text{ S m}^{-1}$. Therefore, $\tau_C = 0.00035 - 3.5 \text{ ms}$. If a characteristic hydrodynamic time $\tau_H \gg \tau_C$, then the fluid behavior is that of a perfect conductor in spite of the fact that it is actually a poor conductor (leaky dielectric) compared to such good conductors as metals. In the present section, $\tau_H \sim 1 \text{ s}$ is associated with the residence time of fluid particles in the droplets which is of the order of 1 s in the experiments. Therefore, $\tau_H \gg \tau_C$ and the approximation of a perfect conductor is fully justified.

Under the influence of an applied potential difference, excess charge flows to or from the liquid. Anions and cations are distributed non-uniformly on the surface of the liquid. The free surfaces of the liquids are always equipotential surfaces with the charges distributed in a way that maintains a zero electric field inside the liquid.

To establish the self-similar nature of the solution corresponding to the Taylor cone, we consider an axisymmetric liquid body kept at a potential $(\varphi_0 + \text{const})$ with its tip at a distance a_0 from an equipotential plane (Fig. 4.1). The distribution of the electric potential $\Phi = \varphi + \text{const}$ is described in the spherical coordinates R and θ , and in the cylindrical coordinates ρ and z (see Fig. 4.1). The shape of the free surface is assumed to

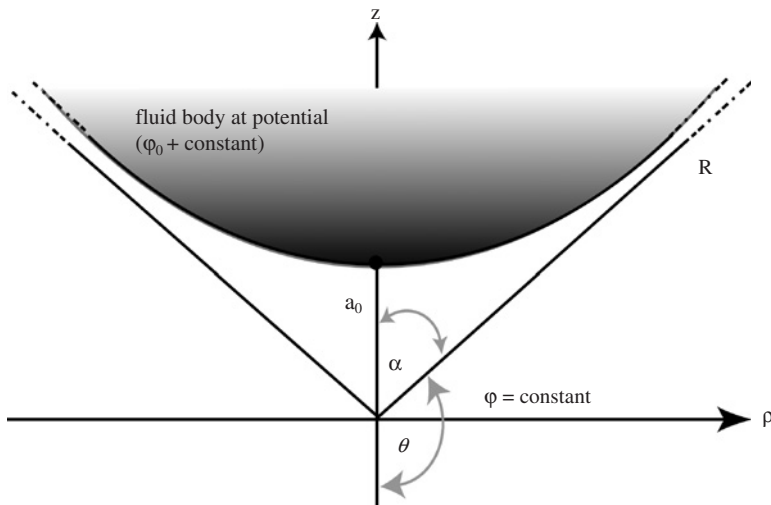


FIG. 4.1. Axisymmetric “infinite” fluid body kept at potential $\Phi_0 = \varphi_0 + \text{const}$ at a distance a_0 from an equipotential plane kept at $\Phi = \text{const}$. After Yarin et al. (2001b) with permission from AIP.

be that of equilibrium, which means that the electrical forces acting on the droplet in Fig. 4.1 are balanced by the surface tension forces. The potential φ_0 can, in such a case, always be expressed in terms of the surface tension coefficient σ and of a_0 , specifically as $\varphi_0 = C(\sigma a_0)^{1/2}$, where C is a dimensionless factor. Owing to the dimensional arguments, the general representation of φ is, in the present case, $\varphi = \varphi_0 F_1(R/a_0, \theta)$, where F_1 is a dimensionless function. The value of the potential Φ throughout the space that surrounds the liquid body is given by

$$\Phi = (\sigma a_0)^{1/2} F\left(\frac{R}{a_0}, \theta\right) + \text{const}, \quad (4.1)$$

where $F = C F_1$ is a dimensionless function.

At distances, $R > > a_0$, where it can be assumed that the influence of the gap a_0 is small, the function F should approach a specific power-law scaling

$$F\left(\frac{R}{a_0}, \theta\right) = \left(\frac{R}{a_0}\right)^{1/2} \Psi(\theta) \quad (4.2)$$

($\Psi(\theta)$ being a dimensionless function), whereupon Eq. (4.1) takes the asymptotic self-similar form, independent of a_0

$$\Phi = (\sigma R)^{1/2} \Psi(\theta) + \text{const.} \quad (4.3)$$

Power-law scalings leading to self-similar solutions are common in boundary-layer theory (cf., for example, Schlichting, 1979; Zel'dovich, 1992, and references therein). In particular, such self-similar solutions for jets and plumes, considered as issuing from a pointwise source, in reality correspond to the non-self-similar solutions of the Prandtl equations for the jets and plumes being issued from finite-size nozzles, at distances much larger than the nozzle size (Dzhaugashin and Yarin, 1977). The remote-asymptotic and self-similar solution (Yarin and Weiss, 1995) for capillary waves generated by a weak impact of a droplet of diameter D onto a thin liquid layer, emerges at distances much greater than D from the center of impact. The self-similar solution for the electric field Eq. (4.3) is motivated by precisely the same idea, and is expected to be the limit to all non-self-similar solutions at distances $R \gg a_0$.

This solution should also satisfy the Laplace equation, which enables us to find Ψ as in Taylor (1964)

$$\Psi(\theta) = P_{1/2}(\cos \theta), \quad (4.4)$$

where $P_{1/2}(\cos \theta)$ is a Legendre function of order 1/2.

The free surface becomes equipotential only when θ corresponds to the only zero of $P_{1/2}(\cos \theta)$ in the range $0 \leq \theta \leq \pi$, which is $\theta_0 = 130.7^\circ$ (Taylor, 1964). Then the fluid body shown in Fig. 4.1. is enveloped by a cone with the half angle at its tip equal to $\alpha = \alpha_T = \pi - \theta_0 = 49.3^\circ$, which is the Taylor cone. The shape of the liquid body in Fig. 4.1 would then approach the Taylor cone asymptotically as $R \rightarrow \infty$. (Note that Pantano et al., 1994 considered a finite drop attached to a tube). Taylor's self-similarity assumption leading to Eqs. (4.2) and (4.3) also specifies that $\Phi \rightarrow \infty$ as $R \rightarrow \infty$, which is quite peculiar. In Section IV.B, we show that relevant non-self-similar solutions do not follow this trend as $R \rightarrow \infty$, which means that these solutions are fundamentally different from the solution corresponding to the Taylor cone.

B. NON-SELF-SIMILAR SOLUTIONS FOR HYPERBOLOIDAL LIQUID BODIES

Experimental data of Taylor (1964) and numerous subsequent works show that droplets acquire a static shape that does not depend on the initial shape. This static shape is stable if the strength of the electric field does not exceed a certain critical level. As the electric field approaches the critical value, the droplet shape approaches that of a cone with a rounded tip. The radius of curvature of the tip can become too small to be seen in an ordinary photograph (to be discussed in Section IV.D). Nevertheless, the tip should be rounded, since otherwise the electric field would become infinite at the tip. Detailed calculation of the exact droplet shape near the tip is an involved non-linear integro-differential problem, since the field depends on the droplet shape and *vice versa* (this is briefly discussed in Section IV.E). To simplify such calculations, approximate methods were proposed (e.g., Taylor, 1964). In those approximate methods a likely shape for a droplet is chosen that would satisfy the stress balance between the electric field and surface tension in an approximate way. In the present problem any likely droplet shape must be very close to a hyperboloid of revolution. Therefore, the first theoretical assumption is that the droplet shape is a hyperboloid of revolution. We will show that such a hyperboloidal droplet approaches a static shape that is very close to that of a cone with a rounded tip. The tip has a very small radius of curvature. This hyperboloid corresponds to the experimental evidence (discussed in Section IV.D).

In calculating an electric field about a body shaped as a hyperboloid of revolution, like the one denoted BCD in Figs. 4.2.(b) and (c), it is natural to use the prolate spheroidal coordinate system ξ, η .

We assume that the tip of the hyperboloid BCD is situated at a distance a_0 from the equipotential surface $z = 0$, and the range in which a solution is sought corresponds to $0 \leq \xi \leq \xi_0 < 1$, $1 \leq \eta \leq \infty$. The surface of hyperboloid

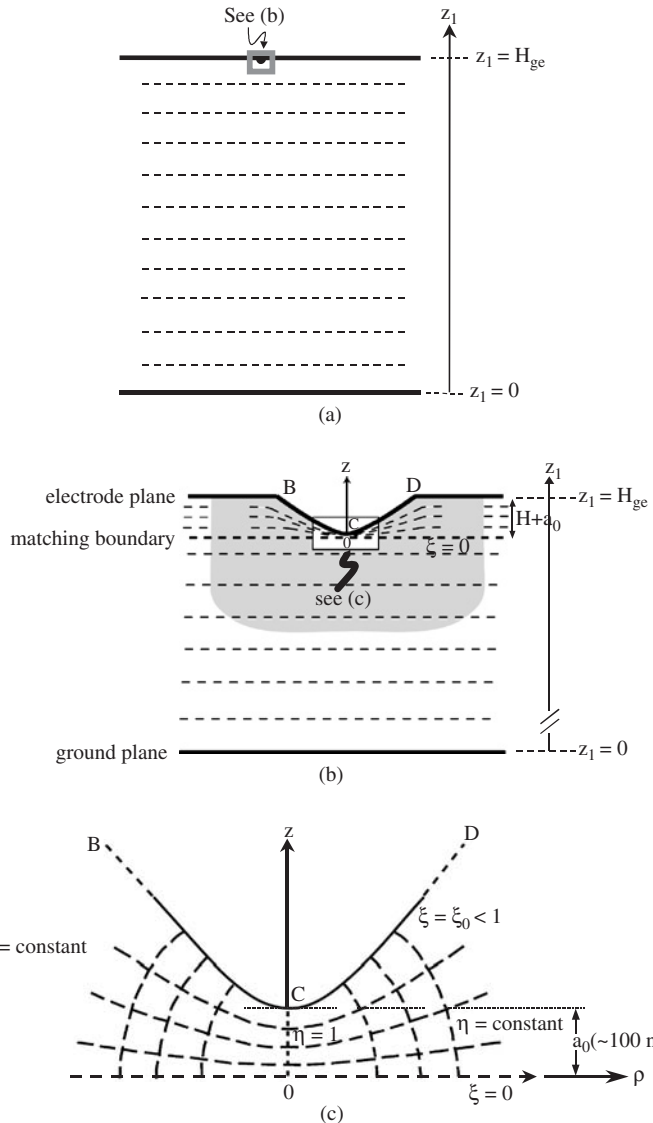


FIG. 4.2. Prolate spheroidal coordinate system about a hyperboloidal liquid body BCD. (a) Equipotential lines are shown for $0 \leq z_1 \leq H_{ge} - (H + a_0)$. (c) Equipotential lines ($\xi = \text{const}$) are shown for $H_{ge} - (H + a_0) \leq z_1 \leq H_{ge}$. After Yarin et al. (2001b) with permission from AIP.

BCD is represented by ξ_0 (see Fig. 4.2(c)). Coordinate isolines are also shown in Fig. 4.2, with the lines $\eta = \text{const}$ representing ellipsoids, and the lines $\xi = \text{const}$ representing hyperboloids.

The second theoretical assumption is that the space charge effects are negligible. This assumption is discussed in detail in Section IV.D. Then the electric potential Φ satisfies the Laplace equation. In prolate spheroidal coordinates it takes the form (Smythe, 1968)

$$\frac{\partial}{\partial \xi} \left[(1 - \xi^2) \frac{\partial \Phi}{\partial \xi} \right] + \frac{\partial}{\partial \eta} \left[(\eta^2 - 1) \frac{\partial \Phi}{\partial \eta} \right] = 0, \quad (4.5)$$

which has the general solution,

$$\Phi = \sum_{m=0}^{\infty} [A_m P_m(\xi) + B_m Q_m(\xi)] [A'_m P_m(\eta) + B'_m Q_m(\eta)] + \text{const}, \quad (4.6)$$

where $P_m(\cdot)$ and $Q_m(\cdot)$ are Legendre functions and associated Legendre functions of integer order m , respectively, and A_m , B_m , A'_m and B'_m are the constants of integration.

Since in the present case the range of interest includes $\eta = 1$ (cf. Fig. 4.2) where $Q_m(1) = \infty$, to have a finite solution we should take $B'_m = 0$. Also in the present case, it suffices to consider only the first term of Eq. (4.6) corresponding to $m = 0$. We then obtain from Eq. (4.6)

$$\Phi = A''_0 P_0(\eta) [P_0(\xi) + B''_0 Q_0(\xi)] + \text{const}, \quad (4.7)$$

where, $A''_0 = A_0 A'_0$, $B''_0 = B_0 / A_0$, $P_0(\eta) = P_0(\xi) = 1$, and $Q_0(\xi) = (1/2) \ln[(1 + \xi)/(1 - \xi)]$.

Expression (4.7) then takes the form

$$\Phi = D \ln \left(\frac{1 + \xi}{1 - \xi} \right) + \text{const}, \quad (4.8)$$

where D is a constant, determined by the circumstance that the free surface of the hyperboloid BCD at $\xi = \xi_0$ is kept at a potential $\Phi_0 = \varphi_0 + \text{const}$. Then $D = \varphi_0 / \ln[(1 + \xi_0)/(1 - \xi_0)]$, and

$$\Phi = \varphi_0 \frac{\ln[(1 + \xi)/(1 - \xi)]}{\ln[(1 + \xi_0)/(1 - \xi_0)]} + \text{const}. \quad (4.9)$$

Hyperboloid BCD is given by the expression

$$\frac{z^2}{a_0^2} - \frac{\rho^2}{b_0^2} = 1, \quad (4.10)$$

where

$$a_0^2 = c^2 \xi^2, \quad b_0^2 = c^2(1 - \xi^2), \quad (4.11a,b)$$

and c is a constant.

The normal derivative of the electric potential at its surface is given by

$$\left. \frac{\partial \Phi}{\partial n} \right|_{\xi=\xi_0} = \frac{1}{c} \left(\frac{1 - \xi^2}{\eta^2 - \xi^2} \right)^{1/2} \left. \frac{\partial \Phi}{\partial \xi} \right|_{\xi=\xi_0}, \quad (4.12)$$

which yields, using Eq. (4.9)

$$\left. \frac{\partial \Phi}{\partial n} \right|_{\xi=\xi_0} = \frac{2\varphi_0}{\ell n[(1 + \xi_0)/(1 - \xi_0)]} \cdot \frac{1}{c[(\eta^2 - \xi_0^2)(1 - \xi_0^2)]^{1/2}}. \quad (4.13)$$

From Eq. (4.11a) it is seen that for the hyperboloid considered $c = a_0/\xi_0$.

Expression (4.13) characterizes the charge distribution over the free surface BCD with the maximal charge at the tip, where $\eta = 1$. The only non-zero stress of electric origin acting on BCD is the normal stress,

$$\sigma_{nn} = \frac{1}{8\pi} \left(\left. \frac{\partial \Phi}{\partial n} \right|_{\xi=\xi_0} \right)^2, \quad (4.14)$$

which yields the stress distribution over the surface of the hyperboloid ξ_0

$$\sigma_{nn}|_{\xi=\xi_0} = \frac{\varphi_0^2}{2\pi\ell n^2[(1 + \xi_0)/(1 - \xi_0)]} \cdot \frac{1}{[(z^2/\xi_0^2 - a_0^2)(1 - \xi_0^2)]}. \quad (4.15)$$

The z -coordinates of points on the free surface are z .

It is emphasized that to arrive at Eq. (4.15) we also use Eq. (4.11a) and the first formula relating the cylindrical and the prolate spheroidal coordinates

$$z = c\eta\xi, \quad (4.16a)$$

$$\rho = c[(1 - \xi^2)(\eta^2 - 1)]^{1/2}. \quad (4.16b)$$

From Eq. (4.15) it follows that the stresses σ_{nn} at the tip of hyperboloid BCD at $z = a_0$ and $H \gg a_0$ are given by

$$\sigma_{nn}|_{z=a_0} = \sigma_{nn,\max} = \frac{\varphi_0^2}{2\pi\ell n^2[(1 + \xi_0)/(1 - \xi_0)]} \left(\frac{\xi_0}{a_0} \right)^2 \frac{1}{(1 - \xi_0^2)^2}, \quad (4.17a)$$

$$\sigma_{nn}|_{z=H} = \sigma_{nn,\min} = \frac{\varphi_0^2}{2\pi\ell n^2 \left[(1 + \xi_0)/(1 - \xi_0) \right]} \cdot \frac{1}{\left[(H^2/\xi_0^2 - a_0^2)(1 - \xi_0^2) \right]}. \quad (4.17b)$$

It should be noted that the solutions obtained above for the electric field about hyperboloidal bodies are exact. However, for liquid bodies the shape of the free surface cannot, *a priori*, be expected to be a perfect hyperboloid and should be calculated separately.

Assuming a hyperboloidal shape as an approximation, its curvature is given by

$$K = \frac{(b_0 z/a_0)^2 - b_0^2 + (b_0^2 z/a_0^2)^2 + b_0^4/a_0^2}{\left[(b_0 z/a_0)^2 - b_0^2 + (b_0^2 z/a_0^2)^2 \right]^{3/2}}. \quad (4.18)$$

Therefore, the capillary pressure $p_\sigma = \sigma K$ at the tip and at a height H above the tip (see Fig. 4.2) is given by

$$p_\sigma|_{z=a_0} = \sigma \frac{2a_0}{b_0^2}, \quad (4.19a)$$

$$p_\sigma|_{z=H} = \sigma \frac{(b_0 H/a_0)^2 - b_0^2 + (b_0^2 H/a_0^2)^2 + b_0^4/a_0^2}{\left[(b_0 H/a_0)^2 - b_0^2 + (b_0^2 H/a_0^2)^2 \right]^{3/2}}. \quad (4.19b)$$

Similar to the first spheroidal approximation used in Taylor (1964), we approximate the force balance at the hyperboloidal surface by the expressions

$$\sigma K|_{z=a_0} - \Delta p = \sigma_{nn}|_{z=a_0}, \quad (4.20a)$$

$$\sigma K|_{z=H} - \Delta p = \sigma_{nn}|_{z=H}. \quad (4.20b)$$

Assuming that Δp , the difference between the pressure inside and that outside the surface, is the same at the tip $z = a_0$ and “bottom” $z = H$, we obtain

$$\sigma_{nn}|_{z=a_0} - \sigma_{nn}|_{z=H} = \sigma K|_{z=a_0} - \sigma K|_{z=H}. \quad (4.21)$$

Substituting Eqs. (4.17) and (4.19) into Eq. (4.21), we find the dependence of φ_0 on the surface tension coefficient σ ,

$$\begin{aligned} & \frac{\varphi_0^2}{2\pi\ell n^2[(1+\xi_0)/(1-\xi_0)]} \left[\left(\frac{\xi_0/a_0}{1-\xi_0^2} \right)^2 - \frac{1}{[(H/a_0)^2 - a_0^2] (1-\xi_0^2)} \right] \\ &= \sigma \left(\frac{2a_0}{b_0^2} - \frac{(b_0H/a_0)^2 - b_0^2 + (b_0^2H/a_0^2)^2 + b_0^4/a_0^2}{[(b_0H/a_0)^2 - b_0^2 + (b_0^2H/a_0^2)^2]^{3/2}} \right). \end{aligned} \quad (4.22)$$

Also from Eq. (4.11) we obtain

$$b_0^2 = a_0^2 \frac{(1-\xi_0^2)}{\xi_0^2}. \quad (4.23)$$

Substituting Eq. (4.23) into Eq. (4.22) and rendering Eq. (4.22) dimensionless, we rearrange it as follows

$$\begin{aligned} \frac{\varphi_0^2}{\sigma a_0} &= 2\pi\ell n^2 \left(\frac{1+\xi_0}{1-\xi_0} \right) \left[2\xi_0^2 - \frac{\xi_0(1-\xi_0)^{1/2} \left[(\bar{H}^2 + 1)/\xi_0^2 - 2 \right]}{\left[(\bar{H}/\xi_0)^2 - 1 \right]^{3/2}} \right] \\ &\quad \times \left\{ \frac{\xi_0^2}{1-\xi_0^2} - \frac{1}{\left[(\bar{H}/\xi_0)^2 - 1 \right]} \right\}^{-1}. \end{aligned} \quad (4.24)$$

For a given $\bar{H} = H/a_0$, we obtain from expression (4.24) a dependence of $\varphi_0^2/\sigma a_0$ on ξ_0 for a stationary liquid body assumed to have a hyperboloidal shape. In the case of an “infinite” hyperboloid ($\bar{H} \gg 1$), with its tip at a distance a_0 from the equipotential surface $z = 0$, expression (4.24) yields

$$\varphi_0 = (\sigma a_0)^{1/2} (4\pi)^{1/2} \ell n \left(\frac{1+\xi_0}{1-\xi_0} \right) (1-\xi_0^2)^{1/2}, \quad (4.25)$$

which is analyzed in Section IV.C.

The temptation is to assign the equipotential surface $z = 0$ to the ground plate at $z_1 = 0$. This assignment is ruled out, because a_0 would then be much larger than the droplet size. Then the electric field adjoining the droplet (which is only a small detail of the practically uniform, capacitor-like field between the electrode and the ground; cf., Fig. 4.2(a)) would be grossly in error because this calculation does not account for the presence of the electrode at $z_1 = H_{ge}$. To eliminate this difficulty, we assume that the equipotential surface $z = 0$ is situated very close to the droplet tip, at a distance a_0 , which is yet to be determined. The electric field between the matching boundary (cf., Fig. 4.2(b)) and the free surface of the droplet was already determined, and was described above.

The electric field between the matching boundary and the ground plate at distances from the tip much larger than a_0 is practically unaffected by the droplet. Thus the electric field in the region between the ground plate and the matching boundary may be assumed to be that of a parallel-plate capacitor (cf., Fig. 4.2(a)). The parallel-capacitor field and the field of the potential Φ found here in Section IV.B (cf. Fig. 4.2(c)) are to be matched at $z = 0$, which enables us to calculate a_0 (cf. Fig. 4.2(b)). We can call the space between the surface $z = 0$ and the hyperboloid the boundary layer, which is characterized by the scale a_0 . The space below $z = 0$ is then the “outer field” using a fluid-mechanical analogy. It is emphasized that this procedure is only a crude first approximation, since the normal derivatives of the potentials (the electric field intensities) are not automatically matched at $z = 0$. A much better representation of the field and potential in the intermediate region could be achieved by matching asymptotic expansions or computer modeling (cf. Section IV.E). The region where the potential is not predicted with much precision is shown in gray in Fig. 4.2(b).

We now consider in detail matching of the approximate solutions for the electric potential. If z_1 is the coordinate directed from the ground plate (at $z_1 = 0$) toward the droplet, then the capacitor-like field is given by

$$\Phi = \frac{\Phi_0}{H_{ge}} z_1. \quad (4.26)$$

Here H_{ge} is the distance between the ground plate and an electrode attached to the droplet (at potential Φ_0).

Given that the droplet height in the z direction is H , that the borderline equipotential surface where $z = \xi = 0$ is situated at $z_1 = H_{ge} - H - a_0$, and matching the solutions for the potential, we find from Eqs. (4.9) and (4.26) that the constant in Eq. (4.9) is

$$\text{const} = \frac{\Phi_0}{H_{ge}} (H_{ge} - H - a_0). \quad (4.27)$$

Thus, Eqs. (4.9) and (4.27) yield

$$\Phi = \varphi_0 \frac{\ell n[(1 + \xi)/(1 - \xi)]}{\ell n[(1 + \xi_0)/(1 - \xi_0)]} + \Phi_0 \frac{(H_{ge} - H - a_0)}{H_{ge}}. \quad (4.28)$$

For the droplet surface at $\xi = \xi_0$, the potential is $\Phi = \Phi_0$ and thus from Eq. (4.28) we find

$$\varphi_0 = \frac{\Phi_0}{H_{ge}} (H + a_0). \quad (4.29)$$

Combining Eq. (4.29) with Eq. (4.25), we obtain the equation for a_0

$$(\sigma a_0)^{1/2} (4\pi)^{1/2} \ell n \left(\frac{1 + \xi_0}{1 - \xi_0} \right) (1 - \xi_0^2)^{1/2} = \frac{\Phi_0}{H_{ge}} (H + a_0), \quad (4.30)$$

which has two solutions. The solution relevant here reads

$$a_0 = \frac{1}{2} \left(\frac{1}{\beta^2} - 2H \right) - \left[\frac{1}{4} \left(\frac{1}{\beta^2} - 2H \right)^2 - H^2 \right]^{1/2}, \quad (4.31a)$$

$$\beta = \frac{\Phi_0}{H_{ge} (4\pi\sigma)^{1/2} \ell n [(1 + \xi_0)/(1 - \xi_0)] (1 - \xi_0^2)^{1/2}}, \quad (4.31b)$$

whereas the other one is irrelevant, since it yields $a_0 > H_{ge}$.

Expression (4.31a) permits calculation of a_0 for any given hyperboloidal droplet (given ξ_0 and H) at any given potential Φ_0 . It should be noted that the results will be accurate if the calculated value of a_0 is sufficiently small relative to H .

C. FAILURE OF THE SELF-SIMILARITY ASSUMPTION FOR HYPERBOLOIDAL SOLUTIONS

The electric potential between the free surface of a hyperboloidal liquid body and the equipotential surface $z = 0$ is given by Eq. (4.9) with φ_0 as per Eq. (4.25). To visualize the asymptotic behavior of Eq. (4.9), we should follow a straight line with a constant slope θ , while R tends to infinity (see Fig. 4.1). Then using Eqs. (4.16a,b) we find

$$R = (z^2 + \rho^2)^{1/2} = c(\eta^2 + \xi^2 - 1)^{1/2}. \quad (4.32)$$

Also

$$-\tan \theta = \frac{\rho}{z} = \frac{[(1 - \xi^2)(\eta^2 - 1)]^{1/2}}{\eta \xi}, \quad (4.33)$$

which yields

$$\eta^2 = \frac{1 - \xi^2}{1 - (\xi / \cos \theta)^2}. \quad (4.34)$$

Substituting the latter into Eq. (4.32), we find

$$R = c \frac{\xi}{-\cos \theta} \left[\frac{1 - \xi^2}{1 - (\xi / \cos \theta)^2} \right]^{1/2}. \quad (4.35)$$

It is seen that $R \rightarrow \infty$ as $\xi \rightarrow -\cos \theta$. Then we obtain from Eqs. (4.9) and (4.25) the potential Φ as $R \rightarrow \infty$ in the following form:

$$\Phi|_{R \rightarrow \infty} = (\sigma a_0)^{1/2} (4\pi)^{1/2} (1 - \xi_0^2)^{1/2} \ln \left(\frac{1 - \cos \theta}{1 + \cos \theta} \right) + \text{const}, \quad \frac{\pi}{2} \leq \theta \leq \pi, \quad (4.36)$$

which shows that the asymptotic value, Φ , is finite. Φ does not tend towards infinity as the self-similarity of Section IV.A implies. Also, in spite of the fact that $R \gg a_0$, the dependence on a_0 does not disappear from Eq. (4.36) in contrast with the self-similar behavior of Taylor's solution given by Eq. (4.3). Thus, we have an example of a non-self-similar solution with a non-fading influence of the value of a_0 , even when $R \gg a_0$. Details of the shape of the tip at small distances of the order of a_0 , affect the solution for Φ at any $R \gg a_0$. In other words, the solution for the field about a hyperboloid depends on the value of a_0 everywhere, while the field surrounding the Taylor cone does not depend on a_0 at $R \gg a_0$. The field surrounding the hyperboloidal bodies is always affected by the value of a_0 , even when R approaches ∞ . This behavior is quite distinct from that of the boundary-layer theory cases of jets from a finite orifice and of plumes originating at a finite source, where the influence of the size of the orifice or source rapidly fades out.

The following observation should be mentioned. In the case of the parabolic governing equations (the boundary layer theory, [Dzhaugashtin and Yarin, 1977](#); [Schlichting, 1979](#); [Zel'dovich, 1992](#)), or the equation with a squared parabolic operator (the beam equation describing self-similar capillary waves, [Yarin and Weiss, 1995](#)), self-similar solutions attract the non-self-similar ones and thus are realizable. On the other hand, in the present case the governing Laplace equation is elliptic, and its self-similar solution does not attract the non-self-similar one and therefore could hardly be expected to be realizable. Moreover, a similar phenomenon was found in the problem described by the biharmonic (the elliptic operator squared) equation, namely in the problem on a wedge under a concentrated couple. The later is known in the elasticity theory as the Sternberg-Koiter paradox ([Sternberg and Koiter, 1958](#)).

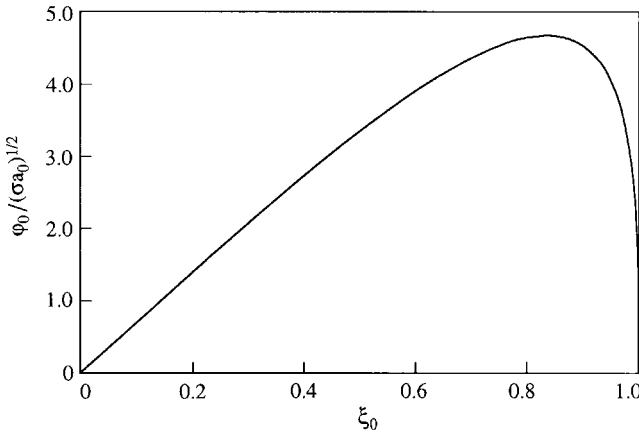


FIG. 4.3. Dependence of the shape parameter ξ_0 on the electric potential ϕ_0 of an infinite hyperboloid. After Yarin et al. (2001b) with permission from AIP.

The calculated cone, which is tangent to the critical hyperboloid just before a jet is ejected, is definitely not the Taylor cone. Indeed, in Fig. 4.3 the dependence of $\phi_0/(\sigma a_0)^{1/2}$ on ξ_0 according to Eq. (4.25) is shown. The maximal potential at which a stationary shape can exist corresponds to $\xi_{0*} = 0.834$ and $\phi_{0*} = 4.699(\sigma a_0)^{1/2}$. The value ξ_{0*} corresponds to the critical hyperboloid. An envelope cone for any hyperboloid can be found using the derivative

$$\left. \frac{dz}{d\rho} \right|_{\rho \rightarrow \infty} = \frac{a_0}{b_0}, \quad (4.37)$$

which follows from Eq. (4.10).

For the critical hyperboloid, using Eq. (4.23), we find

$$\frac{a_0}{b_0} = \frac{\xi_{0*}}{\left(1 - \xi_{0*}^2\right)^{1/2}} = 1.51. \quad (4.38)$$

Therefore, the half angle at the tip of the cone is given by (cf. Fig. 4.1)

$$\alpha_* = \frac{\pi}{2} - \arctan(1.51), \quad (4.39)$$

which yields $\alpha_* = 33.5^\circ$, which is significantly smaller than the angle for the Taylor cone $\alpha_T = 49.3^\circ$. Note also that the Taylor cone is asymptotic to a

hyperboloid possessing a value of $\xi = \xi_{0T}$ which should be less than ξ_* . Indeed, similar to Eq. (4.38)

$$\frac{a_{0T}}{b_{0T}} = \frac{\xi_{0T}}{(1 - \xi_{0T}^2)^{1/2}} = \tan\left(\frac{\pi}{2} - \alpha_T\right), \quad (4.40)$$

which yields $\xi_{0T} = \cos \alpha_T = 0.65$. Comparing this value with that for the critical hyperboloid, $\xi_{0*} = 0.834$, we see once more that the critical hyperboloid is much “sharper” than the one corresponding to the Taylor cone, since this sharpness increases with ξ .

The left part of the curve with a positive slope in Fig. 4.3 can be realized pointwise, since there higher potentials correspond to sharper hyperboloids. By contrast, the right-hand part represents still sharper hyperboloids for lower potentials, which cannot be reached in usual experiments with a stable fluid body. The latter means that the right-hand part corresponds to unstable solutions. It is also emphasized that the critical angle $\alpha_* = 33.5^\circ$ is much closer to the experimental values reported in Section IV.D than that of the Taylor cone.

The results of Sections IV.B and IV.C are equally relevant for inviscid, for Newtonian or for viscoelastic liquids after the stress has relaxed. All these manifest in stationary states with zero deviatoric stresses. In the hypothetical case of a non-relaxing purely elastic liquid or for a viscoelastic liquid with weak relaxation effects the elastic stresses affect the half-angle value, which increases (Yarin et al., 2001b).

D. EXPERIMENTAL RESULTS AND COMPARISON WITH THEORY

Two experiments, using sessile and pendant droplets, were performed for comparison with the theory. In the sessile drop experiment (Fig. 4.4) a droplet was created at the tip of an inverted pipette by forcing the liquid through the pipette slowly with a syringe pump. The liquid used was an aqueous solution of polyethylene oxide (PEO) with a molecular weight of 400,000 and a weight concentration of 6%.

Fluid properties of such solutions including shear and elongational viscosity, surface tension and conductivity/resistivity are published elsewhere (Fong and Reneker, 1999; Reneker et al., 2000; Yarin et al., 2001a). Their evaporation rate can be described using the standard dependence of saturation vapor concentration on temperature (Yarin et al., 2001a). For droplet sizes of the order of 0.1 cm, the evaporation process lasts not less than 600 s (Yarin et al., 1999). This is much more than the time required to

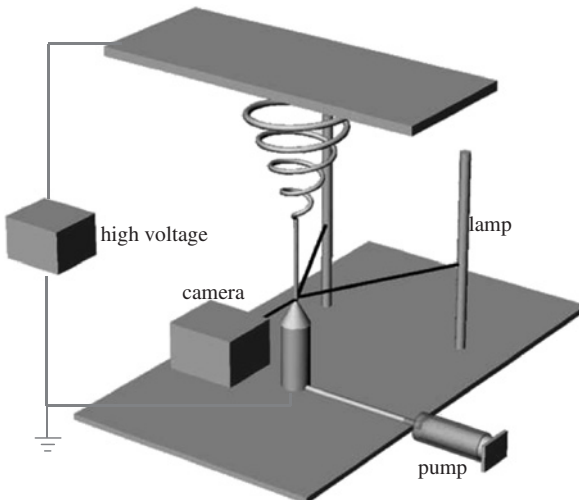


FIG. 4.4. Sessile drop experiment. After Yarin et al. (2001b) with permission from AIP.

reach steady state and make measurements (of the order of 1 s). Therefore, evaporation effects when the photographs were taken are negligible. All the experiments were done at room temperature. Elevated temperatures were not studied. Droplet configurations are quite reproducible for a given capillary size, which was not varied in the present experiments. The effect of pH was not studied in detail. Addition of sodium chloride to the solution was discussed in Fong et al. (1999). The electrode material, usually copper, had no important effect on the ionic conductivity of the solutions (Fong et al., 1999; Reneker, et al., 2000; Yarin et al., 2001a).

The electric potential was applied between the droplet and a flat metal collector plate held above the droplet. The droplet was kept at ground potential for convenience. The potential difference was increased in steps of about 200 V, each step a few seconds long, until a jet formed at the tip of the droplet. Images of the droplet were made with a video camera. The shape of the droplet during the step that preceded the formation of the jet was called the critical shape. Two linear lamps were mounted vertically, behind and on either side of the droplet. The shape and diameter of the droplet were demarcated by reflection of the lights, seen as white line on the image recorded by the video camera. Diffuse back lighting was used for the pendant drop (Fig. 4.5).

The drops were photographed at a rate of 30 frames s^{-1} . The observed shape of the droplet is compared with the calculated shape in Fig. 4.6(a).

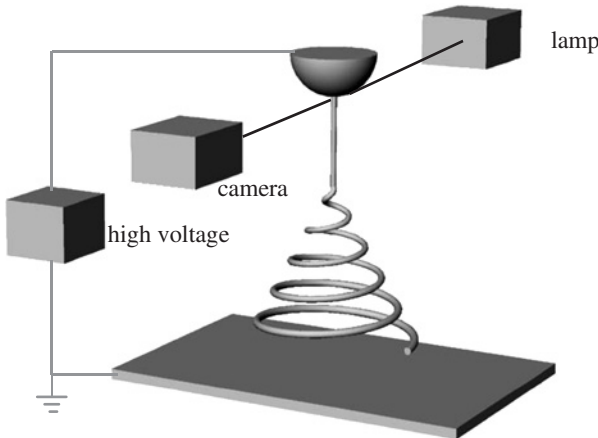


FIG. 4.5. Pendant drop experiment. After Yarin et al. (2001b) with permission from AIP.

In the pendant droplet experiment (Fig. 4.5) the polymer solution was placed in a spoon with a 1 mm hole in its bowl. The potential was applied between the drop and a flat plate. The experimental result is shown in Fig. 4.6(b).

The sessile droplet, which was attracted toward a flat electrode at a distance $H_{ge} = 13$ cm, became critical at the potential $\Phi_0 = 19.34$ kV = $64.47(\text{g cm})^{1/2}\text{s}^{-1}$. The drop had a height of $H = 0.128$ cm. When Φ_0 was slightly increased by a step of about 200 V, a jet emerged from the top of the droplet. Using these data, as well as $\xi_0 = \xi_{0*} = 0.834$ (cf. Section IV.C), and taking $\sigma = 70 \text{ g/s}^2$, the value of a_0 was found from Eq. (4.31) to be $a_0 = 0.00026$ cm. Since the value of a_0 is much smaller than H , the hyperboloidal approximation not accounting for perturbations due to the electrode, is self-consistent and satisfactory (see earlier discussion near the end of Section IV.B).

The pendant droplet became critical at the potential $\Phi_0 = 19.5$ kV = $65.6(\text{g cm})^{1/2}\text{s}^{-1}$ at $H_{ge} = 17.3$ cm (see Fig. 4.6(b)). The height of the droplet was $H = 0.30$ cm. The value of a_0 was found to be 0.00021 cm, which is also sufficiently small relative to H . The corresponding value of the potential difference between the droplet and the equipotential surface at the matching boundary is $\varphi_{0*} = 4.699(\sigma a_0)^{1/2} = 0.57(\text{g cm})^{1/2}\text{s}^{-1} = 171$ V.

The hyperboloids calculated using Eqs. (4.10) and (4.25) approach the conical asymptotes with a half angle of $\alpha_* = 33.5^\circ$, which are shown by the solid lines in Fig. 4.6. Cones with a half angle of $\alpha_T = 49.3^\circ$, which is characteristic of the Taylor cone, are shown in Fig. 4.6 by dashed lines. The half angle at the tip shown in the photographs of Figs. 4.6(a) and (b) in region C,

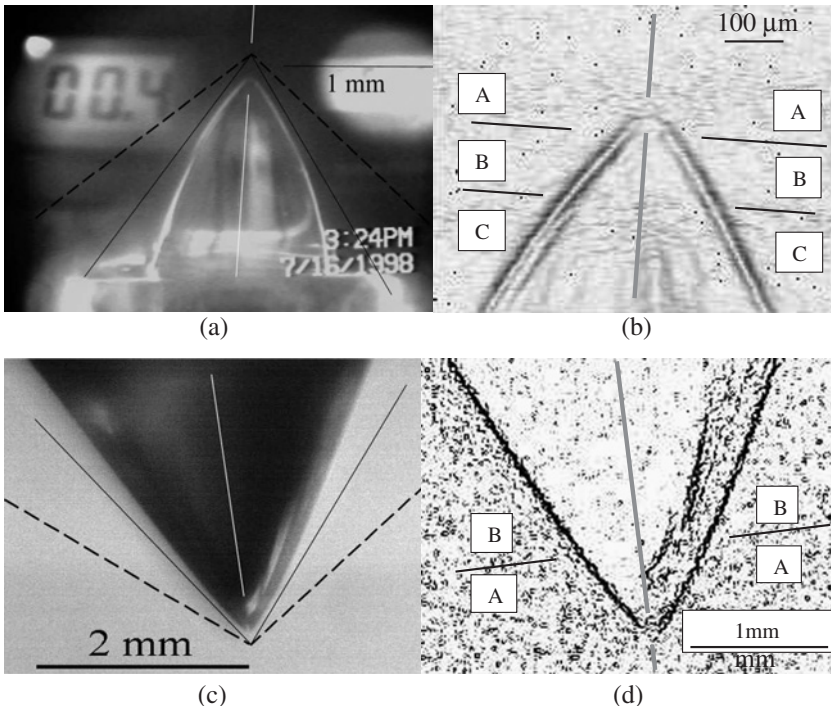


FIG. 4.6. (a) Videograph of the critical droplet shape observed for a sessile droplet. The bottom of the drop was constrained to the inner diameter of the pipette on which it sat. The drop is symmetrical about the white line. The symmetry axis is not exactly vertical due to camera tilt, the tilt of the pipette and the tilt of the electric field direction. The half angles predicted in this section are indicated by the solid lines. The half angle associated with the Taylor cone is indicated by the dashed lines. This image was not enhanced or cropped. The outlines of the pipette can be seen at the bottom, and information on the experimental parameters is visible in the background. (b) Part of the image in (a), processed with Scion image “find edges” (<http://www.scioncorp.com/>). No useful data about the location of the edge were found in region A. Lines tangent to the boundary segments in region B indicate a half angle of 37.5°. Lines tangent to the boundary segments in region C indicate a half angle of 30.5°. The lower parts of the boundary were not used because they were constrained by the pipette. (c) Critical droplet shape observed for a pendant drop. (d) Part of the image in (c). The enlarged droplet tip from (c), processed with Scion image “find edges.” Lines tangent to the boundary segments in region A indicate a half angle of 31°. Lines tangent to the boundary segments in region B indicate a half angle of 26°. After Yarin *et al.* (2001b) with permission from AIP.

where the influence of the pipette is small, is 30.5°. Even closer to the tip in region B an observed half angle is 37.5°. Both of these angles are closer to the hyperboloidal solution (33.5°) than to the Taylor solution (49.3°). Calculation predicts that the hyperboloid approaches within 5 μm of the intersection of the asymptotes, but there is not enough resolution in the images that this can be

seen. Half angles were measured as shown in [Fig. 4.6](#). For the sessile drop, the measured half angle near the tip in region B was 37.5° and in region C it was 30.5° . For the pendant drop, the measured half angle near the tip in region A was 31° and in region B was 26° . All these angles are closer to the hyperboloidal solution than to the Taylor cone.

Notice that the electrode used in the experiments was submerged in the liquid inside the pipette so the influence of the actual electrode on the shape of the droplet is minimal. The lower part of the droplet shown in [Fig. 4.6\(a\)](#) is also affected mechanically by the pipette wall, which restricts the diameter of the base of the droplet. That is the reason why the free surface deviates from the predicted solid line in [Fig. 4.6\(a\)](#) near the bottom.

According to experimental data, a stable cone can be obtained for a range of angles, but typically the half angle was close to 45° as stated in [Michelson \(1990\)](#). Both [Taylor \(1964\)](#) and [Michelson \(1990\)](#) worked with low molecular weight liquids, which are prone to perturbations and atomization. These perturbations might lead to premature jetting before a true critical shape can be achieved. This can explain the larger (and varying) values of α recorded in their experiments.

In [Harris and Basaran \(1993\)](#), critical configurations of liquid droplets affected by the electric field in a parallel capacitor were calculated numerically using the boundary element method. One of the arrangements considered, the initially hemispherical droplet supported by an electrode, is close to the experimental situation in the present work. The numerical predictions for this case (Fig. 42 in [Harris and Basaran, 1993](#)) showed that the apparent cone angle is less than or about 40° , which is closer to the critical angle $\alpha_* = 33.5^\circ$ predicted by the above theory than to $\alpha_T = 49.3^\circ$. [Wohlhuter and Basaran \(1992\)](#) using finite-element analysis calculated steady-state shapes of pendant/sessile droplets in an electric field. [Cheng and Miksis \(1989\)](#) considered steady-state shapes of droplets on a conducting plane. Their droplets, however, were considered as polarizable dielectrics (non-conductors) with no free charges embedded at the free surface. In the situation characteristic of electrospinning, the fluid behavior corresponds to that of ionic conductors. Therefore, neither the electric context in the electrospinning nor the droplet shapes can be related to those predicted in the above-mentioned works.

The numerically predicted value of the half angle of the calculated shape, which is significantly less than 49.3° , may be an indication of failure of the self-similarity assumption, similar to what was discussed in [Section IV.C](#). However, owing to inaccuracies intrinsic in numerical methods in cases in which a singularity is formed, a definite statement cannot be made.

According to Stone *et al.* (1999), in which both boundary and finite element calculations related to the present problem were characterized, “all the numerical studies either assume a rounded end and/or cannot resolve the structure in the neighborhood of a nearly pointed end”. As usual, close to singularities, insight can be gained by approximate models, for example, the slender body approximation (Sherwood, 1991; Li *et al.*, 1994; Stone *et al.*, 1999), or the hyperboloidal approximation considered above.

It is emphasized that following Taylor (1964), most of the works assume the liquid in the droplet to be a perfect conductor. In a number of works, however, cases where liquid in the drop is an insulator, were considered (Li *et al.*, 1994; Ramos and Castellanos, 1994; Stone *et al.*, 1999). Two self-similar conical solutions with half angles of $0^\circ \leq \alpha^* \leq 49.3^\circ$ exist when the ratio of the dielectric constants is in the range of $17.59 \leq \epsilon_d/\epsilon_s \leq \infty$, where ϵ_d corresponds to the droplet and ϵ_s corresponds to a surrounding fluid (the ratio $\epsilon_d/\epsilon_s = \infty$ corresponds to the fully conductive droplet). For $\epsilon_d/\epsilon_s < 17.59$ equilibrium conical solutions do not exist. Deviation of the experimental half angles to values significantly below 49.3° can, in principle, be attributed to one of the two solutions for the range of ϵ_d/ϵ_s where two solutions exist. The choice between these solutions based on the stability argument leads to the rather puzzling outcome that the Taylor cone branch is unstable, and that very small half angles should be taken in contradiction to experiments (Li *et al.*, 1994; Stone *et al.*, 1999). However, the assumption that liquids could be considered as insulators actually holds only on time scales shorter than the charge relaxation times, $\tau_H < \tau_C$. The latter are of the order of 10^{-10} – 10^{-3} s according to the estimates of Ramos and Castellanos (1994) and in Section IV.A. Since in the experiments, the residence time of a liquid in the cone τ_H is of the order of 1 s and is much longer than the charge relaxation time, conductivity effects should dominate the dielectric effects (Ramos and Castellanos, 1994). In insulating dielectric liquids, due to non-zero electric shear stress at the cone surface, flow is inevitable inside the droplet (Ramos and Castellanos 1994). In the experiments discussed above such a flow was not seen. The absence of such a flow is consistent with the fact that the behavior of the polymer solutions could be closely approximated by that of a perfectly conductive liquid, as was assumed.

It is of interest to estimate the radius of curvature r_c at the tip at the potential which corresponds to the onset of instability. From Eq. (4.19a), we have $r_c = b_0^2/2a_0$. Using Eq. (4.23) we find

$$r_c = a_0 \frac{(1 - \xi_0^2)}{2\xi_0^2}. \quad (4.41)$$

Substituting $\zeta_0 = 0.834$ and $a_0 = 0.00026$ cm, which are the values found above, we find $r_c = 5.69 \times 10^{-5}$ cm, which is near the wavelength of light and is too small to be seen in an ordinary photograph. Dimensions of polymer molecules, such as the radius of gyration in the solution, are typically around 10 nm(10^{-6} cm), and therefore can be neglected.

In a group of works related to the development of pure liquid alloy ion sources (LAIS), for example, [Driesel et al. \(1996\)](#) and references therein, several additional physical processes, which may be relevant within the context of Taylor cone formation, were revealed. The most important of them is field evaporation of metal ions from the tip of the cone leading to the emergence of ion emission currents and space charge. These phenomena are totally irrelevant in the present context for the following reasons. According to [Driesel et al. \(1996\)](#) field evaporation is impossible unless a jet-like protrusion is formed on top of the Taylor cone. The characteristic radius of curvature of the protruding tip should be of the order of 1–1.5 nm, and the corresponding field strength of the order of 1.5×10^5 kV cm $^{-1}$. These conditions could never be realized in the electrospinning experiments. In the present case, unlike in LAIS, the huge fields needed for field evaporation could not even be approached. Moreover, the apex temperatures corresponding to field evaporation and the accompanying effects are of the order of 600–1000°C. Such temperatures would produce drastic chemical changes in a polymer solution.

In the course of the present work space charge and electrical currents in the air were occasionally measured. It was shown that the occurrence of these phenomena was always a consequence of corona discharge, and could always be reduced to a very low level. All the above taken together allows us to conclude that field evaporation and ion current effects on the half-angle of the observed cones can be totally disregarded.

For low-viscosity liquids, as already mentioned, tiny droplets can easily be emitted from the cone tip. Sometimes droplet emission begins at α_* close to 45° ([Michelson, 1990](#)), sometimes close to 49° ([Fernandez de la Mora, 1992](#)). It should be emphasized that single tiny protrusions, jets and droplets of submicron size at the top of the Taylor cone are invisible in ordinary photographs. It is difficult to judge when the jet emerges (cf. Section IV.E) since the cone tip may oscillate as each droplet separates. At higher voltage, atomization of the cone tip can lead to significant space charge from the electrically charged droplets emitted. In [Fernandez de la Mora \(1992\)](#), it was shown that the backward electric effect of the charged droplets on the tip of the cone leads to reduction of its half angle to a range of $32^\circ < \alpha_* < 46^\circ$. For the highly viscoelastic liquids used in electrospinning, atomization is

virtually impossible. Breakup of tiny polymer jets, threads and filaments is always prevented by viscoelastic effects and the huge elongational viscosity associated with them (Reneker *et al.*, 2000; Stelter *et al.*, 2000; Yarin *et al.*, 2001a; Yarin, 1993). Therefore, it is highly improbable that the reduced values of the half angle α_* found in the experiments described above can be attributed to a space charge effect similar to that in Fernandez de la Mora (1992).

E. TRANSIENT SHAPES AND JET INITIATION

An early attempt (Suvorov and Litvinov, 2000) to simulate numerically dynamics of Taylor cone formation revealed the following. In one of the two cases considered, the free surface developed a protrusion, which did not approach a cone-like shape before the calculations were stopped. In the second case, a cone-like structure with a half angle of about 50.5° was achieved after the calculations were started from a very large initial perturbation. It should be mentioned that the generatrix of the initial perturbation was assumed to be given by the Gaussian function, and liquid was assumed to be at rest. These assumptions are arbitrary and non-self-consistent. Also, the assumed initial shape was far from a spherical droplet relevant within the context of polymeric fluids. Moreover, the value assumed for the electric field was chosen arbitrarily and could have exceeded the critical electric field for a stationary Taylor cone. All these made the results rather inconclusive.

The shape evolution of small droplets attached to a conducting surface and subjected to relatively strong electric fields was studied both experimentally and numerically in Reznik *et al.* (2004) in relation to the electrospinning of nanofibers. Three different scenarios of droplet shape evolution were distinguished, based on numerical solution of the Stokes equations for perfectly conducting droplets. (i) In sufficiently weak (subcritical) electric fields the droplets are stretched by the electric Maxwell stresses and acquire steady-state shapes where equilibrium is achieved by means of the surface tension. (ii) In stronger (supercritical) electrical fields the Maxwell stresses overcome the surface tension, and jetting is initiated from the droplet tip if the static (initial) contact angle of the droplet with the conducting electrode is $\theta_s < 0.8\pi$; in this case the jet base acquires a quasi-steady, nearly conical shape with vertical semi-angle $\alpha \leq 30^\circ$, which is significantly smaller than that of the Taylor cone ($\alpha_T = 49.3^\circ$). (iii) In supercritical electric fields acting on droplets with contact angle in the range $0.8\pi < \theta_s < \pi$ there is no jetting and almost the whole droplet jumps off, similar to the gravity or drop-on-demand dripping. Reznik *et al.* (2004) used

the boundary integral equations to describe the flow field corresponding to the axisymmetric creeping flow inside the conducting droplet and the electric field surrounding it. The equations were solved using the boundary element method. The parameter representing the relative importance of the electric and capillary stresses is the electric Bond number, defined as $Bo_E = \ell E_\infty^2 / \sigma$, where ℓ is the characteristic droplet size and E_∞ the applied electric field. Supercritical scenarios mentioned above correspond to Bo_E larger than a certain critical value $Bo_{E,cr}$ depending on the value of the contact angle θ_s . In the supercritical cases jetting from the droplet tip emerges. In Fig. 4.7, the predicted and measured shapes of the polycaprolactone (PCL) droplet are shown at different moments. In this case, the theory slightly underestimates the stretching rate, but the overall agreement is fairly good. The shift could be attributed to the neglect of inertia in the calculations. However, that is

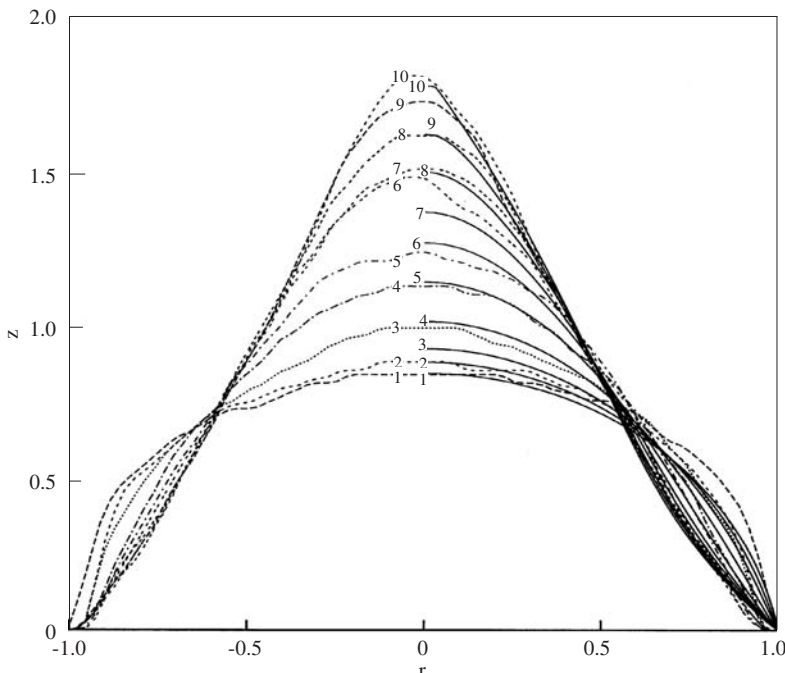


FIG. 4.7. Measured and predicted shapes of the PCL droplet at different time moments: (i) $t = 0$, (ii) 101.5, (iii) 201.5, (iv) 351.5, (v) 501.5, (vi) 601.5, (vii) 651.5, (viii) 701.5, (ix) 731.5 and (x) 756.5. Time is given in milliseconds. The calculation results are shown by solid lines for the right-hand side of the droplet only. Their numerals are located at their tip points (corresponding to $r = 0$). The experimental shapes are plotted as dotted lines. On the left-hand side the values of r are artificially made negative. After Reznik et al. (2004) with permission from Cambridge University Press.

not the case: the values of the tip velocity u_z measured in the experiments are: for curve (i) in Fig. 4.7, 0 cm s^{-1} , (ii) 0.058 cm s^{-1} , (iii) 0.110 cm s^{-1} , (iv) 0.142 cm s^{-1} , (v) 0.167 cm s^{-1} , (vi) 0.221 cm s^{-1} , (vii) 0.353 cm s^{-1} , (viii) 0.485 cm s^{-1} , (ix) 0.638 cm s^{-1} and (x) 0.941 cm s^{-1} ; the corresponding values in the calculations are quite similar. The viscosity of PCL $\mu = 212 \text{ P}$, the density $\rho \simeq 1.32 \text{ g cm}^{-3}$, and the droplet size $\ell \simeq 0.1 \text{ cm}$. Therefore, the highest value of the Reynolds number corresponding to Fig. 4.7 is $\text{Re} = 5.86 \times 10^{-4}$ which hardly gives any inertial effects. Experiments on drop evolution in a high-voltage electric field were also conducted by [Zhang and Basaran \(1996\)](#). They used low-viscosity fluid (water). The flow behavior of the droplets in their case was quite distinct from that of the highly viscous fluids used for electrospinning of nanofibers.

The predicted droplet shapes corresponding to the above-mentioned scenarios (i) and (ii) are shown in Fig. 4.8; in the present case the critical value of the electric Bond number $\text{Bo}_{E,\text{cr}}$ is about 3.04.

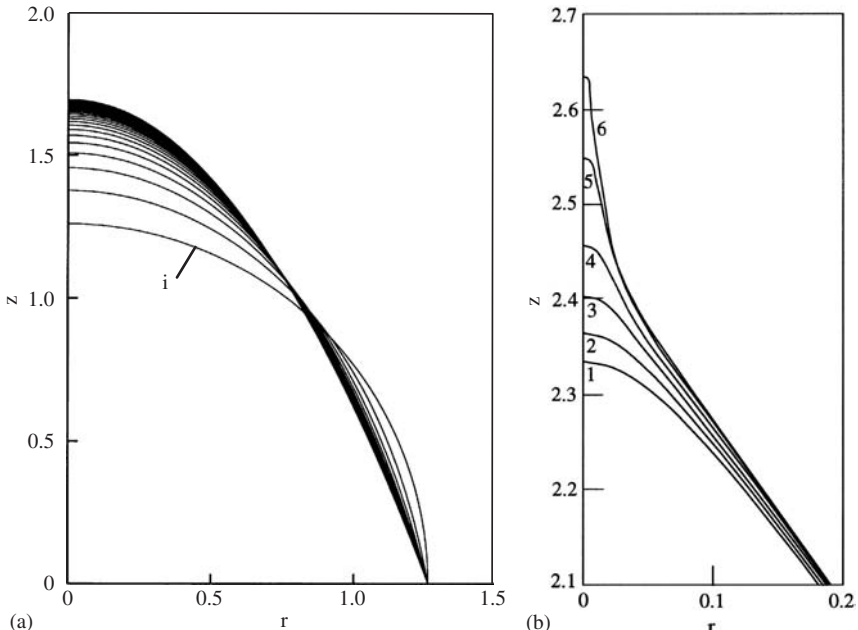


FIG. 4.8. Droplet evolution corresponding to the contact angle $\theta_s = \pi/2$; (a) $\text{Bo}_E = 3.03$: the subcritical case, curve (i) shows the initial droplet shape at $t = 0$, the subsequent curves correspond to the time intervals $\Delta t = 1$; (b) $\text{Bo}_E = 3.24$: the jetting stage emerging in the supercritical case, (i) $t = 12.001$, (ii) 12.012 , (iii) 12.022 , (iv) 12.03 , (v) 12.037 and (vi) 12.041 . Time is rendered dimensionless by $\tau_H = \mu\ell/\sigma$, where μ is viscosity. After [Reznik et al. \(2004\)](#) with permission from Cambridge University Press.

It is emphasized that the average semi-angle α of the cone below the jet base in Fig. 4.8(b) is approximately 25–30°. Reznik et al. (2004) have not been able to find an approach to the Taylor cone from the subcritical regimes in their dynamical numerical simulations. The fact that the early supercritical regimes exhibit jets protruding from the cones with $\alpha = 25\text{--}30^\circ$ favors the assumption that the critical drop configurations (which are very difficult to achieve numerically) are closer to those predicted by Yarin et al. (2001b) with semi-vertical angle of 33.5° than to $\alpha_T = 49.3^\circ$. The assumption, however, should be treated with caution, since all the examples considered correspond to slightly supercritical dynamical cases, where semi-angles α can be smaller because of the presence of the protrusion. It should be added that Taylor (1964) and Yarin et al. (2001b) considered infinite liquid bodies: a cone or a hyperboloid of revolution, respectively. Comparison of these two idealized models with the experimental or less-idealized numerical situations, where droplets are finite and attached to a nozzle or a plane surface, should be made with caution. The base parts of the droplets are mechanically affected by the nozzle wall, which restricts the diameter of the droplet (Yarin et al., 2001b). Such a restriction is, however, much less important for a droplet attached to a plane surface, as in Reznik et al. (2004). On the other hand, near the droplet tip any effect of mechanical restrictions and the electric stresses resulting from charge distribution in the areas far from the tip, should be small. That is the reason why both Taylor cones and hyperboloids could be compared with experiments and numerical calculations for finite droplets.

Notz and Basaran (1999) carried out a numerical analysis of drop formation from a tube in an electric field. The flow in the droplets was treated as an inviscid potential flow. In a subcritical electric field when no jetting is initiated such a model predicts undamped oscillations of the droplet. Obviously, such behavior, as well as that in supercritical jetting, is incompatible with the creeping flow case, characteristic of electrospinning. Experiments with levitated droplets, also corresponding to the low-viscosity limit, revealed thin jets issuing from droplet poles and totally disintegrating during 5 μs (Duft et al., 2003). This case is also incompatible with the present one, dominated by the high-viscosity characteristic of spinnable polymer solutions.

When the critical potential for static cone formation is exceeded and jetting begins, in the case of polymer solutions the jets are stable to capillary perturbations, but are subject to bending instability, which is usually observed in the electrospinning process (see Section V). On the other hand, in the case of low-viscosity liquids or removal of the charge (Fong et al., 1999), the jets are subject to capillary instability, which sometimes leads to an almost immediate disappearance of the jet (Fernandez de la Mora, 1992). Sometimes, however, in

the case of bending or capillary instability a visible, almost straight section of a jet exists, where the growing perturbations are still very small. Therefore, it is of interest to describe the jet profile corresponding to the almost straight section. As noted above, the cone angle in the transient region, where the viscous inertialess flow transforms into a jet, is $\alpha \leq 30^\circ$. Then, for a description of the flow in the transient region and in the jet it is natural to use the quasi-one-dimensional equations, which has been done in a number of works (Cherney, 1999a,b; Feng, 2002, 2003; Ganan-Calvo, 1997a,b, 1999; Hohman *et al.*, 2001a; Kirichenko *et al.*, 1986; Li *et al.*, 1994; Melcher and Warren, 1971; Stone *et al.*, 1999) with different degree of elaboration. The solution of these equations should also be matched to the flow in the drop region. Cherney (1999a,b) used the method of matched asymptotic expansions to match the jet flow with a conical semi-infinite meniscus. As a basic approximation for the droplet shape the Taylor cone of $\alpha_T = 49.3^\circ$ was chosen. This choice seems to be rather questionable in light of finding that the Taylor cone represents a self-similar solution of the Laplace equation to which non-self-similar solutions do not necessarily tend even in the case of a semi-infinite meniscus (cf. Sections IV.A–IV.D). Moreover, even in the situation considered, complete asymptotic matching has never been achieved. Figs. 2(b), 3 and 4 in Cherney (1999a) depict discontinuities in the transition region from the meniscus to the jet. Namely, the solutions for the velocity, the potential and the field strength and the free-surface configuration are all discontinuous. A similar discontinuity in the distribution of the free-surface charge density is depicted in Fig. 2 in Cherney (1999b). In that work it is mentioned that “rigorous studies of the whole transition region require significant effort and must be a subject of separate work”. The rigorous asymptotic matching is not yet available in the literature, to the best of our knowledge. Moreover, Higuera (2003) pointed out a formal inconsistency of Cherney’s (1999a,b) analysis. Approximate approaches were tested to tackle the difficulty. In particular, Ganan-Calvo (1997a,b, 1999), Hohman *et al.* (2001a) and Feng (2002, 2003) extended the quasi-one-dimensional jet equations through the whole droplet up to its attachment to the nozzle. Such an approach is quite reasonable, but only as a first approximation, since the equations are formally invalid in the droplet region, where the flow is fully two-dimensional. Also, in the electric part of the problem there is a need to take into account the image effects at the solid wall, which is not always done. When done, however (e.g. Hohman *et al.*, 2001a), it does not necessarily improve the accuracy of the results. Fortunately, Feng (2002) showed that all the electrical prehistory effects are important only in a very thin boundary layer, adjacent to the cross-section where the initial conditions are imposed (in his case at the nozzle exit). As a result, there is a temptation to apply the

quasi-one-dimensional jet equations similar to those of [Feng \(2002\)](#) but moving the jet origin to a cross-section $z_* > 0$ in the droplet (the value of z_* is of the order of the apparent height of the droplet tip). Based on this idea, [Reznik et al. \(2004\)](#) matched the flow in the jet region with that in the droplet. By this means, they predicted the current-voltage characteristic $I = I(U)$ and the volumetric flow rate Q in electrospun viscous jets, given the potential difference applied. The predicted dependence $I = I(U)$ is nonlinear due to the convective mechanism of charge redistribution superimposed on the conductive (ohmic) one. For $U = O(10\text{ kV})$ the fluid conductivity $\sigma_e = 10^{-4}\text{ S m}^{-1}$, realistic current values $I = O(10^2\text{ nA})$ were predicted.

Two-dimensional calculations of the transition zone between the droplet and the electrically pulled jet at its tip were published in [Hayati \(1992\)](#), [Higuera \(2003\)](#) and [Yan et al. \(2003\)](#).

F. SUMMARY

The hyperboloidal approximation considered in the present section permits prediction of the stationary critical shapes of droplets of inviscid, Newtonian and viscoelastic liquids. It was shown, both theoretically and experimentally, that as a liquid surface develops a critical shape, its configuration approaches the shape of a cone with a half angle of 33.5° , rather than a Taylor cone of 49.3° . The critical half angle does not depend on fluid properties, since an increase in surface tension is always accompanied by an increase in the critical electric field.

V. BENDING INSTABILITY OF ELECTRICALLY CHARGED LIQUID JETS OF POLYMER SOLUTIONS IN ELECTROSPINNING

In the present section, the physical mechanism of the electrospinning process is explained and described following [Reneker et al. \(2000\)](#) and [Yarin et al. \(2001a\)](#). It is shown that the longitudinal stress caused by the external electric field acting on the charge carried by the jet stabilizes the straight jet for some distance. Then a lateral perturbation grows in response to the repulsive forces between adjacent elements of charge carried by the jet. This is the key physical element of the electrospinning process responsible for enormously strong stretching and formation of nanofibers. A localized approximation is developed to calculate the bending electric force acting on an electrified polymer jet. Using this force, a far-reaching analogy between the electrically

driven bending instability and the aerodynamically driven instability was established. Continuous, quasi-one-dimensional, partial differential equations are derived and used to predict the growth rate of small electrically driven bending perturbations of a liquid column. A discretized form of these equations, that accounts for solvent evaporation and polymer solidification, is used to calculate the jet paths during the course of non-linear bending instability leading to formation of large loops and resulting in nanofibers. The results of the calculations are compared to the experimental data. The mathematical model provides a reasonable representation of the experimental data, particularly of the jet paths determined from high-speed videographic observations in set-ups with single and multiple jets.

In Section V.A, the experimental electrospinning single-jet set-up is described. The experimental observations are presented in Section V.B. In Section V.C, a model of the rectilinear part of the electrified jet is presented. The basic physics of bending instability in electrospinning is explained in Section V.D. Localized approximation for calculation of electrostatic repulsive forces in bending instability is introduced in Section V.E. Using it, the continuous quasi-one-dimensional equations of the dynamics of electrified jets are introduced in Section V.F, and the corresponding discretized equations – in Section V.G. Solvent evaporation and jet solidification are incorporated in the model in Section V.H. Growth rate and wavelength of small bending perturbations of an electrified liquid column are discussed in Section V.I. Non-linear dynamics of bending and looping in single-jet electrospinning predicted theoretically is discussed and compared to the experimental data in Section V.J. Section V.K treats the experimental and theoretical aspects of multiple-jet electrospinning intended to increase production rate. Conclusions are drawn in Section V.L.

The international system of units (Système International (SI)) is used to report the values of experimental measurements. Gaussian units that are customary in fluid mechanics and electrostatics have also been used, as well as dimensionless combinations of parameters to provide concise coverage of the multi-dimensional parameter space. The numerical results from the calculations were converted to SI units for comparison with the experimental observations. Table 5.1 of symbols and Table 5.2 of dimensionless groups of parameters are provided.

A. EXPERIMENTAL SET-UP FOR ELECTROSPINNING

Fig. 5.1 is a sketch of the experimental apparatus. In this section, words such as up, down, top and bottom, are used to simplify the description of the

Table 5.1. Symbols employed and their definitions.

Symbol	Definition	Unit (CGS)
a	Cross-sectional radius	cm
a_0	Initial cross-sectional radius	cm
e	Charge	$(\text{g}^{1/2}\text{cm}^{3/2})/\text{s}$
f_a	Air friction force per unit length	g/s^2
f_g	Gravity force per unit length	g/s^2
G	Elastic modulus	$\text{g}/(\text{cm s}^2)$
h	Distance from pendant drop to grounded collector	cm
L_{el}	Length scale, $L_{\text{el}} = (e^2/\pi a_0^2 G)^{1/2}$	cm
L_z	Length of the straight segment	cm
ℓ	Length of the ideal rectilinear jet	cm
m	Mass	g
t	Time	s
v	Velocity	cm/s
U_0	Voltage	$\text{g}^{1/2}\text{cm}^{1/2}/\text{s}$
W	Absolute value of velocity	cm/s
ζ	Initial segment length	cm
λ	Perturbation wavelength	cm
μ	Viscosity	$\text{g}/(\text{cm s})$
ν	Kinematic viscosity	cm^2/s
σ	Surface tension	g/s^2
σ_{ij}	Stress	$\text{g}/(\text{cm s}^2)$
ρ	Density	g/cm^3
ρ_a	Air density	g/cm^3
θ	Relaxation time ($= \mu/G$)	s
ω	Frequency of the perturbation	s^{-1}

experimental arrangements and the observations. The jet flowed downward from the surface of a pendant drop of fluid towards a collector at the distance h below the droplet. An electrical potential difference, which was around 20 kV, was established between the surface of the liquid drop and the collector. The distance, h , was around 0.2 m. The nanofibers formed a mat on the collector. The coordinates used in the mathematical description are also shown. A magnified segment of the jet near the top of the envelope cone shows the electrical forces that cause the growth of the bending instability. These forces are described in detail in Section V.D and Fig. 5.27.

In general, the pendant drop may be replaced by other fluid surfaces such as films on a solid or shapes generated by surface tension and flow. The collector is usually a good electric conductor. The charged nanofibers may be collected on an insulator, although a way to neutralize the charge carried by nanofibers must be provided in order to collect many layers of nanofibers. Airborne ions from a corona discharge provide an effective

Table 5.2. Dimensionless groups and parameters employed and their definitions.

Symbol	Dimensionless group	Dimensionless parameter	Definition
A	Surface tension		$(\sigma\pi a_0^2\mu^2)/(mL_{\text{el}}^2G^2)$
H	Distance from pendant drop to grounded collector		h/L_{el}
K_s	Perturbation frequency		$\omega\mu/G$
Q	Charge		$(e^2\mu^2)/(L_{\text{el}}^3mG^2)$
V	Voltage		$(eU_0\mu^2)/(hL_{\text{el}}mG^2)$
F_{ve}	Elastic modulus		$(\pi a_0^2\mu^2)/(mL_{\text{el}}G)$
\bar{t}	Time		$t/(\mu/G)$
\bar{W}	Absolute value of velocity		$W/(L_{\text{el}}G/\mu)$
$\bar{\ell}$	Length of the rectilinear part of the jet		ℓ/L_{el}
\bar{v}	Velocity		$v/(L_{\text{el}}G/\mu)$
$\bar{\sigma}_{ij}$	Stress		σ_{ij}/G

way to neutralize the charge on the jets and on the nanofibers. Nanofibers may also be collected on the surface of a liquid.

Experiments on electrospinning (Reneker and Chun, 1996; Reneker et al., 2000) typically use set-ups similar to that sketched in Fig. 5.1. All experiments were performed at room temperature, which was about 20°C. PEO with a molecular weight of 400,000, at a weight concentration of 6%, was dissolved in a mixture of around 60% water and 40% ethanol. Fresh solutions produced jets that traveled further before the first bending instability appears. The solution was held in a glass pipette with an internal diameter of about 1 mm. At the beginning of the experiment, a pendant droplet of polymer solution was supported at the tip of the capillary. The liquid jet formed on the surface of the pendant drop of solution.

When the electrical potential difference (measured in volts, and often referred to as the applied voltage) between the capillary and the grounded collector is increased, the surface of the liquid becomes charged by the electrical field-induced migration of ions through the liquid. Instability of the droplet set in when the potential difference was high enough that electrical forces overcame the forces associated with surface tension (cf.

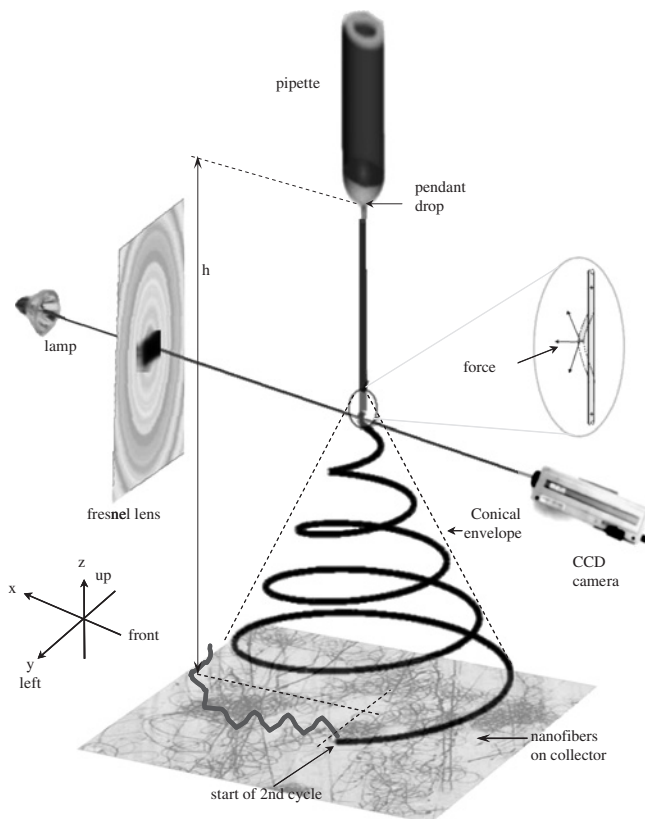


FIG. 5.1. Schematic drawing of the electrospinning process, showing the jet path, reference axes, relative arrangement of parts of the apparatus at different scales and the region where the bending instability grew rapidly. After Reneker et al. (2000) with permission from AIP.

Section IV). Above this threshold, a stable liquid jet emerged. The jet carried away excess ions that migrated to the surface when the potential was applied. A higher potential difference created a higher charge on the jet. For low-conductivity solutions, a significant time may be required for the charge to reach a saturation value after the applied potential changes, since charge transport within the fluid is limited by the finite mobility of the ions.

A region about 5 mm across near the vertex of the envelope cone was imaged with a lens that had a focal length of 86 mm and an *f* number of 1.0. The lens was placed about 20 cm from the jet to avoid disturbing the electrical field near the jet. The image produced by this lens was observed using a 12.5–75 mm, *f* 1.8 zoom lens on an electronic camera that recorded

up to 2000 frames s^{-1} with exposure times as short as 0.0125 ms, although the exposure times used in this work were longer.

The light source was a 50 W halogen lamp with a faceted parabolic reflector. A Fresnel condenser lens was used to project an image of the halogen lamp and its reflector onto the region occupied by the cone. The Fresnel lens had a focal length of 19 cm and a diameter of 30 cm. The central 15 cm diameter part of the Fresnel lens was covered so that the camera received the light scattered from the jet superimposed upon the dark background produced by the covered part of the Fresnel lens.

Images for stereographic viewing were obtained by removing the 86 mm lens, which reduced the magnification so that a region about 1 cm wide is shown in each image in Fig. 5.2. A pair of wedge prisms that were 40 mm high and 55 mm wide were placed about 20 cm in front of the jet. Each prism deflected the light beam that passed through it by 5° . The zoom lens on the electronic camera, viewing the jet through the two prisms, produced side-by-side images of the jet from two directions that were 10° apart on each frame that was recorded. These paired images were viewed stereoscopically during playback to produce a slowed down, three-dimensional image of the moving jet. Image processing and analysis were done with Adobe Photoshop, Corel Photopaint and the software supplied with the electronic camera.

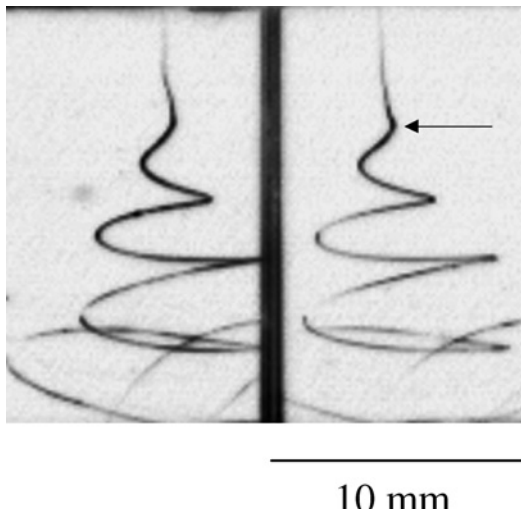


FIG. 5.2. Stereographic images of an electrically driven bending instability. The exposure time was 0.25 ms. The arrow marks a maximum lateral excursion of a loop. After Reneker *et al.* (2000) with permission from AIP

B. EXPERIMENTAL OBSERVATIONS

1. Jet Paths

The electrospinning jets typically have an almost straight section of the order of several centimeters followed by a number of bending loops as depicted in [Fig. 5.1](#). The straight section will be discussed in more detail in Section V.B.4. In the present section and in Sections V.B.2 and 3, we discuss the bending part of the jet. The region near the vertex of the envelope cone was imaged at $2000 \text{ frames s}^{-1}$. These images showed the time evolution of the shape of the jet clearly and in detail. Stereographic images such as those in [Fig. 5.2](#) showed the shape in three dimensions. The expanding spiral in [Fig. 5.2](#) is a simple example of the kinds of paths that were observed. After a short sequence of unstable bending back and forth, with growing amplitude, the jet followed a bending, winding, spiraling and looping path in three dimensions. The jet in each loop grew longer and thinner as the loop diameter and circumference increased. Some jets, which are shown in [Figs. 5.3–5.5](#), drifted downward at a velocity much slower than the downward velocity of the smaller loops close to the vertex of the envelope cone. After some time, segments of a loop suddenly developed a new bending instability,

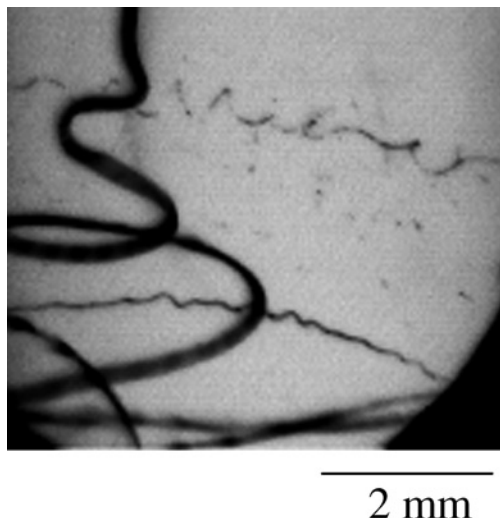


FIG. 5.3. Image of the end of the straight segment of the jet. The exposure time was 0.25 ms. After [Reneker et al. \(2000\)](#) with permission from AIP.

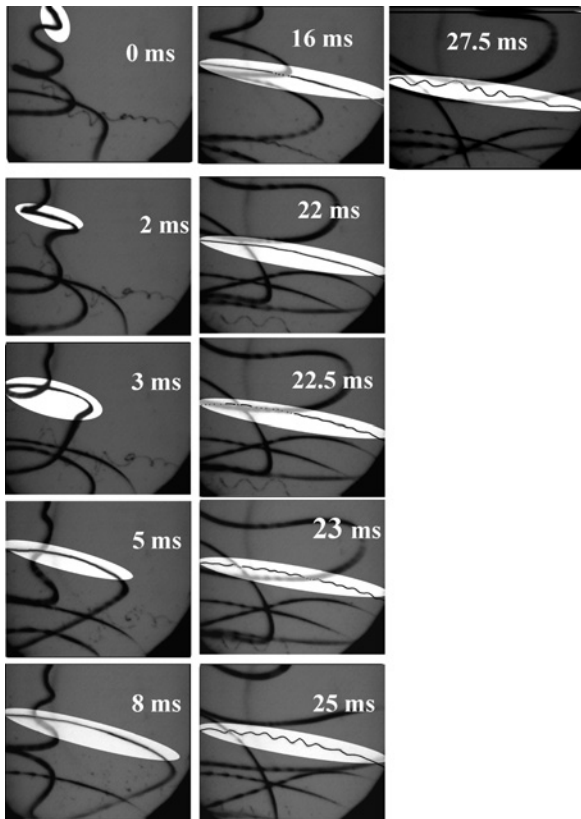


FIG. 5.4. Evolution of electrical bending instability. The exposure times were 0.25 ms. The width of each image was 5 mm. After Reneker *et al.* (2000) with permission from AIP.

similar to, but at a smaller scale than the first. Each cycle of bending instability can be described in three steps.

Step (1) A smooth segment that was straight or slightly curved suddenly developed an array of bends.

Step (2) The segment of the jet in each bend elongated and the array of bends became a series of spiraling loops with growing diameters.

Step (3) As the perimeter of the loops increased, the cross-sectional diameter of the jet forming the loop grew smaller. The conditions for step (1) were established on a smaller scale, and the next cycle of bending instability began.

This cycle of instability was observed to repeat at an even smaller scale. It was inferred that more cycles occur, reducing the jet diameter even more and creating nanofibers. After the second cycle, the axis of a particular segment

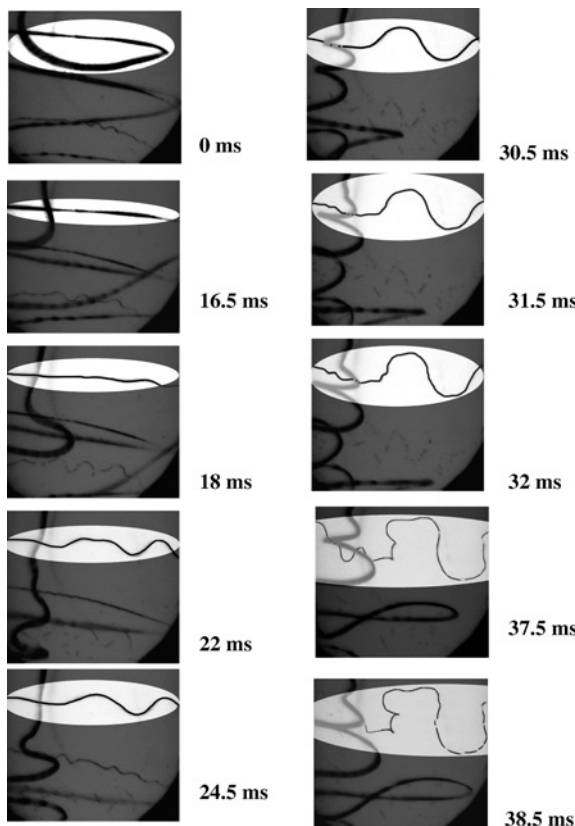


FIG. 5.5. Images of secondary and tertiary cycles of bending instabilities. The exposure time was 0.25 ms. The width of each image is 5 mm. After Reneker et al. (2000) with permission from AIP.

may point in any direction. The fluid jet solidified as it dried and electrospun nanofibers were collected at some distance below the envelope cone.

The vector sum of forces from the externally applied field, the charge momentarily held in space by the jet and air drag caused the charged segments to drift towards the collector. Except for the creation of the pendant droplet, the electrospinning process discussed in this section depends only slightly on the gravity force.

Fig. 5.3 shows the jet entering the upper-left corner, near the end of the straight segment of a jet, and the vertex of the envelope cone, where the first bending instability grew. Several segments of the jet are shown, including segments from slow moving loops that formed earlier. All these segments are connected by segments that are not shown. Two smooth segments cross each

other in this image as they run nearly horizontally across the bottom of the image. These two segments are noticeably thinner than the jet entering the image because the jet elongated as time evolved. These slow moving segments were a part of large loops and were affected both by air drag and by the disturbance of the applied electrical field caused by the presence of both charged segments of the jet and charged nanofibers below the region being observed. Such slow moving segments remained in view for many frames.

Two thinner segments that formed even earlier are also included in [Fig. 5.3](#). One runs across the top half of the image, and the other runs across the bottom half. In the lower of these segments, the successive bends (step (1) of the second cycle) were apparent. In the upper segments, the bends had already developed into spiraling loops (step (2) of the second cycle). The pattern of dots visible in the lower left corners of [Figs. 5.3–5.5](#) was caused by the pattern of facets of the reflector of the halogen lamp used to illuminate this experiment. These dots are not evidence of the familiar varicose instability that may cause a liquid jet to become a series of droplets ([Yarin, 1993](#)). No varicose instability was observed in this experiment.

Using a set of image files created by the electronic camera it was often possible to follow the evolution of the shape of spiraling segments, such as those shown in [Fig. 5.3](#), back to the straight segment that entered the upper-left-hand corner of the image. In [Figs. 5.4 and 5.5](#), the light ellipse in the first image marks a segment that evolved in an interesting way. The selected segment of the jet was followed forward in time, from the moment it entered the region contained in the images until it elongated, looped, became unstable, bend, entered the next cycle and ultimately became too thin to form an image.

[Fig. 5.4](#) starts with a bend near the end of the straight segment of a jet entering the image at the upper left. The onset of the electrically driven bending instability occurred just before the jet entered the image. The straight segment of the jet extended upward, and is not shown. The segment of the jet that is highlighted by the white ellipse was followed for 27.5 ms in a series of images that were recorded at 0.5 ms intervals. The thinner segments of the jet were emphasized by using the Photopaint 6 software to reproduce them. Places where the faint image of the jet was ambiguous are indicated by dots, seen, for example, in the image at 22.5 ms.

Eleven images were selected from this series of 55 images to show the evolution of the highlighted segment. The time intervals between the images that are shown vary. Many images that show only a gradual evolution of the path were omitted to simplify [Fig. 5.4](#). The time at which the first image was

captured is taken as time zero. The elapsed time at which each of the following images was recorded is given in [Fig. 5.4](#).

The looping segment being observed at zero time elongated for 10 ms in [Fig. 5.4](#). Its further elongation was not followed, because the loop had extended entirely across the image. The rate of increase in the length of the highlighted segment was around 120 mm s^{-1} . After 22 ms the visible part of the highlighted segment still appeared in [Fig. 5.4](#) as a smooth, slightly curved line. In the short time interval between 22.0 and 22.5 ms, this long, slightly curved smooth segment suddenly became unstable. A linear array of bends appeared, marking the beginning of the second cycle. The lateral amplitude of the bends grew to about 1 mm, and the spatial period of the bends along the segment was also about 1 mm.

These smaller bent segments of the jet continued to elongate, but the images of the trajectories grew fainter and soon were ambiguous. The elongation and the associated thinning presumably continued as long as the charge on the jet supplied enough force. Meanwhile, the elongational viscosity increased as the jet stretched and dried. Eventually the jet solidified and the elongation stopped.

The first image in [Fig. 5.5](#) shows a selected segment that was tracked back to the highlighted area near the bottom of the straight segment. This loop grew in diameter as the jet elongated and became thinner. After 18 ms, an array of bends that had a relatively long wavelength developed. These bends evolved gradually to the path shown at 30.5 ms. Then a tertiary array of bends developed on the highlighted segment during the next 0.5 ms, and quickly evolved to the path shown at 31.5 ms. The growth of the tertiary excursions was followed until 38.5 ms after the first image, at which point the jet was so thin that its image could no longer be followed.

2. Jet Splaying/Branching and Garlands

The circled region in [Fig. 5.6](#) shows a jet that split into two jets that splayed apart, with the axis of the thinner branch generally perpendicular to the axis of the primary jet (Reneker et al., 2000); cf. with several similar photographs in Shkadov and Shutov (2001). The thinner jet disappeared in a few milliseconds, in some cases because it rapidly became even thinner, and in other cases because its path left the field of view. No bending instability was observed on the thinner segment, probably because it was not observed long enough for an instability to develop. Only a few such events were observed in the thousands of images of PEO solution examined.

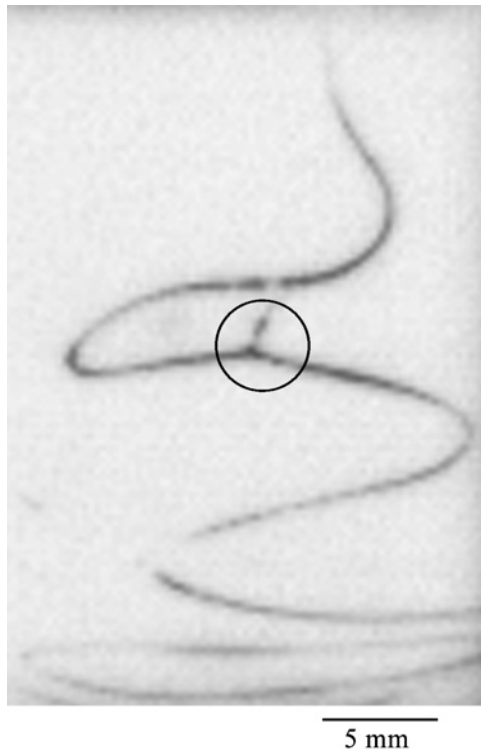


FIG. 5.6. A jet splits off the primary jet and splay to a different direction. After Reneker *et al.* (2000) with permission from AIP.

Before the high frame rate, short exposure time images of Figs. 5.4 and 5.5 were available, visual observations and video images of electrically driven PEO solution jets were interpreted as evidence of a process that splayed the primary jet into many smaller jets. The smaller jets were supposed to emerge from the region just below the apex of the envelope cone. Fig. 5.7(a) shows an image from a video frame with an exposure of 16.7 ms. The envelope cone was illuminated with a single bright halogen lamp that projected a narrow beam through the envelope cone, towards, but not directly into, the lens, so that most of the light that entered the video camera was scattered from the jets.

Fig. 5.7(b) shows a jet similar to that shown in Fig. 5.7(a) that was illuminated with light from two halogen lamps and photographed with a video camera. The two lamps were above and behind the jet. One was to the left and the other to the right. This provided a broader source of illumination than that used for Fig. 5.7(a), but not as uniform as the

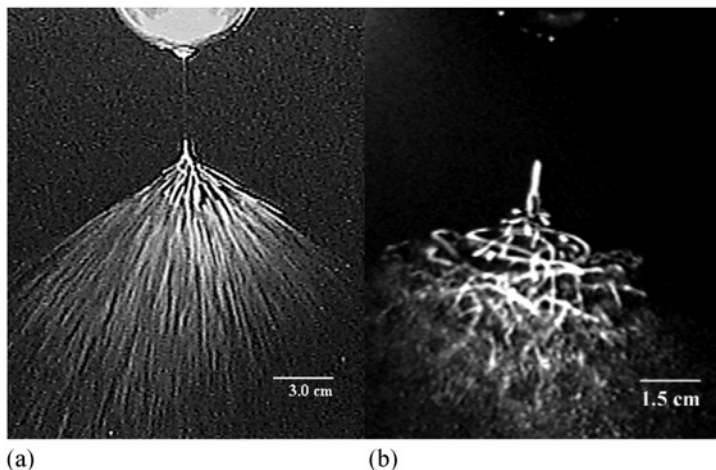


FIG. 5.7. Images of electrospinning jet with longer camera exposure times: (a) 16.7 ms and (b) 1.0 ms. After [Reneker et al. \(2000\)](#) with permission from AIP.

Fresnel lens arrangement shown in [Fig. 5.1](#). An exposure time of 1 ms was used. The part of the straight jet with small bending amplitude is visible as are the loops containing segments, which had turned so that the axis of the segment formed a high angle with the axis of the straight segment. The parts of the jet nearer the vertex of the envelope cone appeared only as short, unconnected lines. Spectacular reflections of the beam of light, called glints, from one or the other of the two halogen lamps off nearly horizontal segments of downward moving loops, were shown to be the cause of these bright spots. Similar bright spots moved downward during longer exposure, and created the lines that are prominent in [Fig. 5.7\(a\)](#).

The video frame rate of 30 frames s^{-1} was not fast enough to follow the smooth development of the jet path. At this frame rate, for any particular frame, the preceding and the following frames showed loops and spirals in completely different positions. Only after the illumination was improved, described in [Section V.A](#), and the high frame rate electronic camera used, was obvious that the envelope cone was occupied by one long, flowing, continuous and ever thinner PEO solution jet. The repeated cycles of ever smaller electrically driven bending instabilities created a complex path in which the directions of the axes of the connected segments were often different and changing, sometimes by large angles.

Being a dominating phenomenon, bending instability, under certain conditions, is accompanied by a sequence of secondary jet branches emanating from the primary jet. [Yarin et al. \(2005\)](#) described an experiment

in which many closely spaced branches along the jet were observed during the electrospinning of a PCL solution. The apparatus was similar to the one described above. PCL, chemical formula $[O(CH_2)_5CO]_n$, with a molecular weight of 120,000 g mol⁻¹ was dissolved in acetone at concentrations near 15%. The observations were not sensitive to small variations in concentration. Polymer solutions were electrospun from a drop hanging from a glass pipette with a tip opening in the range from 300 to 400 μ m. Dried polymer at the tip sometimes formed a short, tube-like extension of the pipette, which affected the size and shape of the droplet, but branches were still observed. Branching jets, of 15 wt% PCL solutions, were produced when the electrical potential difference between the tip and collector was in the range from 3 to 15 kV and the distance between the spinneret and ground was in the range from 15 to 70 mm (cf. Figs. 5.8 and 5.9). No stable jets were produced at 2 kV, even after a jet was started by touching the drop with an insulating rod and pulling out a charged fluid segment. The electric field strengths for these experiments ranged from 57 to 500 V mm⁻¹. Adjacent branches can lower their electrostatic interaction energy by extending in different azimuthal directions. Interactions between branches and the charges on nearby loops of the primary jet may also affect the direction of a branch. The jet and the branches are tapered. Bending and branching may occur together. The stereographic image of the azimuthal directions of the branches provided reliable information about the location and direction of the branches in three-dimensional space. All the measurements of the distance between branches, however, were determined from two-dimensional images, since the collection of the stereographic information is laborious and produces only moderate improvement in the accuracy of the measurements of this distance. For several typical jets, the distance between two adjacent branches was measured as a function of time, starting at the frame in which the two branches were first observed and continuing until one of the branches passed out of the field of view. The increase in the distance between adjacent branches was rapid at first and became much slower after the distance had doubled.

The branches did not occur continuously. As time progressed, the flow shown in Fig. 5.8 showed the following sequence of three types of events: (1) a straight segment, (2) the onset of the bending instability which usually generated a garland discussed below in more detail, and (3) a nearly straight and relatively long segment from which the branches appeared and grew rapidly that extended more than half way across the field of view of the segment where the branches grew. Branches grew rapidly after small branches appeared. This sequence of three events repeated about 10 times

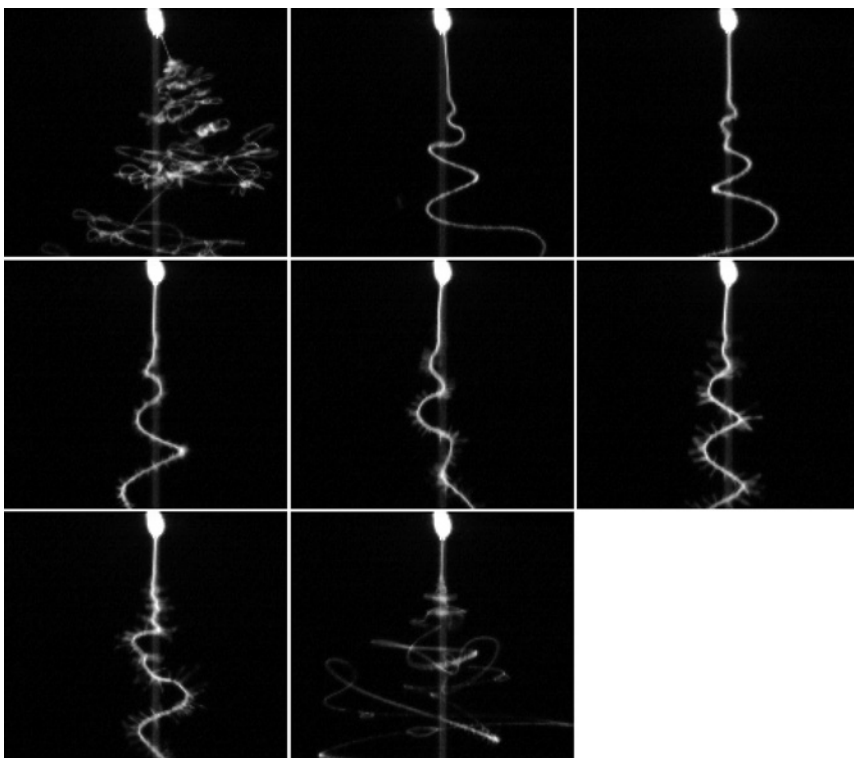


FIG. 5.8. Lateral jets from PCL solution. These “stopped motion” images of a jet were taken by a high-speed camera at a frame rate of 2000 frame s^{-1} . Every 24th frame is shown here, so the time separation between the frames shown was about 12 ms. The 15% PCL solution was electrospun at 5 kV, and gap distance from pipette to copper plate collector was 70 mm. The width of each frame is about 14 mm. The exposure time of each frame was 0.1 ms. Branches are usually initiated in the straight segment and continue to elongate while the primary jet undergoes the electrically driven bending instability. The vertical gray line is due to light from the drop scattered by the camera. This line is not part of the jet. Stereographic images show that every segment of the primary jet including those segments where a branch is present moved radially outward and downward as the segment elongated. After Yarin et al. (2005) with permission from AIP.

per second. The reasons for this repeating sequence are not presently known. Many such branching events were photographed. Branches were observed when the dried nanofibers were observed microscopically, but the tangled paths of the collected nanofibers made it impractical to measure the relatively long distance between the branches. For a particular branching event, a frame that showed a number of branches was selected. The spacings between adjacent branches were determined. Two significant figures were kept, which are consistent with the precision of the measurement. This

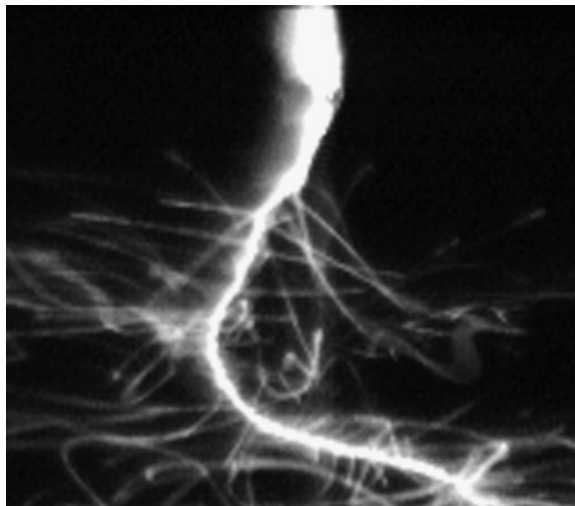


FIG. 5.9. A thick jet with many closely spaced branches and a high-taper rate is shown. The still images of PCL solution were taken by a high-speed camera at a frame rate of 2000 frame s^{-1} . Bending and branching began after only a short distance from the tip. The 15% PCL solution was electrospun with 10 kV, and the gap distance from pipette to the copper plate collector was 70 mm. The width of this frame is about 12 mm. The exposure time was 0.1 ms. After [Yarin *et al.* \(2005\)](#) with permission from AIP.

measurement was repeated for each of the five to ten events that occurred within about 1 s. At each electrical field, the observed spacing between adjacent branches was calculated for each sequential pair of branches. Branching can be profuse, with many long, closely spaced and rapidly growing branches. Jets with larger diameters corresponding to higher voltage values tend to have more branches. The bending instability and the occurrence of branching coexist with only minor interactions, even when both instabilities are fully developed as in Fig. 5.9.

Reneker *et al.* (2002) reported that electrospinning of a PCL solution in acetone caused the dramatic appearance of a fluffy, columnar network of fibers that moved slowly in large loops and long curves. The name “garland” was given to the columnar network. Open loops of the single jet came into contact just after the onset of the bending instability and then merged into a cross-linked network that created and maintained the garland. Side branches can also contribute to the garland formation. Contacts between loops occurred when the plane of some of the leading loops of the jet rotated around a radius of the loop. Then a small following loop, expanding in a different plane, intersected a leading loop that was as many as several turns ahead. Mechanical forces overcame the repulsive forces

from the charge carried by the jet, the open loops in flight made contact and merged at the contact point, to form closed loops. The merged contacts were established when the momentum of the segments and the tension in the jet forced a fluid segment to contact another segment, in spite of the repulsive Coulomb forces. Upon contact, surface tension immediately tended to hold the jets together, while the charge tended to flow away from the point of contact. Since the electric charge moved almost with the motion of liquid, the large elongation of the jet segments led to a dramatic decrease in the charge per unit length of the jet. Segments separated by relatively large distances along the path of the jet contacted each other during the complicated motions associated with the bending and branching. The two liquid sections in contact merged, due to the effect of surface tension, if the reduction of the surface energy due to merging was greater than the local increase of the energy of the electric field.

Jets carrying higher charge (PEO) do not create garlands, while PCL jets carrying lower charge (Theron et al., 2003, 2004) result in garlands under certain conditions. The closed loops constrained the motion to form a fluffy network that stretched and became a long roughly cylindrical column a few millimeters in diameter. This garland, which was electrically charged, developed a path of large open loops that are characteristic of a large-scale electrically driven bending instability (Fig. 5.10). Over a long period of time, the fluffy

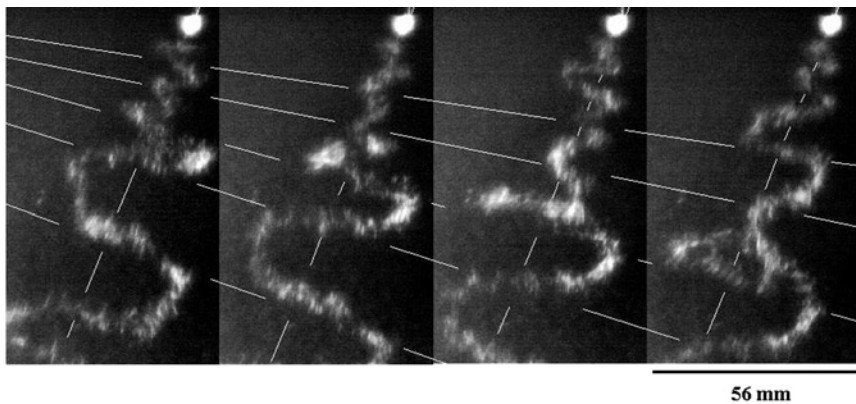


FIG. 5.10. Motion of a curly garland from a 15% PCL solution is shown. The white lines demarcate segments of a garland that advanced downward. The slope of the top line corresponds to 0.58 ms^{-1} , and the slope of the lower lines, successively, to 0.7 , 1.05 , 1.36 and 2.04 ms^{-1} . Since only every fifth frame is shown, the time separation between the frames shown was about 20 ms . (7.5 kV , 140 mm gap, $250 \text{ frames s}^{-1}$, 2 ms exposure time). After Reneker et al. (2002) with permission from Elsevier.

garland never traveled outside a conical envelope similar to, but larger than the conical envelope associated with the bending instability of a single jet.

3. Coiled and Looped Jets Captured on a Hard Surface

Nanofibers electrospun from PEO solutions were sometimes collected by moving a glass microscope slide, a metal screen, or other solid surfaces through the conical envelope. Fig. 5.11 shows that coiled and looped nanofibers collected in this way were similar in shape to the bending instabilities photographed with the high-speed camera. The abundance and single coil of the coiled loops depended on the distance below the vertex at which they were collected.

The well-known tendency of a straight liquid jet moving in its axial direction to coil when it impacts a hard, stationary surface and buckles (Yarin, 1993) could account for some of the observed coils. This mechanical effect is easily observed when a gravity-driven jet of honey falls onto a hard surface. The occurrence of mechanical buckling during impact is likely to be infrequent because most of the long segments of the jet were moving in a sidewise direction as they encountered the collector. It is interesting to hypothesize that in these experiments the coils and loops solidified before collection. Then, the collected coils and loops provide information about the smallest bending instabilities that occurred.

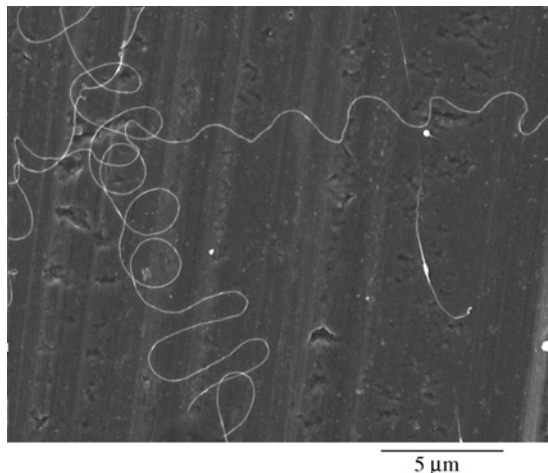


FIG. 5.11. Scanning electron micrograph of coiled and looped nanofibers on the surface of an aluminum collector. After Reneker et al. (2000) with permission from AIP.

Cross-sections of the as-spun nanofibers are typically roughly circular. However, non-circular cross-sectional shapes (presumably due to collapse of the polymer matrix during solvent evaporation) were also revealed by the morphological analysis shown by Koombhongse et al. (2001). The collapse may be so strong that electrospun ribbons appear.

4. Diameter of the Straight Part of the Jet

Xu et al. (2003) developed optical methods for measuring the diameter of a jet. Diffraction of laser beam is a convenient method for observing the diameter of the straight segment as a function of position. The tapered shape of a typical jet is shown in the plot of jet diameter versus distance in Fig. 5.12. A person can easily monitor the changes in diameter of an electrospinning jet by observing the position along the path of a distinctive

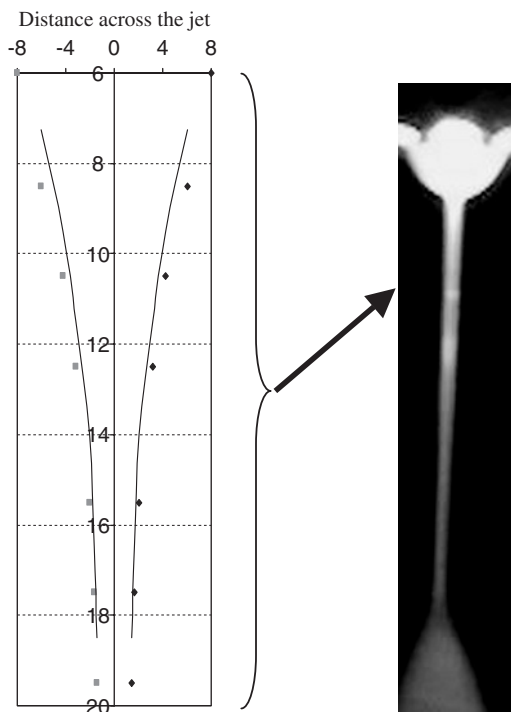


FIG. 5.12. Diameter of the straight segment of a jet as a function of position along the jet. The graph shows the results of a series of measurements of the diffraction of a laser beam. The photograph shows the corresponding range of interference colors (Xu, 2003). (see Color plate section).

color band. With proper illumination, the distinctive colors can be observed inside the envelope cone, which is caused by the bending instability.

The length along the path, of a distinctive color band, provides a visual indication of the taper rate of the jet. A higher taper rate produces a narrow color band (see Section V.B.6).

Xu *et al.* (2003) also showed that when a jet is illuminated with a beam of white light, the interference colors are produced by the jet a few degrees from the direction of the incident beam. The pastel interference colors are similar to those seen in a soap bubble, see the photograph in Fig. 5.12. Some of the colors are quite distinctive. For a given spectral distribution of the white light, and a set measuring direction along a tapered jet, the observation of a distinctive color reveals the region along the jet at which it has diameter associated with that color. As the diameter of the segment varies, the position of the distinctive color moves along the jet.

5. Particle Tracing Technique in Electrospinning: Jet Velocity

Xu *et al.* (2003) applied a particle tracing technique to characterize the electrospinning jet velocity. Tracer particles were incorporated into the polymer solution for electrospinning and the particle speeds were measured by observing the particle movement during electrospinning, using high-speed photography.

Glass beads purchased from Sigma Chemical Company were washed with Alconox Precision Cleaning Detergent to remove any grease left on the surface of the beads during manufacturing or handling. The washed beads were mixed with the 6% PEO/water solution. The solution was then sonicated for three hours in order to disperse the glass beads. The mixture of glass beads and PEO solution was loaded into a glass pipette and electrospun immediately after the sonication. Glass beads were carried by the fluid flow during electrospinning. The largest beads were 106 μm in diameter. The video images show that the size of the beads was close to the diameter of the electrospinning jet at its origin. A camera running at 2000 frames s^{-1} was used to follow the movement of the glass beads during the electrospinning. A Fresnel lens focused the light from a xenon arc source onto the electrospinning jet to produce illumination for high-speed photography. The center of the Fresnel lens was blocked to provide a dark background in the camera's field of view. Owing to the spherical lens effect, glass beads in the jet were much brighter than the surrounding fluid. The movement of the beads could be easily identified.

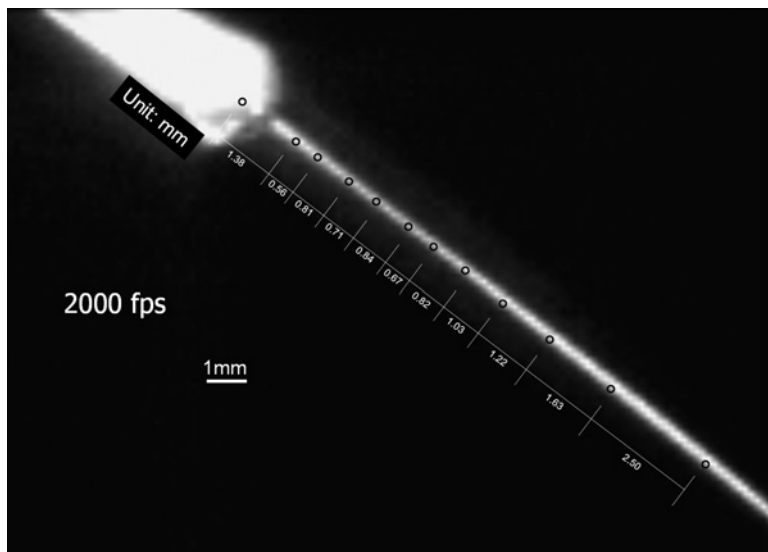


FIG. 5.13. Successive positions of a glass particle in a jet. After Xu et al. (2003).

The glass pipette was set in a plane perpendicular to the camera axis. The video images were calibrated by photographing graph paper set in the same plane as the pipette. Fig. 5.13 shows the successive bead positions in 12 video frames during electrospinning. The position of the particle in each frame was marked by circle. The particle speed was calculated by dividing the distance between circles by the time elapsed between neighbor frames. Fluid velocity as a function of position along the jet axis was measured.

The speed of the beads was measured. Video showed that glass beads carried by the fluid flow came out of the pipette one by one. Gravity was negligible compared with electric force applied during electrospinning. The jet velocities were assumed to be equal to the velocities of the beads.

The jet velocities versus time in different electric fields are shown in Fig. 5.14. The acceleration is 590 m s^{-2} for voltage of 42 V mm^{-1} , 499 m s^{-2} for voltage of 52 V mm^{-1} , 497 m s^{-2} for voltage of 67 V mm^{-1} and 130 m s^{-2} for voltage of 75 V mm^{-1} . These high acceleration values show that the gravity acceleration of 9.8 m s^{-2} can be neglected during electrospinning (which agrees with the theoretical estimates at the end of Section V.G). These measurements also show that fluid jets spun at lower voltage have a higher acceleration.

In Fig. 5.15, the velocities are plotted against distance from the spinneret. It shows that, when spun at lower voltages, an electrospinning jet tends to have a higher velocity at the same position along the jet axis. The elongation

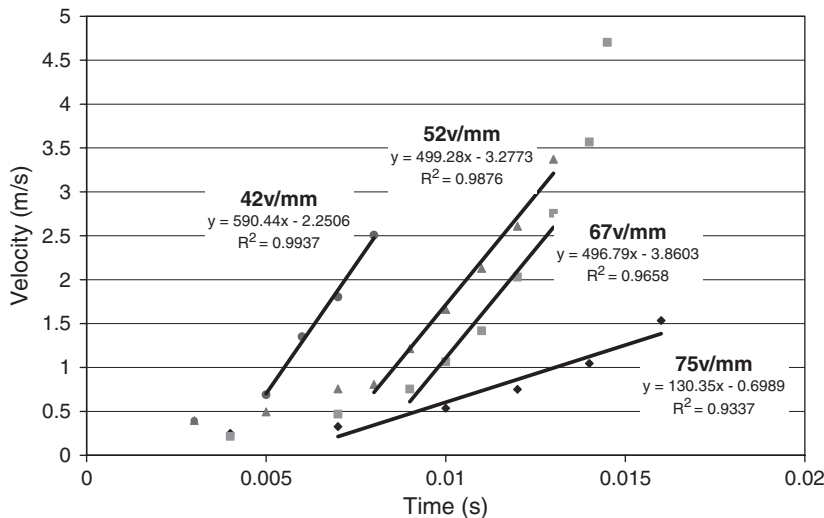


FIG. 5.14. Jet velocity versus time in different electric fields. Straight section of the jet (Xu, 2003).

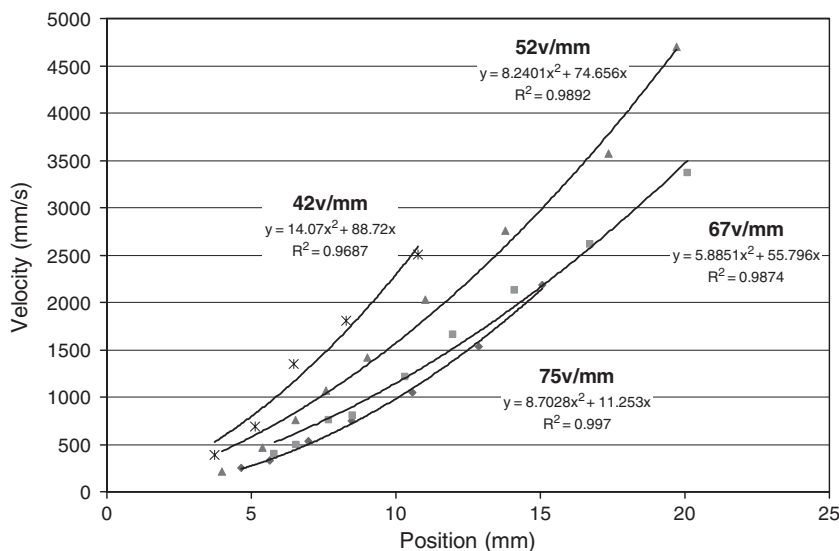


FIG. 5.15. Jet velocity versus position along the jet axis in different electric fields (Xu, 2003).

of the jet is mainly induced by the repulsive forces produced by the charges in the neighboring segments of the jet. From the interference colors shown in Fig. 5.12, it can be seen that lower voltage results in a thinner fluid jet. Therefore, at lower spinning voltages, there is less fluid drawn from the solution reservoir, which is a glass pipette in this case. Therefore, it is easier for charges to elongate the fluid jet and produce a higher fluid velocity, when there is less fluid carried in the jet.

6. Strain Rate of the Electrospinning Jets

The rate of uniaxial elongation in a segment of the straight part of the jet is $\dot{e} = -2(da/dt)/a = -2(da/dx)V/a$, where a is its cross-sectional radius, t time, x longitudinal coordinate and V velocity (Yarin, 1993). The interference color technique described in detail in Section V.B.4 was used to measure diameter distribution along electrospinning jets, $d = 2a(x)$. It is emphasized, that since volumetric flow rate Q in the jet is constant and can be measured, radius $a(x)$ can also be found using the data on jet velocity $V(x)$ of Section V.B.5, as $a(x) = [Q/(\pi V)]^{1/2}$ (Yarin, 1993). However, the advantage of the interference color technique consists in the fact that it allows an immediate estimate of local values of $d = 2a$ just by naked eye observation. Indeed, colors seen along the jet are associated with local jet diameters. Fig. 5.16 shows the interference color on electrospinning jets spun at different voltages. The diameter of the lower part of the jet is smaller than that of the higher part. Decreasing the voltage caused the colors shift

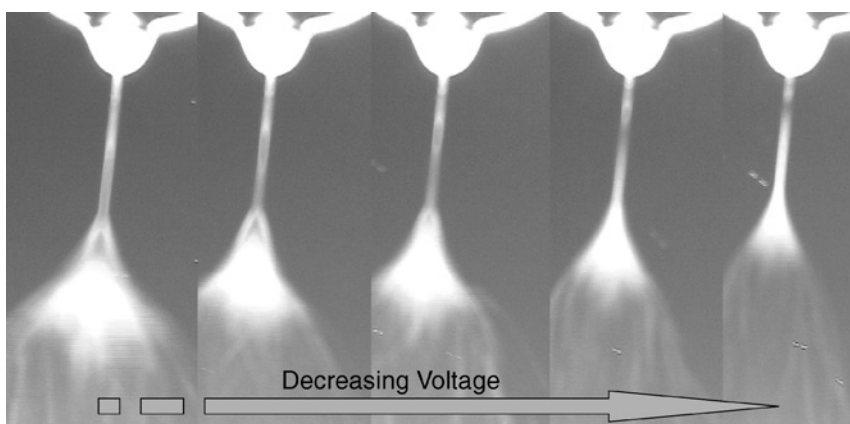


FIG. 5.16. Interference colors provide live information on jet diameter and taper rate change during electrospinning. After Xu et al. (2003). (see Color plate section).

upwards. Fig. 5.16 reveals that jets have smaller diameters at a particular location along the axis when spun at lower voltages, which agrees with the correspondingly higher velocities at the same location as shown in Fig. 5.15. Lengths of the interference color bands also decrease and colors concentrate at the top part of the jet when the electrospinning voltage is decreased. The observations show an increase in the taper rate as the spinning voltage is decreased. In summary, these experimental results show that a^{-1} , da/dx and V all increase with decreasing spinning voltage. Consequently, the strain rate increases when the spinning voltage is decreased. The data obtained allow calculation of the strain rate along the straight segment of the jet. Fig. 5.17 shows the diameters along the jet axis when spun at voltages of 42, 52 and 67 V/mm. The results for $a(x)$, together with those for $V(x)$ from Fig. 5.15, yield the distribution of the elongation rate $\dot{\epsilon}$ depicted in Fig. 5.18.

At the same positions (e.g. $x < 6$ mm) the strain rate has higher values when spinning voltage is low. The capability of the flow in orienting molecular chains will be discussed in the following sections. It is interesting to see that the strain rate does not increase monotonically along the straight section of the jet. Instead, it reaches a maximum and then decreases. However, the fluid velocity and the reciprocal of the jet diameter increase monotonically along the jet axis. This behavior determines the taper rate, da/dx , and its distribution along the straight section of the jet. Fig. 5.19

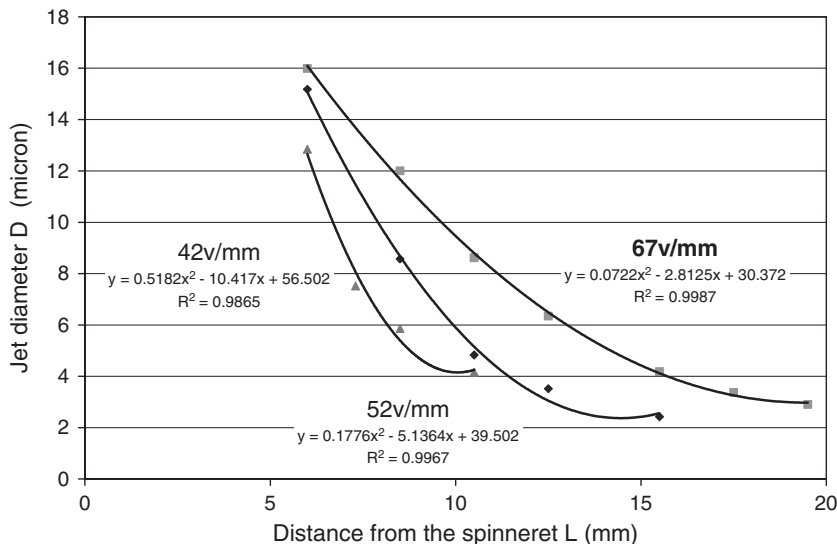


FIG. 5.17. Jet diameter measured under different voltages (Xu, 2003).

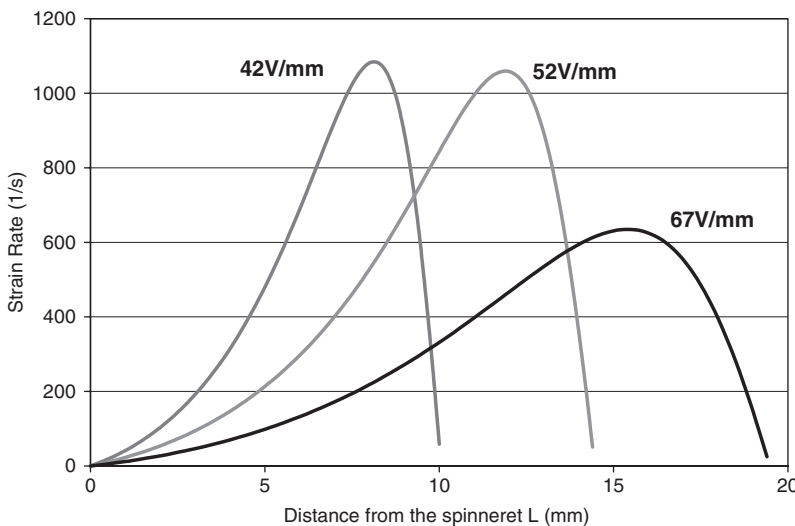


FIG. 5.18. Calculated strain rate $\dot{\varepsilon}$ along the jet axis at different voltages (Xu, 2003).

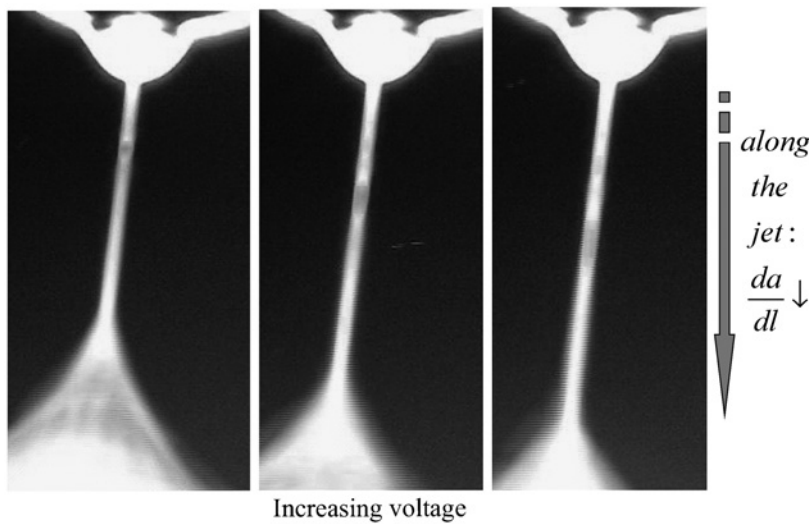


FIG. 5.19. The trend of da/dx observed from the interference colors along the jet axis (Xu, 2003). (see Color plate section).

shows the interference colors of the electrospinning jets spun at different voltages. Color bands on the top part of the jets always have a shorter length than those on the bottom. The taper rate decreases along the jet axis for all

electrospinning voltages. The jet taper rate decreases for the following reasons: first, a certain degree of molecular chain alignment was achieved during the early stage of the stretching, making further elongation more difficult. Second, solvent evaporation caused the elongational viscosity to increase. Third, the envelope cone below the straight part of the jet is electrically repulsive, which should decrease tapering. Therefore, when the decrease of the taper rate exceeds the increase of the fluid velocity and the reciprocal of the jet diameter, the strain rate starts to decrease.

7. Flow-Induced Molecular Chain Orientation in the Electrospinning Jets

Since the extensional component of the velocity gradient dominates the shear component in the elongational flow in the electrospinning jets, they must be very effective in stretching the polymer chains. Polymer chains coil up in theta or good solvents due to entropy contribution to the free energy. A strong elongational flow is able to stretch polymer chains resulting in coil–stretch transition (de Gennes, 1974). In this case, viscous forces exerted by the flow overbear the entropic elasticity of polymer chains. The strength of the flow in electrospinning is characterized by the elongational strain rate. The response of the molecular chains to the flow field depends on the relaxation time, which characterizes entropic elasticity of macromolecular chains. The product of the strain rate and the relaxation time determines whether stretching or relaxation will dominate in the elongation process (de Gennes, 1974; cf. Section V.J.7). If the flow is weak and molecular chains are able to return to their original conformation in a short time, the product of strain rate and relaxation time will be small and relaxation dominates. Thus, the coiled conformations prevail. If the flow is strong and polymer chains need a long time to come back to their original conformation, the product of strain rate and relaxation time will be large. Molecular chains have no time to rearrange in the flow field. Deformation is stored and added up. In this case, a coil–stretch transition occurs and the coil quickly reaches a stretched state.

Fig. 5.20 shows the product of the relaxation time of the polymer solution and the strain rates of the electrospinning jets spun at different voltages. PEO/water solutions for this experiment had an initial concentration of 6%. In Fig. 5.20, the jet spun at the lowest voltages shows the highest value of the product of strain rate $\dot{\varepsilon}$ and the relaxation time θ . Larger value of the product $\dot{\varepsilon}\theta$ signify a better molecular chain stretching and alignment by the flow. It is emphasized that coil–stretch transition is expected for the values of

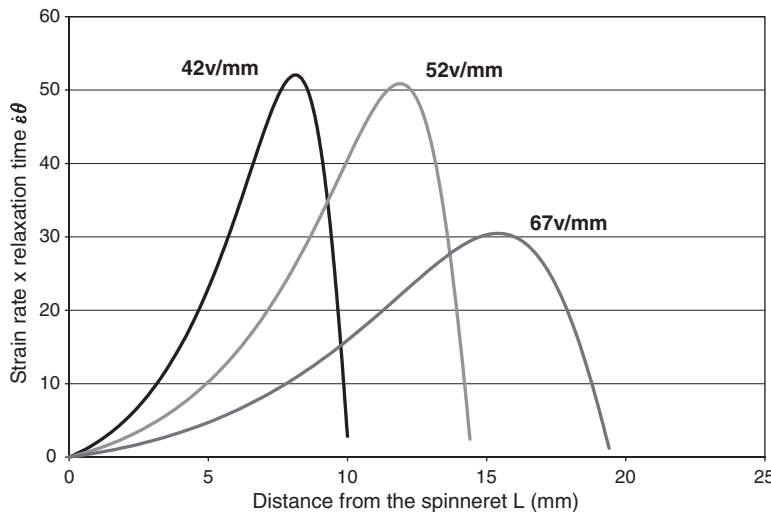


FIG. 5.20. The product of the strain rate and the relaxation time at positions along the straight section of the jet (Xu, 2003).

$\dot{\epsilon}\theta > 0.5$ (de Gennes, 1974). The latter shows that the three jets of Fig. 5.20 are already strong at their straight sections and should result in stretched macromolecules. In the next section, birefringence experiment will be used to investigate the molecular chain alignment under different spinning voltages.

8. Birefringence of the Electrospinning Jets

From the experimental point of view, the coil-stretch transition has been studied using birefringence phenomenon. There are some difficulties in observing the birefringence on electrospinning jets. First, the jet diameter even at the straight section is only a few microns, which may result in extremely low birefringence intensity. Second, the liquid in the jet is highly charged. A certain distance must be maintained, so that the apparatus does not affect the electric field. To solve the above problems, a set-up as shown in Fig. 5.21 has been used. In the set-up, light from a 15 mW YAG laser traveled along the z -axis in space. The electric field vector has two components in the x and y direction. The orientation of the polymer molecules in the jet will cause the polarizability to become anisotropic. A sample with oriented molecules should have a different propagation velocity of light with its electric field vector in the x and the y directions, which

should result in a change of phase difference as the light travels through the jet.

A crossed polarizer-analyzer pair was oriented at -45° and 45° with respect to the vertical direction. Only the light with its electric field vector oriented at 45° could pass through the polarizer. If the media in between the polarizer and analyzer is isotropic, there would be no light passing through the analyzer with a polarization direction of -45° . If molecular chains in the electrospinning jet are oriented by the flow field, there should be a larger refractive index along the preferred chain orientation direction than in the direction perpendicular to the chain axis. In the experiment of Fig. 5.21, the preferred chain orientation direction was vertical. Therefore, the electric field of the incident beam interacted with the electrospinning jet differently in the vertical and horizontal directions as the light passed through the jet. There were preferred losses of the electric field of the light in vertical or horizontal direction due to the difference in absorption and scattering by the jet. After the polarized light passes through the jet, the summation of the electric field vectors was no longer 45° . Therefore, a fraction of the light was able to pass through the analyzer with a polarization direction of -45° . In summary, if the macromolecular chains in the jet were aligned by the flow field, observation of light passing through the analyzer would be possible.

A high magnification optical train is required to observe the birefringence on electrospinning jets. A conventional microscope has its image plane several millimeters away from the objective lens. The electrically charged jet cannot be brought so close to the microscope. Hence, a long working distance polarized microscope was built, as shown in Fig. 5.21. A

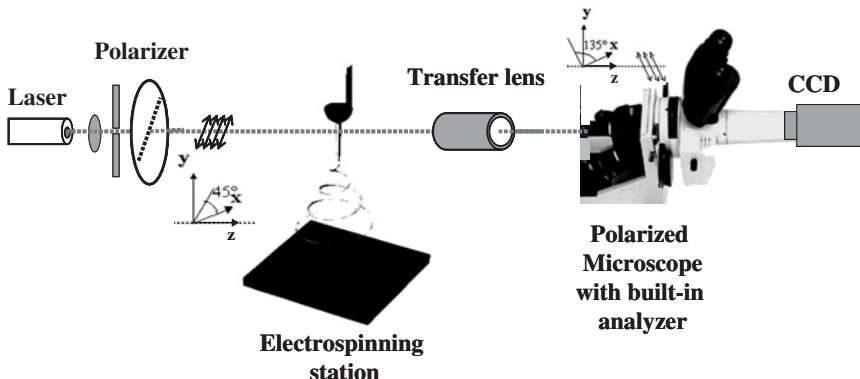


FIG. 5.21. Long working distance polarized microscope. Field of view: $540 \mu\text{m} \times 720 \mu\text{m}$. After Xu *et al.* (2003).

conventional polarized microscope was modified. A long focal length lens, used as a transfer lens, was set in between the object and the objective lens of the microscope. The back focal plane of the transfer lens was superimposed on the image plane of the objective lens. The transfer lens delivered the image of the object to the microscope. The working distance of the modified microscope was twice the focal length of the transfer lens, which was around 20 cm in this experiment. The polarizer and analyzer used were the built-in polarizers in the original microscope. The electrospinning jet was safely set on the focal plane of the transfer lens.

A laser was used to provide illumination. Advantages of using monochromatic laser include high intensity and no chromatic aberration effect. Chromatic aberration arises because light with different wavelengths travels at different speeds in the media. When the light passes through a lens, shorter wavelength light travels faster and bends more towards the optical axis than longer wavelength light. Thus, it has a shorter focal length than long wavelength light. This chromatic aberration makes it impossible to simultaneously focus all wavelengths of the light in a single lens system. Halo on the edge of the object shows up as an effect of chromatic aberration. This effect becomes severe in observing submicron size objects.

A monochrome CCD camera manufactured by Supercircuits with 0.0003 lx sensitivity was attached to the long working distance polarized microscope. The field of view in this set-up was $540\text{ }\mu\text{m} \times 720\text{ }\mu\text{m}$. Electrospinning was conducted at different voltages. The straight segment of the jet was observed. Fig. 5.22a shows birefringence on a jet spun at 44 V mm^{-1} , which is the lowest field at which the electrospinning jet could be maintained in this experiment. Dying jets usually show birefringence before spinning stops. In both situations, flow rates were very low. The thinner jet was stretched more easily by the electric field. Fig. 5.22b showed that when the electrospinning voltage was increased, the jet birefringence became smaller but was detectable in the original image. The lower spinning voltage facilitates chain alignment in the electrospinning process. This result complies with the data on the rate of strain $\dot{\epsilon}$ and the product $\dot{\epsilon}\theta$ shown in Figs. 5.18 and 5.20, respectively.

Birefringent jets observed during electrospinning always have outer layer brighter than the core. The following points are the possible reasons: First, drying happens at the outer edges due to evaporation. A shell structure with a higher polymer concentration and a higher relaxation time could be expected to appear there. This shell can support most of the stress and thus result in better stretching and orientation in the outer layer. Second, molecules on the outer surface of the jet have fewer degrees of freedom than

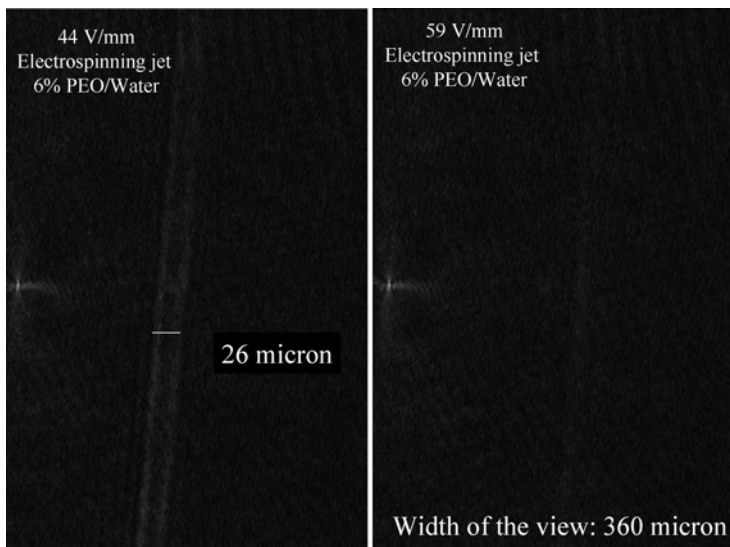


FIG. 5.22. Jet birefringence observed at different electrospinning voltages (Xu, 2003).

those in the bulk. Chains with less freedom are easier to be aligned by the flow. Third, like charges always stay away from each other due to the repulsion forces. Since the electrical relaxation time across the jet is rather short, essentially all of the charge is concentrated on the surface layer. There is a higher charge density at the outer surface than in the bulk. Thus, stronger electrical stretching forces are exerted on the surface layer of the jet.

Fig. 5.23 shows the birefringence of the as-spun fiber obtained under the same conditions and from the same jet as in Fig. 5.22. Although the fiber diameter is much smaller than that of the straight section of the jet, birefringence intensity is a lot stronger. It implies that further chain alignment took place in the bending loops inside the envelope cone.

The results can be summarized as follows. The ultra-low-intensity birefringence on the jets during electrospinning was observed. Jets spun at the very low voltages and the (unstable) dying jets show birefringence. When increasing the electrospinning voltage, the jet birefringence disappeared. Birefringence observation complies with the theoretical prediction in Section V.J.7. Electrospun fibers got under the same condition showed relatively strong birefringence compared with the straight section of the jet during electrospinning, which reveals that further chain alignment took place in the envelope cone area. The strength of the stretching is not the dominant effect on final fiber diameter. Instead, solidification plays a more important role.

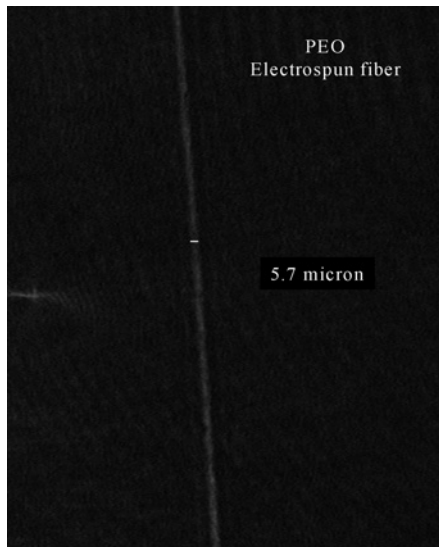


FIG. 5.23. Birefringence on the electrospun fiber (Xu, 2003).

Lower electric field produces thinner jets. The large surface area per unit mass of the thin jet allows solvent to evaporate faster. Hence, thinner jets experience less time to elongate than thicker ones. Then, the overall effect makes the electric field effects on the final fiber diameter rather small.

C. VISCOELASTIC MODEL OF A RECTILINEAR ELECTRIFIED JET

Estimates based on the Maxwell equations, show that all possible magnetic effects can be safely neglected and the conditions of the electrohydrodynamics can be assumed.

Consider first a rectilinear electrified liquid jet in an electric field parallel to its axis. We model a segment of the jet by a viscoelastic dumbbell as shown in Fig. 5.24. In the mathematical description, we use the Gaussian electrostatic system of units. Corresponding SI units are given when parameters are evaluated. Table 5.1 lists the symbols and their units.

Each of the beads, A and B, possesses a charge e and mass m . Let the position of bead A be fixed by non-Coulomb forces. The Coulomb repulsive force acting on bead B is $-e^2/\ell^2$. The force applied to B due to the external

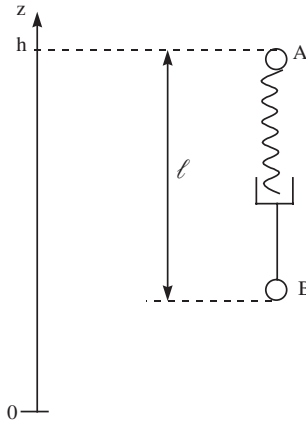


FIG. 5.24. Viscoelastic dumbbell representing a segment of the rectilinear part of the jet. After [Reneker et al. \(2000\)](#) with permission from AIP.

field is $-eV_0/h$. The dumbbell, AB, models a viscoelastic Maxwellian liquid jet. Therefore the stress, σ , pulling B back to A is given by (Bird et al., 1987)

$$\frac{d\sigma}{dt} = G \frac{d\ell}{\ell dt} - \frac{G}{\mu} \sigma, \quad (5.1)$$

where t is the time, G and μ are the elastic modulus and viscosity, respectively, and ℓ the filament length. It should be emphasized that according to [Yarin \(1990, 1993\)](#), the phenomenological Maxwell model adequately describes rheological behavior of concentrated polymeric systems in strong uniaxial elongation, which is the case in the present work.

The momentum balance for bead B is

$$m \frac{dv}{dt} = -\frac{e^2}{\ell^2} - \frac{eU_0}{h} + \pi a^2 \sigma, \quad (5.2)$$

where a is the cross-sectional radius of the filament, and v the velocity of bead B which satisfies the kinematics equation

$$\frac{d\ell}{dt} = -v. \quad (5.3)$$

We adopt dimensionless descriptions, as is customary in fluid mechanics (see Table 5.2). We define the length scale $L_{el} = (e^2/\pi a_0^2 G)^{1/2}$, where a_0 is the initial cross-sectional radius at $t = 0$, and render ℓ dimensionless by L_{el} , and assume L_{el} to be also an initial filament length which is not restrictive. To

make them dimensionless, we divide t by the relaxation time μ/G , stress σ by G , velocity v by $L_{\text{el}}G/\mu$, and radius a by a_0 . Denoting $W = -v$ and applying the condition that the volume of the jet is conserved,

$$\pi a^2 \ell = \pi a_0^2 L_{\text{el}}, \quad (5.4)$$

we obtain Eqs. (5.1)–(5.3) in the following dimensionless forms:

$$\frac{d\bar{\ell}}{d\bar{t}} = \bar{W}, \quad (5.5a)$$

$$\frac{d\bar{W}}{d\bar{t}} = V - F_{\text{ve}} \frac{\bar{\sigma}}{\bar{\ell}} + \frac{Q}{\bar{\ell}^2}, \quad (5.5b)$$

$$\frac{d\bar{\sigma}}{d\bar{t}} = \frac{\bar{W}}{\bar{\ell}} - \bar{\sigma}, \quad (5.5c)$$

where the dimensionless parameters are denoted by bars, and the dimensionless groups are given by

$$Q = \frac{e^2 \mu^2}{L_{\text{el}}^3 m G^2}, \quad (5.6a)$$

$$V = \frac{e U_0 \mu^2}{h L_{\text{el}} m G^2}, \quad (5.6b)$$

$$F_{\text{ve}} = \frac{\pi a_0^2 \mu^2}{m L_{\text{el}} G}. \quad (5.6c)$$

It is emphasized, that in this momentum balance, we temporarily neglect the secondary effects of the surface tension, gravity and the air drag force. Note also that using the definition of L_{el} , we obtain from Eqs. (5.6a) and (5.6c) that $Q \equiv F_{\text{ve}}$. It should also be mentioned that here in Eq. (5.4) and hereinafter in this model, we neglect mass losses due to evaporation. In principle, they can be accounted for using a specific expression for the evaporation rate. Evaporation is not expected to introduce qualitative changes in jet dynamics in the main part of the jet path. However, the effect of solvent evaporation on the values of the rheological parameters of the polymer solution ultimately leads to the solidification of the jet into a polymer fiber. Evaporation and solidification are discussed in detail in Section V.H.

Numerical solutions of the system, Eqs. (5.5), may be found using the following initial conditions $\bar{t} = 0$:

$$\bar{\ell} = 1, \quad (5.7a)$$

$$\bar{W} = 0, \quad (5.7b)$$

$$\bar{\sigma} = 0. \quad (5.7c)$$

Rheological and electrical parameters of the polymer solution are at present not fully known from experiments. Therefore, here and hereinafter, the calculations were done with the best values available for the dimensionless groups. In certain cases, the values were chosen as close as possible to plausible estimates of the physical parameters involved. In these cases, we list the values of the physical parameters along with the values of the dimensionless groups based on them. In Section V.K, however, measured values of the rheological parameters are used. The calculated results in Fig. 5.25 show that the longitudinal stress $\bar{\sigma}$ first increases over time as the filament stretches, passes a maximum and then begins to decrease, since the relaxation effects always reduce the stress at long times. The dimensionless longitudinal force in the filament, $F_{ve}\bar{\sigma}/\bar{\ell}$, passes its maximum before $\bar{\sigma}$ does. At the conditions corresponding to the maximum of $\bar{\sigma}$ the value of the force is already comparatively small and decreasing rapidly. We will see below that this small value of the longitudinal force allows the onset of an electrically driven bending instability. Therefore, we identify the filament length, $\bar{\ell}_*$, at the condition when $\bar{\sigma}$ passes the maximum and the longitudinal

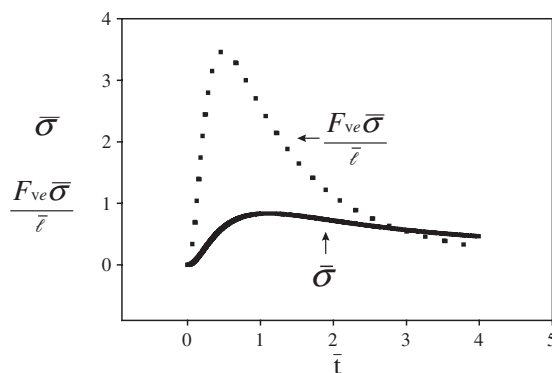


FIG. 5.25. Longitudinal stress $\bar{\sigma}$ in the rectilinear part of the jet, and the longitudinal force $F_{ve}\bar{\sigma}/\bar{\ell}$. $Q = 12$, $V = 2$, $F_{ve} = 12$. After Reneker et al. (2000) with permission from AIP.

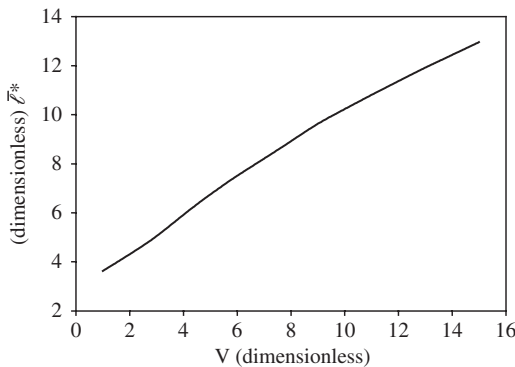


FIG. 5.26. Length of the rectilinear part of the jet $\bar{\ell}^*$ as a function of the dimensionless voltage V . $Q = 12$ and $F_{ve} = 12$. After Reneker et al. (2000) with permission from AIP.

force is already small, as the length of the rectilinear segment of the electrospun jet at which the bending instability begins to grow rapidly. The relationship of this theoretically defined segment to the observed length of the straight segment is not yet determined. The length, $\bar{\ell}^*$, increases with applied voltage as is seen in Fig. 5.26. Near the pendant drop, the longitudinal force is also small, but the jet does not bend, since its radius there is large, and the corresponding bending stiffness is large.

The rectilinear liquid jets are unstable to capillary (varicose) perturbations driven by surface tension. Longitudinal stretching can stabilize the jet in the presence of these perturbations (Khakhar and Ottino, 1987). In electrospinning, jets are stretched along their axis by the external electric field and are elongated further by the repulsive force between charges on adjacent segments. The resulting tensile forces prevent development of capillary instability in the experiments described here.

D. BENDING INSTABILITY OF ELECTRIFIED JETS

Dealing with the bending instability of electrospun jets, we consider the polymer solutions to be perfect dielectrics with frozen charges. This is justified by the fact that the bending instability we are going to tackle is characterized by the characteristic hydrodynamic time, $\tau_H \cong 1$ ms, and thus $\tau_C > \tau_H$ ($\tau_C = 3.5$ ms for $\sigma_e = 10^{-7}$ S m⁻¹). Under such conditions the same fluid, which behaved as a perfect conductor in Taylor's cone, behaves as a perfect dielectric in the bending jet. The conductive electric current along the jet can be neglected, and charge transport can be attributed entirely to the jet flow (the charge is “frozen” in the liquid).

The reason for the observed bending instability may be understood in the following way. In the coordinates that move with a rectilinear electrified jet, the electrical charges can be regarded as a static system of charges interacting mainly by Coulomb's law (without the external field). Such systems are known to be unstable according to Earnshaw's theorem (Jeans, 1958). To illustrate the instability mechanism that is relevant in the electrospinning context, we consider three point-like charges each with a value e and originally in a straight line at A, B and C as shown in Fig. 5.27. Two Coulomb forces having magnitudes $F = e^2/r^2$ push against charge B from opposite directions. If a perturbation causes point B to move off the line by a distance δ to B' , a net force $F_1 = 2F \cos \theta = (2e^2/r^3)\delta$ acts on charge B in a direction perpendicular to the line, and tends to cause B to move further in the direction of the perturbation away from the line between fixed charges, A and C. The growth of the small bending perturbation that is characterized by δ is governed in the linear approximation by the equation

$$m \frac{d^2\delta}{dt^2} = \frac{2e^2}{\ell_1^2} \delta, \quad (5.10)$$

where m is the mass.

The growing solution of this equation, $\delta = \delta_0 \exp[(2e^2/m\ell_1^3)^{1/2} t]$, shows that small perturbations increase exponentially. The increase is sustained because electrostatic potential energy of the system depicted in Fig. 5.27 decreases as e^2/r when the perturbations, characterized by δ and r , grow. We

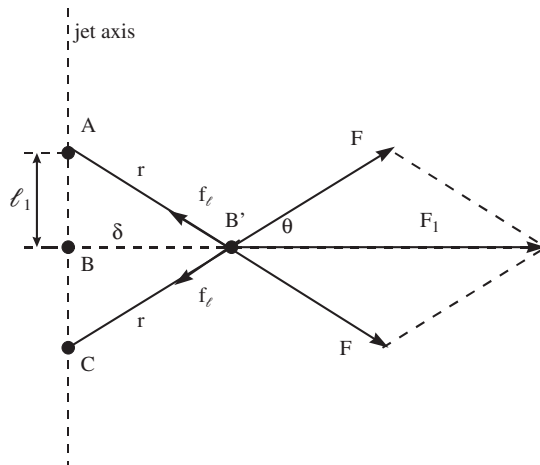


FIG. 5.27. Illustration of the Earnshaw instability, leading to bending of an electrified jet. After Reneker et al. (2000) with permission from AIP.

believe that this mechanism is responsible for the observed bending instability of jets in electrospinning.

If charges A , B and C are attached to a liquid jet, forces associated with the liquid tend to counteract the instability caused by the Coulomb forces. For very thin liquid jets, the influence of the shearing force related to the bending stiffness can be neglected in comparison with the stabilizing effect of the longitudinal forces since the shearing forces are of the order of $O(a^4)$, which is much smaller than the longitudinal forces (Yarin, 1993), which are of the order of $O(a^2)$. The longitudinal force, at the moment when the bending instability sets in, was calculated above for the stretching of a rectilinear filament. Its value is given by $f_\ell = \pi a^2 \sigma^*$ (or in dimensionless form by $F_{ve} \bar{\sigma}^* / \bar{\ell}^*$). The values of σ and $\bar{\ell}$ at the moment when σ (or $\bar{\sigma}$) passes its maximum are denoted by asterisks. The forces f_ℓ are directed along BC or BA in Fig. 5.27, and are opposite to the local Coulomb force F . If F is larger than the viscoelastic resistance, f_ℓ , the bending perturbation continues to grow, but at a rate decelerated by f_ℓ .

It might be thought that bending perturbations of very short lengths can always overcome the viscoelastic resistance f_ℓ , since the Coulomb force increases when the wavelength of the perturbation decreases. The surface tension always counteracts the bending instability because bending always leads to an increase of the area of the jet surface (Yarin, 1993). Surface tension resists the development of too large a curvature by the perturbation ABC in Fig. 5.27, and therefore limits the smallest possible perturbation wavelengths. All these factors are accounted for in the description of the three-dimensional bending instability of electrospun jets in Sections V.F and V.G.

E. LOCALIZED APPROXIMATION

In the dynamics of thin vortices in fluids the localized-induction approximation is widely used to describe velocity induced at a given vortex element by the rest of the vortex line (Arms and Hama, 1965; Batchelor, 1967; Aref and Flinchem, 1984; Pozrikidis, 1997; Yarin, 1997). A similar approach may be used to calculate the electric force imposed on a given element of an electrified jet by the rest of it. Consider an enlarged element of a curved jet shown in Fig. 5.28. We assume that the arc length ξ is reckoned along the jet axis from the central cross-section of the element where $\xi = 0$. We denote the coordinates reckoned along the normal and binormal by y and z , so that the position vector of point A on the surface of the element

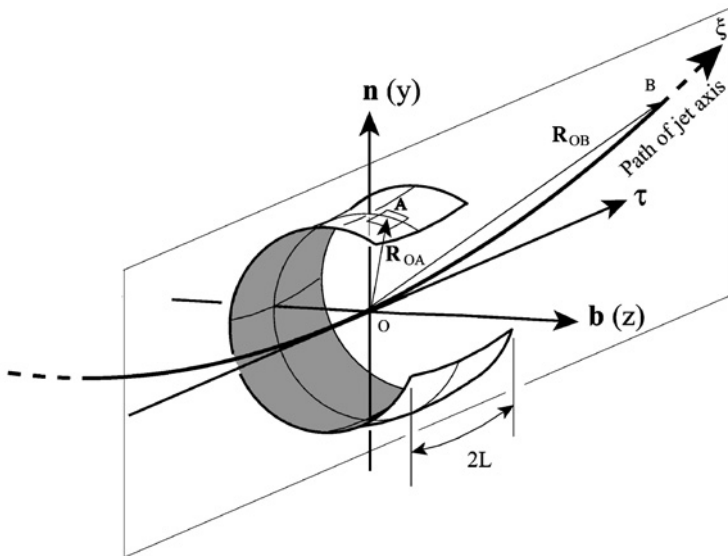


FIG. 5.28. Sketch of an enlarged element of a curved jet and the associated normal, binormal and tangent vectors \mathbf{n} , \mathbf{b} , and τ . After Yarin et al. (2001a) with permission from AIP.

$\mathbf{R}_{OA} = y\mathbf{n} + z\mathbf{b}$. The position vector of point B at the jet axis close enough to the element considered is thus given by

$$\mathbf{R}_{OB} = \tau\xi + \frac{1}{2}|k_0|\xi^2\mathbf{n}, \quad (5.11)$$

where k_0 is the curvature of the jet axis at point O and τ is a unit tangent vector. Therefore

$$\mathbf{R}_{BA} = \mathbf{R}_{OA} - \mathbf{R}_{OB} = \left[y - \frac{1}{2}|k_0|\xi^2 \right] \mathbf{n} + z\mathbf{b} - \tau\xi. \quad (5.12)$$

Denote the cross-sectional radius of the jet element by a , assume that charge is uniformly distributed over the jet surface with the surface density Δe and denote the charge per unit jet length by $e = 2\pi a \Delta e$. Then the Coulomb force acting at a surface element near point A from the jet element situated near point B is given by

$$d\mathbf{F}_{BA} = \frac{e d\xi \Delta e a d\theta d\xi}{|\mathbf{R}_{BA}|^3} \mathbf{R}_{BA}, \quad (5.13)$$

where θ is the polar angle in the jet cross-section. Substituting Eq. (5.12) into Eq. (5.13) and accounting for the fact that $y = a \cos \theta$, and $z = a \sin \theta$ we obtain from Eq. (5.13)

$$d\mathbf{F}_{BA} = e d\xi \Delta e a d\theta d\xi \frac{[(a \cos \theta - |k_0| \xi^2/2) \mathbf{n} + a \sin \theta \mathbf{b} - \tau \xi]}{[a^2 - a \cos \theta |k_0| \xi^2 + |k_0|^2 \xi^4/4 + \xi^2]^{3/2}}. \quad (5.14)$$

For a thin jet, as $a \rightarrow 0$ all the terms containing a in the numerator of Eq. (5.14) can be safely neglected, also in the denominator the term $a \cos \theta |k_0| \xi^2$ is negligibly small as compared to ξ^2 . Then using Eq. (5.14) we calculate the electric force acting on a particular element of the jet, assuming that the length of the element is $2L$, with L being a cut-off for the integral, to be determined later on

$$\mathbf{F}_{el} = \int_0^{2\pi} d\theta \int_{-L}^L d\mathbf{F}_{AB} = e^2 d\xi \int_{-L}^L d\xi \frac{-\tau \xi - |k_0| \xi^2 \mathbf{n}/2}{[a^2 + \xi^2 + |k_0|^2 \xi^4/4]^{3/2}}. \quad (5.15)$$

The latter yields

$$\mathbf{F}_{el} = e^2 d\xi \int_{-L/a}^{L/a} dx \left[\frac{-\tau x}{a(1+x^2)^{3/2}} - \frac{|k_0| x^2 \mathbf{n}/2}{(1+x^2)^{3/2}} \right]. \quad (5.16)$$

The force in the axial direction obviously cancels, whereas the force becomes

$$\mathbf{F}_{el} = -e^2 \ell n \left(\frac{L}{a} \right) |k| \mathbf{n} d\xi. \quad (5.17)$$

This shows that the net electric force acting on a jet element is related to its curvature $k = k_0$, and acts in the normal (lateral) direction to the jet axis. The magnitude of the net force acting on a jet element due to the action of the surface tension forces is equal to

$$\mathbf{F} = \pi a \sigma \tau|_{\xi+d\xi} - \pi a \sigma \tau|_{\xi} = \pi a \sigma |k| \mathbf{n} d\xi, \quad (5.18)$$

where σ is the surface tension coefficient.

Therefore, the net normal (lateral) force acting on a jet element is given by the sum of the electric and surface tension forces, Eqs. (5.17) and (5.18), as

$$d\mathbf{F} = |k| \mathbf{n} d\xi \left[\pi a \sigma - e^2 \ell n \frac{L}{a} \right]. \quad (5.19)$$

The cut-off length L is still to be found. It will be done below in Section V.I.

F. CONTINUOUS QUASI-ONE-DIMENSIONAL EQUATIONS OF THE DYNAMICS OF ELECTRIFIED LIQUID JETS

For very thin jets we can neglect, in the first approximation, the effect of the shearing force in the jet cross-section, as well as the bending stiffness (Yarin, 1993, p. 49). If we use a Lagrangian parameter s “frozen” into the jet elements, then the momentless quasi-one-dimensional equations of the jet dynamics (Yarin, 1993, p. 49, Eq. (4.19)) take the form

$$\lambda f = \lambda_0 f_0, \quad (5.20a)$$

$$\rho \lambda_0 f_0 \frac{\partial \mathbf{V}}{\partial t} = \tau \frac{\partial P}{\partial s} + \lambda |k| P \mathbf{n} - \rho g \lambda_0 f_0 \mathbf{k} + \lambda |k| \left(\pi a \sigma - e^2 \ell n \frac{L}{a} \right) \mathbf{n} - \lambda e \frac{U_0}{h} \mathbf{k}. \quad (5.20b)$$

Equation (5.20a) is the continuity equation with λ being the geometrical stretching ratio, so that $\lambda ds = d\xi$, and $f = \pi a^2$ the cross-sectional area. Subscript zero denotes the parameter values at time $t = 0$. Equation (5.20b) is the momentum balance equation with ρ being the liquid density, \mathbf{V} its velocity, P the longitudinal force in the jet cross-section (of viscoelastic origin in the case of electrospinning of polymer jets), $g\mathbf{k}$ gravity acceleration, U_0/h the outer field strength (the outer field is assumed to be parallel to the unit vector \mathbf{k} , with U_0 being the value of electrical potential at the jet origin, and h the distance between the origin and a ground plate). It is emphasized that on the right-hand side of the momentum Eq. (5.20b) we account for the longitudinal internal force of rheological origin acting on the jet (the first two terms), the gravity force (the third term), the bending electrical force and the stabilizing effect of the surface tension (the fourth term following from Eq. (5.19)), and for the electric force acting on the jet from an electric field created by the potential difference of the starting point of the jet and the collector.

Equations (5.20a,b) are supplemented by the kinematic relation

$$\frac{\partial \mathbf{R}}{\partial t} = \mathbf{V}, \quad (5.21)$$

where \mathbf{R} is the radius vector of a point on the axis of the jet.

Introducing the Cartesian coordinate system associated with a capillary (the jet origin) or a ground plate, with unit vectors \mathbf{i} , \mathbf{j} , and \mathbf{k} , and accounting for

$$\mathbf{R} = \mathbf{i}X + \mathbf{j}Y + \mathbf{k}Z, \quad (5.22a)$$

$$\mathbf{V} = \mathbf{i}u + \mathbf{j}v + \mathbf{k}w, \quad (5.22b)$$

we obtain from the projections of Eqs. (5.20b) and (5.21) the following system of scalar equations:

$$\rho\lambda_0f_0\frac{\partial u}{\partial t} = \tau_X\frac{\partial P}{\partial s} + \lambda|k|Pn_X + \lambda|k|\left(\pi a\sigma - e^2\ell n\frac{L}{a}\right)n_X, \quad (5.23a)$$

$$\rho\lambda_0f_0\frac{\partial v}{\partial t} = \tau_Y\frac{\partial P}{\partial s} + \lambda|k|Pn_Y + \lambda|k|\left(\pi a\sigma - e^2\ell n\frac{L}{a}\right)n_Y, \quad (5.23b)$$

$$\begin{aligned} \rho\lambda_0f_0\frac{\partial w}{\partial t} = & \tau_Z\frac{\partial P}{\partial s} + \lambda|k|Pn_Z + \lambda|k| \\ & \times \left(\pi a\sigma - e^2\ell n\frac{L}{a}\right)n_Z - \rho g\lambda_0f_0 - \lambda e\frac{U_0}{h}, \end{aligned} \quad (5.23c)$$

$$\frac{\partial X}{\partial t} = u, \quad (5.23d)$$

$$\frac{\partial Y}{\partial t} = v, \quad (5.23e)$$

$$\frac{\partial Z}{\partial t} = w. \quad (5.23f)$$

The following geometric relations should be added:

$$\lambda = (X_s^2 + Y_s^2 + Z_s^2)^{1/2}, \quad (5.24a)$$

$$\tau_X = \frac{1}{\lambda}\frac{\partial X}{\partial s}, \quad (5.24b)$$

$$\tau_Y = \frac{1}{\lambda}\frac{\partial Y}{\partial s}, \quad (5.24c)$$

$$\tau_Z = \frac{1}{\lambda}\frac{\partial Z}{\partial s}, \quad (5.24d)$$

$$n_X = \frac{1}{|k|\lambda}\frac{\partial \tau_X}{\partial s}, \quad (5.24e)$$

$$n_Y = \frac{1}{|k|\lambda}\frac{\partial \tau_Y}{\partial s}, \quad (5.24f)$$

$$n_Z = \frac{1}{|k|\lambda} \frac{\partial \tau_Z}{\partial s}, \quad (5.24g)$$

$$|k| = \left[\frac{\left(X_{,s}^2 + Y_{,s}^2 + Z_{,s}^2 \right) \left(X_{,ss}^2 + Y_{,ss}^2 + Z_{,ss}^2 \right) - \left(X_{,s} X_{,ss} + Y_{,s} Y_{,ss} + Z_{,s} Z_{,ss} \right)^2}{\left(X_{,s}^2 + Y_{,s}^2 + Z_{,s}^2 \right)^3} \right]^{1/2} \quad (5.24h)$$

Also assuming the simplest linear version of the upper-convected Maxwell (UCM) model of viscoelasticity properly fitted to describe uniaxial elongation (Yarin, 1990, 1993), we obtain the equation for the normal stress in the jet cross-section $\sigma_{\tau\tau}$

$$\frac{\partial \sigma_{\tau\tau}}{\partial t} = G \frac{1}{\lambda} \frac{\partial \lambda}{\partial t} - \frac{G}{\mu} \sigma_{\tau\tau}, \quad (5.25)$$

where G is the modulus of elasticity, and μ the viscosity, and

$$\frac{1}{\lambda} \frac{\partial \lambda}{\partial t} = \frac{X_{,s} u_{,s} + Y_{,s} v_{,s} + Z_{,s} w_{,s}}{\lambda^2} \quad (5.26)$$

It is emphasized that any other reliable rheological constitutive equation could replace Eq. (5.25) in the framework of the present model. In Section V.K, for example, the non-linear UCM model is used as well, while it is shown that the difference between the predictions based on the linear and non-linear UCM models is not large.

The longitudinal force P is given by

$$P = \frac{\lambda_0 f_0}{\lambda} \sigma_{\tau\tau}. \quad (5.27)$$

It is emphasized that in Eq. (5.27) should actually stand the normal stress $\sigma_{\tau\tau} - \sigma_{nm}$ instead of $\sigma_{\tau\tau}$. However, in strong uniaxial elongational flows (electrospinning is an example of such a flow) the axial component $\sigma_{\tau\tau} \gg \sigma_{nm}$, and the latter can be neglected. Detailed proof of this fact can be found in Stelter et al. (2000).

Also the equation of the charge conservation in a jet element holds

$$e\lambda = e_0 \lambda_0 \quad (5.28)$$

The system of the equations presented in this subsection allows one to find the jet configuration in space at any moment of time. The equations will be

discretized and solved numerically. It is emphasized that the discretized equations can also be obtained directly considering the jet to be a locus of inertial electrically charged beads connected by the spring and dashpot viscoelastic elements (similar to Section V.D). This is done in the following subsection.

G. DISCRETIZED THREE-DIMENSIONAL EQUATIONS OF THE DYNAMICS OF THE ELECTROSPUN JETS

In the present section, we account for the whole integral responsible for the electric force. This is the only difference with Section V.F where the bending electric force is calculated using the localized approximation.

We represent the electrospun jets by a model system of beads possessing charge e and mass m connected by viscoelastic elements as shown in Fig. 5.29, which generalizes the models of Figs. 5.24 and 5.27. It needs to be mentioned that these imaginary beads are not the same as the physical beads (Fong et al., 1999) resulting from the varicose instability. The parameters corresponding to the element connecting bead i with bead $(i+1)$ are denoted by subscript u (up), those for the element connecting bead i with $(i-1)$ by subscript d (down). The lengths ℓ_{ui} and ℓ_{di} of these elements are given by

$$\ell_{ui} = [(X_{i+1} - X_i)^2 + (Y_{i+1} - Y_i)^2 + (Z_{i+1} - Z_i)^2]^{1/2}, \quad (5.29a)$$

$$\ell_{di} = [(X_i - X_{i-1})^2 + (Y_i - Y_{i-1})^2 + (Z_i - Z_{i-1})^2]^{1/2}, \quad (5.29b)$$

respectively, where X_i, Y_i, Z_i, \dots , are the Cartesian coordinates of the beads.

The rates of strain of the elements are given by $(d\ell_{ui}/dt)/\ell_{ui}$ and $(d\ell_{di}/dt)/\ell_{di}$. The viscoelastic forces acting along the elements are similar to Eq. (5.1),

$$\frac{d\sigma_{ui}}{dt} = G \frac{1}{\ell_{ui}} \frac{d\ell_{ui}}{dt} - \frac{G}{\mu} \sigma_{ui}, \quad (5.30a)$$

$$\frac{d\sigma_{di}}{dt} = G \frac{1}{\ell_{di}} \frac{d\ell_{di}}{dt} - \frac{G}{\mu} \sigma_{di}. \quad (5.30b)$$

The total number of beads, N , increases over time as new electrically charged beads are inserted at the top of Fig. 5.29 to represent the flow of

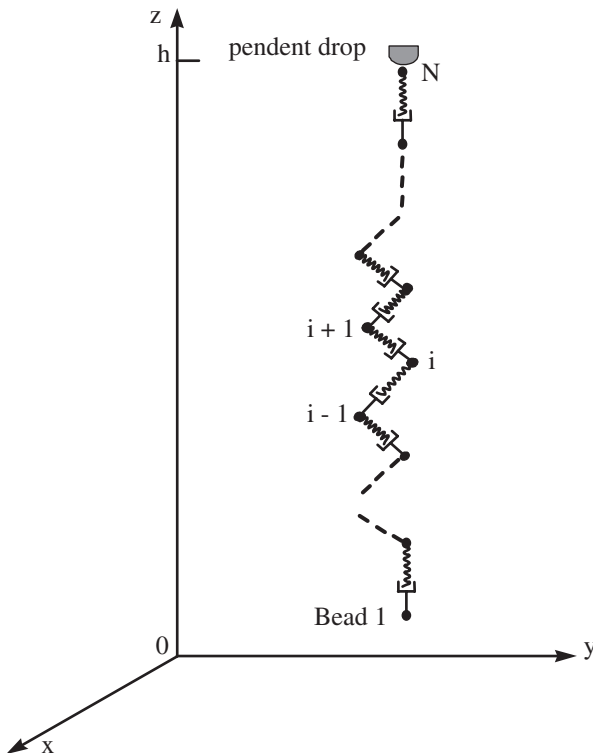


FIG. 5.29. Bending electrospun jet modeled by a system of beads connected by viscoelastic elements. After Reneker et al. (2000) with permission from AIP.

solution into the jet. The net Coulomb force acting on the i th bead from all the other beads is given by

$$\mathbf{f}_C = \sum_{j=1, j \neq i}^N \frac{e^2}{R_{ij}^2} \left[\mathbf{i} \frac{X_i - X_j}{R_{ij}} + \mathbf{j} \frac{Y_i - Y_j}{R_{ij}} + \mathbf{k} \frac{Z_i - Z_j}{R_{ij}} \right], \quad (5.31)$$

where \mathbf{i} , \mathbf{j} and \mathbf{k} are unit vectors along the x -, y - and z -axis, respectively, and

$$R_{ij} = \left[(X_i - X_j)^2 + (Y_i - Y_j)^2 + (Z_i - Z_j)^2 \right]^{1/2}. \quad (5.32)$$

The electric force imposed on the i th bead by the electric field created by the potential difference between the pendant drop and the collector is

$$\mathbf{f}_0 = -e \frac{V_0}{h} \mathbf{k}. \quad (5.33)$$

It is clear that the gravitational force may be included in \mathbf{f}_0 .

The net viscoelastic force acting on the i th bead of the jet is

$$\begin{aligned} \mathbf{f}_{ve} = \pi a_{ui}^2 \sigma_{ui} & \left[\mathbf{i} \frac{X_{i+1} - X_i}{\ell_{ui}} + \mathbf{j} \frac{Y_{i+1} - Y_i}{\ell_{ui}} + \mathbf{k} \frac{Z_{i+1} - Z_i}{\ell_{ui}} \right] \\ & - \pi a_{di}^2 \sigma_{di} \left[\mathbf{i} \frac{X_i - X_{i-1}}{\ell_{di}} + \mathbf{j} \frac{Y_i - Y_{i-1}}{\ell_{di}} + \mathbf{k} \frac{Z_i - Z_{i-1}}{\ell_{di}} \right], \end{aligned} \quad (5.34)$$

where, when mass is conserved and evaporation neglected, the filament radii a_{ui} and a_{di} are given by

$$\pi a_{ui}^2 \ell_{ui} = \pi a_0^2 L_{el}, \quad (5.35a)$$

$$\pi a_{di}^2 \ell_{di} = \pi a_0^2 L_{el}, \quad (5.35b)$$

which is similar to Eq. (5.4).

The surface tension force acting on the i th bead, and tending to restore the rectilinear shape of the bending part of the jet, is given by

$$\mathbf{f}_{cap} = -\frac{\sigma \pi (a^2)_{av} k_i}{(X_i^2 + Y_i^2)^{1/2}} [\mathbf{i} |X_i| \text{sign}(X_i) + \mathbf{j} |Y_i| \text{sign}(y_i)], \quad (5.36)$$

where σ is the surface tension coefficient, k_i the jet curvature calculated using the coordinates of beads $(i-1)$, i and $(i+1)$, and $(a^2)_{av} = (a_{ui} + a_{di})^2/4$. The meaning of “sign” is as follows:

$$\text{sign}(x) = \begin{cases} 1, & \text{if } x > 0, \\ -1, & \text{if } x < 0, \\ 0, & \text{if } x = 0. \end{cases} \quad (5.37)$$

Setting the forces described in Eqs. (5.31), (5.33), (5.34) and (5.36) equal to mass times acceleration, according to Newton's second law, we obtain the

equation governing the radius vector of the position of the i th bead $\mathbf{R}_i = \mathbf{i}X_i + \mathbf{j}Y_i + \mathbf{k}Z_i$ in the following form:

$$m \frac{d^2 \mathbf{R}_i}{dt^2} = \sum_{\substack{j=1 \\ j \neq i}}^N \frac{e^2}{R_{ij}^3} (\mathbf{R}_i - \mathbf{R}_j) - e \frac{U_0}{h} \mathbf{k} + \frac{\pi a_{ui}^2 \sigma_{ui}}{\ell_{ui}} (\mathbf{R}_{i+1} - \mathbf{R}_i) - \frac{\pi a_{di}^2 \sigma_{di}}{\ell_{di}} (\mathbf{R}_i - \mathbf{R}_{i-1}) - \frac{\sigma \pi (a^2)_{av} k_i}{(X_i^2 + Y_i^2)^{1/2}} [\mathbf{i}|X_i|\text{sign}(X_i) + \mathbf{j}|Y_i|\text{sign}(Y_i)]. \quad (5.38)$$

For the first bead, $i = 1$, the total number of beads, N , is also 1. As more beads are added, N becomes larger and the first bead $i = 1$ remains at the bottom end of the growing jet. For this bead, all the parameters with subscript d should be set equal to zero since there are no beads below $i = 1$. Equation (5.38) is essentially a discretized form of Eq. (5.20b) or of its scalar counterparts, Eqs. (5.23a–f).]

It is easy to show that the aerodynamic drag force and gravity have a negligibly small effect on the electrospinning. Indeed, for an uncharged jet moving in air at high speed, an aerodynamically driven bending instability may set in if $\rho_a V_0^2 > \sigma/a$, where ρ_a is the air density, V_0 the jet velocity, and σ the surface tension coefficient (Entov and Yarin, 1984; Yarin, 1993). Taking, for example, $\rho_a = 1.21 \text{ kg m}^{-3}$, $V_0 \sim 0.5 \text{ m s}^{-1}$, $\sigma \sim 0.1 \text{ kg s}^{-2}$ and $a \sim 10^{-4} \text{ m}$, we estimate $\rho_a V_0^2 \sim 0.3 \text{ kg m} \cdot \text{s}^{-2}$, which is much smaller than $\sigma/a \sim 10^3 \text{ kg m} \cdot \text{s}^{-2}$. Therefore, under the conditions characteristic of the experiments on electrospinning, the aerodynamically driven bending instability does not occur.

The air drag force per unit jet length, which tends to compress the jet along its axis, is given by (Ziabicki and Kawai, 1985)

$$f_a = \pi a \rho_a V_0^2 0.65 \left(\frac{2V_0 a}{\nu_a} \right)^{-0.81}, \quad (5.39)$$

where ν_a is the air kinematic viscosity. The gravity force per unit length pulling the jet downward in the experimental geometry shown in Fig. 5.1 is

$$f_g = \rho g \pi a^2, \quad (5.40)$$

where ρ is the liquid density and g the acceleration due to gravity.

In the momentum balance, Eqs. (5.2) or (5.5b), we neglected f_g as a secondary effect. The air drag force f_a is even smaller than f_g . Taking $\rho_a = 1.21 \text{ kg m}^{-3}$, $\nu_a = 0.15 \times 10^{-4} \text{ m}^2 \text{s}^{-1}$, $\rho = 1000 \text{ kg/m}^3$, $V_0 = 0.5 \text{ m} \cdot \text{s}^{-1}$ and $a = 150 \mu\text{m}$ we obtain from Eqs. (5.39) and (5.40) $f_a = 1.4 \times 10^{-5} \text{ kg/s}^2$ and

$f_g = 6.9 \times 10^{-4} \text{ kg/s}^2$. The compressive stress along the jet axis of the air drag is negligibly small in comparison with the stretching due to gravity, and is much smaller than the stretching due to the electrical forces. Buckling of the electrospun jet due to the compressive force from air drag does not occur, since the electrical forces that tend to elongate the jet are larger and dominate any perturbation that might lead to buckling.

H. EVAPORATION AND SOLIDIFICATION

The systems of governing equations in Sections V.F and V.G do not account for the evaporation and solidification effects. We account for them in the present subsection.

In Ziabicki (1976), the following correlation is given for the Nusselt number for a cylinder moving parallel to its axis in air

$$\text{Nu} = 0.42 \text{ Re}^{1/3}, \quad (5.41)$$

where the Reynolds number $\text{Re} = V_0 2a / v_a$, a is the cross-sectional radius, and v_a the kinematic viscosity of air.

Taking the Prandtl number of air to be $\text{Pr} = 0.72$, we can generalize correlation (5.41) for an arbitrary value of the Prandtl number as

$$\text{Nu} = 0.495 \text{ Re}^{1/3} \text{ Pr}^{1/2}. \quad (5.42)$$

Similarly, to (5.42), we take the following correlation for the Sherwood number

$$\text{Sh} = 0.495 \text{ Re}^{1/3} \text{ Sc}^{1/2}, \quad (5.43)$$

where $\text{Sh} = h_m 2a / D_a$, h_m is the mass transfer coefficient for evaporation, D_a the vapor diffusion coefficient in air, and the Schmidt number $\text{Sc} = v_a / D_a$. The Sherwood number is the dimensionless mass transfer coefficient describing the evaporation rate.

Correlations of the type of Eqs. (5.41)–(5.43) are valid for air ($\text{Pr} = 0.72$) for Reynolds number in the range $1 \leq \text{Re} \leq 60$. For $a \leq 10^{-2} \text{ cm}$, $V_0 \sim 10^2 - 10^3 \text{ cm s}^{-1}$ and $v_a = 0.15 \text{ cm}^2 \text{ s}^{-1}$, the Reynolds number is $10 \leq \text{Re} \leq 10^2$ which corresponds approximately to the range of validity.

The initial mass of polymer in a jet element is given by

$$M_{p0} = \rho f_0 \lambda_0 \text{ ds } c_{p0}, \quad (5.44)$$

where c_{p0} is the initial polymer mass fraction. The variable solvent content in the element is

$$M_s = \rho f \lambda \, ds - \rho f_0 \lambda_0 \, ds \, c_{p0} \quad (5.45)$$

which corresponds to the solvent mass fraction

$$c_s = 1 - \frac{f_0 \lambda_0}{f \lambda} c_{p0}. \quad (5.46)$$

The solvent mass decreases due to evaporation according to the equation

$$\frac{\partial M_s}{\partial t} = -\rho h_m [c_{s,eq}(T) - c_{s\infty}] 2\pi a \lambda \, ds, \quad (5.47)$$

where $c_{s,eq}(T)$ is the saturation vapor concentration of solvent at temperature T , and $c_{s\infty}$ the vapor concentration in atmosphere far from the jet.

For water as a solvent, for example, Seaver et al. (1989) recommend the following expression for $c_{s,eq}(T)$:

$$c_{s,eq} = \frac{1}{1013} \{ a_0 + T[a_1 + T(a_2 + T(a_3 + T(a_4 + T(a_5 + a_6 T))))] \}, \quad (5.48)$$

$$\begin{aligned} a_0 &= 6.107799961, \\ a_1 &= 4.436518521 \times 10^{-1}, \\ a_2 &= 1.428945805 \times 10^{-2}, \\ a_3 &= 2.650648731 \times 10^{-4}, \\ a_4 &= 3.031240396 \times 10^{-6}, \\ a_5 &= 2.034080948 \times 10^{-8}, \\ a_6 &= 6.136820929 \times 10^{-11}, \end{aligned}$$

where T is taken in degrees Celsius.

Concentration $c_{s\infty}$ is equal to a relative humidity in the atmosphere.

Substituting Eqs. (5.43) and (5.45) into Eq. (5.47), we obtain the equation describing the variation of the jet volume

$$\frac{\partial f \lambda}{\partial t} = -D_a 0.495 \text{Re}^{1/3} \text{Sc}^{1/2} [c_{s,eq}(T) - c_{s\infty}] \pi \lambda. \quad (5.49)$$

Solvent mass decreases until the solvent mass ratio defined by Eq. (5.47) becomes small enough (say, $c_s = 0.1$), at which point the evaporation part of the calculation is stopped and viscosity remains a constant value. This cut-off can be rationalized by the assumption that further evaporation is reduced because the diffusion coefficient of solvent in the remaining polymer is small.

When evaporation is accounted for as per Eq. (5.49), the left-hand sides of Eqs. (5.20b), and (5.23a)–(5.23c) become, respectively

$$\rho \frac{\partial f \lambda \mathbf{V}}{\partial t}, \quad (5.50a)$$

$$\rho \frac{\partial f \lambda u}{\partial t}, \quad (5.50b)$$

$$\rho \frac{\partial f \lambda v}{\partial t}, \quad (5.50c)$$

$$\rho \frac{\partial f \lambda w}{\partial t}. \quad (5.50d)$$

Also the gravity term in Eq. (5.23c) should contain $f\lambda$ instead of $f_0\lambda_0$, since due to evaporation $f\lambda$ is not equal to $f_0\lambda_0$ any more.

If the discretized version of the model described in Section V.G is used, λ in Eq. (5.49) is replaced by the distance between two adjoining beads.

The local polymer mass ratio in the jet is given by

$$c_p = c_{p0} \frac{f_0 \lambda_0}{f \lambda}. \quad (5.51)$$

We account for the solidification process due to solvent evaporation employing the following correlation for the viscosity dependence on polymer concentration (Ziabicki, 1976)

$$\mu = 10^4 \times 10^{B c_p^m}, \quad (5.52)$$

with $m = 0.1$ to 1.

The value of parameter B is estimated as follows. According to Ziabicki (1976, p. 32), when c_p is doubled, viscosity of the solution increases by a factor of 10 – 10^2 . Using the value 10^2 and assuming that c_p increased from 0.1 to 0.2, we find for $m = 1$ that $B = 20$. The value of $B = 17.54$ corresponds to the factor of 10 and $m = 0.1$. Therefore the order of magnitude estimate of B yields the value $B = O(10)$. The value of A is unimportant, since the initial value of the viscosity $\mu_0 = 10^4 \times 10^{B c_{p0}^m}$ is

assumed to be known and is used for scaling. On the other hand, the relaxation time θ is proportional to c_p (Yarin, 1993). Therefore

$$\frac{\theta}{\theta_0} = \frac{c_p}{c_{p0}}, \quad (5.53)$$

where the initial relaxation time is known.

The modulus of elasticity $G = \mu/\theta$. Rendering the equations of the problem dimensionless, we obtain the rheological constitutive Eq. (5.25) in the following dimensionless form:

$$\frac{\partial \bar{\sigma}_{\tau\tau}}{\partial \bar{t}} = \bar{G} \frac{\partial \lambda}{\lambda \partial \bar{t}} - \frac{\bar{G}}{\bar{\mu}} \bar{\sigma}_{\tau\tau}. \quad (5.54)$$

Here G is rendered dimensionless by $G_0 = \mu_0/\theta_0$, and μ by μ_0 . Therefore,

$$\bar{G} = \frac{10^B (c_p^m - c_{p0}^m)}{c_p / c_{p0}}, \quad (5.55)$$

$$\bar{\mu} = 10^{B(c_p^m - c_{p0}^m)}, \quad (5.56)$$

with $B = O(10)$.

I. GROWTH RATE AND WAVELENGTH OF SMALL BENDING PERTURBATIONS OF AN ELECTRIFIED LIQUID COLUMN

In the works of Yarin (1993) and Entov and Yarin (1984), the theory of the aerodynamically driven jet bending was described. In that case, due to the jet curvature, a distributed lift force acts on the jet (because of the Bernoulli equation for airflow), which enhances perturbations and makes the perturbations grow. The aerodynamic bending force per jet length $d\xi$ in the case of small bending perturbations is given by (Entov and Yarin, 1984; Yarin, 1993)

$$\mathbf{F}_{\text{aer}} = -\rho_a V_0^2 \pi a_0^2 |k| \mathbf{n} d\xi, \quad (5.57)$$

where ρ_a is the air density, V_0 the jet velocity and a_0 the jet cross-sectional radius which does not change for small perturbations.

This force is the only difference between the aerodynamic- and electric-driven bending. Comparing Eq. (5.17) (with $e = e_0$) with Eq. (5.57), we see that all the results obtained in the above-mentioned references for the aerodynamic bending may also be used here in the case of electric bending, if

one replaces the factor $\rho_a V_0^2$ by $e_0^2 \ell n(L/a_0)/\pi a_0^2$. Dynamics of small bending perturbations was studied in the above-mentioned references accounting for the shearing force and moment in jet cross-section (thus, accounting for the bending stiffness in the equations generalizing Eq. (5.23)). For example, the case of viscous Newtonian fluid was considered. We recast these results here for the case of an electrified-liquid column of Newtonian fluid of viscosity μ . In particular, this generalizes the results of [Taylor \(1969\)](#) to the viscous case, and allows us to find the cut-off length L .

Recasting the results of [Yarin \(1993\)](#) and [Entov and Yarin \(1984\)](#), we find that the destabilizing electric force overcomes the stabilizing effect of the surface tension if

$$e_0^2 \ell n \left(\frac{L}{a_0} \right) > \pi a_0 \sigma. \quad (5.58)$$

If we assume $a_0 = 0.015 \text{ cm}$, and the jet charge of 1 C L^{-1} , then $e_0 = 2120.5 \text{ (g cm)}^{1/2} \text{ s}^{-1}$. Below, we show that a reasonable value of L is $L = 0.0325 \text{ cm}$. Using it for the estimate, we find that $e_0^2 \ell n(L/a_0) = 3.465 \times 10^6 \text{ g cm s}^{-2}$, whereas $\pi a_0 \sigma = 3.3 \text{ g cm s}^{-2}$ for $\sigma = 70 \text{ g s}^{-1}$. Therefore, in this case the inequality (5.58) definitely holds and the bending instability should set in and grow.

From the results of [Yarin \(1993\)](#) and [Entov and Yarin \(1984\)](#), we obtain in the present case that the wavenumber χ_* and the growth rate γ_* of the fastest growing bending perturbation are given by

$$\chi_* = \left\{ \frac{8 \rho a_0^2}{9 \mu^2} \left[\frac{e_0^2 \ell n(L/a_0)}{\pi a_0^2} - \frac{\sigma}{a_0} \right] \right\}^{1/6}, \quad (5.59a)$$

$$\gamma_* = \frac{[e_0^2 \ell n(L/a_0)/\pi a_0^2 - \sigma]^{2/3}}{(3 \mu \rho a_0^4)^{1/3}}. \quad (5.59b)$$

Here $\chi_* = 2\pi a_0 / \ell_*$, where ℓ_* is the wavelength of the fastest growing perturbation.

Results (5.59) correspond to the maximum of the spectrum $\gamma(\chi)$ given by the characteristic equation

$$\gamma^2 + \frac{3 \mu \chi^4}{4 \rho a_0^2} \gamma + \left[\frac{\sigma}{\rho a_0^3} - \frac{e_0^2 \ell n(L/a_0)}{\pi \rho a_0^4} \right] \chi^2 = 0. \quad (5.60)$$

This equation is to be compared with the characteristic equation for electrically driven bending perturbations of an inviscid liquid ($\mu = 0$) column derived by [Taylor \(1969, his Eq. \(12\)\)](#). Expanding that equation in

the long-wave limit as the dimensionless wavenumber $\chi \rightarrow 0$, we find that it reduces to Eq. (5.60) with the term $\ell n(1/\chi_*)$ instead of $\ell n(L/a_0)$. This fact defines the cut-off length L , since the result of Taylor (1969) is exact. Thus, taking $\ell n(L/a_0) = \ell n(1/\chi_*)$ and neglecting the minor surface tension effect in Eq. (5.59a), we reduce the latter to the form

$$\chi_* = \left[\frac{8}{9} \frac{\rho}{\mu^2} \frac{e_0^2}{\pi} \ell n \left(\frac{1}{\chi_*} \right) \right]^{1/6}, \quad (5.61)$$

which is the equation defining χ_* (and thus, L). Taking the same values of the parameters as before, as well as $\rho = 1 \text{ g cm}^{-3}$ and $\mu = 10^4 \text{ g (cm s)}^{-1}$ (remember that $e_0 = 2120.5 \text{ (g cm)}^{1/2} \text{ s}^{-1}$), we reduce Eq. (5.61) to the form

$$\chi_* = 0.483 \left[\ell n \left(\frac{1}{\chi_*} \right) \right]^{1/6} \quad (5.62)$$

which yields $\chi_* = 0.462$.

Therefore, the wavelength of the fastest growing perturbation $\ell_* = 2\pi 0.015/0.462 = 0.204 \text{ cm}$, and the cut-off length $L = \ell_*/2\pi = 0.0325 \text{ cm}$. Comparing the latter with the jet cross-sectional radius $a_0 = 0.015 \text{ cm}$, we see that the cut-off length is very short, of the order of a_0 .

Based on the results of Yarin (1993) and Entov and Yarin (1984), it also follows that the bending perturbations of highly viscous liquids grow much faster than the capillary ones (driven by the surface tension), if the condition

$$\frac{\pi\mu^2}{\rho e_0^2 \ell n(L/a_0)} \gg 1 \quad (5.63)$$

is fulfilled. For the values of the parameters used in the present subsection, the left-hand side of Eq. (5.63) is equal to 90.7, which shows that inequality (5.63), indeed, holds. Therefore, such a jet bends with a nearly constant radius.

J. NON-LINEAR DYNAMICS OF BENDING ELECTROSPUN JETS

To model the way a spatial perturbation develops, we denote the last bead pulled out of the pendant drop and added at the upper end of the jet by $i = N$. When the distance $\ell_{d,N}$ between this bead and the pendant drop becomes long enough, say, $h/25,000$, a new bead $i = N+1$ is inserted at a

small distance, say, $h/50,000$, from the previous one. At the same time a small perturbation is added to its x and y coordinates,

$$X_i = 10^{-3} L_{\text{el}} \sin(\omega t), \quad (5.64\text{a})$$

$$Y_i = 10^{-3} L_{\text{el}} \cos(\omega t). \quad (5.64\text{b})$$

Here, ω is the perturbation frequency. The condition that the collector at $z = 0$ is impenetrable is enforced numerically, and the charge on each element of the jet is removed as it arrives at the collector. Such a calculation mimics the development of the electrically driven bending instability. The calculation begins with only two beads, $N = 2$. As the jet flows, the number of beads in the jet, N , increases. In the cases when evaporation and solidification were not accounted for, the system of Eqs. (5.30) and (5.38) was solved numerically, assuming that the stresses σ_{ui} and σ_{di} , and the velocity $d\mathbf{R}_i/dt$ were zero at $t = 0$. The equations were made dimensionless by the same scale factors as those in Section V.C. Since here it is necessary to account for the surface tension and for the perturbing displacements, two new dimensionless groups emerge in addition to those of Eqs. (5.6)

$$A = \frac{\sigma \pi a_0^2 \mu^2}{m L_{\text{el}}^2 G^2}, \quad (5.65\text{a})$$

$$K_s = \omega \mu / G. \quad (5.65\text{b})$$

The last dimensionless group needed in this case is formed by dividing the distance h , from the collector to the pendant droplet, by L_{el} ,

$$H = \frac{h}{L_{\text{el}}}. \quad (5.66)$$

In cases when evaporation and solidification are accounted for, all the dimensionless groups of Eqs. (5.6), (5.65) and (5.66) now contain μ_0 and G_0 . Two new dimensionless groups appear: the Deborah number

$$\text{De} = \frac{\mu_0 / G_0}{a_0^2 / D_a} \quad (5.67)$$

representing the ratio of the relaxation time $\theta_0 = \mu_0/G_0$ to the diffusional characteristic time a_0^2/D_a , and

$$\delta = \frac{L_{\text{el}} a_0}{(\mu_0/G_0) v_a}. \quad (5.68)$$

The latter, as well as A in Eq. (5.65a) and H , in Eq. (5.66), is based on the “electric” characteristic length L_{el} introduced in Section V.C. The group δ is involved in the calculation of the Reynolds number Re introduced in Section V.H.

1. Jet Path Calculated for the Electrically Driven Bending Instability without Accounting for Evaporation and Solidification

Now consider the development of small perturbations into a bending instability in a jet without accounting for evaporation and solidification. We estimate the charge carried by the jet to be 1 C L^{-1} , which is of the same order as the values measured in Fong *et al.* (1999). We also estimate that the relaxation time θ is 10 ms, a_0 is $150 \mu\text{m}$, ρ is 10^3 kg/m^3 , h is 2 m, U_0 is 10 kV, σ is 0.07 kg s^{-2} , and μ is $10^3 \text{ kg (m s)}^{-1}$. The value of μ is taken to be much larger than the zero-shear viscosity μ_0 reported in Fong *et al.* (1999), since the strong longitudinal flows we are dealing with in the present work lead to an increase, by several orders of magnitude, of the elongational viscosity from μ_0 (Chang and Lodge, 1972; de Gennes, 1974; Yarin, 1990, 1993). The assumption is actually immaterial, as the results in Section V.K show. The dimensionless parameters are as follows: $Q = F_{\text{ve}} = 78359.6$, $V = 156.7$, $A = 17.19$ and $H = 626.9$. The length scale is $L_{\text{el}} = 3.19 \text{ mm}$. The charge on the bead $e = 8.48(\text{g}^{1/2}\text{cm}^{3/2})/\text{s} = 2.83 \times 10^{-9} \text{ C}$. The mass on each bead is $m = 0.283 \times 10^{-8} \text{ kg}$. The value of K_s is taken as 100. Since $\theta = \mu/G = 10 \text{ ms}$, this value corresponds to $\omega = 10^4 \text{ s}^{-1}$, which is in the frequency range of typical noise in the laboratory.

Figs. 5.30(a)–(e) illustrate the development of a typical jet path. The time periodic perturbation, Eqs. (5.64), that grows along the jet develops non-linear loops of the bending instability. The jet flows continuously from the pendant drop in response to the electric field established by the externally applied potential between the droplet and the collector. This electric field also causes the jet to be charged as it leaves the pendant drop. At $\tilde{t} = 0.99$ in Fig. 5.30(e) the instantaneous path of the jet is similar to the patterns recorded in experiments using a high-speed video camera such as those

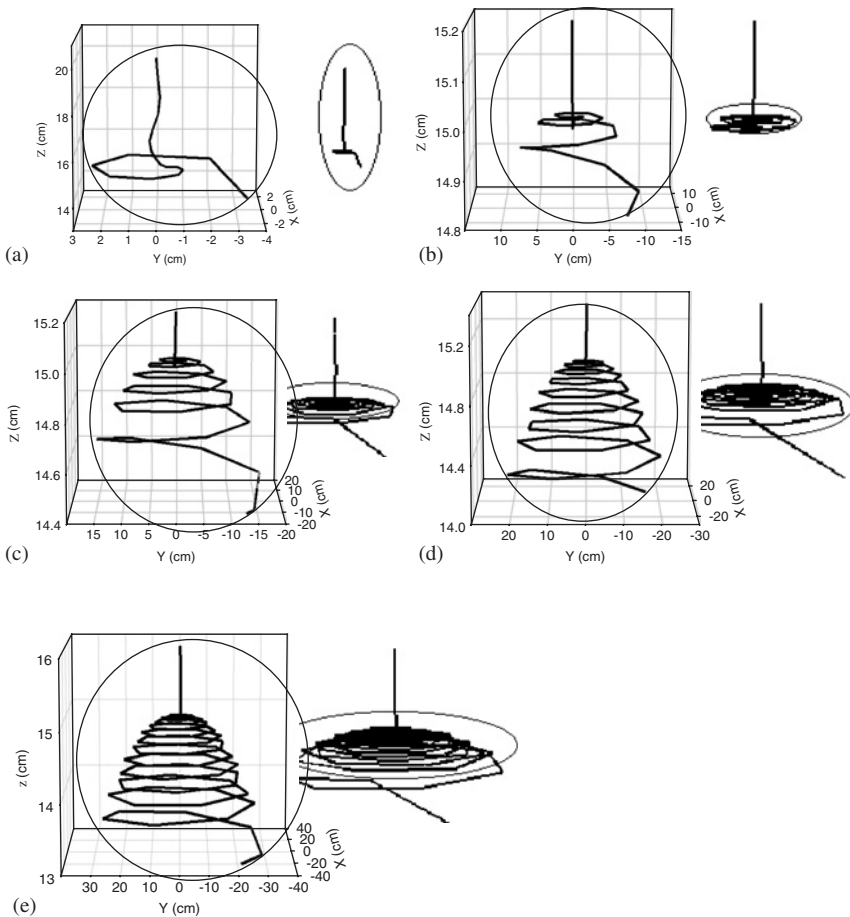


FIG. 5.30. Perturbations develop into a bending instability. The dimensionless groups have the following values: $Q = F_{ve} = 78359.6$, $V = 156.7$, $A = 17.19$, $K_s = 100$, $H = 626.9$. (a) $\bar{t} = 0.19$, (b) 0.39, (c) 0.59, (d) 0.79 and (e) 0.99. After [Reneker et al. \(2000\)](#) with permission from AIP.

shown in Fig. 5.2. It is emphasized that the stresses σ_{ui} and σ_{di} are positive along the entire jet in Figs. 5.30(a)–(e), which means that the whole jet is stretched continuously.

In Fig. 5.30, a long segment near the vertex of the envelope cone is plotted in the x , y and z coordinates at various times and scales to show details of the jet path. The entire length of both the straight segment and the spiral part is shown at the same scale in the inset at the upper right of each part of Fig. 5.30. An ellipse in each inset encloses the part of the jet path shown in

the corresponding coordinate box. The pendant drop was always at $x = 0$, $y = 0$ and $z = h$.

The experimental evidence shows a self-similar, fractal-like process of development of the electrically driven bending instabilities. The diameter of the first generation of bending loops becomes larger and the jet becomes thinner. Then much smaller bending perturbations set in on these loops and begin to grow also. This self-similar process continues at smaller and smaller scales until viscoelastic force, surface tension or solidification of the jet arrest further bending. The numerical results in Fig. 5.30 describe only the emergence and growth of the first cycle of the loops. This is a consequence of the fact that the distances between the beads increase enormously in the simulation of the development of the first cycle. No new beads were added except at the top of the rectilinear segment. Therefore, the capability of the computer code to elucidate smaller details in the path decreases as the jet elongates enormously.

Fig. 5.31 shows the path of a charged jet calculated from a realistic but different set of dimensionless parameters and perturbations than was used in Fig. 5.30. The path displays a bending instability generally similar to that shown in Fig. 5.30.

To show that the bending instability is driven by the Coulomb interaction, the charge e on the beads is taken to be zero so that $Q = 0$. The electrical

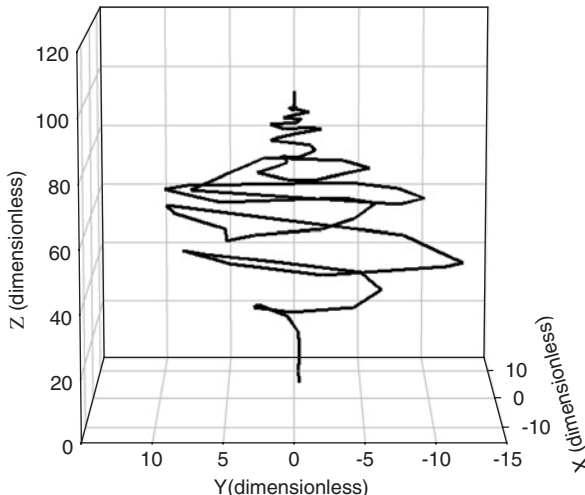


FIG. 5.31. Charged jet with values of the dimensionless parameters that are realistic but different from those used in Fig. 5.30. $Q = F_{ve} = 12$, $V = 2$, $A = 0.9$, $K_s = 100$, $H = 100$, $\tilde{t} = 4.99$. After Reneker et al. (2000) with permission from AIP.

driving force for the bending instability is then zero, but the other parameters are exactly the same as those in Fig. 5.31. If a jet were to be pulled downward by gravity, which can supply a downward component of force that acts on the segment in the same way as the downward component of the electrical force from the electrical field, one would expect the uncharged jet to be almost straight in spite of the small perturbations applied to it, since the perturbations would not develop into a bending instability. The calculated result with the same parameters as those in Fig. 5.31, but $Q = 0$, is in fact a straight jet growing downward, even at a later time ($\tilde{t} = 8.99$). Increasing the ratio of the surface tension to the Coulomb force also stabilizes a charged jet. If A is increased to 9, by increasing the surface tension while all the other parameters are kept the same as those in Fig. 5.31 practically no bending occurs. The results for the gravity driven jet and for the high-surface tension jet are not shown because the calculated jet path cannot be distinguished from a straight line at the scale in Fig. 5.31.

2. Jet Path Calculated for the Electrically Driven Bending Instability Accounting for Evaporation and Solidification

As was shown in Section V.J.1, the qualitative pattern of the jet behavior in the electrospinning process can be drawn without accounting for evaporation and solidification. A quantitative comparison with experiment can be made only accounting for evaporation and solidification. Such a comparison is the aim of the following sections. Also, a comparison between the results obtained with and without accounting for evaporation and solidification will be made here.

Calculations of the present work were done for an aqueous solution with an initial 6% concentration of PEO studied experimentally as described in Section V.B. The following values of the dimensional parameters were established: the initial cross-sectional radius $a_0 = 150 \mu\text{m}$ the density $\rho = 10^3 \text{ kg m}^{-3}$, the surface tension $\sigma = 0.07 \text{ kg s}^{-2}$, the initial viscosity $\mu_0 = 10^3 \text{ kg (m \cdot s)}^{-1}$, the initial relaxation time $\theta_0 = 10 \text{ ms}$, the charge density 1 C L^{-1} and the distance to the collecting plate $h = 20 \text{ cm}$. In the calculations of the present work, we took the field strength $U_0/h = 1.5 \text{ kV m}^{-1}$. In the experiment the electric field was 50 kV m^{-1} . The values of the dimensionless groups introduced in Eqs. (5.6), (5.65) and (5.69) are now based on the initial values of the dimensional parameters and are equal to $Q = F_{\text{ve}} = 78359.57$, $V = 47.02$, $A = 17.19$, $K_S = 100$ and $H = 626.88$, whereas $L_{\text{el}} = 0.319 \text{ cm}$. We also took the humidity of 16.5%, $c_{\text{s}\infty} = 0.165$, and the temperature of 20°C . The best representation

of the envelope cone of the bending loops (see below) was found at $B = 7$ and $m = 0.1$ in the solidification law (5.52), (5.55) and (5.56), which agrees with the estimates known from the literature and those discussed in the previous sections. These values were used in the present calculations.

Fig. 5.32(a) shows the path of the jet accounting for evaporation and solidification, whereas Fig. 5.32(b) was calculated without accounting for

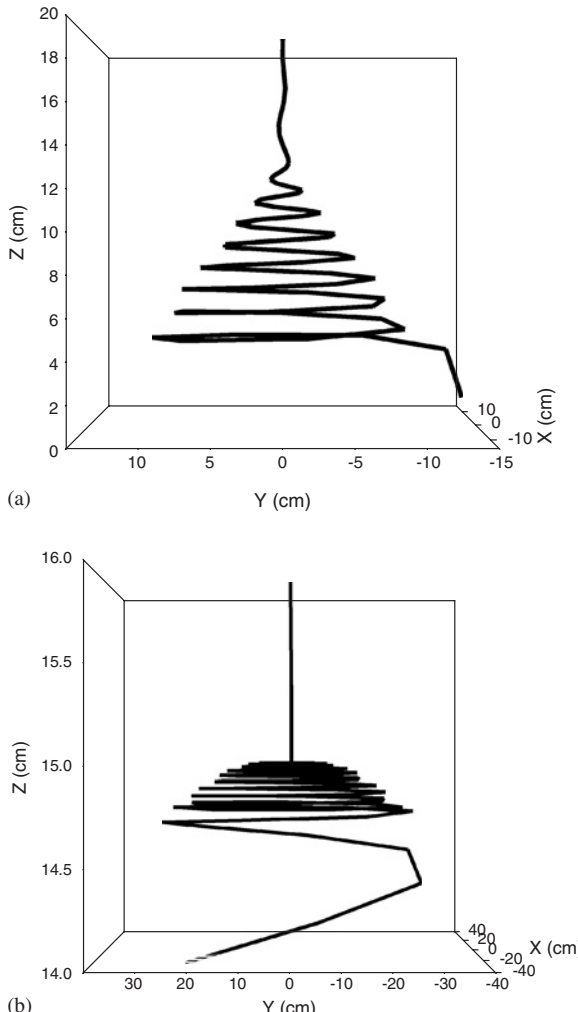


FIG. 5.32. (a) Jet path calculated accounting for evaporation and solidification. (b) Jet path calculated without accounting for evaporation and solidification. After Yarin et al. (2001a) with permission from AIP.

these effects. Owing to evaporation and solidification each loop of the jet becomes more viscous with time, and its elastic modulus increases. As a result, the resistance to bending increases, and the radius of the bending loops in Fig. 5.32(a) (with evaporation and solidification) is smaller than that of Fig. 5.32(b) (without evaporation and solidification). The radius of the bending perturbations of the jet calculated accounting for the evaporation and solidification effects is well comparable with that found in the experiment (cf. Fig. 5.2), which is illustrated in the following section.

3. Envelope Cone

Shape of the envelope cone can be easily seen by a naked eye, or using a camera with long exposure time (cf. Fig. 5.33). The two bright lines bifurcating in Fig. 5.33 from a point emphasized by the arrow resulted from a specular reflection of light from segments near the maximum lateral excursion of each loop. Each loop moved downward during a long exposure time of the camera and created the bright lines seen in Fig. 5.33, which define the envelope cone of the bending jet during the electrospinning process. For comparison with the results of the calculations, the generatrix of the envelope cone in Fig. 5.33 is also represented in Fig. 5.34.

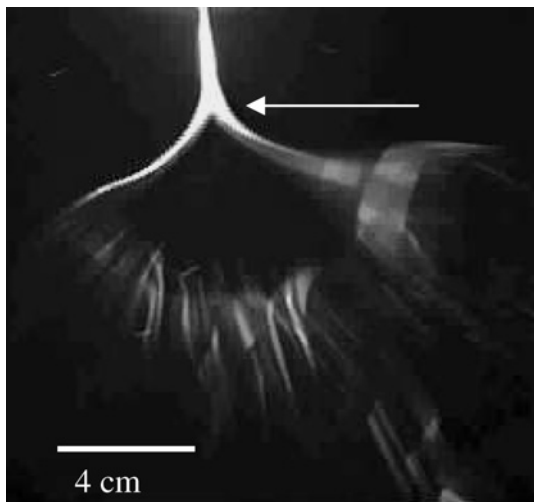


FIG. 5.33. Shape of the envelope cone created by the electrically driven bending instability. The complicated image in the lower part of the figure is a consequence of the long exposure time (~ 16 ms) used to observe the envelope cone, and the time varying path of the jet in that region. After Yarin et al. (2001a) with permission from AIP.

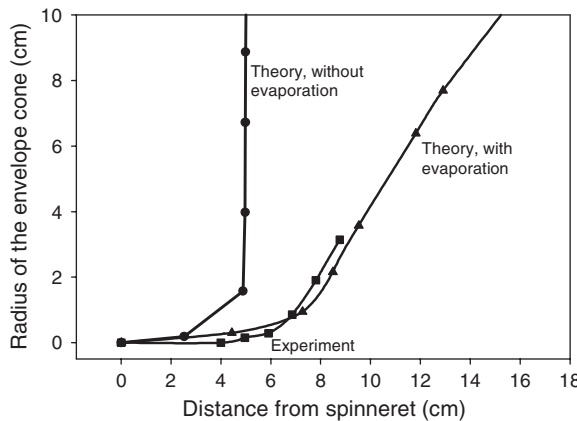


FIG. 5.34. Shape of the envelope cone: experiment vs. theory. Points show calculated radii of successive loops. Experimental points were measured from a photograph. After Yarin *et al.* (2001a) with permission from AIP.

The calculations showed that the evaporation and solidification have a strong effect on the predicted shape of the envelope cone. Two theoretical curves: without evaporation and solidification, and with these effects accounted for ($m = 0.1$) are presented in Fig. 5.34. It is clearly seen that the result accounting for evaporation and solidification agrees fairly well with the experimental data.

The envelope visible in the experiment does not extend beyond a radius of about 3 cm, whereas the theory allowed for further growth of a radius until 10 cm. The reason may be that after the jet had solidified in the experiment, it became much more rigid, i.e. unstretchable. On the other hand, in the theoretical calculations the solidified jet is still described as a liquid (albeit highly viscous, with a high-elastic modulus), which still allows for some additional stretching. Actually, the comparison in Fig. 5.34 shows that the calculations should be stopped as the radius of the envelope cone has achieved the value of 3–4 cm.

4. Jet Velocity

Downward velocity in the electrified jet was measured by following the downward motion of a loop. The comparison of the experimental and theoretical results is shown in Fig. 5.35. The velocity is practically independent on time in both experiment and theory. The theoretical value of the velocity overestimates the measured value by a factor of four. Given the fact that the values of several governing parameters used in the experiments are only an order of magnitude estimates, the discrepancy represented by the factor of four is not dramatic.

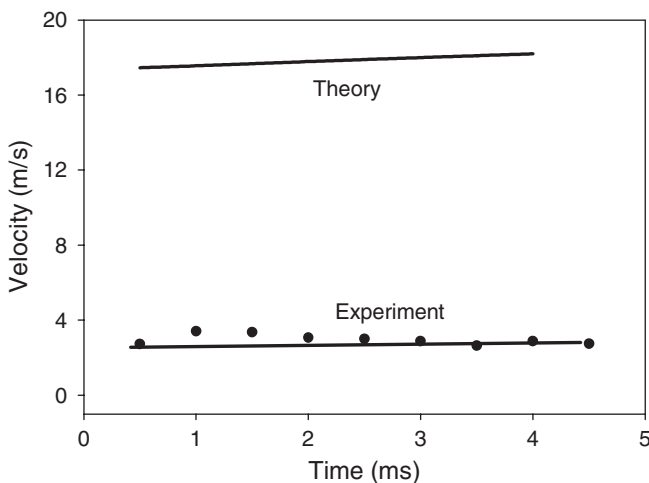


FIG. 5.35. Downward velocity of the jet: experiment vs. theory. $B = 7$, $m = 0.1$. After Yarin et al. (2001a) with permission from AIP.

5. Elongation and Drying of the Jet

The theoretical results suggest that the stretching of material elements along the jet makes it possible to achieve very high draw ratio values in the electrospinning process. In the calculation the initial distance between two successive beads was 3.99×10^{-4} cm, whereas the final distance was 13.92 cm. Assuming that the initial polymer concentration in the jet was 6%, the cross-sectional radius of a dry fiber (a_f), after elongation and solvent evaporation have been completed, is related to the initial radius of the jet (a_0), by the material balance equation

$$\pi a_f^2 13.92 = \pi a_0^2 3.99 \times 10^{-4} \times 0.06. \quad (5.69)$$

For $a_0 = 150 \mu\text{m}$ this yields $a_f = 196.7 \text{ nm}$. The corresponding draw ratio due to elongation is equal to $(a_0/a_f)^2 0.06 = 34815$. It is emphasized that if the jet would be straight and stationary, like in the ordinary fiber spinning processes, the ratio of the fiber velocity at the winding bobbin V_f to the initial one in the spinline V_0 becomes

$$V_f = V_0 \frac{\pi a_0^2 0.06}{\pi a_f^2} = 34815 V_0. \quad (5.70)$$

For the experimentally measured value of $V_0 \cong 0.1 \text{ m s}^{-1}$ the velocity V_f would be

$$V_f = 3481.5 \text{ m s}^{-1} = 10 \text{ (speed sound)} \quad (5.71)$$

Obviously, this is not true. The paradoxical value of V_f in Eq. (5.71) results from the fact that huge elongation of the fiber cannot be achieved at the distance of about 10 cm along a straight line. The electrically driven bending instability supplies the mechanism of strong elongation via fractal-like looping which allows reduction of the final radius a_f to the range of nanofibers, even though $V_f \cong 1 \text{ m s}^{-1}$.

Fig. 5.36 shows the trajectories of two successive beads of the jet in the course of electrospinning. The trajectories are shown by solid lines, and the positions of the beads by black squares and circles. The lines that have longer dashes connect the positions of the adjacent beads. To simplify, not every connection is shown. The projections of the dashed line onto the X - Y plane are shown by the lines with shorter dashes. The X - Y projections of the bead positions are shown by gray squares or circles. The dashed lines

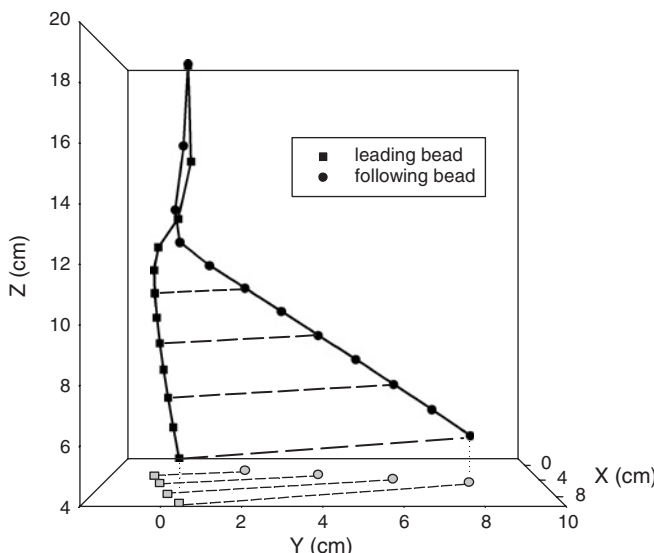


FIG. 5.36. Stretching of a segment of the jet. Each solid line represents a trajectory of one of the two successive beads. The dashed lines represent the segment of the jet between the successive beads. The length of the segment increases with time as a result of the jet stretching during the course of electrospinning. $B = 7$, $m = 0.1$. The projections of the bead positions onto the X - Y plane are shown by the gray symbols. After [Yarin et al. \(2001a\)](#) with permission from AIP.

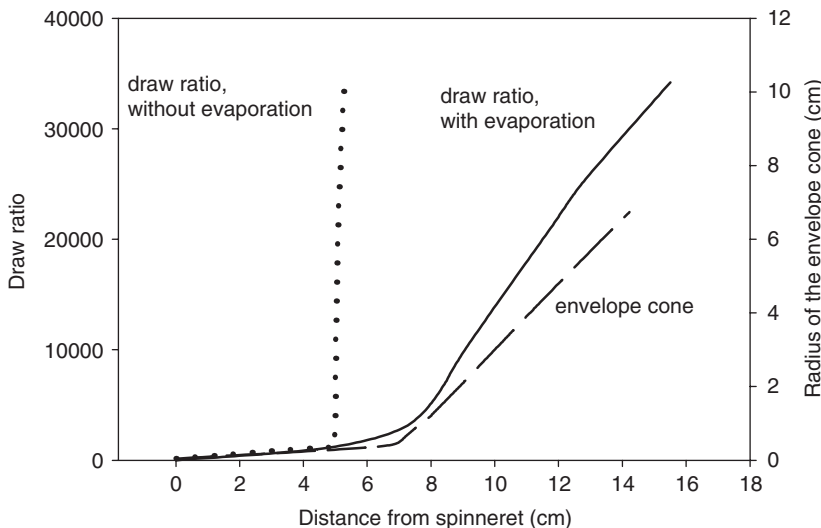


FIG. 5.37. Calculated draw ratio of a segment of the jet along its length. $B = 7$, $m = 0.1$. The dotted line was generated using the results not accounting for evaporation and solidification. After Yarin et al. (2001a) with permission from AIP.

connecting the two beads at a given time represent the elongating segment. Its increase in length, illustrates stretching of the jet element between the two beads. The initial distance between the beads was 3.99×10^{-4} cm, as mentioned above. The time interval covered by Fig. 5.36 is 6.5 ms. A corresponding draw ratio is shown in Fig. 5.37 versus the vertical distance of the segment from the tip. It is instructive to see the envelope cone, too (the dashed line in Fig. 5.37), since it shows where the draw ratio grows.

Along the straight part of the jet, which is about 6 cm long, the draw ratio achieves a value of about 1000. In the bending loops inside the envelope cone the draw ratio increases by another factor of 25, to the value of 25,000. Without evaporation and solidification being accounted for in the model, the draw ratio extracted from the calculation increased very rapidly, as shown in Fig. 5.37.

6. Viscosity Profile in the Bending Jet

The distribution of the viscosity along the jet at $t = 6$ ms is shown by solid line in Fig. 5.38. Viscosity slowly increases along the straight part of the jet. When bending perturbations begin to grow rapidly, velocity of the motion increases, and the evaporation process strongly intensifies. It is clearly seen

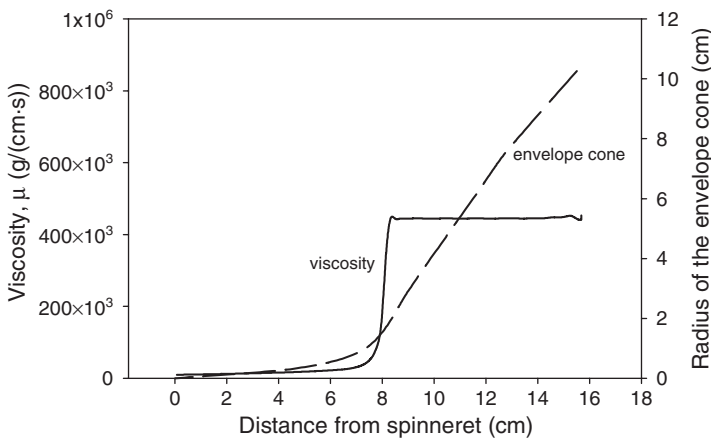


FIG. 5.38. Calculated viscosity along the jet; $t = 6\text{ ms}$, $B = 7$ and $m = 0.1$. The calculated radius of the envelope cone continued to grow after the viscosity reached the plateau. After Yarin *et al.* (2001a) with permission from AIP.

when comparing the viscosity profile with that of the envelope cone shown in Fig. 5.38 by the dashed line. Fast evaporation strongly increases the polymer fraction in the jet, which leads to solidification manifested by the appearance of the high-viscosity plateau at a distance of about 2 cm from the beginning of the envelope cone. The calculation showed that at the beginning of the plateau, nanofibers have already been formed, since the cross-sectional radius of the fiber is already about 640 nm.

7. Longitudinal Strain Rate and Molecular Orientation

The high value of the area reduction ratio and the associated high longitudinal strain rate imply that the macromolecules in the nanofibers should be stretched and axially oriented. Most electrospun nanofibers, even those made from a styrene–butadiene–styrene triblock copolymer, are birefringent (Fong and Reneker, 1999).

The longitudinal strain rate was different at different places along the jet. The longitudinal strain rate for three different parts of the jet was determined.

- (1) The jet velocity in the downward direction was determined from the sequential images by determining the velocity of particular

maxima of the growing bending instability and the length of the straight segment. The length of the straight segment (L_z) was 5 cm and the velocity was 1 m s^{-1} . Therefore, the longitudinal strain rate was $(\delta L_z/L_z \delta t)$,

$$\delta L_z/L_z \delta t = V \delta t/L_z \delta t = V/L_z = (1 \text{ m s}^{-1})(1/0.05 \text{ m}) = 20 \text{ s}^{-1}, \quad (5.72)$$

which is a rough estimate of the strain rate in the straight segment of the jet. Detailed measurements shown in Fig. 5.18 yield the values of the order of several hundreds reciprocal seconds.

- (2) The observation of expanding loops provided a second measure of the longitudinal strain rate for the segment that formed the loop. A typical loop grew from a diameter of 1 to 8 mm in 7 ms. The resulting longitudinal strain rate in such a loop was 1000 s^{-1} .
- (3) The overall longitudinal strain rate can be estimated using the data in Section V.J.5. The time that a typical segment of the electrospun jet is in flight (δt) can be estimated as the distance between the pendant droplet and the collector (20 cm) divided by the average downward velocity of the jet (1 m s^{-1}). The resulting δt is 0.2 s. The longitudinal strain rate is $\delta\zeta/(\delta t \cdot \zeta)$, where ζ is the initial segment length, and $\delta\zeta$ is the growth in length. Since $\delta\zeta$ is much greater than ζ , $\delta\zeta$ is approximately the final segment length. The ratio $\delta\zeta/\zeta$ was around 10^5 , and therefore the longitudinal strain rate was around $0.5 \times 10^6 \text{ s}^{-1}$. Using the estimate, Eq. (5.72), we find that in the straight segment the length of a liquid element has been approximately doubled, and the cross-sectional radius decreased by a factor of four. Then the longitudinal strain rate in the loops becomes of the order of 10^5 s^{-1} . The actual value will be lower due to the effects of evaporation and solidification.

Theory suggests that the transformation from a random coil to a stretched macromolecule occurs when the strain rate multiplied by the conformational relaxation time of the molecule is greater than 0.5 (Chang and Lodge, 1972; de Gennes, 1974). Since the relaxation time of the polymer solution is about 0.01 s – 0.1 s , then $\delta\zeta/(\delta t \cdot \zeta)$ multiplied by the relaxation time was equal to 10 – 10^4 , which is much greater than 0.5. Therefore, the longitudinal flow in the electrospun jet is strong, and the macromolecules are likely to be stretched in the direction of the jet axis.

8. Theory of Branching on Electrospun Jets

An infinitely long static jet of incompressible fluid with a uniform circular cross-section, in a radial electric field, is the theoretical model used in [Yarin et al. \(2005\)](#) as a starting point to describe a mechanism that leads to quasi-periodic branching of an electrospinning jet. This approximation is related to the fact that branching takes place on the background of bending, albeit quite independently of it (cf. Section V.B.2). The electrical conductivity is supposed to be large enough to assume that excess charge is always at the surface.

The surface of the jet can respond to the presence of the electrical Maxwell forces in the following interesting way. If any element of the charged surface moves outward in response to the electrical forces, the motion of that element will extract energy from the electrical field, in order to form a “hill”. The lateral surface area associated with the growing hill must increase because volume is conserved, since flow from the ends cannot occur in an infinitely long jet of incompressible fluid. The energy required to form the undulating surface of hills, saddle points and valleys is provided by the electric field. The resulting static undulations may be quite complicated. The distribution of electrical charge on the surface of the jet is similarly complicated.

Consider a segment of a cylindrical fluid jet with a straight axis surrounded by a coaxial hollow cylindrical electrode. The liquid in the jet is assumed to be a perfect electrical conductor, which means that the time intervals required for changes in the shape of the surface are much longer than the characteristic charge relaxation time τ_C , which is of the order of 0.155×10^{-2} ms for acetone. If the jet were to be a perfect non-conductor of electricity, the redistribution of charge on the surface that is required to stabilize an undulating surface by an intricate balance of electrical and surface tension forces might not be possible.

Assume that the surface of the jet is kept at an electrical potential $\varphi = 0$, and the concentric cylindrical electrode is kept at $\varphi = \varphi_0$. Note that for a solid circular cylinder, this condition defines both the charge per unit area and the electric field normal to the surface of the cylinder, which are parameters often used in electrical engineering and physics to characterize the electrostatic conditions of this coaxial geometry, but that approach does not encompass the changes in the shape of the surface that are considered in this section.

To find a mathematical expression for these undulating shapes, the solution of the partial differential equation that describes the shape of the

surface of the jet and the electric field in the linear approximation is written as a two-dimensional Fourier series that depends on the azimuthal angle and the distance along the axis of the jet. Substituting the assumed Fourier series into the partial differential equation, and using the boundary conditions to evaluate the coefficients of the various terms in the Fourier series leads to the identification of terms in the series that are in equilibrium, static and non-zero. The sum of these non-zero modes determines the shape of the undulating surface of the jet. Since only a subset of the Fourier modes is static, there is a finite wavelength associated with the static mode that has the longest wavelength along the axis.

In the stability analysis in [Yarin et al. \(2005\)](#), which is related to the earlier results of [Saville \(1971\)](#) and [Yarin \(1979\)](#), it is argued that the longest allowed static wavelength along the jet axis leads to the observed quasi-regular spacing of the branches.

A smooth jet with a circular cross-section is the only stable shape at low electrical potential differences. Not every undulating shape can occur in equilibrium as the potential is increased, but some static undulations of the jet surface inevitably occur. Near the highest peaks of the static undulations, shape perturbations, which increase the radius of curvature (cf. [Fig. 5.39](#)), grow rapidly and give rise to branching.

The calculations were made for all four potentials for which measurements were made, and the predicted branch spacings ℓ_N are compared with the measured ones in [Table 5.3](#) ([Yarin et al., 2005](#)). The predictions at the higher voltage values (7.5 and 10 kV) are commensurate with the measurements. The comparison at the lower voltage values is not so good, especially at 5 kV, which might be related to the wide distribution of observed spacings at the lower voltage values caused by variations (perhaps a factor of 2) due to the elongation of the distance between branches that occurs after the branches start growing. The experimentally observed spacing distributions at 7.5 and 10 kV suggest narrower distributions of the distance between branches.

K. MULTIPLE-JET ELECTROSPINNING

Electrospinning of multiple, mutually interacting jets was investigated in [Theron et al. \(2005\)](#). Several experimental settings were used. In the first set-up nine identical syringes, containing identical solutions, were arranged in a 3×3 matrix ([Fig. 5.40\(a\)](#)). In the second, the set-up in [Fig. 5.40\(b\)](#), nine and seven syringes were arranged in a row. Numerical simulation of the multiple-jet electrospinning was conducted within the framework the model described in Sections V.C–V.J.

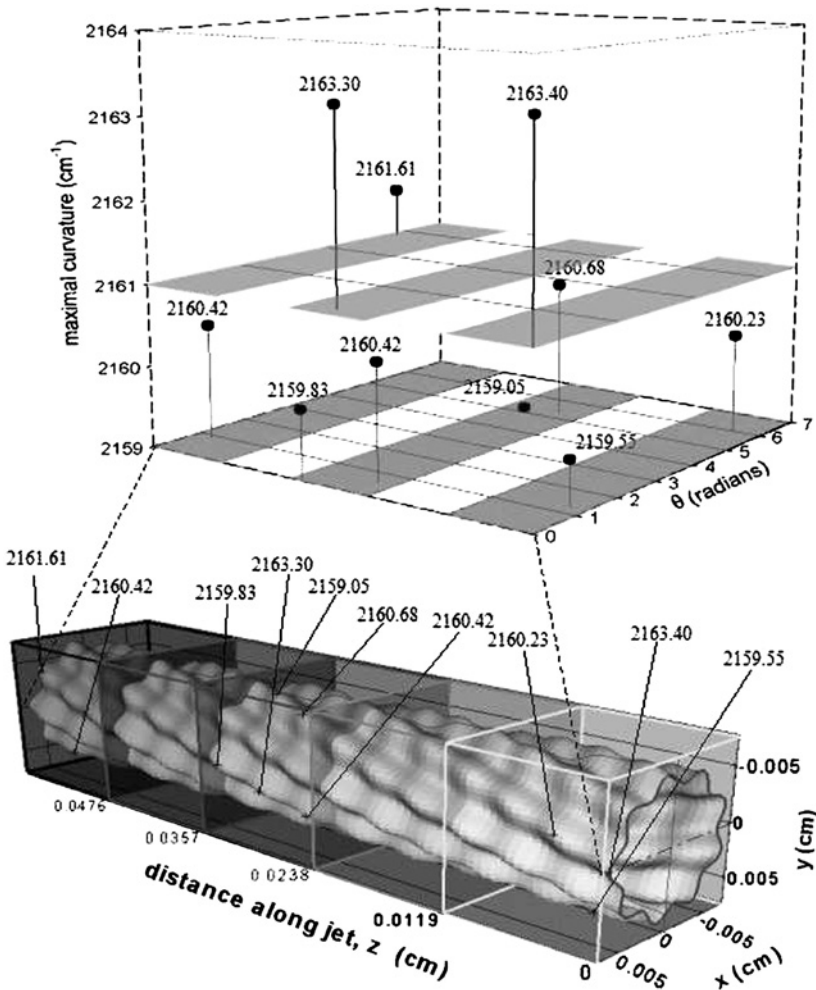


FIG. 5.39. The lower part shows a shaded perspective drawing of 5 cycles of the longest wavelength mode on the calculated surface of the jet, for $\phi_0 = 5$ kV, with the dimensionless undulation amplitudes of the modes involved $\tilde{\zeta}_2 = 0.03$ and $\tilde{\zeta}_9 = 0.1$, and $\tilde{\zeta}_n = 0$ for $n = 3-8$. Each cycle is equal to ℓ_9 in length with ℓ_9 being the wavelength of the 9th mode. The maximum curvatures in the cross-sections along the jet were also calculated and values of the highest curvatures were plotted on the “unrolled” θ, z surface in the upper part of the figure. The locations of the highest curvatures of the surface are identified by arrows in the shaded drawing. In the θ, z planes for curvatures of 2159 cm^{-1} and 2161 cm^{-1} , successive cycles are alternately shaded and unshaded. After Yarin et al. (2005) with permission from AIP.

A number of additional new elements introduced in the model are as follows. First, the uniform capacitor electric field was replaced with the electric field that exists between a sharp electrified nozzle and a large flat ground collector. In the

Table 5.3. The calculated and observed distance between branches along the jet.

Applied voltage (kV)	Average electric field between tip and collector (V/mm)	ℓ_N (calculated) (μm)	ℓ_N (measured) (μm)
4	57	379	294
5	71	119	353
7.5	107	118	118
10	143	124	118

simplest form this field can be represented by the field between a point-wise charge opposite to a conducting plate (or a mirror image of a charge of an opposite sign). Also, mutual Coulombic interactions between the charged jet elements were accounted not only for a given jet, but for all the jets in the array. To describe the rheological behavior of polymer solutions, the non-linear UCM model was used in addition to the linear Maxwell model.

In all the cases, viscosity $\mu = 100$ P and the relaxation time $\theta = 0.1$ s were used in accordance with the data of Reznik et al. (2004). It was demonstrated experimentally and with the help of numerical simulations that the mutual Coulombic interactions influence the paths of individual electrified jets in electrospinning. Mutual repulsion of the jets is highlighted by arrows in Figs. 5.40(a), (b) and is reproduced by the simulation results shown in Fig. 5.41. Furthermore, the semi-vertical angle of the electrospinning envelope cones, of the two jets on the edges, is larger than for the inner jets (#2–8 in Fig. 5.40(b)). The values of the latter angles were obtained by measuring the semi-angle between the two bright lines bifurcating for a specific jet envelope in Fig. 5.40(b). In Fig. 5.40(b), the measured angle for jet #5 is indicated by a double-headed arrow. The semi-vertical angle of the electrospinning envelope for the inner jets lies between 25° and 30°, whereas for jet #1 it is about 40°.

When rotating Fig. 5.40(b) by 90°, the semi-vertical angle of the envelope cone in the direction perpendicular to the line on which the nozzles are located is revealed. The latter angle, estimated from Fig. 5.40(c), is between 50° and 75°. This confirms that the inner envelope cones are, in fact, squeezed along the line on which the nozzles are located. A similar result is revealed by the simulations (cf. Fig. 5.41(c)). Although the electrospinning envelopes are squeezed, the electrically driven bending instability of all the jets is similar to the one familiar for single jets. The results of the modeling suggest that both the non-linear UCM model and the linear Maxwell model provide a reasonable and quite close description of the viscoelastic behavior of jets in electrospinning.

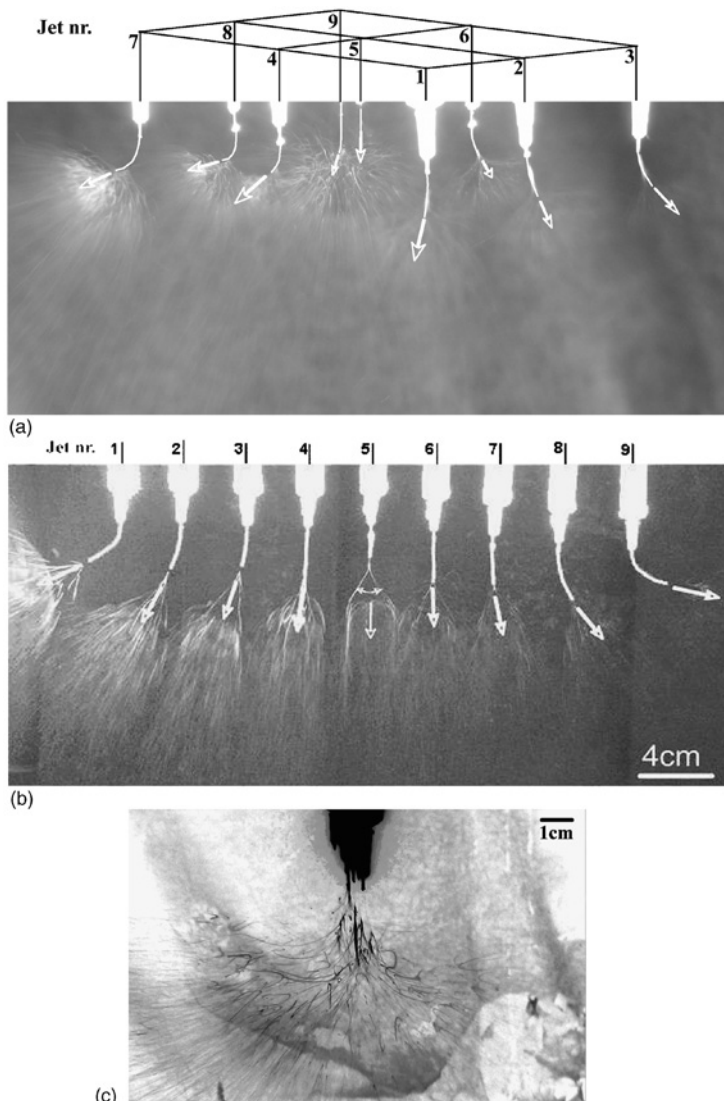


FIG. 5.40. (a) A photograph of a nine-jet electrospinning process where the jets were arranged in a 3×3 matrix (set-up A). The photograph was taken with a slow shutter speed (200 ms). Arrows indicate the three-dimensional directions of the jets' axes. The distance, d_s , between the nozzles in the image was 5 cm. (b) Photographs were taken at long exposure times (200 ms) of a nine-jet electrospinning process using set-up B. The distance between the individual syringes $d_s = 4$ cm. Front view of jets #1–9 with arrows to indicate the direction of the main axes of the electrospinning envelopes. (c) A side view of all the jets in set-up B. Jet #1 is the foremost jet in the image. After Theron *et al.* (2005) with permission from Elsevier.

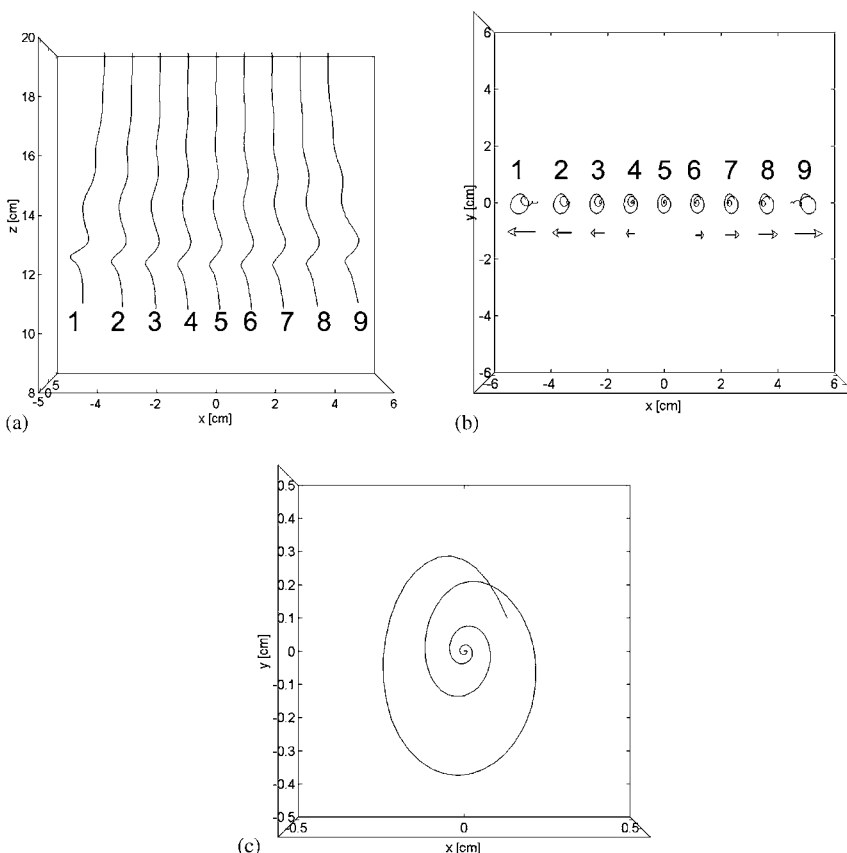


FIG. 5.41. The paths of nine jets in a multiple-jet electrospinning process, where the jets were arranged in a row. These jet paths were obtained from the calculations at $t = 3.4$ ms. (a) Side view of all the jets. (b) Top view corresponding to (a). Arrows show the directions of jet deviations. (c) Top view of jet #5. After [Theron et al. \(2005\)](#) with permission from Elsevier.

Reasonable stability of the process and uniformity of the as-spun nanofiber mats can be achieved with an inter-nozzle distance of about 1 cm and nine nozzles on a square of about 4 cm^2 . This results in the jet distribution density of 2.25 jets cm^{-2} , and in the production rate of the order of $4\text{ mL/(cm}^2\text{ min)}$.

When a single jet is issued from a single nozzle in a multiple-jet set-up, one needs to use many needles to achieve a high production rate. This is technologically inconvenient due to the complexity of the system involved and high probability of clogging.

A new approach to electrospinning of polymer nanofibers was proposed in [Yarin and Zussman \(2004\)](#). A two-layer system, with the lower layer

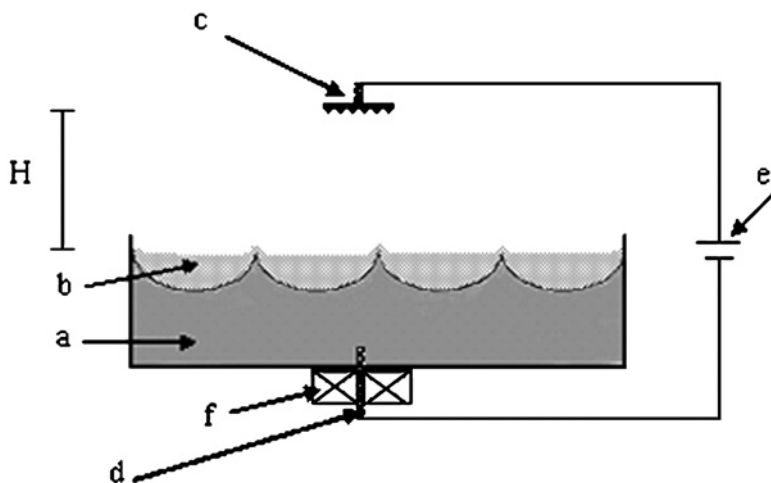


FIG. 5.42. Schematic drawing of the experimental setup. (a) Layer of magnetic liquid, (b) layer of polymer solution, (c) counter-electrode located at a distance H from the free surface of the polymer, (d) electrode submerged into magnetic fluid, (e) high-voltage source, and (f) strong permanent magnet or electromagnet. After [Yarin and Zussman \(2004\)](#) with permission from Elsevier.

being a ferromagnetic suspension and the upper layer a polymer solution, was subjected to a normal magnetic field provided by a permanent magnet or a coil (Fig. 5.42). As a result, steady vertical spikes of magnetic suspension perturbed the inter-layer interface, as well as the free surface of the uppermost polymer layer. When a normal electric field was applied in addition, the perturbations of the free surface become sites of jetting directed upward. Multiple-electrified jets underwent strong stretching by the electric field and bending instability, solvent evaporated and solidified nanofibers were deposited on the upper counter-electrode, as in an ordinary electrospinning process. The jet density in such a process was estimated as 26 jets cm^{-2} instead of the above-mentioned value of $2.25 \text{ jets cm}^{-2}$. As a result, a 12-fold increase in the production rate is expected when this method is used instead of separate nozzles. In addition, the design problems related to multiple nozzles, as well as clogging can be eliminated.

L. CONCLUDING REMARKS

The entire electrospinning process and the electrically driven bending instabilities of an electrospun fluid can each be viewed as particular

examples of the very general Earnshaw theorem in electrostatics. This theorem leads to the conclusion that it is impossible to create a stable structure in which the elements of the structure interact only by Coulomb's law. Charges on or embedded in a polymer fluid move the fluid in quite complicated ways to reduce their Coulomb interaction energy. Electrospinning, and perhaps other useful processes, utilizes this behavior to produce interesting and useful polymer objects.

The localized approximation introduced in the present section utilized a far-reaching analogy between the electrically driven bending instability in the electrospinning process and the aerodynamically driven bending instability studied before. The quasi-one-dimensional partial differential equations of the jet dynamics that describe the paths of the electrified jets in electrospinning were established.

A reasonable quantitative description of the experimental data was achieved, which allows one to calculate the shape of the envelope cone, which surrounds the bending loops of the jet in electrospinning. The downward velocity of the jet can also be calculated to be within an order of magnitude of the observed velocity. The theoretical results also allow for the calculation of the elongation of material elements of the jet. The calculated results also illustrate the increase in viscosity of segments of the jet as the solvent evaporates during the course of electrospinning. Multiple-jet configurations were studied both experimentally and via numerical modeling.

It is emphasized that presently, information on the rheological material behavior of polymer solution being elongated at the rate and other conditions encountered during electrospinning, is rather scarce. Data on evaporation and solidification of polymer solutions in the electrospinning process are practically unavailable. Therefore, at present a number of parameters in the simulations can only be estimated by the order of magnitude, or found from experimental observations of the electrospinning process. Material science data acquired for the electrospinning process will allow researchers to avoid such obstacles in future. A more detailed description of the nature of the solvents (in many cases, mixtures of several miscible fluids with a variable evaporation rate) may also be very helpful for a further upgrading of the modeling capabilities.

Note also that a physically similar approach to bending instability of a single jet of inelastic Newtonian viscous liquids was developed in [Shin et al. \(2001a,b\)](#), [Hohman et al. \(2001a,b\)](#) and [Fridrikh et al. \(2003\)](#). In these works the phenomenon was called whipping instability.

VI. Scientific and Technological Challenges in Producing Nanofibers with Desirable Characteristics and Properties

Electrospinning has been shown to be an effective method for the production of nanofibers. For most applications, it is desirable to control, in addition to the diameter of the fibers, also the architecture, the internal composition, the internal morphology and the surface topology as well as fibers alignment in a structure. Porous fibers are of interest, for instance, for filter applications. Core-shell fibers, or fibers which are hollow, are of interest for storage, release systems and insulation. A given surface topology and chemical structure will affect, for instance, the wetting behavior (super-hydrophobicity), as well as specific adsorption processes (Busscher *et al.*, 1984; Jiang *et al.*, 2004; Ma *et al.*, 2005; Oner and McCarthy, 2000; Youngblood and McCarthy, 1999), and it will couple very effectively to the surrounding matrix in the case of reinforcement (Huang *et al.*, 2003). The objective is to tailor the fiber formation during electrospinning in such a way that fibers with specific diameters, architectures, internal structures and surface topologies are manufactured and aligned specifically for the targeted application.

A further objective is the inclusion of additives – drugs, catalysts (i.e. TiO₂ nanoparticles or enzymes), non-linear optical materials, electrically conducting and photosensitive materials, chromophores, for example into the fibers, possibly only in well-defined compartments within the fibers. Chemical modifications and functionalizations of fibers, again directed at optimizing the properties for specific applications, are highly desirable (Kedem *et al.*, 2005; Kim *et al.*, 2005a; Li *et al.*, 2005).

First successes in preparation of conductive and photosensitive nanofibers from electronic and photonic polymers (Drew *et al.*, 2002; MacDiarmid *et al.*, 2001; MacDiarmid, 2002; Norris *et al.*, 2000) show that electrically conducting and light-emitting nanofibers and nanotubes are achievable via electrospinning.

Electrical conductivity and strength of nanofibers are significantly improved when single- and multi-wall carbon nanotubes, CNTs (Rakov, 2000) are incorporated into them. The attempts in this direction show that nanofibers containing CNTs can be electrospun from a polymer-based solution of CNTs (Dror *et al.*, 2003; Ko *et al.*, 2003; Seoul *et al.*, 2003; Salalha *et al.*, 2004; Ye *et al.*, 2004). Both multi-walled (MWCNT) and single-walled (SWCNT) carbon nanotubes were oriented and embedded inside nanofibers during electrospinning. The most important issue to be tackled when electrospinning polymer-CNT solutions is the achievement of

a fine and stable dispersion of CNTs. This is accomplished by dissolving CNTs in solutions of surfactants (e.g. in sodium dodecyl sulfate, SDS (Vigolo et al., 2000), or in a non-ionic surfactant like Triton X at low concentration). In these systems, the amphiphilic character of the surfactant or polysoap stabilizes a colloidal suspension in water. There is no evidence that this process always separates the CNT bundles into individual tubes. In fact, viscosity measurements performed on these systems revealed a low viscosity as that of water, Vigolo et al. (2000), which demonstrates the aggregated character of CNTs in these suspensions.

Another way to disperse nanotubes is to modify them with attached polymers (Dalton et al., 2001; McCarthy et al., 2000; O'Connell et al., 2001). The dispersion of CNTs in an amphiphilic alternating copolymer of styrene and sodium maleate generically named polysoap is particularly effective (Salalha et al., 2004).

A simple one-step process was reported for using a natural polysaccharide, gum arabic, to disperse SWCNTs in aqueous solutions (Bandyopadhyaya et al., 2002). Combination of both electrostatic and steric repulsion interaction in aqueous dispersion can be achieved by attaching amphiphilic block or grafted copolymers with a charged hydrophilic block to the CNT (Hamley, 2000).

Dror et al. (2003) used the electrospinning process to fabricate nanofibers of PEO in which MWCNTs are embedded. The initial dispersion of MWCNTs in water was achieved using amphiphiles, either as small molecules (SDS) or as a high molecular weight, highly branched polymer (gum arabic). These dispersions separate the MWCNTs for incorporation into the PEO nanofibers by subsequent electrospinning. The focus of that work was on the development of axial orientations in these multi-component nanofibers. Continuous nanofibers of controlled diameter were thus obtained either as an unoriented mat on a flat collector or as an oriented rope by deposition on a rotating wheel.

Transmission electron microscope (TEM) images of nanofibers containing SWCNTs in PEO/SDS are shown in Fig. 6.1. It is evident that individual SWCNTs were successfully embedded in the dispersing polymer/surfactant matrix. This indicates that the original dispersion contained individual nanotubes rather than aggregates or bundles. In many regions of the electrospun nanofibers the embedded nanotubes appeared to be well-oriented along the fiber axis. Good axial alignment of the embedded SWCNTs was revealed by etching the as-spun nanofibers in Salalha et al. (2004). Polymer nanofibers reinforced by an embedded oriented system of CNTs will allow development of advanced materials possessing ultimate tensile strength and significant electric conductivity.

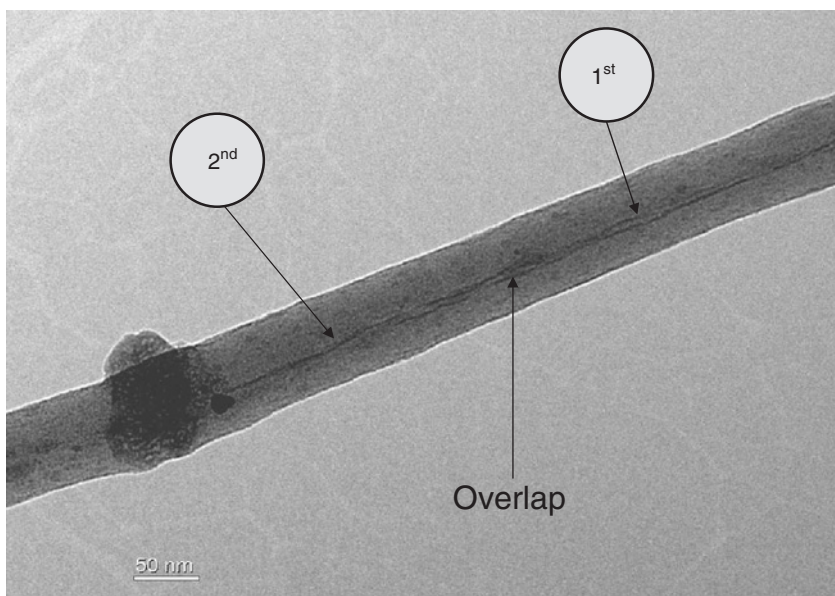


FIG. 6.1. TEM image of composite nanofibers after etching in oxygen flow for 1 min. Bar = 50 nm. A catalyst particle is seen on the left. After Salalha *et al.* (2004) with permission from ACS.

Ge *et al.* (2004) developed highly oriented, large area continuous composite nanofiber sheets made from surface-oxidized MWCNTs and polyacrylonitrile (PAN) using electrospinning (Fig. 6.2). They reported the highest degree of orientation of nanotubes in electrospun composite nanofibers, which was determined with transmission electron microscopy and electron diffraction. This degree of orientation in the electrospun PAN/MWCNTs nanofiber sheets approaches that observed in the PAN/SWCNT microfibers made by a dry-jet spinning method when the draw ratio reaches the value of 4.3. They observed that the orientation of the CNTs within the nanofibers was much higher than that of the PAN polymer crystal matrix as detected by two-dimensional wide-angle X-ray diffraction (WAXD) experiments. This suggests that not only jet elongation but also the slow relaxations of the CNTs in the nanofibers are determining factors in the orientation of CNTs. They revealed that the formation of charge transfer complexes between the surface-oxidized nanotubes and negatively charged functional groups in PAN during electrospinning leads to a strong interfacial bonding between the nanotubes and surrounding polymer chains. As a result of the highly anisotropic orientation and the formation of

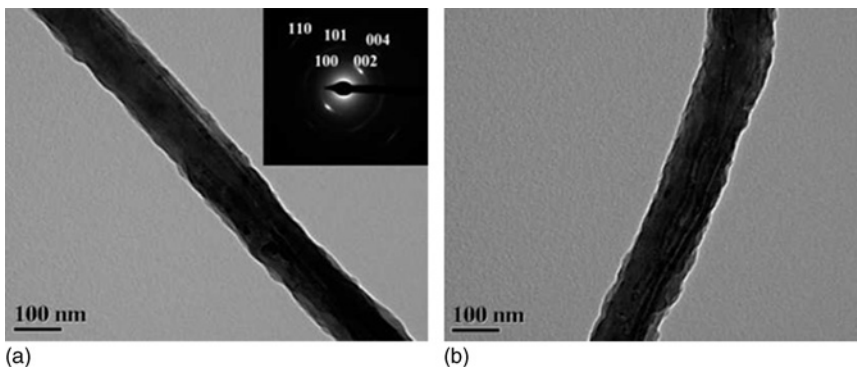


FIG. 6.2. High magnification bright field TEM images of electrospun MWCNT/PAN composite nanofibers containing (a) 10 wt% and (b) 20 wt% oxidized MWCNTs (the scale bar of 100 nm). The inset in part (a) is an SAED pattern obtained from this nanofiber. After [Ge et al. \(2004\)](#) with permission from ACS.

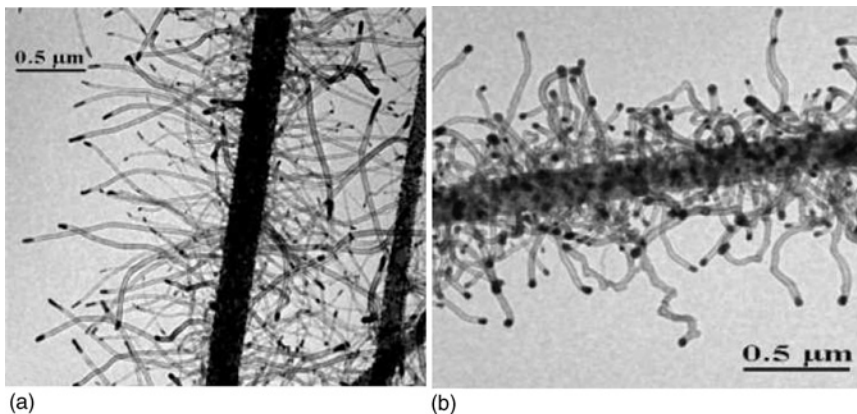


FIG. 6.3. Transmission electron micrographs of carbon nanostructures. (a) Long, slightly curved carbon nanotubes formed at 850°C, (b) Curved and bent CNTs formed at 700°C. After [Hou and Reneker \(2004\)](#) with permission from Wiley-VCH Verlag.

complexes, the composite nanofiber sheets possessed enhanced electrical conductivity, mechanical properties, thermal deformation temperature, thermal stability and dimensional stability.

[Hou and Reneker \(2004\)](#) reported electrospun PAN nanofibers carbonized and used as substrates for the formation of MWCNTs (Fig. 6.3). The MWCNTs were formed by an ion-catalyzed growth mechanism. Electrospun polymer nanofibers, produced using electrospinning, were made with diameters

ranging from a few nanometers to several micrometers and collected in a highly porous thin sheet. Multi-walled CNTs with metal particles on the tips grown on such carbonized nanofiber substrates form a characteristic hierarchical structure. This unique hierarchical carbon structure, with dimensions that can be controlled during synthesis, promises to become important in fuel-cells, redox-reaction electrodes and in nanoscale engineering of other systems in which electrical, mechanical and chemical interactions are integrated to produce macroscale effects.

Conducting and photosensitive nanofibers can be obtained not only by electrospinning, but also via different chemical and electrochemical synthesis methods and template methods (Jerome *et al.*, 1999; Demoustier-Champagne *et al.*, 1999; Wan *et al.*, 1999; Hsu *et al.*, 1999; Pomfret *et al.*, 1999). However, these nanofibers are always very short (\sim several μm) as compared to the electrospun nanofibers (\sim 10 cm and more).

Magnetic nanoparticles were embedded in the electrospun nanofiber mats in Li *et al.*, (2003), Yang *et al.* (2003) and Wang *et al.* (2004a). Magnetic-field-responsive non-woven electrospun fabrics were produced.

Piezoelectric polymer poly(vinylidene fluoride), PVDF, which also has such properties as pyroelectricity and ferroelectricity was successfully electrospun in Bates *et al.* (2003), Yang *et al.* (2003) and Gupta and Wilkes (2003).

Beaded electrospun nanofibers result from capillary instability in the process where polymer concentration, molecular weight or electric charge, are insufficient. Lee *et al.* (2002, 2003c) showed that bead formation can be controlled by using different solvents or solvent compositions. Fong *et al.* (1999) examined other parameters, including reduction of charge on the jet, which is very effective in producing beads. Beaded electrospun nanofiber mats represent a perfect superhydrophobic surface (Jiang *et al.*, 2004) attractive for many applications. Beads appear to be helpful to strengthen binding between the fibers and a matrix in fiber-reinforced composites (Huang *et al.*, 2003).

Some additional details on scientific and technological challenges related to electrospinning of biofunctional, conducting and photosensitive nanofibers, will be given below in the subsections devoted to these particular topics.

To overcome technological challenges in fabrication of microdevices, techniques for *in situ* alignment of as-spun nanofibers/nanotubes using electrostatic repulsion forces have recently been demonstrated (Theron *et al.*, 2001; Deitzel *et al.*, 2001; Zussman *et al.*, 2003b; Sundaray *et al.*, 2004; Li *et al.*, 2004).

A sketch of the experimental apparatus used by Theron *et al.* (2001) and Zussman *et al.* (2003b) is shown in Fig. 6.4. The jet flowed downward from

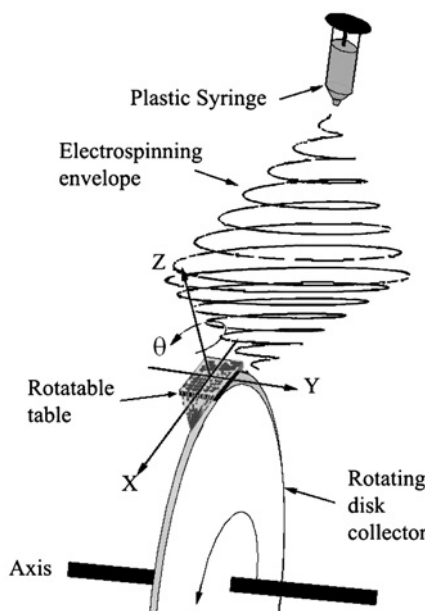


FIG. 6.4. Schematic drawing of the electrospinning process, showing the double-cone envelope of the jet. The collector disk is equipped with a table that assists to collect the nanofibers. The table can be rotated about the Z-axis when the disk rotation is temporarily stopped to enable layer-by-layer collection at a desired angle between the nanofiber array layers. After Zussman et al. (2003b) with permission from AIP.

the surface of a pendant drop of polymer solution toward a rotating disk collector at a distance of 120 mm below the droplet. The disk (with a diameter of 200 mm) was made of aluminum and had a tapered edge with a half angle of 26.6° in order to create a strongly converging electrostatic field. An electric potential difference of around 8 kV was created between the surface of the liquid drop and the rotating disk collector. When the potential difference between the pendant droplet and the grounded wheel was increased, the droplet acquired a cone-like shape (the Taylor cone). At a high enough potential difference, a stable jet emerged from the cone and moved downward toward the wheel. The jet flowed away from the droplet in a nearly straight line and then bent into a complex path that was contained within a nearly conical region, with its apex at the top, which is called the envelope cone. Then, at a certain point above the wheel the envelope cone started to shrink, resulting in an inverted envelope cone with its apex at the wheel's edge.

During the electrospinning process, the disk was rotated at a constant speed to collect the developing nanofibers onto its sharp edge. The linear speed at the tip of the disk collector was $V = 11\text{ m s}^{-1}$. As the as-spun fiber reached the wheel's edge, it was wound around the wheel.

A small table ($5 \times 4\text{ mm}$) made of aluminum was attached to the disk edge to facilitate the collection of the nanofibers and to detach them further on. The table can be rotated about its Z -axis when the disk rotation is temporarily stopped, hence the direction of the collected nanofibers can be controlled. The nanofibers were collected over a 10 s period. The resulting two-dimensional nanofiber arrays are shown in Fig. 6.5. The diameter of the nanofibers was not uniform and varies from 100 to 300 nm in Fig. 6.5(a) and from 200 to 400 nm in Fig. 6.5(b). The separation between the parallel nanofibers also varies from 1 to 2 μm in Fig. 6.5(a) and from 1 to 1.5 μm in Fig. 6.5(b). Typical three-dimensional nanofiber arrays (crossbars) are depicted in Fig. 6.6. A single junction is shown in Fig. 6.7. The collected nanofibers show a high order of alignment. The diameter of the nanofibers in this case is also non-uniform and varies in the range 10–80 nm. When nanofibers were electrospun onto the wheel's sharp edge without the table, nanoropes of nanofibers were obtained. A typical image of a rope of nanofibers is shown in Fig. 6.8 (Theron *et al.*, 2001). The duration of the collection process was 60 s. The rope was manually detached from the wheel edge. Two HR-SEM images of nanoropes are shown in Fig. 6.9. The nanofibers are in contact, and nearly parallel for long distances.

Arrays similar to those shown in Figs. 6.5–6.7 are periodic arrays of dielectric scatterers in a homogeneous dielectric matrix. Such arrays can interact strongly with photons, which have commensurate wavelengths. Such photonic structures have band structures, localized defect modes and surface modes that can interact with and modify or direct photons. A variety of novel applications of nanofibers and nanotubes in such fields as microelectronics, telecommunications, solar energy conversion, medical and pharmaceutical industry are developing rapidly.

For short nanofibers and nanowires prepared by methods other than electrospinning, various assembly methods were proposed, e.g. electric-field assisted assembly (Smith *et al.*, 2000) and micro-fluidics methods (Huang *et al.*, 2001b).

Core-shell nano/meso fibers were first produced by co-electrospinning of two materials in Sun *et al.* (2003). Essentially, the same process was adopted elsewhere (Li and Xia 2004a,b; Loscertales *et al.*, 2004; Yu *et al.*, 2004; Zhang *et al.*, 2004). In this approach two different solutions flow through concentric annular nozzles (Fig. 6.10). The experiments showed that for a

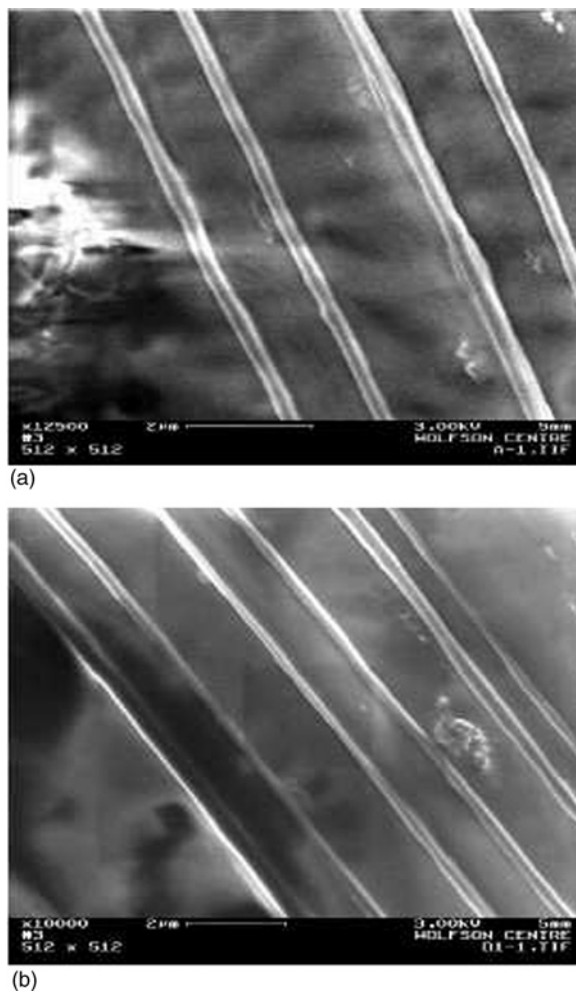


FIG. 6.5. HR-SEM images of aligned NFs that were collected on a carbon tape attached to the edge of the disc collector. In (a), the diameter of the fibers varies from 100 to 300 nm. The pitch (center to center) varies from 1 to 2 μ m. In (b), the diameter of the fibers varies from 200 to 400 nm. The pitch varies from 1 to 1.5 μ m. After Theron et al. (2001) with permission from IOP.

stable co-electrospinning process both fluids should be electrified as shown in Fig. 6.10. Only then the electrical pulling forces create compound jets, since purely viscous entrainment of one of the fluids by another one appears to be insufficient for a stable process. Two polymer solutions or a combination of polymer solution and a non-polymeric liquid or even a powder may be used. A compound droplet sustained at the edge of such

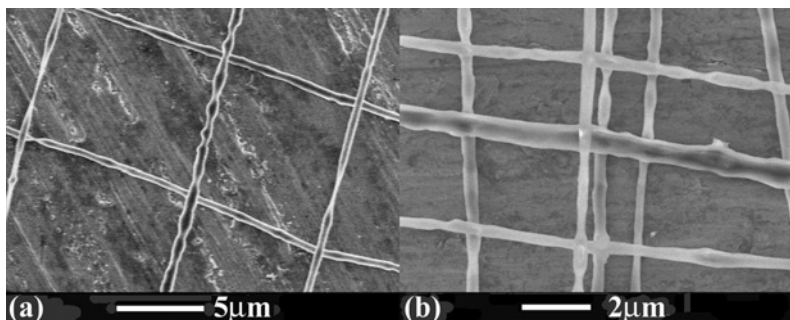


FIG. 6.6. Typical SEM images of crossed arrays of PEO based nanofibers collected on an aluminum table. The structures were obtained in a sequential assembly process with orthogonal placement directions. (a) A two-step assembly (b) a four-step assembly. After Zussman *et al.* (2003b) with permission from AIP.

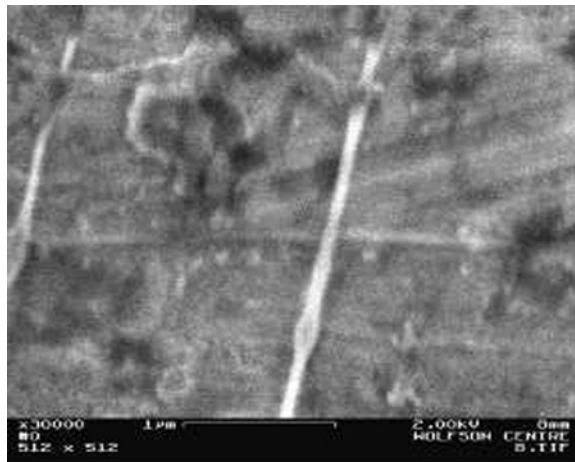


FIG. 6.7. A junction of the nanofiber crossed array. After Zussman *et al.* (2003b) with permission from AIP.

concentric nozzles transforms into a compound Taylor cone with a core-shell jet co-electrospun from its tip. As in the ordinary electrospinning process, the jet is separately, sequentially and simultaneously pulled, stretched and elongated and bent by the electric forces. Solvent evaporates and the compound jet solidifies resulting in compound core-shell nanofibers. Compound nanofibers electrospun from PEO/PSU (Polysulfone) solutions had an outer diameter of the order of 60 nm, and a core diameter of about 40 nm as apparent from Fig. 6.11. The compound nanofibers shown in Fig. 6.11 have a relatively smooth core-shell interface. The co-electrospinning of

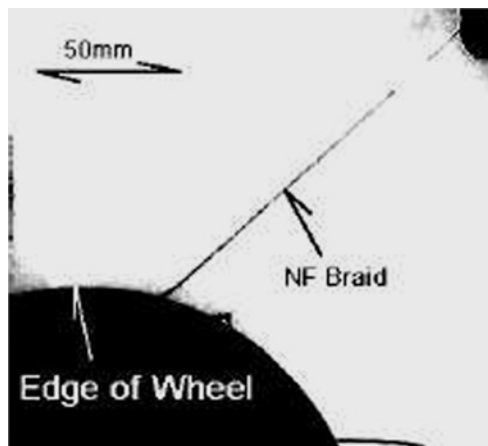


FIG. 6.8. A rope of aligned NFs manually pulled from the collector. Almost all the NFs were collected on the edge of the sharpened disc collector. After Theron et al. (2001) with permission from IOP.

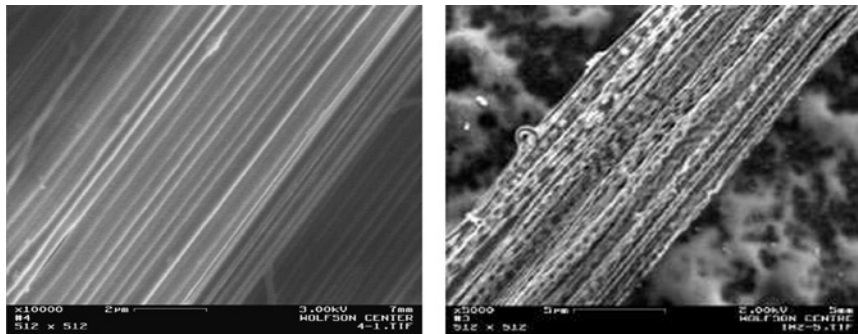


FIG. 6.9. Typical HR-SEM images of two ropes of aligned NFs. The density is about $100 \text{ NFs } \mu\text{m}^{-2}$. After Theron et al. (2001) with permission from IOP.

fluids is very versatile and will certainly foster new materials design. It can also result in a two-stage method of fabrication of hollow nanofibers (nanotubes) instead of the previously used three-stage one (Bognitzki et al., 2000, 2001; Liu et al., 2002). Co-electrospinning should be followed by a selective removal of the core material in the compound fiber via selective solvents or heat treatment. Calcination and pyrolysis of polymers containing metal atoms transform nanofibers and nanotubes into ceramic, and metal ones (Liu et al., 2002; Li and Xia, 2003, 2004b; Li et al., 2004). Carbonization of co-electrospun nanofibers yields turbostratic carbon

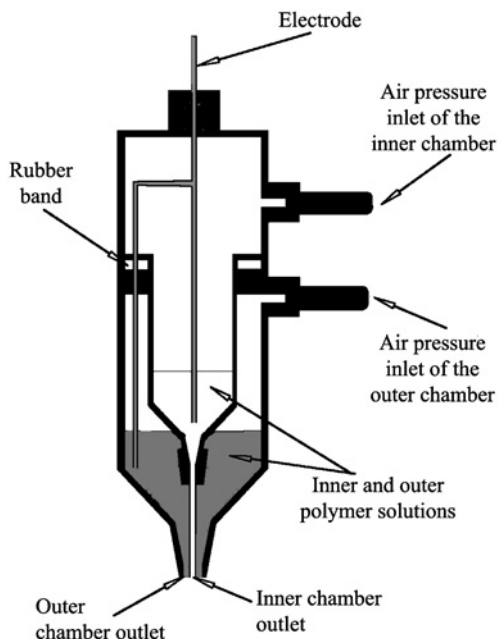


FIG. 6.10. Experimental set-up used for co-electrospinning of compound core-shell nanofibers. After Sun *et al.* (2003) with permission from Wiley-VCH Verlag.

nanotubes (Zussman *et al.*, 2006). The preparation of organic, inorganic materials, of semiconductor systems, which are functionalized by a structuring process taking place on the submicrometer scale, is a promising goal of the co-electrospinning process. The manufacturing of structured yet compact polymer fibers with diameters down to less than 10 nm is of growing interest.

Bi- and multi-component as-spun nanofiber mats can be produced by electrospinning where different polymers are supplied through different nozzles side by side (Gupta and Wilkes, 2003).

VII. Characterization Methods and Tools for Studying the Nanofiber Properties

Morphological characterization of nanofibers and nanotubes describes their crystalline or amorphous structure, spherulites, internal defects and complex internal structures such as incorporated solid particles, CNTs. The crystal orientations and the crystal modifications present can be observed.

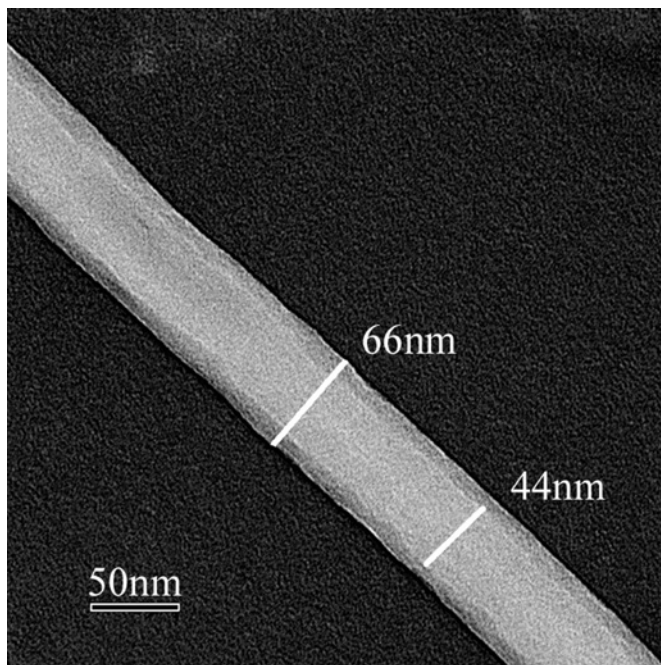


FIG. 6.11. TEM picture of a compound nanofiber. The core and shell solutions are PSU and PEO, respectively. After [Sun et al. \(2003\)](#) with permission from Wiley-VCH Verlag.

X-ray scattering and diffraction, traditionally employed for textile fibers, has already been demonstrated as a useful tool in characterization of nanofibers. Wide-angle X-ray scattering (WAXS), wide-angle X-ray diffraction (WAXD) and small-angle scattering are useful. In particular, Phillips diffractometer for WAXD with the Bragg-Brentano scheme for beam focusing is helpful.

With only X-ray scattering it is difficult to completely characterize nanoparticles, CNTs and structures such as cracks, necks and internal boundaries. Scanning electron microscopy and transmission electron microscopy provide much useful information about compound nanofibers and nanotubes, as well as nanofibers containing CNTs ([Theron et al., 2001](#); [Bognitzki et al., 2000, 2001](#); [Dror et al., 2003](#)).

Characterization of tensile stress and elastic and plastic properties of nanofibers, as well as fractographic analysis ([Poza et al., 2002](#)), are important for some applications. Various microstages and low-load commercial instruments are needed (an example is the Housfield H1KS machine with a 5 N load cell, [Fang et al., 2001](#)). Composites of nanofibers in

epoxy resin were tested using a double torsion fracture method in Kim and Reneker (1999) and Dzenis (2004). Three points bending tests were carried out using atomic force microscopy (Cuenot *et al.*, 2000). Atomic force microscope was also used to measure nanofiber dimensions and nanofiber-array structures by Theron *et al.* (2001). Using microstages and tensile machines (even the smallest ones), it is possible to make measurements only with samples of non-woven nanofiber-based materials or oriented nanofiber ropes (Theron *et al.*, 2001). At present appropriate methods for observing mechanical properties of a single nanofiber are being developed (Gu *et al.*, 2005; Inai *et al.*, 2005; Kim *et al.*, 2005b; Tan and Lim, 2004; Tan *et al.*, 2005; Zussman *et al.*, (2006)).

Mechanical properties of electrospun fiber mats of polyblends of poly(vinyl chloride) and polyurethane, PVC/PU, yield the Young's modulus up to 11.8 MPa, the yield stress of 1.03 MPa, the ultimate tensile stress of 3.73 MPa and the elongation at break of 456% for 50/50 blends (Lee *et al.*, 2003b). For blends with higher content of PU, fully elastic behavior was recorded up to the ultimate strength of 7.04 MPa, and the elongation at break of 1210% for pure PU mats. The Young's modulus of the PU mats was, however, much lower, namely 0.62 MPa (Lee *et al.*, 2003b). For non-woven PU mats, the ultimate tensile stress of the order of 40 MPa at the elongation of about 700% was reported (Pedicini and Farris 2003). For non-woven mats of poly(trimethylene terephthalate), PTT, nanofibers with diameters ranging from 200 to 600 nm the ultimate tensile stress was about 4 MPa at an elongation of about 300% (Khil *et al.*, 2004). For mats of gelatin nanofibers with diameters in the range from 100 to 340 nm, the tensile modulus was of the order of 117–134 MPa and the ultimate tensile strength was in the range from 2.93 to 3.40 MPa (Huang *et al.*, 2004).

A natural material, spider silk, is both strong and biologically compatible in certain cases (Lazaris *et al.*, 2002; Poza *et al.*, 2002). Spider dragline silk is stronger than Kevlar and stretches better than nylon. This combination of properties is seen in no other fiber. Numerous trials to domesticate spiders and to raise spiders on a farm have not achieved success. However, there is a way to utilize spider silk, which was recently developed via gene engineering and polymer science. Spider dragline silk genes were spliced into mammalian cells. It was shown that this resulted in secreting soluble silk proteins outside the cells where they could easily be collected (Lazaris *et al.*, 2002). For example, a goat or a cow can secrete spider silk proteins into milk. Spider silk proteins produced using this route have been made into fibers of 50 μm in diameter. These fibers are not as strong and sophisticated as the natural spider silk. Electrospinning of the solutions of these proteins is obviously

called for, since such nanofibers could become one of the good candidates for scaffolds for tissue engineering and artificial organs. The recent works of [Zarkoob et al. \(2004\)](#) and [Wang et al. \(2004b\)](#) describe electrospinning of spider and silkworm silk.

The elastic modulus of SWCNTs and of whisker-like graphite crystals is of the order of 1000 GPa ([Ciferri and Ward, 1979](#); [Harris et al., 2001](#)). For carbon fibers made from mesophase pitch $E \cong 700$ GPa ([Ciferri and Ward, 1979](#)), tensile strengths of SWCNTs of the order of 200 GPa have been claimed. Since these values are much higher than those for polymer nanofibers, there is significant interest in electrospinning of composite polymer nanofibers containing SWCNTs and MWCNTs. For PAN nanofibers with SWCNTs force–displacement curves obtained by indentation of atomic force microscope tip indicated a Young's modulus in the range 60–140 GPa at 0–4% weight of SWCNTs in PAN nanofibers with the diameters of about 50–200 nm ([Ko et al., 2003](#)).

The above-mentioned results demonstrate a significant effect of chosen material on mechanical properties of nanofibers. The effect of the fiber size may also be dramatic. Measurements of the elastic modulus of poly(pyrrole) nanotubes made by a template-based method, showed that the elastic modulus increases, as the outer diameter decreases under 70 nm ([Cuenot et al., 2000](#)). Namely, an increase from 1–3 GPa (at the outer diameter larger than 100 nm) to about 60 GPa (at the outer diameter of 35 nm) was reported for poly(pyrrole) in the latter work. This value is of the order of those for the Young's modulus of ultra-high modulus polymer macroscopic fibers obtained by different methods ([Ciferri and Ward, 1979](#)). On the other hand, ordinary textile fibers have Young's modulus of the order of 30–100 cN/tex, which is about 300–1000 MPa ([Perepelkin, 1985](#)). [Tan et al. \(2005\)](#) reported increasing tensile strength of PCL microfibers as their diameter decreases.

Stretching of individual nanofibers by a rotating wheel electrode similar to those of [Theron et al., \(2001\)](#) and [Zussman et al. \(2003b\)](#) revealed that the nanofibers fail by a multiple necking mechanism, sometimes followed by the development of a fibrillar structure (Figs. 7.1 and 7.2, [Zussman et al., 2003a](#)); also, cf. [Ye et al. \(2004\)](#). This phenomenon was attributed to the high-force stretching of solidified nanofibers by the wheel, if the rotation speed becomes high. Necking has not been observed in nanofibers collected in other ways. [Fig. 7.3](#) shows a WAXD pattern obtained for PEO nanofiber microrope. The pattern shows six diffraction arcs with a high degree of orientation. Analysis of this pattern indicates a monoclinic crystalline structure of PEO with a helical molecular conformation. Correlation

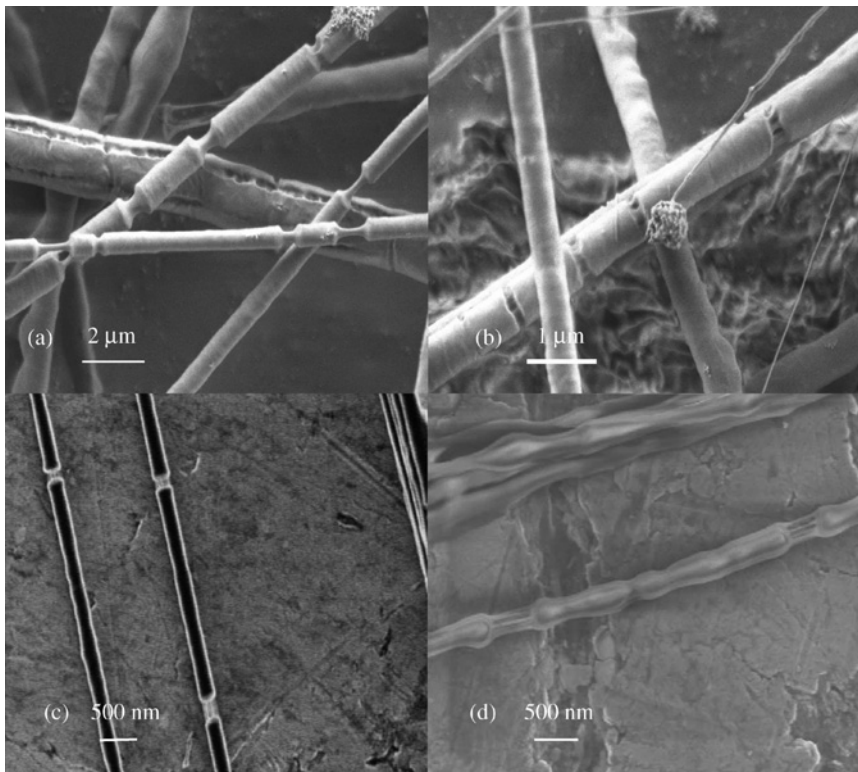


FIG. 7.1. Electron micrographs of multiple neck formation in electrospun nanofibers. (a) and (b) 7% PEO electrospun nanofibers, (c) and (d) 4% PEO electrospun nanofibers. After [Zussman *et al.* \(2003a\)](#) with permission from AIP.

between crystalline structure of nanofibers and their failure modes is an interesting problem.

Characterization of surfaces and porosity of electrospun nanofibers and nanotubes can be achieved using SEM images ([Bognitzki *et al.*, 2000, 2001](#); [Buchko *et al.*, 2001](#)).

The surface energy and the wetting behavior are studied by observation of drop spreading on the fiber mats. Functionalized nanofibers and nanotubes containing specific groups such as dipolar groups or chromophores can be characterized by absorption and fluorescence spectroscopy and dielectric relaxation studies.

The presence and orientation of nanofibers containing CNTs can be observed by Raman spectroscopy ([Ko *et al.*, 2003](#); [Wood *et al.*, 2001](#)). In the case of conducting and photosensitive nanofibers, electrical and optical

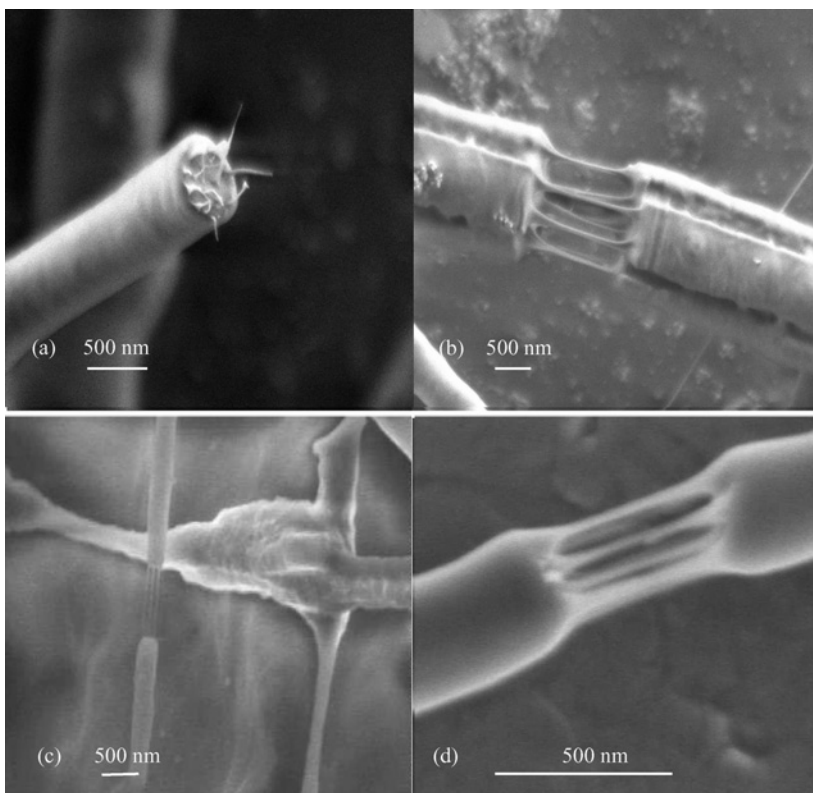


FIG. 7.2. Electron micrographs of fibrillar structures. (a) failed 7% PEO electrospun nanofiber, (b) fibrillar structure in 7% PEO electrospun nanofiber, (c) and (d) fibrillar structures in 4% PEO electrospun nanofibers. After [Zussman et al. \(2003a\)](#) with permission from AIP.

measurements are called for. Current voltage curves of polyaniline-based nanofibers were measured using a non-woven mat collected on a silicon wafer (MacDiarmid et al., 2001). Two gold electrodes separated by 60.3 μm were deposited on a fiber after its deposition on the substrate. Additional details on challenges in electrospinning of conducting and photosensitive nanofibers will be given below in the section devoted to them.

Rheological characterization of the viscoelastic polymer solutions used for electrospinning is elementary at present. Zero-shear viscosity and flow curves in simple shear could be characterized using rotational viscometers. Measurements of the relaxation time should utilize uniaxial elongational rheometry at high-strain rates. In this context elongational rheometers based on uniaxial elongation flow arising in self-thinning threads discussed in Yarin (1993), Stelter et al. (1999, 2000, 2002), Wunderlich et al. (2000), McKinley

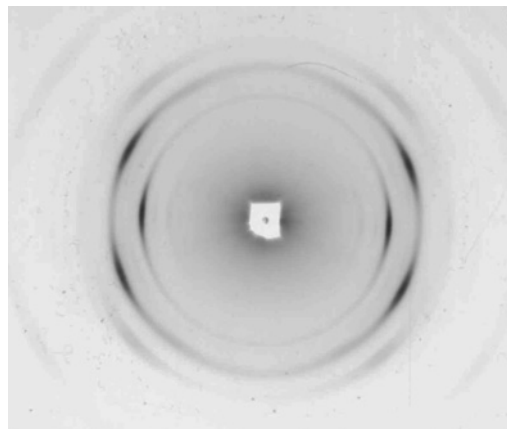


FIG. 7.3. Typical X-ray pattern of the oriented nanofiber rope made of 6% PEO ($M_w = 600,000 \text{ g mol}^{-1}$) aqueous solution with 40% ethanol. After Zussman *et al.* (2003a) with permission from AIP.

and Tripathi (2000) and Yarin *et al.* (2004) can be very helpful to characterize spinnability and rheological parameters of the solutions depending on polymer type and concentration. It is absolutely necessary to characterize rheological behavior of the polymer solutions used in electrospinning both in shear and elongation, since their effective viscosity actually depends on several other basic parameters (like zero-shear viscosity and the relaxation time) which are responsible for viscoelasticity. Such an approach was demonstrated by Theron *et al.*, (2004). The solutions listed in Table 7.1 were studied. Shear viscosities of the fluids were measured at different shear rates using a Coutte viscometer (Brookfield DV- II + programmable viscometer). Measurements of the shear viscosity at different shear rates for different solutions of PEO ($M_w = 6 \times 10^5 \text{ g mol}^{-1}$) demonstrate a pronounced shear thinning, as shown in Fig. 7.4. The values of the zero-shear viscosity μ are presented in Table 7.1. Relaxation times, θ characterizing viscoelastic properties of the electrospun solutions are also presented in Table 7.1. Relaxation times of PCL solutions could not be measured because of the high evaporation rates of the solvents, acetone and methylene chloride (MC). Surface tension measurements were conducted with a pulsating bubble surfactometer. Comparison of the surface tension of solutions of PEO ($M_w = 6 \times 10^5 \text{ g mol}^{-1}$) in ethanol/water (40/60) suggests that the surface tension is mainly a function of the solvent in the solutions and tends to be less sensitive to variation in the polymer concentration. Therefore, the values of surface tension are given in Table 7.2 as the solvent properties.

Table 7.1. Characteristic properties of test fluids.

Polymer	M_w (g mol ⁻¹)	Solvents	C (%)	ϵ_r	σ_e (mS m ⁻¹)	μ (cP)	θ (ms)
PEO	$6 \cdot 10^5$	Ethanol/water (40/60)	2	67.09	0.85	285	21
			3	61.44	1.38	1200	25
			4	66.57	1.15	3000	28
			6	57.63	1.67	43200	33
PEO	10^6	Ethanol/water (40/60)	2	66.71	0.81	1590	142
			3	67.97	1.28	9600	183
PEO	$4 \cdot 10^6$	Ethanol/water (40/60)	1	66.12	1.102	4250	217
			2	70.07	1.45	90,000	298
			3	65.07	0.88	335,000	359
PEO	10^6 $4 \cdot 10^6$	Water	2	81.96	9.43	570	—
			1	110.6	8.49	2600	128
PAA	$2.5 \cdot 10^5$ $4.5 \cdot 10^5$	Ethanol/water (40/60)	6	79.5	24.47	455	48.1
			5	74.14	17.95	255	22.75
PVA	10^4	Ethanol/water (50/50)	6	65.99	3.73	355	29.6
PU	Tecoflex	THF/ethanol (50/50)	6	16.75	0.093	25	—
			8	14.45	0.069	82	1.77
			8	25.2	0.142	107	—
PCL	$8 \cdot 10^4$	Acetone	10	25.38	0.141	165	—
			14	24.8	0.12	400	—
			10	18.55	0.191	670	—
PCL	$8 \cdot 10^4$	MC/DMF (75/25) MC/DMF (40/60)	10	24.49	0.36	950	—

Note: Molecular weight (M_w), polymer weight concentration (C), relative permittivity (ϵ_r), electric conductivity (σ), zero-shear viscosity (μ) and relaxation time (θ).

Xu et al., (2003) designed a liquid-stretching apparatus similar to the one used in Stelter et al. (1999, 2000, 2002) shown in Fig. 7.5. The apparatus was able to generate extensional flows mechanically for relatively low viscosity liquids. During the test approximately 0.2 mL of polymer solution was placed in a reservoir located on the bottom plate of the rheometer. A cylindrical tip mounted on a horizontal arm was dipped in the polymer solution initially. The arm could move vertically at a constant speed for a certain distance. The motion stopped after a distance that could be chosen by the experimenter when the horizontal arm ran in between the infrared emitter and the sensor pair and blocked the infrared emission. The tip picked up a portion of the polymer fluid and moved 21 mm upward at a constant speed of 350 mm s⁻¹. A fluid filament was created between the bottom plate and the tip. Then, self-thinning of the filament had started. A high frame rate camera monitored the decreasing diameter of this self-thinning jet. Two linear halogen lights were adjusted to provide proper illumination to the filament and a dark background. The liquid filament was outlined by the specular reflection of two linear lights from its lateral

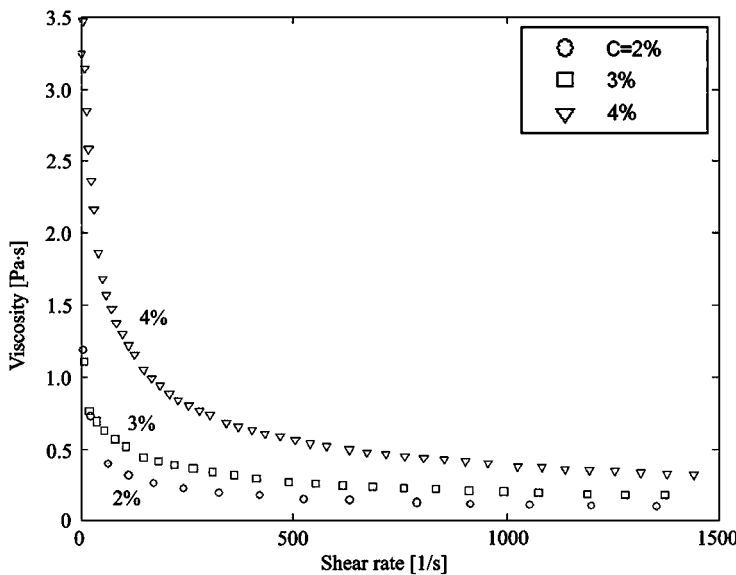


FIG. 7.4. Shear viscosity versus shear rate. Plots for solutions of PEO ($M_W = 6 \cdot 10^5$ g/mol) in ethanol/water (40%/60%) at different weight concentrations. After Theron *et al.* (2004) with permission from Elsevier.

Table 7.2. Characteristic properties of solvents.

Solvents	ε_r	σ_e (mS m ⁻¹)	η (cP)	σ (mN m ⁻¹)
Distilled water	88.75	0.447	1.12	72
Ethanol (95%)	24.55*	0.0624	1.1*	22.3*
Acetone	20.7*	0.0202	0.36*	23.3*
Ethanol/water (40/60)	69.47	0.150	2.49	30 [†]
MC/DMF (40/60)	29.82	0.505	0.93	31.6
MC/DMF (75/25)	21.3	0.273	0.73	28.9
THF/ethanol (50/50)	15.79	0.037	0.89	23.7

Note: Relative permittivity (ε_r), electric conductivity (σ_e), viscosity (η) and surface tension (σ). (*) <http://www.bandj.com/Home.html>.

Source: Wohlfarth and Wohlfarth (1997).

surface. The contour of the filament was seen as two bright lines on a dark background. Fig. 7.6 shows the reflections of the two linear light sources from the lateral surface of the liquid filament.

The high-speed camera was run at 500 frames s⁻¹. The field of view was approximately 2 mm \times 2 mm. A calibration procedure was carried out to

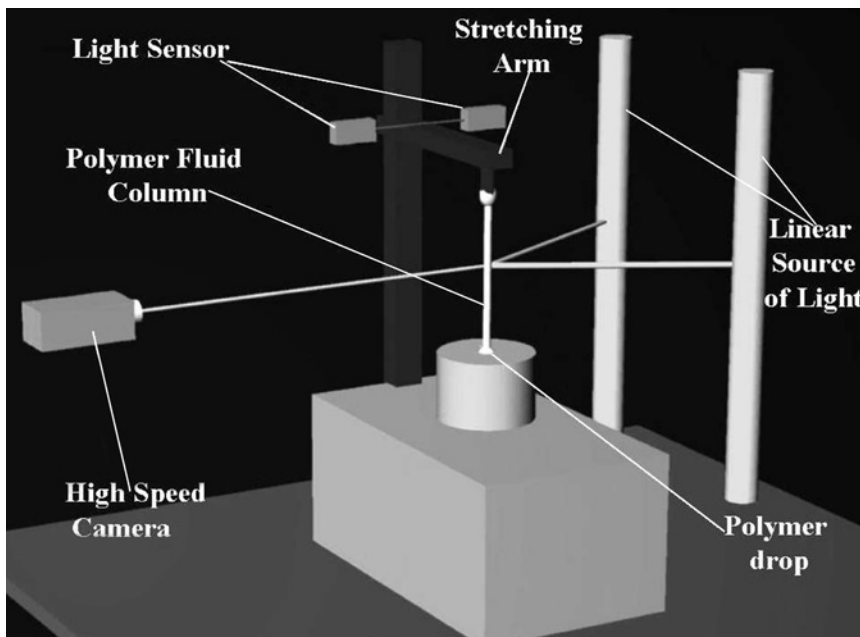


FIG. 7.5. The illustration of the fluid stretching apparatus. After Xu et al. (2003).

correlate the distance between pixels on screen with the dimensions in real space. Jet diameter was calculated from the distance between two contour lines. The initial jet diameter d_0 was recorded when the probe tip reached its highest position at time $t_0 = 0$ ms. Fluid jets with diameters as small as $80\text{ }\mu\text{m}$ could be accurately measured.

The whole set-up was mounted on a vibration-damped imaging bench. A special sample fluid holder was designed to minimize filament vibration during the thinning process. Various shapes of tips were tested. A flat-faced tip was used to minimize the end region of the liquid filament.

The polymer concentrations were much higher than those used by Stelter et al. (1999, 2000, 2002). In the latter works filament self-thinning was due to surface tension, which results in the following expressions for the filament diameter $d = 2a$ and the elongational viscosity μ_{el}

$$d = d_0 \exp(-t/3\theta), \quad (7.1\text{a})$$

$$\mu_{\text{el}} = \frac{3\theta\sigma}{d_0} \exp(t/3\theta), \quad (7.1\text{b})$$

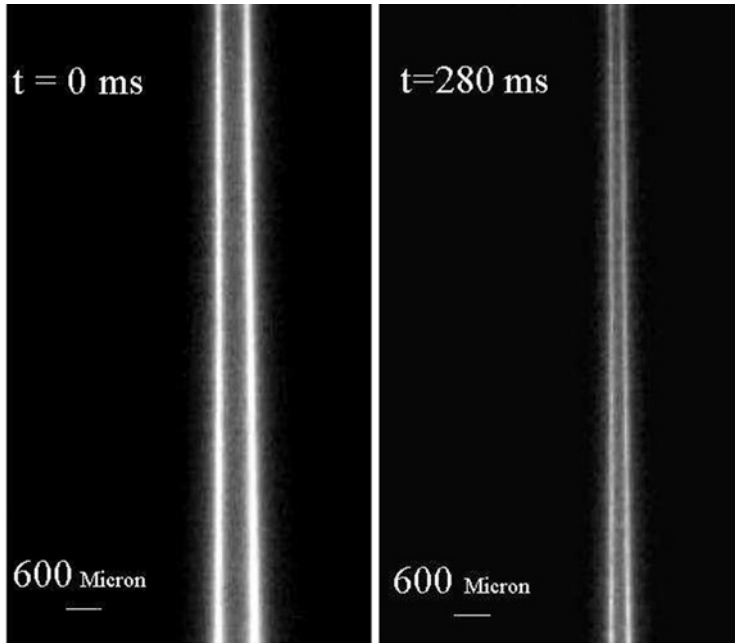


FIG. 7.6. Reflections of two linear light sources from the lateral surface of the liquid filament (Xu, 2003).

where σ is the surface tension. Note, that the values of the relaxation time given in Table 7.1 were obtained by fitting Eq. (7.1a) to the experimental data.

On the contrary, concentrated polymer solutions studied by Xu et al. (2003) thinned mostly due to gravity, which resulted in the following expressions

$$d = d_0 \exp(-t/2\theta), \quad (7.2a)$$

$$\mu_{\text{el}} = \rho g l_0 \theta \exp(t/\theta), \quad (7.2b)$$

where ρ is the solution density, l_0 the initial filament length, and g gravity acceleration.

Fig. 7.7 shows the entire filament during stretching and self-thinning. The cylindrical shape of the filament reflects that a uniform elongational flow was produced. At the middle part of the filament pure extensional deformation was created. The diameter decrease was monitored at this position. The large strain was produced by long residence time of the filament during the thinning process. The optical system allowed filaments

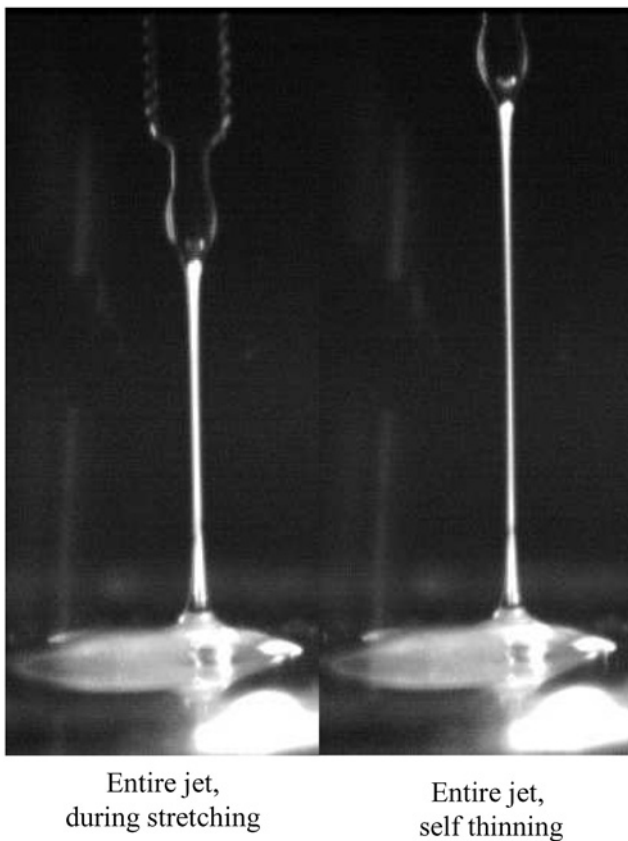


FIG. 7.7. The entire filament during stretching and self-thinning (Xu, 2003).

with diameters as small as $80\text{ }\mu\text{m}$ to be accurately measured. The time evolution of the filament diameter was studied for a series of concentrations of PEO in water. As can be seen from Fig. 7.8, the rate of decrease of diameter during the self-thinning process was higher for solutions with lower concentrations of polymer.

The relaxation time is found by fitting Eq. (7.2a) to the experimental data. As shown in Fig. 7.9, the relaxation time window suitable for electrospinning of PEO solutions is in the range from 20 to 80 ms, which agrees with the data for PEO in Table 7.1. The logarithm of the relaxation time decreases linearly with polymer concentration.

Fig. 7.10 summarizes the elongational viscosities of PEO/water solutions with different concentrations calculated from Eq. (7.2b). Extensional elongational flows strongly orient polymer macromolecules. Elongational

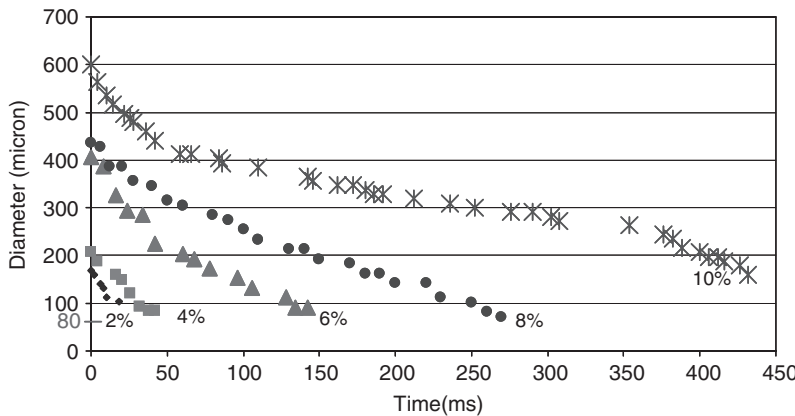


FIG. 7.8. Time evolution of the liquid filament (Xu, 2003).

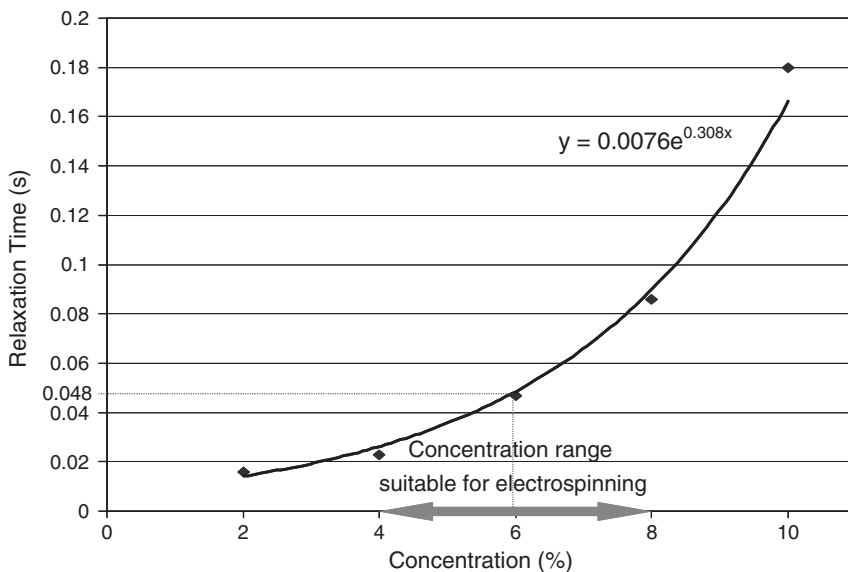


FIG. 7.9. Relaxation time of aqueous PEO solutions (Xu, 2003).

viscosities increase during the self-thinning process. The figure also shows that the low-concentration solution has a lower initial elongational viscosity. However, the viscosity increases at a much faster speed, during the self-thinning process, compared with the high-concentration solution. The fast building up of the elongational viscosity of the low-concentration solution corresponds to the faster diameter decrease.

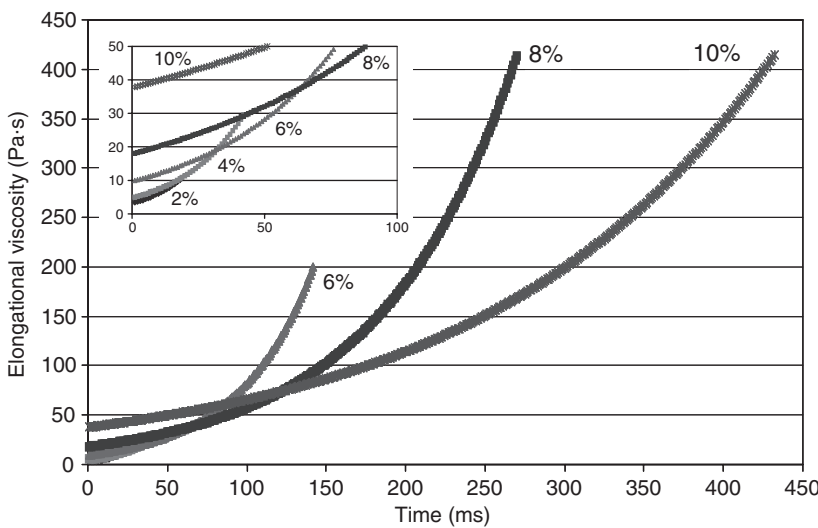


FIG. 7.10. Elongational viscosity of aqueous PEO solutions (Xu, 2003).

Xu et al. (2003) also used the birefringence observation set-up (Fig. 5.21) to study the molecular chain alignment during the filament self-stretching. In the birefringence experiment, aqueous PEO solutions with concentrations of 2%, 4%, 6% and 8% did not show observable birefringence before the filaments broke. For 10% solution, as shown in Fig. 7.11, strong birefringence took place 508 ms after the stretcher tip reached its highest position. This indicates that a critical strain rate had been surpassed and the polymer chains passed from a slightly distorted random coil to a nearly fully extended state. The chain extension in the elongational flow field took place suddenly while the strain is continuously increased during the self-thinning process.

Polymer solutions used in electrospinning can be characterized as leaky dielectrics (Melcher and Taylor, 1969; Saville, 1997). In other words, they are poor conductors. For such fluids the charge relaxation time τ_C is either larger or of the order of a characteristic hydrodynamic time τ_H (as it happens in the bending part of the electrospinning jets, cf. Section V.D). It is emphasized, however, that the same liquid could be considered as a perfect conductor in the case where the opposite is true, i.e. $\tau_H \gg \tau_C$, as it happens in the droplet wherefrom the jet originates (cf. Section IV.A). The nature of the ions involved is typically unknown. Therefore, electric characterization of the solutions intended for measuring their electric conductivity and dielectric permeability is highly desirable. In Theron et al. (2004), the electric

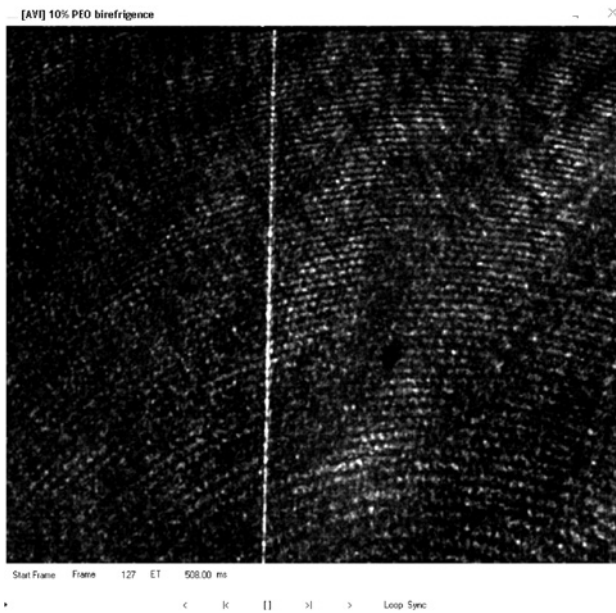


FIG. 7.11. Birefringence of 10% filament during self-thinning (Xu, 2003).

conductivity and permittivity of the polymer solutions (σ_e and ε_r , respectively) were determined by measuring the complex impedance of a small cylindrical volume of fluid (Heinrich *et al.*, 2000). Values of these parameters for the solutions used in this work are summarized in Table 7.1 for different polymer concentrations C (in wt%); the parameters for the solvents are shown in Table 7.2. The permittivity (ε_r) measurements for solvents and polymer solutions suggest that the solvent properties dominate the solution values of ε_r . The conductivities of the solutions increase slightly with the addition of polymers. With the exception of PAA, the ordinary bulk polymers are dielectrics; therefore it is assumed that conductivity σ_e of polymer solutions is mostly a function of the ionic conductivity of slightly impure solvents.

Electric field and current affect the shape of the transitional region connecting the Taylor cone and the jet. Experimental studies should reveal a relation between the electric and fluid mechanical parameters, which is also affected by the electric conductivity and dielectric permeability of the leaky dielectrics (Demir *et al.*, 2002). Such studies can be facilitated by the theoretical solutions for the transition region found in Kirichenko *et al.* (1986), Spivak and Dzenis (1998), Shin *et al.* (2001b), Hohman *et al.* (2001a)

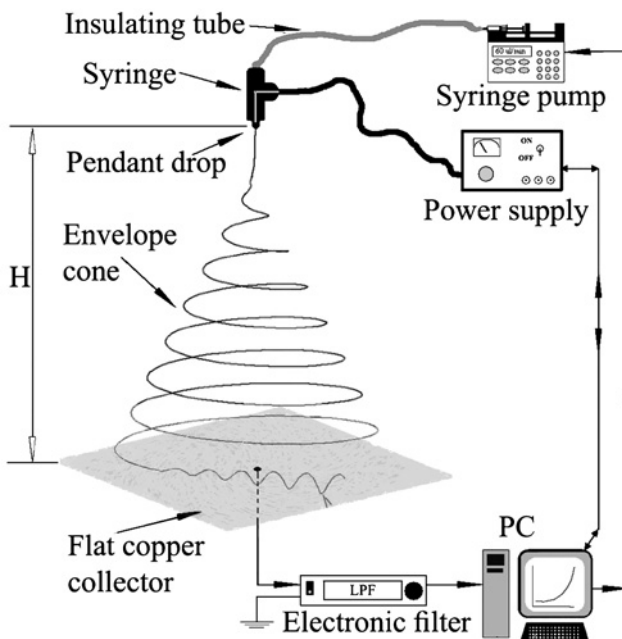


FIG. 7.12. Sketch of the experimental setup for measuring the electric current in electrospun jets. Nominal voltage at the source was about 10 kV, and at the syringe exit—about 600 V lower. Electrical current through the liquid was suitably small and ohmic heating and sparking to ground were eliminated. After Theron et al. (2004) with permission from Elsevier.

and Feng (2002, 2003). In Theron et al. (2004) experiments on electrospinning were performed with an apparatus shown in Fig. 7.12. The electrospun nanofibers were collected on a large flat copper collector (400 mm \times 400 mm). The collector was connected to ground through a resistor. The potential drop across the resistor was measured and translated to electric current using Ohm's law. The volume charge density, ρ , was calculated using the equation $\rho = I/Q$, where I is the electric current and Q the volumetric flow rate. The initial surface charge density was calculated as $q = (\rho d/4)10^{-7}$ where d (μm) is the measured diameter of the jet close to the tip of the Taylor cone, and q (C cm^{-2}) the surface charge density calculated at the point of the diameter measurements. The volume charge density is a useful parameter even though the charge is almost always on the surface of the jet. Total charge per total volume can only change by processes that are highly improbable during electrospinning (due to relatively low strengths of the electric field involved and suppression of liquid atomization by the elastic forces) if airborne charges

are eliminated. For the polymer solutions listed in Table 7.1 the charge density can be described by the following expression

$$\rho = k_{\text{exp}} U_0^{p_U} Q^{p_{\rho Q}} C^{p_C} M_w^{p_M} e^{-H/h} C_{\text{et}}^{p_{C_{\text{et}}}} \quad (7.3)$$

where $k_{\text{exp}} = 0.0128 \pm 0.00556$, U is the applied voltage in kV, Q is the volumetric flow rate in $\mu\text{L min}^{-1}$, C is the polymer concentration in weight %, M_w is the molecular weight of the polymer in g mol^{-1} , H is the nozzle-to-ground distance in cm and C_{et} is the ethanol concentration in weight% (this factor should be accounted only for PEO solutions). In Eq. (7.3),

$$p_U = 3; p_{\rho Q} = -0.8; p_C = 0.75; p_M = 0.5; p_{C_{\text{et}}} = -0.11 \quad (7.4)$$

and h in cm is given by the expression

$$h(M_w) = k_{hM} \cdot M_w^{p_{hM}}, \quad (7.5)$$

where $k_{hM} = 43.66$ and $p_{hM} = -0.496$.

VIII. Development and Applications of Several Specific Types of Nanofibers

A. BIOFUNCTIONAL (BIOACTIVE) NANOFIBERS FOR SCAFFOLDS IN TISSUE ENGINEERING APPLICATIONS AND FOR DRUG DELIVERY AND WOUND DRESSING

Electrospun nanofiber mats are attractive for tissue engineering mainly as a scaffold forming a matrix for cell proliferation or for the extracellular matrix (ECM) deposition. The matrix is, *in vivo*, a 3D scaffold for cells, and provides them with a tissue with specific environment and architecture. Furthermore, it serves as a reservoir of water, nutrients, cytokines and growth factors (Salgado *et al.*, 2004). Tissue engineering *in vitro* and *in vivo* involves the interaction of cells with a material surface and with substances that can be transported through the fibers. The nature of the surface and the chemical constitution of the fiber can directly influence cellular response, ultimately affecting the rate and quality of new tissue formation. Nanofibers formed by electrospinning attract attention of the research community by virtue of their structural similarity to natural ECM. By controlling the electrospinning process, many essential properties of the as-spun scaffold can be adjusted, such as the gross morphology, the microtopography, the porosity and the chemistry of the surface. All these properties which will be discussed herein determine which molecules can adsorb and how cells will attach and align themselves on a scaffold.

1. Processing Techniques

Electrospinning of scaffolds for tissue engineering applications follows the trends characteristic of electrospinning of the other polymer materials. For scaffold applications, polymer solutions are electrospun from the tip of a pendant or sessile drop at the edge of a syringe needle by applying electric potential differences of the order of 10 kV, or the field strengths of the order of 1 kV cm^{-1} (Boland et al., 2001; Buchko et al., 2001; Li et al., 2002). Nanofibers are collected on a ground plate as a non-woven mat as usual, or on a rotating mandrel as in Matthews et al. (2002). The latter introduces slight orientation in the electrospun mats, which is beneficial for cell attachment and growth. Kidoaki et al. (2005) developed multi-layering and mixing methods shown in Fig. 8.1. In the multi-layering electrospinning technique a layer-by-layer method is employed, such that a multi-layered nanofiber mesh is created. The structure can consist of different materials and with different porosity. In the mixing technique different polymer can be spun simultaneously which results in a mixed scaffold. An example of a product created by sequential multi-layering is shown in Fig. 8.1. A multi-layered product is a tube that was produced from segmented polyurethane SPU and collagen (see Fig. 8.2). This design is of a potential use for small-diameter compliant artificial vascular graft.

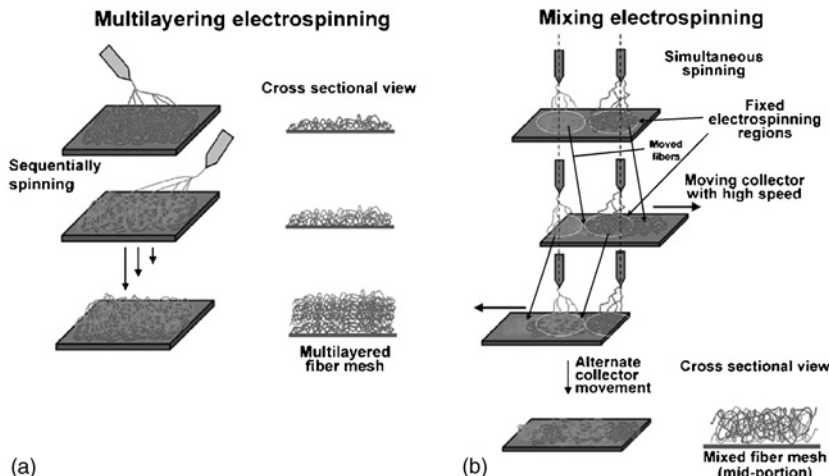


FIG. 8.1. The electrospinning techniques for scaffold formation: (a) multi-layering and (b) mixing. After Kidoaki et al. (2005) with permission from Elsevier.

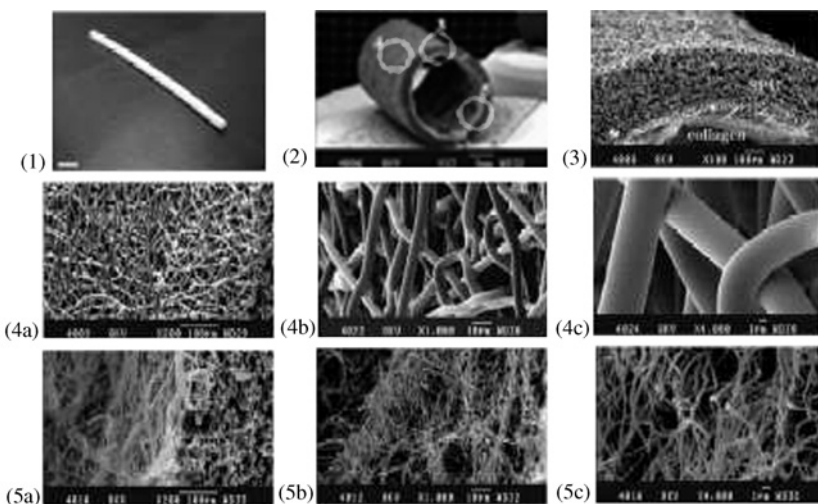


FIG. 8.2. Fabricated bilayered tubular construct of SPU/collagen. (1) Appearance of the tube (scale bar 1 mm). (2) SEM micrograph of the tube. (3) Magnified image of region 3 in the photo (2). (4a–c) Magnified images of the outer layer of region 4 in the photo (2). (5a–c) Magnified images of the inner layer of region 5 in the photo (2). After Kidoaki *et al.* (2005) with permission from Elsevier.

Additional applications of the electrospun nanofiber mats as soft-tissue prostheses were recently presented. Espy *et al.* (2004) used as-spun elastin fibers in bladders tissue engineering. Boland *et al.* (2004) have demonstrated the electrospinning of micro- and nano-fibrous scaffoldings from collagen and elastin and applied these to development of biomimicking vascular tissue-engineered constructs.

Biodegradable scaffolds can be made from poly(glycolic acid) (PGA), poly(L-lactic acid), (PLA), poly(ϵ -caprolactone) (PCL), and their copolymers (e.g. PLGA) (e.g. Zheng *et al.*, 2003). An example of the as-spun PCL nanofibers is shown in Fig. 8.3. These materials have many favorable properties, although these polymers have not performed up to the expectation in a clinical setting (Matthews *et al.*, 2002). That is the reason that natural materials like collagen prepared from calfskin and from human placenta were used to electrospin skin scaffolds (Huang *et al.*, 2001a; Matthews *et al.*, 2002).

Solution drying at the nozzle exit is quite common in electrospinning of PCL (Reneker *et al.*, 2002) and PLA (Larsen *et al.*, 2004). In the latter work, coaxial solvent vapor flow was demonstrated to be capable of preventing premature drying, solidification and clogging of the nozzle.

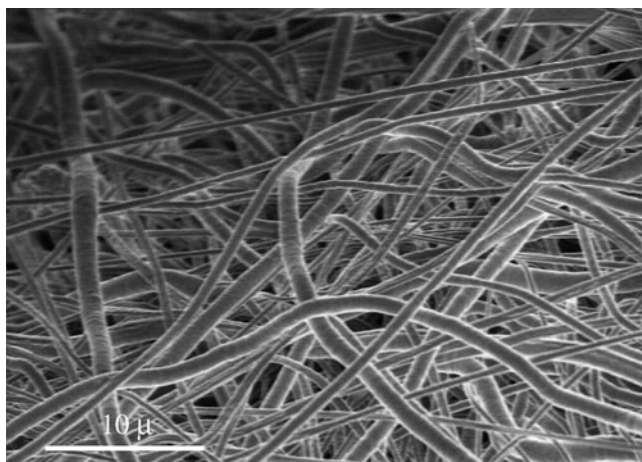


FIG. 8.3. SEM micrograph of electrospun PCL poly(ϵ -caprolactone) nanofibers. The fibers were spun from a 15 wt.% PCL solution in DMF/DCM (25:75) with applied electrostatic field of 1 kV/cm (Zussman et al., 2004).

Fang and Reneker (1997) reported producing calf thymus Na-DNA fibers with beads structure through electrospinning from aqueous solutions with concentration from 0.3 to 1.5%. Scanning electron micrographs showed that the fibers had diameters as small as 30 nm and beads with diameters from 80 to 200 nm. The beads suggest that some of the DNA retracted into droplets at intervals along the fiber. In the fiber with diameter of 62 nm about 600 DNA molecules could pass through each cross-section. Transverse striations on the fibers, about 3–6 nm wide, were also found.

There are some indications that smooth muscle cells can better infiltrate a slightly oriented matrix (Matthews et al., 2002). This conclusion could be checked using fully oriented matrixes produced by the method of Theron et al. (2001); cf. Section VI, Yang et al. (2005) and Ramakrishna et al. (2005). This has been recently done in Xu et al. (2004), where favorable interaction of such scaffolds with human coronary artery smooth muscle cells was demonstrated. To the best of our knowledge, nanofibers or oriented nanofiber ropes still have not been used for nerve regeneration. The method of Theron et al. (2001) can easily be applied for fabrication of oriented ropes of conducting nanofibers, which can be tested as nerve substitutes. Nanofiber mats have great potential as scaffolds for artificial skin and artificial organs.

Electrostatic spinning was applied to the preparation of drug-laden non-biodegradable nanofibers for potential use in topical drug administration and wound healing. The specific aim of these studies was to assess whether

these systems might be of interest as delivery systems for poorly water-soluble drugs. Antifungal agents (itraconazole and ketanserin) were selected as model compounds while a segmented PU was selected as the non-biodegradable polymer (Verreck *et al.*, 2003). For both itraconazole and ketanserin, an amorphous nanodispersion with PU was obtained when the drug/polymer solutions were electrospun from dimethylformamide (DMF) and dimethylacetamide (DMAc), respectively. The collected non-woven fabrics were shown to release the drugs at various rates and profiles based on the nanofiber morphology and drug content. The electrospinning of colloidal particles such as fungicides blended in polymer solutions results in the production of nanofibers with incorporated nanoparticles. The water insoluble polymer, PCL, was used for producing nanofibers ranging 200–1000 nm in diameter. Acetone suspensions of the fungicides Benomyl or Ciclopirox containing the antifungal agents were added to PCL solutions and the mixture was electrospun using electrostatic field strength of about 3 kV cm^{-1} . Fungicide granules could be observed, by scanning electron microscopy, to be associated with the produced nanofibers (see Fig. 8.4). The effect of different electrospinning conditions on antifungal activity (against *Penicillium digitatum*, and *Sclerotinia sclerotiorum*) was determined by diffusion assays.

Electrospinning as encapsulation of various drugs inside as-spun nanofibers was also demonstrated by Kenawy *et al.* (2002) and Sanders *et al.* (2003). The drugs can further be released when nanofiber mats have been implanted or attached to a human body. Prediction, measurement and control of the release rate pose interesting unsolved applied mechanical problems. Viruses can also be encapsulated in the electrospun nanofibers (Lee and Belcher, 2004).

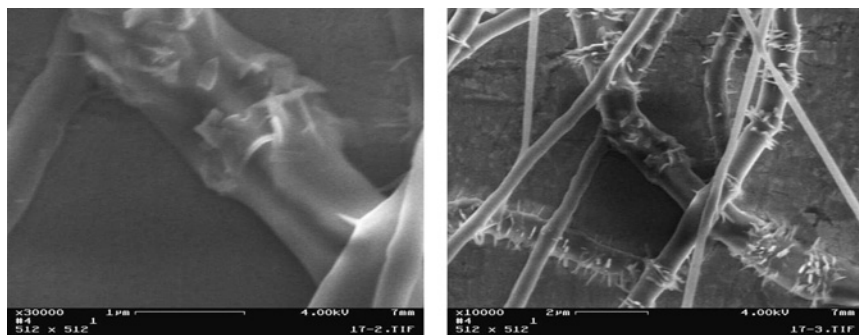


FIG. 8.4. SEM micrographs of fungicide-embedded electrospun nanofibers made from solution of PCL 10 wt.% in acetone and Ciclopirox powder (Zussman *et al.*, 2004).

2. Surface Properties

The physical and chemical characteristics of the scaffold surface mediate the adsorption of biological molecules that regulate cell activities, such as adhesion and migration (Boyan et al., 1996). Cells are able to attach to the electrospun mat and proliferate into it. Therefore, design criteria of an ideal engineering scaffold include favorable cell–matrix interactions, and biocompatibility of the structure (Li et al., 2002). The results of the latter work show suitable biocompatibility for mouse fibroblasts and human bone-marrow-derived mesenchymal stem cells on poly(D,L-lactide-*co*-glycolide) (PLGA) nanofibers. This opens possibilities for scaffolding human skin, cartilage, cardiovascular and bone-like materials. To make bones, cells should be calcium-producing, which is an essential structural element.

The hydrophilicity (wettability) of the electrospun scaffolds is related to the static contact angles between the scaffold and the buffer solution containing MC3T3-E1 (mouse calvaria osteoblast) cells; Kim et al. (2003). The contact angle of the cell-containing solution with an electrospun scaffold made of pure PLGA, poly(lactide-*co*-glycolide) (LA/GA = 75/25, M_w = 75,000) was 105°. The contact angle value between purified water and the same electrospun mat was also 105°. That suggested that the presence of the cells did not alter wettability of this electrospun mat.

The feasibility of obtaining a hydrophobic electrospun mat from high-molecular weight polymer was demonstrated by Deitzel et al. (2002). They electrospun polymer blends composed of PMMA with a varying amount of tetrahydroperfluoroctyl acrylate (TAN) with the concentration of TAN in the range from 0 to 10%. The fiber diameters were in the range from 0.1 to 2 μ m. Beads, due to capillary instability, were observed along the fibers. Jiang et al. (2004) demonstrated that an electrospun mat fabricated from a 25 wt% solution of polystyrene PS in DMF created a superhydrophobic surface with water, with a contact angle of 160.4°. This work resulted in nanofibers, which create a mat with two scales, the fiber scale and the beads scale. Such morphology reveals superhydrophobic behavior as in the famous lotus effect.

To tackle the hydrophobic properties of polymer mats which are normally resistant to infiltration of water into their pores, a surface treatment with ethanol was suggested (Stitzel et al., 2001). The treatment was demonstrated on an electrospun PLA mat, which was wetted by immersion in ethanol followed by immersion in water. In particular, the mat was wetted with 100% ethanol for 30 min, rinsed once with sterile water and placed in fresh sterile water for 30 min. The wetting procedure allows an effective penetration of

cells into the interstices of the matrix, as well as simultaneously sterilizing the matrix/fiber structure.

3. Porosity

Porosity and interconnectivity are essential in scaffolds for diffusion of nutrients and gasses and/or for removal of metabolic waste (Salgado *et al.*, 2004). Scaffolds must possess open pores and a fully inter-connected geometry in a highly porous structure with a large surface area to volume ratio. That will aid migration of growing cells throughout the porous structure. Furthermore, the scaffolds should also exhibit adequate microporosity in order to allow capillary ingrowth. Pore sizes and flexibility are also very important.

An electrospun nanofiber mat of copolymer PLGA [85:15; PL:GA] resulted in porosity of 91.63%. The pore diameter distribution measured by a mercury porosimeter indicated that pore diameter ranged broadly from 2 to 465 μm . The effective pore diameters for cell ingrowth into a non-woven mat are between 20 and 60 μm while for bone ingrowth 75–150 μm are required (Li *et al.*, 2002). If in a non-woven mat of nanofibers the fibers are not attached at contact points, cells are able to push nanofibers aside. Therefore, even the smallest pores could become appropriate for cell ingrowth. Salgado *et al.* (2004) argue that for bone tissue engineering purposes, pore size should be within the 200–900 μm range. Holy *et al.* (2000) reported an application of electrospinning for bone tissue engineering where they investigated a scaffold made of biodegradable PLGA 75/25. The scaffold exhibited a regular distribution of inter-connected macropores with diameters in the range from 1.5 to 2.2 mm.

4. Mechanical Properties

The strength and elasticity of a scaffold are other important aspects for its design. The scaffold should withstand the expected mechanical stresses and ideally match the mechanical behavior of its immediate environment. In bone tissue engineering, because the bone is subjected to varying stress, the mechanical properties of the implanted construct should ideally match those of the living bone (Hutmacher, 2000). Zong *et al.* (2003) showed that electrospun PLGA membranes are promising scaffolds for applications such as regeneration of heart tissue. Cardiac myocytes were found to remodel the flexible electrospun matrix by pulling on fibers and moving into the scaffold to form dense multiple layers.

Stress-strain curves measured for polymer nanofiber mats of interest in the tissue engineering field, PGA and PLGA revealed mechanical properties of their non-woven mats comparable to those of human cartilage and skin. The tensile (Young's) modulus E was of the order of 300 MPa, the ultimate (maximal) tensile stress was about 23 MPa and the strain at breakup was about 96% (Boland et al., 2001; Li et al., 2002). For non-woven mats of poly(ϵ -caprolactone), PCL, the ultimate tensile stress and strain were found to be of about 1–2 MPa and 200%, respectively (Lee et al., 2003a). The Young's modulus was of the order of 3–5 MPa, and the yield stress was 0.5–0.6 MPa (Lee et al., 2003a). Measurements done for quasi-parallel fiber mats of polylactide, PLA, using 250–1000 nm nanofibers, revealed an ultimate tensile stress of about 0.1 MPa and an ultimate tensile strain of about 14% (Dersh et al., 2003).

B. CONDUCTING NANOFIBERS: DISPLAYS, LIGHTING DEVICES, OPTICAL SENSORS, THERMOVOLTAIC APPLICATIONS

Electrospinning of conducting nanofibers was considered briefly in Section VI. In the present section, we extend the discussion. Poly(pyrrole), polyaniline, PEDOT, PPV and MEH-PPV (poly(2-methoxy, 5-(2'-ethylhexoxy)-*p*-phenylenevinylene) are the conducting conjugated polymers which received the most attention from the researchers dealing with fiber and nanofiber applications. The interest is related first of all to their possible applications in micro- and opto-electronics. LEDs made of conjugated polymers have been examined for such applications as displays and lighting (Weder et al., 1998; Ho et al., 1999). The intrinsic anisotropy of the electronic structure of such molecules means that provided they can be oriented into a specific direction, emission of polarized light will occur. A polarization ratio 200:1 would not require power inefficient external polarizers to produce useful polarized light (Whitehead et al., 2000). In order to optimize the broad range of the electrical properties of conjugated polymers, a variety of processing techniques were developed to improve the structural order to the point that the intrinsic properties of the macromolecular chains can be achieved. These techniques include mechanical alignment by rubbing, stretching (Grell and Bradley, 1999) or alignment of luminescent "guest" molecules in a "host" polymer matrix (Hagler et al., 1991). Further improvement in material quality is expected in the intrinsic electronic properties of conjugated polymers, as well as improvement of the ability to fabricate thin media for creating power efficient devices that operate at low voltage.

Srinivasan and Reneker (Srinivasan, 1994) reported electrospun polyaniline (VERSICON[®]) fibers from solutions in concentrated sulfuric acid (95–98%) containing 15–18% by weight of the polymer. The electrospun fibers were green in color in the conducting state. They were often curved and looped. Roughness of the surface of the fibers measured with an STM on a $100 \times 100 \text{ nm}^2$ area was about 18. The diameter of the polyaniline fibers ranges from about 40 nm to about a micron. These diameters are the lowest reported for polyaniline. Such fibers can potentially be used in electro-mechanical actuators, which convert electrical energy to mechanical energy using doping/dedoping or charge transfer reactions that cause large dimensional changes in the system. Srinivasan and Reneker proved by the successful imaging of the surface of the fibers using an STM that the fibers were electrically conducting.

Electrospinning represents a very promising technique for fabrication of luminescent nanofibers based on conducting, photosensitive polymers. The high value of the area reduction ratio and the associated high longitudinal strain rate ($\sim 1000 \text{ s}^{-1}$) imply that macromolecules in the nanofibers should be elongated and oriented in the direction of the jet axis. In the present context, the aim is to electrospin spinnable “host” polymer nanofibers containing light-emitting “guest” conjugated polymers, and conjugated polymers are typically not spinnable. Utilizing the high degree of chain extension, chain alignment and structural order attainable, in principle, in electrospinning of the “host” polymer, one can expect to induce a similar order in the “guest” conjugated macromolecules incorporated in the nanofiber. This will allow a combination of the mechanical properties of electrospun “host” polymer nanofiber with the electric conductivity and the anisotropic linear and non-linear optical properties of the conjugated “guest” polymer.

Electrospinning of a blend of polyaniline doped with camphorsulfonic acid (PAn.HCSA) and PEO was previously demonstrated (MacDiarmid *et al.*, 2001; Norris *et al.*, 2000; MacDiarmid, 2001). The electrospun nanofibers had diameters ranging between 950 and 2100 nm, with a generally uniform thickness along the fiber. The fibers formed a non-woven mat with high porosity and a relatively low conductivity compared to cast films. The method proposed in Theron *et al.* (2001) and Zussman *et al.* (2003b) allows assembly of the individual electrospun nanofibers aligned with a preferable orientation relative to the substrate, as well as nanofiber crossbars. In this method, both high molecular orientation of the nanofibers and a structural orientation are guaranteed. Photovoltaic diodes, which could be based on such nanofibers, are described in Granstrom *et al.* (1998).

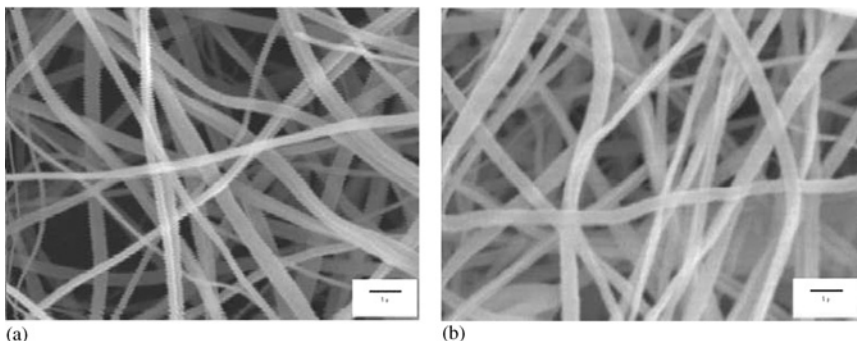


FIG. 8.5. Scanning electron microscope images of self-supporting and continuous titania nanofibers after pyrolysis. These structures result from electrospinning TPT/PVP solutions with ratios of (a) 0.2 and (b) 0.4 by weight. The scale bar in both panels is 1 μ m. After Teye-Mensah et al. (2004) with permission from IOP.

Teye-Mensah et al. (2004) and Tomer et al. (2005) reported erbium (III) oxide particles hybridized with titania nanofibers electrospun from mixed solution of tetraisopropyl titanate (TPT) and polyvinylpyrrolidone (PVP); Fig. 8.5. The electrospun nanofibers were thermally annealed at 900°C to pyrolyse the PVP, leaving nanofibres of rutile-phase titania. The erbium (III) oxide particles modify the near-infrared optical properties of the titania nanofibres as are verified both by absorption and emission spectra. They demonstrated that the diameters of the nanofibers can be controlled by adjusting the precursor solution, and the crystal structure can be adjusted by annealing at different temperatures. Temperature-dependent near-infrared emission spectra demonstrate that the erbia-containing nanofibers emit selectively in the range 6000–7000 cm^{-1} . These high-temperature optically functionalized nanostructures with large surface to volume ratios and narrow-band optical emission can be used in a thermophotovoltaic energy conversion system.

C. PROTECTIVE CLOTHING, CHEMICAL AND BIOSENSORS AND SMART FABRICS

Protective clothing is expected to employ polymer nanofibers as a key element (Schreuder-Gibson et al., 2002, 2003). The advantages of using nanofibers in protective clothing are twofold: (i) Nanofiber mats have a huge internal surface, which allows an enhanced contact area between the protective medium and dangerous and aggressive environment. Examples of such an environment are lethal gases such as mustard gas, sarin and nerve gases, as well

as aerosols of contagious disease spores, which could be used in chemical and biological warfare. (ii) It is relatively easy to incorporate different chemical agents into polymer solutions and, via electrospinning, into polymer nanofibers. These agents could effectively deactivate dangerous chemical and biological compounds in contact with them, and thus protect personnel. Nanofibers containing deactivating agents can also be used in gas masks. For all these applications, as well as for such applications as nanofiber-based filters, mass production of nanofibers at fast rate becomes crucial. This both makes scale-up of the manufacturing process based on electrospinning and the search for appropriate stable deactivating agents compatible with nanofiber-forming polymer solutions important activities.

Bulletproof vests incorporating nanofibers could become more effective and stronger than the ordinary Kevlar-based ones given the fact that spider dragline silk is stronger than Kevlar and stretches better than nylon (cf. Section VIII.A).

Srinivasan and Reneker (Srinivasan, 1994) reported electrospun KEVLAR[®] fibers from solutions in concentrated sulfuric acid (95–98%) containing 2–3% by weight of the polymer, PPTA. Small diameter fibers ranging from 40 nm to a few hundreds of nanometers were successfully spun by the electrospinning technique. These fibers were at least one order of magnitude smaller in diameter than available textile fibers. The PPTA molecules were shown to be oriented along the fiber axis. The electron diffraction patterns obtained from the PPTA fibers were similar to the electron diffraction patterns obtained from fibers spun commercially from the liquid crystalline state. The annealing allowed the crystallites to rearrange themselves to a more thermodynamically stable state as opposed to a more kinetically determined arrangement in as-spun fibers. Although PPTA is a rod-like polymer, solutions of PPTA in this process have enough extensional flow to orient the chain molecules. Dark-field imaging revealed crystallites whose size and orientation was characterized. High magnification bright field images of an annealed fiber revealed alternate bright and dark stripes suggesting the stacking of coin-shaped layers with slightly different orientation along the fiber axis.

The tensile modules and the strength of polymers depend on the degree of chain orientation. Achievement of a high degree of chain orientation is an ongoing goal in the technology of high-performance polymer fibers. The high draw ratios achieved in electrospinning (of the order of 1000) offer an opportunity to obtain novel highly oriented nanofibers with fully extended polymer chain conformation without recourse to rigid or ultra-long chain architecture (cf. e.g., Kahol and Pinto, 2002).

In the work of Zussman et al. (2002), micro-aerodynamic decelerators based on air permeable nanofiber mats were studied. The nanofibers were obtained via electrospinning of polymer solutions. The mats were electrospun directly onto light pyramid-shaped frames. These platforms were released and fell freely through the stagnant air, apex down, at a constant velocity. The motivation of Zussman et al. (2002) stems from a necessity to develop very light air-borne platforms of weight less than 1 g, capable of carrying relatively large payloads up to several grams. The platforms should be capable of delivering various chemical, biological, thermal and radioactivity sensors to the locations otherwise difficult to reach. This is of crucial importance in the cases of spillage or other dissemination of hazardous materials, and for atmospheric studies. In spite of the fact that different platform configurations could be imagined, their feasibility is rooted in the same question: whether or not a permeable and thus very light parachute could possess the same drag as the corresponding impermeable one? It was demonstrated in Zussman et al. (2002) that terminal velocity of such permeable structures is of the order of $30\text{--}50\text{ cm s}^{-1}$ with payloads of up to several grams. The reduced settling velocity of the mats with porosities of the order of 0.8–0.9 shows that permeable wings or parachutes based on nanofibers are feasible. Passive platforms similar to those of the above-mentioned work would be easily transported by wind to large distances. Active flapping or jet-propulsion-based light flying objects fabricated via electrospinning are also possible (Pawlowski et al., 2003). The inter-fiber spaces constitute a significant part of their area. This fact allows for a significant reduction in the weight of these structures compared to the corresponding impermeable structures. Permeable non-woven nanofiber networks are sufficiently strong and have negligible weight even compared to the light frames or to light plastic wrap. Therefore, the role of the non-woven fiber mats attached at the frames is twofold: (i) to generate drag force, while (ii) to reduce the weight. The ultimate aim of such a construction is to reduce the terminal settling velocity while carrying a useful payload (e.g. a sensor). The nanofiber mats for this purpose may ultimately be electrospun from photo-sensitive polymers, which can generate electric power for sensors from the sunlight, thus making the wings also a source of energy for the sensors and their transmitters (cf. Teye-Mensah et al., 2004; Tomer et al., 2005).

Different chemical and biological indicators can easily be incorporated in polymers. As a continuation of the work in Zussman et al. (2002), one of the chemical indicators, bromophenol, was incorporated into nanofibers-based airborne platforms (WMD Sensitive, 2004). It was shown that the platforms changed their color when subjected to an appropriate acidic or basic environment thus serving as chemical indicators. In Wang et al. (2002),

non-woven nanofiber mats containing pyrene methanol were used as a highly sensitive fluorescence-based optical sensor for detection of explosives.

Acknowledgment

Support for this work was provided by the National Science Foundation under Grants Nos. DMI-9813098 and CTS-9900949, by the U.S. Army Research Office MURI Grant No. 95-0950-01-06, by the U.S. Army Soldier and Biological Systems Command, by the Nonmetallic Materials Division of the U.S. Air Force Research Laboratory, Wright Patterson Air Force Base, by the GIF-German-Israeli Foundation for Scientific Research and Development under Grant No. I-536-097.14/97, by the Israel Academy of Sciences under Grants No. 287/00-1 and 26/03, and by a Grant from VolkswagenStiftung, Germany. The authors gratefully acknowledge their research collaboration with Y. Cohen, Y. Dror, H. Fong, W. Kataphinan, R. Khalfin, S. Koombhongse, S.N. Reznik, W. Salalha and A. Theron.

References

Aref, H., and Flinchem, E. P. (1984). Dynamics of a vortex filament in a shear flow. *J. Fluid Mech.* **148**, 477–497.

Arms, R. J., and Hama, F. R. (1965). Localized-induction concept on a curved vortex and motion of an elliptic vortex ring. *Phys. Fluids* **8**, 533–559.

Bandyopadhyaya, R., Nativ-Roth, E., Regev, O., and Yerushalmi-Rozen, R. (2002). Stabilization of individual carbon nanotubes in aqueous solutions. *Nano Letters* **2**, 25–28.

Batchelor, G. K. (1967). *An Introduction to Fluid Dynamics*. Cambridge University Press, Cambridge.

Bates, W. D., Barnes, C. P., Ounaies, Z., and Wnek, G. E. (2003). Electrostatic processing of PVDF. *Polym. Preprints*, **44**, 114–114.

Baumgarten, P. K. (1971). Electrostatic spinning of acrylic microfibers. *J. Colloid. Interface Sci.* **36**, 71–79.

Bird, R. B., Armstrong, R. C., and Hassager, O. (1987). *Dynamics of Polymeric Liquids*, 2nd ed. Wiley, New York.

Bognitzki, M., Czado, W., Freze, T., Schaper, A., Hellwig, M., Steinhart, M., Greiner, A., and Wendorff, J. H. (2001). Nanostructured fibers via electrospinning. *Adv. Mat.* **13**, 70–72.

Bognitzki, M., Hou, H., Ishaque, M., Frese, T., Hellwig, M., Schwarte, C., Schaper, A., Wendorff, J. H., and Greiner, A. (2000). Polymer, metal and hybrid nano- and mesotubes by coating degradable polymer template fibers (TUFT process). *Adv. Mat.* **12**, 637–640.

Boland, E. D., Matthews, J. A., Pawlowski, K. J., Simpson, D. G., Wnek, G. E., and Bowlin, G. L. (2004). Electrospinning collagen and elastin: preliminary vascular tissue engineering. *Front. Biosci.* **9**, 1422–1432.

Boland, E. D., Wnek, G. E., Simpson, D. G., Pawlowski, K. J., and Bowlin, G. L. (2001). Tayloring tissue engineering scaffolds using electrostatic processing techniques: a study of poly(glycolic acid) electrospinning. *J. Macromol. Sci. – Pure Appl. Chem.* **A38**, 1231–1243.

Boyan, B. D., Hummert, T. W., Dean, D. D., and Schwartz, Z. (1996). Role of material surfaces in regulating bone and cartilage cell response. *Biomaterials* **17**, 137–146.

Braun, E., Eichen, Y., Sivan, U., and Ben-Yoseph, G. (1998). DNA-templated assembly and electrode attachment of a conducting silver wire. *Nature* **391**, 775–778.

Buchko, C. J., Kozloff, K. M., and Martin, D. C. (2001). Surface characterization of porous, biocompatible protein polymer thin films. *Biomaterials* **22**, 1289–1300.

Busscher, H. J., van Pelt, A. W. J., de Boer, P., de Jong, H. P., and Arends, J. (1984). The effect of surface roughening of polymers on measured contact angles of liquids. *Colloid. Surface* **9**, 319–331.

Caruso, R. A., Schattka, J. H., and Greiner, A. (2001). Titanium dioxide tubes from sol–gel coating of electrospun polymer fibers. *Adv. Mat.* **13**, 1577–1579.

Chang, H., and Lodge, A. S. (1972). Comparison of rubberlike–liquid theory with stress-growth data for elongation of a low-density branched polyethylene melt. *Rheol. Acta* **11**, 127–129.

Cheng, K. J., and Miksis, M. J. (1989). Shape and stability of a drop on a conducting plane in an electric field. *Physicochem. Hydron.* **11**, 9–20.

Cherney, L. T. (1999a). Structure of Taylor cone-jets: limit of low flow rates. *J. Fluid Mech.* **378**, 167–196.

Cherney, L. T. (1999b). Electrohydrodynamics of electrified liquid menisci and emitted jets. *J. Aerosol Sci.* **30**, 851–862.

Ciferri, A., and Ward, I. M., eds. (1979). *Ultra-High Modulus Polymers*. Applied Science Publishers, London.

Cobden, D. H. (2001). Molecular electronics – nanowires begin to shine. *Nature* **409**, 32–33.

Cuenot, S., Demoustier-Champagne, S., and Nysten, B. (2000). Elastic modulus of polypyrrole nanotubes. *Phys. Rev. Lett.* **85**, 1690–1693.

Dalton, A. B., Blau, W. J., Chambers, G., Coleman, J. N., Henderson, K., Lefrant, S., McCarthy, B., Stephan, C., and Byrne, H. J. (2001). A functional conjugated polymer to process, purify and selectively interact with single wall carbon nanotubes. *Synth. Met.* **121**, 1217–1218.

de Gennes, P. G. (1974). Coil-stretch transition of dilute flexible polymers under ultrahigh velocity gradients. *J. Chem. Phys.* **60**, 5030–5042.

Deitzel, J. M., Kleimeyer, J. D., Hirvonen, J. K., and Tan, N. C. B. (2001). Controlled deposition of electrospun poly(ethylene oxide) fibers. *Polymer* **42**, 8163–8170.

Deitzel, J. M., Kosik, W., McKnight, S. H., Tan, N. C. B., DeSimone, J. M., and Crette, S. (2002). Electrospinning of polymer nanofibers with specific surface chemistry. *Polymer* **43**, 1025–1029.

Demir, M. M., Yilgor, I., Yilgor, E., and Erman, B. (2002). Electrospinning of polyurethane fibers. *Polymer* **43**, 3303–3309.

Demoustier-Champagne, S., Duchet, J., and Legras, R. (1999). Chemical and electrochemical synthesis of polypyrrole nanotubes. *Synth. Met.* **101**, 20–21.

Dersh, R., Liu, T., Schaper, A. K., Greiner, A., and Wendorff, J. H. (2003). Electrospun nanofibers: internal structure and intrinsic orientation. *J. Polym. Sci., Polym. Chem. Ed.* **A41**, 545–553.

Doshi, J., and Reneker, D. H. (1995). Electrospinning process and applications of electrospun fibers. *J. Electrostat.* **35**, 151–160.

Drew, C., Wang, X. Y., Senecal, K., Schreuder-Gibson, H., He, J. N., Kumar, J., and Samuelson, L. A. (2002). Electrospun photovoltaic cells. *J. Macromol. Sci. – Pure Appl. Chem.* **A39**, 1085–1094.

Driesel, W., Dietzsch, Ch., and Muhle, R. (1996). *In situ* observation of the tip shape of AuGe liquid alloy ion sources using a high voltage transmission electron microscope. *J. Vac. Sci. Technol.* **B14**, 3367–3380.

Dror, Y., Salalha, W., Khalfin, R., Cohen, Y., Yarin, A. L., and Zussman, E. (2003). Carbon nanotubes embedded in oriented polymer nanofibers by electrospinning. *Langmuir* **19**, 7012–7020.

Duan, X., Huang, Y., Cui, Y., Wang, J., and Lieber, C. M. (2001). Indium phosphide nanowires as building blocks for nanoscale electronic and optoelectronic devices. *Nature* **409**, 66–69.

Duft, D., Achtzehn, T., Muller, R., Huber, B. A., and Leisner, T. (2003). Rayleigh jets from levitated microdroplets. *Nature* **421**, 128–128.

Dzenis, Y. (2004). Spinning continuous fibers for nanotechnology. *Science* **304**, 1917–1919.

Dzhaugashin, K. E., and Yarin, A. L. (1977). Numerical simulation of nonself-similar wall jet. *J. Eng. Phys.* **32**, 420–426.

Edelman, F. T. (1999). Fullerene pipes, tube-in-tube membranes, and carbon-nanotube tips: adding new dimensions to molecular technology. *Angew. Chemie – Int. Ed.* **38**, 1381–1387.

Entov, V. M., and Yarin, A. L. (1984). The dynamics of thin liquid jets in air. *J. Fluid Mech.* **140**, 91–111.

Espy, P. G., McManus, M. C., Bowlin, G. L., and Koo, H. P. (2004). Electrospun elastin scaffolds for use in bladder tissue engineering. *J. Urol.* **171**, 457–457.

Evans, E., Brownman, H., Leung, A., Needham, D., and Tirrell, D. (1996). Biomembrane templates for nanoscale conduits and networks. *Science* **273**, 933–935.

Fang, Q., Chetwynd, D. G., and Gardner, J. W. (2001). Tensile properties of conducting polymer fibres. *Proc. of 2nd EUSPEN Internat. Conf., Turin, Italy* 27–31(May), 32–35.

Fang, X., and Reneker, D. H. (1997). DNA fibers by electrospinning. *J. Macromol. Sci. Phys. Ed.* **B36**, 169–173.

Feng, J. J. (2002). The stretching of an electrified non-Newtonian jet: a model for electrospinning. *Phys. Fluids* **14**, 3912–3926.

Feng, J. J. (2003). Stretching of a straight electrically charged viscoelastic jet. *J. Non-Newtonian Fluid Mech.* **116**, 55–70.

Fernandez de la Mora, J. (1992). The effect of charge emission from electrified liquid cones. *J. Fluid Mech.* **243**, 561–574.

Fong, H., Chung, I., and Reneker, D. H. (1999). Beaded nanofibers formed during electrospinning. *Polymer* **40**, 4585–4592.

Fong, H., and Reneker, D. H. (1999). Elastomeric nanofibers of styrene–butadiene–styrene triblock copolymer. *J. Polym. Sci., Polym. Phys. Ed.* **37**, 3488–3493.

Fong, H., and Reneker, D. H. (2000). Electrospinning and formation of nanofibers. In *Structure Formation in Polymeric Fibers* (D. R., Salem, and M. V., Sussman, eds.), pp. 225–246. Hanser, Munich.

Formhals, A. (1934). Process and apparatus for preparing artificial threads. U.S. Patent No. 1,975,504.

Frenot, A., and Chronakis, I. S. (2003). Polymer nanofibers assembled by electrospinning. *Curr. Opinion Colloid Interface Sci.* **8**, 64–75.

Fridrikh, S. V., Yu, J. H., Brenner, M. P., and Rutledge, G. C. (2003). Controlling the fiber diameter during electrospinning. *Phys. Rev. Lett.* **90** Art. No. 144502.

Ganan-Calvo, A. M. (1997a). On the theory of electrohydrodynamically driven capillary jets. *J. Fluid Mech.* **335**, 165–188.

Ganan-Calvo, A. M. (1997b). Cone-jet analytical extension of Taylor's electrostatic solution and the asymptotic universal scaling laws in electrospraying. *Phys. Rev. Lett.* **79**, 217–220.

Ganan-Calvo, A. M. (1999). The surface charge in electrospraying: its nature and its universal scaling laws. *J. Aerosol Sci.* **30**, 863–872.

Ge, J. J., Hou, H. Q., Li, Q., Graham, M. J., Greiner, A., Reneker, D. H., Harris, F. W., and Cheng, S. Z. D. (2004). Assembly of well-aligned multiwalled nanotubes in confined polyacrylonitrile environments. Electrospun composite nanofiber sheets. *J. Am. Chem. Soc.* **126**, 15754–15761.

Ghadiri, M., Granja, J. R., and Buechler, L. (1994). Artificial transmembrane ion channels from self-assembling peptide nanotubes. *Nature* **369**, 301–304.

Granstrom, M., Petritsch, K., Arias, A. C., Lux, A., Andersson, M. R., and Friend, R. H. (1998). Laminated fabrication of polymeric photovoltaic diodes. *Nature* **395**, 257–260.

Grell, M., and Bradley, D. D. C. (1999). Polarized luminescence from oriented molecular materials. *Adv. Mat.* **11**, 895–905.

Gu, S. Y., Wu, Q. L., Ren, J., and Vansco, G. J. (2005). Mechanical properties of a single electrospun fiber and its structures. *Macromol. Rapid Commun.* **26**, 716–720.

Gupta, P., and Wilkes, G. L. (2003). Some investigations on the fiber formation by utilizing a side-by-side bicomponent electrospinning approach. *Polymer* **44**, 6353–6359.

Hagler, T. W., Pakbaz, K., Voss, K. F., and Heeger, A. J. (1991). Enhanced order and electronic delocalization in conjugated polymers oriented by gel processing in polyethylene. *Phys. Rev. B* **44**, 8652–8666.

Hamley, I. W. (2000). *Introduction to Soft Matter*. Wiley, Chichester.

Harris, C. E., Starnes Jr., J. H. & Stuart, M. J. (2001). NATA/TM-2001-210844, April 2001.

Harris, M. T., and Basaran, O. A. (1993). Capillary electrohydrostatics of conducting drops hanging from a nozzle in an electric field. *J. Colloid Interface Sci.* **161**, 389–413.

Hatzor, A., and Weiss, P. S. (2001). Molecular rulers for scaling down nanostructures. *Science* **291**, 1019–1020.

Hayati, I. (1992). Eddies inside a liquid cone stressed by interfacial electrical shear. *Colloid. Surf.* **65**, 77–84.

Heinrich, R., Bonisch, S., Pommerenke, D., Jobava, R., & Kalkner, W. (2000). Broadband measurement of the conductivity and the permittivity of semiconducting materials in high voltage XLPE cables. *8th Int. Conf. Dielect. Mater. Meas. Appl. Edinburgh, IEE Conf. Publ.* No. 473, 212–217.

Higuera, F. J. (2003). Flow rate and electric current emitted by a Taylor cone. *J. Fluid Mech.* **484**, 303–327.

Ho, P. K. H., Thomas, D. S., Friend, R. H., and Tessler, N. (1999). All-polymer optoelectronic devices. *Science* **285**, 233–236.

Hohman, M. M., Shin, M., Rutledge, G., and Brenner, M. P. (2001a). Electrospinning and electrically forced jets: I. Stability theory. *Phys. Fluids* **13**, 2201–2220.

Hohman, M. M., Shin, M., Rutledge, G., and Brenner, M. P. (2001b). Electrospinning and electrically forced jets: II. Applications. *Phys. Fluids* **13**, 2221–2236.

Holy, C. E., Schochet, M. S., and Davies, J. E. (2000). Engineering three-dimensional bone tissue in vitro using biodegradable scaffolds: investigating initial cell-seeding density and culture period. *J. Biomed. Mater. Res.* **51**, 376–382.

Hou, H., and Reneker, D. H. (2004). Carbon nanotube on carbon nanofibers: a novel structure based on electrospun nanofibers. *Adv. Mat.* **16**, 69–73.

Hsu, C. H., Shih, H., Subramoney, S., and Epstein, A. J. (1999). High tenacity, high modulus conducting polyaniline composite fibers. *Synth. Met.* **101**, 677–680.

Huang, L., Apkarian, R. P., and Chaikof, E. L. (2001a). High-resolution analysis of engineered type I collagen nanofibers by electron microscopy. *Scanning* **23**, 372–375.

Huang, Y., Duan, X. F., Wei, Q. Q., and Lieber, C. M. (2001b). Directed assembly of one-dimensional nanostructures into functional networks. *Science* **291**, 630–633.

Huang, Z. M., Zhang, Y. Z., Kotaki, M., and Ramakrishna, S. (2003). A review on polymer nanofibers by electrospinning and their applications in nanocomposites. *Composite Sci. Technol.* **63**, 2223–2253.

Huang, Z. M., Zhang, Y. Z., Ramakrishna, S., and Lim, C. T. (2004). Electrospinning and mechanical characterization of gelatin nanofibers. *Polymer* **45**, 5361–5368.

Hutmacher, D. W. (2000). Scaffolds in tissue engineering bone and cartilage. *Biomaterials* **21**, 2529–2543.

Iijima, S. (1991). Helical microtubules of graphitic carbon. *Nature* **354**, 56–58.

Inai, R., Kotaki, M., and Ramakrishna, S. (2005). Structure and properties of electrospun PLLA single nanofibers. *Nanotechnology* **16**, 208–213.

Jaeger, R., Schonherr, H., and Vancso, G. J. (1996). Chain packing in electrospun poly(ethylene oxide) visualized by atomic force microscopy. *Macromolecules* **29**, 7634–7636.

Jeans, J. (1958). *The Mathematical Theory of Electricity and Magnetism*. Cambridge University Press, Cambridge.

Jerome, C., Labaye, D., Bodart, I., and Jerome, R. (1999). Electrosynthesis of polyacrylic polypyrrole composites: formation of polypyrrole wires. *Synth. Met.* **101**, 3–4.

Jiang, L., Zhao, Y., and Zhai, J. (2004). A lotus-leaf-like superhydrophobic surface: a porous micropshere/nanofiber composite film prepared by electrohydrodynamics. *Angew. Chem.-Int. Ed.* **43**, 4338–4341.

Kahol, P. K., and Pinto, N. J. (2002). Electron paramagnetic resonance investigations of electrospun polyaniline fibers. *Solid State Commun.* **124**, 195–197.

Kedem, S., Schmidt, J., Paz, Y., and Cohen, Y. (2005). Composite polymer nanofibers with carbon nanotubes and titanium dioxide particles. *Langmuir* **21**, 5600–5604.

Kenawy, E. R., Bowling, G. L., Mansfield, K., Layman, J., Simpson, D. G., Sanders, E. H., and Wnek, G. E. (2002). Release of tetracycline hydrochloride from electrospun poly(ethylene-co-vinylacetate), poly(lactic acid), and a blend. *J. Contr. Release* **81**, 57–64.

Khakhar, D. V., and Ottino, J. M. (1987). Breakup of liquid threads in linear flows. *Int. J. Multiphase Flow* **13**, 71–86.

Khil, M. S., Kim, H. Y., Kim, M. S., Park, S. Y., and Lee, D. R. (2004). Nanofibrous mats of poly(trimethylene terephthalate) via electrospinning. *Polymer* **45**, 295–301.

Kidoaki, S., Kwon, I. K., and Matsuda, T. (2005). Mesoscopic spatial designs of nano- and microfiber meshes for tissue-engineering matrix and scaffold based on newly devised multilayering and mixing electrospinning techniques. *Biomaterials* **26**, 37–46.

Kim, B. C., Nair, S., Kim, J., Kwak, J. H., Grate, J. W., Kim, S. H., and Gu, M. B. (2005a). Preparation of biocatalytic nanofibres with high activity and stability via enzyme aggregate coating on polymer nanofibres. *Nanotechnology* **16**, S382–S388.

Kim, G. M., Lach, R., Michler, G. H., and Chang, Y. W. (2005b). The mechanical deformation process of electrospun polymer nanocomposite fibers. *Macromol. Rapid Commun.* **26**, 728–733.

Kim, J. S., and Reneker, D. H. (1999). Mechanical properties of composites using ultrafine electrospun fibers. *Polym. Composite* **20**, 124–131.

Kim, K., Yu, M., Zong, X., Chiu, J., Fang, D., Seo, Y. S., Hsiao, B. S., Chu, B., and Hadjigiyrou, M. (2003). Control of degradation rate and hydrophilicity in electrospun non-woven poly(D,L-lactide) nanofibers scaffolds for biomedical applications. *Biomaterials* **24**, 4977–4985.

Kirichenko, V. M., Petrianov-Sokolov, I. V., Suprun, N. N., and Shutov, A. A. (1986). Asymptotic radius of a slightly conducting liquid jet in an electric field. *Sov. Phys. Dokl.* **31**, 611–614.

Ko, F., Gogotsi, Y., Ali, A., Naguib, N., Ye, H. H., Yang, G. L., Li, C., and Willis, P. (2003). Electrospinning of continuous carbon nanotube-filled nanofiber yarns. *Adv. Mat.* **15**, 1161–1165.

Koombhongse, S., Liu, W., and Reneker, D. H. (2001). Flat polymer ribbons and other shapes by electrospinning. *J. Polym. Sci., Polym. Phys. Ed.* **39**, 2598–2606.

Larrondo, L., and Manley, R. S. J. (1981a). Electrostatic fiber spinning from polymer melts. I. Experimental observations on fiber formation and properties. *J. Polym. Sci., Polym. Phys. Ed.* **19**, 909–920.

Larrondo, L., and Manley, R. S. J. (1981b). Electrostatic fiber spinning from polymer melts. II. Examination of the flow field in an electrically driven jet. *J. Polym. Sci., Polym. Phys. Ed.* **19**, 921–932.

Larrondo, L., and Manley, R. S. J. (1981c). Electrostatic fiber spinning from polymer melts. III. Electrostatic deformation of a pendant drop of polymer melt. *J. Polym. Sci., Polym. Phys. Ed.* **19**, 933–940.

Larsen, G., Spretz, R., and Velarde-Ortiz, R. (2004). Use of coaxial gas jackets to stabilize Taylor cones of volatile solutions and to induce particle-to-fiber transitions. *Adv. Mat.* **16**, 166–169.

Lazaris, A., Arcidiacono, S., Huang, Y., Zhou, J. F., Duguay, F., Chretien, N., Welsh, E. A., Soares, J. W., and Karatzas, C. N. (2002). Spider silk fibers spun from soluble recombinant silk produced in mammalian cells. *Science* **295**, 472–476.

Lee, K. H., Kim, H. Y., Bang, H. J., Jung, Y. H., and Lee, S. G. (2003c). The change of bead morphology formed on electrospun polystyrene fibers. *Polymer* **44**, 4029–4034.

Lee, K. H., Kim, H. Y., Khil, M. S., Ra, Y. M., and Lee, D. R. (2003a). Characterization of nano-structured poly(ϵ -caprolactone) nonwoven mats via electrospinning. *Polymer* **44**, 1287–1294.

Lee, K. H., Kim, H. Y., La, Y. M., Lee, D. R., and Sung, N. H. (2002). Influence of a mixing solvent with tetrahydrofuran and N,N-di-methylformamide on electrospun poly(vinyl chloride) nonwoven mats. *J. Polym. Sci., Polym. Phys. Ed.* **B40**, 2259–2268.

Lee, K. H., Kim, H. Y., Ryu, Y. J., Kim, K. W., and Choi, S. W. (2003b). Mechanical behavior of electrospun fiber mats of poly(vinyl chloride)/polyurethane polyblends. *J. Polym. Sci., Polym. Phys. Ed.* **B41**, 1256–1262.

Lee, S. W., and Belcher, A. M. (2004). Virus-based fabrication of micro- and nanofibers using electrospinning. *Nano Letters* **4**, 387–390.

Li, D., Herricks, T., and Xia, Y. (2003). Magnetic nanofibers of nickel ferrite prepared by electrospinning. *Appl. Phys. Lett.* **83**, 4586–4588.

Li, D., McCann, J. T., and Xia, Y. (2005). Use of electrospinning to directly fabricate hollow nanofibers with functionalized inner and outer surfaces. *Small* **1**, 83–86.

Li, D., Wang, Y., and Xia, Y. (2004). Electrospinning nanofibers as uniaxially aligned arrays and layer-by-layer stacked films. *Adv. Mat.* **16**, 361–365.

Li, D., and Xia, Y. (2003). Fabrication of titania nanofibers by electrospinning. *Nano Lett.* **3**, 555–560.

Li, D., and Xia, Y. (2004a). Direct fabrication of composite and ceramic hollow nanofibers by electrospinning. *Nano Letters* **4**, 933–938.

Li, D., and Xia, Y. (2004b). Electrospinning of nanofibers: reinventing the wheel? *Adv. Mat.* **16**, 1151–1170.

Li, H., Halsey, T. C., and Lobkovsky, A. (1994). Singular shape of a fluid drop in an electric or magnetic field. *Europhys. Lett.* **27**, 575–580.

Li, W. J., Laurencin, C. T., Caterson, E. J., Tuan, R. S., and Ko, F. K. (2002). Electrospun nanofibrous structure: a novel scaffold for tissue engineering. *J. Biomed. Mater. Res.* **60**, 613–621.

Liu, W., Graham, M., Evans, E. A., and Reneker, D. H. (2002). Poly(meta-phenylene isophthalamide) nanofibers: coating and post processing. *J. Mater. Res.* **17**, 1–8.

Loscortales, I. G., Barrero, A., Marquez, M., Spretz, R., Velarde-Ortiz, R., and Larsen, G. (2004). Electrically forced coaxial nanojets for one-step hollow nanofiber design. *J. Am. Chem. Soc.* **126**, 5376–5377.

Ma, M., Hill, R. M., Lowery, J. L., Fridrikh, S. V., and Rutledge, G. C. (2005). Electrospun poly(styrene-block-dimethylsiloxane) block copolymer fibers exhibiting superhydrophobicity. *Langmuir* **21**, 5549–5554.

MacDiarmid, A. G. (2002). “Synthetic metals”: a novel role for organic polymers (Nobel lecture). *Angew. Chemie. – Int. Ed.* **40**, 2581–2590. Also in *Synth. Met.* **125**, 11–22.

MacDiarmid, A. G., Jones, W. E., Jr., Norris, I. D., Gao, J., Johnson, A. T., Jr., Pinto, N. J., Hone, J., Han, B., Ko, F. K., Okuzaki, H., and Llaguno, M. (2001). Electrostatically generated nanofibers of electronic polymers. *Synth. Met.* **119**, 27–30.

Martin, C. R. (1994). Nanomaterials – a membrane-based synthetic approach. *Science* **266**, 1961–1966.

Martin, C. R. (1995). Template synthesis of electronically conductive polymer. *Acc. Chem. Res.* **28**, 61–68.

Matthews, J. A., Wnek, G. E., Simpson, D. G., and Bowlin, G. L. (2002). Electrospinning of collagen nanofibers. *Biomacromolecules* **3**, 232–238.

Mbindyo, J. K. N., Reiss, B. D., Martin, B. R., Keating, C. D., Natan, M. J., and Mallouk, T. E. (2001). DNA-directed assembly of gold nanowires on complementary surfaces. *Adv. Mat.* **13**, 249–254.

McCarthy, B., Coleman, J. N., Curran, S. A., Dalton, A. B., Davey, A. P., Konya, Z., Fonseca, A., Nagy, J. B., and Blau, W. J. (2000). Observation of site selective binding in a polymer nanotube composite. *J. Mat. Sci. Lett.* **19**, 2239–2241.

McKinley, G. H., and Tripathi, A. (2000). How to extract the Newtonian viscosity from capillary breakup measurements in a filament rheometer. *J. Rheol.* **44**, 653–670.

Melcher, J. R., and Taylor, G. I. (1969). Electrohydrodynamics: a review of the role of interfacial shear stresses. *Annu. Rev. Fluid Mech.* **1**, 111–146.

Melcher, J. R., and Warren, E. P. (1971). Electrohydrodynamics of a current-carrying semi-insulating jet. *J. Fluid Mech.* **47**, 127–143.

Michelson, D. (1990). *Electrostatic Atomization*. Adam Higler, Bristol and New York.

Norris, I. D., Shaker, M. M., Ko, F. K., and MacDiarmid, A. G. (2000). Electrostatic fabrication of ultrafine conducting fibers: polyaniline/polyethylene oxide blends. *Synth. Met.* **114**, 109–114.

Notz, P. K., and Basaran, O. A. (1999). Dynamics of drop formation in an electric field. *J. Colloid Interface Sci.* **213**, 218–237.

O'Connell, M. J., Boul, P., Ericson, L. M., Huffman, C., Wang, Y. H., Haroz, E., Kuper, C., Tour, J., Ausman, K. D., and Smalley, R. E. (2001). Reversible water-solubilizaiton of single-walled carbon nanotubes by polymer wrapping. *Chem. Phys. Lett.* **342**, 265–271.

Ondarcuhu, T., and Joachim, C. (1998). Drawing a single nanofiber over hundreds of microns. *Europophys. Lett.* **42**, 215–220.

Oner, D., and McCarthy, T. J. (2000). Ultrahydrophobic surfaces. Effects of topography length scales on wettability. *Langmuir* **16**, 7777–7782.

Ozin, G. A. (1992). Nanochemistry – synthesis in diminishing dimensions. *Adv. Mat.* **4**, 612–649.

Pantano, C., Ganan-Calvo, A. M., and Barrero, A. (1994). Zeroth-order, electrohydrostatic solution for electrospraying in cone-jet mode. *J. Aerosol Sci.* **25**, 1065–1077.

Pawlowski, K. J., Belvin, H. L., Raney, D. L., Su, J., Harrison, J. S., and Siochi, E. J. (2003). Electrospinning of a micro-air vehicle wing skin. *Polymer* **44**, 1309–1314.

Pedicini, A., and Farris, R. J. (2003). Mechanical behavior of electrospun polyurethane. *Polymer* **44**, 6857–6862.

Perepelkin, K. E. (1985). *Structure and Properties of Fibers*. Chemistry, Moscow (in Russian).

Pomfret, S. J., Adams, P. N., Comfort, N. P., and Monkman, A. P. (1999). Advances in processing routes for conductive polyaniline fibres. *Synth. Met.* **101**, 724–725.

Poza, P., Perez-Rigueiro, J., Elices, M., and Llorca, J. (2002). Fractographic analysis of silkworm and spider silk. *Eng. Fracture Mech.* **69**, 1035–1048.

Pozrikidis, C. (1997). *Introduction to Theoretical and Computational Fluid Dynamics*. Oxford University Press, New York.

Rakov, E. G. (2000). The chemistry and application of carbon nanotubes. *Russ. Chem. Rev.* **70**, 827–863.

Ramakrishna, S., Fujihara, K., Teo, W. E., Lim, T. C., and Ma, Z. (2005). *An Introduction to Electrospinning of Nanofibers*. World Scientific, Singapore.

Ramos, A., and Castellanos, A. (1994). Conical points in liquid–liquid interfaces subjected to electric fields. *Phys. Lett.* **A184**, 268–272.

Reneker, D. H., and Chun, I. (1996). Nanometer diameter fibers of polymer, produced by electrospinning. *Nanotechnology* **7**, 216–223.

Reneker, D. H., Kataphinan, W., Theron, A., Zussman, E., and Yarin, A. L. (2002). Nanofiber garlands of polycaprolactone by electrospinning. *Polymer* **43**, 6785–6794.

Reneker, D. H., Yarin, A. L., Fong, H., and Koombhongse, S. (2000). Bending instability of electrically charged liquid jets of polymer solutions in electrospinning. *J. Appl. Phys.* **87**, 4531–4547.

Reznik, S. N., Yarin, A. L., Theron, A., and Zussman, E. (2004). Transient and steady shapes of droplets attached to a surface in a strong electric field. *J. Fluid Mech.* **516**, 349–377.

Salalha, W., Dror, Y., Khalfin, R. L., Cohen, Y., Yarin, A. L., and Zussman, E. (2004). Single-walled carbon nanotubes embedded in oriented polymeric nanofibers by electrospinning. *Langmuir* **20**, 9852–9855.

Salgado, A. J., Coutinho, O. P., and Reis, R. L. (2004). Bone tissue engineering: state of the art and future trends. *Macromol. Biosci.* **4**, 743–765.

Sanders, E. H., Kloefkorn, R., Bowlin, G. L., Simpson, D. G., and Wnek, G. E. (2003). Two-phase electrospinning from a single electrified jet: microencapsulation of aqueous reservoirs in poly(ethylene-co-vinyl acetate) fibers. *Macromolecules* **36**, 3803–3805.

Saville, D. A. (1971). Stability of electrically charged viscous cylinders. *Phys. Fluids* **14**, 1095–1099.

Saville, D. A. (1997). Electrohydrodynamics: the Taylor–Melcher leaky dielectric model. *Annu. Rev. Fluid Mech.* **29**, 27–64.

Schllichting, H. (1979). *Boundary Layer Theory*, 7th ed. McGraw-Hill, New York.

Schnur, J. M. (1993). Lipid tubules – paradigm for molecularly engineered structures. *Science* **262**, 1669–1676.

Schreuder-Gibson, H., Gibson, P., Senecal, K., Sennett, M., Walker, J., Yeomans, W., Ziegler, D., and Tsai, P. P. (2002). Protective textile materials based on electrospun nanofibers. *J. Adv. Mat.* **34**, 44–55.

Schreuder-Gibson, H. L., Truong, Q., Walker, J. E., Owens, J. R., Wander, J. D., and Jones, W. E. (2003). Chemical and biological protection and detection in fabrics for protective clothing. *MRS Bull.* **28**, 574–578.

Seaver, M., Galloway, A., and Manuccia, T. J. (1989). Acoustic levitation in a free-jet wind tunnel. *Rev. Sci. Instrum.* **60**, 3452–3459.

Seoul, C., Kim, Y. T., and Baek, C. K. (2003). Electrospinning of poly(vinylidene fluoride)/dimethylformamide solutions with carbon nanotubes. *J. Polym. Sci., Polym. Phys. Ed.* **41**, 1572–1577.

Sherwood, J. D. (1991). The deformation of a fluid drop in an electric field – A slender-body analysis. *J. Phys. A* **24**, 4047–4053.

Shin, Y. M., Hohman, M. M., Brenner, M. P., and Rutledge, G. C. (2001a). Electrospinning: a whipping fluid jet generates submicron polymer fibers. *Appl. Phys. Lett.* **78**, 1149–1151.

Shin, Y. M., Hohman, M. M., Brenner, M. P., and Rutledge, G. C. (2001b). Experimental characterization of electrospinning: the electrically forced jet and instabilities. *Polymer* **42**, 9955–9967.

Shkadov, V. Y., and Shutov, A. A. (2001). Disintegration of a charged viscous jet in a high electric field. *Fluid Dyn. Res.* **28**, 23–39.

Smith, P. A., Nordquist, C. D., Jackson, T. N., and Mayer, T. S. (2000). Electric-field assisted assembly and alignment of metallic nanowires. *Appl. Phys. Lett.* **77**, 1399–1401.

Smythe, W. R. (1968). *Static and Dynamic Electricity*, 3rd ed. McGraw-Hill, New York.

Spivak, A. F., and Dzenis, Y. A. (1998). Asymptotic decay of radius of a weakly conductive viscous jet in an external electric field. *Appl. Phys. Lett.* **73**, 3067–3069.

Srinivasan, G. (1994). Structure and morphology of electrospun polymer fibers. PhD thesis. Dept. of Polymer Sci., the University of Akron.

Stelter, M., Brenn, G., Yarin, A. L., Singh, R. P., and Durst, F. (2000). Validation and application of a novel elongational device for polymer solutions. *J. Rheol.* **44**, 595–616.

Stelter, M., Brenn, G., Yarin, A. L., Singh, R. P., and Durst, F. (2002). Investigation of the elongational behavior of polymer solutions by means of an elongational rheometer. *J. Rheol.* **46**, 507–527.

Stelter, M., Wunderlich, J., Rath, S. K., Brenn, G., Yarin, A. L., Singh, R. P., and Durst, F. (1999). Shear and extensional investigations in solutions of grafted/ungrafted amylopectin and polyacrylamide. *J. Appl. Polym. Sci.* **74**, 2773–2782.

Sternberg, E., and Koiter, W. T. (1958). The wedge under a concentrated couple: a paradox in the two-dimensional theory of elasticity. *J. Appl. Mech.* **25**, 575–581.

Stitzel, J. D., Pawlowski, K. J., Wnek, G. E., Simpson, D. G., and Bowlin, G. L. (2001). Arterial smooth muscle cell proliferation on a novel biomimicking, biodegradable vascular graft scaffold. *J. Biomat. Appl.* **16**, 22–33.

Stone, H. A., Lister, J. R., and Brenner, M. P. (1999). Drops with conical ends in electric and magnetic fields. *Proc. Roy. Soc. London A* **455**, 329–347.

Subbiah, T., Bhat, G. S., Tock, R. W., Parameswaran, S., and Ramkumar, S. S. (2005). Electrospinning of nanofibers. *J. Appl. Polym. Sci.* **96**, 557–569.

Sun, Z., Zussman, E., Yarin, A. L., Wendorff, J. H., and Greiner, A. (2003). Compound core-shell polymer nanofibers by co-electrospinning. *Adv. Mat.* **15**, 1929–1932.

Sundaray, B., Subramanian, V., Natarajan, T. S., Xiang, R. Z., Chang, C. C., and Fann, W. S. (2004). Electrospinning of continuous aligned polymer fibers. *Appl. Phys. Lett.* **84**, 1222–1224.

Suvorov, V. G., and Litvinov, E. A. (2000). Dynamic Taylor cone formation on liquid metal surface: numerical modeling. *J. Phys.* **D33**, 1245–1251.

Tan, E. P. S., and Lim, C. T. (2004). Physical properties of a single polymeric nanofiber. *Appl. Phys. Lett.* **84**, 1603–1605.

Tan, E. P. S., Ng, S. Y., and Lim, C. T. (2005). Tensile testing of a single ultrafine polymer fiber. *Biomaterials* **26**, 1453–1456.

Taylor, G. I. (1964). Disintegration of water drops in an electric field. *Proc. Roy. Soc. London A* **280**, 383–397.

Taylor, G. I. (1969). Electrically driven jets. *Proc. Roy. Soc. London A* **313**, 453–475.

Teye-Mensah, R., Tomer, V., Kataphinan, W., Tokash, J. C., Stojilovic, N., Chase, G. G., Evans, E. A., Ramsier, R. D., Smith, D. J., and Reneker, D. H. (2004). Erbia-modified electrospun titania nanofibers for selective infrared emitters. *J. Phys. – Condens. Matter* **16**, 7557–7564.

Theron, A., Zussman, E., and Yarin, A. L. (2001). Electrostatic field-assisted alignment of electrospun nanofibers. *Nanotechnology* **12**, 384–390.

Theron, A., Zussman, E., and Yarin, A. L. (2003). Measurements of the governing parameters in the electrospinning of polymer solutions. *Polym. Preprints* **44**, 61–62.

Theron, S. A., Yarin, A. L., Zussman, E., and Kroll, E. (2005). Multiple jets in electrospinning: experiment and modeling. *Polymer* **46**, 2889–2899.

Theron, S. A., Zussman, E., and Yarin, A. L. (2004). Experimental investigation of the governing parameters in the electrospinning of polymer solutions. *Polymer* **45**, 2017–2030.

Tomer, V., Teye-Mehsah, R., Tokash, J. C., Stojilovic, N., Kataphinan, W., Evans, E. A., Chase, G. G., Ramsier, R. D., Smith, D. J., and Reneker, D. H. (2005). Selective emitters for thermophotovoltaics: erbia-modified electrospun titania nanofibers. *Sol. Energ. Mater. Sol. Cells* **85**, 477–488.

Tseng, G. Y., and Ellenbogen, J. C. (2001). Nanotechnology – toward nanocomputers. *Science* **294**, 1293–1294.

Verreck, G., Chun, I., Rosenblatt, J., Peeters, J., Dijck, A. V., Mensch, J., Noppe, M., and Brewster, M. E. (2003). Incorporation of drugs in an amorphous state into electrospun

nanofibers composed of a water-insoluble, nonbiodegradable polymer. *J. Control Release* **92**, 349–360.

Vigolo, B., Renicaud, A., Coulon, C., Sauder, C., Pailler, R., Journet, C., Bernier, P., and Poulin, P. (2000). Macroscopic fibers and ribbons of oriented carbon nanotubes. *Science* **290**, 1331–1334.

Wan, M., Huang, J., and Shen, Y. (1999). Microtubes of conducting polymers. *Synth. Met.* **101**, 708–711.

Wang, A., Singh, H., Hatton, T. A., and Rutledge, G. C. (2004a). Field-responsive superparamagnetic composite nanofibers by electrospinning. *Polymer* **45**, 5505–5514.

Wang, M., Jin, H. J., Kaplan, D. L., and Rutledge, G. C. (2004b). Mechanical properties of electrospun silk fibers. *Macromolecules* **37**, 6856–6864.

Wang, X., Lee, S. H., Drew, C., Senecal, K. J., Kumar, J., and Samuelson, L. A. (2002). Fluorescent electrospun polymer films for detection of explosives. *Polym. Preprints* **43**, 130–131.

Weder, C., Sarwa, C., Montali, A., Bastiaansen, G., and Smith, P. (1998). Incorporation of photoluminescent polarizers into liquid crystal displays. *Science* **279**, 835–837.

Whitehead, K. S., Grell, M., Bradley, D. D. C., Jandke, M., and Strohriegl, P. (2000). Highly polarized blue electroluminescence from homogeneously aligned films of poly(9, 9-diptylfluorene). *Appl. Phys. Lett.* **76**, 2946–2948.

Whitesides, G. M., Mathias, J. P., and Seto, C. T. (1991). Molecular self-assembly and nanochemistry – a chemical strategy for the synthesis of nanostructures. *Science* **254**, 1312–1319.

WMD Sensitive (2004). *Technion Focus*. <http://www.focus.technion.ac.il>, January, 2004.

Wohlfarth, B., Wohlfarth, Ch. (1997). Surface Tension of Pure Liquids and Binary Liquid Mixtures, In: *Landolt-Bornstein Numerical Data and Functional Relationships in Science and Technology*, v. IV/16. (M.D. Lechner, Ed.). Springer, New York

Wohlhuter, F. K., and Basaran, O. A. (1992). Shapes and stability of pendant and sessile dielectric drops in an electric field. *J. Fluid Mech.* **235**, 481–510.

Wood, J. R., Zhao, Q., and Wagner, H. D. (2001). Orientation of carbon nanotubes in polymers and its detection by Raman spectroscopy. *Composites, Part A – Appl. Sci. Manuf.* **32**, 391–399.

Wunderlich, T., Stelter, M., Tripathy, T., Nayak, B. R., Brenn, G., Yarin, A. L., Singh, R. P., Brunn, P. O., and Durst, F. (2000). Shear and extensional rheological investigations in solutions of grafted and ungrafted polysaccharides. *J. Appl. Polym. Sci.* **77**, 3200–3209.

Xu, C. Y., Inai, R., Kotaki, M., and Ramakrishna, S. (2004). Aligned biodegradable nanofibrous structure: a potential scaffold for blood vessel. *Biomaterials* **25**, 877–886.

Xu, H. (2003). Formation and characterization of polymer jets in electrospinning. PhD thesis. Dept. of Polymer Sci., the University of Akron.

Xu, H., Yarin, A. L., and Reneker, D. H. (2003). Characterization of fluid flow in jets during electrospinning. *Polym. Preprints* **44**, 51–52.

Yan, F., Farouk, B., and Ko, F. (2003). Numerical modeling of an electrically driven liquid meniscus in the cone-jet mode. *Aerosol Sci.* **34**, 99–116.

Yang, H., Loh, L., Han, T., and Ko, F. (2003). Nanomagnetic particle filled piezoelectric polymer nanocomposite wires by co-electrospinning. *Polym. Prepr.* **44**, 163–163.

Yang, F., Murugan, R., Wang, S., and Ramakrishna, S. (2005). Electrospinning of nano/micro scale poly(L-lactic acid) aligned fibers and their potential in neural tissue engineering. *Biomaterials* **26**, 2603–2610.

Yarin, A. L. (1979). Stability of a jet of viscoelastic liquid in the presence of a mass flux at its surface. *J. Eng. Phys.* **37**, 904–910.

Yarin, A. L. (1990). Strong flows of polymeric liquid: I. Rheological behavior. *J. Non-Newton. Fluid Mech.* **37**, 113–138.

Yarin, A. L. (1993). *Free Liquid Jets and Films: Hydrodynamics and Rheology*. Longman, Harlow and Wiley, New York.

Yarin, A. L. (1997). On the mechanism of turbulent drag reduction in dilute polymer solutions: dynamics of vortex filaments. *J. Non-Newton. Fluid Mech.* **69**, 137–153.

Yarin, A. L., Brenn, G., Kastner, O., Rensink, D., and Tropea, C. (1999). Evaporation of acoustically levitated droplets. *J. Fluid Mech.* **399**, 151–204.

Yarin, A. L., Kataphinan, W., and Reneker, D. H. (2005). Branching in electrospinning of nanofibers. *J. Appl. Phys.* **98**, 064501.

Yarin, A. L., Koombhongse, S., and Reneker, D. H. (2001a). Bending instability in electrospinning of nanofibers. *J. Appl. Phys.* **89**, 3018–3026.

Yarin, A. L., Koombhongse, S., and Reneker, D. H. (2001b). Taylor cone and jetting from liquid droplets in electrospinning of nanofibers. *J. Appl. Phys.* **90**, 4836–4846.

Yarin, A. L., and Weiss, D. A. (1995). Impact of drops on solid surfaces: self-similar capillary waves, and splashing as a new type of kinematic discontinuity. *J. Fluid Mech.* **283**, 141–173.

Yarin, A. L., and Zussman, E. (2004). Upward needleless electrospinning of multiple nanofibers. *Polymer* **45**, 2977–2980.

Yarin, A. L., Zussman, E., Theron, A., Rahimi, S., Sobe, Z., and Hassan, D. (2004). Elongational behavior of gelled propellant simulants. *J. Rheol.* **48**, 101–116.

Ye, H., Lam, H., Tichenal, N., Gogotsi, Y., and Ko, F. (2004). Reinforcement and rupture behavior of carbon nanotubes-polymer nanofibers. *Appl. Phys. Lett.* **85**, 1775–1777.

Youngblood, J. P., and McCarthy, T. J. (1999). Ultrahydrophobic polymer surfaces prepared by simultaneous ablation of polypropylene and sputtering of poly(tetrafluoroethylene) using radio frequency plasma. *Macromolecules* **32**, 6800–6806.

Yu, J. H., Fridrikh, S. V., and Rutledge, G. C. (2004). Production of submicrometer diameter fibers by two-fluid electrospinning. *Adv. Mat.* **16**, 1562–1566.

Zach, P. M., Ng, K. H., and Penner, R. M. (2000). Molybdenum nanowires by electrodeposition. *Science* **290**, 2120–2123.

Zarkoob, S., Eby, R. K., Reneker, D. H., Hudson, S. D., Ertley, D., and Adams, W. W. (2004). Structure and morphology of electrospun silk nanofibers. *Polymer* **45**, 3973–3977.

Zel'dovich, Ya. B. (1992). Limiting laws of freely rising convective currents. *Selected Works of Ya.B. Zel'dovich, Vol. I. Chemical Physics and Hydrodynamics*. Princeton University Press, Princeton. First published in 1937.

Zhang, X., and Basaran, O. A. (1996). Dynamics of drop formation from a capillary in the presence of an electric field. *J. Fluid Mech.* **326**, 239–263.

Zhang, Y., Huang, Z. M., Xu, X., Lim, C. T., and Ramakrishna, S. (2004). Preparation of core-shell structured PCL-r-Gelatin bi-component nanofibers by coaxial electrospinning. *Chem. Mater.* **16**, 3406–3409.

Zheng, J., Chen, X., Xu, X., Liang, Q., Bian, X., Yang, L., and Jing, X. (2003). Ultrafine fibers electrospun from biodegradable polymers. *J. Appl. Polym. Sci.* **89**, 1085–1092.

Ziabicki, A. (1976). *Fundamentals of Fibre Formation*. Wiley, London.

Ziabicki, A., and Kawai, H., eds. (1985). *High-Speed Fiber Spinning*. Wiley, New York.

Zong, X., Bien, H., Chungb, C. Y., Yin, L., Kim, K., Fang, D. F., Chu, B., Hsiao, B. S., and Entcheva, E. (2003). Electrospun non-woven membranes as scaffolds for heart tissue constructs. *Proceedings of the American Chemical Society*, New York, pp. 96–97.

Zussman, E., Burman, M., Yarin, A. L., Khalfin, R., and Cohen, Y. (2006). Tensile deformation of electrospun nylon-6,6 nanofibers. *J. Polym. Sci., Polym. Phys. Ed.* **44**, 1482–1489.

Zussman, E., Rittel, D., and Yarin, A. L. (2003a). Failure modes of electrospun nanofibers. *Appl. Phys. Lett.* **82**, 3958–3960.

Zussman, E., Theron, A., and Yarin, A. L. (2003b). Formation of nanofiber crossbars in electrospinning. *Appl. Phys. Lett.* **82**, 973–975.

Zussman, E., Yarden, O., Yarin, A. L. and Chervinsky, S. (2004). Developing a nanofiber-based platform for application of antifungal compounds. *Internal Report #23 – Technion—Faculty of Mechanical Engineering*.

Zussman, E., Yarin, A. L., and Weihs, D. (2002). A micro-aerodynamic decelerator based on permeable surfaces of nanofiber mats. *Exp. Fluids* **33**, 315–320.

Zussman, E., Yarin, A. L., Bazilevsky, A. V., Avrahami, R., and Feldman, M. (2006). Electrospun polyacrylonitrile/poly(methylmethacrylate)-derived turbostratic carbon micro-/nanotubes. *Adv. Mat.* **18**, 348–353.

This page intentionally left blank

A Bibliography of Vortex Dynamics 1858–1956

VYACHESLAV V. MELESHKO^{a,1} and HASSAN AREF^{b,c,2}

^a *Department of Theoretical and Applied Mechanics, Faculty of Mechanics and Mathematics, Kiev National Taras Shevchenko University, 01030 Kiev, Ukraine*

^b *Center for Fluid Dynamics and Department of Physics, Technical University of Denmark, Kgs. Lyngby, DK-2800, Denmark*

^c *Department of Engineering Science and Mechanics, College of Engineering, Virginia Polytechnic Institute & State University, Blacksburg, VA 24061, USA*

Every great man of the first rank is unique. Each has his own office and his own place in the historic procession of the sages. That office did not exist even in the imagination, till he came to fill it, and none can succeed to his place when he has passed away. Others may gain distinction by adapting the exposition of science to the varying language of each generation of students, but their true function is not so much didactic as pedagogic – not to teach the use of phrases which enable us to persuade ourselves that we understand a science, but to bring the student into living contact with the two main sources of mental growth, the fathers of the sciences, for whose personal influence over the opening mind there is no substitute, and the material things to which their labours first gave a meaning.

J. C. Maxwell [640]

1. Introduction

The subject of vortex dynamics³ can fairly be said to have been initiated by the seminal paper [393] of Hermann Ludwig Ferdinand Helmholtz (1821–1894) now nearly 150 years ago⁴. In this paper Helmholtz established his three “laws” of vortex motion in roughly the form they are found today in textbooks on fluid mechanics (often without attribution). His motivations for taking up this new research interest remain unclear, for at that time Helmholtz was professor of physiology and anatomy at the University of Bonn, and the memoir appeared in the year of his coming to the University of Heidelberg as a professor of physiology. One moti-

¹ Email address: meleshko@univ.kiev.ua

² Email address: horef@vt.edu

³ For an accessible, widely-ranging introduction to the entire “universe” of vortex motions across an immense range of scales and physical phenomena we recommend the book by Lugt [606].

⁴ Helmholtz was ennobled and added ‘von’ to his name in 1882. As this occurred later, he appears throughout this review simply as Helmholtz. The life and scientific work of this outstanding natural philosopher of the 19th century – upon his death obituary notices appeared in more than 50 scientific journals all over the world – has been praised by his contemporaries [270, 274, 507, 641, 816, 887] and by modern scientists [109, 188, 520, 969]. There exist many books in many languages devoted to Helmholtz, e.g. [239, 557, 558, 508, 652, 1016].

vation seems to have been his interest in frictional phenomena [969], carried over from his interest in energetics; another was his growing awareness of the power of Green's theorem in hydrodynamics. In a speech [399] at a banquet on the occasion of his 70th birthday – an event that brought together 260 friends and admirers at Kaiserhof on November 2, 1891 – Helmholtz gave the following expanded account:

I have also been in a position to solve several problems in mathematical physics, some of which the great mathematicians since the time of Euler had worked on in vain — for example, problems concerning vortex motion and the discontinuity of motion in fluids, the problem of the motion of sound waves at the open ends of organ pipes, and so on. But the pride which I might have felt about the final result of these investigations was considerably lessened by my knowledge that I had only succeeded in solving such problems, after many erroneous attempts, by the gradual generalization of favorable examples and by a series of fortunate guesses. I would compare myself to a mountain climber who, not knowing the way, ascends slowly and painfully and is often compelled to retrace his steps because he can go no farther; who, sometimes by reasoning and sometimes by accident, hits upon signs of a fresh path, which leads him a little farther; and who finally, when he has reached the summit, discovers to his annoyance a royal road on which he might have ridden up if he had been clever enough to find the right starting point at the beginning. In my papers and memoirs I have not, of course, given the reader an account of my wanderings, but have only described the beaten path along which one may reach the summit without trouble.

Until the appearance of Helmholtz's paper the integrals of the hydrodynamical equations had been determined almost exclusively on the assumption that the cartesian components of the velocity of each fluid particle are partial first derivatives – “differential coefficients”, in the terminology of the time – with respect to the cartesian coordinates of a certain function, the *velocity potential*. This assumption is valid so long as the motion of the fluid results from the action of forces that have a potential of their own. Helmholtz eliminated this limitation, and took into account the possible friction between different elements of the fluid or between the fluid and a solid boundary. At the time the effect of friction had not been fully understood mathematically. Helmholtz endeavored to identify some of the aspects of the motion that frictional forces can produce in fluids.

It is somewhat rare that a subject in a rather “mature” science such as fluid mechanics has so clear a starting date. Usually when this happens it is due to a seminal paper by a luminary of the field, a paper that is far ahead of anything else produced by the contemporaries of said luminary, and a paper that is immediately embraced by the community and sets the stage for developments for decades to come. The early papers in the new field of vortex dynamics were scattered among many journals in many countries and were written in a multitude of languages, primarily English, French, German, Italian and Russian. This diversity of publication venue and language, unfortunately, often makes the literature rather difficult to

identify and access for the modern researcher⁵. About a century after Helmholtz's paper two major journals devoted to fluid mechanics would be started, *Journal of Fluid Mechanics* in 1956 and *Physics of Fluids* in 1957. After their initiation these journals attracted many of the major papers in vortex dynamics. Furthermore, the vast literature on the subject of vortex dynamics since the 1950's may be accessed through serial publications such as *Advances in Applied Mechanics* (published since 1948), *Progress in Aeronautical Sciences* (published since 1961), *Annual Review of Fluid Mechanics* (published since 1969), and several volumes devoted to "Strömungsmechanik" of the extensive *Handbuch der Physik* (published since 1956). Other valuable sources are the proceedings of the International Congresses of Theoretical and Applied Mechanics (held every four years since 1924), along with other topical symposia, conferences and workshops. There also exist many general treatises, surveys, textbooks, Ludwig Prandtl and (since 1957) Lanchester Memorial Lectures [3, 471, 582], etc., a rather complete list of which can be found in the extensive bibliography⁶ in Schlichting's book [835].

Hence – and this may be a somewhat optimistic assessment – the period that is most in need of a comprehensive bibliography is the century from 1858 to about 1956. It is such a bibliography that we have tried to provide in this paper. (We have also included some more recent references which either contain historical perspective on the papers of that period or essentially use and further develop classical results in vortex dynamics.) We hope the bibliography will be found useful by researchers working in vortex dynamics – that it may even on occasion improve the scholarship of this field by drawing attention to earlier and sometimes neglected works – and that it will be of interest to the general reader with an affinity for the history of mechanics. We have also included a few quotations and older illustrations (see Figs. 1, 2, 3 and 4) intended to give the flavor of vortex dynamics as an international scientific endeavor with a long history, sometimes simply to amuse the reader, but also to compensate those readers who do not have easy access to a library with an extensive collection of older books and journals.

The bibliography was compiled by the first author during an extended visit in the Department of Theoretical & Applied Mechanics at University of Illinois, Urbana-Champaign, almost a decade ago. Extensive use was made of the remarkable holdings of the library of that institution. Some additional references related to older studies in Russian were collected at the National Vernadskii Library of Ukraine and the Library of the Institute of Hydromechanics, both in Kiev. We have greatly

⁵ Indeed, while the authors can claim fluent command of English and Russian, the multitude of languages has been a challenge even when assembling this bibliography.

⁶ Oddly neither the first German edition [834] nor the seventh American edition [835] of this classic text on boundary layer theory, a subject closely related to vortex dynamics, reference Helmholtz's paper [393]. Helmholtz's name is not even among the extensive list of authors mentioned! The ninth German edition [836] does reference Helmholtz but the citation is to a later paper [398].

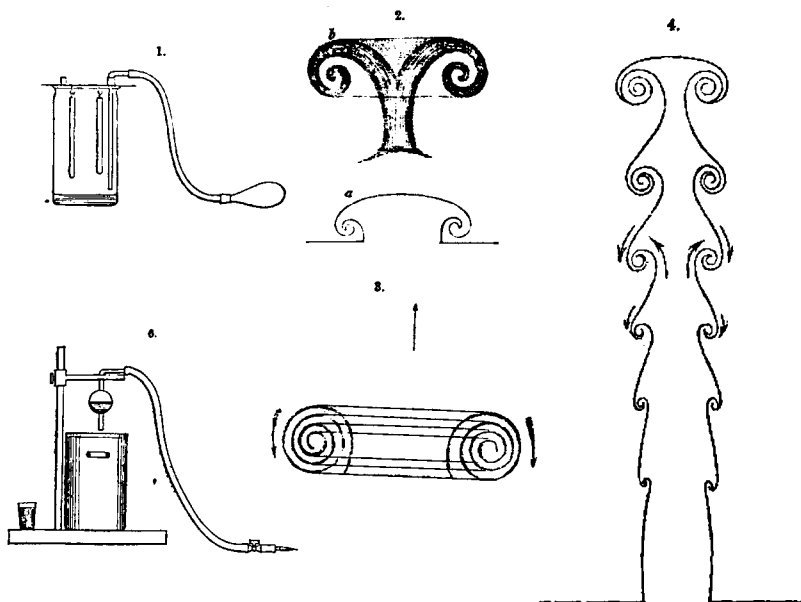


FIG. 1. Illustrations from experiments “[on] the formation of rotating rings by air and liquids under certain conditions of discharge” by W. B. Rogers [789], published in 1858, the same year as Helmholtz’s seminal paper, see also §2.5.

benefitted from the skill and prescience of the librarians in these institutions in assembling and caring for this literature.

We do not claim that the current bibliography is complete, but we do believe it brings to light many important works that ought to be better known and to be more frequently cited than they are today. At the end of the 19th century, Karl Pearson wrote on this issue in the preface to the monumental treatise [951, pp. x–xi]:

The use of a work of this kind is twofold. It forms on the one hand the history of a peculiar phase of intellectual development, worth studying for the many side lights it throws on general human progress. On the other hand it serves as a guide to the investigator in what has been done, and what ought to be done. In this latter respect the individualism of modern science has not infrequently led to a great waste of power; the same bit of work has been repeated in different countries at different times, owing to the absence of such histories as Dr. Todhunter set himself to write. It is true that the various *Jahrbücher* and *Fortschritte* now reduce the possibility of this repetition, but besides their frequent insufficiency they are at best but indices to the work of the last few years; an enormous amount of matter is practically stored out of sight in the *Transactions* and *Journals* of the last century and of the first half of the present century. It would be a great aid to science, if, at any rate, the innumerable mathematical journals could be to a great extent specialized, so that we might look to any of them for a special class of memoir. Perhaps this is too great a collectivist

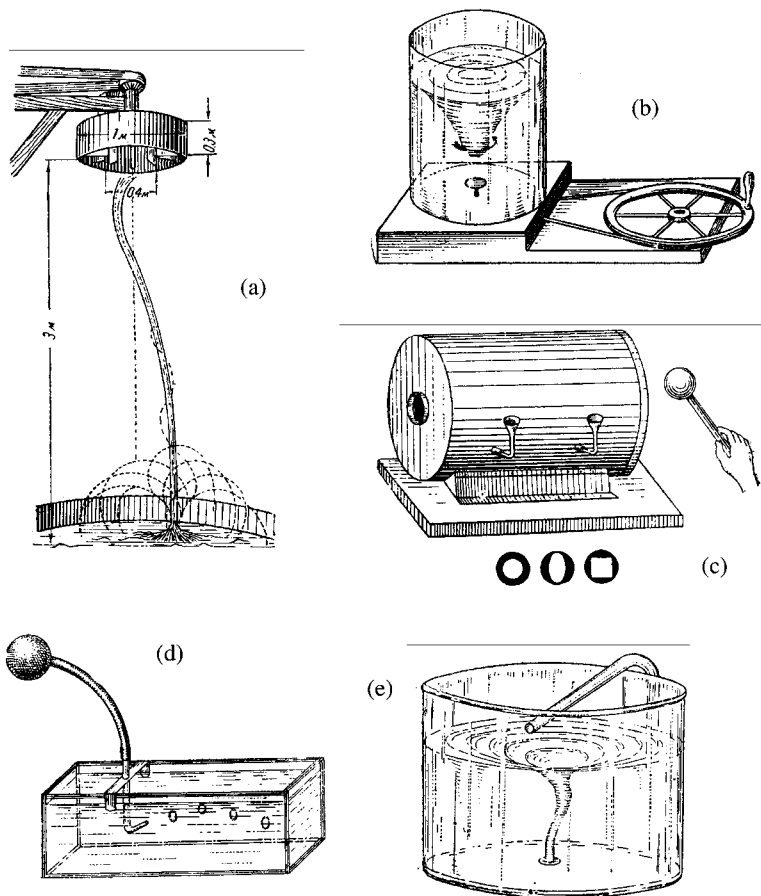


FIG. 2. Various examples of vortex generators. From [439].

reform to expect in the near future from even the cosmopolitan spirit of modern science. As it is, the would-be researcher either wastes much time in learning the history of his subject, or else works away regardless of earlier investigators. The latter course has been singularly prevalent with even some first class British and French mathematicians.

There are, of course, other bibliographies to which the reader might turn. Some older review papers [34, 35, 99, 226, 403, 404, 595, 600–603] contain many references to concrete problems in the dynamics of concentrated vorticity and vortices, with special attention to experimental studies. The 1954 monograph by Truesdell [964] contains a rich and scholarly bibliography covering nominally the same subject and with virtually the same “upper bound” in terms of the period in time. (Truesdell’s first reference is Newton’s *Principia* so his bibliography covers

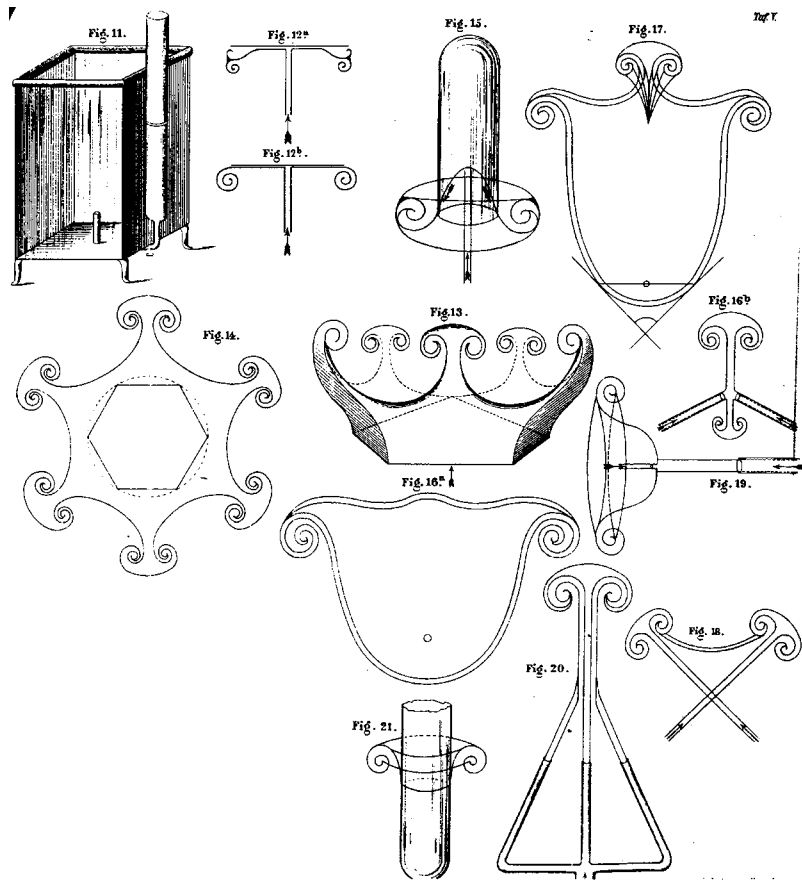


FIG. 3. Experiments on interaction of vortex rings with plates of various shapes. After Kötschau [518].

almost two centuries more than ours.) There is considerable overlap between Truesdell's bibliography and ours. There are also major differences. Truesdell includes a number of papers that, while dealing with basic issues of fluid mechanics, are not particularly – and certainly not solely – addressed to vortex dynamics. Similarly, Truesdell's bibliography is essentially devoid of references to any kind of discrete vortex models, such as point vortices, line vortices, vortex sheets, or so-called “vortex patches” (finite regions of vortical fluid embedded in otherwise irrotational flow), and so on. Thus, the papers [467, 468] by von Kármán – let alone those by Bénard [56–58] – on vortex streets, are not cited by Truesdell. Hill's paper of 1893 [422] on the vortices that today bear his name is not cited. Truesdell's bibliography is also weak on literature from the Eastern block: Russia and the

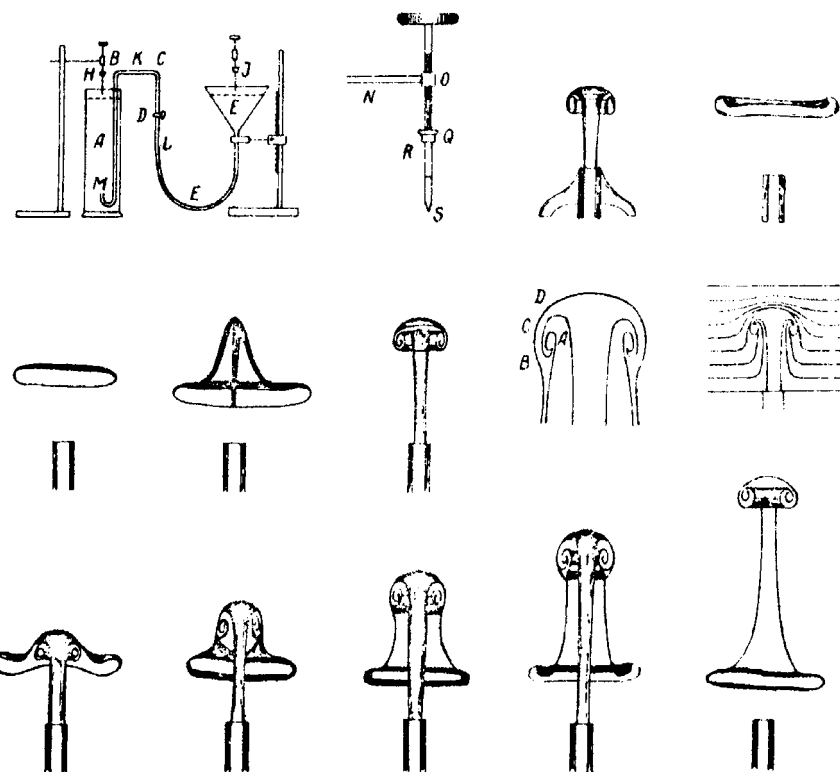


FIG. 4. Experiments on vortex ring formation by injecting one fluid into another through an orifice. After Mack [609].

several republics of the former Soviet Union⁷. (We realize that much of this literature may simply not have been accessible to him.) For example, no work of Chaplygin, such as [127, 129], is cited. Even for the literature where Truesdell's bibliography is strong – mainly the countries of Western Europe – the more physical investigations, such as the papers by Lagally [531–533], are not cited although his 1928 lectures on vector calculus make the list. These examples of the difference between the two bibliographies are given not to detract in any way from Truesdell's work but to stress that the outlook and content of the two bibliographies is quite different. Ideally, the reader will find the two collections to complement one another and to both be useful for further research.

We call attention to the unique *Catalogue of Scientific Papers (1800–1900)* compiled and published by the Royal Society of London in 19 volumes during the period

⁷ References to this vast literature may be found to some extent in the bibliographies [16, 200, 607].

1867–1925 (freely available in electronic form via <http://gallica.bnf.fr>) where a complete list of journal papers of every(!) 19th century author is given in chronological order with complete references. In addition, the subject index to this edition contains short titles of papers (with names of the authors, abbreviated title of the journal, volume, year and first page of the publication) arranged according to the following topics: Volume 2 *Mechanics*, 2450 – Vortex motion. Vortex atoms (130 titles); Volume 3, Part 1 *Physics*, 0500 – Theories of the Constitution of Matter, Vortex theories (20 titles), 0600 – Theories of the Ether (4 titles related to the vortex ether).

We also cite a number of books that have particularly good discussions on aspects of vortex dynamics paying particular attention to several relatively unknown textbooks in French, German, Italian, and Russian. When an English translation exists, we provide a citation to this translation.

In many cases the main work has been reviewed or abstracted elsewhere. Papers written in the 1930's were reviewed in detail in *Zentralblatt für Mechanik* published 1934–1941⁸. Later publications in this area are extensively reviewed in *Applied Mechanics Reviews*, published since 1948 (with S. P. Timoshenko, Th. von Kármán and L. H. Donnell as founding editors). Moreover, some mathematical review journals, such as *Jahrbuch über die Fortschritte der Mathematik* (published in 1875–1942), *Zentralblatt für Mathematik und ihre Grenzgebiete* (published since 1931; both journals are included in the *Zentralblatt MATH* Database which contains about 2.3 million entries drawn from about 3500 journals and 1100 serials from 1868 to the present and is freely available in electronic form via <http://www.zentralblatt-math.org/zmath/en/>), and *Mathematical Reviews* (published since 1940) also contain sections devoted to vortex dynamics. In some cases the abstract or review is in a different language from the original. When we are aware of such a review or abstract, we have included a citation of it along with the citation of the original work.

In the bibliography we have abbreviated the names of most of the journals. Some of these names and abbreviations will be familiar to the reader (although we may have chosen shorter or different abbreviations than are in common use). Others will be to journals and other periodicals that are no longer in circulation. Thus, we give here a list of the full names of the periodicals (as printed on the title page) and other sources where the various papers have appeared, ordered alphabetically by the abbreviations used in the bibliography. The abbreviations are generally formed

⁸ It should be noted that the editorial board of the first several volumes was truly international. It included A. Betz (Göttingen), C. B. Biezeno (Delft), J. M. Burgers (Delft), R. Grammel (Stuttgart), E. Hahn (Nancy), Th. von Kármán (Aachen, Pasadena), T. Levi-Civita (Rome), E. L. Nicolai (Leningrad), L. Prandtl (Göttingen), G. I. Taylor (Cambridge), and S. P. Timoshenko (Ann Arbor). For political reasons of the time later issues were edited solely by German editors, W. Flügge and O. Neugebauer, both from Göttingen.

by abbreviating the principal words in the title in the order in which they occur; the place of publication and other pertinent information is given when desirable for clarity.

Abh. Geb. Naturw. Hamburg – Abhandlungen aus dem Gebiet der Naturwissenschaften herausgegeben van Naturwissenschaftlichen Verein in Hamburg.

Adv. Appl. Mech. – Advances in Applied Mechanics.

Aeronaut. J. – Aeronautical Journal.

AIAA. J. – AIAA Journal.

Am. J. Math. – American Journal of Mathematics.

Am. J. Phys. – American Journal of Physics.

Am. J. Sci. – American Journal of Science and Arts.

Ann. Fac. Sci. Univ. Toulouse – Annales de la Faculté des Sciences de l’Université de Toulouse pour les sciences mathématiques et physiques.

Ann. Phys. – Annalen der Physik.

Ann. Phys. Chem. – Annalen der Physik und Chemie.

Ann. Sci. – Annals of Science.

Ann. Sci. Éc. Norm. Super. – Annales scientifiques de l’École Normale supérieure.

Ann. Scu. Norm. Sup. Pisa – Annali della Scuola normale superiore di Pisa. Scienze Fisiche e Matematiche.

Annu. Rev. Fluid Mech. – Annual Review of Fluid Mechanics.

Appl. Mech. Rev. – Applied Mechanics Reviews.

Arch. Hist. Exact Sci. – Archive for the History of Exact Sciences.

Arch. Math. Phys. – Archiv der Mathematik und Physik.

Atti Accad. Naz. Lincei. Mem. Cl. Sci. Fis. Mat. Nat. – Atti dell’Accademia Nazionale dei Lincei. Memorie. Classe di Scienze Fisiche, Matematiche e Naturali.

Atti Accad. Naz. Lincei. Rend. Cl. Sci. Fis. Mat. Nat. – Atti dell’Accademia Nazionale dei Lincei. Rendiconti. Classe di Scienze Fisiche, Matematiche e Naturali.

Atti Accad. Pontif. Nuovi Lincei – Atti dell’Accademia Pontificia dei Nuovi Lincei.

Atti Accad. Sci. Lett. Arti Padova – Atti dell’Accademia delle Scienze, Lettere ed Arti di Padova.

Atti Accad. Sci. Torino. Cl. Sci. Fis. Mat. Nat. – Atti dell’Accademia delle Scienze di Torino. Classe di Scienze Fisiche, Matematiche e Naturali.

Atti Ist. Veneto Sci. Lett. Arti. Cl. Mat. Nat. – Atti dell’Istituto Veneto di Scienze, Lettere ed Arti. Classe di Scienze Matematiche e Naturali.

Atti Soc. Ital. Prog. Sci – Atti della Società Italiana per il progresso delle scienze.

Beitr. Geophys. – Beiträge zur Geophysik.

Biogr. Mem. Notes FRS – Biographical Memoirs of Fellows of the Royal Society.

Boll. Un. Mat. Ital. – Bollettino della Unione Matematica Italiana.

Bull. Am. Math. Soc. – Bulletin of the American Mathematical Society.

Bull. Calcutta Math. Soc. – Bulletin of the Calcutta Mathematical Society.

Bull. Inst. Aérodyn. Koutchino – Bulletin de l’Institut aérodynamique de Koutchino.

Byull. Mosk. Obshch. Vozdukhopl. – Byulleten’ Moskovskogo obshchestva vozdukhoplavaniya.

Bull. Nat. Res. Council – Bulletin of the National Research Council.

Cambr. Dubl. Math. J. – The Cambridge and Dublin Mathematical Journal

Can. J. Math. – Canadian Journal of Mathematics.

Chem. News J. Ind. Sci. – Chem News and Journal of Industrial Science.

Comment. Math. Helvet. – Commentarii Mathematici Helvetici.

C. R. Acad. Bulg. Sci. – Comptes Rendus de l'Académie Bulgare des Sciences.

C. R. Acad. Sci. Crac. – Comptes Rendus de l'Academie des Sciences Cracovie.

C. R. Acad. Sci. Paris – Comptes rendus hebdomadaires des séances de l'Académie des Sciences.

Dokl. Akad. Nauk SSSR – Doklady Akademii Nauk SSSR.

F. d. M. – Jahrbuch über die Fortschritte der Mathematik

Fluid Dyn. – Fluid Dynamics.

Fluid Dyn. Res. – Fluid Dynamics Research.

Forsch. Geb. IngWes. – Forschung auf dem Gebiet des Ingenieurswesens.

G. Mat. Battaglini – Giornale di Matematiche di Battaglini.

Geophys. Mag. – Geophysical Magazine.

Geofys. Publ. – Geofysiske publikationer.

God. Sof. Univ. – Godishnik na Sofiiskiya Universitet. Fiz-Mat Fakultet.

Helv. Phys. Acta – Helvetica Physica Acta.

Ill. Aeronaut. Mitt. – Illustrierte aeronautische Mitteilungen.

Ing.-Arch. – Ingenieur-Archiv.

Ing. Grav. – Ingenieur. 's Gravenhage.

Izv. Akad. Nauk SSSR. Mekh. Zhid. Gaza – Izvestiya Akademii Nauk SSSR. Mekhanika zhidkosti i gaza.

Izv. Akad. Nauk SSSR. Otd Mat. Estest. Nauk – Izvestiya Akademii Nauk SSSR. Otdelenie matematicheskikh i estestvennykh nauk.

Izv. Akad. Nauk SSSR. Otd. Tekh. Nauk – Izvestiya Akademii Nauk SSSR. Otdelenie tekhnicheskikh nauk.

Izv. Imp. Obshch. Lyub. Estest. Antrop. Etnogr. Imp. Mosk. Univ. – Izvestiya Imperatorskogo obshchestva lyubitelei estestvoznaniiya, antropologii i etnografii pri Imperatorskom Moskovskom universitete.

Izv. RAN. Mekh. Zhid. Gaza – Izvestiya Rossiiskoi Akademii Nauk. Mekhanika zhidkosti i gaza.

Jahrb. Wiss. Ges. Luftf. – Jahrbuch der Wissenschaftlichen Gesellschaft für Luftfahrt.

Jahresber. Dt. Mat. Verein. – Jahresbericht der Deutschen Matematiker-vereinigung.

J. Aeronaut. Sci. – Journal of the Aeronautical Sciences.

J. Appl. Math. Mech. – Journal of Applied Mathematics and Mechanics.

J. Appl. Phys. – Journal of Applied Physics.

J. Chem. Soc. – Journal of the Chemical Society.

J. Coll. Sci. Imp. Univ. Tokyo – Journal of the College of Science, Imperial University of Tokyo.

J. Fluid Mech. – Journal of Fluid Mechanics.

J. Franklin Inst. – Journal of the Franklin Institute.

J. Japan Soc. Mech. Engrs – Journal of the Japan Society of Mechanical Engineers.

J. Lond. Math. Soc. – Journal of the London Mathematical Society.

J. Math. Phys. – Journal of Mathematics and Physics.

J. Math. Pures Appl – Journal de mathématiques pures et appliquées.

J. Phys. Soc. Japan – Journal of the Physical Society of Japan.

J. R. Aeronaut. Soc. – Journal of the Royal Aeronautical Society.

J. Reine Angew. Math. – Journal für die reine und angewandte Mathematik.

J. Sci. Instrum. – Journal of Scientific Instruments.

J. Soc. Appl. Mech. Japan – Journal of the Society of Applied Mechanics of Japan.

Mat. Sbor. – Matematicheskii Sbornik.

Math. Ann. – Mathematische Annalen.

Math. Naturwiss. Unterr. – Mathematische und naturwissenschaftliche Unterricht.

Math. Rev. – Mathematical Reviews

Math. Z. – Mathematische Zeitschrift.

Mem. Accad. Pontif. Nuovi Lincei – Memorie dell'Accademia Pontificia dei Nuovi Lincei.

Mem. R. Accad. Sci. Ist. Bologna – Memorie della R. Accademia delle scienze dell'Istituto di Bologna.

Mess. Math. – Messenger of Mathematics.

Met. Z. – Meteorologische Zeitschrift.

Mitt. math.-naturwiss. Ver. Württemberg – Mitteilungen des mathematisch-naturwissenschaftlichen Vereins ins Württemberg.

Monatsber. Akad. Wiss. Berlin – Monatsberichte der Akademie der Wissenschaften in Berlin.

Nachr. Ges. Wiss. Göttingen Math.-Phys. Kl. – Nachrichten von der (Königliche) Gesellschaft der Wissenschaften zu Göttingen. Mathematisch-physikalische Klasse.

NACA Tech. Memo. – National Advisory Committee for Aeronautics. Technical Memoranda.

NACA Tech. Notes – National Advisory Committee for Aeronautics. Technical Notes.

Note Esercit. Mat. Catania – Note ed esercitazioni matematiche. Circolo matematico di Catania.

Phil. Mag. – Philosophical Magazine.

Phil. Trans. R. Soc. London – Philosophical Transactions of the Royal Society of London.

Phys. Fluids – Physics of Fluids.

Phys. Z. – Physikalische Zeitschrift.

Popul. Sci. Rev. – Popular Science Reviews.

Prikl. Mat. Mekh. – Prikladnaya Matematika i Mekhanika.

Pod Znam. Marxisma – Pod Znamenem Marxisma.

Proc. Am. Acad. Arts Sci. – Proceedings of the American Academy of Arts and Sciences.

Proc. Benares Math. Soc. – Proceedings of the Benares Mathematical Society.

Proc. Camb. Phil. Soc. – Proceedings of the Cambridge Philosophical Society.

Proc. Dublin Sci. Soc. – Proceedings of the Dublin Scientific Society.

Proc. Edinb. Math. Soc. – Proceedings of the Edinburgh Mathematical Society.

Proc. Glasgow Phil. Soc. – Proceedings of the Glasgow Philosophical Society.

Proc. Ind. Acad. Sci. – Proceedings of the Indian Academy of Sciences.

Proc. Inst. Automob. Eng. – Proceedings of the Institution of Automobil Engineers.

Proc. Inst. Mech. Engrs – Proceedings of the Institution of Mechanical Engineers.

Proc. Lit. Phil. Soc. Manch. – Proceedings of the Literary and Philosophical Society of Manchester.

Proc. Lond. Math. Soc. – Proceedings of the London Mathematical Society.

Proc. Nat. Acad. Sci. USA – Proceedings of the National Academy of Sciences of the United States of America.

Proc. Phys.-Math. Soc. Japan – Proceedings of the Physico-Mathematical Society of Japan.

Proc. R. Dublin Soc. – Proceedings of the Royal Dublin Society.

Proc. R. Instn Gt Brit. – Proceedings of the Royal Institution of Great Britain.

Proc. R. Irish Acad. – Proceedings of the Royal Irish Academy.

Proc. R. Soc. Edinb. – Proceedings of the Royal Society of Edinburgh.

Proc. R. Soc. London – Proceedings of the Royal Society of London.

Proc. Sect. Sci. K. Ned. Akad. Wet – Proceedings of the Section of Sciences Koninklijke Nederlandse Akademie van Wetenschappen.

Publ. Scient. Tech. Minist. Air – Publications scientifiques et techniques du Ministère de l'Air. Paris.

Quart. J. Math. – Quarterly Journal of Mathematics. Oxford ser.

Quart. J. Pure Appl. Math. – Quarterly Journal of Pure and Applied Mathematics.

Rend. Circ. Mat. Palermo – Rendiconti del Circolo matematico di Palermo.

Rend. Ist. Lomb. Sci. Lett. – Rendiconti dell'Istituto Lombardo di scienze e lettere. Milano.

Rend. Semin. Mat. Fis. Milano – Rendiconti del Seminario matematico e fisico di Milano.

Rend. Semin. Mat. Univ. Padova – Rendiconti del Seminario matematico della Università Padova.

Rep. Aeronaut. Res. Inst. Tokyo – Report of the Aeronautical Research Institute, Tokyo Imperial University.

Rep. Brit. Ass. Advmt Sci. – Report of the British Association for the Advancement of Science.

Rep. David Taylor Model Basin – Reports David Taylor Model Basin. United States Navy Department.

Rep. Memo. Advis. Comm. Aeronaut. – Reports and Memoranda. Advisory Committee for Aeronautics. London.

Sb. Inst. Inzh. Put. Soobshch. – Sbornik Instituta inzhenerov putei soobshcheniya. St. Petersburg (Leningrad).

SchReihe ForschInst Math. – Schriftenreihe des Forschungsinstituts für Mathematik.

Scient. Am. Suppl. – Scientific American Supplement.

Sber. Akad. Wiss. Wien – Sitzungsberichte der Akademie der Wissenschaften in Wien. Abh. IIa. Mathematik, Physik, Astronomie.

Sber. Bayer. Akad. Wiss. – Sitzungsberichte der Bayerischen Akademie der Wissenschaften zu München. Mathematische-physikalische Klasse.

Sber. Preuss. Akad. Wiss. – Sitzungsberichte der Preussischen Akademie der Wissenschaften zu Berlin.

Sci. Abs. – Scientific Abstracts.

Spis. Bulg. Akad. Nauk. – Spisanie na Bulgarskato akademiya na naukite.

Tech. Rep. Advis. Comm. Aeronaut. – Technical Report of the Advisory Committee for Aeronautics.

Trans. Cambr. Phil. Soc. – Transactions of the Cambridge Philosophical Society.

Trans. R. Irish Acad. – Transactions of the Royal Irish Academy.

Trans. R. Soc. Canada – Transactions of the Royal Society of Canada.

Trans. R. Soc. Edinb. – Transactions of the Royal Society of Edinburgh.

Trudy Avia. Rasch.-Ispyt. Byuro – Trudy Aviacionnogo raschetno-ispytatel'nogo byuro. Moskva.

Trudy Glav. Geofiz. Obs. – Trudy Glavnogo geofizicheskogo observatorii imeni A.I. Voeikova, Leningrad.

Trudy Inst. Istor. Estestv. Tekhn. – Trudy Instituta istorii estestvoznanija i tekhniki. Moskva.

Trudy Otd. Fiz. Nauk. Mosk. Obshch. Lyub. Estest. Antr. Etn. – Trudy otdela fizicheskikh nauk Moskovskogo obshchestva lyubitelei estestvoznaniya, antropologii i etnografii.

Trudy Sev.-Kavkaz. Assoc. – Trudy Severo-Kavkazskoi Asociacii. Rostov-na-Donu.

Trudy Tsentr. Aero-Gidrodin. Inst. – Trudy Tsentral'nogo Aero-Gidrodinamicheskogo Instituta. Moskva.

Uchen. Zap. Imp. Kazan. Univ. – Uchenye zapiski Imperatorskogo Kazanskogo universiteta.

Uchen. Zap. Imp. Moskov. Univ. – Uchenye zapiski Imperatorskogo Moskovskogo universiteta.

Uchen. Zap. Moskov. Gos. Univ. – Uchenye zapiski Moskovskogo gosudarstvennogo universiteta imeni M.V. Lomonosova.

Uchen. Zap. Saratov. Gos. Univ. – Uchenye zapiski Saratovskogo gosudarstvennogo universiteta imeni N.G. Cherynshevskogo.

Unterrbl. Math. Naturw. – Unterrichtsblätter für Mathematik und Naturwissenschaften.

Usp. Mat. Nauk – Uspekhi matematicheskikh nauk. Moskva.

Verh. Naturh.-med. Ver. Heidelb. – Verhandlungen des Naturhistorisch-medizinischen Vereins zu Heidelberg.

Vest. AN SSSR – Vestnik Akademii Nauk SSSR. Moskva.

Vest. Moskov. Univ. – Vestnik Moskovskogo universiteta.

Vierteljschr. Naturf. Ges. Zürich – Vierteljahrsschrift der Naturforschenden Gesellschaft in Zürich.

Zap. Imp. Novoross. Univ. – Zapiski Imperatorskogo Novorossiiskogo universiteta. Odessa. Fiz-mat fakultet.

Zap. Mat. Otd. Novoross. Obshch. Estest. – Zapiski matematicheskogo otdeleniya Novorossiiskogo obshchestva estestvoispytatelei. Odessa.

Z. Angew. Math. Mech. – Zeitschrift für angewandte Mathematik und Mechanik.

Z. Flugtech. Motorluftschiff. – Zeitschrift für Flugtechnik und Motorluftschiffahrt.

Z. Flugwiss. – Zeitschrift für Flugwissenschaften.

Z. Ges. Naturw. – Zeitschrift für die gesamte Naturwissenschaft.

Z. Math. Phys. – Zeitschrift für Mathematik und Physik.

Z. Phys. – Zeitschrift für Physik.

Z. Tech. Phys. – Zeitschrift für technische Physik.

Z. VDI – Zeitschrift des Vereins deutscher Ingenieure.

Zentr. Math. – Zentralblatt für Mathematik.

Zentr. Mech. – Zentralblatt für Mechanik.

ZhETF – Zhurnal eksperimental'noi i teoreticheskoi fiziki. Moskva.

Zh. Nauchno-issled. Kafedr Odessa – Zhurnal nauchno-issledovatel'skikh kafedr v Odesse.

Zh. Russk. Fiz.-Khim. Obshch. – Zhurnal Russkogo fiziko-khimicheskogo obshchestva pri Imperatorskom St-Peterburgskom universitete. Chast' fizicheskaya.

2. Case studies

Some of the older papers collected in this bibliography have maintained themselves into modern research while others have been long forgotten. For example, the thesis of Gröbli [365, 366] and the later paper by Synge [892] on the solution of the three-vortex problem were revived about 30 years ago through the independent rediscoveries by Novikov [697] and Aref [26]. For a review of the history

of solution, neglect and re-discovery see [30]. While the three-vortex problem is very interesting of its own accord, the discovery of chaos in the four-vortex problem (cf. [27]) immediately propelled this problem to the front lines of “modern science”. See also §2.2 below.

Another example of this kind may be found in the extensive series of works by Da Rios, [171–186], on vortex filament motion under the so-called *localized induction approximation*. In spite of having been done as a thesis under T. Levi-Civita, one the most illustrious mathematicians of his day, this work, somehow, never “took”. It was not until the 1960’s when Arms & Hama [31] and Betchov [73] re-introduced this idea – and Batchelor included it in his well known text [46] – that it finally became a standard part of the subject. The beautiful transformation of Hasimoto [385], and the idea that vortex filaments can support soliton waves, also played a role in this “assimilation” into modern research. The history of Da Rios’ work has been reviewed by Ricca [784, 785].

2.1. HELMHOLTZ’S PAPER

Helmholtz must rank as the discoverer of a series of fundamental propositions in hydrodynamics that had entirely escaped his predecessors. He pointed out that already Euler had mentioned cases of fluid motion in which no velocity-potential exists, for example, the rotation of a fluid about an axis where every element has the same angular velocity. A minute sphere of fluid may move as a whole in a definite direction, and change its shape, all while rotating about an axis. This last motion is the distinguishing characteristic of vorticity. Helmholtz was the first to elucidate key properties of those portions of a fluid in which vorticity occurs. His investigation was restricted to a frictionless, incompressible fluid. He proved that in such an ideal substance vortex motion could neither be produced from irrotational flow nor be destroyed entirely by any natural forces that have a potential. If vorticity exists within a group of fluid particles, they are incapable of transmitting it to particles that have none. They cannot be entirely deprived of their vorticity themselves (although the vorticity of any individual particle may change in three-dimensional flow; in two-dimensional flow the vorticity of each particle is a constant of the motion). For an ideal fluid the laws of vortex motion establish a curious and indissoluble fellowship between fluid particles and their state of rotation.

In the Introduction to his paper Helmholtz⁹ states:

Hence it appeared to me to be of importance to investigate the species of motion for which there is no velocity-potential.

⁹ According to Tait’s translation [394, p. 486] of his paper.

The following investigation shows that when there is a velocity-potential the elements of the fluid have no rotation, but that there is at least a portion of the fluid elements in rotation when there is no velocity-potential.

By *vortex-lines* (*Wirbellinien*) I denote lines drawn through the fluid so as at every point to coincide with the instantaneous axis of rotation of the corresponding fluid element.

By *vortex-filaments* (*Wirbelfäden*) I denote portions of the fluid bounded by vortex-lines drawn through every point of the boundary of an infinitely small closed curve.

The investigation shows that, if all the forces which act on the fluid have a potential, —

1. No element of the fluid which was not originally in rotation is made to rotate.

2. The elements which at any time belong to one vortex-line, however they may be translated, remain on one vortex-line.

3. The product of the section and the angular velocity of an infinitely thin vortex-filament is constant throughout its whole length, and retains the same value during all displacements of the filament. Hence vortex-filaments must either be closed curves, or must have their ends in the bounding surface of the fluid.

According to Truesdell [964, p. 58] the name *vorticity* was introduced by Lamb [542, §30] for the vector, ω , whose Cartesian components, (ξ, η, ζ) , are given in terms of the components (u, v, w) of the (Eulerian) velocity vector \mathbf{u} by

$$\xi = \frac{\partial w}{\partial y} - \frac{\partial v}{\partial z}, \quad \eta = \frac{\partial u}{\partial z} - \frac{\partial w}{\partial x}, \quad \zeta = \frac{\partial v}{\partial x} - \frac{\partial u}{\partial y}. \quad (1)$$

In modern vector notation

$$\omega = \nabla \times \mathbf{u}. \quad (2)$$

Helmholtz [393] and Stokes [883] used the symbols ξ, η, ζ and $\omega', \omega'', \omega''''$, respectively, to denote the quantities:

$$\frac{1}{2} \left(\frac{\partial w}{\partial y} - \frac{\partial v}{\partial z} \right), \quad \frac{1}{2} \left(\frac{\partial u}{\partial z} - \frac{\partial w}{\partial x} \right), \quad \frac{1}{2} \left(\frac{\partial v}{\partial x} - \frac{\partial u}{\partial y} \right). \quad (3)$$

Helmholtz called these *Rotationsgeschwindigkeiten*, Stokes *angular velocity*; and W. Thomson [937] called them *component rotations*. Basset [44] called the entities (3) *molecular rotations*. For the general case of motion in which ω does not vanish Helmholtz [393] used the term *Rotationsbewegung*, which was translated by Tait [394] as *vortex motion*.

The notion of vorticity had already appeared in earlier works by d'Alembert (1749), Euler (1752–1755), Lagrange (1760), and Cauchy (1815) – in Truesdell's view [964, p. 59], “all these early works are purely formal and somewhat mystifying” – where the vorticity vector is described either as a mean value of the rates of rotation about all or several directions by Cauchy [126] or as a local angular

velocity by Stokes [883]. Subsequently, additional interpretations as a circulation per unit area were given by Hankel [377] and W. Thomson [1937].

Helmholtz's result in §1 of his paper that an arbitrary instantaneous state of continuous motion of a deformable medium is at each point the superposition of a uniform velocity of translation, a motion of extension, a shearing motion, and a rigid rotation, is called by Truesdell [964, p. 66] the “Cauchy-Stokes decomposition theorem” (referring to [126] and [883]). Saint-Venant in a letter of 22 January 1862 to Stokes, cited in [966], insisted on the clear priority of Cauchy in this regard.

In 1867 the French academician Bertrand published [69] various criticisms regarding the universality of Helmholtz's use of the word *rotation* and the correctness of Helmholtz's result. Bertrand contended that in some cases *oblique*, infinitesimal parallelepipeds could be chosen that would transform into other parallelepipeds, whose edges would remain parallel with those of the former, i.e., the continuous motion would consist of the superposition of a translation and an extension (or contraction) along three *nonorthogonal* axes, without rigid rotation of any element of the fluid. He also pointed out that in a simple shearing motion, $u = y, v = 0, w = 0$, fluid particles move along straight lines, while according to Helmholtz's notation the motion is rotational, $\zeta = -\frac{1}{2}$. These examples produced an animated discussion [70–72, 395–397], “an acrimonious public controversy” as Truesdell [964, p. 58] calls it. Helmholtz proved that any extension (or contraction) along three *nonorthogonal* axes is equivalent to the superposition of an extension (or contraction) along three *orthogonal* axes and a rotation. Concerning Bertrand's example, while the fluid particles, which are *points*, do indeed not rotate in orbits like planets about the sun, any *volume*, however small, suffers rotation with respect to its initial configuration, and to an (Eulerian) observer a small rigid object convected by this motion would appear to rotate.

In §2 of his paper [393] Helmholtz gives proofs of his three laws of vortex motion based upon kinematical considerations and ingenious transformations of the dynamical equations for incompressible, homogeneous, inviscid fluid into his now famous vorticity equations.

The first law of Helmholtz is closely related to the celebrated Lagrange-Cauchy velocity-potential theorem. Lagrange [537, §§17–19] and [538, Part II, Section 11, §§16–17] stated that if a velocity potential exists at one time in a motion of an inviscid incompressible fluid, subject to conservative extraneous forces, it will exist at all future times, i.e., a motion once irrotational is always irrotational. Some objections to Lagrange's proof were put forward by Power [727] and especially by Stokes [883, Section II], (see Truesdell [964, §§104–107] for a thorough discussion). Cauchy [126] gave a clear statement and correct proof of the proposition that in a continuous motion of such a fluid, a particle once in irrotational motion is at all times in irrotational motion. The argument was later repeated by Stokes [884]. Later, Stokes [886] added to his paper [884] a note “that two of Helmholtz's

fundamental propositions respecting vortex motion follow immediately from Cauchy's integrals" and gave the proof.

The third law contains two statements, *viz* that "vortex-filaments must either be closed curves", or that they "must have their ends in the bounding surface of the fluid". The first statement excludes the possibility of vortex lines that wander aperiodically and never close, as one finds, for example, in a chaotic, three-dimensional flow¹⁰. The second is, in principle, correct only for vortex lines, although an example of a thin vortex filament that ends at a point in the interior of the fluid has, so far as we are aware, never been given. The vorticity distribution in such a structure would be near-singular.

In §3 of his paper [393] Helmholtz addresses the inverse problem of finding the components of the velocity u, v, w from the components of vorticity ξ, η, ζ (up to a potential flow that covers the boundary conditions). He independently obtains the representations of Stokes [885] for the classical problem of vector analysis of determining a vector field of known divergence ("hydrodynamic integrals of the first class" in his terminology) and curl ("hydrodynamic integrals of the second class"). Determination of the velocity field for incompressible fluid leads to the *Biot-Savart law* of electromagnetism, which in the present case reads that each rotating element of fluid induces in every other element a velocity with direction perpendicular to the plane through the second element that contains the axis of the first element. The magnitude of this induced velocity is directly proportional to the volume of the first element, its angular velocity, and the sine of the angle between the line that joins the two elements and the axis of rotation, and is inversely proportional to the square of the distance between the two elements.

Helmholtz also establishes analogies between the induced velocity and the forces on magnetized particles. Most of these relations would today come under the heading of potential theory.

In §4 of his paper [393] Helmholtz derives an elegant expression for the conserved kinetic energy – "vis viva" in his terminology – of infinite fluid with a compact distribution of vorticity within it.

In §5, entitled "Straight parallel vortex-filaments", Helmholtz studies certain simple cases in which the rotation of the elements occurs only in a set of parallel rectilinear vortex-filaments. In particular, he considers several infinitely thin, parallel vortex-filaments each of which carries a finite, limiting value, m , of the product of the cross-sectional area and the angular velocity. This is the now celebrated concept of a *point vortex*. Helmholtz considers simple cases of the dynamics of such vortices. He establishes the law of conservation of the *center of vorticity* of

¹⁰The best known examples may be the *ABC flows* studied by several authors ever since their introduction in 1965–66 by Arnold and Hénon; see [28] for a brief description in the context of "chaotic advection". There are many other instances where vortex lines do not close. Indeed, closed vortex lines are the exception.

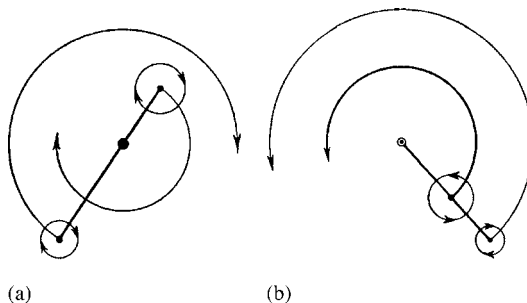


FIG. 5. Motion of two parallel rectilinear vortices (or point vortices) (a) circulations of the same sign; (b) circulations of opposite sign. From [439].

an assembly of point vortices. The discussion is phrased in terms of the “center of gravity” of the vortices (considering their values of m as the analog of “masses”): “The centre of gravity of the vortex-filaments remains stationary during their motions about one another, unless the sum of the masses be zero, in which case there is no centre of gravity.” Without further explanation Helmholtz notes the following two consequences:

1. If there be a single rectilinear vortex-filament of indefinitely small section in a fluid infinite in all directions perpendicular to it, the motion of an element of the fluid at finite distance from it depends only on the product ($\zeta da db = m$) of the velocity of rotation and the section, not on the form of that section. The elements of the fluid revolve about it with tangential velocity $= \frac{m}{\pi r}$, where r is the distance from the centre of gravity of the filament. The position of the centre of gravity, the angular velocity, the area of the section, and therefore, of course, the magnitude m remain unaltered, even if the form of the indefinitely small section may alter.
2. If there be two rectilinear vortex-filaments of indefinitely small section in an unlimited fluid, each will cause the other to move in a direction perpendicular to the line joining them. Thus the length of this joining line will not be altered. They will thus turn about their common centre of gravity at constant distances from it. If the rotation be in the same direction for both (that is, of the same sign) their centre of gravity lies between them. If in opposite directions (that is, of different signs), the centre of gravity lies in the line joining them produced. And if, in addition, the product of the velocity and the section be the same for both, so that the centre of gravity is at an infinite distance, they travel forwards with equal velocity, and in parallel directions perpendicular to the line joining them.

See Figs. 5 and 6 for later illustrations of these motions.

In addition to introducing this notion of a “vortex pair” Helmholtz describes the motion of a single vortex-filament near an infinite plane to which it is parallel. He states that the boundary condition will be fulfilled if instead of the plane there is an infinite mass of fluid with another vortex-filament as the image (with respect to the plane) of the first, and concludes: “From this it follows that the

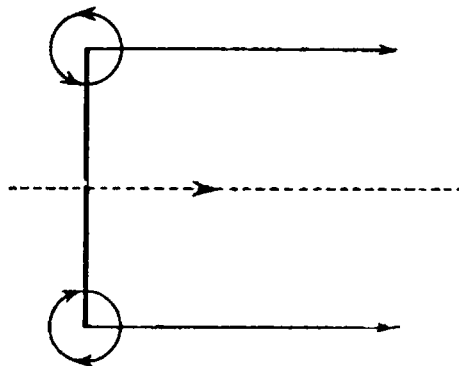


FIG. 6. Motion of a vortex pair. From [439].

vortex-filament moves parallel to the plane in the direction in which the elements of the fluid between it and the plane move, and with one-fourth of the velocity which the elements at the foot of a perpendicular from the filament on the plane have.”

In §6, entitled “Circular vortex-filaments”, Helmholtz studies the axisymmetric motion of several circular vortex-filaments whose planes are parallel to the xy -plane, and whose centers are on the z -axis. Here he considers the problem in full detail (with some minor errors in the formulae corrected in later translations – see [394] and, especially, [401] – without changing the final results) and arrives at the conclusion that “in a circular vortex-filament of very small section in an indefinitely extended fluid, the centre of gravity of the section has, from the commencement, an approximately constant and very great velocity parallel to the axis of the vortex-ring, and this is directed towards the side to which the fluid flows through the ring.” (See Fig. 7 for a later illustration.)

When two such rings of infinitesimal cross-section have a common axis and the same direction of rotation, they travel in the same direction. As they approach, the first ring widens and travels more slowly, the second contracts and travels faster. Finally, if their velocities are not too different, the second ring overtakes the first and travels through it. (For a later illustration see Fig. 10. The corresponding and simpler case for vortex pairs is shown in Fig. 8.) This same process of “leapfrogging” is then repeated indefinitely (in principle – in reality the finite cores of the rings and the effects of viscosity will only allow one or two cycles of this motion). If two vortex rings have equal radii and opposite angular velocities, they will approach each other and widen one another; and when they are very near to one another, their velocity of approach becomes smaller and smaller, and their rate of widening faster and faster. Just as in the case of the straight vortex filament near the plane wall, this motion is similar to the motion of a single vortex ring running up against a plane wall. The image of the ring in the wall is another similar ring with the opposite sense of circulation.

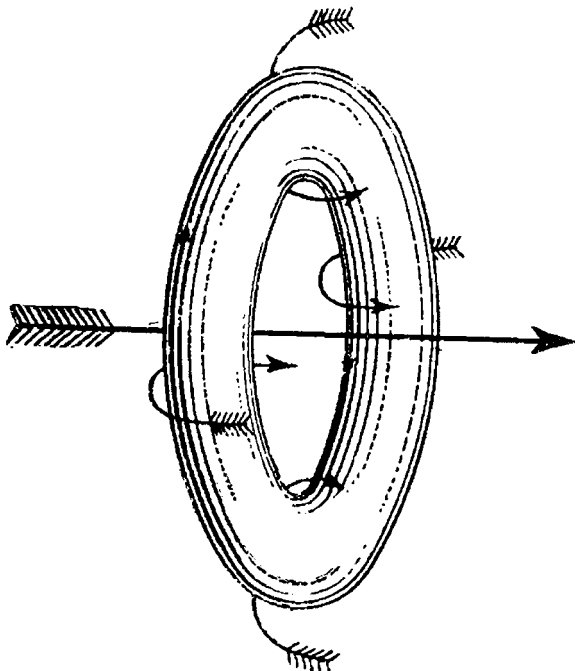


FIG. 7. Self-induced forward motion of a vortex ring. From [439].

Lanchester saw this type of motion involving several vortices to be relevant to vortex formation behind a wing of finite span (cf. Fig. 9). He wrote [545, p. 122]:

Groups of filaments or rings behave in a similar manner to pairs: thus a group of rings may play “leap-frog” collectively so long as the total number of rings does not exceed a certain maximum; congregations of vortex filaments likewise by their mutual interaction move as a part of a concentrated system, like waltzers in a ball-room; when the number exceeds a certain maximum the whole system consists of a number of lesser groups.

This quote seems to embody the mechanism of leap-frogging along with the ultimate merging of vortices with cores of finite size.

Helmholtz concludes his paper with the following interesting thought experiment:

In addition it may be noticed that it is easy in nature to study these motions of circular vortex-rings, by drawing rapidly for a short space along the surface of a fluid a half-immersed circular disk, or the nearly semicircular point of a spoon, and quickly withdrawing it. There remain in the fluid half vortex-rings whose axis is in the free surface. The free surface forms a boundary plane of the fluid through the axis, and thus there is no essential change in the motion. These vortex-rings travel on, widen when they come to a wall, and are widened or contracted by other vortex-rings, exactly as we have deduced from theory.

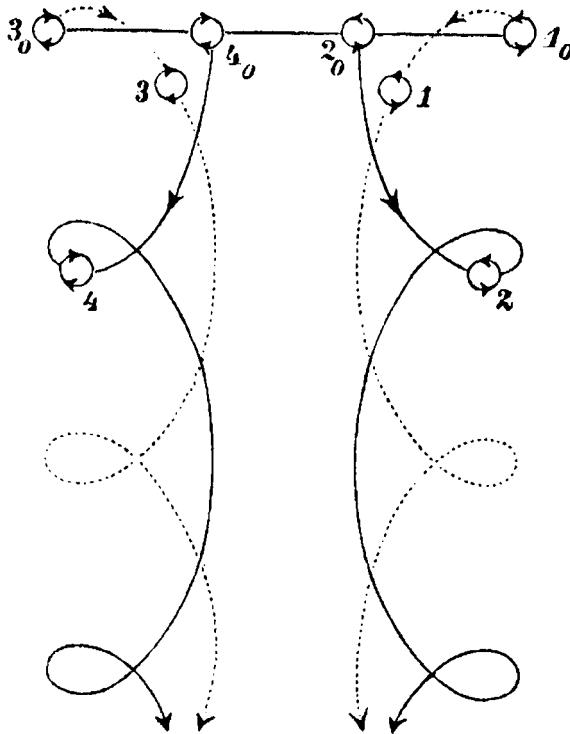


FIG. 8. Illustration of “leapfrogging” by two vortex pairs. The induced velocities are indicated by arrows. From [439] based upon Gröbli’s calculations [365, 366].

This experiment was also described qualitatively by Klein [495] and this led to discussions [2, 79, 82] on the possibility of vortex generation in an inviscid fluid. Quantitative calculations were performed by Taylor [909]; see also his excellent review paper [910]¹¹.

English translations of Helmholtz’s paper [393] have been published at least twice [394, 402]. The paper was included in the well known *Ostwalds Klassiker der exakten Wissenschaften* series [400] (edited by A. Wangerin). In turn, this book was translated into Russian [401] (edited by S. A. Chaplygin, with extensive comments). In view of the widespread use of vector notation today it is interesting to note that when P. G. Tait, Professor of Natural Philosophy at the University of Edinburgh, an intimate friend of Sir W. Thomson and J. C. Maxwell, and a champion of using quaternions (which were flatly rejected by Thomson), wanted to translate Helmholtz’s work for his own use and wrote to Helmholtz on the

¹¹ The remarkable life, career and many seminal contributions to fluid dynamics by G. I. Taylor are chronicled with great scholarship and affection by Batchelor [47, 48].

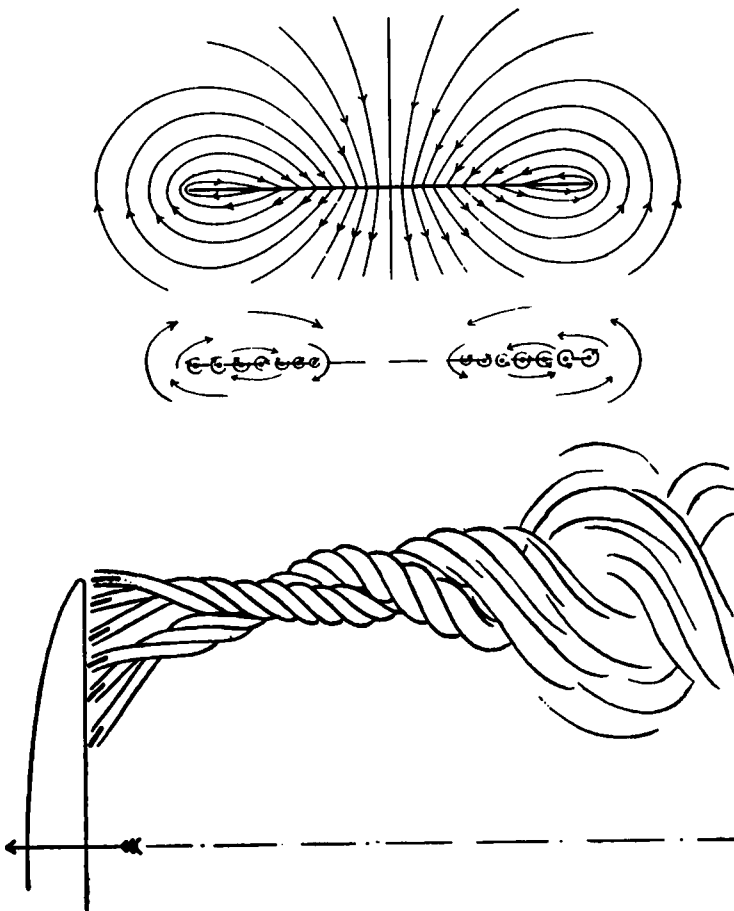


FIG. 9. One of the early major applications of vortex dynamics was to the vortex system of a wing and the generation of lift. These illustrations of the streamlines and vortex formation behind a wing of finite span are from Lanchester's work, see [545].

subject, Helmholtz replied [508, p. 170]:

If you find quaternions useful in this connection, it would be highly desirable to draw up a brief introductory explanation of them, so far as is necessary in order to make their application to vortex-motion intelligible. Up to the present time I have found no mathematician, in Germany at any rate, who was able to state what quaternions are, and personally I must confess that I have always been too lazy to form a connected idea of them from Hamilton's innumerable little notes on this subject.

Only in rare cases does a single paper put forward so many profound ideas and open so many avenues for further investigation. Almost fifty years later, in 1906,

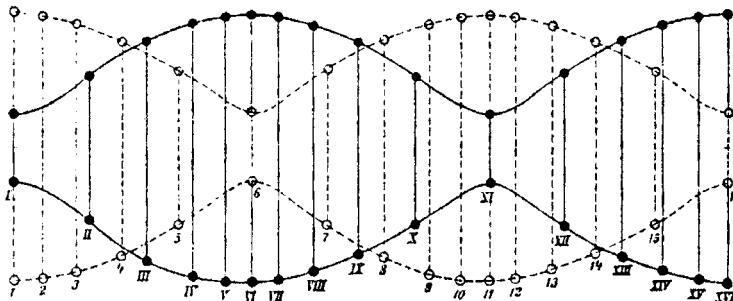


FIG. 10. Illustration of “leapfrogging” by two vortex rings. The trajectories of the two rings have been calculated in detail. This is the analog of the vortex pair motion illustrated in Fig. 8. From [34].

Lord Kelvin, who had himself conducted many great studies developing vortex dynamics further, wrote in the preface to a book about Helmholtz [508] that “his admirable theory of vortex rings is one of the most beautiful of all the beautiful pieces of mathematical work hitherto done in the dynamics of incompressible fluids.” Surprisingly Helmholtz never continued his investigations of the topic established in his ground-breaking paper [393]. Instead he wrote another remarkable paper [398] on discontinuous motion of an inviscid fluid in which he used the notion of a vortex sheet from [393] (see [1025] for details).

In the following century Helmholtz’s theory of vortices was described in great detail in articles in leading general and specialized encyclopedias in various countries [13, 19, 34–36, 96, 261, 264, 339, 341, 348, 361, 592, 600–603, 642, 730]. Note the appearance of the great Maxwell among the authors. Also note that the articles [339, 341, 592] carefully avoided referencing Helmholtz by name because this was considered bad form by the ruling Marxist-Leninist philosophy of the time in the Soviet Union – politics sometimes has unusual influences on science! The theory was elaborated in major German courses of theoretical physics by (in chronological order) Kirchhoff [491], Planck [717], Haas [372], Schaefer [831] and Sommerfeld [866] resulting in now classic texts.

The Helmholtz theory of vortex motion was described, mainly from a qualitative point of view, in several popular courses of general physics [243, 364, 489, 720], and found its place in important treatises on the history of mathematics¹² [496] and physics [428, 791]. In 1866 Maxwell set Helmholtz’s theorems as a question on the Cambridge Mathematical Tripos [637]! The vortex theorems were also treated in important lectures presented on various occasions in various places [8, 18, 76, 77, 95, 106, 108, 265, 392, 410, 439, 453, 571, 593, 604, 605, 639, 728, 736, 738, 759, 771, 775, 782, 787, 807], including the famous 1904 lecture by Prandtl.

¹² Klein [496] points out that the same vortex theorems were independently discovered by Dirichlet [201] at approximately the same time.

Many of these were accompanied by illustrative experiments. Here is a partial list of studies where the results of Helmholtz's paper [393] were used in one way or another: Classical textbooks and monographs on fluid mechanics and aerodynamics [23, 44, 298, 306, 448, 455, 504, 542, 655–657, 740, 742, 743, 809]; general textbooks and monographs on fluid mechanics and aerodynamics [33, 37, 45, 83, 86, 148, 244, 280, 283, 287, 288, 376, 478, 580, 594, 662, 678, 716, 729, 739, 745, 753, 1021, 1024]; review papers [99, 100, 81, 147, 150, 187, 300, 307, 349, 535, 595, 724, 734, 735, 403, 404, 472, 684, 685, 876, 903]; chapters or sections of popular books [275, 712, 896, 930, 931, 993–995]; early specialized books on vortex dynamics [51, 278, 721, 1001]; dissertations [67, 75, 352, 365, 367, 436, 585, 752, 714, 814, 815, 976, 978, 1012]. We also mention the following books in Russian that are less well known in the West¹⁴ [14, 32, 253, 320, 335, 437, 460–463, 487, 505, 506, 530, 591, 658–660, 700, 708, 723, 746, 820, 826, 830, 985, 986].

2.2. POINT VORTICES

A vast area of research started by Helmholtz's paper is the study of the motion of straight, parallel, infinitely thin vortex filaments (rectilinear vortices) in incompressible inviscid fluid or, equivalently, the two-dimensional problem of point vortices on a plane. Through pioneering work of Rosenhead [799] and Westwater [1018] in the 1930's the discretization of two-dimensional hydrodynamics provided by such vortex elements became the foundation for an entire family of numerical methods for flow simulation today collectively known as *vortex methods*.

The problem of N interacting point vortices on the unbounded xy -plane, with vortex $\alpha = 1, \dots, N$ having strength Γ_α (which is constant according to Helmholtz's theorems) and position (x_α, y_α) , consists in solving the following system of $2N$ first-order, nonlinear, ordinary differential equations

$$\begin{aligned} \frac{dx_\alpha}{dt} &= -\frac{1}{2\pi} \sum_{\beta=1}^N \Gamma_\beta \frac{y_\alpha - y_\beta}{l_{\alpha\beta}^2}, \\ \frac{dy_\alpha}{dt} &= \frac{1}{2\pi} \sum_{\beta=1}^N \Gamma_\beta \frac{x_\alpha - x_\beta}{l_{\alpha\beta}^2}, \end{aligned} \tag{4}$$

¹³ Apparently, Lamb [540] (see also the review essay by Reynolds [773] and Lamb's reply [541]) was the first author to treat vortex dynamics in a separate chapter in a major textbook on fluid mechanics.

¹⁴ Many of the authors are also less well known, not to say unknown, in the West. For example, A.A. Satkevitch (1869–1938) was a professor at many St. Petersburg high schools, a corresponding member of the USSR Academy of Sciences (since 1933), and the author of several excellent (text)books on hydromechanics, hydraulics, and gas dynamics, published between 1903 and 1934. He was also a Lieutenant-General in the army of the Russian Empire. In February 1938 he was arrested in Leningrad and accused in the “white-guard officers’ conspiracy” and was executed in July 1938.

where $\alpha = 1, 2, \dots, N$, $l_{\alpha\beta} = \sqrt{(x_\alpha - x_\beta)^2 + (y_\alpha - y_\beta)^2}$ is the distance between vortices α and β , and the prime on the summation indicates omission of the singular term $\beta = \alpha$. Typically, an initial value problem is addressed with the initial positions of the vortices and their strengths given so as to capture or model some flow situation of interest.

The system (4) can also be written as N ordinary differential equations (ODEs) for N complex coordinates $z_\alpha = x_\alpha + iy_\alpha$

$$\frac{dz_\alpha^*}{dt} = \frac{1}{2\pi i} \sum_{\beta=1}^N' \frac{\Gamma_\beta}{z_\alpha - z_\beta}, \quad \alpha = 1, 2, \dots, N, \quad (5)$$

where the asterisk denotes complex conjugation.

In his lectures [491, Lecture 20] Kirchhoff demonstrated that the system (4) can be cast in Hamilton's canonical form ¹⁵:

$$\Gamma_\alpha \frac{dx_\alpha}{dt} = \frac{\partial H}{\partial y_\alpha}, \quad \Gamma_\alpha \frac{dy_\alpha}{dt} = -\frac{\partial H}{\partial x_\alpha}, \quad \alpha = 1, 2, \dots, N, \quad (6)$$

where the Hamiltonian,

$$H = -\frac{1}{4\pi} \sum_{\alpha, \beta=1}^N' \Gamma_\alpha \Gamma_\beta \log l_{\alpha\beta}, \quad (7)$$

is conserved during the motion of the point vortices. (Here \log denotes the natural logarithm.)

In addition to H the Hamiltonian system (6) has three independent first integrals:

$$Q = \sum_{\alpha=1}^N \Gamma_\alpha x_\alpha, \quad P = \sum_{\alpha=1}^N \Gamma_\alpha y_\alpha, \quad I = \sum_{\alpha=1}^N \Gamma_\alpha (x_\alpha^2 + y_\alpha^2). \quad (8)$$

Regardless of the values of the vortex strengths, the integrals H , I , and $P^2 + Q^2$ are *in involution*, that is, the Poisson bracket between any two of them is zero; see the review paper [27] or the monograph [690] ¹⁶. According to Liouville's theorem in analytical dynamics the Hamiltonian system (6) for $N = 3$ is then integrable regardless of the values of the vortex strengths. A terse general statement to this effect was included by Poincaré in his lectures [721, §77] during the second semester of 1891–1892 at the Sorbonne.

¹⁵ A complete correspondence follows by setting the “generalized coordinates” $q_\alpha = x_\alpha$ and the “generalized momenta” $p_\alpha = \Gamma_\alpha y_\alpha$. This results in the remarkable insight that the “phase space” – in the sense of Hamiltonian dynamics – for a point vortex system is, in essence, its configuration space, a fact later exploited by Onsager in a seminal paper [701] on the statistical mechanics of a system of point vortices.

¹⁶ This recent monograph also contains a very useful bibliography connecting vortex dynamics and dynamical systems theory.

An extensive analytical study of integrability and of several special cases of three-vortex motion had already been performed by Gröbli¹⁷ in his noteworthy 1877 Göttingen dissertation [365] (later also published as an extensive paper [366]) that must rightly be considered a classic of the vortex dynamics literature. The solution of the three-vortex problem and the dissertation itself were mentioned in footnotes by Kirchhoff in the third (1883) edition of his lectures [491, Lecture 20, §3] and in the fundamental treatise by Lamb [543, §155] (although in a way that does not fully reveal the comprehensive nature of Gröbli's investigations). Based on these cursory citations it is not difficult to understand that almost a century later Batchelor would write in his important text [46] that the details of motion of three point vortices "are not evident". A lengthy excerpt (in English translation) from Gröbli's dissertation is given in [30].

The Hamiltonian (7) depends only on the mutual distances $l_{\alpha\beta}$ between the vortices which suggests that one can write equations of motion that involve only these distances. Such equations were obtained by Gröbli and later by Laura [553] who also expounded on the canonical formalism. They are

$$\frac{dl_{\alpha\beta}^2}{dt} = \frac{2}{\pi} \sum_{\lambda=1}^N \Gamma_\lambda \epsilon_{\alpha\beta\lambda} A_{\alpha\beta\lambda} \left(\frac{1}{l_{\beta\lambda}^2} - \frac{1}{l_{\lambda\alpha}^2} \right), \quad \alpha, \beta = 1, 2, \dots, N, \quad (9)$$

where the two primes on the summation sign now mean that $\lambda \neq \alpha, \beta$. The quantity $\epsilon_{\alpha\beta\lambda} = +1$ if vortices α, β and λ appear counterclockwise in the plane, and $\epsilon_{\alpha\beta\lambda} = -1$ if they appear clockwise. Finally, $A_{\alpha\beta\lambda}$ is the area of the vortex triangle $\alpha\beta\lambda$ which can, in turn, be expressed in terms of the three vortex separations (the sides of the vortex triangle) by Hero's formula. Interestingly, Eqs.(9) were re-discovered independently at least twice: by Syng [892] in 1949 and by Novikov [697] in 1975. For N vortices one has $\frac{1}{2}N(N-1)$ quantities $l_{\alpha\beta}$ and, thus, $\frac{1}{2}N(N-1)$ equations of the form (9). However, only $2N-3$ of these are independent.

It can be shown that

$$\frac{1}{2} \sum_{\alpha, \beta=1}^N \Gamma_\alpha \Gamma_\beta l_{\alpha\beta}^2 = \left(\sum_{\alpha=1}^N \Gamma_\alpha \right) I - P^2 - Q^2. \quad (10)$$

The equations (9), then, have two general first integrals, *viz* the Hamiltonian (7) and the quantity on the left hand side of (10). Using these two integrals the three ODEs for l_{12} , l_{23} and l_{31} may be reduced to a single ODE that can be solved by quadrature, and this was, in essence, the solution method outlined by Gröbli in his dissertation [365, 366]. The case $N = 3$ thus appears as a critical

¹⁷ An account of the life, scientific achievements and tragic death of the Swiss scientist and mathematician Walter Gröbli (1852–1903) may be found in [30].

one since for more vortices additional “scales of motion” appear without any obvious integrals to constrain them. One may, therefore, expect the problem to become non-integrable. Indeed, this is what happens and the connection to the recent interest in the emergence of chaos in nonlinear dynamics is established. The appearance of chaos in point vortex dynamics as one goes from three to four vortices is analogous to the appearance of chaos in the gravitational N -body problem of celestial mechanics as one goes from two to three bodies. For the case of point masses the appearance of chaos or the absence of integrability became part of the legacy of Poincaré. For inexplicable reasons the analogous discussion for point vortices had to wait for more than a century after the solution of the three-vortex problem. Both Gröbli [365, 366] and later Laura [552, 553] outlined how to determine the “absolute motion” of the vortices provided the solution for the “relative motion” as given by equations (9) was already known.

Over the years the equations for point vortex motion on the unbounded plane have been extensively analyzed in most textbooks and monographs on fluid dynamics, e.g., [23, 45, 148, 306, 455, 459, 504, 542, 543, 655–657, 742, 808] just to mention a few. Several dissertations, e.g., [67, 352, 365, 752, 976, 1012], also addressed various problems of integrable motion of a small number of point vortices.

The nature of the motion of two vortices had already been outlined by Helmholtz [393]. The motion of three vortices – both the relative and the absolute motion – with various intensities and initial conditions was extensively analyzed by Gröbli [365, 366]. The relative motion of three arbitrary vortices, based upon Eqs.(9), was studied and classified by Syng [892] by introducing triangular coordinates in a “phase space” of the three distances between the vortices. Gröbli had actually found such a representation for the case of three identical vortices, and this construction was found independently a century later by Novikov [697]. Syng’s comprehensive analysis was re-discovered independently in [26]. Thus, today the three-vortex problem may be considered to have a rather complete solution. Gröbli [365, 366] also discovered an unusual case where the three vortices converge on a point in a *finite time*. Except for Syng’s study [892], which was itself overlooked, this intriguing case of *vortex collapse* also went unnoticed for a century. It is admittedly a somewhat special case requiring both that the harmonic mean of the three vortex strengths be zero and that the integral of motion (10) vanish.

The problem of stability of uniformly rotating configurations of three vortices with general values of the strengths was addressed by Morton [672] and Sona [867–869]. In our opinion, the papers of the Italian school from the 1920’s and 1930’s on point vortices by Agostinelli [4, 6, 7], Caldonazzo [111–118], Laura [554–556], and Masotti [615–628] deserve to be better known. A “revival” of this large and poorly cited body of work was started in the German dissertation by Wehner [1012], possibly with political motivations considering the time at which it was written.

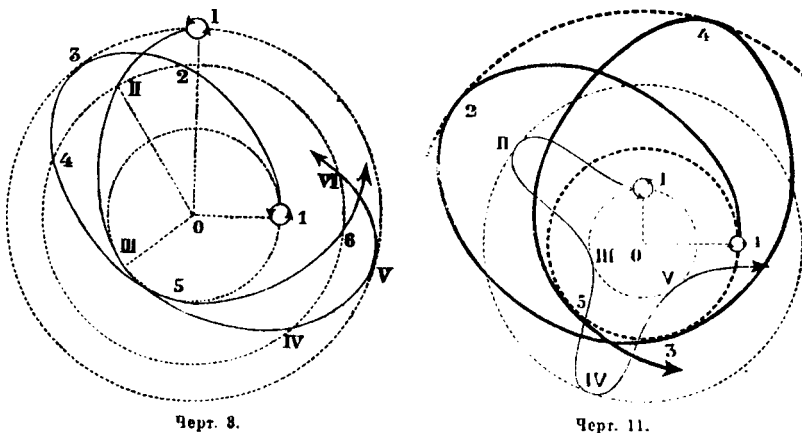


FIG. 11. Results on 4- and 5-vortex motion from Goriachev's 1898 doctoral thesis [352] at Moscow University done under Joukovskii's supervision. The figures show motion of vortices with center of symmetry. Thus, only two trajectories need to be shown. For five vortices, one vortex is at the origin and there are two pairs with a center of symmetry.

The integrable problem of four vortices arranged as two coaxial pairs has been addressed in many papers. Gröbli [365, 366] investigated the case of “leapfrogging” when all vortices have the same absolute strength, and obtained an analytical representation for the vortex trajectories, cf. Fig. 8. His analysis was repeated independently by Love [598] and Hicks [416].

Centrally symmetric configurations of vortices either of equal strengths or of two vortex pairs were studied in detail by Goriachev [351, 352], cf. Fig. 11. The stability problem for a certain configuration of four point vortices that rotates like a rigid body was addressed in [253]¹⁸.

The case of uniform rotation of a regular polygon of N vortices was addressed in the Adams Prize essay of J. J. Thomson [923]. He proved that the regular N -gon is stable to infinitesimal perturbations for $N = 2, 3, 4, 5, 6$ but becomes unstable for $N > 7$. (For $N = 7$ the polygon is marginally stable to linear order and one must go to the next order to decide the stability issue.) This study was extended by Havelock [388], Laura [554] and Morton [673, 674] and the problem continues to be addressed in the literature in various forms.

Helmholtz was also the first to address problems of point vortices interacting with rigid boundaries [393]. As we have seen, he considered the case of a point vortex in the space bounded by a plane wall. Using an “image” vortex of opposite strength situated at the reflection of the original vortex in the plane boundary he reduced the problem to that of the motion of a vortex pair on the unbounded plane.

¹⁸ Note the review of this paper in *Appl. Mech. Rev.* written by a then very young M. J. Lighthill.

This use of the “method of images” has since been widely employed in various problems of the motion of a single point vortex in various bounded domains: in a wedge with an opening angle less than 180° [365, 366, 359, 440], in a parallel channel [498, 679], in a triangle [596], in a rectangle [17, 359, 679], within and outside a circular cylinder [359, 501]; see also [404, 595] for review. Many of these problems appeared either as examples or exercises in textbooks by Basset [44], Lamb [540, 542, 543], Milne-Thomson [655, 656], Kochin and co-authors [504–506], Villat [1001, 1002], and others. Symmetric motion of a vortex pair (two point vortices of opposite strengths) inside and outside a circular cylinder was first studied in [359]. A particular case of an equilibrium of a vortex pair behind a cylinder in a uniform potential flow is known as the “Föppl problem” after the seminal paper [279]. This problem is also frequently discussed in textbooks [504–506, 543, 655, 656, 1001, 1002].

The general case of the motion of point vortices in an arbitrary domain was studied by Routh [810] using the theory of conformal mappings. The velocity of a point vortex in the transformed plane is not equal to the velocity obtained by simple substitution of the conformal mapping into the expression for the velocity in the original plane – one requires also the influence of the images which is captured by the so-called “Routh correction”. Later this approach was extended by Joukovskii [440], Lagally [533] and Caldonazzo [111, 116]. A complete mathematical theory was developed by Lin [583–585] who showed that the problem is always Hamiltonian with a Hamiltonian function that is a hybrid of Kirchhoff’s Hamiltonian (7) for the unbounded plane and the Hamiltonian that Routh found for motion of a single vortex in a bounded domain [810]. This technique has since been applied by several authors [43, 375, 440, 663–666, 709, 975] to study the problem of motion of a point vortex outside and near a sharp wedge. In order to prevent infinite velocity at the apex of the wedge (which occurs for inviscid potential flow) the authors introduce certain conditions on the flow velocity at infinity, some of which seem quite artificial and are, in some sense, equivalent to introducing a time-dependent circulation for the vortex. An improved theory based upon vortex shedding from the sharp edge was developed in [101].

The paper [440] by Joukovskii is considered [877–881] to be one origin of the *Kutta-Joukovskii condition* on flow at the trailing edge of a wing¹⁹. The development of the Kutta [527–529]-Joukovskii [441, 442, 444–447]-Lanchester [545, 546, 547] theory for lift on a wing and what is today usually called the Kutta-Joukovskii condition at the trailing edge of an airfoil has a long and col-

¹⁹ Besides these papers a detailed overview of the voluminous contributions made by Nikolai Egorovich Joukovskii (1847–1921) – alternatively spelled Zhukovskii, Joukowski, Joukovsky, or Žukovskij – in the fields of hydromechanics, aerodynamics, general mechanics, etc., may be found in the books [221, 324, 516, 561] and in the review articles [294, 329, 330, 332, 334, 342, 464, 513, 363, 989]. A detailed bibliography of his works with short comments is collected in [845].

orful history with many contributors. An important early contribution was made by Robins in 1771, well before the period covered by this bibliography. The term *Magnus force* for the side force experienced by a spinning body refers to work by Magnus [610] published in 1853; see also [10, 49, 737] for details. Lord Rayleigh [758] codified much of this early work and provided a derivation of a formula for the lift force, later corrected slightly by Greenhill [360]. Important contributions were also made by Blasius [93] and Chaplygin [130]. This pre-history is extensively reviewed in [294, 863] and also by Khristianovich [488] in a paper that was later criticized by Stepanov [878] who took exception to Khristianovich's proposal that the condition of smooth flow at the trailing edge of an airfoil not be named for Joukovskii!

A classical paper by Joukovskii [442] concerns the important problem of equilibrium of a symmetrical vortex pair behind a finite thin plate placed normally to a flow that is uniform at infinity. It is clearly shown that obtaining stationary positions of the two vortices and at the same time achieving finite velocities of the flow at the sharp edges of the plate (i.e., satisfying the Kutta-Joukovskii condition) is impossible. Interestingly, this key problem has since been reconsidered many times: some authors [102, 781] claimed the existence of solutions (and even stated finding these as an exercise [50, p. 254]), others [381, 998, 1001] flatly ruled out the possibility of a solution. The discussion was re-visited in the 1970's [164, 812, 865].

Various practical problems of point vortex interaction with rigid obstacles and airfoils were studied in the main aviation centers of the USSR (TsAGI and VVA imeni Zhukovskogo) by the famous Russian scientists Sergei Alekseevich Chaplygin (1869–1941)²⁰ [130–131, 134–137] and Vladimir Vasil'evich Golubev (1884–1954)²¹ [308–310, 313–318, 320–323, 344, 345] and in a few of their joint publications [138–140]. Being written mainly in Russian (sometimes with a short English summary and/or a German abstract) these papers remain almost unknown in the West.

W. Thomson [935] was the first to show that a vortex pair in steady motion on the unbounded plane is accompanied by an “atmosphere”, i.e., a fixed, closed volume (area) of fluid particles that move forward with the vortex pair. The bounding curve of this “atmosphere” is today sometimes called the “Kelvin oval”. Figure 12

²⁰ A detailed overview of the life and work of Chaplygin (Tschaplygin, Tchaplyguine) in the fields of hydromechanics and aerodynamics may be found in the book [331] (in Russian) and in the review articles [294, 325, 336, 340, 347, 362, 653, 873, 877, 878, 879, 990, 991]. A detailed bibliography of his work with short comments is collected in [846].

²¹ A detailed overview of the life and work of Golubev in the field of aerodynamics may be found in the books [749, 974] (in Russian), in an interesting autobiography [747], a lecture [346], and in review articles [53, 514, 517, 515, 748].

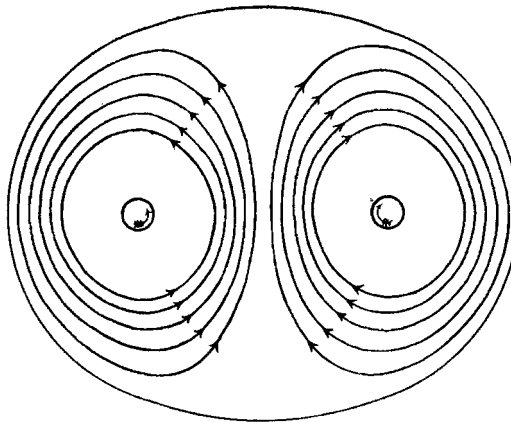


FIG. 12. The “atmosphere” traveling with a vortex pair. From [935].

reproduces the original drawing from [935] where we find this description:

The diagram represents precisely the convex outline referred to, and the lines of motion of the interior fluid carried along by the vortex, for the case of a double vortex consisting of two infinitely long, parallel, straight vortices of equal rotations in opposite directions. The curves have been drawn by Mr. D. McFarlane, from calculations which he has performed by means of the equation of the system of curves, which is

$$\frac{y^2}{a^2} = \frac{2x}{a} \frac{N+1}{N-1} - \left(1 + \frac{x^2}{a^2} \right), \text{ where } \log_e N = \frac{x+b}{a}.$$

The motion of the surrounding fluid must be precisely the same as it would be if the space within this surface were occupied by a smooth solid.

Hicks [415] generalized the result and proved that when a configuration of point vortices moves steadily through otherwise irrotational fluid, it is possible to distinguish three definite regions of fluid motion: (i) a region of rotational motion (the point vortices), which conserves its identity; (ii) a region of irrotational cyclic motion surrounding the first, which also retains its identity and volume and travels uniformly through the fluid with an undeformed boundary; and (iii) a region of irrotational acyclic motion, outside the second region. The fluid in this region remains at rest at infinity and is never displaced over more than a small distance.

Each passive fluid particle may be considered “a point vortex of zero strength”, and the equations of motion for all particles advected by the translating vortex system are integrable. The deformation of a line of fluid connecting two vortices within the moving body was studied analytically by Riecke [788]; see [654] for additional illustrations.

2.3. VORTEX ATOMS

In the 1860's William Thomson, later Lord Kelvin²² became very interested in vortex dynamics since he was convinced that atoms were to be modeled as vortex configurations in the aether. According to [864, p. 417] no evidence exists that Thomson knew of Helmholtz's paper [393] prior to early 1862 when Tait mentioned it to him²³. Tait made a complete English translation [394] of Helmholtz's paper [393] for his own use. He also devised some extremely clever experiments to illustrate the vortex theory using smoke vortex rings in air. Following completion of their famous *Treatise on Natural Philosophy*, referred to simply as "Thomson and Tait", and the successful laying of the Atlantic cable in 1866 (for which Thomson was knighted and became Sir William Thomson), Thomson visited Tait in Edinburgh in mid-January 1867 and saw the smoke rings with his own eyes. On 22nd January he wrote to Helmholtz [920, pp. 513–515]:

... Just now, however, *Wirbelbewegungen* have displaced everything else, since a few days ago Tait showed me in Edinburgh a magnificent way of producing them. Take one side (or the lid) off a box (any old packing-box will serve) and cut a large hole in the opposite side. Stop the open side *AB* loosely with a piece of cloth, and strike the middle of the cloth with your hand. If you leave anything smoking in the box, you will see a magnificent ring shot out by every blow. A piece of burning phosphorus gives very good smoke for the purpose; but I think nitric acid with pieces of zinc thrown into it, in the bottom of the box, and cloth wet with ammonia, or a large open dish of ammonia beside it, will answer better. The nitrite of ammonia makes fine white clouds in the air, which, I think, will be less pungent and disagreeable than the smoke from the phosphorus. We sometimes can make one ring shoot through another, illustrating perfectly your description; when one ring passes near another, each is much disturbed, and is seen to be in a state of violent vibration for a few seconds, till it settles again into its circular form. The accuracy of the circular form of the whole ring, and the fineness and roundness of the section, are beautifully seen. If you try it, you will easily make rings of a foot in diameter and an inch or so in section, and be able to follow them and see the constituent rotary motion. The vibrations make a beautiful subject for mathematical work. The solution for the longitudinal vibration of a straight vortex column comes out easily enough. The absolute permanence of the rotation, and the unchangeable relation you have proved between it and the portion of the fluid once acquiring such motion in a perfect fluid, shows that if there is a perfect fluid all through space, constituting the substance of all matter, a vortex-ring would be as permanent as the solid hard atoms assumed by Lucretius

²² For a popular survey of Kelvin's long and adventuresome life (1824–1907) we may direct the reader to several books [273, 356, 586, 852, 864, 920, 1028] written at various times, to the obituary notice [919], to the century jubilee notes [245, 702] (the second in a rather unusual journal), and to one among many encyclopedia articles [104]. Kelvin was one of the greatest scientists of the 19th century – his grave is in Westminster Abbey, next to Newton's – and is credited with having foreseen in his lecture at the Royal Institution on April 27, 1890, [486] two major discoveries in theoretical physics of the 20th century, *viz* the special theory of relativity and quantum mechanics.

²³ Helmholtz and Thomson had met for the first time in 1855. In a letter of August 30, 1859, Helmholtz reported to Thomson that he had been working on hydrodynamic equations including friction, but did not mention his *Wirbelbewegungen* study.

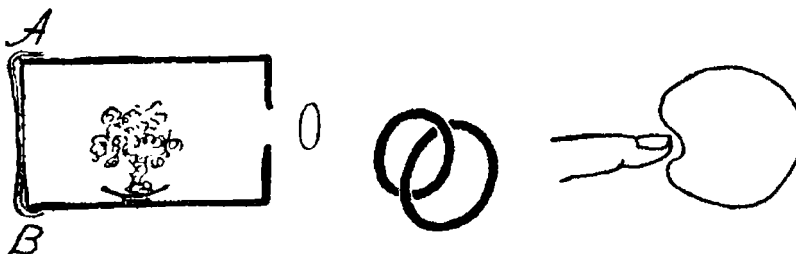


FIG. 13. Illustrations to accompany Kelvin's letter to Helmholtz of 22nd January, 1867 [920].

and his followers (and predecessors) to account for the permanent properties of bodies (as gold, lead, etc.) and the differences of their characters. Thus, if two vortex-rings were once created in a perfect fluid, passing through one another like links of a chain, they never could come into collision, or break one another, they would form an indestructible atom; every variety of combinations might exist.

Thus a long chain of vortex-rings, or three rings, each running through each of the other, would give each very characteristic reactions upon other such kinetic atoms. I am, as yet, a good deal puzzled as to what two vortex-rings through one another would do (how each would move, and how its shape would be influenced by the other). By experiment I find that a single vortex-ring is immediately broken up and destroyed in air by enclosing it in a ring made by one's fingers and cutting it through. But a single finger held before it as it approaches very often does not cut it and break it up, but merely causes an indentation as it passes the obstacle, and a few vibrations after it is clear.

Tait's translation of Helmholtz's paper was published that same year in *Philosophical Magazine* [394]. One must imagine that Kelvin encouraged his friend and colleague to prepare this translation for publication.

Thomson's prodigious talent produced several first rate studies of vortex dynamics which, although ultimately wrong-headed in terms of atomic physics, have had a lasting influence on fluid dynamics. The idea of *circulation*, for example, is from this period. The circulation is defined as the contour integral of the projection of the flow velocity on the tangent to the contour,

$$\Gamma = \oint_C \mathbf{V} \cdot d\mathbf{s}. \quad (11)$$

He showed that for any material contour moving according to Euler's equation for incompressible flow, the circulation is an integral of the motion, a result known today as *Kelvin's circulation theorem*²⁴. This profound insight has continued to

²⁴This theorem was considered by Einstein [245] among the most important scientific results of W. Thomson (Lord Kelvin).

exert an influence on the entire field of fluid mechanics, including in such areas as the assessment of the accuracy of numerical methods and in turbulence modeling. Circulation is a distinctly topological entity, independent of the shape of the vortex and measurable by integration along any circuit that loops around the vortex. In this sense, the notion of circulation may be taken as one of the earliest introductions of topological considerations into fluid mechanics²⁵. For a broader discussion see [248]. Today the intersection of fluid mechanics and topology, in its multiple forms, has matured into a subfield often referred to as topological fluid dynamics. The permanence of circulation in an ideal fluid was one of the cornerstones of vortex atom theory. Like atoms, vortices in the aether could neither be created nor destroyed.

Thomson's fascination with the floating magnet experiments by Mayer [643–648], and his role in the re-publication of these works in journals such as *Nature* and *Philosophical Magazine*, were also outgrowths of his conviction that vortices and atoms are intimately related. See Snelders' article [861] for a comprehensive historical review of this topic.

It is interesting to trace Thomson's presentations at the meetings of the *Royal Society of Edinburgh* and their subsequent publication:

1. “On vortex atoms” (read 18th February 1867 – with an abstract in the newspaper the *Scotsman* on February 19, 1867!); published as [935].
2. “On vortex motion” (read 29th April 1867); published as [937] (abstract in *Proc. R. Soc. Edinb.* **7**, 576–577).
3. “On vortex motion” (read 18th December 1871).
4. “On vortex motion” (read 3rd March 1873); title in *Proc. R. Soc. Edinb.* **8**, 80.
5. “On the oscillation of a system of bodies with rotating portions. Part II. Vibrations of a stretched string of gyrostats (dynamics of Faraday's magneto-optic discovery) with experimental illustrations” (read 19th April 1875); title in *Proc. R. Soc. Edinb.* **8**, 521.
6. “Vortex statics” (read 20th December 1875); published as [938].
7. “On two-dimensional motion of mutually influencing vortex-columns, and on two-dimensional approximately circular motion” (read 3rd January 1876); title in *Proc. R. Soc. Edinb.* **9**, 98.
8. “On the vortex theory of gases, of the condensation of gases, and of the continuity between the gaseous and liquid state of matter” (read 3rd April 1876); title in *Proc. R. Soc. Edinb.* **9**, 144.

²⁵Tait's seminal work on the classification of knots on closed curves is a spin-off of his interest in vortex atoms. It has stood the test of time and is today recognized as an important contribution to topology, knot theory and graph theory. Maxwell was an important catalyst for Tait's work on knots, since he had also become interested in topological ideas. There is a letter from Maxwell to Tait of 13 November 1867 [638] in which he points out the importance of linking of vortices, see [502].

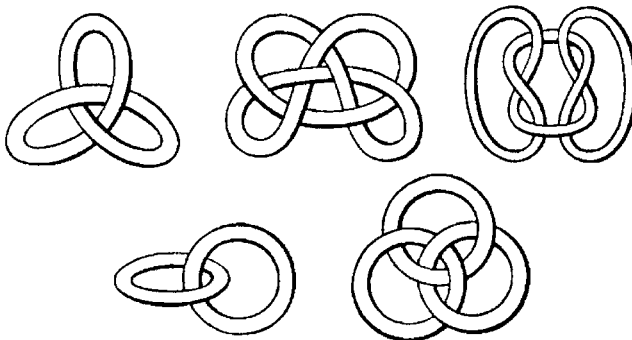


FIG. 14. Tait's drawings, reproduced in [937], that capture Thomson's ideas on how atoms arise as vortex structures in the aether.

9. "On vortex vibrations, and on instability of vortex motion" (read 15th April 1878); title in *Proc. R. Soc. Edinb.* **9**, 613.
10. "A mechanical illustration of the vibrations of a triad of columnar vortices" (read 20th May 1878); title in *Proc. R. Soc. Edinb.* **9**, 660.
11. "On vortex motion: Gravitational oscillations in rotating water" (read 17th March 1879).
12. "Vibrations of a columnar vortex" (read 1st March 1880); published as [940].
13. "On vortex sponge" (read 21st February 1881); title in *Proc. R. Soc. Edinb.* **11**, 135.
14. "On the average pressure due to impulse of vortex rings on a solid" (read 18th April 1881²⁶); title in *Proc. R. Soc. Edinb.* **11**, 204; published as [944].
15. "On energy in vortex motion" (read 16th February 1885); title in *Proc. R. Soc. Edinb.* **13**, 114.
16. "On the instability in fluid motion" (read 18th April 1887); title in *Proc. R. Soc. Edinb.* **14**, 194.
17. "On a mechanism for the constitution of Ether; illustrated by a model" (read 17th March 1890).

The famous quote from Thomson that "Helmholtz's [vortex] rings are the only true atoms" summarizes the theme of this research thrust. Figure 14 depicts the kind of things he envisioned.

Although it ultimately faded, the vortex atom idea maintained itself for many years and through Kelvin's boundless energy and great influence spread widely in the scientific community. Schuster [840, p. 34] recounts that Kirchhoff, who otherwise was not easily excited about physical theories, once told him: "I like it... because it excludes everything else," to which he added with a sigh: "If only it could explain gravitation." The work by J. J. Thomson, discoverer of the electron, on vortex dynamics in [922–932], and [934] was stimulated by vortex atom theory.

²⁶ Helmholtz was the second speaker at this meeting according to [248].

Even in his great paper of 1897 entitled “Cathode Rays”, in which the discovery of the electron is announced, we find these remarks: “If we regard the system of magnets as a model of an atom, the number of magnets being proportional to the atomic weight, ... we should have something quite analogous to the periodic law...”, where by “periodic law” he means the periodic table of the elements. The reference to the floating magnets is to Mayer’s experiments mentioned above. We see what a profound role these demonstration experiments played in the thinking of these great scientists. We should not forget that at the time analog experiments were one of the only ways of exploring solutions to nonlinear equations that did not easily yield to analytical methods. Computers and numerical solutions were still many years in the future.

The vortex atom theory received considerable attention from Maxwell [642] in his article on the atom written for the 1878 edition of *Encyclopedie Britannica*. He provided a detailed description of properties of vortices in ideal fluid and strongly supported the idea of vortex atoms. Apparently, he was reminded of his own earlier articles [633, 634, 635, 636] in which his celebrated electromagnetic theory was initially formulated based upon a mechanical model that also made reference to Helmholtz’s paper [393]. Here the energy of a magnetic system was represented by the rotation of an inviscid fluid about the lines of magnetic force, each unit tube of force being depicted as a circular Rankine vortex [755]. Maxwell concluded:

His [Thomson’s] primitive fluid has no other properties than inertia, invariable density, and perfect mobility, and the method by which the motion of this fluid is to be traced is pure mathematical analysis. The difficulties of this method are enormous, but the glory of surmounting them would be unique.

As one might expect, Boltzmann thought deeply about molecular vortices. In the translations of Maxwell’s papers into German, that Boltzmann produced and annotated, one finds extensive, penetrating comments on two-dimensional vortices elucidated in terms of pressure, velocity, energy, and so on, all very enlightening of the physical properties of this model. These translations and comments are mentioned in the bibliography in conjunction with [633–636].

Accounts of the vortex atom theory may be found in the books [220, pp. 28–33], [229, pp. 169–176], [896, pp. 294–301], [1022, pp. 290–295], and in the papers [855, 861, 1027]. See also [519] for a recent account.

Much recent work has transpired on the problem of *Vortex Statics*, as Kelvin called it (see item 6 above and [938]). The reader may be interested in a recent review in this series [29]. The term “vortex crystals” appears to be gaining favor in current research. The terminology of celestial mechanics would suggest the term “relative equilibria” for the states being investigated.

We conclude this brief description of vortex atoms by citing the following poem which appeared in *Nature* **26** (1882) 297:

THE LAY OF THE LAST VORTEX-ATOM

(*Vide THE UNSEEN UNIVERSE*)

Melody — *Lorelei*

The Vortex-Atom was dying
The last of his shivering race —
With lessening energy flying
Through the vanishing realms of Space.

No more could he measure his fleeting —
No milestones to mark out his way;
But he knew by his evident heating
His motion was prone to decay.

So he stayed in his drift rectilinear
For Time had nigh ceased to exist,
And his motion grew ever less spinnier
Till he scattered in infinite mist.

But as his last knot was dissolving
Into the absolute nought —
“No more,” so sighed he resolving,
“Shall I as atom be caught.

“I’ve capered and whirled for ages,
“I’ve danced to the music of spheres,
“I’ve puzzled the brains of the sages —
“Whose lives were but reckoned by years.

“They thought that my days were unending,
“But sadly mistaken were they;
“For, alas! my ‘life-force’ is expending
“In asymptotic decay!”

2.4. VORTEX RINGS

In spite of the great popularity of Tait's [896, pp. 291–294], smoke box for generating vortex rings in air, the first observation of vortex rings probably corresponds with the introduction of smoking tobacco! Northrup²⁷ [695, p. 211] writes:

It is not improbable that the first observer of vortex motions was Sir Walter Raleigh; if popular tradition may be credited regarding his use of tobacco, and probably few smokers since his day have failed to observe the curiously persistent forms of white rings of tobacco smoke which they delight to make. But some two hundred eighty years went by, after the romantic days of Raleigh and Sir Francis Drake, who made tobacco popular in England, before a scientific explanation of smoke rings was attempted.

By curious coincidence the first experimental observations of the generation of vortex rings in air were performed by Rogers²⁸ [789] in the same year (1858) that Helmholtz published his seminal paper [393], see Fig. 1.

Later Ball [38–40], provided a detailed description of the experimental set-up and gave some data concerning the uniform velocity of propagation of single vortex rings of various sizes. Using the smoke-box apparatus Dolbear carefully repeated all Tait's experiments and produced [220, pp. 28–31], a long list of characteristics of smoke vortex rings:

1. It retains its ring form and the same material rotating as it starts with.
2. It can travel through the air easily twenty or thirty feet in a second without disruption.
3. Its line of motion when free is always at right angles to the plane of the ring.
4. It will not stand still unless compelled by some object. If stopped in the air, it will start up itself to travel on without external help.
5. It possesses momentum and energy like a solid body.
6. It is capable of vibrating like an elastic body, making a definite number of such vibrations per second, – the degree of elasticity depending upon the rate of vibration. The swifter the rotation, the more rigid and elastic it is.
7. It is capable of spinning on its own axis, and thus having rotary energy as well as translatory and vibratory.
8. It repels light bodies in front of it, and attracts into itself light bodies in its rear.
9. If projected along parallel with the top of a long table, it will fall upon it every time, as a stone thrown horizontally will fall to the ground.

²⁷ Edwin Fitch Northrup (1866–1940) was a professor of physics at Princeton and author of a science fiction book entitled "Zero to Eighty: Being my Lifetime Doings, Reflections, and Inventions; also my Journey around the Moon." The book was published in Princeton in 1937 under the pseudonym Akkad Pseudoman. It gives a fictional account, supported by valid scientific data, of a Morris County resident's trip around the moon. It appears to have a sustained following in the world of science fiction.

²⁸ William Barton Rogers (1804–1882) will be better known today as the founder of MIT. Indeed, he was heavily engaged in this enterprise at about the time his paper on vortex rings was written.

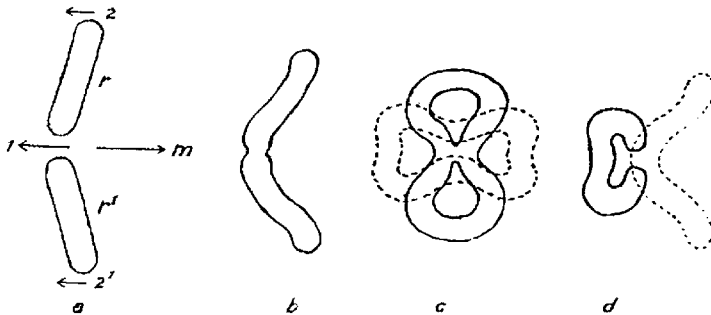


FIG. 15. Sketch of interaction of two identical vortex rings launched on a collision course. From Northrup [696].

10. If two rings of the same size be traveling in the same line, and the rear one overtakes the other, the front one will enlarge its diameter, while the rear one will contract its own till it can go through the forward one, when each will recover its original diameter, and continue on in the same direction, but vibrating, expanding, and contracting its diameter with regularity.
11. If two rings be moving in the same line, but in opposite directions, they will repel each other when near, and thus retard their speed. If one goes through the other, as in the former case, it may quite lose its velocity, and come to a standstill in the air till the other has moved on to a distance, when it will start up its former direction.
12. If two rings be formed side by side, they will instantly collide at their edges, showing strong attraction.
13. If the collision does not destroy them, they may either break apart at the junction of the collision, and then weld together into a single ring, with twice the diameter, and then move on as if a single ring had been formed, or they may simply bound away from each other; in which case they always rebound *in a plane at right angles* to the plane of collision. That is, if they collided on their sides they would rebound so that one went up and the other down.
14. Three may in like manner collide, and fuse into a single ring.

Experiments in water on the generation and interaction of vortex rings were started independently by Rogers [789] and Reusch [768] and then reported in a long series of papers including [41, 42, 52, 97, 170, 196–198, 384, 433, 518, 521, 544, 608, 609, 698, 699, 704, 750, 751, 769–772, 776, 790, 888, 901, 904, 934, 953, 954, 962, 963, 1011, 1019, 1020, 1032]. The extensive study by Northrup [695, 696] should also be mentioned here. It contains a very detailed description of a “vortex gun”, including all the parameters, together with beautiful photos of interacting vortex rings and vortex rings interacting with rigid obstacles, e.g., with a small watch chain. The modern reader may be intrigued to see in these near-century old papers an essentially contemporary elucidation of the interaction of two circular vortex rings tilted towards one another so as to interact after having propagated for some distance, cf. Fig. 15.

Theoretical studies of the motion of a circular vortex ring of closed toroidal shape with core radius a and radius R of the center line of the torus, where $a \ll R$,

in an ideal fluid led to a formula for the self-induced translational velocity V_{ring} , directed normally to the plane of the ring:

$$V_{ring} = \frac{\Gamma}{4\pi R} \left(\log \frac{8R}{a} - C \right) + O(a/R) \quad (12)$$

Here Γ is the (constant) intensity of the vortex ring, equal to the circulation along any closed path around the vortex core, and C is a constant. There was some disagreement in the literature concerning the value of C . The value $C = \frac{1}{4}$ was given (without proof) by W. Thomson [936] and later by Hicks [407], Basset [44], Dyson [238] and Gray [358]. This corresponds to the case where the vorticity inside the core varies directly as the distance from the centerline of the ring. The value $C = 1$ was given by Lewis [577], J. J. Thomson [923], Chree [142], Joukovskii [443], and Lichtenstein [579] for a uniform distribution of vorticity within the core. Detailed discussion of both these hypotheses and also the circular form of the core is given in [847, 543, 579] and later repeated by Fraenkel [281]. For a hollow vortex core, or if one assumes the fluid inside the core is stagnant, the value $C = \frac{1}{2}$ results [719].

The reader may wish to consult the more recent review by Shariff and Leonard [851] on vortex ring dynamics for the further evolution of this intriguing subject.

2.5. VORTEX STREETS

Most students of fluid mechanics know that the common staggered array of vortices that forms in the wake of a cylinder (or any bluff body) is called the *Kármán vortex street*. The concept of the vortex street is among the best known in all of fluid mechanics, in the same “league” as *Reynolds number*, *Bernoulli’s equation* and the concept of the *boundary layer*. The formation and structure of vortex wakes downstream of bluff bodies had been studied extensively in experiments (see Fig. 16 for an example) going back to Leonardo da Vinci [292, 382, 383, 562] but von Kármán’s theory was the first real analysis of the phenomenon. In his charming book [470] he explains that his interest was aroused by an early picture of such vortices in a fresco in one of the churches in Bologna, Italy, where St. Christopher is shown carrying the child Jesus across a flowing stream. Alternating vortices are seen behind the saint’s foot; see [667] for a beautiful color picture of this fresco at the Church of St Dominic, entitled *Madonna con bambino tra I Santi Domenico, Pietro Martire e Critofooro*, painted by an unknown artist of the fourteenth century.

Alternating vortices in air were observed and imaged by the British scientist Mallock [612, 613] (cf. Fig. 16) while impressive photos of such vortices in water were obtained by the German scientist Ahlborn [8]. The French scientist Bénard [56] also observed the alternating formation of detached vortices on the two sides of

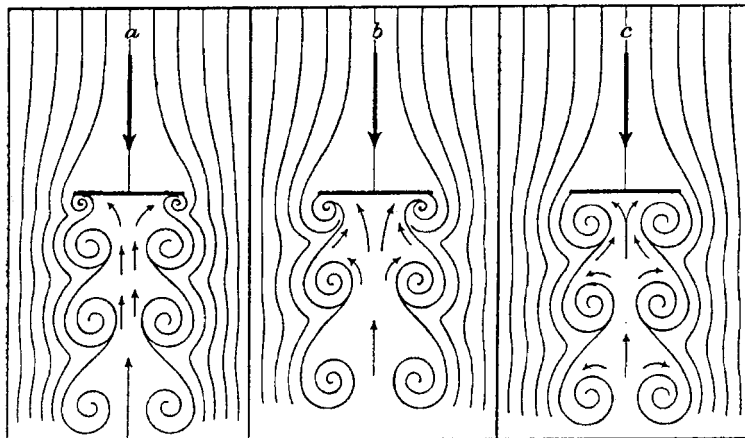


FIG. 16. Sketch of vortex wake formation downstream of a flat plate. After Mallock [612].

a bluff obstacle in water and later in many viscous fluids and in colloidal solutions:

Pour une vitesse suffisante, au-dessous de laquelle il n'y a pas de tourbillons (cette vitesse limite croît avec la viscosité et décroît quand l'épaisseur transversale des obstacles augmente), les tourbillons produits périodiquement se détachent alternativement à droite et à gauche du remous d'arrière qui suit le solide; ils gagnent presque immédiatement leur emplacement définitif, de sorte qu'à l'arrière de l'obstacle se forme une double rangée alternée d'entonnoirs stationnaires, ceux de droite dextrogyres, ceux de gauche lévogyres, séparés par des intervalles égaux.

Analysis shows that only two such configurations will propagate in the streamwise direction: The vortices must either be arranged in a symmetric or in a staggered configuration. Numerically the intensities of the vortices, Γ , are all equal, but the vortices on the two horizontal rows have opposite signs. In remarkable theoretical investigations [467, 468] von Kármán examined the question of stability of such processions in unbounded, incompressible, inviscid, two-dimensional flow with embedded point vortices²⁹. He became interested in this problem when he was appointed as a graduate assistant in Göttingen in Prandtl's laboratory in 1911. Prandtl had a doctoral candidate, K. Hiemenz, to whom he had given the task of constructing a water channel in order to observe the separation of the flow behind a cylinder. Much to his surprise, Hiemenz found that the flow in his channel oscillated violently, and he failed to achieve symmetrical flow about a circular cylinder.

²⁹Contrary to von Kármán's reminiscences (see later) the first paper was submitted to the *Königlichen Gesellschaft der Wissenschaften zu Göttingen* by Felix Klein on September 14, 1911 and the second paper by Carl Runge on December 23, 1911.

Von Kármán wrote [470, p. 70]

When he [Hiemenz] reported this to Prandtl, the latter told him: “Obviously your cylinder is not circular.”

However, even after very careful machining of the cylinder, the flow continued to oscillate. Then Hiemenz was told that possibly the channel was not symmetric, and he started to adjust it.

I was not concerned with this problem, but every morning when I came into the laboratory I asked him, “Herr Hiemenz, is the flow steady now?”

He answered very sadly, “It always oscillates.”

Von Kármán addressed the model problem of two infinite rows of point vortices and derived a criterion for when such a configuration is not unstable to *linearized* perturbations. He showed that the symmetric configuration, cf. Fig. 17, is always unstable and that the staggered configuration is also unstable unless the spacing between successive vortices in either row and the distance between the rows has a definite ratio.

Later he reminisced [470, p. 70]:

One weekend I tried to calculate the stability of the system of vortices, and I did it in a very primitive way. I assumed that only one vortex was free to move, while all other vortices were fixed, and calculated what would happen if this vortex were displaced slightly. The result I got was that, provided a symmetric arrangement was assumed, the vortex always went off from its original position. I obtained the same result for asymmetric arrangements but found that, for a definite ratio of the distances between the rows and between two consecutive vortices, the vortex remained in the immediate neighborhood of its original position, describing a kind of small closed circular path around it.

I finished my work over the weekend and asked Prandtl on Monday, “What do you think about this?”

“You have something,” he answered. “Write it up and I will present your paper in the Academy.”

This was my first paper [467] on the subject. Then, because I thought my assumption was somewhat too arbitrary, I considered a system in which all vortices were movable. This required a little more complicated mathematical calculation, but after a few weeks I finished the calculation and wrote a second paper [468].

If the spacing between successive vortices in the same row is called l , and if the distance between the two parallel rows is called h , von Kármán’s criterion [468] is

$$\cosh \frac{\pi h}{l} = \sqrt{2}, \quad \text{or} \quad \frac{h}{l} = 0.283. \quad (13)$$

The velocity, U , of horizontal translation of the infinite rows is found to be

$$U = \frac{\Gamma}{2l} \tanh \frac{\pi h}{l}. \quad (14)$$

This is today very well known. What is probably less well known is that in the original paper [467] von Kármán found the criterion (13) with $\sqrt{3}$ (or $h/l = 0.365$)

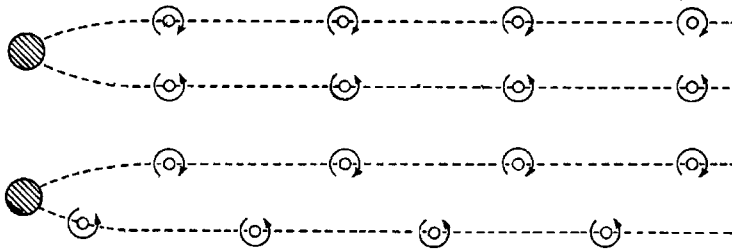


FIG. 17. Schematic of a symmetric and a staggered vortex street downstream of a bluff body. From [470].

on the right hand side rather than (the correct) $\sqrt{2}$, which was confirmed subsequently in [474, 814] (with reference to the then newly created theory of an infinite system of linear differential equations due to O. Toeplitz in 1907)³⁰ and by Lord Rayleigh [760]. The original drawings [474] of the streamlines in a coordinate system moving steadily with the vortices are reproduced in Fig. 18. (When the ratio h/l is given by Eq.(13), the propagation speed of the street, U , in Eq.(14) is $\Gamma/l\sqrt{8}$.)

Von Kármán commented [470, p. 71]: “Some people asked, ‘Why did you publish two papers in three weeks? One of them must be wrong.’ Not exactly wrong, but I first gave a crude approximation and afterwards refined it. The result was essentially the same; only the numerical value of the critical ratio was different.”

The erroneous value was, for example, later used by Synge [891] in his re-derivation of the Kármán drag formula, although the analysis is easily corrected³¹.

Measurements by H. Rubach [474, 814] gave the values $h = 1.8$ cm, $l = 6.4$ cm ($h/l = 0.282$) for a circular cylinder of diameter 1.5 cm, and $h = 3.0$ cm, $l = 9.8$ cm ($h/l = 0.305$) for a thin plate of width 1.75 cm.

On the other hand, Joukovskii in a talk in November 1913 [451] and in lectures [459, §29] read in 1911–1912 at Moscow High Technical School, later translated into French [455], repeated the concise derivation of von Kármán’s first paper [467] in full detail and naturally arrived at the condition $\cosh(\frac{\pi h}{l}) = \sqrt{3}$ and $h/l = 0.365$ for the stability condition of a vortex street. (All publications contain a photo of Prandtl in front of the small water channel in Göttingen where the discovery of vortex streets was made.) His measurements at the laboratory of Moscow High Technical School [459, p. 185] provided the following values: $h/l = 0.320; 0.337; 0.366; 0.363$ for thin plates of various widths placed perpendicular to the flow. Later this work led to an intensive discussion in Russia [1, 309, 311, 312].

³⁰ It may appear strange but in his book [470] von Kármán did not mention Rubach’s name at all.

³¹ The authors have a version of the paper [891] with Prof. Synge’s annotations effecting the necessary changes.

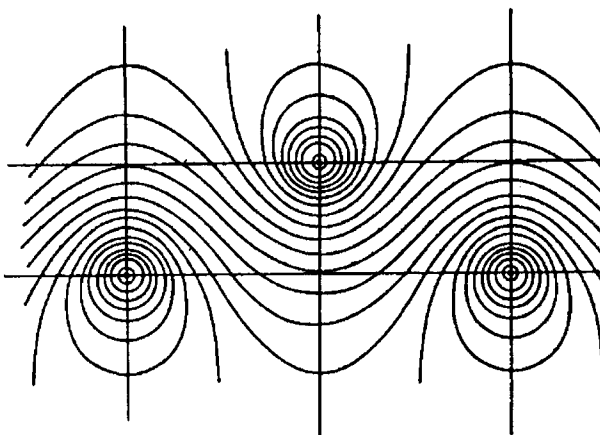


FIG. 18. Streamlines of a vortex street in the co-moving frame based on the point vortex model [474].

The problems considered by von Kármán [467] – Joukovskii [451, 455, 459] and von Kármán [468] are essentially different: in the latter case *all* vortices are “free” and may be perturbed, while in the former case only one vortex is “free” while the others are all fixed at their positions in the street configuration. These two problems are not equivalent and so the stability conditions are different.

Von Kármán’s analysis precipitated huge amounts of work, both experimental, analytical – and much later – numerical; see the review papers [523, 801]. On July 18, 1922, a young Heisenberg, then a student of Sommerfeld at the Institute for Theoretical Physics at University of München, submitted an article [389] in which he tried to define an absolute size of the Kármán vortex street behind a flat plate of width d placed perpendicularly to the oncoming flow of velocity U_∞ far upstream³². Based on physical arguments he arrived at the numerical values $l/d = 5.45$ and $h/d = 1.54$. These values fit von Kármán’s second value for the ratio of width to intra-row spacing, $h/l = 0.283$ and the ratio of the speed of propagation of the row relative to the flow speed at infinity, $U/U_\infty = 0.229$. In a short Appendix (written on July 29, 1922) to this paper Prandtl put forward three objections to the analysis of Heisenberg and concluded:

In my opinion, Mr. Heisenberg’s computation, though very instructive, is only adapted to yield definite conclusions when used in connection with experimental data concerning the correction factors referred to above.

³²The editors of Heisenberg’s collected works call this “the apprentice work of [a] second semester student”.

Heisenberg's thoughts at this time were already turning to other topics, most notably the creation of a new "matrix" version of quantum mechanics for which he was to receive the Nobel prize in 1933 (together with Schrodinger and Dirac). Nevertheless, his doctoral dissertation, completed in July 1923, was on hydrodynamics, in particular stability theory and turbulence, and he would return briefly to the topic of fully developed turbulence in the period following World War II.

The necessary condition for absence of linear instability was generalized to vortex streets moving obliquely to the direction of the "free stream" by Dolaptschiew and Maue. While the paper by Maue [630] will probably be familiar, in part because this work was highlighted in the well-known lectures of Sommerfeld [866], the extensive work of Dolaptschiew [202–219] is less well known than it ought to be. Insofar as assimilation into the literature in the West is concerned, the situation was not helped by several of Dolaptschiew's papers being published in Bulgarian and Russian, albeit usually with an abstract or summary in German.

2.6. COHERENT VORTEX STRUCTURES

The theoretical analysis of solutions of the Euler equations that represent isolated regions of distributed vorticity in a two- or three-dimensional flow domain has attracted the attention of several investigators since the mid-19th century. A detailed survey of the results obtained up to the beginning of the 20th century may be found in the books [44, 542] and the review articles [34, 595, 601]. However, the number of analytically known solutions to the nonlinear Euler or Helmholtz equations is quite limited. For two-dimensional patches of uniform vorticity in an ambient unbounded potential flow, the circular Rankine vortex [755, §633]³³ and the Kirchhoff elliptical vortex [491, Lecture XX] are examples of such exact solutions. Rankine's model of the so-called "molecular vortices" [754, 756] was used by Maxwell [633–636] in his early attempts to understand the nature of electrical and magnetic phenomena. In contrast to the circular Rankine vortex, which represents a steady flow about a stationary vortex, the flow associated with the Kirchhoff elliptical vortex is unsteady since the elliptical patch performs a steady rotation about its center while preserving its shape. The elliptical vortex in a shear flow, a generalization of the Kirchhoff vortex, was first considered by Chaplygin [127]:

In this paper we consider the following case of motion in an unbounded mass of fluid: all motion is parallel to the coordinate plane OXY ; the velocity components u and v are

³³ The year of publication is 1858! Rankine worked on vortices in conjunction with his use of "molecular vortices" in the then emerging theory of thermodynamics.

continuous in the entire flow domain; all the fluid contains vortices; vortex lines are parallel to the OZ axis; the angular velocity Ω of vortex rotation inside an elliptical cylinder with OZ axis is constant and equals $A + \omega$, and in the rest of the fluid $\Omega = A$; the velocity infinitely far from OZ is parallel to OX and $u = -2Ay$. We will show that the inner vortex cylinder will change its form according to a certain law, rotating with a variable angular velocity around the OZ -axis.

Chaplygin provided a complete analytical solution to this problem, see [653] for details. Although Chaplygin's paper [127] was mentioned in review papers by Love [601, p. 123] and Auerbach³⁴ [34, p. 1061], it seems to have escaped the attention of later fluid dynamicists. Thus, many years later this solution was rediscovered and generalized by Moore and Saffman [668] and Kida [490] for an elliptical patch of uniform vorticity in both irrotational strain and in a simple external shear flow. For an arbitrary two-dimensional compact vorticity distribution a general approach based on Clebsch variables was introduced by Hill [417–421]. Even after more than a century this method has not received any attention and seems to deserve further extension and application.

A considerable simplification in the analysis of two-dimensional vortex flows is obtained by considering the case of steady motion. In this case Stokes [882] proved that any flow field represented by a stream function, $\psi(x, y)$, is a solution of the two-dimensional Euler equations provided the stream function satisfies an equation of the form

$$\frac{\partial^2 \psi}{\partial x^2} + \frac{\partial^2 \psi}{\partial y^2} = f(\psi), \quad (15)$$

where $f(\psi)$ is an arbitrary function of ψ . An important question of stability of any steady solution was formulated by the young Maxwell in a draft [631] and in a letter to William Thomson [632] (we use modern notation for partial derivatives):

I have been investigating fluid motion with reference to stability and I have got results when the motion is confined to the plane xy . I do not know whether the method is new. It only applies to an incompressible fluid moving in a plane. Put $\chi = \frac{\partial^2 \psi}{\partial x^2} + \frac{\partial^2 \psi}{\partial y^2}$. Hence, (A) $\frac{d\chi}{dt} = 0$ or $\chi = f(\psi)$ is the condition of steady motion as is otherwise known. (B) $f'(\psi)$ or $\frac{d\chi}{d\psi}$ must be negative for stability.

When $f'(\psi)$ is positive the motion is unstable.

When $f'(\psi) = 0$, χ is constant or 0.

When χ is constant I think equilibrium is neutral.

When $\chi = 0$ the whole motion is determined by the motion at a limiting curve so that there can be no finite displacement.

³⁴Felix Auerbach (1856–1933) was Jewish and committed suicide when Hitler came to power. There is a novel [651] based upon his life.

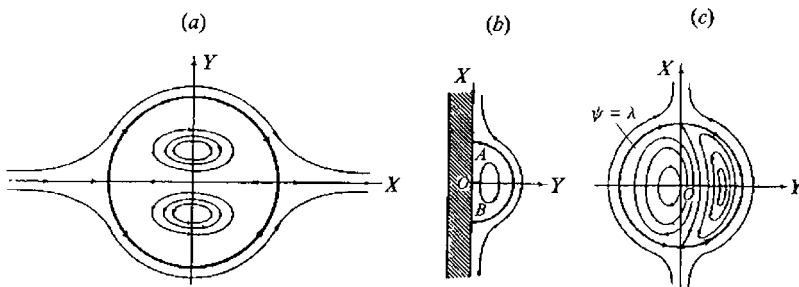


FIG. 19. Streamlines of various coherent vortex structures determined analytically by Chaplygin.

In 1895 and later in 1906 Lamb [542] was the first to try to solve (15) for a non-uniform vorticity distribution for the case of a linear relationship $f(\psi)$. Chaplygin [129] addressed the problem of steady motion of a compact vorticity distribution in two-dimensional unbounded inviscid flow:

Consider an unbounded mass of incompressible fluid in which the motion is parallel to the OXY plane; let the motion outside some circular cylinder be irrotational, the velocity being equal to zero at infinity. The question is to find a distribution of vortex lines inside the cylinder that gives rise to a uniformly translating vortex column with a continuous velocity distribution and with a positive pressure all around.

Chaplygin presented an extensive analysis of the characteristics of this solution, see [653] for details. Since no cross-references exist, it is assumed that Chaplygin and Lamb arrived at the same vortex dipole solution independently. This solution is now generally referred to as the *Lamb dipole* (or sometimes the *Batchelor dipole* because of the description of this vortex structure in the influential text [46, §7.3]). According to the chronological order of publication, the name *Chaplygin-Lamb dipole* would seem to be more appropriate³⁵. Figure 19 gives examples of the type of coherent vortex solutions Chaplygin was able to determine both in unbounded flow and in flow with a solid, plane wall.

Three-dimensional compact vortex structures are even more complicated. There exists a single exact solution, known as *Hill's spherical vortex* [422, 423], with a special non-uniform distribution of vorticity inside a sphere that moves rectilinearly at constant speed. This solution has been used by Synge and Lin [893] in their model of three-dimensional turbulence. So far attempts [379, 380] to generalize such a solution to an ellipsoidal vortex have failed.

³⁵ One of us (H.A.) recalls a meeting where the issue of a name for these solutions came up. George Batchelor was present and immediately stated that whatever the resolution might be, attributing them to him was certainly not appropriate. The attribution of names to physical phenomena, equations and the like often has deeper roots in sociology than in the history of science!

3. Conclusion

History, to paraphrase Leibnitz, is a useful thing, for its study not only gives to the researchers of the past their just due but also provides those of the present with a guide for the orientation of their own endeavors. While Helmholtz's 1858 paper on vortex dynamics and vorticity is of great importance and spawned the new subfield of vortex dynamics, one must admit that in the greater scheme of things Helmholtz is today primarily remembered for other contributions to science. The bibliography below contains several names that would not today be immediately associated with the field of vortex dynamics since the individual did work in other fields – often well outside of fluid mechanics – that became of even greater importance. In this category we may list Dirichlet, Friedmann, Hankel, Heisenberg, Klein, Lin, Love, J.J. Thomson, Zermelo and probably even Lord Kelvin. Considering the caliber of these scientists and mathematicians, it may be appropriate to recall Abel's statement, quoted in the remarkable lecture by Truesdell [965, p. 39], that he had reached the front rank quickly "by studying the masters, not their pupils."

In the "case studies" in Section 2 we have focused on what one may call the classical applications of Helmholtz's vortex theory. It is the test of any significant advance that it elicits interest far beyond the boundaries anticipated by its creator. Thus, the importance of vortex dynamics was realized in meteorology and oceanography by such towering figures as Vilhelm Bjerknes [247, 266, 890] whose seminal work [92] bears the title "On the dynamics of the circular vortex: with applications to the atmosphere and atmospheric vortex and wave motions." At the other end of the size-scale spectrum we may cite the application of classical vortex dynamics to superfluid Helium [263], where the famous footnote in [701] announced the quantization of circulation in this case. As one surveys the now vast literature in vortex dynamics some 150 years after Helmholtz's paper one is struck by the richness of the subject matter, and by how the various aspects enter different applications in almost infinitely varied ways. Küchemann's figurative characterization of vortices as "the sinews and muscles of fluid motions" [525] is no less apt today than it was when it was written 40 years ago.

The period we are covering, 1858–1956, begins with Helmholtz's seminal paper and concludes in the year of publication of the intriguing paper by Domm [224]. In his paper Domm considered the dynamics of four point vortices, two of either sign, all with the same absolute circulation, in a strip with periodic boundary conditions. This work showed *inter alia* that even when the Kármán criterion is satisfied, the vortex street is unstable to higher order perturbations. (It is only marginally stable to linear perturbations.) Von Kármán's collected works were also published in 1956, in celebration of his 75th birthday, and so – along with the reasons stated previously – this year forms a fitting closing for our bibliography.

Acknowledgements

Both authors acknowledge financial support through NSF Grant No. CTS-9311545 which, in part, supported VVM's visit at University of Illinois during the period 1995–1997. VVM also acknowledges INTAS project 04-80-7297 entitled “Vortex Dynamics”. HA also acknowledges support of a Niels Bohr Visiting Professorship at the Technical University of Denmark provided by the Danish National Research Foundation.

VVM thanks G.J.F. van Heijst, Eindhoven University of Technology, The Netherlands, for providing complete copies of the dissertations by Quint [752] and van den Berg [67], and L. Zannetti, Politecnico di Torino, Italy, for many copies of papers by Italian authors, several obtained from the Library of the *Accademia delle Scienze di Torino* founded by Giuseppe Luigi Lagrangia³⁶, today better known as Joseph Louis Lagrange.

HA thanks N. Rott for spurring on his interest in the work of W. Gröbli, and H. Thomann for his exceptional “detective work” in assembling Gröbli's biography, cf. [30].

References

- [1] N. Akhieser, On the question of stability of vortex streets, *Mat. Sbor.* **34** (1927) 5–8 (in Russian, German summary). Abstract: *F. d. M.* **53** 788.
- [2] J. Ackeret, Über die Bildung von Wirbeln in reibungslosen Flüssigkeit, *Z. Angew. Math. Mech.* **15** (1935) 3–4. Abstract: *F. d. M.* **61** 920. *Sci. Abs.* **A38** No 1410.
- [3] J.D.A. Ackroyd, The 31st Lanchester Lecture. Lanchester – the Man, *Aeronaut. J.* **87** (1992) 119–140.
- [4] C. Agostinelli, Moto generato da una sorgente liquida piana addossata a un profilo rigido rettilineo con formazione di vortici, *Atti Accad. Naz. Lincei. Rend. Cl. Sci. Fis. Mat. Nat.* (ser. 6) **23** (1936) 317–322. Abstract: *F. d. M.* **62** 975. *Sci. Abs.* **A39** No 4518.
- [5] C. Agostinelli, Sul vortice elicoidale, *Atti Accad. Naz. Lincei. Rend. Cl. Sci. Fis. Mat. Nat.* (ser. 6) **23** (1936) 670–676. Abstract: *F. d. M.* **62** 973. *Sci. Abs.* **A39** No 4519.
- [6] C. Agostinelli, Sopra alcuni notevoli moti fluidi vorticosi, *Rend. Circ. Mat. Palermo* **60** (1936) 169–184. Abstract: *F. d. M.* **63** 773.
- [7] C. Agostinelli, Applicazione del metodo delle immagini alla determinazione del moto liquido piano in una corona circolare in cui si formino dei vortici puntiformi. Problemi elettrostatici corrispondenti, *Rend. Ist. Lomb. Sci. Lett.* (ser. 3) **6** (1942) 669–689. Abstract: *F. d. M.* **68** 573. *Math. Rev.* **8** 294.
- [8] F. Ahlborn, Über den Mechanismus des hydrodynamischen Widerstandes, *Abh. Geb. Naturw. Hamburg* **17** (1902) 1–57. Abstract: *F. d. M.* **35** 773.
- [9] F. Ahlborn, Die Theorie der diskontinuierlichen Flüssigkeitsbewegungen und die Wirklichkeit, *Phys. Z.* **29** (1928) 34–41. Abstract: *F. d. M.* **54** 923. *Sci. Abs.* **A31** No 1130.
- [10] F. Ahlborn, Der Magnus Effekt in Theorie und Wirklichkeit, *Z. Flugtech. Motorluftschiff.* **20** (1929) 642–653. English translation: Magnus effect in theory and reality, *NACA Tech. Memo.* (1930) No 567.

³⁶ According to <http://www-gap.dcs.st-and.ac.uk/history/Biographies/Lagrange.html>, Lagrange's baptismal name was Giuseppe Lodovico Lagrangia.

- [11] F. Ahlborn, Zur Dynamik des Regens, *Phys. Z.* **32** (1931) 139–147.
- [12] F. Ahlborn, Turbulenz und Mechanismus des Widerstandes an Kugeln und Zylindern, *Z. Tech. Phys.* **12** (1931) 482–491. English translation: Turbulence and mechanism of resistance on spheres and cylinders, *NACA Tech. Memo.* (1934) No 653. Abstract: *Sci. Abs. A***35** No 678.
- [13] V. Alexandrov, Vortex theory, in: L.K. Martens, ed., *Tekhnicheskaya Enciklopediya (Technical Encyclopedia)* (Sovetskaya Enciklopediya, Moscow, 1928) **3** 774–779 (in Russian).
- [14] V. Alexandrov, *Tekhnicheskaya gidromekhanika (Technical Hydromechanics)* 3rd edn (GITTL, Moscow-Leningrad, 1946) (in Russian).
- [15] W. Alexandrow, Die Joukowskysche Wirbeltheorie des Propellers und ihre Verwendung zur Berechnung von Luftschrauben, *Z. Flugtech. Motorluftschiff.* **20** (1929) 633–642.
- [16] V.P. Alexeeva, *Matematika i mekhanika v izdaniakh Akademii Nauk SSSR. Bibliografiia. 2. 1936–1947. (Mathematics and mechanics in the editions of the Academy of Sciences of the USSR. Bibliography. 2. 1936–1947.)* (AN SSSR, Moscow-Leningrad, 1955) (in Russian).
- [17] J.F.C. Andrade, Sur le mouvement d'un vortex rectiligne dans un liquide contenu dans un prisme rectangle de longueur indéfinie, *C. R. Acad. Sci. Paris* **112** (1891) 418–421. Abstract: *F. d. M.* **23** 969.
- [18] E.N.C. Andrade, Whirlpools and vortices, *Proc. R. Instn Gt Brit.* **29** (1936) 320–338.
- [19] N.N. Andreev, Vortex motions, in: O.Yu. Shmidt, ed., *Bol'shaya Sovetskaya Enciklopediya (Large Soviet Encyclopedia)* (Soviet Encyclopedia, Moscow, 1930) **11** 339–350 (in Russian).
- [20] L. Anton, Ausbildung eines Wirbels an der Kante einer Platte, *Ing.-Arch.* **10** (1939) 411–427. Abstract: *F. d. M.* **65** 981. *Math. Rev.* **1** 286. *Zentr. Mech.* **10** 130.
- [21] P. Appell, Sur les équations de l'hydrodynamique et la théorie des tourbillons, *J. Math. Pures Appl.* (ser. 5) **3** (1897) 5–16. Abstract: *F. d. M.* **28** 681.
- [22] P. Appell, Lignes correspondantes dans la déformation d'un milieu; extension des théorèmes sur les tourbillons, *J. Math. Pures Appl.* (ser. 5) **5** (1899) 137–153. Abstract: *F. d. M.* **30** 681.
- [23] P. Appell, *Traité de mécanique rationnelle, III. Équilibre et mouvement des milieux continus* (Gauthier-Villars, Paris, 1903).
- [24] P. Appell, Sur une extension des équations de la théorie des tourbillons et des équations de Weber, *C. R. Acad. Sci. Paris* **164** (1917) 71–74.
- [25] H. Arakawa, On the force between two cylindrical vortices in an incompressible fluid, *Proc. Phys.-Math. Soc. Japan* (ser. 3) **13** (1931) 61–64. Abstract: *F. d. M.* **62** 973. *Sci. Abs. A***34** No 1754.
- [26] H. Aref, Motion of three vortices, *Phys. Fluids* **22** (1979) 393–400.
- [27] H. Aref, Integrable, chaotic and turbulent vortex motion in two-dimensional flows, *Annu. Rev. Fluid Mech.* **15** (1983) 345–389.
- [28] H. Aref, The development of chaotic advection, *Phys. Fluids* **14** (2002) 1315–1325.
- [29] H. Aref, P.K. Newton, M.A. Stremler, T. Tokieda and D.L. Vainchtein, Vortex crystals, *Adv. Appl. Mech.* **39** (2002) 1–79.
- [30] H. Aref, N. Rott and H. Thomann, Gröbli's solution of the three-vortex problem, *Annu. Rev. Fluid Mech.* **24** (1992) 1–20.
- [31] R.J. Arms and F.R. Hama, Localized-induction concept on a curved vortex and motion of an elliptic vortex ring, *Phys. Fluids* **8** (1965) 553–559.
- [32] N.S. Arzhanikov and V.N. Maltcev, *Aerodinamika (Aerodynamics)* (Oborongiz, Moscow, 1952) (in Russian).
- [33] F. Auerbach, *Die theoretische Hydrodynamik. Nach dem Gange der Entwicklung in der neuesten Zeit in Kürze dargestellt* (Vieweg, Braunschweig, 1881). Abstract: *F. d. M.* **13** 717.
- [34] F. Auerbach, Wirbelbewegung, in: A. Winkelmann, ed., *Handbuch der Physik* (Barth, Leipzig, 1908) **1** 1047–1074.
- [35] F. Auerbach, Wirbelbewegung, in: F. Auerbach and W. Hort, eds, *Handbuch der Physikalischen und Technischen Mechanik* (Barth, Leipzig, 1927) **5** 115–156.

- [36] A. Bachinskii, Vortex motions, in: Yu.S. Gambarov, V.Ya. Zhelezov, M.M. Kovalevskii and K.A. Timiryazev, eds, *Enciklopedicheskii Slovar'* (Encyclopedic Dictionary) 7th edn (Granat, Moscow, 1913) **10** 376–378 (in Russian).
- [37] L. Bairstow, *Applied Aerodynamics* (Longmans, London, 1920).
- [38] R.S. Ball, On vortex-rings in air, *Phil. Mag.* (ser. 4) **36** (1868) 12–14.
- [39] R.S. Ball, Account of experiments upon the resistance of air to the motion of vortex-rings, *Phil. Mag.* (ser. 4) **42** (1871) 208–210.
- [40] R.S. Ball, Account of experiments upon the retardation experienced by vortex rings of air when moving through air, *Trans. R. Irish Acad.* **25** (1872) 135–155.
- [41] S.K. Banerji, On Oberbeck's vortices, *Phil. Mag.* (ser. 7) **13** (1932) 865–869.
- [42] S.K. Banerji and R.V. Barave, On Oberbeck's vortices, *Phil. Mag.* (ser. 7) **11** (1931) 1057–1081. Abstract: *Sci. Abs.* **A34** No 2911.
- [43] W. Barth, Wirbelbahnen um Wände und Platten von unendlich kleiner Wandstärke, *Z. Angew. Math. Mech.* **10** (1930) 247–251. Abstract: *F. d. M.* **56** 1253. *Sci. Abs.* **A33** No 3621.
- [44] A.B. Basset, *A Treatise on Hydrodynamics* (Deighton Bell, Cambridge, 1888). Reprinted: (Dover, New York, 1961). Abstract: *F. d. M.* **20** 970.
- [45] A.B. Basset, *An Elementary Treatise on Hydrodynamics and Sound* (Deighton Bell, Cambridge, 1890).
- [46] G.K. Batchelor, *An Introduction to Fluid Dynamics* (Cambridge University Press, Cambridge, 1967).
- [47] G.K. Batchelor, Geoffrey Ingram Taylor. 7 March 1886 – 27 June 1975, *Biogr. Mem. Notes FRS* **22** (1976) 565–633.
- [48] G.K. Batchelor, *The Life and Legacy of G.I. Taylor* (Cambridge University Press, Cambridge, 1996).
- [49] H. Bateman, Rotating cylinders and rectilinear vortices, *Bull. Am. Math. Soc.* (ser. 2) **25** (1919) 359–374.
- [50] H. Bateman, *Partial Differential Equations of Mathematical Physics* (Cambridge University Press, Cambridge, 1932). Reprinted: (Dover, New York, 1944).
- [51] G. Bauer, *Die Helmholtzsche Wirbeltheorie für Ingenieurbearbeitet* (Oldenbourg, München-Berlin, 1919).
- [52] P.E. Belas, A simple method of showing vortex motion, *Nature* **70** (1904) 31.
- [53] S.M. Belotserkovskii, A.Yu. Ishlinskii, P.Ya. Kochina and B.V. Shabat, Vladimir Vasil'evich Golubev (on the centenary of his birth), *Usp. Mat. Nauk* **40** (1985) 225–229 (in Russian). English translation: *Russian Math. Surveys* **40** (1985) 251–255.
- [54] E. Beltrami, Sui principii fondamentali dell'idrodinamica razionale. Ricerche sulla cinematica dei fluidi, *Mem. R. Accad. Sci. Ist. Bologna* **1** (1871) 431–476; **2** (1872) 381–437; **3** (1873) 349–407; **5** (1874) 443–483. Reprinted in: *Opere matematiche di Eugenio Beltrami* (Hoepli, Milano, 1904) **2** 202–379.
- [55] E. Beltrami, Considerazioni idrodinamiche, *Nuovo Cimento* (ser. 3) **25** (1888) 212–222. Also: *Rend. Ist. Lomb. Sci. Lett.* (ser. 2) **22** (1889) 121–130. Reprinted in: *Opere matematiche di Eugenio Beltrami* (Hoepli, Milano, 1920) **4** 300–309. Abstract: *F. d. M.* **20** 949.
- [56] H. Bénard, Formation de centres de giration à l'arrière d'un obstacle en mouvement, *C. R. Acad. Sci. Paris* **147** (1908) 839–842, 970–972.
- [57] H. Bénard, Sur la zone de formation des tourbillons alternés derrière un obstacle, *C. R. Acad. Sci. Paris* **156** (1913) 1003–1005.
- [58] H. Bénard, Sur la marche des tourbillons alternés derrière un obstacle, *C. R. Acad. Sci. Paris* **156** (1913) 1225–1228.
- [59] H. Bénard, Sur les lois de la fréquence des tourbillons alternés détachés derrière un obstacle, *C. R. Acad. Sci. Paris* **182** (1926) 1375–1377. Abstract: *Sci. Abs.* **A39** No 2516.
- [60] H. Bénard, Sur l'inexactitude, pour liquides réels, de lois théoriques de Kármán relatives à la stabilité des tourbillons alternés, *C. R. Acad. Sci. Paris* **182** (1926) 1523–1526. Abstract: *Sci. Abs.* **A29** No 2517.

- [61] H. Bénard, Sur les écarts des valeurs de la fréquence alternés à la loi de similitude dynamique, *C. R. Acad. Sci. Paris* **183** (1926) 20–22.
- [62] H. Bénard, Sur la limite de régime laminaire et du régime turbulent, révélée par l'apparition de tourbillons alternés nets, *C. R. Acad. Sci. Paris* **182** (1926) 1523–1526. Abstract: *Sci. Abs.* **A29** No 2518.
- [63] H. Bénard, Sur les lois de fréquence des tourbillons alternés détachés à l'arrière d'un obstacle mobile, in: E. Meissner, ed., *Proceedings of the 2nd International Congress for Applied Mechanics. Zürich 12–17 September 1926* (Füssli, Zürich-Leipzig, 1927) 495–501.
- [64] H. Bénard, Sur l'inexactitude expérimentale, pour les liquides réels, des lois théoriques de Kármán relatives à la stabilité des tourbillons alternés dans un fluide parfait, in: E. Meissner, ed., *Proceedings of the 2nd International Congress for Applied Mechanics. Zürich 12–17 September 1926* (Füssli, Zürich-Leipzig, 1927) 502–503.
- [65] H. Bénard, Sur les tourbillons alternés dus à des obstacles en lame de couteau, *C. R. Acad. Sci. Paris* **187** (1928) 1028–1030. Abstract: *Sci. Abs.* **A32** No 1410.
- [66] H. Bénard, Les tourbillons alternés et la loi de similitude dynamique, *C. R. Acad. Sci. Paris* **187** (1928) 1123–1125. Abstract: *Sci. Abs.* **A32** No 1411.
- [67] J.C. van den Berg, *De wervelbeweging* (dissertation) (De Haarlemsche Boek-en Muziekhandel, Haarlem, 1888). Abstract: *F. d. M.* **20** 979–980.
- [68] F.A. Berson, A synoptic-aerological study of interaction between vortices, *Tellus* **3** (1951) 172–190.
- [69] J. Bertrand, Théorème relatif au mouvement le plus général d'un fluide, *C. R. Acad. Sci. Paris* **66** (1867) 1227–1230.
- [70] J. Bertrand, Note relatif à la théorie des fluides. Réponse à la communication de M. Helmholtz, *C. R. Acad. Sci. Paris* **67** (1868) 267–269.
- [71] J. Bertrand, Observations nouvelles sur un mémoire de M. Helmholtz, *C. R. Acad. Sci. Paris* **67** (1868) 469–472.
- [72] J. Bertrand, Réponse à la note de M. Helmholtz, *C. R. Acad. Sci. Paris* **67** (1868) 773–775.
- [73] R. Betchov, On the curvature and torsion of an isolated vortex filament, *J. Fluid Mech.* **22** (1965) 471–479.
- [74] A. Betz, Einführung in die Theorie der Flugzeug-Tragflügel, *Naturwissenschaften* **6** (1918) 557–562, 573–578.
- [75] A. Betz, *Beiträge zur Tragflügeltheorie* (dissertation) (Oldenbourg, Göttingen, 1919).
- [76] A. Betz, Wirbel und im Zusammenhang damit stehende Begriffe der Hydrodynamik, *Z. Flugtech. Motorluftschiff.* **12** (1921) 193–198. English translation: Vortices and the related principles of hydrodynamics, *NACA Tech. Notes* (1923) No 68.
- [77] A. Betz, Der Wirbelbegriff und seine Bedeutung für die Flugtechnik, *Unterrbl. Math. Naturw.* **34** (1928) 351–358, 388–393. English translation: The vortex theory and its significance in aviation, *NACA Tech. Memo.* (1930) No 576.
- [78] A. Betz, Eine anschauliche Ableitung des Biot-Savartschen Gesetzes, *Z. Angew. Math. Mech.* **8** (1928) 149–151.
- [79] A. Betz, Wirbelbildung in idealen Flüssigkeiten und Helmholtzscher Wirbelsatz, *Z. Angew. Math. Mech.* **10** (1930) 413–415. Abstract: *F. d. M.* **56** 705.
- [80] A. Betz, Die v. Kármánsche Ähnlichkeitsüberlegung für turbulente Vorgänge in physikalischer Auffassung, *Z. Angew. Math. Mech.* **11** (1931) 391. Abstract: *F. d. M.* **57** 1113.
- [81] A. Betz, Verhalten von Wirbelsystem, *Z. Angew. Math. Mech.* **12** (1932) 164–174. English translation: Behaviour of vortex systems, *NACA Tech. Memo.* (1933) No 713. Abstract: *F. d. M.* **58** 877.
- [82] A. Betz, Wie entsteht ein Wirbel in einer wenig zähen Flüssigkeit?, *Naturwissenschaften* **37** (1950) 193–195. Abstract: *Appl. Mech. Rev.* **4** No 2091.
- [83] A. Betz, ed., *Naturforschung und Medizin in Deutschland 1939–1946. Für Deutschland bestimmte Ausgabe der FIAT Review of German Science. Bd. 11: Hydro- und Aerodynamik* (Chemie, Berlin, 1953).

[84] A. von Bezold, Experimentaluntersuchungen über rotierende Flüssigkeiten, *Sber. Preuss. Akad. Wiss.* (1887) 261–273.

[85] W.G. Bickley, Influence of vortices upon the resistance experienced by solids moving through a liquid, *Proc. R. Soc. London A* **119** (1928) 146–156. Abstract: *F. d. M.* **54** 902. *Sci. Abs.* **31** No 2050.

[86] G. Birkhoff, *Hydrodynamics* (Princeton University Press, Princeton, 1950). Abstract: *Appl. Mech. Rev.* **3** No 2692.

[87] G. Birkhoff, A new theory of vortex streets, *Proc. Nat. Acad. Sci. USA* **38** (1951) 409–410. Abstract: *Appl. Mech. Rev.* **5** No 3130. *Math. Rev.* **14** 102.

[88] G. Birkhoff, Formation of vortex streets, *J. Appl. Phys.* **24** (1953) 98–103. Abstract: *Math. Rev.* **14** 918.

[89] V. Bjerknes, Das dynamische Prinzip der Cirkulationsbewegungen in der Atmosphäre, *Met. Z.* **17** (1900) 97–106, 145–146.

[90] V. Bjerknes, Zirkulation relativ zu der Erde, *Met. Z.* **37** (1902) 97–108. Abstract: *F. d. M.* **33** 967.

[91] V. Bjerknes, Über Wirbelbildung in reibunglosen Flüssigkeiten mit Anwendung auf die Analogie der hydrodynamischen Erscheinungen mit den elektrostatischen, *Z. Math. Phys.* **50** (1904) 422–443. Abstract: *F. d. M.* **35** 751.

[92] V. Bjerknes, On the dynamics of the circular vortex: with applications to the atmosphere and atmospheric vortex and wave motions. *Geofys. Publ.* **2** (1921) No 4.

[93] H. Blasius, Funktionentheoretische Methoden in der Hydrodynamik, *Z. Math. Phys.* **58** (1910) 90–110.

[94] H. Blenk, Theodore von Kármán, zum 75. Geburtstag am 11. Mai 1956, *Z. Flugwiss.* **4** (1956) 161–162.

[95] D. Bobylev, On advances in the theory of fluid motion in the past 30 years, *Sb. Inst. Inzh. Put. Soobshch.* **8** (1887) 1–23 (in Russian). Abstract: *F. d. M.* **20** 971.

[96] D. Bobylev, Vortex motions, in: K.K. Arsen'ev and F.F. Petrushevskii, eds, *Enciklopedicheskii Slovar'* (Encyclopedic Dictionary) (Brockhaus and Efron, St-Petersburg, 1892) VI^a(12) 860–863 (in Russian).

[97] A. Bock, Ueber die objektive Demonstration der Wirbelbewegung, *Ann. Phys. Chem.* (new ser.) **56** (1895) 131–132.

[98] J. Bonder and S. Neumark, Einige Bemerkungen zu der Abhandlungen “Über die Bewegung einzelner Wirbel in einer strömenden Flüssigkeit” von M. Lagally, *Math. Z.* **32** (1930) 600–604. Abstract: *F. d. M.* **56** 705.

[99] M. Brillouin, Questions d'hydrodynamique, *Ann. Fac. Sci. Univ. Toulouse* **1** (1887) 1–72. Abstract: *F. d. M.* **19** 978.

[100] M. Brillouin, *Recherches récentes sur diverses questions d'hydrodynamique* (Gauthier-Villars, Paris, 1891).

[101] C.E. Brown and W.H. Michael, Effect of leading edge separation on the lift of a delta wing, *J. Aeronaut. Sci.* **21** (1954) 690–706.

[102] G.H. Bryan, Eddy formation in the wake of projecting obstacles, *Nature* **82** (1910) 408–409.

[103] L.W. Bryant and D.N. Williams, An investigation of the flow of air around an aerofoil of infinite span, *Phil. Trans. R. Soc. London A* **225** (1926) 199–237.

[104] J.Z. Buchwald, Thomson, Sir William (Baron Kelvin of Largs), in: C.C. Gillispie, ed., *Dictionary of Scientific Biography* (Scribner's Sons, New York, 1976) **XIII** 374–388.

[105] E. Budde, Kleine Bemerkung zur Helmholtzschen Wirbeltheorie, *Arch. Math. Phys.* **3** (1902) 21–22.

[106] J.M. Burgers, *De hydrodynamische druk* (Waltman, Delft, 1918).

[107] J.M. Burgers, The formation of vortex sheets in a simplified type of turbulent motion, *Proc. Sect. Sci. K. Ned. Akad. Weten.* **53** (1950) 122–133. Abstract: *Math. Rev.* **11** 625.

[108] J.M. Burgers, *Terugblik op de hydrodynamica* (THDelft, Delft, 1955).

[109] D. Cahan, ed., *Hermann von Helmholtz and the Foundation of Nineteenth Century Science* (University of California Press, Berkeley, 1993).

- [110] G. Calapaj, Sul moto di un vortice rettilineo in un fluido limitato da una parete piana, *Atti Ist. Veneto Sci. Lett. Arti. Cl. Sci. Mat. Nat.* **99** (1940) Pt 2 691–705. Abstract: *F. d. M.* **66** 1066. *Zentr. Mech.* **11** 416.
- [111] B. Caldonazzo, Sul moto di un vortice puntiforme, *Atti Accad. Naz. Lincei Rend. Cl. Sci. Fis. Mat. Nat.* (ser. 5) **28** (1919) 191–195, 301–303, 325–329. Abstract: *F. d. M.* **47** 996.
- [112] B. Caldonazzo, Sopra alcune proprietà di moti liquidi permanenti i cui vortici sono normali alle velocità, *Atti Accad. Naz. Lincei Rend. Cl. Sci. Fis. Mat. Nat.* (ser. 6) **6** (1927) 288–291. Abstract: *F. d. M.* **53** 787.
- [113] B. Caldonazzo, I moti di Viterbi ed i sistemi tripli ortogonali di superfici da essi determinati, *Atti Accad. Naz. Lincei Rend. Cl. Sci. Fis. Mat. Nat.* (ser. 6) **6** (1927) 407–412. Abstract: *F. d. M.* **53** 788.
- [114] B. Caldonazzo, Vortice spirale in un canale, *Note Esercit. Mat. Catania* **5** (1929) 224–235. Abstract: *F. d. M.* **57** 1107.
- [115] B. Caldonazzo, Onda solitaria provocata da un vortice in un canale, *Note Esercit. Mat. Catania* **6** (1931) 61–74. Abstract: *F. d. M.* **57** 1108.
- [116] B. Caldonazzo, Sui moti liquidi piani con un vortice libero, *Rend. Circ. Mat. Palermo* **55** (1931) 369–394. Abstract: *F. d. M.* **57** 1108.
- [117] B. Caldonazzo, Vortice in un campo limitato da una cardioide, *Atti Accad. Naz. Lincei Rend. Cl. Sci. Fis. Mat. Nat.* (ser. 6) **13** (1931) 869–873. Abstract: *F. d. M.* **57** 1107. *Sci. Abs.* **A34** No 4063.
- [118] B. Caldonazzo, Vortice libero regolarizzatore nel problema della lamina, *Atti Accad. Naz. Lincei Rend. Cl. Sci. Fis. Mat. Nat.* (ser. 6) **23** (1936) 36–40. Abstract: *F. d. M.* **62** 976.
- [119] C. Camichel, Sur les tourbillons provoqués par un obstacle immergé dans un courant liquide, *C. R. Acad. Sci. Paris* **184** (1927) 1509–1512.
- [120] C. Camichel, P. Dupin and M. Teissié-Solier, Sur l’application de la loi de similitude aux périodes de formation des tourbillons alternés de Bénard-Kármán, *C. R. Acad. Sci. Paris* **185** (1927) 1556–1559. Abstract: *F. d. M.* **53** 810.
- [121] E. Carafoli, Confrontation des théories aérodynamique moderne avec les loi de la mécanique rationnelle, *L’Aérophile* **35** (1927) 71–77.
- [122] H.S. Carslaw, The fluted vibrations of a circular vortex ring with a hollow core, *Proc. Lond. Math. Soc.* **28** (1897) 97–119.
- [123] H.S. Carslaw, The steady motion of a spherical vortex, *Proc. Edinb. Math. Soc.* **15** (1897) 76–80.
- [124] H.T. Carter, On unstable vortex motion, *J. Aeronaut. Sci.* **2** (1935) 159–161.
- [125] L. Castagnetto, Contribution à l’étude des tourbillons alternés de Bénard-Kármán, *Ann. Fac. Sci. Univ. Toulouse* (ser. 4) **3** (1939) 71–153. Abstract: *Zentr. Mech.* **11** 231.
- [126] A.-L. Cauchy, Mémoire sur les dilatations, les condensations, et les rotations produites par un changement de forme dans un système de points matériels, *Exercices d’Analyse et de Physique Mathématique* **2** (1841) 71–153. Reprinted in: *Oeuvres Complètes d’Augustin Cauchy* (II ser.) (Gauthier-Villars, Paris, 1916) **12** 343–377.
- [127] S.A. Chaplygin, On a pulsating cylindrical vortex, *Trudy Otd. Fiz. Nauk Mosk. Obshch. Lyub. Estest.* **10** (1899) No 1 13–22 (in Russian). Reprinted in: A.N. Krylov, ed., *Polnoe sobranie sochinenii* (Collected Works) (AN SSSR, Leningrad, 1933) **1** 264–275. Reprinted in: V.V. Golubev, ed., *Sobranie sochinenii* (Collected Papers) (Gostekhizdat, Moscow-Leningrad, 1948) **2** 138–154. Abstract: *F. d. M.* **30** 683.
- [128] S.A. Chaplygin, Comments on Helmholtz’s life and works, in: H. Helmholtz, *Dva issledovaniya po gidrodinamike* (Two Studies in Hydrodynamics) (Palas, Moscow, 1902) 69–108 (in Russian).
- [129] S.A. Chaplygin, A case of vortex motion in a fluid, *Trudy Otd. Fiz. Nauk Mosk. Obshch. Lyub. Estest.* **11** (1903) No 2 11–14 (in Russian). Reprinted in: A.N. Krylov, ed., *Polnoe sobranie sochinenii* (Collected Works) (AN SSSR, Leningrad, 1933) **1** 276–282. Reprinted in: V.V. Golubev, ed., *Sobranie sochinenii* (Collected Papers) (Gostekhizdat, Moscow-Leningrad, 1948) **2** 155–165. Abstract: *F. d. M.* **34** 809.
- [130] S.A. Chaplygin, On the pressure exerted by a plane-parallel flow upon an obstructing body (contribution to the theory of aircraft), *Mat. Sbor.* **28** (1910) No 1 120–166 (in Russian). Reprinted

in: A.N. Krylov, ed., *Polnoe sobranie sochinenii* (Collected Works) (AN SSSR, Leningrad, 1933) **2** 144–178. Reprinted in: V.V. Golubev, ed., *Sobranie sochinenii* (Collected Papers) (Gostekhizdat, Moscow-Leningrad, 1948) **2** 184–229. Reprinted in: S.A. Khristianovich, ed., *Izbrannye stat'i po teorii kryla* (Selected Papers on Wing Theory) (Gostekhizdat, Moscow-Leningrad, 1949) 184–229. Reprinted in: M.V. Keldysh, ed., *Izbrannye trudy po mekhanike i matematike* (Selected Papers on Mechanics and Mathematics) (Gostekhizdat, Moscow, 1954) 90–120. English translation in: *Selected Works on Wing Theory of Sergei A. Chaplygin* (Garbell Research Foundation, San Francisco, 1956) 1–16. Abstract: *F. d. M.* **42** 823–824.

[131] S.A. Chaplygin, Results of theoretical investigations on the motion of aircraft, *Byull. Mosk. Obshch. Vozdukhopl.* (1911) No 3 105–116 (in Russian). Reprinted in: A.N. Krylov, ed., *Polnoe sobranie sochinenii* (Collected Works) (AN SSSR, Leningrad, 1933) **2** 179–190. Reprinted in: V.V. Golubev, ed., *Sobranie sochinenii* (Collected Papers) (Gostekhizdat, Moscow-Leningrad, 1948) **2** 230–245. Reprinted in: S.A. Khristianovich, ed., *Izbrannye stat'i po teorii kryla* (Selected Papers on Wing Theory) (Gostekhizdat, Moscow-Leningrad, 1949) 57–72. Reprinted in: M.V. Keldysh, ed., *Izbrannye trudy po mekhanike i matematike* (Selected Papers on Mechanics and Mathematics) (Gostekhizdat, Moscow, 1954) 121–130. English translation in: *Selected Works on Wing Theory of Sergei A. Chaplygin* (Garbell Research Foundation, San Francisco, 1956) 17–22.

[132] S.A. Chaplygin, On the action of a plane-parallel air flow upon a cylindrical wing moving within it, *Trudy Tsentr. Aero-Gidrodin. Inst.* (1926) No 19 1–67 (in Russian). Reprinted in: A.N. Krylov, ed., *Polnoe sobranie sochinenii* (Collected Works) (AN SSSR, Leningrad, 1935) **3** 3–64. Reprinted in: V.V. Golubev, ed., *Sobranie sochinenii* (Collected Papers) (Gostekhizdat, Moscow-Leningrad, 1948) **2** 300–382. Reprinted in: S.A. Khristianovich, ed., *Izbrannye stat'i po teorii kryla* (Selected Papers on Wing Theory) (Gostekhizdat, Moscow-Leningrad, 1949) 126–210. Reprinted in: M.V. Keldysh, ed., *Izbrannye trudy po mekhanike i matematike* (Selected Papers on Mechanics and Mathematics) (Gostekhizdat, Moscow, 1954) 165–200. English translation in: *Selected Works on Wing Theory of Sergei A. Chaplygin* (Garbell Research Foundation, San Francisco, 1956) 42–72.

[133] S.A. Chaplygin, The vortex theory of lift (tip effect of a plate) (1913–1914), *Prikl. Mat. Mekh.* **5** (1941) 151–157.

[134] S.A. Chaplygin, Vortex flow around a circular cylindrical obstacle (1921), in: V.V. Golubev, ed., *Sobranie sochinenii* (Collected Papers) (Gostekhizdat, Moscow-Leningrad, 1948) **2** 537–545 (in Russian).

[135] S.A. Chaplygin, Vortex flow around a fence obstacle (1921), in: V.V. Golubev, ed., *Sobranie sochinenii* (Collected Papers) (Gostekhizdat, Moscow-Leningrad, 1948) **2** 546–554 (in Russian).

[136] S.A. Chaplygin, Continuous flow around a fence while forming permanent vortices in front of and behind it (1921), in: V.V. Golubev, ed., *Sobranie sochinenii* (Collected Papers) (Gostekhizdat, Moscow-Leningrad, 1948) **2** 555–566 (in Russian).

[137] S.A. Chaplygin, On the theory of snow-storms (1921), in: V.V. Golubev, ed., *Sobranie sochinenii* (Collected Papers) (Gostekhizdat, Moscow-Leningrad, 1948) **2** 567–575 (in Russian).

[138] S.A. Chaplygin and V.V. Golubev, On the theory of a blow through of cylinders in a combustion engine, *Trudy Tsentr. Aero-Gidrodin. Inst.* (1934) No 175 1–48 (in Russian). Reprinted in: A.N. Krylov, ed., *Polnoe sobranie sochinenii* (Collected Works) (AN SSSR, Leningrad, 1935) **3** 251–308. Reprinted in: V.V. Golubev, ed., *Sobranie sochinenii* (Collected Papers) (Gostekhizdat, Moscow-Leningrad, 1950) **3** 169–242.

[139] S.A. Chaplygin and V.V. Golubev, On the theory of slots and flaps, *Trudy Tsentr. Aero-Gidrodin. Inst.* (1935) No 171 1–39 (in Russian). Reprinted in: V.V. Golubev, ed., *Sobranie sochinenii* (Collected Papers) (Gostekhizdat, Moscow-Leningrad, 1948) **2** 586–639.

[140] S.A. Chaplygin and V.V. Golubev, Works on hydromechanics in the USSR, in: V.V. Golubev, ed., *Matematika i estestvennye nauki v SSSR za poslednie 20 let* (Mathematics and Natural Sciences in the USSR in past 20 years) (ONTI, Moscow-Leningrad, 1938) 101–120 (in Russian).

[141] C. Chree, On vortices, *Proc. Edinb. Math. Soc.* **5** (1887) 52–59.

[142] C. Chree, Vortex rings in a compressible fluid, *Proc. Edinb. Math. Soc.* **6** (1888) 59–68.

- [143] C. Chree, Vortices in a compressible fluid, *Mess. Math.* **17** (1888) 105–118. Abstract: *F. d. M.* **20** 980.
- [144] C. Chree, On vortex motion in a rotating fluid, *Proc. Edinb. Math. Soc.* **7** (1889) 29–41.
- [145] C. Chree, On the equations of vortex motion, with special references to the use of polar coordinates, *Proc. Edinb. Math. Soc.* **8** (1890) 43–64.
- [146] U. Cisotti, Sur les mouvements rigides d'une surface de tourbillons, *C. R. Acad. Sci. Paris* **156** (1913) 539–541. Abstract: *F. d. M.* **44** 855.
- [147] U. Cisotti, Su alcune recenti ricerche in idrodinamica, *Atti Soc. Ital. Prog. Sci.* **1** (1913) 491–511.
- [148] U. Cisotti, *Idromeccanica piana* (Tamburini, Milano, 1921). Abstract: *F. d. M.* **48** 941.
- [149] U. Cisotti, Sul carattere necessariamente vorticoso dei moto regolari, permanenti di un fluido qualsiasi in ambienti limitati, oppure in quiete all'infinito, *Boll. Un. Mat. Ital.* **2** (1923) 170–172. Abstract: *F. d. M.* **49** 599.
- [150] U. Cisotti, Über den Anteil Italiens an dem Fortschritt der klassischen Hydrodynamik in den letzten fünfzehn Jahren, in: Th. von Kármán and T. Levi-Civita, eds, *Vorträge aus dem Gebiete der Hydro- und Aerodynamik*. Innsbruck, 1922 (Springer, Berlin, 1924) 1–17. Abstract: *F. d. M.* **50** 555.
- [151] U. Cisotti, Effetto dinamico di una corrente che fluisce tra un cilindro e una parete piana indefinita, *Atti Accad. Naz. Lincei. Rend. Cl. Sci. Fis. Mat. Nat.* (ser. 6) **1** (1925) 494–499. Abstract: *F. d. M.* **51** 661.
- [152] U. Cisotti, Effetti dinamici di un fluido che circola tra quantisivogliano cilindri sottili ad assi paralleli, *Atti Accad. Naz. Lincei. Rend. Cl. Sci. Fis. Mat. Nat.* (ser. 6) **3** (1926) 517–520. Abstract: *F. d. M.* **52** 854.
- [153] U. Cisotti, Una notevole eccezione del teorema di Kutta-Joukowski, *Atti Accad. Naz. Lincei. Rend. Cl. Sci. Fis. Mat. Nat.* (ser. 6) **5** (1927) 16–21. Abstract: *F. d. M.* **53** 801.
- [154] U. Cisotti, Sui vortici spiralì, *Atti Accad. Naz. Lincei. Rend. Cl. Sci. Fis. Mat. Nat.* (ser. 6) **6** (1927) 183–186. Abstract: *F. d. M.* **53** 788.
- [155] U. Cisotti, Sui vortici elico-conici, *Atti Accad. Naz. Lincei. Rend. Cl. Sci. Fis. Mat. Nat.* (ser. 6) **6** (1927) 446–448. Abstract: *F. d. M.* **53** 788.
- [156] U. Cisotti, Azioni dinamiche di correnti traslocircolatorie intorno a una lastra arcuata, *Atti Accad. Naz. Lincei. Rend. Cl. Sci. Fis. Mat. Nat.* (ser. 6) **11** (1930) 335–343. Abstract: *F. d. M.* **56** 708.
- [157] U. Cisotti, Correnti circolatorie locali intorno a regioni di acqua morta, *Atti Accad. Naz. Lincei. Rend. Cl. Sci. Fis. Mat. Nat.* (ser. 6) **13** (1931) 85–92. Abstract: *F. d. M.* **57** 1097. *Sci. Abs.* **A34** No 2532.
- [158] A. Clebsch, Über eine allgemeine Transformation der hydrodynamischen Gleichungen, *J. Reine Angew. Math.* **54** (1857) 293–312.
- [159] A. Clebsch, Über die Integration der hydrodynamischen Gleichungen, *J. Reine Angew. Math.* **57** (1859) 1–10.
- [160] C.V. Coats, Vortex motion in and about elliptic cylinders, I, *Quart. J. Pure Appl. Math.* **15** (1878) 356–365.
- [161] C.V. Coats, Vortex motion in and about elliptic cylinders, II, *Quart. J. Pure Appl. Math.* **16** (1879) 81–88.
- [162] C.V. Coats, On circular vortex rings, *Quart. J. Pure Appl. Math.* **16** (1879) 170–178.
- [163] E.A. Coddington, The stability of infinite differential systems associated with vortex streets, *J. Math. Phys.* **30** (1952) 171–199. Abstract: *Appl. Mech. Rev.* **5** No 3454. *Math. Rev.* **13** 790.
- [164] P.L. Coe, Stationary vortices behind a flat plate normal to the freestream in incompressible flow, *AIAA J.* **10** (1972) 1701.
- [165] A. Consiglio, Ancora una eccezione del teorema di Kutta-Joukowski, *Atti Accad. Naz. Lincei. Rend. Cl. Sci. Fis. Mat. Nat.* (ser. 6) **11** (1930) 813–818. Abstract: *F. d. M.* **56** 709.
- [166] R. Cormazzi, Azioni dinamiche esercitate in un moto piano liquido provocato da vortici liberi in un semipiano, *Note Esercit. Mat. Catania* **6** (1931) 255–259. Abstract: *F. d. M.* **57** 1126.
- [167] J. Courrègelongue, Sur l'existence de deux familles de tourbillons à l'arrière des solides immersés, *C. R. Acad. Sci. Paris* **189** (1929) 972–974.

- [168] J. Courrègelongue, Sur la formation des mouvements tourbillonnaires à l'arrière de solides immersés. *C. R. Acad. Sci. Paris* **190** (1930) 362–365. Abstract: *Sci. Abs.* **A33** No 2390.
- [169] J. Croll, Note on the vortex-atom theory, *Am. J. Sci.* **26** (1883) 339–340.
- [170] P. Czermak, Eine neue Beobachtungsmethode für Luftwirbelringe, *Sber. Akad. Wiss. Wien* **109** (1900) Abh 2a, 878–890.
- [171] L.S. Da Rios, Sul moto d'un liquido indefinito con un filetto vorticoso di forma qualunque, *Rend. Circ. Mat. Palermo* **22** (1906) 117–135. Abstract: *F. d. M.* **37** 764.
- [172] L.S. Da Rios, Sul moto dei filetti vorticosi di forma qualunque. *Atti Accad. Naz. Lincei Rend. Cl. Sci. Fis. Mat. Nat. (ser. 5)* **18** (1909) 75–79. Abstract: *F. d. M.* **37** 764.
- [173] L.S. Da Rios, Sul moto dei filetti vorticosi di forma qualunque, *Rend. Circ. Mat. Palermo* **29** (1910) 354–368. Abstract: *F. d. M.* **41** 819.
- [174] L.S. Da Rios, Sul moto intestino dei filetti vorticosi, *G. Mat. Battaglini* (ser. 3) **2** (1911) 300–308. Abstract: *F. d. M.* **42** 799.
- [175] L.S. Da Rios, Sezioni trasversali stabili dei filetti vorticosi, *Atti Ist. Veneto Sci. Lett. Arti Cl. Sci. Mat. Nat.* **75** (1916) Pt 2 299–308.
- [176] L.S. Da Rios, Sui tubi vorticosi rettilinei posti a raffronto con filetti di forma qualunque, *Atti Accad. Sci. Lett. Arti Padova* **32** (1916) 343–350.
- [177] L.S. Da Rios, Vortici ad elica, *Nuovo Cimento* (ser. 6) **11** (1916) 419–431.
- [178] L.S. Da Rios, Interpretazione dinamica dei movimenti indotti in un liquido da un campo vorticoso, *Atti Ist. Veneto Sci. Lett. Arti Cl. Sci. Mat. Nat.* **78** (1919) Pt 2 331–336.
- [179] L.S. Da Rios, Sulla conclusioni del Weingarten intorno ai vortici, *Atti Ist. Veneto Sci. Lett. Arti Cl. Sci. Mat. Nat.* **79** (1919) Pt 2 93–98.
- [180] L.S. Da Rios, Scie e anelli vorticosi, *Aerotecnica* **8** (1928) 120–126.
- [181] L.S. Da Rios, Sur la théorie des tourbillons, *C. R. Acad. Sci. Paris* **191** (1930) 399–401. Abstract: *F. d. M.* **56** 707; *Sci. Abs.* **A34** No 334.
- [182] L.S. Da Rios, Sui vortici piani indeformabili, *Atti Accad. Pontif. Nuovi Lincei* **84** (1931) 720–731. Abstract: *F. d. M.* **57** 1106. *Sci. Abs.* **A35** No 1076.
- [183] L.S. Da Rios, Anelli vorticosi ruotanti, *Rend. Semin. Mat. Univ. Padova* **9** (1931) 142–151. Abstract: *F. d. M.* **57** 1107.
- [184] L.S. Da Rios, Sui vortici piani indeformabili, *Atti Soc. Ital. Prog. Sci.* **2** (1931) 7–8. Abstract: *F. d. M.* **58** 874.
- [185] L.S. Da Rios, Ancora sugli anelli vorticosi ruotanti, *Atti Accad. Naz. Lincei Rend. Cl. Sci. Fis. Mat. Nat.* (ser. 6) **17** (1933) 924–926.
- [186] L.S. Da Rios, Sui vortici gobbi indeformabili, *Atti Accad. Pontif. Nuovi Lincei* **86** (1933) 162–168. Abstract: *F. d. M.* **59** 1452.
- [187] G. Darrieus, Recent progress in hydrodynamics, *Engineering* **124** (1927) 277–279, 294–295, 405–406, 440–441, 500–501.
- [188] O. Darrigol, From organ pipes to atmospheric motion: Helmholtz on fluid mechanics, *Hist. Stud. Phys. Sci.* **29** (1998) 1–51.
- [189] G.H. Darwin, Mr Preston on vortex atoms, *Nature* **22** (1880) 95–96.
- [190] H.K. Dasgupta, Sur la stabilité de deux files de tourbillons dans un canal de largeur finie, *C. R. Acad. Sci. Paris* **209** (1939) 503–505. Abstract: *Zentr. Mech.* **10** 136.
- [191] B. Datta, On the stability of two coaxial rectilinear vortices of compressible fluid, *Bull. Calcutta Math. Soc.* **10** (1920) 219–228.
- [192] B. Datta, Notes on vortices in a compressible fluid, *Proc. Benares Math. Soc.* **2** (1920) 23–31. Abstract: *F. d. M.* **47** 767.
- [193] B. Datta, On the periods of vibrations of a straight vortex-pair, *Proc. Benares Math. Soc.* **3** (1921) 13–24. Abstract: *F. d. M.* **48** 964.
- [194] K. De, On a case of vortex motion near semicircular boundaries with semicircular projections, *Bull. Calcutta Math. Soc.* **21** (1929) 197–202. Abstract: *F. d. M.* **56** 1253. *Sci. Abs.* **A21** No 1713.
- [195] A. De Faccio, Sulle lamine vorticose in seno a un liquido perfetto, *Atti Ist. Veneto Sci. Lett. Arti Cl. Sci. Mat. Nat.* **72** (1913) Pt 2 971–988.

[196] H. Deacon, Experiments on formation of ring vortices (with secondary phenomena) in water, *Chem. News J. Ind. Sci.* **24** (1871) 60–61.

[197] H. Deacon, Ring vortices, *Chem. News J. Ind. Sci.* **24** (1871) 70–71.

[198] H. Deacon, Ring vortices in water, *Chem. News. J. Ind. Sci.* **24** (1871) 154–155.

[199] L. Derr, A photographic study of Mayer's floating magnets, *Proc. Am. Acad. Arts Sci.* **44** (1909) 525–528.

[200] O.V. Dinze and K.I. Shafranovskii, *Matematika v izdaniakh Akademii Nauk. 1728–1935. (Mathematics in the editions of the Academy of Sciences. 1728–1935.)* (AN SSSR, Moscow–Leningrad, 1936). (in Russian).

[201] G.L. Dirichlet, Untersuchungen über ein Problem der Hydrodynamik, *J. Reine Angew. Math.* **58** (1860) 181–216. Reprinted in: L. Kronecker, ed., *G. Lejeune Dirichlet's Werke* (Reimer, Berlin, 1897) **2** 263–301.

[202] B. Dolaptschiew, Über die Stabilität der Kármánschen Wirbelstraße, *Z. Angew. Math. Mech.* **17** (1937) 313–323. Discussion: *Z. Angew. Math. Mech.* **18** (1938) 261. Abstract: *F. d. M.* **63** 1353. *Zentr. Mech.* **7** 134.

[203] B. Dolaptschiew, Störungsbewegungen (Bahnen) der einzelnen Wirbel der Kármánschen Wirbelstraße, *Z. Angew. Math. Mech.* **18** (1938) 264–271. Abstract: *F. d. M.* **64** 853. *Zentr. Mech.* **8** 177.

[204] B. Dolaptschiew, Beitrag zur Stabilität der Kármánschen Wirbelstraßen und die Bahnen der einzelnen Wirbel, *Spis. Bulg. Akad. Nauk* **57** (1938) 148–211 (in Bulgarian); 212–218 (extended German summary). Abstract: *F. d. M.* **64** 1447.

[205] B. Dolaptschiew, Zweiparametrische Wirbelstraßen, *God. Sof. Univ.* (part 1) **39** (1943) 287–316 (in Bulgarian); 317–320 (extended German summary). Abstract: *Math. Rev.* **12** 214.

[206] B. Dolaptschiew, Über die schräge Fortbewegung der Wirbelstraßen, *God. Sof. Univ.* (part 1) **43** (1947) 137–160 (in Bulgarian); 161–163 (extended German summary). Abstract: *Math. Rev.* **12** 214.

[207] B. Dolaptschiew, Über die Stabilisierung der Wirbelstraßen, *God. Sof. Univ.* (part 1) **43** (1947) 165–176 (in Bulgarian); 177–178 (extended German summary). Abstract: *Math. Rev.* **12** 214.

[208] B. Dolaptchiev, Stabilisation des files de tourbillons, *C. R. Acad. Bulg. Sci.* **191** (1949) No 2/3, 13–16. Abstract: *Appl. Mech. Rev.* **4** No 2988. *Math. Rev.* **12** 367.

[209] B. Dolaptschiew, Anwendung der Methode von N. E. Kotschin zur Bestimmung des Gleichgewichtszustandes der zweiparametrischen Wirbelstraßen, *God. Sof. Univ.* (part 1) **46** (1950) 357–367 (in Bulgarian); 367–368 (German abstract). Abstract: *Appl. Mech. Rev.* **6** No 2281. *Math. Rev.* **14** 422.

[210] B. Dolaptschiew, Verallgemeinertes Verfahren zur Stabilitätsuntersuchung beliebig geordneter Wirbelstraßen, *God. Sof. Univ.* (part 1) **46** (1950) 369–375 (in Bulgarian); 376 (German abstract). Abstract: *Appl. Mech. Rev.* **6** No 2573. *Math. Rev.* **14** 423.

[211] B. Dolaptchiev, A generalized method of definition of the stability of an arbitrarily situated vortex street, *Dokl. Akad. Nauk SSSR* **77** (1951) 985–988 (in Russian). Abstract: *Appl. Mech. Rev.* **4** No 4199. *Math. Rev.* **13** 81.

[212] B. Dolaptchiev, Application of N.E. Kochin's method to the investigation of the equilibrium conditions of two-parameter vortex streets, *Dokl. Akad. Nauk SSSR* **78** (1951) 29–32 (in Russian). Abstract: *Appl. Mech. Rev.* **5** No 161. *Math. Rev.* **13** 81.

[213] B. Dolaptchiev, The stability of vortex streets, *Dokl. Akad. Nauk SSSR* **78** (1951) 225–228 (in Russian). Abstract: *Appl. Mech. Rev.* **5** No 3453. *Math. Rev.* **13** 81.

[214] B. Dolaptchiev, On the stability and oblique flow of two-parameter vortex streets, *Dokl. Akad. Nauk SSSR* **98** (1954) 349–352 (in Russian). Abstract: *Math. Rev.* **16** 1169.

[215] B. Dolaptchiev, On the approximate determination of the vortex drag force, *Dokl. Akad. Nauk SSSR* **98** (1954) 743–746 (in Russian). Abstract: *Math. Rev.* **16** 1169.

[216] B. Dolaptschiew, Verallgemeinerte Föppl'sche Kurven im Zusammenhang mit der Wirbelwiderstandsbestimmung, *Z. Angew. Math. Mech.* **35** (1955) 427–434.

- [217] Bl. Dolaptschiew, Bemerkungen über die Stabilitätsuntersuchungen der Wirbelstraßen, *Sch. Reihe Forsch. Inst. Math.* (1957) No 4 1–28.
- [218] B. Dolaptschiew, Über einen unbekannten klassischen Satz (von Synge) in einem alten hydrodynamischen Problem (von Kármán), *God. Sof. Univ.* **67** (1973) 355–361 (in Bulgarian); 361–362 (German summary).
- [219] B. Dolaptschiew and I. Tschobanow, Über die Integrale der Bewegungleichungen der Flüssigkeit um eine Kármánsche Wirbelstraße, in: *Proceedings of the IX Congrès International de Mécanique Appliquée* (Université de Bruxelles Press, Bruxelles, 1957) **1** 476–482.
- [220] A.E. Dolbear *Modes of Motion or Mechanical Conceptions of Physical Phenomena* (Lee and Shepard, Boston, 1897).
- [221] E.A. Dombrovskaya, *Nikolai Egorovich Joukovskii. 1847–1921* (Oborongiz, Moscow-Leningrad, 1939) (in Russian).
- [222] U. Domm, Ein Beitrag zur Stabilitätstheorie der Wirbelstraßen unter Berücksichtigung endlicher und zeitlich wachsender Wirbeldurchmesser, *Ing.-Arch.* **22** (1954) 400–410. Abstract: *Math. Rev.* **17** 308.
- [223] U. Domm, The stability of vortex streets with consideration of the spread of vorticity of the individual vortices, *J. Aeronaut. Sci.* **22** (1955) 750–754. Abstract: *Math. Rev.* **17** 308.
- [224] U. Domm, Über die Wirbelstraßen von geringster Instabilität, *Z. Angew. Math. Mech.* **36** (1956) 367–371.
- [225] H.L. Dryden, Turbulence, companion of Reynolds number, *J. Aeronaut. Sci.* **1** (1934) 67–75.
- [226] H.L. Dryden, F.L. Murnaghan and H. Bateman, Report of Committee on Hydrodynamics, *Bull. Nat. Res. Council* (1932) No 84.
- [227] H.L. Dryden, F.L. Murnaghan and H. Bateman, *Hydrodynamics* (Dover, New York, 1956).
- [228] H.L. Dryden, Contribution of Theodore von Kármán to applied mechanics, *Appl. Mech. Rev.* **16** (1963) 589–595.
- [229] P. Duhem, *L'Évolution de la mécanique* (Hermann, Paris, 1905).
- [230] P. Dupin, Sur la vibration des tiges cylindriques dans l'eau sous l'influence des tourbillons alternés, *C. R. Acad. Sci. Paris* **191** (1930) 482–484. Abstract: *Sci. Abs. A***34** No 335.
- [231] P. Dupin and E. Crausse, Sur la vibration des tiges cylindriques dans l'eau sous l'influence des tourbillons alternés, *C. R. Acad. Sci. Paris* **192** (1931) 729–731.
- [232] P. Dupin and M. Teissié-Solier, *Les tourbillons alternés et les régimes d'un fluide autour d'un obstacle* (Gauthier-Villars, Paris, 1928).
- [233] P. Dupin and M. Teissié-Solier, Sur les tourbillons alternés en régime non turbulent et en régime turbulent, *C. R. Acad. Sci. Paris* **190** (1930) 920–922.
- [234] P. Dupin and M. Teissié-Solier, Sur les tourbillons alternés de Bénard-Kármán et la loi de similitude dynamique de Reynolds, *C. R. Acad. Sci. Paris* **192** (1931) 1017–1020. Abstract: *Sci. Abs. A***34** No 2539.
- [235] G. Durand, Sur la stabilité des files tourbillonnaires, *C. R. Acad. Sci. Paris* **196** (1933) 382–385. Abstract: *F. d. M.* **59** 761.
- [236] G. Durand, Sur les petits mouvements d'un système infini de tourbillons autour d'un position d'équilibre, *Publ. Scient. Tech. Minist. Air* (1933) No 35.
- [237] F.W. Dyson, The potential of an anchor ring, *Proc. R. Soc. London* **53** (1893) 372–375.
- [238] F. W. Dyson, The potential of an anchor ring. Part II, *Phil. Trans. R. Soc. London* **A184** (1893) 1041–1106.
- [239] H. Ebert, *Hermann von Helmholtz* (Wissenschaftliche Verlagsgesellschaft, Stuttgart, 1949).
- [240] B. Eck, Experimentelle Behandlung der Strömungslehre im physikalischen und technischen Unterricht, *Z. Tech. Phys.* **11** (1930) 506–511.
- [241] C.G. Eden, Apparatus for the visual and photographic study of the distribution of the flow round plates and models in a current of water, *Rep. Memo. Advis. Comm. Aeronaut.* (1911) No 31. Also: *Tech. Rep. Advis. Comm. Aeronaut.* (1910/11) 48–49.

- [242] C.G. Eden, Investigation by visual and photographic methods of the flow past plates and models, *Rep. Memo. Advis. Comm. Aeronaut.* (1912) No 58. Also: *Tech. Rep. Advis. Comm. Aeronaut.* (1911/12) 97–99.
- [243] E. Edser, *General Physics for Students: A textbook on the fundamental properties of matter* (Macmillan, London, 1911).
- [244] G. Eiffel, *La résistance de l'air et l'aviation* (Gauthier-Villars, Paris, 1910). English translation: *The Resistance of the Air and Aviation. Experiments conducted at the Champ de Mars Laboratory* 2nd edn (Constable & Co, London, 1913).
- [245] A. Einstein, Zum hundertjährigen Gedenktag von Lord Kelvin's Geburt. (26. Juni 1824), *Naturwissenschaften* **12** (1924) 601–602.
- [246] A. Einstein, Die Ursache der Mäanderbildung der Flüsse und des so-genannten Baerschen Gesetzes, *Naturwissenschaften* **14** (1926) 223–224.
- [247] A. Eliassen, Vilhelm Bjerknes and his students, *Annu. Rev. Fluid Mech.* **14** (1982) 1–12.
- [248] M. Epple, Topology, matter, and space, I: Topological notions in 19th-century natural philosophy, *Arch. Hist. Exact Sci.* **52** (1998) 297–392.
- [249] H. Ertel, Ein neuer hydrodynamischer Wirbelsatz, *Met. Z.* **59** (1942) 277–281.
- [250] H. Ertel, Über das Verhältnis des neuen hydrodynamischen Wirbelsatzes zum Zirkulationssatz von V. Bjerknes, *Met. Z.* **59** (1942) 385–387.
- [251] H. Ertel, Über hydrodynamische Wirbelsätze, *Phys. Z.* **43** (1942) 526–529.
- [252] L. Fabricesi, Questioni di stabilità relativa ad una configurazione rigida di quattro vortici filiformi, *Atti Ist. Veneto Sci. Lett. Arti Cl. Sci. Mat. Nat.* **106** (1948) Pt 2 67–74. Abstract: *Appl. Mech. Rev.* **3** No 1505. *Math. Rev.* **11** 221.
- [253] N.Ya. Fabrikant, *Aerodinamika (Aerodynamics)* (Gostekhizdat, Moscow-Leningrad, 1949) (in Russian).
- [254] A. Fage, Some recent experiments on fluid motion, *J. R. Aeronaut. Soc.* **32** (1928) 296–321; 322–330 (discussion).
- [255] A. Fage, The behaviour of fluids in turbulent motion, *J. R. Aeronaut. Soc.* **37** (1933) 573–593; 593–600 (discussion).
- [256] A. Fage, Aerodynamic research and hydraulic practice, *Proc. Inst Mech. Engrs* **130** (1935) 3–37; 38–69 (discussion).
- [257] A. Fage and F.C. Johansen, On the flow of air behind an inclined flat plate of infinite span, *Rep. Memo. Advis. Comm. Aeronaut.* (1927) No 1104. Also: *Tech. Rep. Advis. Comm. Aeronaut.* (1927/28) 81–106. Also: *Proc. R. Soc. London A116* (1927) 170–197. Abstract: *Sci. Abs. A31* No 245.
- [258] A. Fage and F.C. Johansen, The structure of vortex sheets, *Rep. Memo. Advis. Comm. Aeronaut.* (1927) No 1143. Also: *Tech. Rep. Advis. Comm. Aeronaut.* (1927/28) 114–130. Also: *Phil. Mag.* (ser. 7) **5** (1928) 417–441. Abstract: *Sci. Abs. A31* No 1135.
- [259] A. Fage and L.J. Jones, Drag of an aerofoil for two-dimensional flow, *Proc. R. Soc. London A111* (1926) 592–603.
- [260] A. Fage and L.F.G. Simmons, An investigation of the air-flow pattern in the wake of an aerofoil of finite span, *Phil. Trans. R. Soc. London A225* (1926) 303–330.
- [261] H. Falkenhagen, Klassische Hydrodynamik, in: L. Schiller, ed., *Handbuch der Experimentalphysik. 4. Hydro- und Aerodynamik* (Akademische Verlagsgesellschaft, Leipzig, 1931) Pt 1 43–237. Abstract: *F. d. M.* **57** 1085.
- [262] W.S. Farren, Air flow, *J. R. Aeronaut. Soc.* **36** (1932) 451–472.
- [263] R.P. Feynman, Application of quantum mechanics to liquid Helium, in: C.J. Gorter, ed., *Progress in Low Temperature Physics* (North Holland, Amsterdam, 1955) **1** 17–53.
- [264] S. Finsterwalder, Aërodynamik, in: F. Klein and C. Müller, eds, *Encyklopädie der mathematischen Wissenschaften* (Teubner, Leipzig, 1903) **IV/3** No 17 150–184.
- [265] S. Finsterwalder, Die Aerodynamik als Grundlag der Luftschiffahrt, *Z. Flugtech. Motorluftschiff.* **1** (1910) 6–10, 30–31.

[266] A. Fiolek, *Pioneers in Modern Meteorology and Climatology: Vilhelm and Jacob Bjerknes. A Selected Bibliography* (U. S. Department of Commerce, National Oceanic and Atmospheric Administration, 2004).

[267] G.F. FitzGerald, On currents of gas in the vortex atom theory of gases, *Proc. Dublin Sci. Soc.* **4** (1885) 339–340.

[268] G.F. FitzGerald, On a model illustrating some properties of the ether, *Proc. Dublin Sci. Soc.* **4** (1885) 407–419. Reprinted in: J. Larmor, ed., *The Scientific Writings of the late George Francis FitzGerald* (Longmans, Green, & Co, London, 1902) 142–156.

[269] G.F. FitzGerald, On an electro-magnetic interpretation of turbulent liquid motion, *Nature* **40** (1889) 32–34. Reprinted in: J. Larmor, ed., *The Scientific Writings of the late George Francis FitzGerald* (Longmans, Green, & Co, London, 1902) 254–261.

[270] G.F. FitzGerald, Helmholtz memorial lecture, *J. Chem. Soc.* **69** (1896) 885–912. Also *Nature* **53** (1896) 296–298. Reprinted in: J. Larmor, ed., *The Scientific Writings of the late George Francis FitzGerald* (Longmans, Green, & Co, London, 1902) 340–377.

[271] G.F. FitzGerald, On the energy per cubic centimetre in a turbulent liquid when transmitting laminar waves, *Rep. Brit. Ass. Advmt Sci.* **69** (1899) 632–634. Reprinted in: J. Larmor, ed., *The Scientific Writings of the late George Francis FitzGerald* (Longmans, Green, & Co, London, 1902) 484–486.

[272] G.F. FitzGerald, On a hydrodynamical hypothesis as to electromagnetic actions, *Proc. Dublin Sci. Soc.* **9** (1899) 50–54. Reprinted in: J. Larmor, ed., *The Scientific Writings of the late George Francis FitzGerald* (Longmans, Green, & Co, London, 1902) 472–477.

[273] G.F. FitzGerald, *Lord Kelvin, Professor of Natural Philosophy in the University of Glasgow 1846–1899* (MacLehose and Sons, Glasgow, 1899).

[274] G.F. FitzGerald, Thoughts on the work of Helmholtz, being an abridgement of the Helmholtz memorial lecture, in: J. Larmor, ed., *The Scientific Writings of the late George Francis FitzGerald* (Longmans, Green, & Co, London, 1902) 378–386.

[275] J.A. Fleming, *Waves and Ripples in Water, Air, and Aether* (Young, London, 1902).

[276] F. Florin, Ebene Bewegung eines Wirbelkranzes am rotierenden radialen Schaufelstern von endlichen Schaufellängen, *Z. Angew. Math. Mech.* **20** (1940) 152–164. Abstract: *F. d. M.* **66** 1066. *Zentr. Mech.* **11** 92.

[277] I. Flügge-Lotz and W. Flügge, Ludwig Prandtl in the nineteen-thirties: reminiscences, *Annu. Rev. Fluid Mech.* **5** (1973) 1–7.

[278] A. Föppl, *Die Geometrie der Wirbelfelder* (Teubner, Leipzig, 1897). Abstract: *F. d. M.* **28** 762.

[279] L. Föppl, Wirbelbewegung hinter einem Kreiszylinder, *Sber. Bayer. Akad. Wiss.* **43** (1913) 1–17.

[280] Ph. Forchheimer, *Hydraulik* (Teubner, Leipzig, 1914). Abstract: *F. d. M.* **45** 1106.

[281] L.E. Fraenkel, On steady vortex rings of small cross-section in an ideal fluid, *Proc. R. Soc. London A* **316** (1970) 29–62.

[282] R.A. Fraser, Juvenile lecture – model aircraft, *J. R. Aeronaut. Soc.* **27** (1923) 105–113.

[283] K.O. Friedrichs, *Special Topics in Fluid Dynamics* (New York University Press, New York, 1953).

[284] A. Friedmann, *Opyt gidromekhaniki szhimaemoi zhidkosti* (An essay on hydrodynamics of compressible fluid) (GIZ, Petrograd, 1922) (in Russian). Abstract: *F. d. M.* **48** 944.

[285] A. Friedmann, Über Wirbelbewegung in einer kompressiblen Flüssigkeit, *Z. Angew. Math. Mech.* **4** (1924) 102–107. Abstract: *F. d. M.* **50** 563.

[286] A. Friedmann and P. Poloubarinova, Über fortschreitende Singularitäten der ebenen Bewegung einer inkompressiblen Flüssigkeit, *Recueil de Géophysique* **5** (1928) No 2 9–23. Translated in: A.A. Fridman, *Izbrannye trudy* (Selected Works) (Nauka, Moscow, 1966) 125–139. Translated in: P.Ya. Kochina, *Izbrannye trudy. Gidrodinamika i teoriya fil'tracii* (Selected Works. Hydrodynamics and Percolation Theory) (Nauka, Moscow, 1991) 28–46.

[287] R. Fuchs and L. Hopf *Aerodynamik* (Schmidt, Berlin, 1922). Abstract: *F. d. M.* **48** 942.

[288] R. Fuchs, L. Hopf and F. Seewald, *Aerodynamik* (Springer, Berlin, 1935). Abstract: *F. d. M.* **61** 905.

- [289] S. Fujiwhara, Experiment on the behaviour of two vortices in water, in: E. Meissner, ed., *Proceedings of the 2nd International Congress for Applied Mechanics. Zürich 12–17 September 1926* (Füssli, Zürich-Leipzig, 1927) 506.
- [290] S. Fujiwhara, Short note on the behaviour of two vortices, *Proc. Phys.-Math. Soc. Japan* (ser. 3) **13** (1931) 106–110. Abstract: *Sci. Abs. A34* No 2538.
- [291] V. Garten, Über die Bewegung von Wirbelfäden endlichen Querschnittes in einer zweidimensionalen idealen Flüssigkeit, *Math. Ann.* **109** (1934) 445–464. Abstract: *F. d. M.* **60** 1381.
- [292] R. Giacomelli, The aerodynamics of Leonardo da Vinci, *J. R. Aeronaut. Soc.* **34** (1930) 1016–1038.
- [293] R. Giacomelli, Flight in nature and in science, *J. R. Aeronaut. Soc.* **36** (1932) 578–597.
- [294] R. Giacomelli and E. Pistolesi, Historical sketch, in: W. Durand, ed., *Aerodynamic Theory* (Springer, New York, 1934) **1** 305–394.
- [295] H. Glauert, Aerofoil theory, *Rep. Memo. Advis. Comm. Aeronaut.* (1921) No 723. Also: *Tech. Rep. Advis. Comm. Aeronaut.* (1921/22) 160–177.
- [296] H. Glauert, Some applications of the vortex theory of aerofoils, *Rep. Memo. Advis. Comm. Aeronaut.* (1921) No 752. Also: *Tech. Rep. Advis. Comm. Aeronaut.* (1921/22) 56–69.
- [297] H. Glauert, Theoretical relationships for the lift and drag of an aerofoil structure, *J. R. Aeronaut. Soc.* **27** (1923) 512–518.
- [298] H. Glauert, *The Elements of Aerofoil and Airscrew Theory* (Cambridge University Press, Cambridge, 1926).
- [299] H. Glauert, The characteristics of a Kármán vortex street in a channel of finite breadth, *Rep. Memo. Advis. Comm. Aeronaut.* (1927) No 1151. Also: *Tech. Rep. Advis. Comm. Aeronaut.* (1927/28) 81–106. Also: *Proc. R. Soc. London A116* (1927) 170–197. Abstract: *Sci. Abs. A31* No 2899.
- [300] H. Glauert, Aerodynamic theory, *J. R. Aeronaut. Soc.* **34** (1930) 409–414.
- [301] H. Glauert, The influence of a uniform jet on the lift of an aerofoil, *Rep. Memo. Advis. Comm. Aeronaut.* (1934) No 1602. Also: *Tech. Rep. Advis. Comm. Aeronaut.* (1934/35) 173–189.
- [302] M. Glauert, Two-dimensional aerofoil theory, *J. R. Aeronaut. Soc.* **27** (1923) 348–366.
- [303] M. Godefroy, Sur la stabilité des files de tourbillons, *C. R. Acad. Sci. Paris* **207** (1938) 770–772. Abstract: *Zentr. Mech.* **9** 419.
- [304] M. Godefroy, Recherches sur les systèmes de tourbillons ponctuels soumis à des liaisons et sur la notion de configuration hydrodynamique stable, *Comment. Math. Helvet.* **11** (1939) 293–320. Abstract: *F. d. M.* **65** 981.
- [305] S. Goldstein, On the vortex theory of screw propellers, *Proc. R. Soc. London A123* (1929) 440–465.
- [306] S. Goldstein, ed., *Modern Developments in Fluid Dynamics* (Clarendon Press, Oxford, 1937). Abstract: *F. d. M.* **64** 1451.
- [307] S. Goldstein, Fluid mechanics in the first half of this century, *Annu. Rev. Fluid Mech.* **1** (1969) 1–28.
- [308] V.V. Golubev, Theory of an aerofoil in a plane-parallel flow, *Trudy Tsentr. Aero-Gidrodin. Inst.* No 29 (1927) 3–207 (in Russian, English summary).
- [309] V.V. Golubev, Theory of an aerofoil of finite span, *Trudy Tsentr. Aero-Gidrodin. Inst.* No 108 (1931) 3–350 (in Russian, English summary).
- [310] V.V. Golubev, On slotted wings, in: *I All-Union Conference on Aerodynamics. 16–21 May 1931* (TsAGI, Moscow, 1932) 166–170 (in Russian). Reprinted in: *Trudy po aerodinamike (Papers on Aerodynamics)* (GITTL, Moscow-Leningrad, 1957) 11–15.
- [311] V.V. Golubev, On the stability of the Kármán vortex streets, *Izv. Akad. Nauk SSSR. Otd. Mat. Estest. Nauk* (ser. 7) (1932) 1103–1108 (in Russian).
- [312] V.V. Golubev, On the theory of the Kármán vortex streets, *Mat. Sbor.* **40** (1933) 73–85 (in Russian). Reprinted in: *Trudy po aerodinamike (Papers on Aerodynamics)* (GITTL, Moscow-Leningrad, 1957) 641–657. Abstract: *F. d. M.* **59** 761.

- [313] V.V. Golubev, Studies on the theory of a finite wing. I. Theory of a slot in a two-dimensional flow, *Trudy Tsentr. Aero-Gidrodin. Inst.* (1933) No 147 1–72 (in Russian). Reprinted in: *Trudy po aerodinamike (Papers on Aerodynamics)* (GITTL, Moscow-Leningrad, 1957) 31–137.
- [314] V.V. Golubev, On the theory of a finite wing, *Trudy Tsentr. Aero-Gidrodin. Inst.* (1935) No 240 14–17 (in Russian). Reprinted in: *Trudy po aerodinamike (Papers on Aerodynamics)* (GITTL, Moscow-Leningrad, 1957) 137–141.
- [315] V.V. Golubev, Theory of a slot in a two-dimensional flow, *J. R. Aeronaut. Soc.* **40** (1936) 681–708.
- [316] V.V. Golubev, On the theory of ground's influence on the lift force of a wing, *Trudy Tsentr. Aero-Gidrodin. Inst.* (1937) No 301 36–38 (in Russian). Reprinted in: *Trudy po aerodinamike (Papers on Aerodynamics)* (GITTL, Moscow-Leningrad, 1957) 657–661.
- [317] V.V. Golubev, Studies on the theory of a finite wing. II. Approximate theory of the slot, *Trudy Tsentr. Aero-Gidrodin. Inst.* (1937) No 306 1–40 (in Russian). Reprinted in: *Trudy po aerodinamike (Papers on Aerodynamics)* (GITTL, Moscow-Leningrad, 1957) 291–348.
- [318] V.V. Golubev, On the influence of a system of unmovable vortices upon the flow around a cylinder, *Uchen. Zap. Moskov. Gos. Univ.* (1937) No 7 3–19 (in Russian). Reprinted in: *Trudy po aerodinamike (Papers on Aerodynamics)* (GITTL, Moscow-Leningrad, 1957) 348–371.
- [319] V.V. Golubev, Nikolai Egorovich Joukovskii. A biographical essay, in: N.E. Joukovskii, *Polnoe sobranie sochinenii. Tom I (Collected Papers. I. General mechanics)* (ONTI, Moscow-Leningrad, 1937) 15–55 (in Russian). Reprinted in: *Trudy po aerodinamike (Papers on Aerodynamics)* (GITTL, Moscow-Leningrad, 1957) 823–864.
- [320] V.V. Golubev, *Teoriia kryla v plosko-parallel'nom potoke (Theory of a wing in a plane-parallel flow)* (GTTI, Moscow, 1938) (in Russian).
- [321] V.V. Golubev, On the influence of flaps on the lift force of a wing, *Trudy Tsentr. Aero-Gidrodin. Inst.* (1938) No 342 24–35 (in Russian). Reprinted in: *Trudy po aerodinamike (Papers on Aerodynamics)* (GITTL, Moscow-Leningrad, 1957) 671–687.
- [322] V.V. Golubev, Theoretical studies of increasing the lift force of an airfoil, *Trudy VVA RKKA im. Joukovskogo* (1939) No 46 3–72 (in Russian). Reprinted in: *Trudy po aerodinamike (Papers on Aerodynamics)* (GITTL, Moscow-Leningrad, 1957) 199–291.
- [323] V.V. Golubev, On the theory of a wing flap closely connected to the wing, *Trudy Tsentr. Aero-Gidrodin. Inst.* (1939) No 398 3–54 (in Russian). Reprinted in: *Trudy po aerodinamike (Papers on Aerodynamics)* (GITTL, Moscow-Leningrad, 1957) 371–396.
- [324] V.V. Golubev, *N.E. Joukovskii* (NKAP, Moscow, 1941) (in Russian).
- [325] V.V. Golubev, Academician S.A. Chaplygin (His life, scientific and public activity), *Vest. AN SSSR* (1944) No 3 50–65 (in Russian). Reprinted in: *Trudy po aerodinamike (Papers on Aerodynamics)* (GITTL, Moscow-Leningrad, 1957) 887–912.
- [326] V.V. Golubev, Theory of a flapping wing and the general problem of thrust and drag, in: V.L. Komarov, ed., *Obshchee sobranie Akademii Nauk SSSR, 14–17 oktyabrya 1944 (General Assembly of the Academy of Sciences of the USSR, 14–17 October 1944)* (AN SSSR, Moscow, 1945) 193–218 (in Russian). Reprinted in: *Trudy po aerodinamike (Papers on Aerodynamics)* (GITTL, Moscow-Leningrad, 1957) 426–450.
- [327] V.V. Golubev, On the thrust of a flapping wing, *Izv. Akad. Nauk SSSR. Otd. Tekh. Nauk* (1946) No 5 641–658 (in Russian). Reprinted in: *Trudy po aerodinamike (Papers on Aerodynamics)* (GITTL, Moscow-Leningrad, 1957) 450–477.
- [328] V.V. Golubev, On the theory of a wing of low aspect ratio, *Izv. Akad. Nauk SSSR. Otd. Tekh. Nauk* (1947) No 3 261–270 (in Russian).
- [329] V.V. Golubev, N.E. Joukovskii and modern technical aeromechanics, in: S.I. Vavilov, ed., *Yubileinyi sbornik, posvyashchennyi 30-letiyu Oktyabr'skoi Revolyutsii (Jubilee Collection dedicated to 30th Anniversary of the October Revolution)* (AN SSSR, Moscow-Leningrad, 1947) **II** 503–523 (in Russian).
- [330] V.V. Golubev, Nikolai Egorovich Joukovskii. Famous scientists of Moscow University, *Uchen. Zap. Moskov. Gos. Univ.* (1947) No 1 3–64 (in Russian).

- [331] V.V. Golubev, *Sergei Alekseevich Chaplygin* (TsAGI-NKAP, Moscow, 1947) (in Russian).
- [332] V.V. Golubev, Nikolai Egorovich Joukovskii, *Usp. Mat. Nauk* **2** (1947) No 1(19) 3–17 (in Russian).
- [333] V.V. Golubev, On the theory of a wing of low aspect ratio, *Uchen. Zap. Moskov. Gos. Univ.* **2** (1948) No 122 3–16 (in Russian). Reprinted in: *Trudy po aerodinamike (Papers on Aerodynamics)* (GITTL, Moscow-Leningrad, 1957) 593–614.
- [334] V.V. Golubev, Nikolai Egorovich Joukovskii. A biographical sketch, in: N.E. Joukovskii, *Izbrannye sochineniya (Selected Papers)* (GITTL, Moscow-Leningrad, 1948) **1** 7–24. Also in: N.E. Joukovskii, *Sobranie sochinenii. Tom I. (Complete Works. I. General mechanics)* (GITTL, Moscow-Leningrad, 1948) 7–24 (in Russian).
- [335] V.V. Golubev, *Lektsii po teorii kryla (Lectures on Wing Theory)* (GITTL, Moscow, 1949) (in Russian).
- [336] V.V. Golubev, Aerofoil and screw of an airplane, in: V.Z. Vlasov, V.V. Golubev and N.D. Moiseev, eds, *Mekhanika v SSSR za tridtsat' let. 1917–1947 (Mechanics in the USSR in the period of 30 years. 1917–1947)* (GITTL, Moscow-Leningrad, 1950) 341–357 (in Russian).
- [337] V.V. Golubev, On some questions of the theory of a flapping wing, *Uchen. Zap. Moskov. Gos. Univ.* **3** (1951) No 152 3–12 (in Russian). Reprinted in: *Trudy po aerodinamike (Papers on Aerodynamics)* (GITTL, Moscow-Leningrad, 1957) 477–491. Abstract: *Appl. Mech. Rev.* **6** No 3470. *Math. Rev.* **14** 595.
- [338] V.V. Golubev, Investigations of the theory of a flapping wing, *Uchen. Zap. Moskov. Gos. Univ.* **4** (1951) No 154 3–53 (in Russian). Reprinted in: *Trudy po aerodinamike (Papers on Aerodynamics)* (GITTL, Moscow-Leningrad, 1957) 491–569. Abstract: *Appl. Mech. Rev.* **6** No 3469. *Math. Rev.* **14** 594–595.
- [339] V.V. Golubev, Vortex motion, in: B.A. Vvedenskii, ed., *Bol'shaya Sovetskaya Enciklopediya (Large Soviet Encyclopedia)* 2nd edn (Sovetskaya Enciklopediya, Moscow, 1951) **8** 209–211 (in Russian).
- [340] V.V. Golubev, Sergei Alekseevich Chaplygin (1869–1942). Famous scientists of Moscow University, *Uchen. Zap. Moskov. Gos. Univ.* (1951) No 2 3–56 (in Russian).
- [341] V.V. Golubev, Hydrodynamics, in: B.A. Vvedenskii, ed., *Bol'shaya Sovetskaya Enciklopediya (Large Soviet Encyclopedia)* 2nd edn (Sovetskaya Enciklopediya, Moscow, 1952) **11** 281–285 (in Russian).
- [342] V.V. Golubev, Joukovskii, in: B.A. Vvedenskii, ed., *Bol'shaya Sovetskaya Enciklopediya (Large Soviet Encyclopedia)* 2nd edn (Sovetskaya Enciklopediya, Moscow, 1952) **16** 227–229 (in Russian).
- [343] V.V. Golubev, On the efficiency of a flapping wing, *Uchen. Zap. Moskov. Gos. Univ.* **5** (1954) No 172 3–7 (in Russian). Reprinted in: *Trudy po aerodinamike (Papers on Aerodynamics)* (GITTL, Moscow-Leningrad, 1957) 477–491.
- [344] V.V. Golubev, On the structure of the wake behind a bluff body, *Izv. Akad. Nauk SSSR. Otd. Tekh. Nauk* (1954) No 12, 19–37 (in Russian). Reprinted in: *Trudy po aerodinamike (Papers on Aerodynamics)* (GITTL, Moscow-Leningrad, 1957) 793–820. Abstract: *Math. Rev.* **16** 1169.
- [345] V.V. Golubev, On the theory of a wing of low aspect ratio, *Prikl. Mat. Mech.* **19** (1955) 143–158 (in Russian). Reprinted in: *Trudy po aerodinamike (Papers on Aerodynamics)* (GITTL, Moscow-Leningrad, 1957) 614–638.
- [346] V.V. Golubev, The concluding words of V.V. Golubev, a professor at the University of Moscow, on his seventieth birthday, 3 December 1954, *Vest. Moskov. Univ.* (1955) No 2 143–158 (in Russian).
- [347] V.V. Golubev, Chaplygin, in: B.A. Vvedenskii, ed., *Bol'shaya Sovetskaya Enciklopediya (Large Soviet Encyclopedia)* 2nd edn (Sovetskaya Enciklopediya, Moscow, 1957) **47** 45–46 (in Russian).
- [348] V.V. Golubev, The Chaplygin – Joukovskii postulate, in: B.A. Vvedenskii, ed., *Bol'shaya Sovetskaya Enciklopediya (Large Soviet Encyclopedia)* 2nd edn (Sovetskaya Enciklopediya, Moscow, 1957) **47** 48 (in Russian).

[349] V.V. Golubev and E.S. Kuznetcov, Hydro-and aeromechanics, in: V.V. Golubev and L.S. Leibenzon, eds, *Mekhanika v SSSR za XV let (Mechanics in the USSR in the period of 15 years)* (GTTI, Moscow-Leningrad, 1932) 33–101 (in Russian).

[350] O.V. Golubeva, On the question of point vortices and vortex-sinks on the surface of a sphere, *Dokl. Akad. Nauk SSSR* **65** (1949) 653–656. (in Russian).

[351] D.N. Goriachev, On a problem of motion of rectilinear vortex filaments, *Izv. Imp. Obshch. Lyub. Estest. Antrop. Etnogr. Imp. Moskov. Univ.* **93** (1898) 14–16 (in Russian). Abstract: *F. d. M.* **29** 642.

[352] D.N. Goriachev, On some cases of motion of rectilinear parallel vortex filaments, (Magister dissertation), *Uchen. Zap. Imp. Moskov. Univ.* **16** (1898) 1–106 (in Russian). Abstract: *F. d. M.* **29** 642.

[353] D.N. Goriachev, Some cases of motion of a liquid with an axis of symmetry, *Trudy Sev-Kavkaz. Assos.* (1930) No 77 9–19 (in Russian).

[354] L. Graetz, Ueber Wirbelbewegungen in compressiblen Flüssigkeiten, *Z. Math. Phys.* **25** (1880) 1–10.

[355] R. Grammel, Über ebene Zirkulationsströmungen und die von ihnen erzeugten Kräfte, (Habilitationsvortrag), *Jahresber. Dt. Mat. Verein* **25** (1917) 16–34.

[356] A. Gray, *Lord Kelvin. An account of his scientific life and work* (Dent, London, 1908).

[357] A. Gray, Notes on hydrodynamics, chiefly on vortex motion, *Trans. R. Soc. Edinb.* **47** (1909) 1–15.

[358] A. Gray, Notes on hydrodynamics, *Phil. Mag.* (ser. 6) **28** (1914) 1–18.

[359] A.G. Greenhill, Plane vortex motion, *Quart. J. Pure Appl. Math.* **15** (1878) 10–29.

[360] A.G. Greenhill, Notes on hydrodynamics. I. On Lord Rayleigh's paper on the irregular flight of a tennis-ball. II. On the motion of a cylinder through frictionless liquid under no forces, *Mess. Math.* **9** (1880) 113–120.

[361] A.G. Greenhill, Hydromechanics, in: *Encyclopaedia Britannica* 11th edn (Cambridge University Press, Cambridge, 1910) **XIV** 115–135.

[362] A.T. Grigorian, Chaplygin, Sergei Alekseevich, in: C.C. Gillispie, ed., *Dictionary of Scientific Biography* (Scribner's Sons, New York, 1971) **III** 194–196.

[363] A.T. Grigorian, Zhukovsky, Nikolay Egorovich, in: C.C. Gillispie, ed., *Dictionary of Scientific Biography* (Scribner's Sons, New York, 1976) **XIV** 619–622.

[364] E. Grimsehl, *Lehrbuch der Physik. Mechanik, Wärmelehre, Akustik und Optik* 6th edn (Teubner, Berlin, 1923). English translation: *A Textbook of Physics* (Blackie and Sons, London-Glasgow, 1932).

[365] W. Gröbli, *Spezielle Probleme über die Bewegung geradliniger paralleler Wirbelfäden* (dissertation) (Zürcher und Furrer, Zürich, 1877).

[366] W. Gröbli, Spezielle Probleme über die Bewegung geradliniger paralleler Wirbelfäden, *Vierteljschr. Naturf. Ges. Zürich* **22** (1877) 37–82, 129–168. Abstract: *F. d. M.* **9** 675.

[367] I.S. Gromeka, *Nekotorye sluchai dvizheniya neszhimaemoi zhidkosti* (Some cases of motion of incompressible fluid) (Doctoral dissertation) (Kazan, 1881) (in Russian).

[368] I.S. Gromeka, Some cases of motion of incompressible fluid, *Uchen. Zap. Imp. Kazan. Univ.* (1882) No 2 1–107 (in Russian). Reprinted in: P.Ya. Kochina, ed., *Sobranie sochinenii (Collected Papers)* (AN SSSR, Moscow, 1952) 76–148.

[369] I.S. Gromeka, On vortex motions of a liquid on a sphere, *Uchen. Zap. Imp. Kazan. Univ.* (1885) No 3 202–236 (in Russian). Reprinted in: P.Ya. Kochina, ed., *Sobranie sochinenii (Collected Papers)* (AN SSSR, Moscow, 1952) 184–205.

[370] A. Guglielmi, Sul moto vorticoso dei liquidi, *Atti Ist. Veneto Sci. Lett. Arti. Cl. Mat. Nat.* **81** (1922) 289–314.

[371] R.F. Gwyther, On cyclic motions in a fluid, and the motion of a vortex ring of varying curvature, *Proc. Lit. Phil. Soc. Manch.* **21** (1881) 32–36.

- [372] A. Haas, *Einführung in die theoretische Physik mit besonderer Berücksichtigung ihrer modernen Probleme* (de Gruyter, Berlin-Leipzig, 1921). English translation: *Introduction to Theoretical Physics* (Constable, London, 1924).
- [373] H. Hahnemann, Neue experimentelle Untersuchungen über Entstehung der turbulenten Rohströmung, *Forsch. Geb. IngWes.* **A8** (1937) 226–237.
- [374] G.E. Hale and G.P. Luckey, Some vortex experiments bearing on the motion of Sun-spots and flocculi, *Proc. Nat. Acad. Sci. USA* **1** (1915) 385–389.
- [375] G. Hamel, Bewegung eines gradlinigen Wirbels um eine Buhne, *Z. Angew. Math. Mech.* **13** (1933) 98–101.
- [376] G. Hamel, *Mechanik der Kontinua* (Teubner, Stuttgart, 1956).
- [377] H. Hankel, *Zur allgemeinen Theorie der Bewegung der Flüssigkeiten* (dissertation) (Dieterichschen Univ.-Buchdruckerei, Göttingen, 1861).
- [378] P.A. Hanle, *Bringing Aerodynamics to America* (The MIT Press, Cambridge MA, 1982).
- [379] R. Hargreaves, The continuity of pressure in vortex motion, *Proc. Lond. Math. Soc.* **27** (1896) 281–299.
- [380] R. Hargreaves, An ellipsoidal vortex, *Proc. Lond. Math. Soc.* **27** (1896) 299–327.
- [381] E.H. Harper, Eddy formation – a correction, *Nature* **83** (1910) 397–398.
- [382] I.B. Hart, Leonardo da Vinci as a pioneer of aviation, *J. R. Aeronaut. Soc.* **27** (1923) 245–269.
- [383] I.B. Hart, Leonardo da Vinci's manuscript on the flight of birds, *J. R. Aeronaut. Soc.* **27** (1923) 289–317.
- [384] T. Hart, On certain phenomena manifested by liquid vortex rings, *Scient. Am. Suppl.* **16** (1883) 400–402.
- [385] H. Hasimoto, A soliton on a vortex filament, *J. Fluid Mech.* **51** (1972) 477–485.
- [386] B. Haurwitz, Die Arbeiten zur Dynamik der Atmosphäre von Diro Kitao, *Beitr. Geophys.* **21** (1929) 81–102. Abstract: *Sci. Abs.* **A32** No 2385.
- [387] B. Haurwitz, Bewegungen von Wirbeln mit vertikaler Achse und endlichen kreisförmigen Querschnitt, *Z. Phys.* **60** (1930) 719–740. Abstract: *F. d. M.* **56** 706. *Sci. Abs.* **A33** No 2388.
- [388] T.H. Havelock, Stability of motion of rectilinear vortices in ring formation, *Phil. Mag.* (ser. 7) **11** (1931) 617–633. Abstract: *F. d. M.* **57** 1109. *Sci. Abs.* **A34** No 2142.
- [389] W. Heisenberg, Die absoluten Dimensionen der Kármánschen Wirbelbewegung, *Phys. Z.* **23** (1922) 363–366. Reprinted in: *Gesammelte Werke (Collected Works)* (Springer, Berlin, 1985) Ser.A, Part 1, 27–30. English translation: Absolute dimensions of Karman vortex motion, *NACA Tech. Notes* (1924) No 126.
- [390] H.S. Hele-Shaw, The flow of water, *Nature* **58** (1898) 34–36.
- [391] H.S. Hele-Shaw, Flow of water, *Nature* **59** (1899) 222–223.
- [392] H.S. Hele-Shaw, The motion of a perfect liquid, *Proc. R. Instn Gt Brit.* **16** (1899) 49–64.
- [393] H. Helmholtz, Über Integrale der hydrodynamischen Gleichungen, welche den Wirbelbewegungen entsprechen, *J. Reine Angew. Math.* **55** (1858) 25–55. Reprinted in: *Wissenschaftliche Abhandlungen von Hermann Helmholtz* (Barth, Leipzig, 1882) **I** 101–134.
- [394] H. Helmholtz, On integrals of the hydrodynamical equations, which express vortex-motion, *Phil. Mag.* (ser. 4) **33** (1867) 485–510.
- [395] H. Helmholtz, Sur le mouvement le plus général d'un fluide. Réponse à une communication précédente de M. J. Bertrand, *C. R. Acad. Sci. Paris* **67** (1868) 221–225. Reprinted in: *Wissenschaftliche Abhandlungen von Hermann Helmholtz* (Barth, Leipzig, 1882) **I** 135–139.
- [396] H. Helmholtz, Sur le mouvement des fluides. Deuxième réponse à M. J. Bertrand, *C. R. Acad. Sci. Paris* **67** (1868) 754–757. Reprinted in: *Wissenschaftliche Abhandlungen von Hermann Helmholtz* (Barth, Leipzig, 1882) **I** 140–144.
- [397] H. Helmholtz, Réponse à la note de M. J. Bertrand, du 19 Octobre, *C. R. Acad. Sci. Paris* **67** (1868) 1034–1035. Reprinted in: *Wissenschaftliche Abhandlungen von Hermann Helmholtz* (Barth, Leipzig, 1882) **I** 145.
- [398] H. Helmholtz, Ueber discontinuirliche Flüssigkeitsbewegungen, *Monatsber. Akad. Wiss. Berlin* (1868) 215–228. Also: *Verh. Naturh.-med. Ver. Heidelb.* **4** (1868) 187–196. English translation:

On discontinuous movements of fluids, *Phil. Mag.* (ser. 4) **36** (1868) 337–346. Reprinted in: *Wissenschaftliche Abhandlungen von Hermann Helmholtz* (Barth, Leipzig, 1882) **I** 146–157. Abstract: *F.d.M.* **1** 341.

[399] H. von. Helmholtz, Autobiographisches Tischrede bei der Feier des 70. Geburtstages, in: *Ansprachen und Reden, gehalten bei der am 2. November 1891 zu Ehren von Hermann von Helmholtz veranstalteten Feier* (Hirschwald, Berlin, 1892) 46–59. English translation: An autobiographical sketch, in R. Kahl, ed., *Selected Writings of Hermann von Helmholtz* (Wesleyan University Press, Middletown, 1971) 466–478.

[400] H. von Helmholtz, *Zwei hydrodynamische Abhandlungen, I. Ueber Wirbelbewegungen(1858). II. Ueber diskontinuirliche Flüssigkeitsbewegungen (1868)*, in: A. Wangerin, ed., *Ostwalds Klassiker der exakten Wissenschaften* (Engelmann, Leipzig, 1896) No 79. Reprinted: (Deutsch, Frankfurt am Main, 1995). Abstract: *F.d.M.* **23** 643.

[401] H. von Helmholtz, *Dva issledovaniya po gidrodinamike (Two studies in hydrodynamics)* (Palas, Moscow, 1902) (in Russian).

[402] H. von Helmholtz, On integrals of the hydrodynamical equations, which express vortex motion, *Int. J. Fusion Energy* **1** (1978) No 3/4, 41–68.

[403] W.M. Hicks, Report on recent progress in hydrodynamics, I, *Rep. Brit. Ass. Advmt Sci.* **51** (1881) 57–88.

[404] W.M. Hicks, Report on recent progress in hydrodynamics, II, *Rep. Brit. Ass. Advmt Sci.* **52** (1882) 39–70.

[405] W.M. Hicks, On the steady motion of a hollow vortex, *Proc. R. Soc. London* **35** (1883) 304–308.

[406] W.M. Hicks, On the steady motion and small vibrations of a hollow vortex. Part I, *Phil. Trans. R. Soc. London A* **175** (1884) 161–195.

[407] W.M. Hicks, Researches on the theory of vortex rings. Part II, *Phil. Trans. R. Soc. London A* **176** (1885) 725–780.

[408] W.M. Hicks, On the construction of the luminiferous ether on the vortex atom theory, *Rep. Brit. Ass. Advmt Sci.* **55** (1885) 930.

[409] W.M. Hicks, A vortex analogue of static electricity, *Rep. Brit. Ass. Advmt Sci.* **58** (1888) 577–578.

[410] W.M. Hicks, Theories of either. (Opening presidential Address to the Mathematical and Physical Section), *Rep. Brit. Ass. Advmt Sci.* **65** (1895) 595–606. Also: *Nature* **52** (1895) 472–477.

[411] W.M. Hicks, On bicyclic vortex aggregates, *Rep. Brit. Ass. Advmt Sci.* **65** (1895) 612.

[412] W.M. Hicks, On Hill's spherical vortex, *Rep. Brit. Ass. Advmt Sci.* **65** (1895) 612–613.

[413] W.M. Hicks, Researches in vortex motion. Part III. On spiral or gyrostatic vortex aggregates, *Proc. R. Soc. London* **62** (1897–1898) 332–338.

[414] W.M. Hicks, Researches in vortex motion. Part III. On spiral or gyrostatic vortex aggregates, *Phil. Trans. R. Soc. London A* **192** (1899) 33–99.

[415] W.M. Hicks, The mass carried forward by a vortex, *Phil. Mag.* (ser. 6) **38** (1919) 597–612.

[416] W.M. Hicks, On the mutual threading of vortex rings, *Proc. R. Soc. London A* **102** (1922) 111–131.

[417] M.J.M. Hill, Some properties of the equations of hydrodynamics, *Quart. J. Pure Appl. Math.* **17** (1881) 1–20, 168–174.

[418] M.J.M. Hill, On some general equations which include the equations of hydrodynamics, *Trans. Cambr. Phil. Soc.* **14** (1883) 1–29.

[419] M.J.M. Hill, On the motion of fluid, part of which is moving rotationally and part irrotationally, *Proc. R. Soc. London* **36** (1883–1884) 276–284.

[420] M.J.M. Hill, On the motion of fluid, part of which is moving rotationally and part irrotationally, *Phil. Trans. R. Soc. London A* **175** (1884) 363–409.

[421] M.J.M. Hill, The differential equations of cylindrical and annular vortices, *Proc. Lond. Math. Soc.* **16** (1885) 171–183.

[422] M.J.M. Hill, On a spherical vortex, *Rep. Brit. Ass. Advmt Sci.* **63** (1893) 695–698.

[423] M.J.M. Hill, On a spherical vortex, *Phil. Trans. R. Soc. London A* **185** (1894) 213–245.

[424] E. Hogner, Über die Wirbeltheorie des Schraubenpropellers, *Ann. Phys.* (ser. 4) **87** (1928) 385–424.

- [425] S.W. Holman, *Matter, Energy, Force and Work* (Macmillan, New York, 1899).
- [426] S.G. Hooker, On the action of viscosity in increasing the spacing ratio of a vortex street, *Proc. R. Soc. London A* **154** (1936) 67–89.
- [427] B. Hopkinson, On discontinuous fluid motions involving sources and vortices, *Proc. Lond. Math. Soc.* **29** (1897) 142–164.
- [428] E. Hoppe, *Geschichte der Physik* (Vieweg, Braunschweig, 1926).
- [429] R.C.J. Howland, Vortex motion behind a circular cylinder, *J. R. Aeronaut. Soc.* **29** (1923) 189–195.
- [430] I. Imai, Sur la stabilité de la double file de tourbillons dans un canal rectiligne, *C. R. Acad. Sci. Paris* **202** (1936) 1908–1910. Abstract: *F. d. M.* **62** 973.
- [431] I. Imai, On the stability of a double row of vortices with unequal strengths in a channel of finite breadth, *Proc. Phys.-Math. Soc. Japan* (ser. 3), **18** (1936) 436–459. Abstract: *F. d. M.* **62** 973.
- [432] I. Imai, On the deformation of a free boundary due to line vortices, *Rep. Aeronaut. Res. Inst. Tokyo* **14** (1939) No 183 397–438. Abstract: *F. d. M.* **65** 982.
- [433] A. Indra, Studien über die Wirbelbewegungen, *Sber. Akad. Wiss. Wien* **110** (1901) Abh 2a 335–357.
- [434] G. Jaffé, Über zweidimensionale Flüssigkeitsströmung zwischen parallelen ebenen Wänden, *Ann. Phys.* (ser. 4), **61** (1920) 173–194. Abstract: *F. d. M.* **48** 1318.
- [435] H. Jeffreys, The wake in fluid flow past a solid, *Proc. R. Soc. London A* **128** (1930) 376–393. Abstract: *F. d. M.* **56** 710. *Sci. Abs. A* **34** No 331.
- [436] N.E. Joukovskii, Kinematics of fluid bodies. (Magister dissertation), *Mat. Sbor.* **8** (1876) No 1 1–79; No 2 163–238 (in Russian). Reprinted in: S.A. Chaplygin, A.I. Nekrasov, V.A. Arkhangelsky, V.P. Vetchinkin and A.P. Kotelnikov, eds, *Polnoe sobranie sochinenii. Tom II (Collected Papers. II. Hydrodynamics)* (ONTI NKTP SSSR, Moscow-Leningrad, 1935) 7–144, 145–148 (English summary). Reprinted in: M.V. Keldysh and S.A. Khristianovich, eds, *Sobranie sochinenii. Tom II (Complete Works. II. Hydrodynamics)* (GTTI, Moscow-Leningrad, 1949) 5–142. Abstract: *F. d. M.* **8** 610; **10** 638.
- [437] N.E. Joukovskii, Lectures on hydrodynamics, *Uchen. Zap. Imp. Moskov. Univ.* (1887) No 7 1–178 (in Russian). Reprinted in: *Trudy Tsentr. Aero-Gidrodin. Inst.* (1929) No 40 1–143. Reprinted in: S.A. Chaplygin, A.I. Nekrasov, V.A. Arkhangelsky, V.P. Vetchinkin and A.P. Kotelnikov, eds, *Polnoe sobranie sochinenii. Tom II. (Collected Papers. II. Hydrodynamics)* (ONTI NKTP SSSR, Moscow-Leningrad, 1935) 149–330, 331 (English summary). Reprinted in: M.V. Keldysh and S.A. Khristianovich, eds, *Sobranie sochinenii. Tom II (Complete Works. II. Hydrodynamics)* (GTTI, Moscow-Leningrad, 1949) 316–488.
- [438] N.E. Joukovskii, On flight theory, *Zh. Russ. Fiz.-Khim. Obshch.* **22** (1890) No 2 3–10; No 3 120–125 (in Russian). Reprinted in: A.P. Kotelnikov and V.P. Vetchinkin, eds, *Polnoe sobranie sochinenii. Tom VI (Collected Papers VI. Propellers. Windmills. Ventilators. Wind tunnels)* (ONTI NKTP SSSR, Moscow-Leningrad, 1937) 9–17, 18–19 (English summary). Reprinted in: V.P. Vetchinkin, V.V. Golubev, V.S. Pyshnov and B.N. Jouriev, eds, *Sobranie sochinenii. Tom IV (Complete Works. IV. Aerodynamics)* (GTTI, Moscow-Leningrad, 1949) 343–351. Abstract: *F. d. M.* **22** 959.
- [439] N.E. Joukovskii, [Helmholtz's] works on mechanics, in: A.G. Stoletov, ed., *Hermann von Helmholtz 1821–1891. Publichnye lekcii, chitannye v Imperatorskom Moskovskom universitete v pol'zu Helmholtzovskogo fonda (Hermann von Helmholtz 1821–1891. Public lectures delivered at the Imperior Moscow University for the Helmholtz fund)* (Moscow University Press, Moscow, 1892) 37–52 (in Russian). Reprinted in: A.P. Kotelnikov, ed., *Polnoe sobranie sochinenii. Tom IX (Collected Papers. IX. Mathematics. Astronomy. Reports. Lectures. Characteristics and biographies)* (ONTI NKTP SSSR, Moscow-Leningrad, 1937) 313–328. Reprinted in: V.V. Golubev and L.N. Sretenskii, eds, *Sobranie sochinenii. Tom VII (Complete Works. VII. Reports and addresses)* (GTTI, Moscow-Leningrad, 1950) 132–149.
- [440] N.E. Joukovskii, On the problem of cutting vortex filaments, *Mat. Sbor.* **17** (1895) No 4 702–719 (in Russian). Reprinted in: *Trudy Tsentr. Aero-Gidrodin. Inst.* (1931) No 95 20–34. Reprinted

in: S.A. Chaplygin, A.I. Nekrasov, V.A. Arhangelsky, V.P. Vetchinkin and A.P. Kotelnikov, eds, *Polnoe sobranie sochinenii. Tom III (Collected Papers. III. Hydrodynamics)* (ONTI NKTP SSSR, Moscow-Leningrad, 1936) 387–404, 405 (English summary). Reprinted in: M.V. Keldysh and S.A. Khristianovich, eds, *Sobranie sochinenii. Tom II (Complete Works. II. Hydrodynamics)* (GTTI, Moscow-Leningrad, 1949) 654–669. Abstract: *F. d. M.* **26** 877.

[441] N.E. Joukovskii, De la chute dans l'air de corps légers de forme allongée, animés d'un mouvement rotatoire, *Bull. Inst. Aérodyn. Koutchino* (1906) No 1 51–65. Reprinted in: A.P. Kotelnikov, ed., *Polnoe sobranie sochinenii. Tom V (Collected Papers. V. Vortices. Aerofoil theory. Aviation)* (ONTI NKTP SSSR, Moscow-Leningrad, 1937) 5, 82–98, 99 (English summary), 100–115 (Russian translation). Reprinted in: V.P. Vetchinkin, V.V. Golubev, V.S. Pyshnov and B.N. Jouriev, eds, *Sobranie sochinenii. Tom IV (Complete Works. IV. Aerodynamics)* (GTTI, Moscow-Leningrad, 1949) 51–68.

[442] N.E. Joukovskii, On annexed [bounded] vortices, *Trudy Otd. Fiz. Nauk. Mosk. Obshch. Lyub. Estest. Antr. Etn.* **13** (1907) No 2 12–25 (in Russian). Reprinted in: A.P. Kotelnikov, ed., *Polnoe sobranie sochinenii. Tom V (Collected Papers. V. Vortices. Aerofoil theory. Aviation)* (ONTI NKTP SSSR, Moscow-Leningrad, 1937) 48–69, 70–71 (English summary). Reprinted in: L.S. Leibenzon and S.A. Khristianovich, eds, *Izbrannye sochineniya (Selected Works)* (GTTI, Moscow-Leningrad, 1948) 2 97–114. Reprinted in: V.P. Vetchinkin, V.V. Golubev, V.S. Pyshnov and B.N. Jouriev, eds, *Sobranie sochinenii. Tom IV (Complete Works. IV. Aerodynamics)* (GTTI, Moscow-Leningrad, 1949) 69–91. Abstract: *F. d. M.* **37** 762.

[443] N.E. Joukovskii, A note on the motion of vortex rings, *Mat. Sbor.* **26** (1907) No 2 483–490 (in Russian). Reprinted in: S.A. Chaplygin, A.I. Nekrasov, V.A. Arkhangelsky, V.P. Vetchinkin and A.P. Kotelnikov, eds, *Polnoe sobranie sochinenii. Tom III (Collected Papers. III. Hydrodynamics)* (ONTI NKTP SSSR, Moscow-Leningrad, 1936) 406–418, 419 (English summary). Reprinted in: M.V. Keldysh and S.A. Khristianovich, eds, *Sobranie sochinenii. Tom II (Complete Works. II. Hydrodynamics)* (GTTI, Moscow-Leningrad, 1949) 689–696. Abstract: *F. d. M.* **38** 743.

[444] N. Joukowsky, Über die Konturen der Tragflächen der Drachenflieger, *Z. Flugtech. Motorluftschiff.* **1** (1910) 281–284; **3** (1912) 81–86. Reprinted in: A.P. Kotelnikov, ed., *Polnoe sobranie sochinenii. Tom V (Collected Papers. V. Vortices. Aerofoil theory. Aviation)* (ONTI NKTP SSSR, Moscow-Leningrad, 1937) 204–231, 232–257 (Russian translation). Reprinted in: L.S. Leibenzon and S.A. Khristianovich, eds, *Izbrannye sochineniya (Selected Works)* (GTTI, Moscow-Leningrad, 1948) 2 115–135. Reprinted in: V.P. Vetchinkin, V.V. Golubev, V.S. Pyshnov and B.N. Jouriev, eds, *Sobranie sochinenii. Tom IV (Complete Works. IV. Aerodynamics)* (GTTI, Moscow-Leningrad, 1949) 92–116. Abstract: *F. d. M.* **42** 810.

[445] N. Joukowsky, Geometrische Untersuchungen über die Kutta'sche Strömung, *Trudy Otd. Fiz. Nauk. Mosk. Obshch. Lyub. Estest. Antr. Etn.* **15** (1911) No 1 10–22; **15** (1912) No 2 36–47. Reprinted in: A.P. Kotelnikov, ed., *Polnoe sobranie sochinenii. Tom V (Collected Papers. V. Vortices. Aerofoil theory. Aviation)* (ONTI NKTP SSSR, Moscow-Leningrad, 1937) 116–159, 160–162 (English summary), 163–203 (Russian translation). Reprinted in: L.S. Leibenzon and S.A. Khristianovich, eds, *Izbrannye sochineniya (Selected Works)* (GTTI, Moscow-Leningrad, 1948) 2 136–167. Reprinted in: V.P. Vetchinkin, V.V. Golubev, V.S. Pyshnov and B.N. Jouriev, eds, *Sobranie sochinenii. Tom IV (Complete Works. IV. Aerodynamics)* (GTTI, Moscow-Leningrad, 1949) 139–178. Abstract: *F. d. M.* **42** 810.

[446] N.E. Joukovskii, Determination of pressure by a two-dimensional flow on a contour, which in the limit reduces to a segment of a straight line, *Mat. Sbor.* **28** (1911) No 1 195–204 (in Russian). Reprinted in: A.P. Kotelnikov, ed., *Polnoe sobranie sochinenii. Tom V (Collected Papers. V. Vortices. Aerofoil theory. Aviation)* (ONTI NKTP SSSR, Moscow-Leningrad, 1937) 258–267, 268 (English summary). Reprinted in: V.P. Vetchinkin, V.V. Golubev, V.S. Pyshnov and B.N. Jouriev, eds, *Sobranie sochinenii. Tom IV (Complete Works. IV. Aerodynamics)* (GTTI, Moscow-Leningrad, 1949) 117–126. Abstract: *F. d. M.* **42** 824.

[447] N.E. Joukovskii, On the lifting planes of the “Antoinette” design, *Trudy Otd. Fiz. Nauk. Mosk. Obshch. Lyub. Estest. Antr. Etn.* **15** (1911) No 2 7–20 (in Russian). Reprinted in: A.P. Kotelnikov, ed., *Polnoe sobranie sochinenii. Tom V (Collected Papers. V. Vortices. Aerofoil theory. Aviation)* (ONTI NKTP SSSR, Moscow-Leningrad, 1937) 281–308, 309–310 (English summary), 311–339 (German translation). Reprinted in: L.S. Leibenzon and S.A. Khristianovich, eds, *Izbrannye sochineniya (Selected Works)* (GTTI, Moscow-Leningrad, 1948) **2** 168–189. Reprinted in: V.P. Vetchinkin, V.V. Golubev, V.S. Pyshnov and B.N. Jouriev, eds, *Sobranie sochinenii. Tom IV (Complete Works. IV. Aerodynamics)* (GTTI, Moscow-Leningrad, 1949) 176–206. Abstract: *F. d. M.* **42** 824; **48** 1448.

[448] N.E. Joukovskii, On snowdrifts, in: *Anniversary Volume for Professor G.K. Suslov* (Saint Vladimir University Press, Kiev, 1911) 357–366 (in Russian). Reprinted in: S.A. Chaplygin, A.I. Nekrasov, V.A. Arkhangelsky, V.P. Vetchinkin and A.P. Kotelnikov, eds, *Polnoe sobranie sochinenii. Tom III (Collected Papers. III. Hydrodynamics)* (ONTI NKTP SSSR, Moscow-Leningrad, 1936) 439–448, 449–450 (English summary). Reprinted in: G.N. Abramovich and L.S. Leibenzon, eds, *Sobranie sochinenii. Tom III (Complete Works. III. Hydraulics. Applied Mechanics)* (GTTI, Moscow-Leningrad, 1949) 214–223.

[449] N.E. Joukovskii, Vortex theory of screw propeller, I, *Trudy Otd. Fiz. Nauk Mosk. Obshch. Lyub. Estest. Antr. Etn.* **16** (1912) No 1 1–31 (in Russian). Reprinted in: A.P. Kotelnikov and V.P. Vetchinkin, eds, *Polnoe sobranie sochinenii. Tom VI (Collected Papers. VI. Propellers. Windmills. Ventilators. Wind tunnels)* (ONTI NKTP SSSR, Moscow-Leningrad, 1937) 75–127, 127–157 (appendix). Reprinted in: L.S. Leibenzon and S.A. Khristianovich, eds, *Izbrannye sochineniya (Selected Works)* (GTTI, Moscow-Leningrad, 1948) **2** 190–229. Reprinted in: V.P. Vetchinkin, V.V. Golubev, V.S. Pyshnov and B.N. Jouriev, eds, *Sobranie sochinenii. Tom IV (Complete Works. IV. Aerodynamics)* (GTTI, Moscow-Leningrad, 1949) 395–444. French translation in: *Théorie tourbillonnaire de l'hélice propulsive* (Gauthier-Villars, Paris, 1929) 1–47.

[450] N.E. Joukovskii, Vortex theory of screw propeller, II, *Trudy Otd. Fiz. Nauk Mosk. Obshch. Lyub. Estest. Antr. Etn.* **17** (1914) No 1 1–33 (in Russian). Reprinted in: A.P. Kotelnikov and V.P. Vetchinkin, eds, *Polnoe sobranie sochinenii. Tom VI (Collected Papers. VI. Propellers. Windmills. Ventilators. Wind tunnels)* (ONTI NKTP SSSR, Moscow-Leningrad, 1937) 158–219, 209–216 (appendix). Reprinted in: L.S. Leibenzon and S.A. Khristianovich, eds, *Izbrannye sochineniya (Selected Works)* (GTTI, Moscow-Leningrad, 1948) **2** 230–269. Reprinted in: V.P. Vetchinkin, V.V. Golubev, V.S. Pyshnov and B.N. Jouriev, eds, *Sobranie sochinenii. Tom IV (Complete Works. IV. Aerodynamics)* (GTTI, Moscow-Leningrad, 1949) 445–493. French translation in: *Théorie tourbillonnaire de l'hélice propulsive* (Gauthier-Villars, Paris, 1929) 48–93.

[451] N.E. Joukovskii, Professor Kármán’s vortex theory of drag, I, *Trudy Otd. Fiz. Nauk Mosk. Obshch. Lyub. Estest. Antr. Etn.* **17** (1914) No 1 48–61 (in Russian). Reprinted in: A.P. Kotelnikov, ed., *Polnoe sobranie sochinenii. Tom V (Collected Papers. V. Vortices. Aerofoil theory. Aviation)* (ONTI NKTP SSSR, Moscow-Leningrad, 1937) 406–427, 428–430 (English summary). Reprinted in: V.P. Vetchinkin, V.V. Golubev, V.S. Pyshnov and B.N. Jouriev, eds, *Sobranie sochinenii. Tom IV (Complete Works. IV. Aerodynamics)* (GTTI, Moscow-Leningrad, 1949) 271–292. Abstract: *F. d. M.* **48** 1145.

[452] N.E. Joukovskii, On the motion of water at the turn of a river, *Mat. Sbor.* **29** (1914) 192–219 (in Russian). Reprinted in: A.P. Kotelnikov, ed., *Polnoe sobranie sochinenii. Tom IV (Collected Papers. IV. Waves. Viscosity. Fluid reaction)* (ONTI NKTP SSSR, Moscow-Leningrad, 1937) 193–230, 231–233 (English summary). Reprinted in: G.N. Abramovich and L.S. Leibenzon, eds, *Sobranie sochinenii. Tom III (Complete Works. III. Hydraulics. Applied Mechanics)* (GTTI, Moscow-Leningrad, 1949) 160–183. Abstract: *F. d. M.* **48** 1448.

[453] N.E. Joukovskii, New scientific achievements in the theory of fluid resistance, *Dnevnik XIII S'ezda Russ. Estest. Vrach.* (1914) No 10 LI-LIX (in Russian). Reprinted in: A.P. Kotelnikov, ed., *Polnoe sobranie sochinenii. Tom IX (Collected Papers. IX. Mathematics. Astronomy. Reports. Lectures. Characteristics and biographies)* (ONTI NKTP SSSR, Moscow-Leningrad, 1937)

233–244. Reprinted in: V.V. Golubev and L.N. Sretenskii, eds, *Sobranie sochinenii. Tom VII (Complete Works. VII. Reports and addresses)* (GTTI, Moscow-Leningrad, 1950) 66–78.

[454] N.E. Joukovskii, Vortex theory of screw propeller, III, *Trudy Otd. Fiz. Nauk Mosk. Obshch. Lyub. Estest. Antr. Etn.* **17** (1915) No 2 1–23 (in Russian). Reprinted in: A.P. Kotelnikov and V.P. Vetchinkin, eds, *Polnoe sobranie sochinenii. Tom VI (Collected Papers. VI. Propellers. Windmills. Ventilators. Wind tunnels)* (ONTI NKTP SSSR, Moscow-Leningrad, 1937) 217–251, 251–253 (appendix). Reprinted in: L.S. Leibenzon and S.A. Khristianovich, eds, *Izbrannye sochineniya (Selected Works)* (GTTI, Moscow-Leningrad, 1948) **2** 270–297. Reprinted in: V.P. Vetchinkin, V.V. Golubev, V.S. Pyshnov and B.N. Jouriev, eds, *Sobranie sochinenii. Tom IV (Complete Works. IV. Aerodynamics)* (GTTI, Moscow-Leningrad, 1949) 494–528. French translation in: *Théorie tourbillonnaire de l'hélice propulsive* (Gauthier-Villars, Paris, 1929) 94–122.

[455] N. Joukowski, *Bases théoriques de l'aéronautique. Aérodynamique: Cours professé a l'École Impériale Technique de Moscou* (Gauthier-Villars, Paris, 1916).

[456] N.E. Joukovskii, Vortex theory of screw propeller, IV, *Trudy Avia Rasch.-Ispyt. Byuro* (1918) No 3 1–97 (in Russian). Reprinted in: A.P. Kotelnikov and V.P. Vetchinkin, eds, *Polnoe sobranie sochinenii. Tom VI (Collected Papers. VI. Propellers. Windmills. Ventilators. Wind tunnels)* (ONTI NKTP SSSR, Moscow-Leningrad, 1937) 254–331, 331–345 (appendix). Reprinted in: L.S. Leibenzon and S.A. Khristianovich, eds, *Izbrannye sochineniya (Selected Works)* (GTTI, Moscow-Leningrad, 1948) **2** 298–355. Reprinted in: V.P. Vetchinkin, V.V. Golubev, V.S. Pyshnov and B.N. Jouriev, eds, *Sobranie sochinenii. Tom IV (Complete Works. IV. Aerodynamics)* (GTTI, Moscow-Leningrad, 1949) 529–612. French translation in: *Théorie tourbillonnaire de l'hélice propulsive* (Gauthier-Villars, Paris, 1929) 123–198.

[457] N.E. Joukovskii, On snowdrifts and on silting of rivers, *Trudy Tsentr. Aero-Gidrodin. Inst.* (1919) No 1 1–26 (in Russian). Reprinted in: S.A. Chaplygin, A.I. Nekrasov, V.A. Arkhangelsky, V.P. Vetchinkin and A.P. Kotelnikov, eds, *Polnoe sobranie sochinenii. Tom III (Collected Papers. III. Hydrodynamics)* (ONTI NKTP SSSR, Moscow-Leningrad, 1936) 451–474, 475–477 (English summary). Reprinted in: G.N. Abramovich and L.S. Leibenzon, eds, *Sobranie sochinenii. Tom III (Complete Works. III. Hydraulics. Applied Mechanics)* (GTTI, Moscow-Leningrad, 1949) 224–245.

[458] N.E. Joukovskii, The vortex theory of drag, II, *Trudy Avia Rasch.-Ispyt. Byuro* (1919) No 8 1–11 (in Russian). Reprinted in: A.P. Kotelnikov, ed., *Polnoe sobranie sochinenii. Tom V (Collected Papers. V. Vortices. Aerofoil theory. Aviation)* (ONTI NKTP SSSR, Moscow-Leningrad, 1937) 473–478, 479–480 (English summary). Reprinted in: V.P. Vetchinkin, V.V. Golubev, V.S. Pyshnov and B.N. Jouriev, eds, *Sobranie sochinenii. Tom IV (Complete Works. IV. Aerodynamics)* (GTTI, Moscow-Leningrad, 1949) 293–298.

[459] N.E. Joukovskii, *Teoreticheskie osnovy vozdukhoplavaniya, chast' I (Theoretical Basis of Aeronautics. Part I)* 2nd edn (GIZ, Moscow, 1925). Reprinted in: V.P. Vetchinkin, ed., *Polnoe sobranie sochinenii. Tom I (Collected Papers. 1. Lectures)*, (ONTI NKTP SSSR, Moscow-Leningrad, 1938) 7–536. Reprinted in: V.P. Vetchinkin, V.S. Pyshnov, V.A. Semenov and B.N. Jouriev, eds, *Sobranie sochinenii. Tom VI (Complete Works. VI. Theoretical Basis of Aeronautics)* (GTTI, Moscow-Leningrad, 1950) 7–456.

[460] N.E. Joukovskii, Hydrodynamics, in: A.P. Kotelnikov, ed., *Polnoe sobranie sochinenii. Tom 7 (Collected Papers. Lectures. 7. Theory of attraction. Hydromechanics)*, (Oborongiz, Moscow-Leningrad, 1939) 169–199 (in Russian). Reprinted in: L.N. Sretenskii, ed., *Sobranie sochinenii. Tom V (Complete Works. V. Theoretical mechanics. Hydrostatics and hydrodynamics. Theory of attraction)*, (GTTI, Moscow-Leningrad, 1949) 837–874.

[461] B.N. Jouriev, *Vozdushnye vinty (Aerial Screws)* (Gosmashizdat, Moscow-Leningrad, 1933) (in Russian).

[462] B.N. Jouriev, *Experimental'naya aerodinamika. 1. Teoreticheskie osnovy experimental'noi aerodinamiki (Experimental Aerodynamics. Part I. Theoretical Foundations of Experimental Aerodynamics)* (ONTI, Moscow-Leningrad, 1936) (in Russian).

[463] B.N. Jouriev, *Experimental'naya aerodinamika. 2. Induktivnoe soprotivlenie (Experimental Aerodynamics. Part II. Inductive Drag)* (Oborongiz, Moscow-Leningrad, 1938) (in Russian).

[464] B.N. Jouriev, L.S. Leibenzon and V.P. Vetchinkin, N.E. Joukovsky (1847–1921), *Prikl. Mat. Mekh.* **11** (1947) 9–40.

[465] H. Kaden, Aufwicklung einer unstabilen Unstetigkeitsfläche, *Ing.-Arch.* **2** (1931) 140–168. Abstract: *F. d. M.* **57** 1135.

[466] G.V. Kamenkov, Vortex theory of drag, in: V. Alexandrov, ed., *III All-Union Conference on Aerodynamics. Part 2* (TsAGI, Moscow, 1935) 166–170 (in Russian). Reprinted in: *Izbrannye trudy (Selected works)* (Nauka, Moscow, 1971) **1** 213–222.

[467] Th.von Kármán, Über den Mechanismus des Widerstandes, den ein bewegter Körper in einer Flüssigkeit erfährt. 1. Teil, *Nachr. Ges. Wiss. Göttingen. Math.-Phys. Kl.* (1911) 509–517. Reprinted in: *Collected works of Theodore von Kármán* (Butterworth, London, 1956) **1** 324–330. Abstract: *F. d. M.* **42** 800.

[468] Th.von Kármán, Über den Mechanismus des Widerstandes, den ein bewegter Körper in einer Flüssigkeit erfährt. 2. Teil, *Nachr. Ges. Wiss. Göttingen. Math.-Phys. Kl.* (1912) 547–556. Reprinted in: *Collected works of Theodore von Kármán* (Butterworth, London, 1956) **1** 331–338. Abstract: *F. d. M.* **43** 854.

[469] Th. von Kármán, Turbulence and skin friction, *J. Aeronaut. Sci.* **1** (1934) 1–20.

[470] Th. von Kármán, *Aerodynamics. Selected Topics in the Light of their Historical Development* (Cornell University Press, Ithaca, 1954).

[471] Th. von Kármán, Lanchester's contributions to the theory of flight and operational research, *J. R. Aeronaut. Soc.* **62** (1958) 80–93.

[472] Th. von Kármán and J.M. Burgers, General aerodynamic theory: Perfect fluids, in: W. Durand, ed., *Aerodynamic Theory* (Springer, New York, 1934) **2** 1–367.

[473] Th. von Kármán and L. Edson, *The Wind and Beyond* (Little & Brown, Boston-Toronto, 1967).

[474] Th. von Kármán and H. Rubach, Über den Mechanismus des Flüssigkeits- und Luftwiderstandes, *Phys. Z.* **13** (1912) 49–59. Reprinted in: *Collected works of Theodore von Kármán* (Butterworth, London, 1956) **1** 339–358. Abstract: *F. d. M.* **43** 853.

[475] N.P. Kasterin, A resolution of F. Klein's hydrodynamical paradox, *Vest. Moskov. Univ.* (1949) No 10 45–52 (in Russian).

[476] N.P. Kasterin, A.K. Timiriazev and T.M. Sviridov, An experimental generation of an aerial vortex tube, *Vest. Moskov. Univ.* (1949) No 10 53–58 (in Russian).

[477] N.P. Kasterin, A.K. Timiriazev and T.M. Sviridov, Vortex hysteresis, *Vest. Moskov. Univ.* (1949) No 10 59–73 (in Russian).

[478] W. Kaufmann, *Angewandte Hydromechanik* (Springer, Berlin, 1931). Abstract: *F. d. M.* **58** 1299.

[479] W. Kaufmann, Die kinetische Energie der vor einem Wirbelpaar erzeugten Flüssigkeitsbewegung, *Sber. Bayer. Akad. Wiss.* **73** (1943) 295–306. Abstract: *Math. Rev.* **8** 103.

[480] W. Kaufmann, Über die Aufwicklung einer instabilen Wirbelschicht von endlicher Breite, *Sber. Bayer. Akad. Wiss.* **75** (1945) 109–130. Abstract: *Math. Rev.* **10** 756.

[481] W. Kaufmann, Die energetische Berechnung des induzierten Widerstandes, *Ing.-Arch.* **17** (1949) 187–192.

[482] W. Kaufmann, Der zeitliche Verlauf des Aufspulvorganges einer instabilen Unstetigkeitsfläche von eindlicher Breite, *Ing.-Arch.* **19** (1951) 1–11. Abstract: *Appl. Mech. Rev.* **4** No 4201. *Math. Rev.* **13** 82.

[483] W. Kaufmann, Über den Mechanismus den Wirbelkerne einer Kármánschen Wirbelstrasse, *Ing.-Arch.* **19** (1951) 192–199. Abstract: *Appl. Mech. Rev.* **4** No 4502. *Math. Rev.* **13** 293.

[484] E.M. Kelly, Maxwell's equations as properties of vortex sponge, *Am. J. Phys.* **31** (1963) 785–791.

[485] Kelvin, Lord, On the doctrine of discontinuity of fluid motion, in connection with the resistance against a solid moving through a fluid, *Nature* **50** (1894) 524–525, 549, 573–575, 597–598.

[486] Kelvin, Lord, Nineteenth century clouds over the dynamical theory of heat and light, *Proc. R. Instn Gt Brit.* **16** (1902) 363–397. Reprinted as Appendix B in: Lord Kelvin, *Baltimore Lectures on Molecular Dynamics and the Wave Theory of Light* (Clay and Sons, London, 1904) 486–527.

- [487] I.G. Khanovich, *Teoriya korablya (Theory of a Ship)* (Voenmorizdat, Moscow, 1938) (in Russian).
- [488] S.A. Khristianovich, S.A. Chaplygin on the lifting force of a wing, *Priroda* (1975) No 4 53–55 (in Russian).
- [489] O.D. Khvol'son, *Kurs fiziki (Course of Physics)* 5th edn (Grschebin, Berlin, 1923) (in Russian). French translation: O.D. Chwolson, *Traite de physique* (Hermann, Paris, 1908).
- [490] S. Kida, Motion of an elliptical vortex in a uniform shear flow, *J. Phys. Soc. Japan* **50** (1981) 3517–3520.
- [491] G. Kirchhoff, *Vorlesungen über mathematische Physik. Mechanik* (Teubner, Leipzig, 1876).
- [492] D. Kitao, Beitrag zur Theorie der Bewegung der Erdatmosphäre und der Wirbelstürme, I, *J. Coll. Sci. Imp. Univ. Tokyo* **1** (1887) 113–209.
- [493] D. Kitao, Beitrag zur Theorie der bewegung der Erdatmosphäre und der Wirbelstürme, II, *J. Coll. Sci. Imp. Univ. Tokyo* **2** (1889) 329–403.
- [494] D. Kitao, Beitrag zur Theorie der bewegung der Erdatmosphäre und der Wirbelstürme, III, *J. Coll. Sci. Imp. Univ. Tokyo* **7** (1895) 293–402.
- [495] F. Klein, Über die Bildung von Wirbel in reibungslosen Flüssigkeiten, *Z. Math. Phys.* **58** (1910) 259–262. Reprinted in: *Gesammelte mathematische Abhandlungen. 2. Anschauliche Geometrie, Substitutionsgruppen und Gleichungstheorie zur mathematischen Physik* (Springer, Berlin, 1922) 710–713.
- [496] F. Klein, *Vorlesungen über die Entwicklung der Mathematik im 19. Jahrhundert* (Springer, Berlin, 1926).
- [497] A. Kneschke, Über die Bewegung eines Wirbels um Quellen, Senken, Doppelquellen und feste Wirbel in der Halbebene, *Ann. Phys.* (ser. 5) **9** (1931) 905–915. Abstract: *F. d. M.* **57** 1106. *Sci. Abs.* **A34** No 3300.
- [498] A. Kneschke, Über die Bewegung von Wirbel in einem einseitig begrenzten Kanal, *Ann. Phys.* (ser. 5) **14** (1932) 655–666. Abstract: *F. d. M.* **58** 874. *Sci. Abs.* **A35** No 4741.
- [499] A. Kneschke, Über die Ruhelage von Wirbeln, *Z. Angew. Math. Mech.* **14** (1934) 178–183. Abstract: *F. d. M.* **60** 725.
- [500] A. Kneschke, Zur Theorie der Wirbelbewegung, *Z. Angew. Math. Mech.* **18** (1938) 343–346. Abstract: *F. d. M.* **64** 852.
- [501] A. Kneschke and S. Matthes, Wirbelbewegung um einem Kreiszylinder, *Ann. Phys.* (ser. 5) **9** (1931) 916–920. Abstract: *F. d. M.* **57** 1106. *Sci. Abs.* **A34** No 3301.
- [502] C.G. Knott, *Life and Scientific Work of Peter Guthrie Tait supplementing the Two Volumes of Scientific Papers published in 1898 and 1900* (Cambridge University Press, Cambridge, 1911).
- [503] N. Kochin, On the instability of von Kármán's vortex streets, *Dokl. Akad. Nauk SSSR* **24** (1939) No 1 18–22 (in Russian). Reprinted in: *Sobranie sochinenii (Collected Papers)* (Nauka, Moscow, 1958) **2** 479–485. English translation in: *C.R. (Doklady) Acad. Sci. URSS* **24** (1939) No 1 19–23. Abstract: *F. d. M.* **65** 981. *Math. Rev.* **2** 26. *Zentr. Mech.* **10** 228.
- [504] N.E. Kochin, I.A. Kibel' and N.W. Roze, *Teoreticheskaya gidromekhanika* 4th edn (Gostekhizdat, Moscow-Leningrad, 1948) (in Russian). English translation: *Theoretical Hydromechanics* (Interscience, London, 1964). German translation: *Theoretische Hydromechanik* (Akademie, Berlin, 1954). Abstract: *Math. Rev.* **17** 911.
- [505] N.E. Kochin and N.W. Roze, *Vvedenie v teoreticheskuyu gidromekhaniku (Introduction to Theoretical Hydromechanics)* (Gostekhizdat, Moscow-Leningrad, 1932) (in Russian).
- [506] N.E. Kochin and N.W. Roze, *Teoreticheskaya gidromekhanika (Theoretical Hydromechanics)* (GONTI, Leningrad-Moscow, 1938)
- [507] L. Koenigsberger, *Hermann von Helmholtz's Untersuchungen über die Grundlagen der Mathematik und Mechanik* (Teubner, Leipzig, 1896). Reprinted: (Sändig, Niederwalluf bei Wiesbaden, 1971). English translation: The investigations of Hermann von Helmholtz on the fundamental principles of mathematics and mechanics, *Smithsonian Institution Annual Report* **51** (1896) 93–123.

- [508] L. Koenigsberger, *Hermann von Helmholtz* (Vieweg & Sohn, Braunschweig, 1902). English abridged translation: *Hermann von Helmholtz* (Clarendon Press, Oxford, 1906). Reprinted: (Dover, New York, 1965).
- [509] W.A. Konstantinov, Über helikoidale Wirbel in Anwendung zur aerodynamischen Berechnung der Luftschauben und Windkraftmaschinen, *Dokl. Akad. Nauk SSSR* **28** (1940) 688–693. Abstract: *Math. Rev.* **2**, 170–171.
- [510] A.A. Kosmodemianskii, Contribution to the drag theory. III. On the vorticity drag, *Trudy Tsentr. Aero-Gidrodin. Inst.* (1935) No 216 1–19 (in Russian, English summary).
- [511] A.A. Kosmodemianskii, Eddy resistance of theoretical aerofoils, *Trudy Tsentr. Aero-Gidrodin. Inst.* (1937) No 317 1–58 (in Russian, English summary).
- [512] A. Kosmodemianskii, Some questions in the aerodynamical theory of resistance, *Uchen. Zap. Moskov. Gos. Univ.* (1940) No 46 39–83 (in Russian). Abstract: *F. d. M.* **66** 1387.
- [513] A.A. Kosmodemianskii, Founders of modern aeromechanics: N.E. Joukovskii and S.A. Chaplygin, *Uchen. Zap. Mosk. Gos. Univ.* (1947) No 91 105–128 (in Russian).
- [514] A.A. Kosmodemianskii, Life and work of V.V. Golubev, in: V.V. Golubev, *Trudy po aerodinamike (Papers on Aerodynamics)* (GITTL, Moscow-Leningrad, 1957) 945–970 (in Russian).
- [515] A.A. Kosmodemianskii, Vladimir Vasil'evich Golubev – his life and scientific work, in: A.A. Kosmodemianskii, *Ocherki po istorii mehaniki (Essays on the History of Mechanics)* (Prosveshchenie, Moscow, 1964) 385–408 (in Russian).
- [516] A.A. Kosmodemianskii, *Nikolai Egorovich Joukovskii (1847–1921)* (Nauka, Moscow, 1984) (in Russian).
- [517] A.A. Kosmodemianskii and Ya.E. Polonskii, Review of the scientific works of V.V. Golubev, *Prikl. Mat. Mech.* **19** (1955) 131–142 (in Russian).
- [518] G. Kötschau, Studien über Flüssigkeitsbewegungen, *Ann. Phys. Chem.* (ser. 3) **26** (1885) 530–546.
- [519] H. Kragh, The vortex atom: A Victorian theory of everything, *Centaurus* **44** (2002) 32–114.
- [520] L. Krüger, ed., *Universalgenie Helmholtz. Rückblick nach 100 Jahren* (Akademie, Berlin, 1994).
- [521] C.H. Krutzsch, Über eine experimentell beobachtete Erscheinung an Wirbelringen bei ihrer translatorischen Bewegung in wirklichen Flüssigkeiten, *Ann. Phys.* (ser. 5) **35** (1939) 497–523.
- [522] M.Z. von Krzywoblocki, Investigation of the wing-wake frequency with application of the Strouhal number, *J. Aeronaut. Sci.* **12** (1945) 51–62.
- [523] M.Z. von Krzywoblocki, Vortex streets in incompressible media, *Appl. Mech. Rev.* **6** (1953) 393–397.
- [524] W. Kucharski, Bewegung eines Wirbels in einem nach auß offenen Kreissektor, *Forsch. Geb. IngWes.* **A8** (1937) 14–20.
- [525] D. Küchemann, Report on the I.U.T.A.M. Symposium on concentrated vortex motions in fluids, *J. Fluid Mech.* **21** (1965) 1–20.
- [526] H. Kurzweg, Neue Untersuchungen über Entstehung der turbulenten Rohströmung, *Ann. Phys.* (ser. 5) **18** (1933) 193–216.
- [527] W.M. Kutta, Auftriebskräfte in strömenden Flüssigkeiten, *Ill. Aeronaut. Mitt.* **6** (1902) 133–135.
- [528] W.M. Kutta, Über eine mit den Grundlagen des Flugproblems in Beziehung stehende zweidimensionale Strömung, *Sber. Bayer. Akad. Wiss.* **40** (1910) No 2, 1–58. Abstract: *F. d. M.* **41** 830.
- [529] W.M. Kutta, Über ebene Zirkulationströmungen nebst flugtechnischen Anwendungen, *Sber. Bayer. Akad. Wiss.* **41** (1911) No 3 65–125. Abstract: *F. d. M.* **42** 825.
- [530] D.S. Kuznetsov, *Gidrodinamika (Hydrodynamics)* (Gidrometeoizdat, Moscow, 1948) (in Russian).
- [531] M. Lagally, Über die Bewegung einzelner Wirbel in einer strömenden Flüssigkeit, *Sber. Bayer. Akad. Wiss.* **44** (1914) 377–432. Abstract: *F. d. M.* **45** 1068.
- [532] M. Lagally, Zur Theorie der Wirbelschichten, *Sber. Bayer. Akad. Wiss.* **45** (1915) 79–107. Abstract: *F. d. M.* **45** 1070.
- [533] M. Lagally, Über ein Verfahren zur Transformation ebener Wirbelprobleme, *Math. Z.* **10** (1921) 231–239. Abstract: *F. d. M.* **45** 949.

- [534] M. Lagally, Über den Druck einer strömenden Flüssigkeit auf eine geschlossene Fläche, *Sber. Bayer. Akad. Wiss.* **51** (1921) 209–226.
- [535] M. Lagally, Ideale Flüssigkeiten. in: H. Geiger and K. Scheel, eds, *Handbuch der Physik* (Springer, Berlin, 1927) **7** 1–90.
- [536] M. Lagally, Bemerkungen zu vorstehender Note der Herren Bonder und Neumark, *Math. Z.* **32** (1930) 605–607. Abstract: *F. d. M.* **56** 706.
- [537] J.L. Lagrange, Mémoire sur la théorie du mouvement des fluides, *Nouv. Mem. Acad. Berlin* (1783) 151–198. Reprinted in: J.A. Serret, ed., *Œuvres de Lagrange* (Gauthier-Villars, Paris, 1867) **4** 695–748.
- [538] J.L. Lagrange, *Mécanique analytique* (Desaint, Paris, 1788).
- [539] H. Lamb, Note on a theorem in hydrodynamics, *Mess. Math.* **7** (1877) 41–42.
- [540] H. Lamb, *A Treatise on the Mathematical Theory of the Motion of Fluids* (Cambridge University Press, Cambridge, 1879).
- [541] H. Lamb, The motion of fluids, *Nature* **22** (1880) 145.
- [542] H. Lamb, *Hydrodynamics* 2nd edn (Cambridge University Press, Cambridge, 1895).
- [543] H. Lamb, *Hydrodynamics* 6th edn (Cambridge University Press, Cambridge, 1932).
- [544] A. Lampa, Über einen Versuch mit Wirbelringen, *Sber. Akad. Wiss. Wien* **112** (1903) Abh 2a 606–614.
- [545] F.W. Lanchester, *Aerodynamics. Constituting the first volume of a complete Work on Aerial Flight* (Constable & Co., London, 1907). German translation: *Aerodynamik; ein Gesamtwerk über das Fliegen* (Teubner, Leipzig-Berlin, 1909). French translation: *Aérodynamique* (Paris, Gauthier-Villars, 1914).
- [546] F.W. Lanchester, The flying machine: the aerofoil in the light of theory and experiment, *Proc. Inst. Automob. Eng.* **9** (1915) 171–259.
- [547] F.W. Lanchester, Sustentation in flight, *J. R. Aeronaut. Soc.* **30** (1926) 587–606.
- [548] F.W. Lanchester, The part played by skin friction in aeronautics, *J. R. Aeronaut. Soc.* **41** (1937) 68–113, 113–131 (discussion).
- [549] L. Landweber, Flow about a pair of adjacent, parallel cylinders normal to a stream. Theoretical analysis, *Rep. David Taylor Model Basin* (1942) No 485 1–27.
- [550] J. Larmor, *Aether and Matter* (Cambridge University Press, Cambridge, 1900).
- [551] J. Larmor, Vortex spirals, *Nature* **66** (1902) 630. Abstract: *F. d. M.* **33** 780.
- [552] E. Laura, Sul moto parallelo ad un piano di un fluido in cui vi sono n vortici elementari, *Atti Accad. Sci. Torino. Cl. Sci. Fis. Mat. Nat.* **37** (1902) 469–476. Abstract: *F. d. M.* **33** 780.
- [553] E. Laura, Sulle equazioni differenziali canoniche del moto di un sistema di vortici elementari, rettilinei e paralleli, in un fluido incompressibile indefinito, *Atti Accad. Sci. Torino. Cl. Sci. Fis. Mat. Nat.* **40** (1905) 296–312. Abstract: *F. d. M.* **36** 799.
- [554] E. Laura, Questioni di stabilità relative al moto di n filetti vorticosi, *Atti Ist. Veneto Sci. Lett. Arti. Cl. Sci. Mat. Nat.* **92** (1933) Pt 2 387–398. Abstract: *F. d. M.* **59** 1451.
- [555] E. Laura, Sulle configurazioni rigide di quattro vortici elementari perpendicolari ad un piano, *Atti Ist. Véneto Sci. Lett. Arti. Cl. Sci. Mat. Nat.* **97** (1938) Pt 2 535–540. Abstract: *F. d. M.* **64** 1446. *Zentr. Math.* **23** 417. *Zentr. Mech.* **11** 33.
- [556] E. Laura, Sulla stabilità delle configurazioni rigide di quattro vortici rettilinei, *Atti Ist. Veneto Sci. Lett. Arti. Cl. Sci. Mat. Nat.* **97** (1938) Pt 2 813–818. Abstract: *F. d. M.* **65** 980. *Zentr. Math.* **23** 417. *Zentr. Mech.* **11** 33.
- [557] P.P. Lazarev, *Helmholtz* (Goskhimizdat, Moscow, 1925) (in Russian).
- [558] A.V. Lebedinskii, U.I. Frankfurt and A.M. Frenk, *Helmholtz* (Nauka, Moscow, 1966) (in Russian).
- [559] L. Lecornu, Sur les mouvements giratoires des fluides, *C. R. Acad. Sci. Paris* **106** (1888) 1654–1657.
- [560] L. Lecornu, Sur les tourbillons d'une veine fluide, *C. R. Acad. Sci. Paris* **168** (1919) 923–926.
- [561] L.S. Leibenzon, *Nikolai Egorovich Joukovskii* (AN SSSR, Moscow-Leningrad, 1947) (in Russian).
- [562] Leonardo da Vinci, *Del moto e misura dell'acqua* (Zanichelli, Bologna, 1923).

- [563] J. Letzmann, Experimentelle Untersuchungen an Wasserwirbeln, *Beitr. Geophys.* **17** (1927) 40–85.
- [564] J. Letzmann, Über die Einflüsse positiver und negativer Beschleunigung auf ortsfest rotierende Flüssigkeitssäulen, *Beitr. Geophys.* **25** (1930) 360–413.
- [565] J. Letzmann, Experimentelle Untersuchungen an Luftwirbeln, *Beitr. Geophys.* **33** (1931) 130–172. Abstract: *Sci. Abs. A***35** No 753.
- [566] J. Letzmann, Zur Kinematik und Dynamik stabiler Luftwirbeln, *Beitr. Geophys.* **39** (1933) 167–205.
- [567] T. Levi-Civita, Sulle azioni meccaniche dovute ad un flusso filiforme di elettricità, *Atti Accad. Naz. Lincei. Rend. Cl. Sci. Fis. Mat. Nat.* (ser. 5) **18** (1909) 41–50. Abstract: *F. d. M.* **40** 938.
- [568] T. Levi-Civita, Attrazione Newtoniana dei tubi sottili e vortici filiformi, *Ann. Scu. Norm. Sup. Pisa* **1** (1932) 1–33, 229–250. Abstract: *F. d. M.* **58** 873.
- [569] T. Levi-Civita, Teoremi di unicità e di esistenza per le piccole oscillazioni di un filetto vorticoso prossimo alla forma circolare, *Atti Accad. Naz. Lincei. Rend. Cl. Sci. Fis. Mat. Nat.* (ser. 6) **15** (1932) 409–416. Abstract: *F. d. M.* **58** 874.
- [570] H. Levy, On the resistance experienced by a body moving in a fluid, *Proc. R. Soc. Edinb.* **35** (1915) 95–109.
- [571] H. Levy, From model to full scale in aeronautics, *Aeronaut. J.* **23** (1919) 326–345, 352–356 (discussion).
- [572] H. Levy, Growth of eddies in a viscous fluid, *Phil. Mag.* (ser. 7) **2** (1926) 844–851. Abstract: *F. d. M.* **52** 863.
- [573] H. Levy and A.G. Forsdyke, The stability of an infinite system of circular vortices, *Proc. R. Soc. London A***114** (1927) 594–604. Abstract: *Sci. Abs. A***30** No 1968.
- [574] H. Levy and A.G. Forsdyke, The vibrations of an infinite system of vortex rings, *Proc. R. Soc. London A***116** (1927) 352–379. Abstract: *Sci. Abs. A***31** No 14.
- [575] H. Levy and A.G. Forsdyke, The steady motion and stability of a helical vortex, *Proc. R. Soc. London A***120** (1928) 670–690. Abstract: *F. d. M.* **54** 902. *Sci. Abs. A***32** No 380.
- [576] H. Levy and S.G. Hooker, On the vortex system in the wake of a cylinder in a fluid, *Phil. Mag.* (ser. 7) **9** (1930) 489–502. Abstract: *F. d. M.* **56** 710. *Sci. Abs. A***32** No 380.
- [577] T.C. Lewis, On the images of vortices in a spherical vessel, *Quart. J. Pure Appl. Math.* **16** (1879) 338–347.
- [578] T.C. Lewis, Some cases of vortex motion, *Mess. Math.* **9** (1880) 93–95.
- [579] L. Lichtenstein, Über einige Existenzprobleme der Hydrodynamik homogener, unzusammendrückbarer, reibungloser Flüssigkeiten und die Helmholtzschen Wirbelsätze, *Math. Z.* (1925) **23** 89–154, 310–316.
- [580] L. Lichtenstein, *Grundlagen der Hydromechanik* (Springer, Berlin, 1929). Abstract: *F. d. M.* **55** 1124.
- [581] A. Liénard, Une généralisation du tourbillon sphérique de Hill, *C. R. Acad. Sci. Paris* **182** (1926) 202–204. Abstract: *F. d. M.* **52** 859.
- [582] G.M. Lilley, Vortices and turbulence, *Aeronaut. J.* **87** (1983) 371–393.
- [583] C.C. Lin, On the motion of vortices in two dimensions – I. Existence of the Kirchhoff-Routh function, *Proc. Nat. Acad. Sci. USA* **27** (1941) 570–575. Reprinted in: *Selected Papers of C.C. Lin* (World Scientific, Singapore, 1987) **1** 267–272. Abstract: *Math. Rev.* **3** 282. *Sci. Abs. A***45** No 708.
- [584] C.C. Lin, On the motion of vortices in two dimensions – II. Some further investigations on the Kirchhoff-Routh function, *Proc. Nat. Acad. Sci. USA* **27** (1941) 575–577. Reprinted in: *Selected Papers of C.C. Lin* (World Scientific, Singapore, 1987) **1** 273–275. Abstract: *Math. Rev.* **3** 282. *Sci. Abs. A***45** No 709.
- [585] C.C. Lin, *On the Motion of Vortices in Two Dimensions* (dissertation) (University of Toronto Press, Toronto, 1943). Abstract: *Math. Rev.* **4** 261.
- [586] D. Lindlay, *Degrees Kelvin. A tale of genius, invention, and tragedy* (Joseph Henry Press, Washington D.C., 2004).

[587] C.N.H. Lock, On the system of vortices generated by a circular cylinder in steady motion through a fluid, *Rep. Memo. Adv. Comm. Aeronaut.* (1925) No 986. Also: *Rep. Memo. Advis. Comm. Aeronaut.* (1925/26) 76–81. Also: *Phil. Mag.* (ser. 6) **50** (1925) 1083–1089.

[588] C.N.H. Lock, Aeroscrew theory; a paper delivered before the Fourth International Congress for Applied Mechanics, 1934. *Rep. Memo. Adv. Comm. Aeronaut.* (1936) No 1746. Also: *Tech. Rep. Adv. Comm. Aeronaut.* (1936) 343–353.

[589] O.J. Lodge, The stream-lines of moving vortex-rings, *Phil. Mag.* (ser. 5) **20** (1885) 67–70.

[590] O.J. Lodge, *The Aether of Space* (Harper & Brothers, New York-London, 1909).

[591] L.G. Loitsyanskii, *Mekhanika zhidkosti i gaza* (Mechanics of Fluid and Gas) (GITTL, Moscow, 1950) (in Russian). English translation: *Mechanics of Liquids and Gases* (Pergamon, Oxford, 1966).

[592] L.G. Loitsyanskii, Hydromechanics, in: B.A. Vvedenskii, ed., *Bol'shaya Sovetskaya Enciklopediya* (Large Soviet Encyclopedia) 2nd edn (Sovetskaya Enciklopediya, Moscow, 1952) **11** 311–318 (in Russian).

[593] H.A. Lorentz, Hydrodynamische vraagstukken, *Ing. Grav.* **30** (1915) 206–217. English translation: Hydrodynamical problems, in: *Collected Papers* (Nijhoff, Den Haag, 1934) **7** 1–34.

[594] H. Lorenz, *Technische Hydromechanik* (Oldenbourg, München, 1910).

[595] A.E.H. Love, On recent English researches in vortex motion, *Math. Ann.* **30** (1887) 326–344.

[596] A.E.H. Love, Vortex motion in certain triangles, *Am. J. Math.* **11** (1889) 158–171. Abstract: *F. d. M.* **20** 982.

[597] A.E.H. Love, On the stability of certain vortex motions, *Proc. Lond. Math. Soc.* **25** (1894) 18–42. Abstract: *F. d. M.* **25** 1467.

[598] A.E.H. Love, On the motion of paired vortices with a common axis, *Proc. Lond. Math. Soc.* **25** (1894) 185–194. Abstract: *F. d. M.* **25** 1468.

[599] A.E.H. Love, Note on elliptic cylindrical vortices, *Quart. J. Pure Appl. Math.* **27** (1895) 89–92. Abstract: *F. d. M.* **25** 1467.

[600] A.E.H. Love, Hydrodynamik: Physikalische Grundlegung, in: F. Klein and C. Müller, eds, *Encyklopädie der mathematischen Wissenschaften* (Teubner, Leipzig, 1901) **IV/3** No 15 48–83.

[601] A.E.H. Love, Hydrodynamik: Theoretische Ausführungen, in: F. Klein and C. Müller, eds, *Encyklopädie der mathematischen Wissenschaften* (Teubner, Leipzig, 1901) **IV/3** No 16 84–147.

[602] A.E.H. Love, Hydrodynamique, in: J. Molk and P. Appell, eds, *Encyclopédie des sciences mathématiques* (Gauthier-Villars – Teubner, Paris-Leipzig, 1913) **IV/5** No 17 61–101.

[603] A.E.H. Love, Développements d'hydrodynamique, in: J. Molk and P. Appell, eds, *Encyclopédie des sciences mathématiques* (Gauthier-Villars – Teubner, Paris-Leipzig, 1913) **IV/5** No 18 102–208.

[604] A.R. Low, Review of airscrew theories, *J. R. Aeronaut. Soc.* **27** (1923) 38–59, 60–72 (discussion).

[605] A.R. Low, Review of airscrew theories, *J. R. Aeronaut. Soc.* **29** (1925) 100–104, 141–144 (discussion).

[606] H. Lügt, *Vortex Flow in Nature and Technology* (Wiley, New York, 1983).

[607] A.M. Lukomskaia, *Bibliograficheskie istochniki po matematike i mehanike, izdannye v SSSR za 1917–1952 gg.* (Bibliographical sources in mathematics and mechanics issued in the USSR, 1917–1952) (AN SSSR, Moscow-Leningrad, 1957) (in Russian).

[608] K. Mack, Experimentelle Beiträge zum Studium der Wirbelbewegungen in den Wolken, *Met. Z.* **15** (1898) 281–298.

[609] K. Mack, Experimentelle Untersuchung gewisser Strömungsgebilde in Flüssigkeiten, *Ann. Phys. Chem.* (new ser.) **68** (1899) 183–195.

[610] G. Magnus, Über die Abweichung der Geschosse, *Ann. Phys. Chem.* **53** (1853) 1–28.

[611] F. Magyar, Das Wirbelsystem der ebenen turbulenten Strömung, *Z. Angew. Math. Mech.* **12** (1932) 157–163. Abstract: *F. d. M.* **58** 887.

[612] A. Mallock, On the resistance of air, *Proc. R. Soc. London A* **79** (1907) 262–273. Abstract: *F. d. M.* **38** 732.

- [613] A. Mallock, Influence of viscosity on the stability of the flow of fluids, *Proc. R. Soc. London A* **84** (1910–1911) 482–491.
- [614] M. Margules, Über discrete Wirbelfäden, *Sber. Akad. Wiss. Wien* **81** (1880) Abh 2a 810–819.
- [615] A. Masotti, Traslazione uniforme di un cilindro rotondo in un canale a sponde piane parallele, *Atti Accad. Naz. Lincei. Rend. Cl. Sci. Fis. Mat. Nat. (ser. 6)* **4** (1926) 359–363. Abstract: *F. d. M.* **52** 856.
- [616] A. Masotti, Osservazioni sui moti di un fluido nei quali è stazionaria la distribuzione del vortice, *Atti Accad. Naz. Lincei. Rend. Cl. Sci. Fis. Mat. Nat. (ser. 6)* **5** (1927) 224–228. Abstract: *F. d. M.* **53** 788.
- [617] A. Masotti, Sopra una forma delle equazioni dinamiche di un sistema di vortici rettilinei, *Atti Accad. Naz. Lincei. Rend. Cl. Sci. Fis. Mat. Nat. (ser. 6)* **8** (1928) 300–301. Abstract: *F. d. M.* **54** 903.
- [618] A. Masotti, Sulle azioni dinamiche in un sistema di vortici rettilinei, *Atti Accad. Naz. Lincei. Rend. Cl. Sci. Fis. Mat. Nat. (ser. 6)* **9** (1929) 301–304. Abstract: *F. d. M.* **55** 1132. *Sci. Abs.* **A32** No 2342.
- [619] A. Masotti, Vortice rettilineo in un canale a sponde piane parallele, *Atti Accad. Naz. Lincei. Rend. Cl. Sci. Fis. Mat. Nat. (ser. 6)* **12** (1930) 321–327. Abstract: *F. d. M.* **56** 1252. *Sci. Abs.* **A34** No 1070.
- [620] A. Masotti, Sul moto di un vortice rettilineo, *Atti Accad. Pontif. Nuovi Lincei* **84** (1931) 235–245. Abstract: *F. d. M.* **57** 1108. *Sci. Abs.* **A34** No 2910.
- [621] A. Masotti, Sopra una proprietà energetica del moto di un vortice rettilineo, *Atti Accad. Pontif. Nuovi Lincei* **84** (1931) 464–467. Abstract: *F. d. M.* **57** 1108. *Sci. Abs.* **A34** No 3677.
- [622] A. Masotti, Sulle una relazione di reciprocità nella idrodinamica, *Atti Accad. Pontif. Nuovi Lincei* **84** (1931) 468–478. Abstract: *F. d. M.* **57** 1109. *Sci. Abs.* **A34** No 3678.
- [623] A. Masotti, Sulle azioni dinamiche dovute ad un vortice rettilineo, *Atti Accad. Pontif. Nuovi Lincei* **84** (1931) 623–631. Abstract: *F. d. M.* **57** 1109.
- [624] A. Masotti, Sul moto dei vortici-sorgenti. *Rend. Ist. Lomb. Sci. Lett. (ser. 2)* **66** (1933) 386–398. Abstract: *F. d. M.* **59** 761.
- [625] A. Masotti, Sul moto piano indotto da una sorgente addossata ad una lamina rettilinea indefinita, *Atti Accad. Pontif. Nuovi Lincei* **87** (1934) 494–501. Abstract: *F. d. M.* **60** 1381.
- [626] A. Masotti, Moto piani in presenza di particolari sistemi di vortici-sorgenti, *Atti Accad. Naz. Lincei. Rend. Cl. Sci. Fis. Mat. Nat. (ser. 6)* **22** (1935) 429–432. Abstract: *F. d. M.* **61** 912.
- [627] A. Masotti, Sui moti piani provocati da due vortici-sorgenti, *Atti Accad. Naz. Lincei. Rend. Cl. Sci. Fis. Mat. Nat. (ser. 6)* **23** (1936) 133–138. Abstract: *F. d. M.* **62** 970. *Sci. Abs.* **A39** No 3012.
- [628] A. Masotti, Sul moto di un vortice nel campo esterno ad una parete parabolica, *Rend. Ist. Lomb. Sci. Lett. (ser. 2)* **70** (1937) 137–147. Abstract: *F. d. M.* **63** 773.
- [629] G.D. Mattioli, Sui moti permanenti rotazionali i cui vortici sono rettilinei e paralleli alla velocità, *Atti Ist. Veneto Sci. Lett. Arti. Cl. Sci. Mat. Nat.* **88** (1929) Pt 2 411–419. Abstract: *F. d. M.* **55** 1132.
- [630] A.W. Maue, Zur Stabilität der Kármánschen Wirbelstraße, *Z. Angew. Math. Mech.* **20** (1940) 129–137. Abstract: *F. d. M.* **66** 1074. *Math. Rev.* **2** 170. *Zentr. Math.* **24** 137. *Zentr. Mech.* **11** 33.
- [631] J.C. Maxwell, Manuscript on the steady motion of an incompressible fluid, in: P.M. Harman, ed., *The Scientific Letters and Papers of James Clerk Maxwell* (Cambridge University Press, Cambridge, 1990) **1** 295–299.
- [632] J.C. Maxwell, Letter to William Thomson, 15 May 1855, in: P.M. Harman, ed., *The Scientific Letters and Papers of James Clerk Maxwell* (Cambridge University Press, Cambridge, 1990) **1** 309–313.
- [633] J.C. Maxwell, On physical lines of force. Part I. The theory of molecular vortices applied to magnetic phenomena, *Phil. Mag. (ser. 4)* **21** (1861) 161–175. Reprinted in: W.D. Niven, ed., *The Scientific Papers of James Clerk Maxwell* (Cambridge University Press, Cambridge, 1890) **1** 451–466. German translation in: L. Boltzmann, ed., *Ueber physikalische Kraftlinien* (Engelmann, Leipzig, 1898).
- [634] J.C. Maxwell, On physical lines of force. Part II. The theory of molecular vortices applied to electric currents, *Phil. Mag.* **21** (1861) 281–291, 338–348. Reprinted in: W.D. Niven, ed., *The*

Scientific Papers of James Clerk Maxwell (Cambridge University Press, Cambridge, 1890) **1** 467–488. German translation in: L. Boltzmann, ed., *Ueber physikalische Kraftlinien* (Engelmann, Leipzig, 1898).

[635] J.C. Maxwell, On physical lines of force. Part III. The theory of molecular vortices applied to statical electricity, *Phil. Mag.* (ser. 4) **23** (1862) 12–24. Reprinted in: W.D. Niven, ed., *The Scientific Papers of James Clerk Maxwell* (Cambridge University Press, Cambridge, 1890) **1** 489–502. German translation in: L. Boltzmann, ed., *Ueber physikalische Kraftlinien* (Engelmann, Leipzig, 1898).

[636] J.C. Maxwell, On physical lines of force. Part IV. The theory of molecular vortices applied to the action of magnetism on polarized light, *Phil. Mag.* (ser. 4) **23** (1862) 85–95. Reprinted in: W.D. Niven, ed., *The Scientific Papers of James Clerk Maxwell* (Cambridge University Press, Cambridge, 1890) **1** 503–513. German translation in: L. Boltzmann, ed., *Ueber physikalische Kraftlinien* (Engelmann, Leipzig, 1898).

[637] J.C. Maxwell, Manuscript fragments on the stability of fluid motion [a question set for the Cambridge Mathematical Tripos in 1866], in: P.M. Harman, ed., *The Scientific Letters and Papers of James Clerk Maxwell* (Cambridge University Press, Cambridge, 1995) **2** 241–244.

[638] J.C. Maxwell, Letter to Peter Guthrie Tait, 13 November 1867, in: P.M. Harman, ed., *The Scientific Letters and Papers of James Clerk Maxwell* (Cambridge University Press, Cambridge, 1995) **2** 392–393.

[639] J.C. Maxwell, Address to the Mathematical and Physical Sections of the British Association, *Rep. Brit. Ass. Advmt Sci.* **40** (1870) 1–9. Reprinted in: W.D. Niven, ed., *The Scientific Papers of James Clerk Maxwell* (Cambridge University Press, Cambridge, 1890) **2** 215–230.

[640] J.C. Maxwell, Faraday [Michael Faraday, born September 22, 1791, died August 25, 1867], *Nature* **8** (1873) 397–399. Reprinted in: W.D. Niven, ed., *The Scientific Papers of James Clerk Maxwell* (Cambridge University Press, Cambridge, 1890) **2** 355–360.

[641] J.C. Maxwell, Hermann Ludwig Ferdinand Helmholtz, *Nature* **15** (1877) 389–391. Reprinted in: W.D. Niven, ed., *The Scientific Papers of James Clerk Maxwell* (Cambridge University Press, Cambridge, 1890) **2** 592–598.

[642] J.C. Maxwell, Atom, in: *Encyclopædia Britannica* 9th edn (London, 1878) **3** 36–48. Reprinted in: W.D. Niven, ed., *The Scientific Papers of James Clerk Maxwell* (Cambridge University Press, Cambridge, 1890) **2** 445–484.

[643] A.M. Mayer, A note on experiments with floating magnets; showing the motions and arrangements in a plane of freely moving bodies, acted on by forces of attraction and repulsion; and serving in the study of the directions and motions of lines of magnetic force, *Am. J. Sci.* (ser. 3) **15** (1878) 276–277. Also: *Phil. Mag.* (ser. 5) **5** (1878) 397–398.

[644] A.M. Mayer, Floating magnets, *Nature* **17** (1878) 487–488.

[645] A.M. Mayer, Note on floating magnets, *Am. J. Sci.* (ser. 3) **15** (1878) 477–478.

[646] A.M. Mayer, Experiments with floating and suspended magnets, illustrating the action of atomic forces, molecular structure of matter, allotropy, isomerism, and the kinetic theory of gases, *Scient. Am. Suppl.* **40** (1878) 2045–2047.

[647] A.M. Mayer, Floating magnets, *Nature* **18** (1878) 258–260.

[648] A.M. Mayer, On the morphological laws of the configuration formed by magnets floating vertically and subjected to the attraction of a superposed magnet; with notes on some of the phenomena in molecular structure which these experiments may serve to explain and illustrate, *Am. J. Sci.* (ser. 3) **16** (1878) 247–256. Also: *Phil. Mag.* (ser. 5) **7** (1879) 98–108.

[649] R. Mazet, Sur l’écoulement permanent avec tourbillons isolés, *C. R. Acad. Sci. Paris* **191** (1930) 600–602. Abstract: *F. d. M.* **56** 707. *Sci. Abs.* **A34** No 702.

[650] R. Mazet, Sur la stabilité de certains tourbillons isolés, *C. R. Acad. Sci. Paris* **191** (1930) 832–834. Abstract: *F. d. M.* **56** 707. *Sci. Abs.* **A34** No 1071.

[651] R. McCormach, *Night Thoughts of a Classical Physicist* (Harvard University Press, Cambridge, MA, 1982).

- [652] J.G. McKendrick, *Hermann Ludwig Ferdinand von Helmholtz* (Longmans, Green & Co, New York, 1899).
- [653] V.V. Meleshko and G.J.F. van Heijst, On Chaplygin's investigations of two-dimensional vortex structures in an inviscid fluid, *J. Fluid Mech.* **272** (1994) 157–182.
- [654] V.V. Meleshko and G.J.F. van Heijst, Interacting two-dimensional vortex structures: Point vortices, contour kinematics and stirring properties, in: H. Aref and M.S. El Naschie, eds, *Chaos Applied to Fluid Mixing* (Oxford, Pergamon, 1994) 233–267.
- [655] L.M. Milne-Thomson, *Theoretical Hydrodynamics* (Macmillan, London, 1938). Abstract: *Appl. Mech. Rev.* **3** No 1972.
- [656] L.M. Milne-Thomson, *Theoretical Aerodynamics* 2nd edn (Macmillan, London, 1952). Abstract: *Appl. Mech. Rev.* **6** No 3127.
- [657] L.M. Milne-Thomson, Theory of the flow of incompressible inviscid fluids, *Appl. Mech. Rev.* **6** (1952) 105–107.
- [658] A.Ya. Milovich, *Osnovy gidromekhaniki. Gidrodinamika (Foundation of Fluid Mechanics. Hydrodynamics)* (Gosenergoizdat, Moscow-Leningrad, 1933) (in Russian).
- [659] A.Ya. Milovich, *Teoriya dinamicheskogo vzaimodeistviya tel i zhidkosti (Theory of the dynamical Interaction of Solids and Fluid)* (Gosenergoizdat, Moscow-Leningrad, 1940) (in Russian).
- [660] A.Ya. Milovich, *Osnovy gidromekhaniki (Foundation of Fluid Mechanics)* (Gosenergoizdat, Moscow-Leningrad, 1946) (in Russian).
- [661] R. von Mises, Über die Umströmung eines Hindernisses in idealer Flüssigkeit, *Z. Angew. Math. Mech.* **15** (1935) 71–76.
- [662] R. von Mises and K.O. Friedrichs, *Fluid Dynamics* (Brown University Press, Providence, 1942) Reprinted: (Springer, Berlin, 1971).
- [663] A. Miyadzu, Path and stability of a local vortex moving round a corner, *Phil. Mag. (ser. 7)* **16** (1933) 553–562.
- [664] A. Miyadzu, Path and stability of a local vortex moving round a corner. (Second paper), *Phil. Mag. (ser. 7)* **17** (1934) 1010–1023. Abstract: *Sci. Abs. A***37** No 1070.
- [665] A. Miyadzu, Path and stability of a local vortex moving round a corner. (Third paper), *Phil. Mag. (ser. 7)* **19** (1935) 644–660. Abstract: *Sci. Abs. A***38** No 1412.
- [666] A. Miyadzu, On the problem of a stationary vortex of a fluid passing the surface of an obtuse angle, *J. Soc. Appl. Mech. Japan* **4** (1951) 10–15. Abstract: *Appl. Mech. Rev.* **5** No 1117.
- [667] T. Mizota, M. Zdravkovich, K.-U. Graw and A. Leder, St Christopher and the vortex, *Nature* **404** (2000) 226.
- [668] D.W. Moore and P.G. Saffman, Structure of a line vortex in an imposed strain, in: J.H. Olsen, A. Goldburg and M. Rogers, eds, *Aircraft Wake Turbulence and its Detection*, (Plenum, New York, 1971) 339–354.
- [669] J.-J. Moreau, Sur deux théorèmes généraux de la dynamique d'un milieu incompressible illimité, *C. R. Acad. Sci. Paris* **226** (1948) 1420–1422.
- [670] W.B. Morton, On the motion near two straight parallel vortices, *Proc. R. Irish Acad. A***41** (1932) 1–7. Abstract: *F. d. M.* **58** 872. *Sci. Abs. A***35** No 4024.
- [671] W.B. Morton, On some permanent arrangements of parallel vortices and their points of relative rest, *Proc. R. Irish Acad. A***41** (1933) 94–101. Abstract: *F. d. M.* **59** 1451. *Sci. Abs. A***37** No 1838.
- [672] W.B. Morton, On the stability and oscillations of certain permanent arrangements of parallel vortices, *Proc. R. Irish Acad. A***42** (1934) 7–14. Abstract: *F. d. M.* **60** 725. *Sci. Abs. A***37** No 4426.
- [673] W.B. Morton, Vortex polygons, *Proc. R. Irish Acad. A***42** (1935) 21–29. Abstract: *F. d. M.* **61** 912.
- [674] W.B. Morton, Centred vortex polygons, *Proc. R. Irish Acad. A***43** (1937) 73–77. Abstract: *F. d. M.* **63** 774. *Sci. Abs. A***38** No 4099.
- [675] W.B. Morton, The paths of the particles in a vortex street, *Proc. R. Irish Acad. A***49** (1944) 289–292. Abstract: *Sci. Abs. A***38** No 1412. *Math. Rev.* **6** 136.
- [676] W. Müller, Wirbelschichten und Zirkulation, *Z. Tech. Phys.* **5** (1924) 450–458.

[677] W. Müller, Über den Einfluß von Wirbeln auf den Strömungsdruck an einem Kreiszylinder, *Z. Tech. Phys.* **8** (1927) 62–68. Abstract: *F. d. M.* **54** 903. *Sci. Abs.* **A30** No 1611.

[678] W. Müller, *Mathematische Strömungslehre* (Springer, Berlin, 1928). Abstract: *F. d. M.* **54** 888.

[679] W. Müller, Bewegung von Wirbeln in einer idealen Flüssigkeit unter dem Einfluß von ebenen Wänden, *Z. Angew. Math. Mech.* **10** (1930) 227–243. Abstract: *F. d. M.* **56** 1252. *Sci. Abs.* **A33** No 3620.

[680] M.M. Munk, On some vortex theorems of hydrodynamics, *J. Aeronaut. Sci.* **5** (1941) 90–96. Abstract: *Math. Rev.* **3** 219.

[681] M.M. Munk, On turbulent fluid motion, *J. Aeronaut. Sci.* **15** (1951) 442–446.

[682] M.M. Munk, On the mechanism of turbulent fluid motion, in: *Proceedings of the Second Midwestern Conference on Fluid Mechanics* (Ohio State University, Columbus, 1951) 19–33.

[683] M.M. Munk, Mechanism of turbulent fluid motion, *Aero Digest* **64** (1952) No 6 32–48.

[684] M.M. Munk, Aerodynamics, *Appl. Mech. Rev.* **8** (1955) 221–223.

[685] M.M. Munk, My early aerodynamic research – thoughts and memories, *Annu. Rev. Fluid Mech.* **13** (1981) 1–7.

[686] E.J. Nanson, Note on hydrodynamics, *Mess. Math.* **3** (1874) 120–121.

[687] E.J. Nanson, Note on hydrodynamics, *Mess. Math.* **7** (1878) 182–185.

[688] J.L. Nayler and R.A. Frazer, Vortex motion. Preliminary report upon an experimental method of investigating, by the aid of cinematographic photography, the history of eddying flow past a model immersed in water, *Rep. Memo. Advis. Comm. Aeronaut.* (1917) No 332. Also: *Tech. Rep. Advis. Comm. Aeronaut.* (1917/18) 18–25.

[689] A.I. Nekrasov, Diffusion of vortex, *Trudy Tsentr. Aero-Gidrodin. Inst.* (1931) No 84 1–27 (in Russian, English summary).

[690] P.K. Newton, *The N-vortex Problem: Analytical Techniques* (Springer, New York, 2001).

[691] H. Nisi and A.W. Porter, On eddies in air, *Phil. Mag.* (ser. 6) **46** (1923) 754–768.

[692] F. Noether, Zur statistischen Deutung der Kármánschen Ähnlichkeitshypothese in der Turbulenztheorie, *Z. Angew. Math. Mech.* **11** (1931) 224–231. Abstract: *F. d. M.* **57** 1112. *Sci. Abs.* **A34** No 3302.

[693] F. Noether, Dynamische Gesichtspunkte zu einer statistischen Turbulenztheorie, *Z. Angew. Math. Mech.* **13** (1933) 115–120. Abstract: *F. d. M.* **59** 769.

[694] O. Nomoto, Y. Sakagami and Y. Fujii, On the character of vortex “to stand perpendicularly on walls”, *Proc. Phys.-Math. Soc. Japan* (ser. 3) **16** (1934) 16–34. Abstract: *Sci. Abs.* **A37** No 965.

[695] E.F. Northrup, An experimental study of vortex motions in liquids, *J. Franklin Inst.* **172** (1911) 211–226, 345–368. Also: *Scient. Am. Suppl.* **74** (1912) 204–205, 215, 238–239, 248–249.

[696] E.F. Northrup, A photographic study of vortex rings in liquids, *Nature* **88** (1912) 463–468.

[697] E.A. Novikov, Dynamics and statistics of a system of vortices, *ZhETF* **68** (1975) 1868–1882. English translation in: *Soviet Phys.-JETP* **41** (1975) 937–943.

[698] A. Oberbeck, Ueber diskontinuierliche Flüssigkeitsbewegungen, *Ann. Phys. Chem.* (new ser.), **2** (1877) 1–17. Abstract: *F. d. M.* **9** 677.

[699] A. Oberbeck, Ueber die Bewegungen der Luft an der Erdoberfläche, *Ann. Phys. Chem.* (new ser.) **17** (1882) 128–148. Abstract: *F. d. M.* **14** 791.

[700] A.P. Ogloblin, *Osnovy gidromekhaniki (Foundations of Fluid Mechanics)* (Oborongiz, Moscow, 1940) (in Russian).

[701] L. Onsager, Statistical hydromechanics, *Nuovo Cimento* **6** (Suppl.) (1949) 279–287. Abstract: *Math. Rev.* **12** 60.

[702] I. Orlov, Scientific works of William Thomson (Kelvin), *Pod Znam. Marxisma* (1924) No 10/11 56–61 (in Russian).

[703] T. Otani, S. Kanzai, S. Fujijwhara and S. Syono, On the behaviour of two coupled vortices and velocity distribution within them, *Geophys. Mag.* **22** (1951) 289–310. Abstract: *Appl. Mech. Rev.* **5** No 560.

[704] H.M. Parker, A dissolving smoke-ring, *Science* **8** (1886) 36.

- [705] M. Pascal, Le ricerche aerodinamiche di Kutta e di Joukowski, *G. Mat. Battaglini* (ser. 3) **15** (1924) 111–214. Abstract: *F. d. M.* **50** 561.
- [706] M. Pascal, Traiettorie di vortici puntiformi, *Rend. Ist. Lomb. Sci. Lett.* (ser. 2) **58** (1925) 471–479. Abstract: *F. d. M.* **51** 662.
- [707] J. Patry, Instabilité d'une rangeé de tourbillons de long d'une paroi, *Helvet. Phys. Acta* **16** (1943) 83–90. Abstract: *Sci. Abs.* **A46** No 1885. *Math. Rev.* **6** 77.
- [708] A.N. Patrashev, *Gidromekhanika (Hydromechanics)* (Voenmorizdat, Moscow, 1953) (in Russian).
- [709] E. Paul, Bewegung eines Wirbels in geradlinig begrenzten Gebieten, *Z. Angew. Math. Mech.* **14** (1934) 105–116. Abstract: *F. d. M.* **60** 725.
- [710] E. Paul, Über die Bewegung eines Wirbels um eine Platte, *Z. Angew. Math. Mech.* **17** (1937) 186. Abstract: *F. d. M.* **63** 774.
- [711] G. Peretti, Vortici nei veli liquidi viscosi, *Atti Accad. Naz. Lincei. Rend. Cl. Sci. Fis. Mat. Nat.* (ser. 6) **29** (1939) 581–584. Abstract: *F. d. M.* **65** 984. *Zentr. Math.* **23** 417.
- [712] J. Perry, *Spinning Tops*, (Young & Co, New York, 1901). Reprinted: *Spinning Tops and Gyroscopic Motion* (Dover, New York, 1957).
- [713] G.I. Petrov, On the stability of vortex sheets, *Trudy Tsentr. Aero-Gidrodin. Inst.* (1937) No 304 1–23 (in Russian).
- [714] F. Pfeiffer, Theorien des Flüssigkeitswiderstandes. (Habilitationsvorlag), *Jahresber. Dt. Mat. Verein.* **22** (1913) 113–126. Abstract: *F. d. M.* **44** 863.
- [715] N.A.V. Piercy, On the vortex pair quickly formed by some aerofoils, *J. R. Aeronaut. Soc.* **27** (1923) 488–500.
- [716] N.A.V. Piercy, *Aerodynamics* (van Nostrand, New York, 1937).
- [717] M. Planck, *Einführung in die theoretische Physik. 2. Einführung in die Mechanik deformierbarer Körper* (Hirzel, Leipzig, 1919). English translation: *Introduction to Theoretical Physics. 2. The Mechanics of Deformable Bodies* (London, Macmillan, 1932).
- [718] H.C. Pocklington, The configuration of a pair of equal and opposite hollow straight vortices, of finite cross-section, moving steadily through fluid, *Proc. Camb. Phil. Soc.* **8** (1895) 178–187.
- [719] H.C. Pocklington, The complete system of the periods of a hollow vortex ring, *Phil. Trans. R. Soc. London A* **186** (1895) 603–619.
- [720] R.W. Pohl, *Einführung in die Mechanik und Akustik* (Springer, Berlin, 1930).
- [721] H. Poincaré, *Théorie des tourbillons* (Carré, Paris, 1893).
- [722] S.G. Popov, On the helical motions of an ideal fluid, *Vest. Moskov. Univ.* (1948) No 8 35–47 (in Russian). Abstract: *Appl. Mech. Rev.* **3** No 1305.
- [723] S.G. Popov, *Nekotorye zadachi i metody experimental'noi aeromekhaniki (Some problems and methods of experimental aeromechanics)* (GITTL, Moscow, 1952) (in Russian).
- [724] H. Poritsky, Vortices in fluid flow, *J. Math. Phys.* **21** (1942) 218–239. Abstract: *Math. Rev.* **4** 261. *Sci. Abs.* **A46** No 2154.
- [725] A.W. Porter, Models of atoms, *Nature* **74** (1906) 563–564.
- [726] C. Possio, Campo di velocità creato da un vortice in un fluido pesante e superficie libera in moto uniforme, *Atti Accad. Sci. Torino. Cl. Sci. Fis. Mat. Nat.* **76** (1941) 365–388.
- [727] J. Power, On the truth of the hydrodynamical theorem, that if $udx + vdy + wdz$ be a complete differential with respect to x, y, z at any one instant, it is always so, *Trans. Camb. Phil. Soc.* **7** (1842) 455–464.
- [728] L. Prandtl, Über Flüssigkeitsbewegung bei sehr kleiner Reibung, in: *Verhandlungen des III. Internationalen Mathematiker-Kongresses, Heidelberg, 1904* (Teubner, Leipzig, 1905) 484–491. Reprinted in: L. Prandtl and A. Betz, eds, *Vier Abhandlungen zur Hydrodynamik und Aerodynamik* (Institut für Strömungsforschung, Göttingen, 1927) 1–8. Reprinted in: W. Tollmien, H. Schlichting and H. Görtler, eds, *Gesammelte Abhandlungen zur angewandten Mechanik, Hydro- und Aerodynamik* (Springer, Berlin, 1961) 2 575–584. English translation: On the motion of fluids of very small viscosity, *NACA Tech. Memo.* (1928) No 452.
- [729] L. Prandtl, *Abriss der Lehre von der Flüssigkeits- und Gasbewegung* (Fischer, Jena, 1913).

[730] L. Prandtl, Flüssigkeitsbewegung, in: *Handwörterbuch der Naturwissenschaften* (Fischer, Jena, 1913) **4** 101–140. Reprinted in: W. Tollmien, H. Schlichting and H. Görtler, eds, *Gesammelte Abhandlungen zur angewandten Mechanik, Hydro- und Aerodynamik* (Springer, Berlin, 1961) **3** 1421–1485.

[731] L. Prandtl, Tragflügeltheorie. I. Mitteilung, *Nachr. Ges. Wiss. Göttingen. Math.-Phys. Kl.* (1918) 151–177. Reprinted in: L. Prandtl and A. Betz, eds, *Vier Abhandlungen zur Hydrodynamik und Aerodynamik* (Institut für Strömungsforschung, Göttingen, 1927) 9–35. Reprinted in: W. Tollmien, H. Schlichting and H. Görtler, eds, *Gesammelte Abhandlungen zur angewandten Mechanik, Hydro- und Aerodynamik* (Springer, Berlin, 1961) **1** 322–345. English translation: Theory of lifting surfaces. Part I, *NACA Tech. Notes* (1920) No 9.

[732] L. Prandtl, Tragflügeltheorie. II. Mitteilung, *Nachr. Ges. Wiss. Göttingen. Math.-Phys. Kl.* (1919) 107–137. Reprinted in: L. Prandtl and A. Betz, eds, *Vier Abhandlungen zur Hydrodynamik und Aerodynamik* (Institut für Strömungsforschung, Göttingen, 1927) 36–65. Reprinted in: W. Tollmien, H. Schlichting and H. Görtler, eds, *Gesammelte Abhandlungen zur angewandten Mechanik, Hydro- und Aerodynamik* (Springer, Berlin, 1961) **1** 346–372. English translation: Theory of lifting surfaces. Part II, *NACA Tech. Notes* (1920) No 10.

[733] L. Prandtl, Tragflächen-Auftrieb und -Widerstand in der Theorie, *Jahrb. Wiss. Ges. Luftf.* **5** (1920) 37–65. Reprinted in: W. Tollmien, H. Schlichting and H. Görtler, eds, *Gesammelte Abhandlungen zur angewandten Mechanik, Hydro- und Aerodynamik* (Springer, Berlin, 1961) **1** 377–406.

[734] L. Prandtl, Applications of modern hydrodynamics to aeronautics, *NACA Tech. Rep.* (1921) No 116 7–61. Reprinted in: W. Tollmien, H. Schlichting and H. Görtler, eds, *Gesammelte Abhandlungen zur angewandten Mechanik, Hydro- und Aerodynamik* (Springer, Berlin, 1961) **1** 433–515.

[735] L. Prandtl, Die neueren Fortschritte der flugtechnischen Strömungslehre, *Z. VDI* **65** (1921) 959–965. Reprinted in: W. Tollmien, H. Schlichting and H. Görtler, eds, *Gesammelte Abhandlungen zur angewandten Mechanik, Hydro- und Aerodynamik* (Springer, Berlin, 1961) **1** 407–424.

[736] L. Prandtl, Über die Entstehung von Wirbeln in der idealen Flüssigkeit, mit Anwendung auf die Tragflügeltheorie und andere Aufgaben, in: T. von Kármán and T. Levi-Civita, eds, *Vorträge aus dem Gebiete der Hydro- und Aerodynamik. Innsbruck 1922* (Springer, Berlin, 1924) 18–33. Reprinted in: W. Tollmien, H. Schlichting and H. Görtler, eds, *Gesammelte Abhandlungen zur angewandten Mechanik, Hydro- und Aerodynamik* (Springer, Berlin, 1961) **2** 692–713.

[737] L. Prandtl, Magnus effect and Windkraftschiff, *Naturwissenschaften* **13** (1925) 93–108. Reprinted in: W. Tollmien, H. Schlichting and H. Görtler, eds, *Gesammelte Abhandlungen zur angewandten Mechanik, Hydro- und Aerodynamik* (Springer, Berlin, 1961) **3** 1503–1530.

[738] L. Prandtl, The generation of vortices in fluids of small viscosity, *J. R. Aeronaut. Soc.* **31** (1927) 718–741. Also: *Engineering* **123** (1927) 627–628. Also: *NACA Tech. Memo.* (1928) No 452. Reprinted in: W. Tollmien, H. Schlichting and H. Görtler, eds, *Gesammelte Abhandlungen zur angewandten Mechanik, Hydro- und Aerodynamik* (Springer, Berlin, 1961) **2** 752–777. German translation: Die Entstehung von Wirbeln in einer Flüssigkeit mit kleiner Reibung, *Z. Flugtech. Motorluftschiff* **18** (1927) 489–496. Abstract: *Sci. Abs. A30* No 2439.

[739] L. Prandtl, *Abriß der Strömungslehre* (Vieweg und Sohn, Braunschweig, 1931).

[740] L. Prandtl, *Führer durch die Strömungslehre* (Vieweg, Braunschweig, 1942). English translation of 3rd edition (1949): *Essentials in Fluid Dynamics: with Applications to Hydraulics, Meteorology and other Subjects* (Blackie, London, 1952).

[741] L. Prandtl and O. Tietjens, Kinematographische Strömungsbilder, *Naturwissenschaften* **13** (1925) 1050–1053. Reprinted in: W. Tollmien, H. Schlichting and H. Görtler, eds, *Gesammelte Abhandlungen zur angewandten Mechanik, Hydro- und Aerodynamik* (Springer, Berlin, 1961) **3** 1531–1537. English translation: Cinematographic flow pictures, *NACA Tech. Memo.* (1926) No 364.

[742] L. Prandtl and O. Tietjens, *Hydro- und Aeromechanik nach Vorlesungen von L. Prandtl. I. Gleichgewicht und reibunglose Bewegung* (Springer, Berlin, 1929). English translation:

Fundamentals of Hydro- and Aeromechanics: based on lectures of L. Prandtl (McGraw-Hill, New York-London, 1934). Reprinted: (Dover, New York, 1957).

[743] L. Prandtl and O. Tietjens, *Hydro- und Aeromechanik nach Vorlesungen von L. Prandtl. II. Bewegung reibender Flüssigkeiten und technische Anwendungen* (Springer, Berlin, 1931). English translation: *Applied Hydro- and Aeromechanics: based on lectures of L. Prandtl* (McGraw-Hill, New York-London, 1934). Reprinted: (Dover, New York, 1957).

[744] S.T. Preston, On the physical aspects of the vortex-atom theory, *Nature* **22** (1880) 56–59.

[745] A. Pröll, *Grundlagen der Aeromechanik und Flugmechanik* (Springer, Wien, 1951).

[746] G.F. Proskura, *Gidrodinamika turbomashin (Hydrodynamics of turbines)* 2nd edn (Mashiz, Kiev, 1954) (in Russian).

[747] L.A. Protasova, On life and activity of V.V. Golubev (an autobiography with comments), in: K.A. Rybnikov and I.A. Tyulina, eds, *Istoriya i metodologiya estestvennykh nauk (History and Methodology of Natural Sciences)* (Moscow University Press, Moscow, 1986) No 32 218–227 (in Russian).

[748] L.A. Protasova, The formation of Soviet educational literature on wing theory, in: K.A. Rybnikov and I.A. Tyulina, eds, *Istoriya i metodologiya estestvennykh nauk (History and Methodology of Natural Sciences)* (Moscow University Press, Moscow, 1986) No 36 166–177 (in Russian).

[749] L.A. Protasova and I.A. Tyulina, *Vladimir Vasil'evich Golubev* (Moscow University Press, Moscow, 1986) (in Russian).

[750] G. Quincke, Ueber Wirbelbewegung bei Flüssigkeitsströmungen und staubfreie Räume, *Verh. Naturh.-med. Ver. Heidelb.* **4** (1892) 468–474.

[751] G. Quincke, Ueber Wirbelbewegung der Luft, *Verh. Naturh.-med. Ver. Heidelb.* **5** (1897) 226–227.

[752] N. Quint, *De wervelbeweging* (dissertation) (van Heteren, Amsterdam, 1888). Abstract: *F. d. M.* **20** 979.

[753] A.S. Ramsay, *A Treatise of Hydromechanics. Part II. Hydrodynamics* (Bell, London, 1913).

[754] W.J.M. Rankine, On the mechanical action of heat, *Trans. R. Soc. Edinb.* **20** (1850) 158–164.

[755] W.J.M. Rankine, *A Manual of Applied Mechanics* (Griffin, London, 1858).

[756] W.J.M. Rankine, On the thermal energy of molecular vortices, *Phil. Mag.* (ser. 4) **39** (1870) 211–221.

[757] M. Ray, Stability of a circular vortex, *Bull. Calcutta Math. Soc.* **27** (1935) 45–54.

[758] Rayleigh, Lord, On the irregular flight of a tennis-ball, *Mess. Math.* **7** (1877) 14–16. Reprinted in: *Scientific Papers by John William Strutt, Baron Rayleigh* (Cambridge University Press, Cambridge, 1899) **I** 344–346.

[759] Rayleigh, Lord, Fluid motions, *Proc. R. Instn Gt Brit.* **21** (1914) 70–83. Also: *Nature* **93** (1914) 364–365. Reprinted in: *Scientific Papers by John William Strutt, Baron Rayleigh* (Cambridge University Press, Cambridge, 1920) **VI** 237–249.

[760] Rayleigh, Lord, Æolian tones, *Phil. Mag.* (ser. 6) **29** (1915) 433–444. Reprinted in: *Scientific Papers by John William Strutt, Baron Rayleigh* (Cambridge University Press, Cambridge, 1920) **VI** 315–325.

[761] Rayleigh, Lord, The travelling cyclone, *Phil. Mag.* (ser. 6) **38** (1919) 420–424. Reprinted in: *Scientific Papers by John William Strutt, Baron Rayleigh* (Cambridge University Press, Cambridge, 1920) **VI** 654–658.

[762] R. Reiff, Ueber Wirbelbewegungen reibender Flüssigkeiten, *Mitt. math.-naturwiss. Ver. Württemberg* **5** (1892) 33–51.

[763] H. Reissner, Stationärer Bewegungszustand einer schraubenförmigen Wirbelfläche, *Jahresber. Dt. Mat. Verein.* **31** (1922) 30–34.

[764] H. Reissner, On the vortex theory of the screw propeller, *J. Aeronaut. Sci.* **5** (1937) 1–7.

[765] E.F. Relf, On the sound emitted by wires of circular section when exposed to an air current, *Phil. Mag.* (ser. 6) **42** (1921) 173–176.

[766] E.F. Relf and E. Ower, The singing of circular and streamline wires, *Rep. Memo. Advis. Comm. Aeronaut.* (1921) No 825. Also: *Tech. Rep. Advis. Comm. Aeronaut.* (1922/23) 56–59.

[767] E.F. Relf and L.F.G. Simmons, The frequency of the eddies generated by the motion of circular cylinders through a fluid, *Rep. Memo. Advis. Comm. Aeronaut.* (1924) No 917. Also: *Tech. Rep. Advis. Comm. Aeronaut.* (1924/25) 658–660. Also: *Phil. Mag.* (ser. 7) **49** (1925) 509–513.

[768] E. Reusch, Ueber Ringbildung in Flüssigkeiten, *Ann. Phys. Chem.* (ser. 2) **110** (1860) 309–316.

[769] O. Reynolds, On the action of rain to calm the sea, *Nature* **11** (1875) 279–280. Reprinted in: *Papers on Mechanical and Physical Subjects* (Cambridge University Press, Cambridge, 1900) **1** 86–88.

[770] O. Reynolds, On the resistance encountered by vortex rings and the relation between vortex rings and the stream-lines of a disc, *Nature* **14** (1876) 477–479.

[771] O. Reynolds, On vortex motion, *Proc. R. Instn Gt Brit.* **8** (1877) 272–279. Also: *Popul. Sci. Rev.* **16** (1877) 276–284. Also: *Scient. Am. Suppl.* **3** (1877) 1353–1354. Reprinted in: *Papers on Mechanical and Physical Subjects* (Cambridge University Press, Cambridge, 1900) **1** 184–191.

[772] O. Reynolds, Vortex motion in fluids, *Nature* **15** (1877) 347.

[773] O. Reynolds, The motion of fluids. [*A Treatise on the Mathematical Theory of the Motion of Fluids*. By Horace Lamb, M.A., formerly Fellow and Assistant Tutor of Trinity College, Cambridge; Professor of Mathematics in the University of Adelaide. (Cambridge University Press, 1879)], *Nature* **21** (1880) 342–344.

[774] O. Reynolds, Vortex rings. [*The Motion of Vortex Rings*. By J.J. Thomson (London: Macmillan and Co., 1883)], *Nature* **29** (1883) 193–195.

[775] O. Reynolds, On the two manners of motion of water, *Proc. R. Instn Gt Brit.* **11** (1884) 44–52. Reprinted in: *Papers on Mechanical and Physical Subjects* (Cambridge University Press, Cambridge, 1900) **2** 153–162.

[776] O. Reynolds, Study of fluid motion by means of coloured bands, *Proc. R. Instn Gt Brit.* **14** (1893) 129–138. Also: *Nature* **50** (1894) 161–164. Reprinted in: *Papers on Mechanical and Physical Subjects* (Cambridge University Press, Cambridge, 1900) **1** 524–534.

[777] O. Reynolds, Flow of water shown by colour bands, *Nature* **58** (1898) 467–468.

[778] D. Riabouchinsky, Sur les mouvements plans des fluides autour de solides avec tourbillons, *Assoc. Fran. l'Advanc. Sci.* **45** (1921) 154–158.

[779] D. Riabouchinsky, Sur quelques cas des mouvements plans des fluides autour de solides avec tourbillons, *C. R. Acad. Sci. Paris* **174** (1921) 1224–1227.

[780] D. Riabouchinsky, Sur les équations du mouvement à deux dimensions de solides dans un liquide avec tourbillons, *C. R. Acad. Sci. Paris* **175** (1921) 442–445.

[781] D. Riabouchinsky, Sur les équations du mouvement à deux dimensions de solides dans un liquide avec tourbillons, *C. R. Acad. Sci. Paris* **175** (1922) 442–445.

[782] D. Riabouchinsky, Thirty years of research in fluid mechanics, *J. R. Aeronaut. Soc.* **39** (1935) 292–348, 377–444.

[783] D. Riabouchinsky, Contribution à l'étude des hélices, *Publ. Scient. Tech. Minist. Air* (1938) No 18.

[784] R.L. Ricca, Rediscovery of Da Rios equations, *Nature* **352** (1991) 561–562.

[785] R.L. Ricca, The contributions of Da Rios and Levi-Civita to asymptotic potential theory and vortex filament dynamics, *Fluid Dyn. Res.* **18** (1996) 245–268.

[786] G.J. Richards, An experimental investigation of the wake behind an elliptic cylinder, *Rep. Memo. Advis. Comm. Aeronaut.* (1933) No 1590. Also: *Tech. Rep. Advis. Comm. Aeronaut.* (1934/35) 387–392. Also: *Phil. Trans. R. Soc. London A* **233** (1934) 279–301.

[787] E.G. Richardson, Recent model experiments in aerodynamics, *J. R. Aeronaut. Soc.* **31** (1927) 810–839, 839–843 (discussion).

[788] E. Riecke, Beiträge zur Hydrodynamik, *Nachr. Ges. Wiss. Göttingen. Math.-Phys. Kl.* (1888) 347–357. Also: *Ann. Phys. Chem.* (new ser.) **36** (1889) 322–334.

[789] W.B. Rogers, On the formation of rotating rings by air and liquids under certain conditions of discharge, *Am. J. Sci.* (ser. 2) **26** (1858) 246–258.

[790] V.L. Rosenberg, Some experiments on vortex motion, *Zh. Russ. Fiz.-Khim. Obshch.* **21** (1889) 21–22 (in Russian).

[791] F. Rosenberger, *Die Geschichte der Physik. 3. Geschichte der Physik in den letzten hundert Jahren* (Vieweg, Braunschweig, 1890).

[792] L. Rosenhead, Sur les tourbillons alternés de Bénard-Kármán dans un canal de largeur finie, *C. R. Acad. Sci. Paris* **189** (1929) 397–398. Abstract: *Sci. Abs.* **A33** No 449.

[793] L. Rosenhead, Double row of vortices with arbitrary stagger, *Proc. Camb. Phil. Soc.* **25** (1929) 132–138. Abstract: *Sci. Abs.* **A32**, No 2344.

[794] L. Rosenhead, Systems of double rows of line vortices in a channel of finite breadth with the axis of the row is parallel to the axis of the channel, *Proc. Camb. Phil. Soc.* **25** (1929) 277–281. Abstract: *F. d. M.* **55** 475. *Sci. Abs.* **A33** No 867.

[795] L. Rosenhead, The Kármán street of vortices in a channel of finite breadth, *Phil. Trans. R. Soc. London* **A228** (1929) 275–329.

[796] L. Rosenhead, The spread of vorticity in the wake behind a cylinder, *Proc. R. Soc. London* **A127** (1930) 590–612. Abstract: *Sci. Abs.* **A33** No 3623.

[797] L. Rosenhead, An experimental investigation of the flow behind circular cylinders in channels of different breadths, *Proc. R. Soc. London* **A129** (1930) 115–135. Abstract: *Sci. Abs.* **A34** No 332.

[798] L. Rosenhead, The effect of wind tunnel interference on the characteristic of an aerofoil, *Proc. R. Soc. London* **A129** (1930) 135–146.

[799] L. Rosenhead, The formation of vortices from a surface of discontinuity, *Proc. R. Soc. London* **A134** (1931) 170–192. Abstract: *F. d. M.* **57** 1109. *Sci. Abs.* **A35** No 1077.

[800] L. Rosenhead, Note on the eddy system in the wake of flat circular plates in three dimensional flow, *Rep. Memo. Advis. Comm. Aeronaut.* (1932) No 1358 (Appendix). Also: *Tech. Rep. Advis. Comm. Aeronaut.* (1931/32) 209–211.

[801] L. Rosenhead, Vortex systems in wakes, *Adv. Appl. Mech.* **3** (1953) 85–195.

[802] A. Roshko, On the development of turbulent wakes from vortex streets, *NACA Tech. Notes* (1953) No 2913.

[803] A. Roshko, On the drag and shedding frequency of two-dimensional bluff bodies, *NACA Tech. Notes* (1954) No 3169.

[804] A. Roshko, On the wake and drag of bluff bodies, *J. Aeronaut. Sci.* **22** (1954) 124–132.

[805] J. Rossignol, Problème touchant des tourbillons cylindriques de section finie, *C. R. Acad. Sci. Paris* **193** (1931) 700–703. Abstract: *F. d. M.* **57** 1110. *Sci. Abs.* **A35** No 677.

[806] J. Rossignol, Recherche de la forme d'équilibre de deux tourbillons cylindriques de densité uniforme et de section finie en rotation uniforme l'un par rapport à l'autre dans un fluide non visqueux, *Publ. Scient. Tech. Minist. Air* (1936) No 109. Abstract: *F. d. M.* **63** 1352. *Zentr. Mech. 7* 321.

[807] N. Rott, Vortex drift: A historical survey, in: K.-Y. Fung, ed., *Symposium on Aerodynamics & Aeroacoustics. Tuscon, Arizona, March 1-2, 1993* (World Scientific, Singapore, 1993) 173–186.

[808] H. Rouse, *Fluid Mechanics for Hydraulic Engineers* (McGraw-Hill, New York, 1938).

[809] H. Rouse and S. Ince, *History of Hydraulics* (Dover, New York, 1963).

[810] E.J. Routh, Some applications of conjugate functions, *Proc. Lond. Math. Soc.* **12** (1881) 73–89.

[811] H.A. Rowland, On the motion of a perfect incompressible fluid when no solid bodies are present, *Am. J. Math.* **3** (1880) 226–268.

[812] M. Roy, Stationnarité et stabilisation de tourbillons rectilignes en écoulement plan, *C. R. Acad. Sci. Paris* **A274** (1972) 1659–1662.

[813] S.K. Roy, Motion of a local vortex round a disturbed corner, *Proc. Benares Math. Soc.* **3** (1941) 71–93. Abstract: *Math. Rev.* **5** 135.

[814] H.L. Rubach, *Ueber die Entstehung und Fortbewegung des Wirbelpaars hinter zylindrischen Körpern* (dissertation), (Göttingen, 1914).

[815] H.L. Rubach, Ueber die Entstehung und Fortbewegung des Wirbelpaars hinter zylindrischen Körpern, *Forsch. Geb. IngWes.* (1916) No 185 1–35.

[816] A.W. Rücker, The physical work of von Helmholtz, *Nature* **51** (1895) 472–475, 493–495.

[817] D.E. Rutherford and J. Caldwell, On Oberbeck's vortices, *Phil. Mag. (ser. 7)* **12** (1931) 1190–1191.

[818] C. Sadron, État actuel des recherches expérimentales sur les anneaux de tourbillons dans les gaz, *Publ. Scient. Tech. Minist. Air* (1933) No 22.

[819] M. Sakuki and H. Arakawa, Mechanism of vortex motion behind an elliptic cylinder, *Proc. Phys.-Math. Soc. Japan* (ser. 3) **13** (1931) 201–207. Abstract: *Sci. Abs.* A**34** No 4065.

[820] A.A. Satkevitch, *Aerodinamika kak teoreticheskaya osnova aviatsii* (Aerodynamics as the Theoretical Basis of Aerial Flight) (Institute of Ways of Communication Press, Petrograd, 1923) (in Russian).

[821] A.A. Satkevitch, A critical study of Prandtl's theory of a finite wing and an inductive drag theory, *Sb. Inst. Inzh. Put. Soobshch.* (1926) No 93 1–25 (in Russian).

[822] A.A. Satkevitch, Method for derivation of a velocity field in vortex flow, *Sb. Inst. Inzh. Put. Soobshch.* (1927) No 96 183–200 (in Russian).

[823] A.A. Satkevitch, Fundamental principles of aerodynamics, re-examined in connection with the varying density of gases, *Sb. Inst. Inzh. Put. Soobshch.* (1927) No 98 49–71 (in Russian, English summary).

[824] A.A. Satkevitch, Calculation of velocities in a plane vortex flow, *Sb. Inst. Inzh. Put. Soobshch.* (1928) No 98 25–44 (in Russian).

[825] A.A. Satkevitch, Distribution of velocities within a circular vortex, *Sb. Inst. Inzh. Put. Soobshch.* (1931) No 100 435–451 (in Russian, English summary).

[826] A.A. Satkevitch, *Teoreticheskie osnovy gidro-aerodinamiki. 1. Kinematika zhidkikh tel* (Theoretical Basis of Hydro-Aerodynamics. 1. Kinematics of Fluids) (Vozdukhoflot, Leningrad, 1932) (in Russian).

[827] A.A. Satkevitch, The vortex problem in hydrodynamics and the organization of the vortical department of the hydraulic laboratory of Leningrad Institute of Water Transport Engineers, *Trudy Leningr. Inst. Inzh. Vodn. Transp.* (1933) No 2 5–22 (in Russian).

[828] A.A. Satkevitch, General analysis of a vortex flow, *Zap. Gos. Gidrolog. Inst.* **9** (1933) 1–16 (in Russian).

[829] A.A. Satkevitch, Natural coordinates in hydrodynamics, *Zap. Gos. Gidrolog. Inst.* **1** (1933) 1–79 (in Russian, French summary).

[830] A.A. Satkevitch, *Teoreticheskie osnovy gidro-aerodinamiki. 2. Dinamika zhidkikh tel* (Theoretical Basis of Hydro-Aerodynamics. 2. Dynamics of Fluids) (ONTI, Leningrad, 1934) (in Russian).

[831] C. Schaefer, *Einführung in die theoretische Physik. 1 Mechanik materieller Punkte, Mechanik starrer Körper und Mechanik der Kontinua (Elastizität und Hydrodynamik)* 2nd edn (de Gruyter, Berlin-Leipzig, 1922).

[832] L. Schiller, Neue quantitative Versuche zur Turbulenzentstehung, *Z. Angew. Math. Mech.* **14** (1934) 36–45.

[833] K. Schlayer, Über die Stabilität der Kármánschen Wirbelstraße gegenüber beliebigen Störungen in drei Dimensionen, *Z. Angew. Math. Mech.* **8** (1928) 352–372. Abstract: *Sci. Abs.* A**32** No 672.

[834] H. Schlichting, *Grenzschicht-Theorie* (Braun, Karlsruhe, 1951).

[835] H. Schlichting, *Boundary-Layer Theory* 7th edn (McGraw-Hill, New York, 1979).

[836] H. Schlichting and K. Gersten, *Grenzschicht-Theorie* 9th edn (Springer, Berlin-Heidelberg, 1997).

[837] F.G. Schmidt, Application of conformal mapping to a study of rectilinear vortex motion in a bounded fluid, *Uchen. Zap. Saratov. Gos. Univ.* **2** (1924) 96–110 (in Russian).

[838] C. Schmieden, Zur Theorie der Kármánschen Wirbelstraße, *Ing.-Arch.* **7** (1936) 215–221, 337–341. Abstract: *F. d. M.* **62** 973.

[839] C. Schmieden, Über Tragflügelströmungen mit Wirbelablösung, *Luftfahrtforschung* **17** (1940) 37–46. Abstract: *Math. Rev.* **2** 171.

[840] A. Schuster, *The Progress of Physics during 33 years (1875–1908)* (Cambridge University Press, Cambridge, 1911). Reprinted: (Arno Press, New York, 1975).

[841] P. Schwarz, Sur le mouvement des tourbillons de Bénard-Kármán dans un canal rectiligne, *C. R. Acad. Sci. Paris* **202** (1936) 629–631.

[842] P. Schwarz, Sur le permanence des tourbillons alternés dans un canal rectiligne, *C. R. Acad. Sci. Paris* **202** (1936) 824–826.

[843] P. Schwarz, Sur les tourbillons de Bénard-Kármán derrière un obstacle, en mouvement dans un canal rectiligne, *C. R. Acad. Sci. Paris* **202** (1936) 1021–1024.

- [844] P. Schwarz, Recherches sur les tourbillons alternés, *Publ. Scient. Tech. Minist. Air* (1936) No 100. Abstract: *F. d. M.* **63** 1353.
- [845] N.M. Semenova, N.M. Koptelova and I.V. Syuganova, *N.E. Joukovskii. Bibliografiya pechatnykh trudov (N.E. Joukovskii. A bibliography of published works)* (TsAGI, Moscow, 1968) (in Russian).
- [846] N.M. Semenova, N.M. Koptelova and I.V. Syuganova, *S.A. Chaplygin. Bibliografiya pechatnykh trudov (S.A. Chaplygin. A bibliography of published works)* (TsAGI, Moscow, 1968) (in Russian).
- [847] N.R. Sen, On circular vortex rings of finite section in incompressible fluids, *Bull. Calcutta Math. Soc.* **13** (1922/23) 117–140.
- [848] N.R. Sen, On vortex rings of finite circular section in incompressible fluid, *Bull. Calcutta Math. Soc.* **14** (1923) 36–48.
- [849] N.R. Sen, On the stability of vortex rings of finite circular section in incompressible fluid, *Bull. Calcutta Math. Soc.* **15** (1923) 23–37.
- [850] B.R. Seth, Vortex motion in rectangular cylinders, *Proc. Ind. Acad. Sci. A***3** (1936) 435–441.
- [851] K. Shariff and A. Leonard, Vortex rings, *Annu. Rev. Fluid Mech.* **24** (1992) 235–279.
- [852] H.I. Sharlin, *Lord Kelvin, the dynamic Victorian* (Pennsylvania State University Press, University Park, 1979).
- [853] D.M. Siegel, Thomson, Maxwell, and the universal ether in Victorian physics, in: G.N. Cantor and M.J.S. Hodge, eds, *Conceptions of Ether. Studies in the History of Ether Theories 1740–1900* (Cambridge University Press, Cambridge, 1981), 239–268.
- [854] D.M. Siegel, Mechanical image and reality in Maxwell's electromagnetic theory, in: P.M. Harman, ed., *Wranglers and Physicists: Studies on Cambridge Physics in the Nineteenth Century* (Manchester University Press, Manchester, 1985) **1** 309–313.
- [855] R.H. Silliman, William Thomson: Smoke rings and nineteenth-century atomism, *Isis* **54** (1963) 461–474.
- [856] N. Simmons, Free stream-line flow past a vortex, *Quart. J. Math.* **10** (1938) 283–298. Abstract: *F. d. M.* **65** 983.
- [857] N. Simmons, Free stream-line flow past vortices and aerofoils, *Quart. J. Math.* **10** (1938) 299–312. Abstract: *F. d. M.* **65** 983.
- [858] L.F.G. Simmons and E. Ower, Note on the application of the vortex theory of aerofoils to the prediction of downwash, *Rep. Memo. Advis. Comm. Aeronaut.* (1924) No 914. Also: *Tech. Rep. Advis. Comm. Aeronaut.* (1924/25) 63–65.
- [859] L.F.G. Simmons and N.S. Dewey, Wind tunnel experiments with circular discs, *Rep. Memo. Advis. Comm. Aeronaut.* (1931) No. 1334. Also: *Tech. Rep. Advis. Comm. Aeronaut.* (1930/31), 227–232.
- [860] K.R. Singh, Path of a vortex round the rectangular bend of a channel with a uniform flow, *Z. Angew. Math. Mech.* **34** (1954) 432–435.
- [861] H.A.M. Snelders, A. M. Mayer's experiments with floating magnets and their use in the atomic theories of matter, *Ann. Sci.* **33** (1976) 67–80.
- [862] R.E. Soloveichik, On motion of vortices on a spherical surface, *Trudy Glav. Geofiz. Obs.* (1937) No 13 46–73 (in Russian).
- [863] G. Smirnov, *Rozhdennye vikhrej (Born by Vortex)* (Znanie, Moscow, 1982) (in Russian).
- [864] C. Smith and M.N. Wise, *Energy and Empire. A biographical study of Lord Kelvin* (Cambridge University Press, Cambridge, 1989).
- [865] J.H.B. Smith and R.W. Clark, Nonexistence of stationary vortices behind a two-dimensional normal plate, *AIAA J.* **13** (1975) 1114–1115.
- [866] A. Sommerfeld, *Vorlesungen über theoretische Physik. 2. Mechanik der deformierbaren Medien* (Becker & Erler, Leipzig, 1943). English translation: *Lectures on theoretical Physics, 2. Mechanics of deformable Bodies* (Academic Press, New York, 1950).
- [867] L. Sona, Sopra alcune configurazioni rigide di filamenti vorticosi perpendicolari a un piano, *Atti Accad. Naz. Lincei. Rend. Cl. Sci. Fis. Mat. Nat.* (ser. 6) **27** (1938) 80–85, 182–184.
- [868] L. Sona, Configurazioni rigide di tre vortici allineati e condizioni di stabilità, *Atti Ist. Veneto Sci. Lett. Arti. Cl. Sci. Mat. Nat.* **98** (1938) Pt 2, 11–26. Abstract: *F. d. M.* **65** 980. *Zentr. Math.* **24** 137. *Zentr. Mech.* **11** 76.

- [869] L. Sona, Sulla stabilità delle configurazioni rigide di tre vortici, *Atti Ist. Veneto Sci. Lett. Arti. Cl. Sci. Mat. Nat.* **100** (1940) Pt 2, 67–73. Abstract: *F. d. M.* **67** 839.
- [870] D. Spataro, *Trattato completo di idraulica teorica e sperimentale (Le basi fisiche dell'idromeccanica). I. Proprietà generali dei liquidi. II. Equilibrio e moto dei liquidi. III. Azioni, reazioni e resistenza dei fluidi* (Hoepli, Milan, 1924).
- [871] H.M. Spivack, Vortex frequency and flow pattern in the wake of two parallel cylinders at varied spacing normal to an air stream, *J. Aeronaut. Sci.* **13** (1946) 289–301.
- [872] L.N. Sretensky, On the diffusion of a vortex pair, *Izv. Akad. Nauk SSSR. Otd. Tekh. Nauk* (1947) No 3 271–300 (in Russian).
- [873] L.N. Sretensky, Scientific activity of S.A. Chaplygin, *Izv. Akad. Nauk SSSR. Otd. Tekh. Nauk* (1953) No 1 106–108 (in Russian).
- [874] T.E. Stanton and D. Marshall, On the eddy system in the wake of flat circular plates in three dimensional flow, *Rep. Memo. Advis. Comm. Aeronaut.* (1930) No 1358. Also: *Tech. Rep. Advis. Comm. Aeronaut.* (1930/31) 202–209. Also: *Proc. R. Soc. London A* **130** (1930) 295–301. Abstract: *Sci. Abs.* **A34** No 1750.
- [875] H.T. Stearn, Vortex sheets, *Quart. J. Pure Appl. Math.* **16** (1879) 271–278.
- [876] W. Stekloff, Questions d'hydrodynamique, *Ann. Fac. Sci. Univ. Toulouse* (ser. 2) **10** (1908) 271–334.
- [877] G.Yu. Stepanov, Theory of hydrodynamic grids in the works of N.E. Zhukovskii and S.A. Chaplygin and its subsequent development (Dedicated to the 125th birthday of N.E. Zhukovskii), *Izv. Akad. Nauk SSSR. Mekh. Zhid. Gaza* (1972) No 2 3–8 (in Russian). English translation: *Fluid Dyn.* **7** (1972) 193–197.
- [878] G.Yu. Stepanov, Inaccuracies in explanation of the theory of a wing, *Izv. Akad. Nauk SSSR. Mekh. Zhid. Gaza* (1975) No 3 188–190 (in Russian). English translation: *Fluid Dyn.* **10** (1975) 532–534.
- [879] G.Yu. Stepanov, Commentaries on the selected works of S.A. Chaplygin, *Izv. Akad. Nauk SSSR. Mekh. Zhid. Gaza* (1977) No 4 180–184 (in Russian). English translation: *Fluid Dyn.* **12** (1977) 636–640.
- [880] G.Yu. Stepanov, Fluid dynamics in the works of N.E. Joukowski (On the 150th anniversary of his birth 5(17).01.1847), *Izv. RAN. Mekh. Zhid. Gaza* (1997) No 2 3–18 (in Russian). English translation: *Fluid Dyn.* **22** (1997) 161–172.
- [881] G.Yu. Stepanov, Nikolai Yegorovich Zhukovskii. On the 150th anniversary of his birth (5(17) January 1847–17 March 1921), *Prikl. Mat. Mekh.* **61** (1997) 3–11 (in Russian). English translation: *J. Appl. Math. Mech.* **61** (1997) 1–8.
- [882] G.G. Stokes, On the steady motion of incompressible fluids, *Trans. Cambr. Phil. Soc.* **7** (1842) 439–453. Reprinted in: *Mathematical and Physical Papers by George Gabriel Stokes* (Cambridge University Press, Cambridge, 1880) **1** 1–16.
- [883] G.G. Stokes, On the theories of the internal friction of fluids in motion, and the equilibrium and motion of elastic solids, *Trans. Cambr. Phil. Soc.* **8** (1845) 287–319. Reprinted in: *Mathematical and Physical Papers by George Gabriel Stokes* (Cambridge University Press, Cambridge, 1880) **1** 75–129.
- [884] G.G. Stokes, Notes on hydrodynamics. IV. – Demonstration of a fundamental theorem, *Cambr. Dubl. Math. J.* **3** (1848) 209–219.
- [885] G.G. Stokes, On the dynamical theory of diffraction, *Trans. Cambr. Phil. Soc.* **9** (1849) 1–62. Reprinted in: *Mathematical and Physical Papers by George Gabriel Stokes* (Cambridge University Press, Cambridge, 1883) **2** 243–328.
- [886] G.G. Stokes, Notes on Hydrodynamics. IV.–Demonstration of a fundamental theorem, in: *Mathematical and Physical Papers by George Gabriel Stokes* (Cambridge University Press, Cambridge, 1883) **2** 36–50.
- [887] A.G. Stoletov, ed., *Hermann von Helmholtz 1821–1891. Publichnye lekci, chitannye v Imperatorskom Moskovskom universitete v pol'zu Helmholtzovskogo fonda (Hermann von Helmholtz 1821–1891. Public lectures delivered at the Imperial Moscow University for the Helmholtz fund)* (Moscow University Press, Moscow, 1892) (in Russian).

- [888] G. Suschning, Neue Experimente mit Wirbelringe, *Sber. Akad. Wiss. Wien* **111** (1902) Abh 2a 830–845.
- [889] A.F. Svanberg, Sur le mouvement des fluides, *J. Reine Angew. Math.* **24** (1842) 153–163.
- [890] H.U. Sverdrup, Vilhelm Bjerknes, in Memoriam, *Tellus* **3** (1951) 217–221.
- [891] J.L. Synge, Mathematical investigation of the thrust experienced by a cylinder in a current, the motion being periodic, *Proc. R. Irish Acad.* **37** (1927) 95–109.
- [892] J.L. Synge, On the motion of three vortices, *Can. J. Math.* **1** (1949) 257–270. Abstract: *Appl. Mech. Rev.* **3** No 725.
- [893] J.L. Synge and C.C. Lin, On a statistical model of isotropic turbulence, *Trans. R. Soc. Canada* **37** (1943) 45–79. Abstract: *Math. Rev.* **4** 263. *Sci. Abs.* **A47** No 1043.
- [894] P. Tait, On the steady motion of an incompressible perfect fluid in two dimensions, *Proc. R. Soc. Edinb.* **7** (1870) 142–143.
- [895] P. Tait, On the most general motion of an incompressible perfect fluid, *Proc. R. Soc. Edinb.* **7** (1870) 143–144.
- [896] P.G. Tait, *Recent Advances in Physical Sciences* 2nd edn (Macmillan, London, 1876).
- [897] P. Tait, On vortex motion, *Proc. R. Soc. Edinb.* **12** (1884) 143–144.
- [898] H. Takeyama, Helical vortices and cylindrical boundaries of circular section, *J. Soc. Appl. Mech. Japan* **3** (1950) 6–8 (in Japanese). Abstract: *Appl. Mech. Rev.* **4** No 2198.
- [899] N.A. Talitskikh, Scientific works of I.S. Gromeka, *Prikl. Mat. Mech.* **15** (1951) 396–408 (in Russian). Also in: I.S. Gromeka, *Sobranie sochinenii* (Collected Papers) (AN SSSR, Moscow, 1952) 10–24.
- [900] F.A. Tarleton, On a problem in vortex motion, *Proc. R. Irish Acad.* **2** (1893) 617–619.
- [901] G.I. Taylor, Motion of solids in fluids when the flow is not irrotational, *Proc. R. Soc. London* **A93** (1917) 99–113. Reprinted in: G.K. Batchelor, ed., *The Scientific Papers of Sir Geoffrey Ingram Taylor. Volume IV. Mechanics of fluids: Miscellaneous papers* (Cambridge University Press, Cambridge, 1971) 3–16.
- [902] G.I. Taylor, On the dissipation of eddies, *Rep. Memo. Advis. Comm. Aeronaut.* (1918) No 598. Reprinted in: G.K. Batchelor, ed., *The Scientific Papers of Sir Geoffrey Ingram Taylor. Volume II. Meteorology, oceanography and turbulent flow* (Cambridge University Press, Cambridge, 1960) 96–101.
- [903] G.I. Taylor, Scientific methods in aeronautics, *Aeronaut. J.* **25** (1921) 474–491. Reprinted in: G.K. Batchelor, ed., *The Scientific Papers of Sir Geoffrey Ingram Taylor. Volume III. Aerodynamics and the mechanics of projectiles and explosions* (Cambridge University Press, Cambridge, 1963) 38–58.
- [904] G.I. Taylor, Motion of solids in fluids when the flow is not irrotational, *Proc. R. Soc. London* **A100** (1921) 114–121. Reprinted in: G.K. Batchelor, ed., *The Scientific Papers of Sir Geoffrey Ingram Taylor. Volume IV. Mechanics of fluids: Miscellaneous papers* (Cambridge University Press, Cambridge, 1971) 17–23.
- [905] G.I. Taylor, The decay of eddies in a fluid (1923), in: G.K. Batchelor, ed., *The Scientific Papers of Sir Geoffrey Ingram Taylor. Volume II. Meteorology, oceanography and turbulent flow* (Cambridge University Press, Cambridge, 1960) 190–192.
- [906] G.I. Taylor, Motion of solids in fluids when the flow is not irrotational, *Phil. Mag.* (ser. 6) **46** (1923) 671–674. Reprinted in: G.K. Batchelor, ed., *The Scientific Papers of Sir Geoffrey Ingram Taylor. Volume IV. Mechanics of fluids: Miscellaneous papers* (Cambridge University Press, Cambridge, 1971) 90–92.
- [907] G.I. Taylor, Note on the connection between the lift on an aerofoil in a wind and the circulation round it, *Phil. Trans. R. Soc. London* **A225** (1926) 238–246. Reprinted in: G.K. Batchelor, ed., *The Scientific Papers of Sir Geoffrey Ingram Taylor. Volume III. Aerodynamics and the mechanics of projectiles and explosions* (Cambridge University Press, Cambridge, 1963) 70–76.
- [908] G.I. Taylor, Production and dissipation of vorticity in a turbulent fluid, *Proc. R. Soc. London* **A164** (1938) 15–23. Reprinted in: G.K. Batchelor, ed., *The Scientific Papers of Sir Geoffrey Ingram*

Taylor. Volume II. Meteorology, oceanography and turbulent flow (Cambridge University Press, Cambridge, 1960) 446–452.

[909] G.I. Taylor, Formation of a vortex ring by giving an impulse to a circular disk and then dissolving it away, *J. Appl. Phys.* **24** (1953) 104. Reprinted in: G.K. Batchelor, ed., *The Scientific Papers of Sir Geoffrey Ingram Taylor. Volume IV. Mechanics of fluids: Miscellaneous papers* (Cambridge University Press, Cambridge, 1971) 206–207.

[910] G.I. Taylor, The interaction between experiment and theory in fluid mechanics, *Annu. Rev. Fluid Mech.* **6** (1974) 1–16.

[911] G.I. Taylor and A.E. Green, Mechanism of the production of small eddies from large ones, *Proc. R. Soc. London A159* (1937) 499–521. Reprinted in: G.K. Batchelor, ed., *The Scientific Papers of Sir Geoffrey Ingram Taylor. Volume II. Meteorology, oceanography and turbulent flow* (Cambridge University Press, Cambridge, 1960) 409–426.

[912] T. Terada and K. Hattori, Some experiments on motion of fluids, I, II, III, *Rep. Aeronaut. Res. Inst. Tokyo* **2** (1926) No 16 87–112.

[913] T. Terada and K. Hattori, Some experiments on motion of fluids, IV, *Rep. Aeronaut. Res. Inst. Tokyo* **3** (1927) No 26 287–326. Abstract: *Sci. Abs.* **31** No 13.

[914] T. Terada and M. Tamano, Further research on periodic columnar vortices produced by convection, *Rep. Aeronaut. Res. Inst. Tokyo* **4** (1929) No 53 447–470.

[915] K. Terazawa, On the decay of vortical motion in a viscous fluid, *Rep. Aeronaut. Res. Inst. Tokyo* **1** (1922) No 4 79–90.

[916] K. Terazawa, On the interference of wind tunnel walls of rectangular cross-section on the aerodynamical characteristics of a wing, *Rep. Aeronaut. Res. Inst. Tokyo* **4** (1928) No 44 69–81.

[917] K. Terazawa, Y. Yamazaki and Y. Akishino, Cinematographic study on aeronautics, *Rep. Aeronaut. Res. Inst. Tokyo* **1** (1924) No 8 213–225.

[918] A. Thom, The strength and position of the eddies behind a circular cylinder, *Rep. Memo. Advis. Comm. Aeronaut.* (1928) No 1373. Also: *Tech. Rep. Advis. Comm. Aeronaut.* (1930/31) 178–185.

[919] S.P. Thompson, Lord Kelvin, *Nature* **77** (1907) 175–177.

[920] S.P. Thompson, *The Life of William Thomson, Baron Kelvin of Largs* (Macmillan, London, 1910).

[921] J.J. Thomson, On the vibrations of a vortex ring, and the action of two vortex rings upon each other, *Proc. R. Soc. London* **33** (1881–1882) 145–147.

[922] J.J. Thomson, On the vibrations of a vortex ring, and the action of two vortex rings upon each other, *Phil. Trans. R. Soc. London A173* (1882) 493–521.

[923] J.J. Thomson, *A Treatise on the Motion of Vortex Rings: an essay to which the Adams prize was adjudged in 1882, in the University of Cambridge* (Macmillan, London, 1883). Reprinted: (Dawsons of Pall Mall, London, 1968).

[924] J.J. Thomson, The vortex ring theory of gases. On the law of the distribution of energy among the molecules, *Proc. R. Soc. London* **39** (1886) 23–36.

[925] J.J. Thomson, *Applications of Dynamics to Physics and Chemistry* (Macmillan, London, 1888).

[926] J.J. Thomson, Cathode rays, *Phil. Mag.* (ser. 5) **44** (1897) 293–316.

[927] J.J. Thomson, On the masses of the ions in gases at low pressures, *Phil. Mag.* (ser. 5) **48** (1899) 547–561.

[928] J.J. Thomson, *Electricity and Matter* (Scribner's Sons, New York, 1904).

[929] J.J. Thomson, On the structure of the atom: an investigation of the stability and periods of oscillation of a number of corpuscles arranged at equal intervals around the circumference of a circle with application of the results to the theory of atomic structure, *Phil. Mag.* (ser. 6) **7** (1904) 667–681.

[930] J.J. Thomson, *The Corpuscular Theory of Matter* (Constable & Co., London, 1907).

[931] J.J. Thomson, *Structure of Light* (Cambridge University Press, Cambridge, 1925).

[932] J.J. Thomson, Analogy between the electromagnetic field and a fluid containing a large number of vortex filaments, *Phil. Mag.* (ser. 7) **12** (1931) 1057–1063.

[933] J.J. Thomson, *Recollections and Reflections* (Macmillan, New York, 1937).

[934] J.J. Thomson and H.F. Newall, On the formation of vortex-rings by drops falling into liquids, *Proc. R. Soc. London* **39** (1885) 417–436.

[935] W. Thomson, On vortex atoms, *Proc. R. Soc. Edinb.* **6** (1867) 94–105. Also: *Phil. Mag.* (ser. 4) **34** (1867) 15–24. Also: *Proc. Glasgow Phil. Soc.* **6** (1868) 197–208. Reprinted in: J. Larmor, ed., *Mathematical and Physical Papers by Sir William Thomson, Baron Kelvin. Volume IV. Hydrodynamics and General Dynamics* (Cambridge University Press, Cambridge, 1910) 1–12.

[936] W. Thomson, The translatory velocity of a circular vortex ring, *Phil. Mag.* (ser. 4) **33** (1867) 511–512. Reprinted in: J. Larmor, ed., *Mathematical and Physical Papers by Sir William Thomson, Baron Kelvin. Volume IV. Hydrodynamics and General Dynamics* (Cambridge University Press, Cambridge, 1910) 67–68.

[937] W. Thomson, On vortex motion, *Trans. R. Soc. Edinb.* **25** (1869) 217–260. Reprinted in: J. Larmor, ed., *Mathematical and Physical Papers by Sir William Thomson, Baron Kelvin. Volume IV. Hydrodynamics and General Dynamics* (Cambridge University Press, Cambridge, 1910) 13–66.

[938] W. Thomson, Vortex statics, *Proc. R. Soc. Edinb.* **9** (1876) 59–73. Also: *Phil. Mag.* (ser. 5) **10** (1880) 97–109. Reprinted in: J. Larmor, ed., *Mathematical and Physical Papers by Sir William Thomson, Baron Kelvin. Volume IV. Hydrodynamics and General Dynamics* (Cambridge University Press, Cambridge, 1910) 115–128.

[939] W. Thomson, Floating magnets [illustrating vortex systems], *Nature* **18** (1878) 13–14. Reprinted in: J. Larmor, ed., *Mathematical and Physical Papers by Sir William Thomson, Baron Kelvin. Volume IV. Hydrodynamics and General Dynamics* (Cambridge University Press, Cambridge, 1910) 135–140.

[940] W. Thomson, Vibrations of a columnar vortex, *Proc. R. Soc. Edinb.* **10** (1880) 443–456. Also: *Phil. Mag.* (ser. 5) **10** (1880) 155–168. Reprinted in: J. Larmor, ed., *Mathematical and Physical Papers by Sir William Thomson, Baron Kelvin. Volume IV. Hydrodynamics and General Dynamics* (Cambridge University Press, Cambridge, 1910) 152–165.

[941] W. Thomson, On maximum and minimum energy in vortex motion, *Rep. Brit. Ass. Advmt Sci.* **50** (1880) 473–476. Also: *Nature* **22** (1880) 618–620. Reprinted in: J. Larmor, ed., *Mathematical and Physical Papers by Sir William Thomson, Baron Kelvin. Volume IV. Hydrodynamics and General Dynamics* (Cambridge University Press, Cambridge, 1910) 172–183.

[942] W. Thomson, On an experimental illustration of minimum energy in vortex motion, *Rep. Brit. Ass. Advmt Sci.* **50** (1880) 473–476. Also: *Nature* **23** (1881) 69–70. Reprinted in: J. Larmor, ed., *Mathematical and Physical Papers by Sir William Thomson, Baron Kelvin. Volume IV. Hydrodynamics and General Dynamics* (Cambridge University Press, Cambridge, 1910) 183–185.

[943] W. Thomson, On a disturbing infinity in Lord Rayleigh's solution for waves in a plane vortex stratum. *Rep. Brit. Ass. Advmt Sci.* **50** (1880) 492–493. Also: *Nature* **23** (1881) 45–46, 70. Reprinted in: J. Larmor, ed., *Mathematical and Physical Papers by Sir William Thomson, Baron Kelvin. Volume IV. Hydrodynamics and General Dynamics* (Cambridge University Press, Cambridge, 1910) 186–187.

[944] W. Thomson, On the average pressure due to impulse of vortex-rings on a solid, *Nature* **24** (1881) 47–48. Reprinted in: J. Larmor, ed., *Mathematical and Physical Papers by Sir William Thomson, Baron Kelvin. Volume IV. Hydrodynamics and General Dynamics* (Cambridge University Press, Cambridge, 1910) 188.

[945] W. Thomson, On the vortex theory of the luminiferous aether, *Rep. Brit. Ass. Advmt Sci.* **57** (1887) 486–495. Also: *Nature* **36** (1887) 550–551.

[946] W. Thomson, On the formation of coreless vortices by the motion of a solid through an inviscid incompressible fluid, *Proc. R. Soc. London* **42** (1887) 83–85. Also: *Phil. Mag.* (ser. 5) **23** (1887) 255–257. Reprinted in: J. Larmor, ed., *Mathematical and Physical Papers by Sir William Thomson, Baron Kelvin. Volume IV. Hydrodynamics and General Dynamics* (Cambridge University Press, Cambridge, 1910) 149–151.

[947] W. Thomson, On the stability of steady and of periodic fluid motion, *Phil. Mag.* (ser. 5) **23** (1887) 459–464, 529–539. Reprinted in: J. Larmor, ed., *Mathematical and Physical Papers by Sir William Thomson, Baron Kelvin. Volume IV. Hydrodynamics and General Dynamics* (Cambridge University Press, Cambridge, 1910) 166–185.

[948] W. Thomson, On the propagation of laminar motion through a turbulently moving inviscid liquid, *Phil. Mag.* (ser. 5) **24** (1887) 342–353. Reprinted in: J. Larmor, ed., *Mathematical and Physical Papers by Sir William Thomson, Baron Kelvin. Volume IV. Hydrodynamics and General Dynamics* (Cambridge University Press, Cambridge, 1910) 308–320.

[949] W. Thomson, On the stability and small oscillation of a perfect liquid full of nearly straight coreless vortices, *Proc. R. Irish Acad.* **1** (1889) 340–342. Reprinted in: J. Larmor, ed., *Mathematical and Physical Papers by Sir William Thomson, Baron Kelvin. Volume IV. Hydrodynamics and General Dynamics* (Cambridge University Press, Cambridge, 1910) 202–204.

[950] M.K. Tikhonravov, *Polet ptic i mashiny s mashushchimi kryl'yami* (Flight of birds and flapping wing machines) 2nd edn (Oborongiz, Moscow, 1949) (in Russian).

[951] I. Todhunter and K. Pearson, *A History of the Theory of Elasticity and of the Strength of Materials from Galilei to Lord Kelvin. Vol. I. Galilei to Saint-Venant, 1639–1850* (Cambridge University Press, Cambridge, 1886). Reprinted: (Dover, New York, 1960).

[952] W. Tollmien, Über die Korrelation der Geschwindigkeitskomponenten in periodisch Schwankenden Wirbelverteilungen, *Z. Angew. Math. Mech.* **15** (1935) 96–100.

[953] C. Tomlinson, On a new variety of the cohesion-figures of liquids, *Phil. Mag.* (ser. 4) **27** (1864) 425–432.

[954] C. Tomlinson, On the cohesion-figures of liquids, *Phil. Mag.* (ser. 4) **28** (1864) 354–364.

[955] S. Tomotika, On the stability of a Kármán vortex street in a channel of finite breadth, I, *Proc. Phys.-Math. Soc. Japan* (ser. 3) **11** (1929) 53–68. Also: *Rep. Aeronaut. Res. Inst. Tokyo* **4** (1929) No 48 213–242. Abstract: *Sci. Abs.* **32** No 3457.

[956] S. Tomotika, On the stability of a Kármán vortex street in a channel of finite breadth, II, *Proc. Phys.-Math. Soc. Japan* (ser. 3) **11** (1929) 149–163. Also: *Rep. Aeronaut. Res. Inst. Tokyo* **4** (1929) No 55 5–46. Abstract: *Sci. Abs.* **33** No 1714.

[957] S. Tomotika, On the resistance experienced by a cylinder moving in a channel of finite breadth, *Rep. Aeronaut. Res. Inst. Tokyo* **5** (1930) No 58 101–142.

[958] S. Tomotika, Vortex motion behind an elliptical cylinder in a stream and some allied problems, *Proc. Phys.-Math. Soc. Japan* (ser. 3) **13** (1931) 61–64. Abstract: *Sci. Abs.* **34** No 4064.

[959] E. Tönnies and J. Bodner, Der Boden-Effekt beim Fluge in Erdnähe, *Z. Flugtech. Motorluftschiff.* **23** (1932) 157–164.

[960] A. Toussaint and E. Carafoli, Sur les spectres cinématographiques de l'écoulement plan des fluides autour d'obstacles variés, *C. R. Acad. Sci. Paris* **183** (1926) 947–948.

[961] T.H. Troller, Zur Wirbeltheorie der Luftschauben, *Z. Angew. Math. Mech.* **8** (1928) 426–430.

[962] J. Trowbridge, On vortex rings in liquids, *Proc. Nat. Acad. Sci. USA* **12** (1877) 131–136. Also: *Am. J. Sci.* (ser. 3) **13** (1877) 327–332.

[963] J. Trowbridge, On liquid vortex-rings, *Phil. Mag.* (ser. 5) **3** (1877) 290–295.

[964] C. Truesdell, *The Kinematics of Vorticity* (Indiana University Press, Bloomington, 1954).

[965] C. Truesdell, Solid body mechanics in relation to mechanical engineering, in: R.M. Rosenberg, ed., *Proceedings of the Fourth U.S. National Congress on Applied Mechanics*, (ASME, New York, 1962) 35–47.

[966] C. Truesdell, The *Mathematical and Physical Papers* of G. G. Stokes, in: C. Truesdell, *An Idiot's Fugitive Essays on Science* (Springer, New York, 1984) 223–235.

[967] Z. Tseitlin, Vortex theory of matter, its development and importance, *Pod Znam. Marxisma* (1924) No 10/11 78–91 (in Russian).

[968] Z. Tseitlin, Vortex theory of electromagnetism, in: J.J. Thomson, *Elektrichestvo i materiya* (Electricity and Matter) (GIZ, Moscow-Leningrad, 1928) 235–263 (in Russian).

[969] R.S. Turner, Helmholtz, Hermann von, in: C.C. Gillispie, ed., *Dictionary of Scientific Biography* (Scribner's Sons, New York, 1972) **VI** 241–253.

[970] E. Tyler, Use of the hot-wire detector in determining the path of vortices, *J. Sci. Instrum.* **3** (1926) 398–400. Abstract: *Sci. Abs.* **30** No 277.

[971] E. Tyler, Vortices behind aerofoil sections and rotating cylinders, *Phil. Mag.* (ser. 7) **5** (1928) 449–463.

[972] E. Tyler, A hot-wire amplifier method for the measurement of distribution of vortices behind obstacles, *Phil. Mag.* (ser. 7) **9** (1930) 1113–1130.

[973] E. Tyler, Vortex formation behind obstacles of various sections, *Phil. Mag.* (ser. 7) **11** (1931) 849–890.

[974] I.A. Tyulina, ed., *Vladimir Vasil'evich Golubev (on the centenary of his birth)* (Znanie, Moscow, 1984) (in Russian).

[975] L. Uslenghi, Sul moto di un vortice puntiforme in un angolo concavo, *Rend. Ist. Lomb. Sci. Lett.* (ser. 2) **68** (1935) 863–879.

[976] N.S. Vasil'ev, *Dvizhenie beskonechno tonkikh vikhrei (Motion of infinitely thin vortices)* (dissertation) (Sapozhnikov, Odessa, 1913) (in Russian).

[977] N.S. Vasil'ev, Reduction of the equations of motion of coaxial vortex rings to canonical form, *Zap. Mat. Otd. Novoross. Obshch. Estestv.* **21** (1913) 1–12 (in Russian).

[978] N.S. Vasil'ev, Motion of infinitely thin vortices, *Zap. Mat. Otd. Novoross. Obshch. Estestv.* **22** (1914) 1–188 (in Russian). Abstract: *F. d. M.* **48** 1443.

[979] N.S. Vasil'ev, On the motion of an infinite row of coaxial circular vortex rings with the same initial radii, *Zap. Fiz.-Mat. Fak. Imp. Novoross. Univ.* **10** (1914) 1–44 (in Russian). Abstract: *F. d. M.* **48** 1444.

[980] N.S. Vasil'ev, A question on the motion of infinite parallel vortices, *Zap. Mat. Otd. Novoross. Obshch. Estestv.* **23** (1916) 99–143 (in Russian). Abstract: *F. d. M.* **48** 1444.

[981] N.S. Vasil'ev, Fluid motion governed by a helical vortex, *Zh. Nauchno-issled. Kafedr Odessa* **23** (1926) 99–143 (in Russian, German summary). Abstract: *F. d. M.* **52** 860.

[982] O.F. Vasil'ev, On a forgotten paper by I.S. Gromeka, *Prikl. Mat. Mekh.* **15** (1951) 261–263 (in Russian).

[983] O.F. Vasil'ev, I.S. Gromeka and his works on hydromechanics, *Izv. Akad. Nauk SSSR. Otd. Tekh. Nauk* (1952) No 7 1095–1103 (in Russian).

[984] O.F. Vasil'ev, Scientific inheritance of I.S. Gromeka, *Trudy Inst. Istor. Estestv. Tekhn.* **10** (1956) 245–268 (in Russian).

[985] O.F. Vasil'ev, *Osnovy mehaniki vintovykh i cirkulyacionnykh potokov (Foundation of mechanics of screw and circulation flows)* (Gosenergoizdat, Moscow-Leningrad, 1958) (in Russian).

[986] M.A. Velikanov, *Dinamika ruslovykh potokov (Dynamics of River Flows)* 3rd edn (GITTL, Moscow, 1954) (in Russian).

[987] W. Veltmann, Die Helmholtz'sche Theorie der Flüssigkeitswirbel, *Z. Math. Phys.* **15** (1870) 450–463.

[988] L. Venturelli, Su una particolare configurazione rigida di quattro vortici rettilinei, *Atti Ist. Veneto Sci. Lett. Arti. Cl. Sci. Mat. Nat.* **98** (1939) Pt 2 43–54. Abstract: *Zentr. Math.* **24** 138.

[989] V.P. Vetchinkin, Printed works of Professor Nikolai Egorovich Joukovsky, in: S.A. Chaplygin, ed., *Pamyati professora Nikolaya Egorovicha Joukovskogo (Nikolai Egorovich Joukovsky. In memoriam)* (TsAGI, Moscow, 1922) 167–181 (in Russian).

[990] V. Vetchinkin, S.A. Chaplygin's works on the induced drag theory, *Prikl. Mat. Mekh.* **5** (1941) 149–160.

[991] V. Vetchinkin, Review of papers by N. Joukovskii and S. Chaplygin forming the basis of wing theory, *Prikl. Mat. Mekh.* **5** (1941) 161–164.

[992] G. Vicentini and G. Pacher, Esperienze sui proiettili gazosi, *Atti Ist. Veneto Sci. Lett. Arti. Cl. Sci. Mat. Nat.* **49** (1900) Pt 2, 1007–1023. Also: *Nature* **63** (1900) 209.

[993] R. de Villamil, *ABC of Hydrodynamics* (Spon, London, 1912).

[994] R. de Villamil, *Motion of Liquids* (Spon, London, 1914).

[995] R. de Villamil, *Resistance of Air* (Spon, London, 1917).

[1996] H. Villat, Sur certains mouvements cycliques avec ou sans tourbillons, *C. R. Acad. Sci. Paris* **170** (1919) 449–451.

[1997] H. Villat, Sur le mouvement d'un fluide indéfinie avec sillage, en pré d'un corps solides, *C. R. Acad. Sci. Paris* **171** (1920) 653–655.

[1998] H. Villat, Sur les mouvements plans tourbillonnaires dans un fluide simplement ou doublement connexe, contenant des parois solides, *C. R. Acad. Sci. Paris* **175** (1922) 445–446.

[1999] H. Villat, Sur les tourbillons alternés de M. H. Bénard dans un canal de largeur finie, *C. R. Acad. Sci. Paris* **188** (1929) 1129–1132.

[2000] H. Villat, La théorie de l'expérience de M. Henri Bénard sur les tourbillons alternés dans une cuve limitée par deux parois fixes parallèles, *Ann. Sci. Éc. Norm. Supér.* **64** (1929) 259–281.

[2001] H. Villat, *Leçons sur la théorie des tourbillons* (Gauthier-Villars, Paris, 1930).

[2002] H. Villat, *Mécanique des fluides* (Gauthier-Villars, Paris, 1933).

[2003] A. Vitterbi, Sopra una classe di moti vorticosi permanenti, *Atti Ist. Veneto Sci. Lett. Arti. Cl. Sci. Mat. Nat.* **61** (1901) Pt 2 449–464.

[2004] A. Vitterbi, Aggiunta alla nota sopra una classe di moti vorticosi permanenti, *Atti Ist. Veneto Sci. Lett. Arti. Cl. Sci. Mat. Nat.* **62** (1902) Pt 2, 175–176.

[2005] J. Vogel-Prandtl, *Ludwig Prandtl: ein Lebensbild, Erinnerungen, Dokumente* (Max-Planck-Institut für Strömungsforschung, Göttingen, 1993).

[2006] W. Voigt, Beiträge zur Hydrodynamik, *Nachr. Ges. Wiss. Göttingen. Math.-Phys. Kl.* (1891) 37–84.

[2007] G.W. Walker, A theorem in vortex motion, *Quart. J. Pure Appl. Math.* **29** (1898) 382–384.

[2008] P.B. Walker, Experiments on the growth of circulation about a wing with a description of an apparatus for measuring fluid motion, *Rep. Memo. Advis. Comm. Aeronaut.* (1931) No 1402. Also: *Tech. Rep. Advis. Comm. Aeronaut.* (1931/32) 97–171.

[2009] E.T.S. Walton, On the motion of vortices near a circular cylinder in a stream of liquid, *Proc. R. Irish Acad. A* **38** (1928) No 3 29–47.

[2010] R.B. Warder and W.P. Shipley, Floating magnets, *Am. J. Sci. (ser. 3)* **20** (1880) 285–288.

[2011] C.S.S. Webster, Novel production of vortex motion, *Chem. News. J. Ind. Sci.* **78** (1898) 269.

[2012] R. Wehner, *Die italienische Literatur über die Bewegung isolierter Wirbel und isolierter Quellen in der Ebene* (dissertation) (Frommhold & Wendler, Leipzig, 1939). Abstract: *F. d. M.* **65** 980. *Zentr. Math.* **23** 416.

[2013] J. Weingarten, Ueber die geometrischen Bedingungen, denen die Unstetigkeiten der Derivierten eines Systems dreier stetigen und ihre Bedeutung in der Theorie Wirbelbewegung, *Arch. Math. Phys. (ser. 3)* **1** (1901) 27–33.

[2014] J. Weingarten, Zur Theorie der Wirbelringe, *Nachr. Ges. Wiss. Göttingen. Math.-Phys. Kl.* (1906) 81–93. Abstract: *F. d. M.* **33** 779.

[2015] P. Welander, Studies of the general development of motion in a two-dimensional, ideal fluid, *Tellus* **7** (1955) 141–156.

[2016] F. Werner, *Hermann Helmholtz' Heidelberger Jahre (1858–1871)* (Springer, Berlin, 1997).

[2017] J.R. Weske and A.H. Planktholt, Discrete vortex systems in the transition range of fully developed flow in a pipe, *J. Aeronaut. Sci.* **20** (1953) 717–718.

[2018] F.L. Westwater, The rolling up of the surface of discontinuity behind an aerofoil of finite span, *Rep. Memo. Advis. Comm. Aeronaut.* (1935) No 1692. Also: *Tech. Rep. Advis. Comm. Aeronaut.* (1935/36) 116–131.

[2019] C. Weyher, Quelques expériences sur les tourbillons aériens, *C. R. Acad. Sci. Paris* **104** (1877) 352–354.

[2020] C. Weyher, Aerial vortices and revolving spheres, *Nature* **35** (1887) 514–515.

[2021] C.L. Weyher, *Sur les tourbillons, trombes, tempêtes, sphères tournantes* (Carré, Paris, 1889).

[2022] E. Whittaker, *A History of the Theories of Aether and Electricity.* **1** (Harper, New York, 1960)

[2023] W. Wien, Ueber zyklonartige Bewegungsformen einer inkompressiblen reibungslosen Flüssigkeit, *Ann. Phys. Chem. (new ser.)* **59** (1896) 753–763.

- [1024] W. Wien, *Lehrbuch der Hydrodynamik* (Hirzel, Leipzig, 1900).
- [1025] W. Wien, Hydrodynamische Untersuchungen von H. v. Helmholtz, *Sber. Preuss. Akad. Wiss.* (1904) 716–736.
- [1026] R. Wille, Kármánsche Wirbelstraßen. Herrn Professor Dr. Th. von Kármán zum 80. Geburtstag gewidmet, *Z. Flugwiss.* **9** (1961) 150–155.
- [1027] D.B. Wilson, Kinetic atom, *Am. J. Phys.* **49** (1981) 217–222.
- [1028] D.B. Wilson, *Kelvin and Stokes: a comparative study in Victorian physics* (Hilger, Bristol, 1987).
- [1029] H.F. Winny, The vortex system generated behind a sphere moving through a viscous fluid, *Rep. Memo. Advis. Comm. Aeronaut.* (1933) No 1531. Also: *Tech. Rep. Advis. Comm. Aeronaut.* (1932/33) 183–197.
- [1030] A. Wintner, Bemerkung über die Eigenwellen der Kármánschen Wirbelstrasse, *Math. Z.* **30** (1929) 283–284.
- [1031] R.W. Wood, Equilibrium-figures formed by floating magnets, *Phil. Mag.* (ser. 5) **46** (1898) 162–164.
- [1032] R.W. Wood, Vortex rings, *Nature* **63** (1901) 418–420.
- [1033] E. Zermelo, Hydrodynamische Untersuchungen über die Wirbelbewegungen in einer Kugelfläche, *Z. Math. Phys.* **47** (1902) 201–237. Abstract: *F. d. M.* **33** 781.
- [1034] M. Zeuli, Sul moto liquido piano con esistenza di vortice in un canale con pareti rigide rettilinee e con variazione di sezione, *Rend. Ist. Lomb. Sci. Lett.* (ser. 2) **71** (1938) 301–317.
- [1035] K. Zorawski, Ueber die Erhaltung der Wirbelbewegung, *C. R. Acad. Sci. Crac.* (1900) 335–341.

Field-Assisted Self-Assembly of Superparamagnetic Nanoparticles for Biomedical, MEMS and BioMEMS Applications

RANJAN GANGULY^a and ISHWAR K. PURI^b

^a*Power Engineering Department, Jadavpur University, Kolkata, 700098, India*

^b*Department of Engineering Science and Mechanics, Virginia Polytechnic Institute and State University, VA 24061, USA*

I.	Practical Significance of Ferrofluids and Magnetic Microspheres	294
A.	Magnetic Nanoparticles	295
B.	Ferrofluids.	296
C.	Magnetic Microspheres.	297
II.	Field-Induced Ferrofluid Aggregation	300
A.	Ferrofluid Hydrodynamics	300
B.	Field-Induced Self-Assembly due to Force Interactions	303
C.	Field-Induced Self-Assembly and Transport in Forced Flow	307
III.	Thermomechanical Ferrofluid Applications	319
IV.	BioMEMS and Biomedical Applications of Magnetic Microspheres	322
A.	Field-Guided Transport	323
B.	Micro Total Analytical Systems.	325
C.	Micro Mixers using Self-Assembled Chains	327
V.	Closing Remarks.	330
	References	331

Single domain nanoparticles of iron oxides ranging 5–15 nm in diameter behave as superparamagnetic materials. These particles can be coated with an adsorbed surfactant layer and be stably suspended in a nonmagnetic-liquid carrier. The resulting suspension, called a ferrofluid, exhibits magnetic behavior when an external magnetic field is imposed, which aligns the thermally disoriented magnetic moments of these particles. The nanoparticles can also be embedded within solid materials, e.g., inside 1–2 μm size polystyrene microspheres, so that the beads respond to magnetic fields. The transport of both ferrofluids and magnetic microspheres (containing superparamagnetic

nanoparticles) can be controlled using suitable guiding magnetic fields. The nanoparticles or microspheres can be functionalized with chemical substances and bioconjugates to accomplish specific tasks. This combination of the (bio)chemical functionalization and the “action-at-a-distance” using the magnetic field has considerable potential for applications of superparamagnetic nanoparticles in MEMS (micro-electromechanical systems) and NEMS (nano-electromechanical systems) (and BioMEMS and BioNEMS) devices. Flowfields established with ferrofluids can be altered by applying external magnetic fields to realize enhanced heat transfer, controlled mass transfer or field-assisted self-organizations and assemblies that form three-dimensional structures, from the nano- to the mesoscale. Magnetic microspheres can be advantageously used as “mobile substrates” for microscale bioassays or *in vivo* applications. This article provides an insight into the magnetic behavior of the nanoparticles and the transport phenomena associated with ferrofluids and magnetic microspheres.

I. Practical Significance of Ferrofluids and Magnetic Microspheres

Ferrofluids have both a fluid nature and exhibit magnetic behavior. Therefore, flowfields containing these magnetic fluids can be remotely controlled by magnetic fields. While the “action-at-a-distance” of a magnetic field can be localized, it can also be induced at a level strong enough to alter an entire flowfield. Consequently, ferrofluids have promising potential for a number of applications.

One such application is the control of convection heat transfer that makes use of the spatial gradient in the ferrofluid magnetic susceptibility that is produced in the presence of a temperature gradient. When an external magnetic field is imposed in such a circumstance, the varying susceptibility results in a nonuniform magnetic body force on the ferrofluid, leading to thermomagnetic convection (Finlayson, 1970). This form of heat transfer can be particularly useful for cases where conventional thermogravitational convection (that measures as the cube of the length scale) fails to provide adequate heat transfer, e.g., in microscale devices or under reduced gravity conditions. It can also be employed to augment or hinder free convection by altering the nature of the imposed field. The recent development of micro-magnets (Ye et al., 1995) and microelectromagnets (Drndić et al., 1998) has made it possible to use thermomagnetic convection in miniature devices.

Likewise, the controlled transport of a ferrofluid or of magnetic microspheres can be utilized for magnetic drug targeting (MDT). Here, chemo-therapeutic agents are bonded to magnetic particles that are placed in a

biocompatible fluid and injected into the vasculature. Thereafter, they are magnetically guided *in vivo* to a target location. This is a promising active biophysical drug-targeting technique for the medical treatment of various diseases and cardiovascular episodes, such as stenosis and thrombosis (Mosbach and Schröder, 1979). In comparison with other drug targeting methods (Lubbe et al., 2001), MDT has several advantages. It is minimally invasive (requiring only injection and, if at all, a very limited surgical procedure). Magnetic carriers can reach the smallest capillaries of the body, which are 5–6 μm in diameter and the carrier particles can be manipulated with high accuracy for relatively large drug concentrations using suitably designed magnetic fields (Rusetski and Ruuge, 1990).

There are advantages to using magnetic fluids in microscale (e.g., MEMS) systems. Unlike many other forces, a magnetic force is effective even from a distance, permitting “action-at-a-distance;” it is also localized; and competition between the magnetic force and other forces, e.g., fluid shear, surface tension or gravity enables unique self-assembled ferrofluid structures. Several types of field-assisted aggregations of ferrofluids (in forced flow or for sessile droplets) are possible. The resulting structures can be made permanent or semi-permanent by mixing suitable curing agents with a ferrofluid.

Magnetic microspheres also have numerous applications. For instance, in microfluidic biosensors the bead surfaces can be functionalized with suitable bioconjugates. Thereafter, the microspheres can be attached to or become engulfed by cells with high selectivity, making it possible to manipulate the cells with external magnetic fields (Ugelstad et al., 1993; Radbruch et al., 1994; Tibbe et al., 1999). Consequently, the beads can be advantageously used as “mobile substrates” for microscale bioassays and even for *in vivo* applications. They can be used to promote mixing in microchannels, recovered from a dispersion by high-gradient magnetic separation (Choi et al., 2001), or can be reversibly redispersed.

A. MAGNETIC NANOPARTICLES

The magnetic behavior of finely divided particles is quite different from their bulk counterparts. McNab et al. (1968) performed Mössbauer spectroscopy on ferro- and ferrimagnetite particles of diameter ranging from 10 to 16 nm and found that although the particles have the same saturation magnetization characteristic of the bulk material, the remnant magnetism is zero. Unlike bulk ferro- or ferrimagnetic materials, nanoparticles often contain a single domain and therefore have a permanent magnetic moment proportional to their volume. At normal temperatures ($\sim 300 \text{ K}$) the thermal

Brownian energy of individual particle magnetic domains is much larger than the magnetocrystalline anisotropy energy. For the particles ranging 10–15 nm in diameter, the blocking temperature (Chen and Zhang, 1998) is much lower than room temperature and, hence, the particles exhibit superparamagnetic behavior (Berkovsky, 1978). The individual particle dipoles are randomly oriented due to thermal agitation and hence, a collection of these nanoparticles do not respond magnetically unless an external magnetic field (that tends to align the individual dipoles of the nanoparticles) is imposed.

B. FERROFLUIDS

Ferrofluids are colloidal suspensions of single domain magnetic nanoparticles, typically of 10 nm diameter, containing Ni, Co, Mg or Zn compositions of ferrite (Fe_2O_4), magnetite (Fe_3O_4) and maghemite ($\gamma\text{-Fe}_2\text{O}_3$) in a nonmagnetic-liquid carrier (Rosensweig, 1985; Odenbach, 2004). Since the particles are superparamagnetic, ferrofluids do not exhibit permanent magnetization but demonstrate magnetic behavior only when an external magnetic field is imposed that aligns the thermally disoriented magnetic moments of the nanoparticles. The nanoparticles are often coated with adsorbed surfactant layers to prevent their agglomeration that would otherwise occur due to the attractive van der Waals forces and dipole–dipole interactions between them (refer to Fig. 1.1). The particles can also be “functionalized”, i.e., they can be coated with suitable inorganic or organic molecules that serve specific chemical or biological tasks (Kouassi et al., 2005).

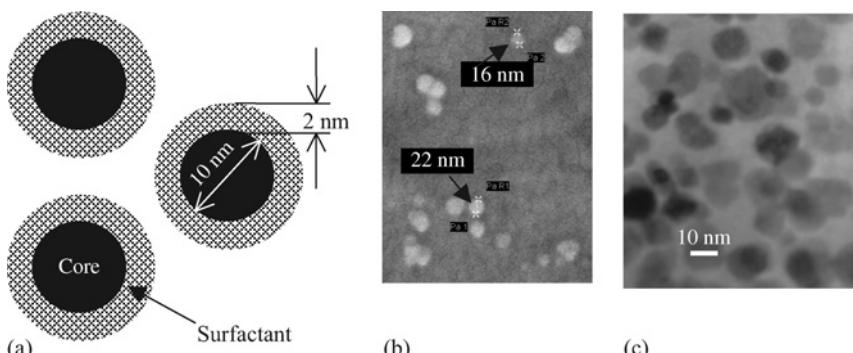


FIG. 1.1. (a) Schematic representation of the suspended nanoparticles in a ferrofluid – the ferro- or ferrimagnetic core is coated with a layer of surfactant. (b) SEM image of a diluted EMG 705 Series ferrofluid. (c) TEM image of the same sample.

Depending upon the nature of the particle materials or the carrier liquids, ferrofluids can have a wide range of physical and magnetic properties (Rosensweig, 1985). The choice of the liquid carrier, which can be water, mineral oil, organic solvent, ester, etc., depends on the application. An earlier method of synthesizing ferrofluids involved size reduction of micron-scale ferro- or ferrimagnetic particles through successive grinding (ball milling). This time consuming (~ 1000 h) and expensive method has been replaced by chemical coprecipitation. For example, magnetite nanoparticles can be prepared by coprecipitating iron (II) and iron (III) chloride salts in the presence of ammonium hydroxide at pH 9–10. Subsequently the nanoparticles are stabilized in oleic acid that prevents particle agglomeration by steric (entropic) repulsion (Harris, 2002).

Since the nanoparticles suspended in ferrofluids show superparamagnetic properties, the magnetization vector \mathbf{M} (i.e., the magnetic moment per unit volume, A/m) of the bulk ferrofluid obeys Langevin equation (Rosensweig, 1985), namely,

$$|\mathbf{M}| = M_{\text{sat}}\varphi \left(\coth(\alpha) - \frac{1}{\alpha} \right), \quad (1.1)$$

where φ denotes the volume fraction of magnetic particles in the fluid, M_{sat} the bulk saturation magnetization of the particle material and the Langevin parameter

$$\alpha = \frac{4\pi a^3 \mu_0 M_{\text{sat}} |\mathbf{H}|}{3 k_B T} \quad (1.2)$$

Here, a denotes radius of a nanoparticle, k_B the Boltzmann constant ($= 1.3807 \times 10^{-23}$ JK $^{-1}$), and T the absolute temperature. Fig. 1.2 shows the representative magnetization curves (normalized with respect to the ferrofluid saturation magnetization) for superparamagnetic ferrite nanoparticles following the Langevin equation at 300 K. As is evident from the magnetization curves, an almost linear magnetization curve is achieved for particles with a diameter smaller than 5 nm. Thus, the particle magnetization at very small diameters approaches the characteristic magnetization of a paramagnetic substance.

C. MAGNETIC MICROSpheres

Another useful form of magnetic nanoparticles consists of ferrous nanoparticles embedded in micron-size polystyrene beads that are commercially available. Functional microparticles (or “microbeads”) prepared, e.g., by

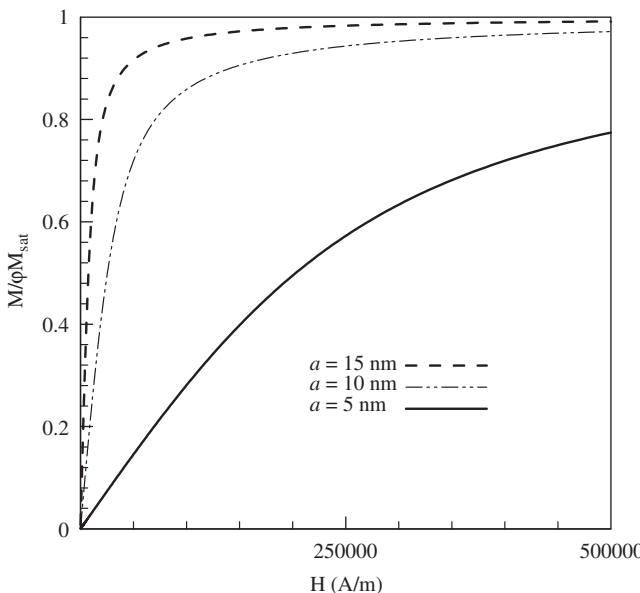


FIG. 1.2. Ferrofluid magnetization curves (normalized with respect to the saturation magnetization) for three different ferrite ($M_{\text{sat}} = 4.46 \times 10^5 \text{ A m}^{-1}$) nanoparticle diameters.

emulsion polymerization or dispersion polymerization can offer a large specific surface for chemical binding. By functionalizing the bead surfaces with antibodies, peptides or lectins, they can be attached to or engulfed by cells with high selectivity, making it possible to manipulate cells with external magnetic fields (Ugelstad et al., 1993; Radbruch et al., 1994; Tibbe et al., 1999).

When magnetic microspheres are suspended in a liquid medium under a homogeneously imposed magnetic field $\mathbf{B}_0 = \mu_0 \mathbf{H}_0$, where, $\mu_0 = 4\pi \times 10^{-7} \text{ N A}^{-2}$, and denotes the permeability in vacuum, there is no net unbalanced force on an isolated particle. However, in a system of particles, a dipole-dipole interaction occurs, since a magnetic dipole moment $\mathbf{m} = 4/3(\pi R^3 \chi_{\text{eff}} \mathbf{H}_0)$ is induced in each microsphere, where R denotes the microsphere radius and χ_{eff} the effective susceptibility of the bead. The effective magnetic susceptibility is different from the intrinsic magnetic susceptibility χ_i (where $\mathbf{M} = \chi_i \mathbf{H}_0$) of the microspheres, since it takes into account the distortion of the magnetic flux lines around a magnetized material placed in a magnetic field. For a uniformly magnetized spherical particle, the magnetic field inside the sphere is $\mathbf{B} = \mu_0(\mathbf{H}_0 + 2/3(\mathbf{M}))$ (Griffiths, 2004), and the effective magnetic susceptibility is linked to the intrinsic susceptibility of the nanoparticles through the relationship $\chi_{\text{eff}} = \chi_i / (1 + (1/3)\chi_i)$.

Since the microspheres consist of nanoparticles that are superparamagnetic, the intrinsic susceptibility can be obtained from the Langevin equation (Eq. (1.1)). When the magnetic microspheres are magnetized, they themselves act like tiny magnets, with fields of their own. If two magnetic beads are not far away from each other (as in the case of a dense bead-suspension), their fields interact. For any two magnetic microspheres of identical dipole strength \mathbf{m} that are separated by a distance r , the magnetic interaction potential is (Biswal and Gast, 2004a) (refer to Fig. 1.3(a))

$$U_{\text{mag}} = \frac{\mu_0 \mu_r}{4\pi} |\mathbf{m}|^2 \frac{(1 - 3\cos^2\delta)}{r^3}, \quad (1.3)$$

where μ_r represents the relative permeability of the liquid in which the beads are suspended and δ the angle between the magnetic field vector and the radius vector connecting the two particles. The relation shows that the dipole–dipole interaction force \mathbf{F} ($\sim \nabla U_{\text{mag}}$) is attractive and scales as $1/r^4$, implying that the force becomes much stronger as two microspheres more closely approach each other. Unlike the nanoparticles in a ferrofluid, the dipole–dipole interaction in a suspension of magnetic microspheres cannot be effectively overcome by adding a surfactant, and the microspheres form chain-like structures (refer to Fig. 1.3(b), Sinha et al., 2005).

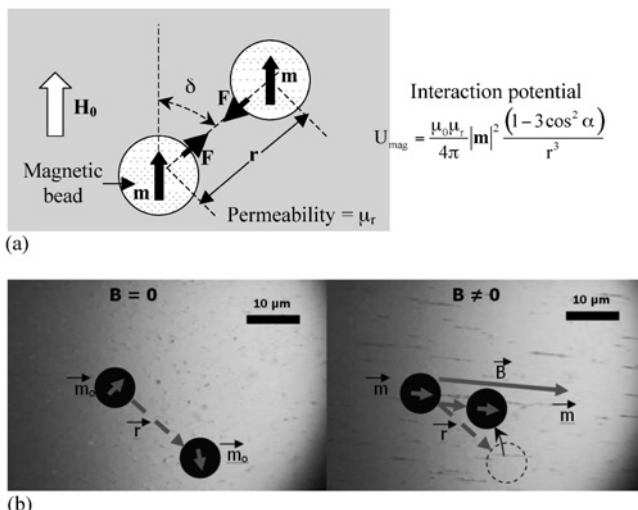


FIG. 1.3. (a) Dipole–dipole interaction potential for magnetic microspheres. (b) Formation of “pearl-chains” by magnetic microspheres suspended in a liquid carrier under a homogeneous magnetic field (Sinha et al., 2005).

II. Field-Induced Ferrofluid Aggregation

A. FERROFLUID HYDRODYNAMICS

Since the particle size of the dispersed phase in a ferrofluid is comparable to the molecular mean free path of the carrier liquid, a stable ferrofluid suspension can be treated through a continuum approach. Here, the nanoparticle concentration in the ferrofluid is considered small enough for the dipole–dipole interactions to be negligible (since the largest volume fraction of the particles does not generally exceed 3%). Therefore, the Langevin equation can describe the fluid magnetization sufficiently accurately (Lange, 2002; van Ewijk et al., 2002). As described by Berkovsky (1978), each nanoparticle in a ferrofluid possesses a finite magnetocrystalline anisotropy energy component (which is a function of the particle size, shape and crystallographic structure) and another thermal Brownian energy component (that is a function of the temperature). While the first component is responsible for the rotation of a magnetic particle, which has a definite particle moment, that aligns it with an imposed magnetic field, the latter produces random thermal fluctuations of the magnetic moment within the particle. Here, we have considered a fluid type for which the total magnetocrystalline anisotropy energy of the nanoparticles is much lower than their thermal fluctuation energy. This implies that the magnetic moment of a domain is not rigidly fixed to the particle body. Therefore, the magnetic field does not influence the particle orientation.

The magnetoviscous effect, which is the change of effective fluid viscosity due to the forced alignment of particles in the direction of imposed magnetic field, and consequent anisotropies in other fluid properties are negligible (Shliomis and Stepanov, 1993). Also, since the magnetic moments are not “frozen” inside the particles, the particle rotation that occurs in a rotational flowfield does not alter the orientation of the individual particle magnetic moment, which tends to align itself with the imposed field. Thus, the viscous torque on the nanoparticles does not have to overcome the magnetic torque so that the fluid is free from magnetodissipation (Müller and Engel, 1999).

The hydrodynamic equations describing the mass, momentum and species equations (for cases involving two or more fluids) can be written as

$$\partial\rho/\partial t + \partial(\rho v_j)/\partial x_j = 0, \quad (2.1)$$

$$\partial(\rho v_i)/\partial t + \partial(\rho v_j v_i)/\partial x_j = -\partial p/\partial x_i + \partial\tau_{ij}/\partial x_j + \mathfrak{I}_i, \quad (2.2)$$

and

$$\partial(\rho Y_f) \partial t + \partial[\rho v_i Y_f - \rho D \partial Y_f / \partial x_j + 1/(6\pi\eta a) \cdot \rho Y_f f_j] / \partial x_j = 0, \quad (2.3)$$

respectively. Here, ρ denotes fluid density, v_i the velocity, p the pressure, D the ferrofluid diffusivity, and Y_f the ferrofluid mass fraction. The viscous stress tensor τ_{ij} that appears in the momentum equation is expressed in terms of the fluid viscosity η and velocity gradient, i.e.,

$$\tau_{ij} = \eta(\partial v_i / \partial x_j + \partial v_j / \partial x_i) - (2/3)\eta\delta_{ij}(\partial v_k / \partial x_k), \quad (2.4)$$

where δ_{ij} denotes the Kronecker delta. The last term in the momentum equation contains the Kelvin body force (KBF) expressed per unit volume $\mathfrak{J}_i = M_f(\partial B_j / \partial x_i)$ that arises from the fluid magnetization (due to the presence of the magnetic nanoparticles) in the imposed magnetic field (Zahn, 1979). As evident from the expression of KBF, this magnetic body force is experienced only under a nonuniform magnetic field (i.e., in a field having a nonzero gradient).

The KBF is responsible for a wide range of interesting hydrodynamic and field-induced self-assembly behaviors exhibited by ferrofluids under different conditions. Self-assembly is characterized by a competition between at least two forces, one attractive and the other repulsive, in systems that are not in thermodynamic equilibrium and is associated with energy dissipation. Magnetic field-induced self-assembly of ferrofluids occurs through the interplay of magnetic, surface tension, gravity and hydrodynamic shear forces. The mass fraction of nanoparticles in the host fluid, Y_f is linked with the particle volume fraction φ through the relation

$$\varphi = \rho^l Y_f / [\rho^p - (\rho^p - \rho^l) Y_f], \quad (2.5)$$

where ρ^p and ρ^l denote the densities of the particles and the host liquid, respectively, and the local fluid density ρ is related to the local volumetric fraction of the nanoparticles through the expression

$$\rho = (\rho^p - \rho^l)\varphi + \rho^l. \quad (2.6)$$

For a dilute ferrofluid, the diffusivity D of the magnetic nanoparticles (having radius a) can be obtained using the Stokes–Einstein equation (Probestein, 1994), i.e.,

$$D = kT / 6\pi\eta a. \quad (2.7)$$

The last term in the species equation (Eq. (2.3)) represents magnetophoretic motion, which arises due to Stokesian migration of superparamagnetic

nanoparticles under the magnetic force $f_j = \mu_0 m^p k \partial H_j / \partial x_k$ (Zahn, 1979).¹ Here, $m^p k$ denotes the component of the particle moment vector along x_k axis.

The force field in a magnetic fluid depend on the magnetic field \mathbf{B} and the magnetization \mathbf{M} (which is related to the variable² \mathbf{H} ($= \mathbf{B}/\mu_0 - \mathbf{M}$) through Langevin equation (Eq. 1.1)), where μ_0 denotes the permeability of vacuum). The vectors \mathbf{B} and \mathbf{H} obey the Maxwell's equations in static form (Griffiths, 2004), i.e.,

$$\varepsilon_{ijk} \partial H_k / \partial x_j = 0 \text{ (no free current),} \quad (2.8)$$

and

$$\partial B_j / \partial x_j = 0, \quad (2.9)$$

where ε_{ijk} denotes the Levi-Civita tensor. At the interface of ferrofluid and another nonmagnetic fluid, we can expect a discontinuity of fluid magnetization at the interface, and Eqs. (2.8) and (2.9) reduce to the following interface conditions for \mathbf{B} and \mathbf{H} (refer to Fig. 2.1)

$$\mathbf{H}_{1t} = \mathbf{H}_{2t} \quad (2.10)$$

and

$$\mathbf{B}_{1n} = \mathbf{B}_{2n}, \quad (2.11)$$

where the suffixes t and n indicate the tangential and normal components along the interface, respectively. Equations (2.10) and (2.11) indicate that when there is a discontinuity in the medium, the tangential components of the \mathbf{H} vector and the normal components of \mathbf{B} vector on either sides of the interface are identical.

¹ Eq. (9) (p-369) of this reference states that for zero free current (i.e., $J_f = 0$), $\mathfrak{I}_i = \mu_0 M_j \cdot (\partial H_i / \partial x_j) + 1/2 \mu_0 \cdot \partial / \partial x_i (M_j M_j)$. Using Maxwell's equation for $J_f = 0$, i.e., $\partial H_i / \partial x_j = \partial H_j / \partial x_i$, one gets, $\mathfrak{I}_i = M_j (\mu_0 \partial H_j / \partial x_i + \mu_0 \partial M_j / \partial x_i) = M_j \partial B_j / \partial x_i$. However, the body force around a single particle is computed from the volume integral $f_i = \int \mathfrak{I}_i dV$, where the particle of volume V is surrounded by the carrier fluid having zero magnetization and Eq. (12) (p-370) leads to the expression of the force on a single particle as $f_i = \mu_0 m^p \partial H_i / \partial x_j$.

² A quote from Griffiths (2004, p. 271) is appropriate in this regard

Many authors call \mathbf{H} , not \mathbf{B} , the “magnetic field”. Then they have to invent a new word for \mathbf{B} : the “flux density”, or magnetic “induction” (an absurd choice, since the term has at least two other meaning in electrodynamics). Anyway, \mathbf{B} is indisputably the fundamental quantity, so I shall continue to call it the “magnetic field”, as everyone does in spoken language. \mathbf{H} has no sensible name: just call it “ \mathbf{H} ”. Also the footnote on the same page of the book quotes from A. Sommerfeld's *Electrodynamics* (Academic Press, New York, 1952, p. 45) the unhappy term “magnetic field” for \mathbf{H} should be avoided as far as possible. It seems to us that this term has led into error none less than Maxwell himself ...

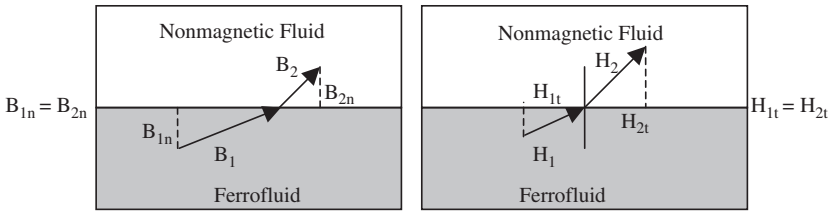


FIG. 2.1. Discontinuity in the fluid magnetization due to the presence of free surface in ferrofluid gives rise to sharp gradient in \mathbf{B} and \mathbf{H} , and large KBF at the interface.

B. FIELD-INDUCED SELF-ASSEMBLY DUE TO FORCE INTERACTIONS

When a ferrofluid and a nonmagnetic liquid share a common interface, the application of a normal magnetic field produces a destabilizing effect on the planar free interface, leading to the formation of free-standing spikes that have a static hexagonal pattern. This is known as the *Rosenstheig instability* (Cowley and Resensweig, 1967; Rosenstheig, 1985). The theory behind the formation of ferrofluid structures in idealized geometries has been addressed by Boudouvis et al. (1993) who solved the magnetically augmented Young–Laplace’s equation to explain this behavior.

Ferrofluids have been used to form patterns on flat substrates (Goldstein et al., 1993). For instance, a thin ferromagnetic film can be patterned into isolated islands and used to direct the assembly of superparamagnetic colloidal particles into two-dimensional arrays (Yellen et al., 2003). However, previous research has focused on the self-assembly of two-dimensional patterns rather than of complex three-dimensional architectures. When a sessile drop of ferrofluid placed on a flat substrate is subjected to a spatially varying magnetic field, the interactions between gravity, surface tension and the magnetic force create different shapes (Boudouvis and Scriven, 1993; Goldstein et al., 1993; Jang et al., 1999).

For systems influenced by the surface tension, magnetic and gravity forces, Boudouvis et al. (1993) proposed two nondimensional numbers, the gravitational Bond number $N_g = g\Delta r L^2/\sigma$, and the magnetic Bond number $N_m = \mu_0 \mathbf{H}_0^2 L/\sigma$, where L is the pertinent length scale (e.g., the size of a ferrofluid droplet), and σ denotes the surface tension coefficient. The first number represents the ratio of the gravitational to the surface tension force, while the latter is the ratio of the magnetic to the surface tension force. If one considers the practical limitation of the magnetic saturation of ferrofluids, i.e., when the magnetization of the ferrofluid does not further increase with increase of \mathbf{H}_0 , and remains constant ($= \varphi M_{\text{sat}}$), the magnetic Bond

number expression can be modified into the form

$$N_m = \mu_0 \chi_m \mathbf{H}_0^2 L / \sigma \text{ (below saturation), and} \quad (2.12)$$

$$N_m = \mu_0 \varphi M_{\text{sat}} \mathbf{H}_0 L / \sigma \text{ (above saturation)} \quad (2.13)$$

If the magnetic field is produced by a line dipole (e.g., by depositing a conducting wire on a substrate during microfabrication) of strength m (Ganguly et al., 2004a), then $\mathbf{H}_0 \sim m L^{-2}$. Consequently, for a given value of m (the dipole strength of the field-inducing circuit), the magnetic Bond number

$$N_m = \mu_0 \chi_m \mathbf{H}_0^2 L / \sigma \text{ (below saturation), and} \quad (2.14)$$

$$N_m = \mu_0 \varphi M_{\text{sat}} \mathbf{H}_0 L / \sigma \text{ (above saturation)} \quad (2.15)$$

With decreasing length scale, the gravitational and magnetic Bond numbers change differently. The gravitational Bond number decreases as the length scale is reduced, since $N_g \propto L^2$. Curve ① in Fig. 2.2 shows the variation of

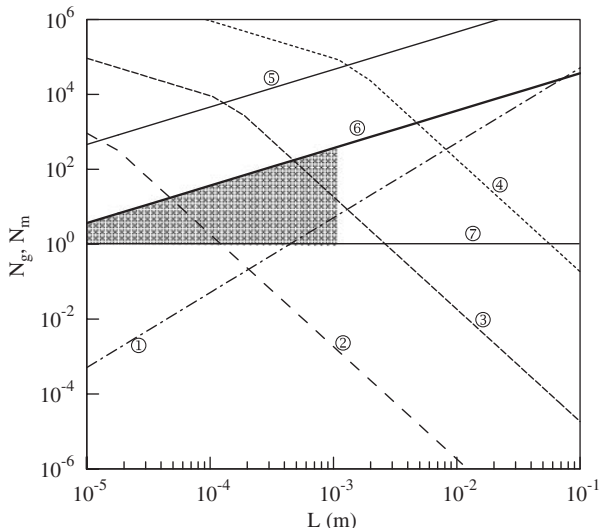


FIG. 2.2. Different regimes of interactions between magnetic, surface tension and gravity forces. Curve ①: Variation of N_g with gravity. Curves ②, ③ and ④: Variation of N_m with L for $m_1 = 2 \times 10^{-4} \text{ A/m}$, $m_2 = 2 \times 10^{-2} \text{ A/m}$ and $m_3 = 2 \text{ A/m}$, respectively. Curve ⑤: Locus of N_m corresponding to magnetic saturation points (i.e., $B = B_{\text{sat}}$). Curve ⑥: Variation of N_m with L under the constraint of a limiting field $B_{\text{max}} < B_{\text{sat}}$. Surface tension force dominates over other force in the region below curve ⑦. Shaded region denotes the regime of field-assisted self-assembly.

N_g as a function of L . On the contrary, for a given value of m , the magnetic Bond number increases as the length scale is increased. When plotted against the length scale, N_m varies in two distinct regimes, one below the magnetic saturation limit ($N_m \propto L^{-3}$), and the other above saturation ($N_m \propto L^{-1}$). Considering representative ferrofluid properties (viz. density $\Delta\rho = 1530 \text{ kg m}^{-3}$ and $\sigma = 2.95 \times 10^{-3} \text{ N m}^{-1}$; Weilepp and Brand, 1996), a set of parallel curves ② ③ and ④ (cf., Fig. 2.2) can be drawn that relate N_m to L for a specified dipole strength. Above saturation, a distinct change in the slopes of the N_m – L curves ② ③ and ④ is observed. Curve ⑤ connects the saturation points of all N_m – L curves at different m values.

The dynamic response of a magnetically saturated ferrofluid structures to a time-varying magnetic field is not as strong as in an unsaturated ferrofluid (N_m scales with \mathbf{H}_0 in a saturated ferrofluid as opposed to \mathbf{H}_0^2 when it is unsaturated). Thus, for applications involving a periodic magnetic field, e.g., a ferrofluid microvalve for a MEMS scale reciprocating flow device (Hartshorne et al., 2004), the design objective is to operate below curve ⑤ of Fig. 2.2. For many practical MEMS applications the magnetic Bond number is also limited by the maximum magnetic field that can be used in the device (this may either be due to the limitation of the MEMS scale electromagnet that produces the field or it may originate from the functional limitations of other electrical/electronic components integrated into the device that are subjected to the magnetic field during its operation). Curve ⑥ denotes the maximum magnetic Bond number achieved for a specified allowable upper limit of the magnetic field $B_{\max} = 200 \text{ mT}$.

Magnetic field-assisted self-assembly occurs under the mutual interaction of the magnetic force and surface tension force while the former exceeds the latter, i.e., above $N_m \sim 1$. However, as the length scale increases, N_g also increases, and the gravitational force becomes important. When these forces exceed the surface tension force by an order of magnitude (i.e., $N_g \sim 10$), magnetic and gravity forces become dominant. Then, field-assisted self-assembly ceases, since surface tension plays an insignificant role. For the case presented in Fig. 2.2 for $B_{\max} = 200 \text{ mT}$ (curve ⑥ denoting the largest achievable N_m at any length scale), $N_m > 1$ and $N_g < 10$ are realized in the length scale region between 10^{-3} m and 10^{-5} m . In Fig. 2.2, which can also be used to choose the design parameters for a MEMS device, the region shaded in grey should be expected to exhibit field-assisted self-assembly. Thus, at the microscale, the magnetic force can effectively compete with the surface tension force to produce aggregates (since at this scale the gravitational force does not play a significant role). It is then intuitive that the formation of three-dimensional structures through ferrofluid field-assisted

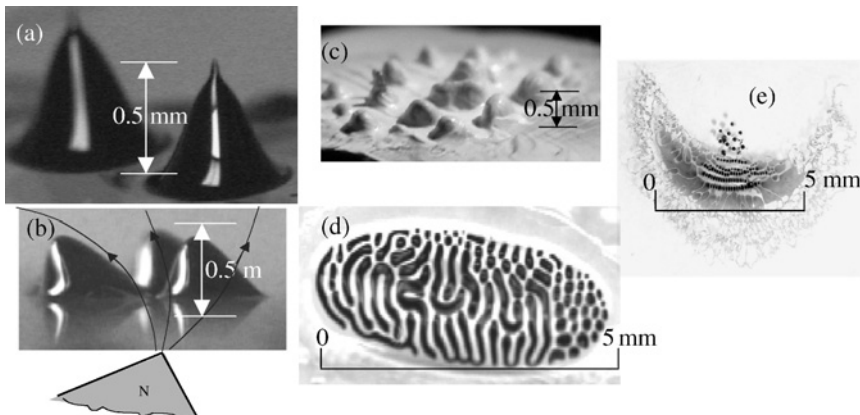


FIG. 2.3. (a) Three-dimensional ferrofluid structures produced on a flat substrate using a bar magnet. (b) Orientations of these structures with respect to the magnetic lines of force. (c) Permanent ferrofluid structures made by mixing a curing agent (Sylgard®) with the ferrofluid and then curing under a magnetic field. (d) Labyrinthine structures formed in a Hele Shaw cell. (e) Patterns exhibited by an oil-based ferrofluid on water surface.

self-assembly is favored at the microscale, which can be exploited for use in various MEMS applications (Mukhopadhyay et al., 2005).

Three-dimensional mesoscopic ferrofluid structures and arrays of various configurations have been created on flat substrates using a magnetic field (Sinha et al., 2004). Fig. 2.3(a) presents an image of a mesoscale 3-D structure produced by a hydrocarbon oil-based EFH 1 ferrofluid (FerroTec USA, NH) that was placed on a wetting glass surface under the influence of the nonuniform magnetic field. The height, shape and orientation of such microliter droplets can be adjusted by altering the nature of the magnetic field, as shown in Fig. 2.3(b). Although such aggregates are semi-permanent (i.e., they disappear when the magnetic field is withdrawn) permanent structures can be created by mixing low-viscosity epoxy resins (e.g., with a fast cure silicone elastomer) with the ferrofluid, applying a magnetic field to create ferrofluid structures and curing them. Since the final size and shape of a hardened structure will depend upon that of an aggregate at the instant of curing, it is important to characterize the shapes of the ferrofluid structures (refer to Fig. 2.3(c)). This technique offers a quick and easy method of creating 3-D MEMS scale features, which could be used in rapid prototyping of MEMS using polydimethylsiloxane (PDMS).

Inside an immiscible liquid medium in a Hele Shaw cell, ferrofluids exhibit labyrinthine patterns (Sinha et al., 2004) under an imposed magnetic field (Fig. 2.3(d)). Field-induced self-assembly of an oil-based ferrofluid on water

surface under a magnetic field is observed to create intriguing structures³ (Fig. 2.3(e)). If suitable means are identified for depositing these structures on a surface and curing those to permanent features, a viable technique for the bottom-up assembly of MEMS devices could emerge.

The field-induced deformation of a ferrofluid surface can be used for micromanipulation of MEM devices, e.g., a micromirror. The structures described in Fig. 2.3 are reversible, i.e., they regain their original shape upon removal of the field. Thus, repeated manipulation cycles are possible without the aid of moving components in a characteristic MEMS device. The magnetically controlled deformation of a ferrofluid surface can offer a unique application in ophthalmology where a metal-like film (MLF) covered ferrofluid acts like a deformable mirror, and can be used to reduced optical aberrations in the human eye (Macpherson et al., 2005).

C. FIELD-INDUCED SELF-ASSEMBLY AND TRANSPORT IN FORCED FLOW

Several ferrofluid applications, e.g., microfabrication, ferrofluid-based switches and valves or MDT, can benefit from the self-assembly of magnetic nanoparticles in forced fluid flows. A ferrofluid can be mixed with wet etching chemicals and introduced into narrow channels (where masking is otherwise difficult). Thereafter, it can be deposited on the substrate wall locally and selectively by imposing a suitably designed magnetic field using microelectromagnets (Drndić et al., 1998). Thus, mask-less etching of micro- or mesoscale channels can be achieved using targeted ferrofluid aggregation.

Three-dimensional ferrofluid aggregates can also be used as microfluidic components in pumps and valves (Hartshorne et al., 2004) or as microsize contact switches. In a ferrofluid micropump, a magnetic field-driven ferrofluid droplet acts as a reciprocating piston in a microchannel to pump another fluid. In microvalves, ferrofluid aggregates (formed by imposing a magnetic field) are used to open or close the flow in a microchannel. In ferrofluid microcontact switches, liquid bridges of electrically conductive ferrofluids are formed under the influence of a magnetic field to establish contacts between two electrodes that are immersed in an immiscible fluid. All these microfluidic applications rely on the phenomenon of ferrofluid aggregation under an imposed magnetic field. For these devices to work, it is

³ This image titled *El Collar del Hierro: The Ferro-Necklace* was a finalist in the 3rd Science and Engineering Visualization Challenge, an annual international visualization competition organized by American Association for the Advancement of Science (AAAS) and the US National Science Foundation (NSF).

important that the ferrofluid structures maintain their integrity against the shear force exerted by another fluid flowing over them.

Similar self-assembled aggregates can be produced for a number of biomedical applications such as MDT (Mosbach and Schröder, 1979; Lubbe et al., 2001), magnetic fluid hyperthermia (Jordan et al., 2001) and magnetic resonance imaging (MRI) contrast enhancement (Pankhurst et al., 2003). MDT is a promising technique of first order, active, biophysical (Lubbe et al., 2001) drug targeting for the medical treatment of various diseases and cardiovascular episodes, such as stenosis and thrombosis (Mosbach and Schröder, 1979). In MDT, magnetically guided droplets of biocompatible ferrofluid with specific chemotherapeutic agents bonded to the nanoparticles are used to carry and release medicinal drugs at target sites *in vivo*. This enhances the efficacy of the drug while simultaneously minimizing its deleterious side effects. Since the US FDA-approved human exposure limit to static magnetic fields is relatively high (e.g., 2 T for the entire body and 5 T for a limb), fairly large magnetic field gradients can be used without detrimental side effects. The magnetic nanoparticles are influenced by magnetic fields generated outside the human body that produce the desired transport characteristics (Gillies et al., 1994). In magnetic fluid hyperthermia, ferrous nanoparticles are targeted to a tumor in a way similar to MDT. Then a high-frequency (~ 100 kHz) ac-magnetic field is imposed to rotate the nanoparticles embedded in the malignant tissue (Johannsen et al., 2005). If the heat generated due to friction between the oscillating magnetic nanoparticles and the malignant tissue can maintain the temperature above the therapeutic threshold of 42°C for 30 min or more, the cancer is destroyed without damaging the neighboring cells. Magnetic nanoparticles have also been proposed for intraocular retinal repair (Dailey et al., 1999; Holligan et al., 2003).

Magnetic fluids used in MDT systems must be biodegradable and non-toxic. They should have strong magnetic polarization and must maintain colloidal stability in biological systems. Recent developments in the synthesis of biocompatible ferrofluids have successfully addressed most of these material issues (Roger et al., 1999). However, very few researchers have addressed the hydrodynamics of MDT (Ruuge and Rusetski, 1993; Volatiras et al., 2002). Therefore, the transport issues related to MDT are yet poorly understood. Magnetic drug delivery requires that a given volume of drug-laden ferrofluid droplet be delivered in the form of an aggregate at a target location *in vivo* through the blood vessel or lymphatic system where it is localized until the medicinal drug disperses from the ferrofluid droplet into the affected area (Lubbe et al., 1999). Here, the challenge is to hold the ferrofluid aggregate in position against the blood (or lymphatic) flow in a

vessel next to the target location. In order to investigate the efficacy of the targeting, drug desorption in the target area must be investigated. Firsthand information on this can be achieved by analyzing the ferrofluid aggregate size that is localized at the target area and its dispersion under the shear force induced by blood (or lymphatic) flow.

Since an actual MDT situation involves several complicating factors including blood rheology and fluid-structure interaction, to begin with a logical stepwise approach should involve laboratory scale studies in simple geometries. Ferrofluid transport in blood vessels is important from two perspectives: first, these vessels lead to tissue-embedded capillaries where the drug may be required; alternately, MDT may be used to cure local damage or stenosis within these vessels themselves. This should be followed by *in vitro* studies and finally *in vivo* experiments. Ganguly et al. (2005a, b, c) characterized the complex hydrodynamic and magnetic force interactions on the aggregation and dispersion of a magnetic fluid that is held stationary by a magnetic field in a steady Poiseuille flow and in a pulsatile flow. They conducted a numerical analysis in a representative 2-D channel to obtain insight into force interactions as well as an experimental study. They investigated the dispersion by analyzing the ferrofluid aggregate size, mean position and frequency spectrum. Although the pulsatile circulation in the human body is complex, e.g., the FFT analysis of blood flow in the carotid artery (Liepsch, 2002) produces frequency peaks at 1.13, 2.26, 3.39, 4.52 and 6.78 Hz, their idealized experiments kept the flow waveform free from the higher harmonics to investigate the important features of the hydrodynamics. The dependence of the dispersion rates on the mean flow Reynolds numbers was examined to develop a generalized relationship that can be used for next-level *in vitro* MDT investigations.

Fig. 2.4(a) shows their computational domain, where ferrofluid is injected steadily from the lower inlet section in a channel flow, and a line dipole is placed next to the lower wall at a downstream location. Fig. 2.4(b) shows the predicted concentration of ferrofluid (in terms of the normalized particle volume fraction Φ^* ($= \varphi/\varphi_{in}$), where φ_{in} corresponds to the particle volume fraction at the inlet). Since the injected ferrofluid has a very low diffusivity ($D \sim 10^{-11} \text{ m}^2 \text{ s}^{-1}$) in water (Blums et al., 1983), very little cross-stream diffusion occurs from the ferrofluid streak. Instead, owing to the magnetic body force, the ferrofluid collects near the line dipole and builds a local structure in the form of a region of high concentration. At the same time, advective-diffusive transport of the nanoparticles takes place from this region to downstream locations. The aggregate initially grows as the ferrofluid supply from the inlet exceeds its washaway rate. However, after it reaches a

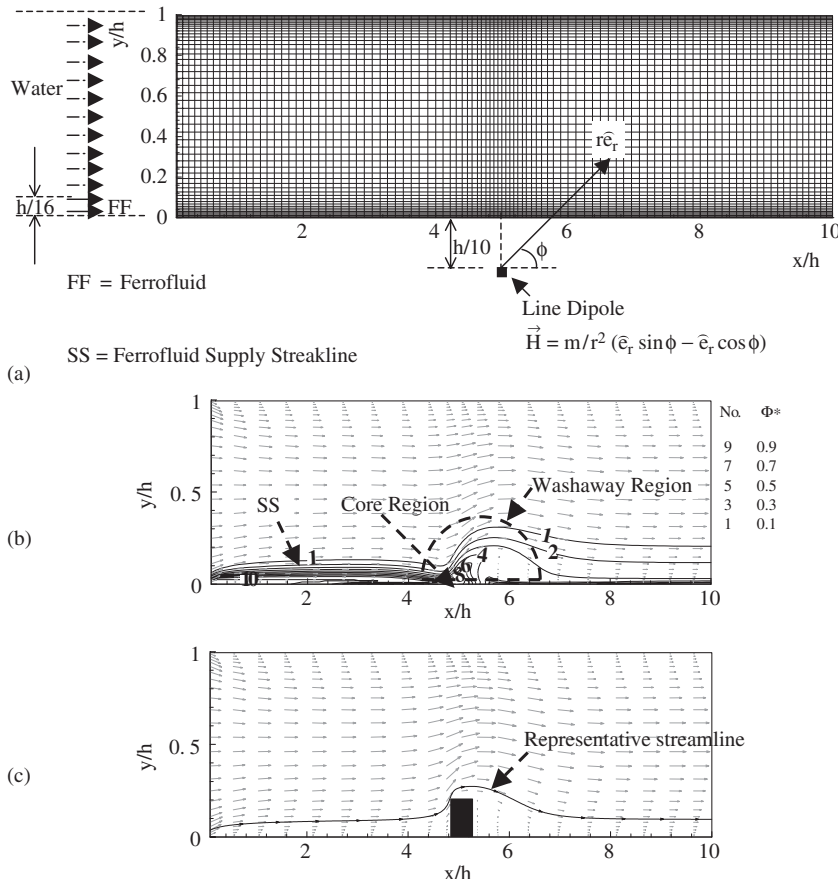


FIG. 2.4. (a) Schematic diagram of the computational domain. (b) Steady-state ferrofluid structures (formed due to the influence of a line dipole with strengths of 0.1 A/m) represented by the normalized particle volume fraction Φ^* contours ($= \phi/\phi_{in}$). Ferrofluid dispersion from the structures due to hydrodynamic shear is steadily replenished through a continuous supply from the inlet. (c) Similar recirculation profile is produced at the wake of a solid obstacle of normalized length \times height $= 0.45 \times 0.2$ placed in a Poiseuille flow of same Re (250).

critical size, the ferrofluid dispersion rate is equal to its influx and stable structure, as described in Fig. 2.4(b) is established. Fig. 2.4(b) also shows that there is a departure from Poiseuille flow, since the streamlines move away from the lower wall at upstream locations before the aggregate. However, the ferrofluid continues to move along the lower wall towards the dipole, since it is attracted in the direction of increasing magnetic field strength. The velocity vectors in Fig. 2.4(b) show that boundary layer separation and flow recirculation occur downstream of the ferrofluid aggregate.

Since both the magnetic field gradient and the ferrofluid concentration are high near the dipole, a large magnetostatic pressure builds up. This induces flow stagnation in a manner similar to that produced by a solid obstacle placed in a flow.

Fig. 2.4(c) compares the flows induced by the ferrofluid aggregate at $m = 0.1$ A/m (Fig. 2.4(b)) and a solid obstacle of normalized length \times height $= 0.45 \times 0.2$ placed on the channel wall with the two flows at identical Reynolds numbers. The ferrofluid dispersing into the flow from the core collects temporarily in this recirculation region and creates the washaway region. Likewise, in Fig. 2.4(c), the streamline adjacent to the solid obstacle is in qualitative agreement with the shape of the washaway region downstream of the ferrofluid aggregate. Since the aggregate size grows as the dipole strength is increased, the flow in the washaway region can also be altered accordingly. This provides evidence that these ferrofluid aggregates, if used in a microfluidic device, can act as a plug or a valve, which can be controlled by externally altering the magnetic field. Depending upon the application, the flow recirculation occurring in the washaway region can have favorable or detrimental effects. For example, in ferrofluid microvalves or pumps, the recirculation is undesirable, since it leads to additional channel pressure loss. On the contrary, in micromixing devices, ferrofluid structures can be constructed to achieve additional recirculation and enhance the cross-stream mixing (which is generally extremely slow in microchannels). In MDT applications, the creation of the washaway region due to the flow recirculation is favorable, since it allows the ferrofluid (and the medicinal drug functionalized with it) to stay longer in the vicinity of the target organ.

Experimental investigations of ferrofluid aggregation and transport in steady (Ganguly et al., 2005a, b) and pulsatile (Ganguly et al., 2005c) flows through pipes have corroborated these predictions. As shown in Fig. 2.5, in these experiments, a known volume (3 μ l) of EMG 705-series (FerroTec USA, NH) water soluble ferrofluid ($\phi_{in} = 4.0$) is released from a microliter syringe pump into a steady or pulsating laminar pipe flow of distilled water through a horizontally mounted glass tube (inner diameter 10 mm, length 1 m). A flow is established for $150 < Re < 400$, which is representative of the mean Re corresponding to hemodynamic flows in human veins and arteries; the mean flow Re in a coronary artery can vary from 100 in a resting state to 400 during exercise (Back and Banerjee, 2000). A rare-earth NdFeB permanent magnet mounted at $\theta = \phi = 45^\circ$ (refer to Fig. 2.5) with one corner of its pole face touching the lower edge of the glass tube establishes the magnetic field. The spatial distribution of the vertical component of magnetic field (measured with a 0.5 mm resolution using a Gaussmeter) shown in

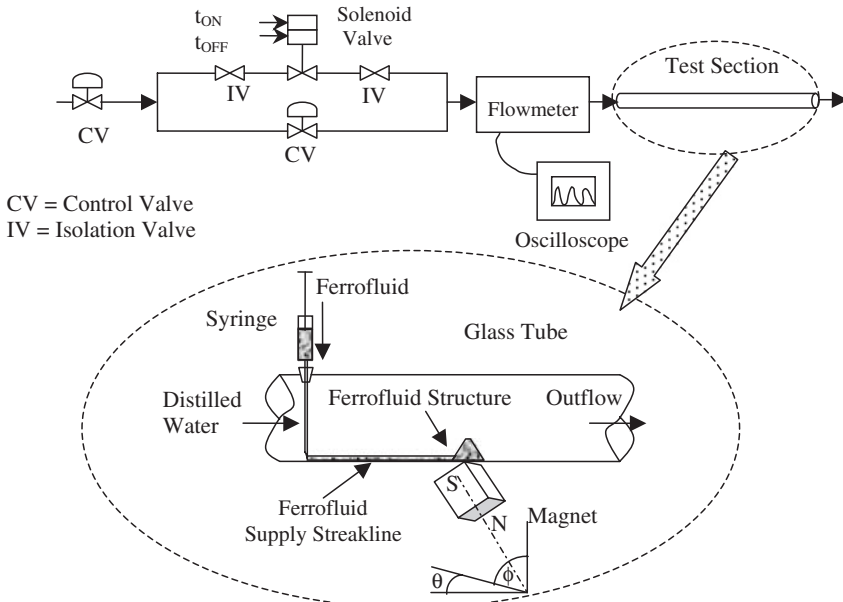


FIG. 2.5. Schematic diagram of the experimental setup. Inset: the enlarged view of the test section.

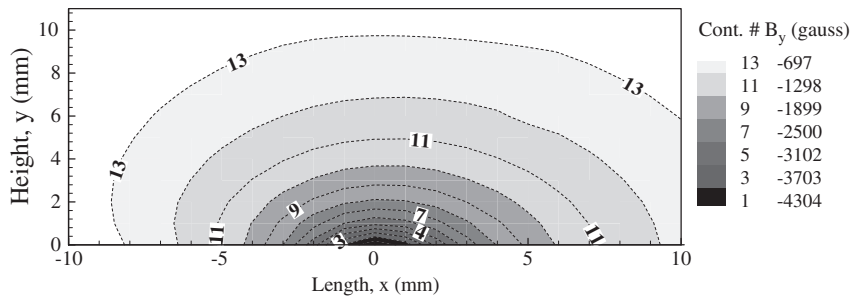


FIG. 2.6. Spatial variation of the vertical component of the magnetic field B_y . The location $y = 0$ denotes the outer edge of the glass tube wall (of 1 mm thickness) and $x = 0$ indicates the point where the bar magnet touches the wall (c.f. Fig. 2.5). The magnetic field is represented in units of gauss ($1 \text{ G} = 10^{-4} \text{ T}$).

Fig. 2.6 indicates that the largest possible gradient is produced at the test section. The field intensity $|\mathbf{B}_y|$ and the corresponding field gradients have large values near the dipole, but diminish quickly moving away from it. The magnitudes of the field gradient components provide an indication of the magnetic body force that the ferrofluid experiences.

The dispersion and localization of the ferrofluid observed from direct images acquired using a CCD camera against a white backlight (since the ferrofluid is dark and opaque) give experimental evidence of field-induced ferrofluid aggregation and subsequent dispersion of ferrofluid structures in pipe flow. The entire ferrofluid mass is transported by advection to the region near the dipole tip and builds up a ferrofluid 3-D mesoscopic accumulation. Initially, the ferrofluid accumulation rate exceeds its wash-away rate and the size of the nanoparticle aggregate grows into a conical shape. The supply streakline and the resulting ferrofluid structure are visible in Fig. 2.7(a) and (b).

Once fresh supply to the aggregate ceases, the advective and diffusive transport of the ferrofluid into the continually flowing host water stream leads to depletion in the ferrofluid aggregate. This phase is presented through the image sequences in Fig. 2.8(a). Both the simulation (Fig. 2.4) and experiment (Figs. 2.7(b) and 2.8(b)) show that a ferrofluid aggregate develops near the dipole, which behaves as a solid obstruction in the flow, creating downstream recirculation. In the region close to the dipole, the magnetic body force on the nanoparticles exceeds the shear force applied by the host fluid flow and causes the magnetic nanoparticles to move closer to the dipole. This further increases the magnetic force that they experience, pushing them more inward. Thus, a tightly bound core region is formed. The front view of this aggregate in Fig. 2.8(c) strongly resembles the simulated core region presented in Fig. 2.4(b). An outward ferrofluid flux

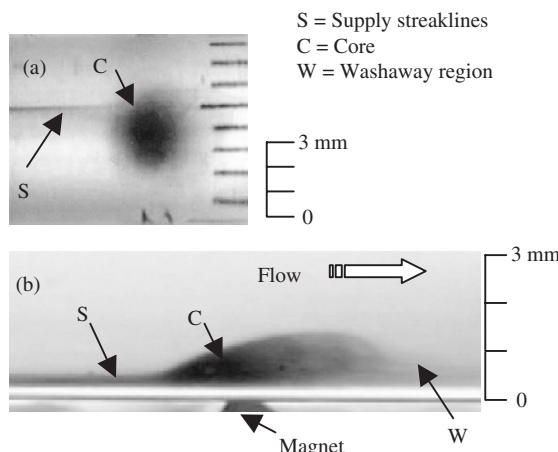


FIG. 2.7. Accumulation of ferrofluid near the dipole at $t = 20$ s: (a) top view, (b) front view. Volume of injected drop = $3 \mu\text{l}$, flow $Re = 250$. Accumulation phase continues till $t = 100$ s.

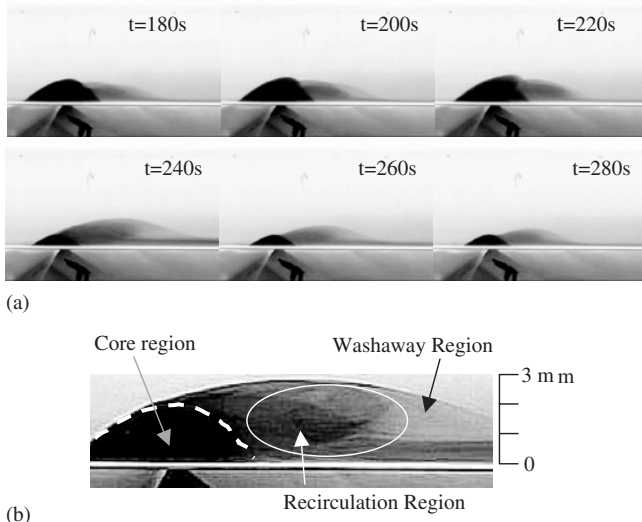


FIG. 2.8. Time evolution during the depletion phase of the ferrofluid structure (the volume of injected ferrofluid is $3 \mu\text{l}$ and the flow $Re = 250$): (a) $t = 180\text{--}280\text{s}$ during one complete washaway cycle and (b) Ferrofluid structure at $t = 240\text{s}$ after injection. The combined advective-diffusive hydrodynamic force competes with the magnetic force to produce a tightly bound core region that is immediately followed by a downstream washaway region. The contrast-enhanced image in the right is provided for better visualization of the flow recirculation.

occurs from the core region due to the presence of a large local concentration gradient at the periphery of this core (Fig. 2.4(b) presents the comparable simulation results). As the nanoparticles travel outward from the core through diffusion, the magnetic force on them weakens. Hence, the shear force exerted by the main flow becomes comparable to the restoring magnetic force. Consequently, ferrofluid dispersion occurs from the boundary demarcating the core. As the core boundary erodes, ferrofluid recirculates in this wake or “washaway” region. In this region, the magnetic body force is much weaker than in the core because of the smaller ferrofluid concentration and larger displacement from the dipole. Hence, ferrofluid is readily transported away from the washaway region through the influence of the host flow.

Fig. 2.9 provides physical insight into the mechanism of ferrofluid dispersion from the aggregate core and the growth of the washaway region. Flow perturbations during the experiment create vortex shedding (Kim and Choi, 2003) in the wake of the ferrofluid structure. There is unstable balance between the magnetic and shear force in the peripheral region because even slight dislocation of a particle away from the core by the shear force causes

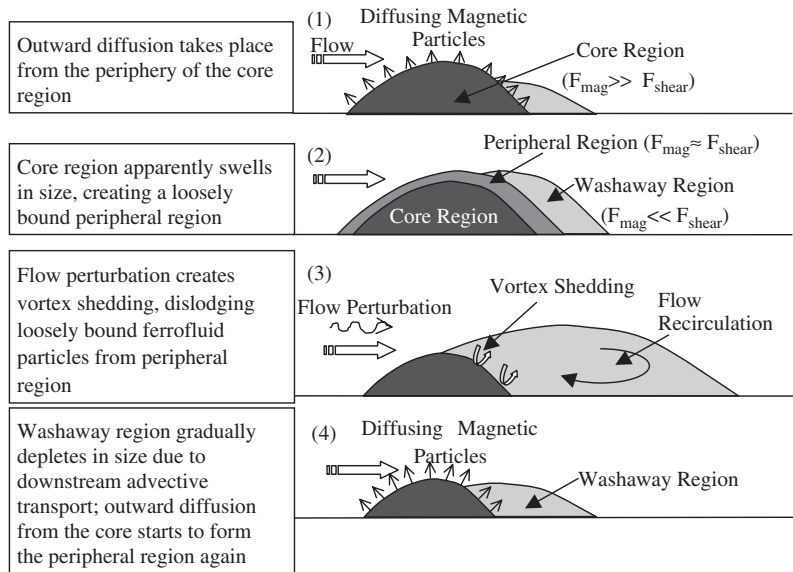


FIG. 2.9. Schematic diagram showing the phases of the ferrofluid washaway that lead to apparent oscillations of the core and washaway regions during one washaway cycle.

the magnetic force to diminish. In that case, small perturbations lead to sudden ferrofluid release from the core periphery, followed by advective washaway. Erosion of the ferrofluid aggregate occurs in cycles, i.e., the projected areas of the core and the washaway region in particular are observed to first increase with time (e.g., the washaway region is observed to swell from $t = 180$ to 240 s in the Fig. 2.8(a)). Then, a substantial amount of ferrofluid is suddenly washed away downstream. This is accompanied by a rapid shrinking of the aggregate size (as seen in Fig. 2.8(a) where the washaway region shrinks quickly between $t = 240$ and 260 s). This behavior is referred to as a washaway cycle. Since there is continuous loss of ferrofluid from the aggregate, its final size after each washaway cycle is progressively smaller.

Fig. 2.10 shows the washaway cycles in a steady flow ($Re = 382$) as the projected area of the ferrofluid aggregate is plotted as a function of time. In a 1 Hz frequency pulsatile flow, an accumulation phase followed by washaway is again observed for the ferrofluid aggregate. However, washaway occurs four times faster than that for the steady flow as shown in Fig. 2.10 and, unlike for the steady flow, this washaway behavior is not periodic. Fig. 2.11(a) illustrates the oscillation of the ferrofluid aggregate during a complete 1 Hz flow cycle by presenting a sequence of images taken at 0.1 s

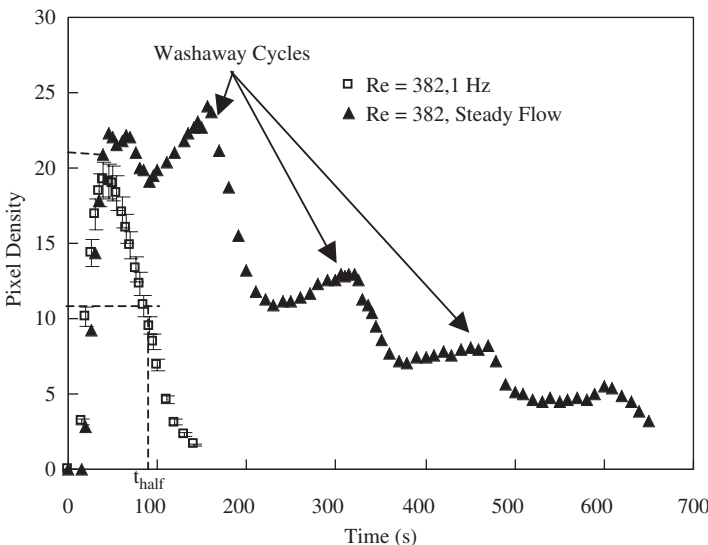


FIG. 2.10. Ferrofluid washaway profile for a steady and for a 1 Hz pulsatile flow ($Re = 382$ for both). The pixel density (in arbitrary units) characterizes the ferrofluid accumulation at the target location in a qualitative manner. Half-life (t_{half}) of the aggregate is described as the time when the projected aggregate area is half of the maximum accumulated size (e.g., for the pulsatile flow at $Re = 382$, $t_{\text{half}} \approx 90$ s).

intervals. In a pulsatile flow, both the mean position of the ferrofluid aggregate and the projected area of the “core + washaway” region oscillate about their mean value. The frequency spectrum of the imposed periodic flow shows in Fig. 2.11(b) a strong 1 Hz component and a weaker 3 Hz component. However, the frequency spectrum of the oscillating aggregate size shows several peaks (e.g., Fig. 2.11(b)). Generation of these extra harmonics in the frequency spectrum of the aggregate size results from a non-linear interaction of the shear and magnetic forces.

The time t_{max} required to reach the maximum integrated pixel intensity A_{max} describes the accumulation phase. Subsequently, the aggregate size decreases due to washaway. The time required for the aggregate size to deplete to half its maximum size (i.e., $A_{\text{max}}/2$) denotes the half-life t_{half} of the aggregate. When experiments are performed in a pulsatile flow of given frequency (e.g., 1 Hz) at several mean Re of the flow, t_{max} and t_{half} are observed to decrease with increasing Re . Parametric investigations yield the relations $A_{\text{max}} \propto Re^{-0.71}$, $t_{\text{max}} \propto Re^{-2.1}$ and $t_{\text{half}} \propto Re^{-2.2}$ (Ganguly et al., 2005c). The relations can be useful to design for the aggregation and dispersion of ferrofluids (e.g., during MDT or in ferrofluid-based pumps and valves), since they provide information about the ferrofluid aggregate

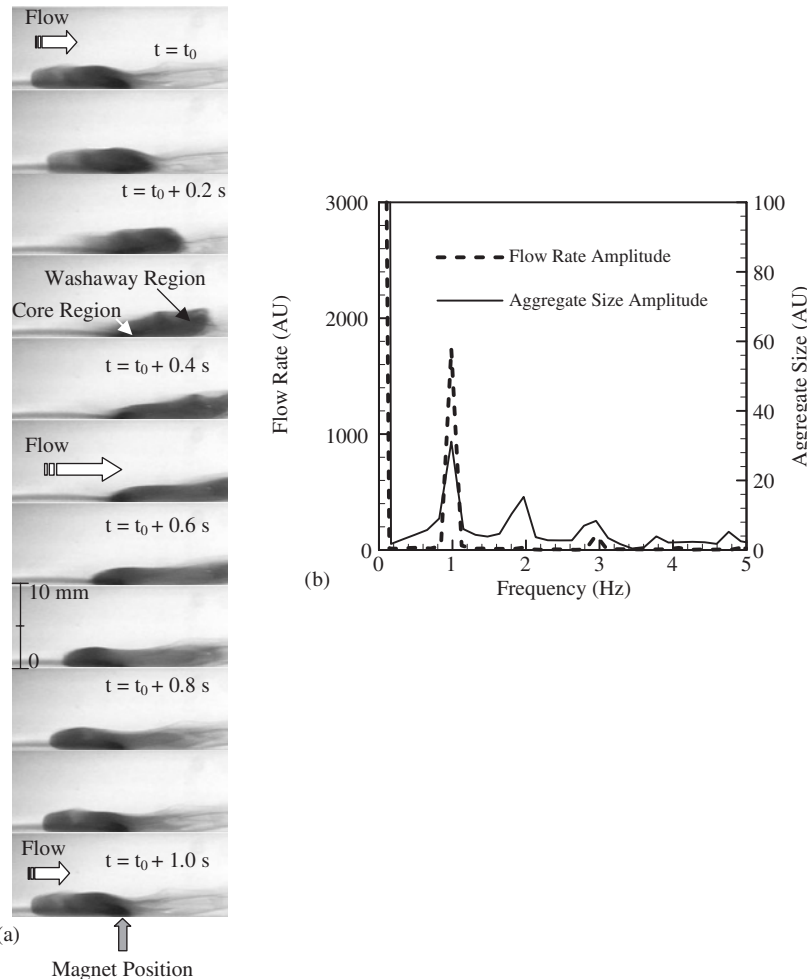


FIG. 2.11. (a) The oscillation of ferrofluid accumulation during a single 1 Hz pulsating flow cycle ($Re = 382$). Images represent the ferrofluid dispersion at 0.1 s intervals ($t = t_0$ represents a condition of minimum instantaneous flow). (b) FFT response of the pulsatile flow rate and projected area of the ferrofluid aggregate in arbitrary units (AU). FFT of the flow profile shows a strong presence of the 1 Hz-imposed frequency along with a higher harmonic at 3 Hz. Oscillation in the aggregate size exhibits peak at 1, 2, 3, 3.8 and 4.8 Hz.

lifetime at a target location. For instance, if MDT efficacy is to be expressed in terms of the aggregate size (that is representative of the total drug supply) and its half-life (that indicates the duration during which the drug is released at the target site), these relationships imply that the local blood flow Reynolds number becomes an important parameter.

Field-induced aggregation of a ferrofluid can be used for wet-etching or targeted deposition of materials inside a prefabricated microchannel. A ferrofluid stream (conjugated with the etchant, or the material to be deposited) can be provided to a microchannel as shown in Fig. 2.12(a). Localization of the ferrofluid can be achieved by a field created by a line dipole as described before. Fig. 2.12(b) shows the ferrofluid aggregation at the target location for a dipole strength $m = 0.5 \text{ A m}^{-1}$ in a $500 \mu\text{m}$ wide channel at $Re = 10$. For particle size of 10 nm , the magnetophoretic components are negligible and the ferrofluid accumulation on the target location takes place mostly by ferrohydrodynamic advection. In Fig. 2.12(b), the largest φ^* at the target spot is 0.25. Higher particle loading of ferrofluid or increasing the particle size would increase the ferrofluid buildup to larger values. However, the colloidal stability of the particles would be seriously affected unless special care is taken (e.g., the particles could be charged so that they repel each other and remain uniformly suspended in the host liquid). A transport analysis of such particles in MEMS applications would require a more elaborate two-phase flow formulation where the particles are considered as

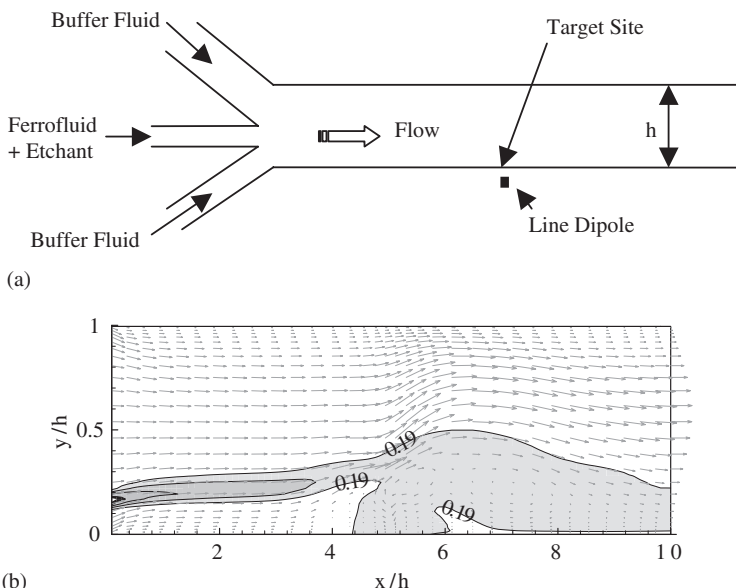


FIG. 2.12. Feasibility of dosing a ferrofluid and an etching fluid (or a material to be deposited) conjugate inside a microchannel of $h = 500 \mu\text{m}$, at $Re = 10$: (a) The schematic diagram of the proposed configuration, (b) targeted deposition of ferrofluid (contours denote the normalized volume fraction (φ/φ_{in}) of the magnetic nanoparticles) using a line dipole of $m = 0.01 \text{ A m}^{-1}$. Particle (10 nm diameter) volume fraction at inlet, $\varphi_{in} = 0.03$.

the dispersed phase in the host liquid. Also, at larger particle size, the particles will no longer remain single domain, and superparamagnetic. Consequently, the particle magnetization would differ from the Langevin equation (Eq. (1.1)).

III. Thermomechanical Ferrofluid Applications

Ferrofluids have promising potential for heat transfer applications, since advective transport in a ferrofluid can be readily controlled by using an external magnetic field. In a nonisothermal flow field, the magnetization of a ferrofluid depends both on the local value of \mathbf{H} and the fluid temperature. Within a small range of temperature variation (about a reference temperature T^* and H^*), the magnetization of the fluid, M , can be expressed in the linearized form (Bashtovoy et al., 1988)

$$M = \mathbf{M}^* + \left(\frac{\partial M}{\partial T} \right)_H (T - T^*) + \left(\frac{\partial M}{\partial H} \right)_T (\mathbf{H} - \mathbf{H}^*), \quad (3.1)$$

and the magnetization vector \mathbf{M} can be related to \mathbf{H} (Ganguly et al., 2004a) through the state relation

$$\mathbf{M} = \chi_m \mathbf{H} \quad (3.2)$$

The susceptibility, χ_m can be assumed as a function of temperature alone. For a small temperature change, the linearized relation

$$\chi_m = \chi_0 [1 + \beta_p (T - T^*)]^{-1} \quad (3.3)$$

can be applied, where β_p denotes the coefficient of thermal expansion of ferrofluid. Thus, it becomes clear how the temperature gradient in ferrofluid causes a spatial gradient in its magnetic susceptibility. With this understanding, the KBF appearing in momentum equation (Eq. (2.2)) simplifies (Mukhopadhyay et al., 2005) into the form

$$\begin{aligned} \mathfrak{I}_i &= \frac{1}{2} \mu_0 \chi_m (1 + \chi_m) \left[\frac{\partial}{\partial x_i} (H_j H_j) \right] + \mu_0 \chi_m \beta_p \left(H_j \frac{\partial \chi_m}{\partial x_j} \right) H_i \\ &= \frac{1}{2} \mu_0 \chi_{m0} \left[1 - \beta_p (T - T^*) \frac{\partial}{\partial x_i} (H_j H_j) \right] - \mu_0 \chi_{m0}^2 \beta_p \left(H_j \frac{\partial T}{\partial x_j} \right) H_i \quad (3.4) \end{aligned}$$

The first term in Eq. (3.4) is analogous to the pressure term and can be referred to as the “magnetostatic pressure”. In the absence of a temperature gradient the second term of Eq. (3.4) is zero and, the first term becomes a

function of gradient (H^2) only. Consequently, the KBF creates a static pressure field in the flow that is symmetric about the line dipole (producing a curl-free force field, i.e., $\text{curl}(\mathfrak{J}) = 0$). Such a symmetric field does not alter the velocity profile. However, for nonisothermal systems with an asymmetric (or biased) temperature distribution about the imposed magnetic field, the resulting KBF is also asymmetric (for such a force field, i.e., $\text{curl}(\mathfrak{J}) \neq 0$). This leads to the self-organized advective motion of the ferrofluid across isotherms. This influences the advective components of the energy equation, i.e.,

$$\partial(\rho C_P T) / \partial t + \partial(\rho v_j C_P T) / \partial x_j = \partial(k \partial T / \partial x_j) / \partial x_j, \quad (3.5)$$

where T represent the ferrofluid temperature, C_P the specific heat and k the thermal conductivity. The resulting convection is called thermomagnetic convection, which can be particularly useful for cases when conventional thermogravitational convection fails to provide adequate heat transfer, e.g., in microscale devices, or under reduced gravity conditions. However, unlike conventional free or forced convection, thermomagnetic convection is not yet well characterized.

Finlayson (1970) first discussed thermomagnetic convection and analytically calculated a critical stability parameter beyond which this form of convection sets in. Schwab et al. (1983) conducted experimental investigation of convective instability in a horizontal layer of ferrofluid under a vertical temperature gradient and a homogeneous vertical magnetic field and determined the influence of the magnetic Rayleigh number on the Nusselt number. Abraham (2002) performed an analytical study on a similar configuration to characterize a relationship between the critical wave number associated with magnetically induced Rayleigh–Bénard convection and the magnetization parameters. Lange (2002) analyzed the origin of the thermomagnetic force in a heated ferrofluid layer. Krakov and Nikiforov (2002) addressed the influence of the relative orientation of the temperature gradient and magnetic field on thermomagnetic convection in a square cavity. Yamaguchi et al. (1999a, b) performed thermomagnetic convection experiments in a square enclosure and characterized the heat transfer in terms of a magnetic Rayleigh number. A comprehensive review of the state of research on thermomagnetic convection can be found in Mukhopadhyay et al. (2005).

A differentially heated square cavity explicitly reveals the role of the thermomagnetic body force in creating convection. It is also relatively

straightforward to compare thermomagnetic heat transfer with the corresponding well-characterized buoyant free convection (de Vahl Davis, 1983) problems in this configuration. The origin of thermomagnetic convection in a differentially heated cavity under the influence of a line dipole is described schematically in Fig. 3.1(a). In the absence of buoyant free convection, the initial temperature gradient is directed horizontally from the cold to the hot wall, and the gradient $\nabla\chi_m$ acts in the reverse direction. If we consider two points ① and ② spaced symmetrically about the line dipole (cf. Fig. 3.1(b)), the value of KBF is larger at point ② than at point ①. Therefore, a net clockwise circulation in the fluid is induced, i.e., by the imbalance in the magnetic pressure term around the line dipole, which develops thermomagnetic

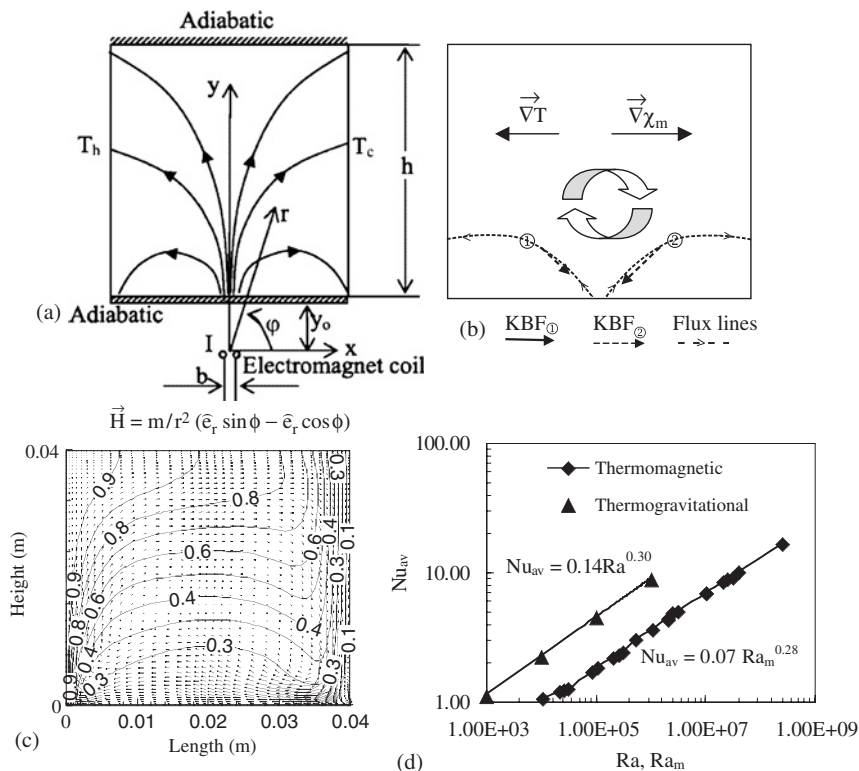


FIG. 3.1. Thermomagnetic convection in square enclosure: (a) The configuration, (b) origin of thermomagnetic convection, (c) normalized isotherm and velocity profile in a purely thermomagnetic flow, (d) average Nu scales with Magnetic Rayleigh number $Ra_m = (\mu_0\rho_0\beta_0\chi_{m,0}m^2\Delta T P r)/(\eta^2 L^2)$ in a manner similar to thermogravitational Nu scales with Ra (de Vahl Davis, 1983).

convection in the cavity. The resulting temperature field is shown in Fig. 3.1(c). A more elaborate analysis is to be found elsewhere (Ganguly et al., 2004b).

Tangthieng et al. (1999) observed that thermomagnetic convection provides up to 45% heat transfer enhancement over buoyant-free convection. Kikura et al. (1993) proposed a magnetic Grashof number, $Gr_m = \rho KL^3 |\nabla \mathbf{H}| \Delta T / \eta^2$ (where K denotes the thermomagnetic coefficient in units of A/m K) to characterize the influence of the thermomagnetic body force in a cubic enclosure. Snyder et al. (2003) simulated combined free and thermomagnetic convection in a cubic enclosure and obtained results in agreement with the measurements of Kikura et al. (1993). Ganguly et al. (2004b) showed (refer to Fig. 3.1(d)) that the height-averaged Nusselt number, Nu_{av} for thermomagnetic convection in a square enclosure using a line dipole is correlated with a dimensionless magnetic Rayleigh number $Ra_m = (\mu_0 \rho_0 \beta_p \chi_{m,0} m^2 \Delta T Pr) / (\eta^2 L^2)$, where Pr denotes the Prandtl number. A scaling analysis by Mukhopadhyay et al. (2005) confirms the results of Fig. 3.1(b). For a given dipole strength, thermomagnetic heat transfer increases when the length scale decreases. This makes thermomagnetic convection a potentially viable option for microscale heat transfer applications. For forced convection configurations, Ganguly et al. (2004a) have shown that thermomagnetic convection can be utilized to enhance the heat transfer by suitable placing one or more field-inducing dipoles.

IV. BioMEMS and Biomedical Applications of Magnetic Microspheres

Magnetic microspheres are well suited for BioMEMS because they can provide relatively large reaction sites, ensuring fast reaction times. Also, since each microsphere can be manipulated in isolation, the analysis and monitoring of small samples can be achieved. Finally, their small size allows integration into “micro-total analysis systems (μ -TAS)”. Magnetic tweezing in biological systems is preferable to electrostatic (e.g., electrophoretic or dielectrophoretic) manipulation (Wong et al., 2004) for several reasons. First, an aqueous medium has a very low relative permeability (i.e., there is no magnetic “screening” with magnetic microspheres). This allows more efficient coupling between an applied field and the magnetically labeled material. Moreover, the relatively low intrinsic magnetic susceptibility of biomaterials provides substantial contrast between labeled and unlabeled materials enabling a high degree of detection and selectivity. Magnetic fields can also be biologically safe, allowing manipulation of living cells using appropriate magnetic chaperons.

Recent advances in photolithography have enabled the magnetic gradients exceeding 10^5 T/m in MEMS devices (Lee et al., 2001). Such fields can be used to either remotely position or selectively filter biological materials attached to magnetic beads. *In vitro* applications of the specific labeling of cells or bio-molecules with magnetic microbeads can lead to advanced developments in cell manipulation and separation (Suzuki et al., 2004), DNA sequencing and separation (Doyle et al., 2002), etc. The predominant transport issue for these μ -TAS devices is the precise magnetic manipulations of the microbeads so that the chemical/biological reactions at the bead/analyte surface are controlled.

Like ferrofluids, magnetic microspheres can also be used for *in vivo* drug targeting, where the beads are used as vectors for carrying a drug and magnetically guiding it to the desired location (Iacob et al., 2004). Magnetic microspheres have larger particle size, greater magnetic moments than the nanoparticles of ferrofluids and hence, are more conveniently guided *in vivo*. Precise targeting of the magnetic microbeads can be achieved even in the interior regions of a subject through the use of an external field that magnetizes the microspheres and a magnetic implant that creates the local field gradient (Iacob et al., 2004; Yellen et al., 2005). Field-induced aggregation of magnetic microspheres can be used to embolize blood vessels inhibiting the blood supply and thus facilitating necrosis of tumors (Rotariu et al., 2004). In addition, owing to the larger magnetic moments of the microscopic particles (which leads to a larger distortion of an imposed magnetic field by them), magnetic microspheres can offer better performance as an MRI contrast enhancement agent compared to ferrofluids (Gijs, 2004).

A. FIELD-GUIDED TRANSPORT

Magnetic microspheres can be advantageously used as “mobile substrates” for bioassays, or even for *in vivo* applications; they are easily recovered from dispersion by high-gradient magnetic separation (Choi et al., 2001), or can reversibly be redispersed. When a single magnetic microsphere is transported in a fluidic device under an imposed magnetic field gradient, it experiences following forces: magnetic force \mathbf{F}_m , drag force \mathbf{F}_d exerted by the fluid (since the particle tends to move with a finite velocity relative to the fluid), and the gravitational force \mathbf{F}_g . The motion of a particle (in terms of its absolute velocity \mathbf{V}_p) under these forces is described by applying Newton’s second law of motion for a particle, i.e.,

$$\left(\frac{4}{3}\pi a^3 \rho_p\right) dV_p/dt = [\mathbf{F}_m + \mathbf{F}_d + \mathbf{F}_g]. \quad (4.1)$$

The force terms appearing on the right hand side of Eq. (4.1) are

$$\mathbf{F}_m = \mu_0 \left(\frac{4}{3} \pi a^3 \right) \left[\chi_i / \left(1 + \frac{1}{3} \chi_i \right) \right] \frac{1}{2} \nabla (\mathbf{H}_0 \cdot \mathbf{H}_0), \quad (4.2)$$

$$\mathbf{F}_d = 6\pi a \eta (\mathbf{V}_l - \mathbf{V}_p), \quad (4.3)$$

and

$$\mathbf{F}_g = \left(\frac{4}{3} \pi a^3 \right) (\rho_p - \rho_l) \mathbf{g}. \quad (4.4)$$

Here, \mathbf{H}_0 correspond to the local (undistorted) value of \mathbf{H} in absence of the microsphere, and \mathbf{V}_p and \mathbf{V}_l the absolute velocities of the particle (of density ρ_p) and the carrier fluid (of density ρ_l) respectively. The three forces result in particle drift, which is shown schematically in Fig. 4.1. The absolute velocity of the particle can be computed from the force-vector polygon shown in Fig. 4.1. The trajectory of the particle (shown by the dotted curve) can be obtained by time-integration of the instantaneous absolute velocity of the particle (refer to the velocity triangle of Fig. 4.1). Thus, by suitably imposing an external magnetic field, magnetic microspheres can be targeted to a desired location, transported in a desired fashion, separated from a stream or redispersed in a stream (by withdrawing the magnetic field).

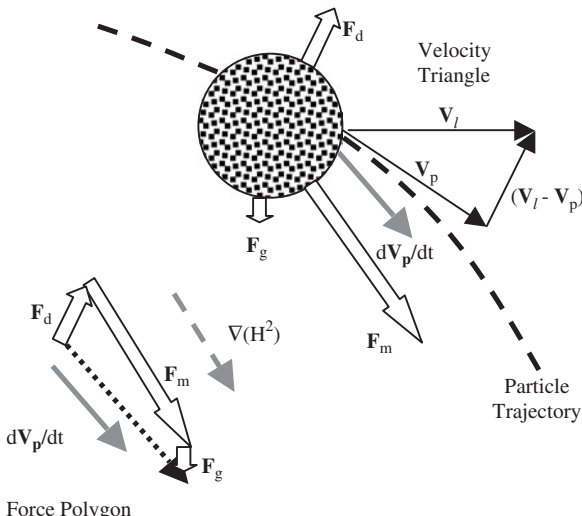


FIG. 4.1. Force dynamics for a single magnetic microsphere in a viscous fluid.

B. MICRO TOTAL ANALYTICAL SYSTEMS

Self-organized, assembled or aggregated magnetic microspheres can achieve several objectives in a μ -TAS device. First, functionalized microspheres can provide the site for biochemical reactions that are vital to the analytical device. For example, immunomagnetic separation (IMS) via mobile suspended magnetic microbeads provides the advantage of relatively rapid antigen capture as compared to enzyme-linked immunosorbent assay (ELISA). It has been used to easily and effectively confine and concentrate bacteria and protozoa from a variety of complex biological media, including foods and waste (Luk and Lindberg, 1991; Fratamico et al., 1992; Wright et al., 1994) and environmental water samples (Morgan et al., 1991; Yu, 1998; Kuczynska et al., 2003; Garcia-Aljaro et al., 2005). A wide variety of bioconjugates are commercially available that can be coated on the microspheres so that the microspheres can act as selective tags. Apart from bioanalysis, such tags can also have biosynthetic use. For example, streptavidin–biotin conjugation or base pairing between oligonucleotide residues can be used for immobilizing DNA targets on magnetic beads for DNA hybridization (Fan et al., 1999). All these bioanalytical features of magnetic microspheres are realizable at the macro- as well as microscale. Since the biochemical binding forces are essentially short-range forces, selective tagging by the magnetic beads is more effective in MEMS scale analyzers.

Second, magnetic microspheres can chaperon biochemical agents to target locations. This property can be used to transport biochemical agents either to a more active reaction zone or to withdraw the agents from a reacting medium thus promoting or inhibiting a specific biochemical reaction. It is also possible to magnetically target the tagged molecules to a specific zone in a microfluidic device to achieve a higher analyte concentration. This can enable detection processes to work above a threshold concentration. Fig. 4.2 describes the targeted localization of magnetic microspheres in a pressure-driven flow ($Re \sim 1$) through a $100 \times 2,000 \mu\text{m}$ capillary tube using a needle magnet. The particle concentration is large enough in the high field gradient region for strong interparticle interaction to induce the formation of self-assembled magnetic beads into chain-like structures. The separation of tagged molecules or biological entities (e.g., bacteria, DNA, protein or living cells) can be subsequently performed by controlling the formation and transport of these beads in microfluidic devices.

Third, momentum exchange between the magnetically transported microspheres and the host fluid can induce mixing in microfluidic devices. The

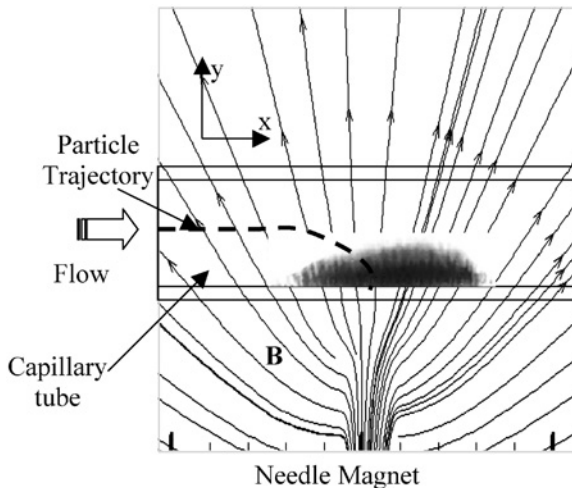


FIG. 4.2. Field-induced capture of magnetic microspheres in a micro-capillary flow. Chain-like structures can be seen at the capture region as the particle–particle interaction grows stronger in the region of high bead concentration. Magnetic field plot is obtained using the Maxwell SV® solver.

use of serpentine and twisted channels has shown promising improvement in microchannel mixing (Liu et al., 2000; Bertsch et al., 2001). Active mixing can be achieved by imparting periodic perturbations to the flowfield. A perturbation can also be generated in the flow field by magnetic actuation (Beebe et al., 2001; Suzuki and Ho, 2002). The advantage of active mixing is that it can be activated whenever required and can be controlled.

All these features make magnetic microspheres a suitable choice for MEMS-based biochemical sensors. Sinha et al. (2005) have proposed a proof-of-concept microfluidic sensor for detecting water-borne pathogenic agents. The sensor is based on a scaled-down version of the standard IMS technique. The microanalyzer component of the sensor consists of a mixing channel followed by a magnetic separation section. Magnetic microspheres coated with suitable bioconjugates (Kawaguchi et al., 1996) are allowed to mix with the sample fluid in a mixer such that pathogens attach themselves to the microspheres (Fig. 4.3(a)). Subsequently, the pathogen–microsphere conjugates are separated from the background water sample that is being tested by suitably placing electromagnetic traps on the channel walls in the first stage separator. After separation, the microspheres (with attached pathogens) can be washed by buffer solutions and be reversibly redispersed by sequentially turning the magnetic traps on and off (Fig. 4.3(b)). The second stage of the mixer and separator deals with detection techniques,

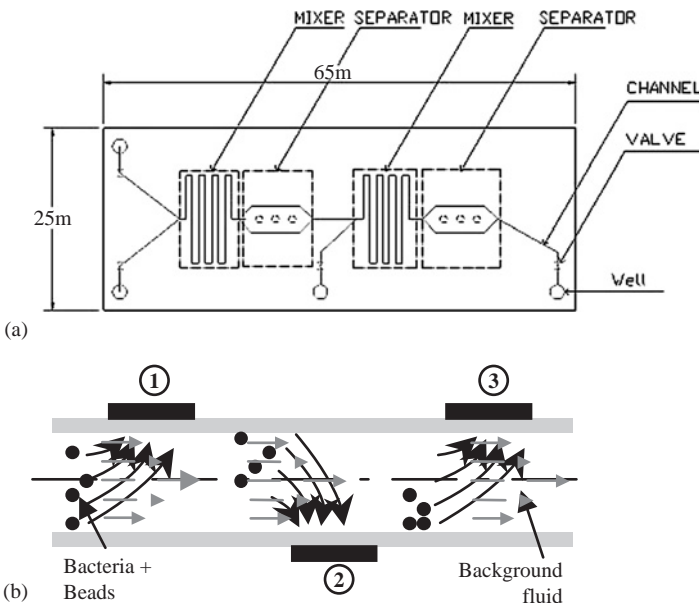


FIG. 4.3. (a) Schematic of a MEMS-based IMS sensor, (b) schematic of the separator section.

where standard electrochemiluminescence (ECL) (Bruno and Yu, 1996) can be implemented after a bead–pathogen conjugate is treated suitably with ECL chemicals (Blackburn et al., 1991) and concentrated in the magnetic traps. Magnetic concentration of the samples can enable good detection even for very dilute analyte solutions.

C. MICRO MIXERS USING SELF-ASSEMBLED CHAINS

Magnetic microspheres form chain-like structures due to the dipole–dipole interaction of the particles under an imposed magnetic field (Biswal and Gast, 2003). The chain strength increases if particles are bonded together with linker molecules. The natural tendency of these microsphere chains is to align themselves along the direction of the imposed magnetic field. The magnetic particles of such a chain are held together by the magnetic interaction energy of the particles (Eq. (1.3)). If the magnetic field is rotated, these chains also follow its orientation. When this occurs, a chain of N spherical particles experiences a magnetic torque Γ_m and an opposing viscous drag Γ_v according to the relations $\Gamma_m = (\mu_0\mu_r/4\pi)/(3|m|^2N^2/2(2a^3))\sin(2\delta)$ and $\Gamma_v = \frac{4}{3}N\pi a^3(2N^2/\ln(N/2))\eta\omega$

(Biswal and Gast, 2004a). Here, ω denotes the angular velocity of the chains. The response of the microbeads to the magnetic force is characterized by the Mason number (Biswal and Gast, 2004a)

$$Ma = \frac{\ln(N/2)}{N} \frac{\Gamma_v}{\Gamma_m} \sin(2\delta) = \frac{32\omega\eta}{\mu_0\mu_r\chi_{\text{eff}}^2 |\mathbf{H}_0^2|} \quad (4.5)$$

that compares the viscous and magnetic forces.

With a strong magnetic field, for magnetic beads of high χ_{eff} , for low-viscosity fluids or at a small angular frequency of rotation, $Ma \ll 1$. Then the microspheres form long unbroken chains rotating in synchronism with the imposed magnetic field with a very small angle δ (i.e., very closely following the orientation of the imposed rotating magnetic field as sketched in Fig. 4.4). Since the viscous torque originates from the interaction between the particles and the host liquid of the droplet, an equal and opposite torque is applied by the particles on the liquid. This induces a rotational motion inside the droplet in the liquid phase. The resulting advection in the droplet can be employed to enhance mixing. Since the advective velocity induced in the droplet is proportional to ω , which scales with Ma , the latter is an important parameter for describing the extent of mixing induced in the droplet by the rotating chains. Intuitively, a large value of Ma would induce more convection in the droplet, but the integrity of the chains and their ability to rotate synchronously with the imposed field deteriorate with an increase of Ma (Biswal and Gast, 2004a). Such chains can be made to rotate under a rotating magnetic field and these microrotors can also induce faster mixing in microchannels (Biswal and Gast, 2004b).

An alternative micromixer design has been proposed by Puri et al. (2006), which manipulates discrete droplets rather than continuous liquid streams. The substances or reactants to be mixed are confined in nano- to picoliter-size droplets, effectively producing a *lab-in-a-droplet* (LID). Magnetic microspheres are premixed in the droplet liquid, and form self-assembled stable

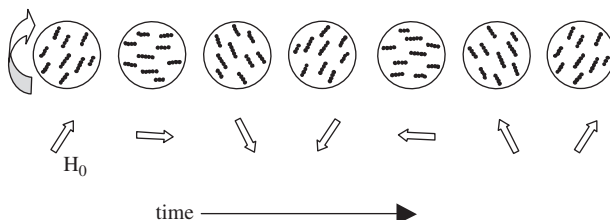


FIG. 4.4. Rotation of the magnetoresponsive chains as the imposed magnetic field rotates.

chains under an imposed magnetic field. When the magnetic field is rotated, the reagents in the droplet mix at a faster rate. Fig. 4.5 illustrates the mixing of a dye using the LID concept. The mixing time is found to be two orders of magnitude faster than purely diffusive mixing. Through independent micromanipulation of discrete droplets, complex procedures can be carried out in a manner that directly mimics traditional bench-top protocols. Because each droplet can be independently controlled, highly integrated flexible architectures can be implemented using this concept. For example, the micro- or nanoliter droplets could rest on a substrate, be immersed in an immiscible buffer, or even be transported through a microchannel by an immiscible host fluid (Shestopalov et al., 2004). The *LID* technique uses active control for mixing in the droplets using magnetic microspheres but does not necessarily require the integration of a power source into a microfluidic device. Microdroplets containing reactants could be used in a freeze-quenching device to trap metastable intermediates obtained during a fast chemical reaction (Lin et al., 2003). Bioanalytical diagnostics involving IMS (Sinha et al., 2005) can also be performed in such a droplet.

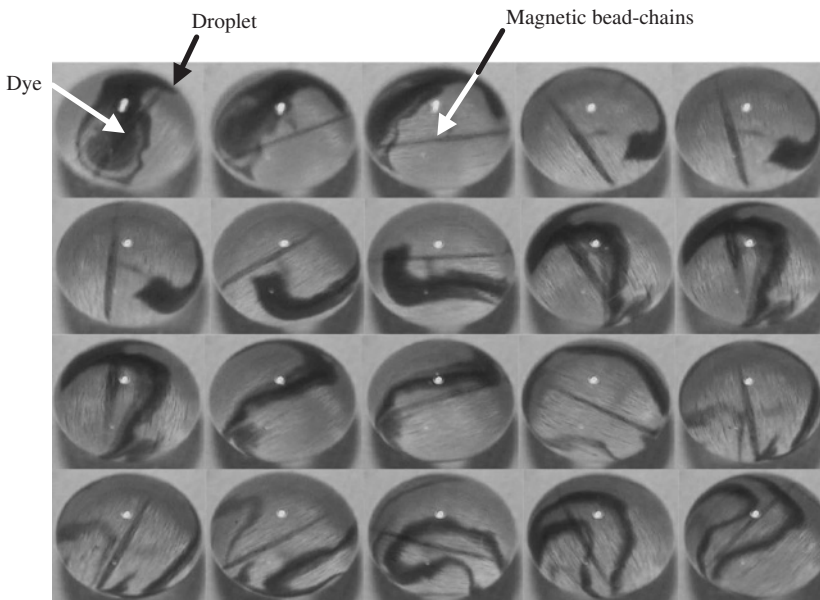


FIG. 4.5. Initial stages of the mixing of a dye using the lab in a droplet concept (image sequence taken over a span of 0.5 s). The dye mixes homogeneously after a few revolutions. This mixing process is much faster than that by pure diffusion alone.

V. Closing Remarks

The article describes the behavior of the superparamagnetic nanoparticles in the context of the transport and field-induced self-assembly of ferrofluids and magnetic microspheres. The current research on applications of ferrofluids and magnetic microspheres in biomedical, MEMS and microscale thermal engineering is then discussed.

Magnetic nanoparticles in a suspension are amenable to a number of forces such as Brownian and Stokes drag forces, van der Waals attraction potential, gravitational force and dipole–dipole interaction in an imposed magnetic field. Therefore, more involved multiscale models, e.g., lattice-Boltzmann method (Calhoun et al., 2006; Sofonea and Frueh, 2001; Xuan et al., 2005), have been deployed to analyze the transport of magnetic nanoparticles and magnetic microspheres. Experimental investigations of magnetic microspheres have been performed using direct imaging (Häfeli et al., 2005; Sinha et al., 2005), fluorescence imaging (Pekas et al., 2005), micro-PIV (Pai et al., 1999), magnetic sensing, e.g., using giant magneto resistive (GMR) sensors (Rife et al., 2003) or superconducting quantum interference device (SQUID) sensors (Katsura et al., 2001). Flow visualization in a ferrofluid flows is challenging at the microscale, since these fluids are generally opaque. The most widely adopted technique for characterizing ferrohydrodynamic flow uses ultrasonic Doppler velocimetry (Kikura et al., 1999). However, the mass transfer of ferrofluids in a transparent fluid can be more easily detected by using a laser or other light extinction method (Trivedi et al., 2004).

Further significant development in μ -TAS design and targeted drug delivery by employing magnetic nanoparticles is expected. The integration of diagnostics and therapeutic devices could also become possible, leading to personalized medication treatments (Bashir, 2004). The integration of magnetic μ -TAS devices with microelectronic devices will enable real-time sampling, analysis, detection and wireless data transfer using a single-chip mounted sensor (DeHennis and Wise, 2005). Such a device could find widespread use for geological surveys, remote monitoring of water and air quality or as a diagnostic tool for bioterrorism threats. Magnetic nanoparticles have significant potential for gene delivery (Dobson, 2006), synthesis of organic molecules, biological systems or intelligent medication procedures (Müller-Schulte and Schmitz-Rode, 2006). The use of magnetic nanoparticles in micro- and nanoscale devices for measurements of protein, mRNA, and the physical and chemical profiles of cells could collectively provide valuable information on the signaling pathways, e.g., for cell division, self-renewal, differentiation and apoptosis (Hood and Galas, 2003). Thus, it is

possible that the field-induced transport of magnetic nanoparticles could help to significantly transform future MEMS and BioMEMS devices.

References

Abraham, A. (2002). Rayleigh–Bénard convection in a micropolar ferromagnetic fluid. *Int. J. Eng. Sci.* **40**, 449–460.

Back, L. H., and Banerjee, R. K. (2000). Estimated flow resistance increase in a spiral human coronary artery segment. *J. Biomech. Eng.* **122**, 675–677.

Bashir, R. (2004). BioMEMS: State-of-the-art in detection, opportunities and prospects. *Adv. Drug Deliv. Rev.* **56**, 1565–1586.

Bashtovoy, V. G., Berkovsky, B. M., and Vislovich, A. N. (1988). *Introduction to Thermomechanics of Magnetic Fluids*. Hemisphere Publishing Corporation, Washington.

Beebe, D. J., Mensing, G., Moorthy, J., Khoury, C. M., and Pearce, T. M. (2001). Alternative approaches to microfluidic systems design, construction and operation. *Proc. Micro Total Analysis Systems (μTAS 2001) Symposium*, Monterey, CA, pp. 453–455.

Berkovsky, B. M. (1978). Some aspects of theoretical modeling of thermomechanics of magnetic fluids. In *Proc. International Advanced Course and Workshop on Thermomechanics of Magnetic Fluids* (B. M., Berkovsky, Ed.), pp. 149–157. Hemisphere, Washington, DC.

Bertsch, A., Heimgartner, S., Cousseau, P., and Renaud, P. (2001). Static micromixers based on large-scale industrial mixer geometry. *Lab Chip* **1**, 56–60.

Biswal, S. L., and Gast, A. P. (2003). Mechanism of semiflexible chains formed by poly(ethylene glycol)-linked paramagnetic particles. *Phys. Rev. E* **69**, 021402 (1–9).

Biswal, S. L., and Gast, A. P. (2004a). Rotational dynamics of semiflexible paramagnetic particle chains. *Phys. Rev. E* **69**, 041406(1–9).

Biswal, S. L., and Gast, A. P. (2004b). Micromixing with linked chains of paramagnetic particles. *Anal. Chem.* **76**, 6448–6455.

Blackburn, G. F., Shah, H. P., Kenten, J. H., Leland, J., Kamin, R. A., Link, J., Peterman, J., Powell, M. J., Shah, A., Talley, D. B., Tyagi, S. K., Wilkins, E., Wu, T. G., and Massey, R. J. (1991). Electrochemiluminescence detection for development of immunoassays and DNA probe assays for clinical diagnostics. *Clin. Chem.* **37**, 1534–1539.

Blums, E., Plaviniš, J., and Chukhrov, A. (1983). High-gradient magnetic separation of magnetic colloids and suspensions. *J. Magn. Magn. Mater.* **39**, 147–151.

Boudouvis, A. G., Puchalla, J. L., and Scriven, L. E. (1988). Interaction of capillary wetting and fringing magnetic field in ferrofluid systems. *J. Coll. Interface Sci.* **124**, 677–687.

Boudouvis, A. G., and Scriven, L. E. (1993). Sensitivity analysis of hysteresis in deformation of ferrofluid drops. *J. Magn. Magn. Mater.* **122**, 254–258.

Bruno, J. G., and Yu, H. (1996). Immunomagnetic–electrochemiluminescent detection of *Bacillus anthracis* spores in soil matrices. *Appl. Environ. Microbiol.* **62**, 3474–3476.

Calhoun, R., Yadav, A., Phelan, P., Vuppu, A., Garcia, A., and Hayes, M. (2006). Paramagnetic particles and mixing in micro-scale flows. *Lab Chip* **6**, 247–257.

Chen, Q., and Zhang, Z. J. (1998). Size-dependent superparamagnetic properties of MgFe_2O_4 spinel ferrite nanocrystallites. *Appl. Phys. Lett.* **73**, 3156–3158.

Choi, J.-W., Liakopoulos, T. M., and Ahn, C. H. (2001). An on-chip magnetic bead separator using spiral electromagnets with semi-encapsulated permalloy. *Biosens. Bioelectron.* **16**, 409–416.

Cowley, M. D., and Resensweig, R. E. (1967). The interfacial stability of a ferromagnetic fluid. *J. Fluid Mech.* **30**(4), 671–688.

Dailey, J. P., Phillips, J. P., Li, C., and Rife, J. S. (1999). Synthesis of silicone magnetic fluid for use in eye surgery. *J. Magn. Magn. Mater.* **194**, 140–148.

de Vahl Davis, G. (1983). Natural convection of air in a square cavity: A benchmark numerical solution. *Int. J. Numer. Meth. Fluids* **3**, 249–264.

DeHennis, A. D., and Wise, K. D. (2005). A wireless microsystem for the remote sensing of pressure, temperature, and relative humidity. *J. MEMS* **14**, 12–22.

Dobson, J. (2006). Gene therapy progress and prospects: magnetic nanoparticle-based gene delivery. *Gene Ther.* **13**, 283–287.

Doyle, P. S., Bibette, J., Bancaud, A., and Viovy, J. -L. (2002). Self-assembled magnetic matrices for DNA separation chips. *Science* **295**(5563), 2237.

Drndić, M., Johnson, K. S., Thywissen, J. H., Prentiss, M., and Westervelt, R. M. (1998). Micro-electromagnets for atom manipulation. *Appl. Phys. Lett.* **72**, 2906–2908.

Fan, Z. H., Mangru, S., Granzow, R., Heaney, P., Ho, W., Dong, Q. P., and Kumar, R. (1999). Dynamic DNA hybridization on a chip using paramagnetic beads. *Anal. Chem.* **71**, 4851–4859.

Finlayson, B. A. (1970). Convective instability of ferromagnetic fluids. *J. Fluid Mech.* **40**, 753–767.

Fratamico, P. M., Schultz, P. J., and Buchanan, R. L. (1992). Rapid isolation of *Escherichia coli* O157:H7 from enrichment cultures of foods using an immunomagnetic separation method. *Food Microbiol.* **9**, 105–113.

Ganguly, R., Gaind, A. P., and Puri I. K. (2005b). A strategy for the assembly of 3-D mesoscopic structures using a ferrofluid. *Phys. Fluids* **17**, 57103(1–9).

Ganguly, R., Gaind, A. P., Sen, S., and Puri, I. K. (2005a). Analyzing ferrofluid transport in magnetic drug targeting. *J. Magn. Magn. Mater.* **289**, 331–334.

Ganguly, R., Sen, S., and Puri, I. K. (2004a). Heat transfer augmentation in a channel with a magnetic fluid under the influence of a line-dipole. *J. Magn. Magn. Mater.* **271**, 63–73.

Ganguly, R., Sen, S., and Puri, I. K. (2004b). Thermomagnetic convection in a square enclosure using a line dipole. *Phys. Fluids* **16**, 2228–2236.

Ganguly, R., Zellmer B., and Puri, I. K. (2005c). Field-induced self-assembled ferrofluid aggregation in pulsatile flow. *Phys. Fluids* **17**, 097104(1–8).

Garcia-Aljaro, C., Bonjoch, X., and Blanch, A. R. (2005). Combined use of an immunomagnetic separation method and immunoblotting for the enumeration and isolation of *E. coli* O157 in wastewaters. *J. Appl. Microbiol.* **98**, 589–597.

Gijs, M. A. M. (2004). Magnetic bead handling on-chip: new opportunities for analytical applications. *Microfluid Nanofluid* **1**, 22–40.

Gillies, G. T., Ritter, R. C., Broaddus, W. C., Grady, M. S., Howard, M. A., III, and McNeil, R. G. (1994). Magnetic manipulation instrumentation for medical physics research. *Rev. Sci. Instrum.* **65**, 533–562.

Goldstein, R. E., Jackson, D. P., and Langer, S. A. (1993). Dynamics of pattern-formation in magnetic fluids. *J. Magn. Magn. Mater.* **122**, 267–270.

Griffiths, D. J. (2004). *Introduction to Electrodynamics*, Fourth Edition. Prentice Hall, India, New Delhi.

Häfeli, U. O., Lobedann, M. A., Steingroewer, J., Moore, L. R., and Riffle, J. (2005). Optical method for measurement of magnetophoretic mobility of individual magnetic microspheres in defined magnetic field. *J. magn. Magn. Mater.* **293**, 224–239.

Harris, L. (2002). *Polymer stabilized magnetite nanoparticles and poly(propylene oxide) modified styrene-dimethacrylate networks*. PhD thesis, Virginia Polytechnic University and State University, Blacksburg, VA.

Hartshorne, H., Backhouse, C. J., and Lee, W. E. (2004). Ferrofluid-based microchip pump and valve. *Sensor. Actuator. B* **99**, 592–600.

Holligan, D. L., Gillies, G. T., and Dailey, J. P. (2003). Magnetic guidance of ferrofluidic nanoparticles in an *in vitro* model of intraocular retinal repair. *Nanotechnology* **14**, 661–666.

Hood, L., and Galas, D. (2003). The digital code of DNA. *Nature* **421**, 444–448.

Iacob, Gh., Rotariu, O., and Häfeli, U. O. (2004). Magnetizable needles and wires – modeling an efficient way to target magnetic microspheres *in vivo*. *Biorheology* **41**, 599–612.

Jang, I. J., Horng, H. E., Chiou, Y. C., Hong, C. -Y., Yu, J. M., and Yang, H. C. (1999). Pattern formation in microdrops of magnetic fluids. *J. Magn. Magn. Mater.* **201**, 317–320.

Johannsen, M., Gneveckow, U., Eckelt, L., Feussner, A., WaldÖFner, N., Scholz, R., Deger, S., Wust, P., Loening, S. A., and Jordan, A. (2005). Clinical hyperthermia of prostate cancer using magnetic nanoparticles: Presentation of a new interstitial technique. *Int. J. Hyperther.* **21**, 637–647.

Jordan, A., Scholz, R., Maier-Hauff, K., Johannsen, M., Wust, P., Nadobny, J., Shirr, H., Schmidt, H., Deger, S., Loening, S., Lanksch, W., and Felix, R. (2001). Presentation of a new magnetic field therapy system for the treatment of human solid tumors with magnetic fluid hyperthermia. *J. Magn. Magn. Mater.* **225**(1–2), 118–126.

Katsura, S., Yasuda, T., Hirano, K., Mizuno, A., and Tanaka, S. (2001). Supercond. *Sci. Technol.* **14**, 1131–1134.

Kawaguchi, H., Fujimoto, K., Nakazawa, Y., Sakagawa, M., Ariyoshi, Y., Shidara, M., Okazaki, H., and Ebisawa, Y. (1996). Modification and functionalization of hydrogel microspheres. *Coll. Surface. A Physicochem. Eng. Aspects* **109**, 147–154.

Kikura, H., Sawada, T., and Tanahashi, T. (1993). Natural convection of a magnetic fluid in a cubic enclosure. *J. Magn. Magn. Mater.* **122**, 315–318.

Kikura, H., Takeda, Y., and Sawada, T. (1999). Velocity profile measurement of magnetic fluid flow using ultrasonic Doppler velocimetry. *J. Magn. Magn. Mater.* **201**, 276–280.

Kim, D., and Choi, H. (2003). Laminar flow past a hemisphere. *Phys. Fluids* **15**, 2457–2460.

Kouassi, G. K., Irudayaraj, J., and McCarty, G. (2005). Activity of glucose oxidase functionalized onto magnetic nanoparticles. *Biomag. Res. Technol.* **3**, 1–10.

Krakov, M. S., and Nikiforov, I. V. (2002). To the influence of uniform magnetic field on thermomagnetic convection in square cavity. *J. Magn. Magn. Mater.* **252**, 209–211.

Kuczynska, E., Boyer, D. G., and Shelton, D. R. (2003). Comparison of immunofluorescence assay and immunomagnetic electrochemiluminescence in detection of *Cryptosporidium parvum* oocysts in karst water samples. *J. Microbiol. Methods* **53**, 17–26.

Lange, A. (2002). Kelvin force in a layer of magnetic fluid. *J. Magn. Magn. Mater.* **241**, 327–329.

Lange, A. (2002). Thermomagnetic convection of magnetic fluids in a cylindrical geometry. *Phys Fluids* **14**(7), 2059–2064.

Lee, C. S., Lee, H., and Westervelt, R. M. (2001). Microelectromagnets for the control of magnetic nanoparticles. *Appl. Phys. Lett.* **79**, 3308–3310.

Liepsch, D. (2002). An introduction to biofluid mechanics – basic models and applications. *J. Biomech.* **35**, 415–435.

Lin, Y., Gerfen, G. J., Rousseau, D. L., and Yeh, S. R. (2003). Ultrafast microfluidic mixer and freeze-quenching device. *Anal. Chem.* **75**, 5381–5386.

Liu, R. H., Stremler, M. A., Sharp, K. V., Olsen, M. G., Santiago, J. G., Adrian, R. J., Aref, H., and Beebe, D. J. (2000). Passive mixing in a three-dimensional serpentine microchannel. *J. Microelectromech. S.* **9**, 190–197.

Lubbe, A. S., Alexiou, C., and Bergemann, C. (2001). Clinical applications of magnetic drug targeting. *J. Surg. Res.* **95**, 200–206.

Lubbe, A. S., Bergemann, C., Brock, J., and McClure, D. G. (1999). Physiological aspects in magnetic drug-targeting. *J. Magn. Magn. Mater.* **194**, 149–155.

Luk, J. C., and Lindberg, A. A. (1991). Rapid and sensitive detection of *Salmonella* (O:6,7) by immunomagnetic monoclonal antibody-based assays. *J. Immunol. Methods*, **137**, 1–8.

Macpherson, J. B., Thibault, S., Borra, E. F., Ritcey, A. M., Carufel, N., Asselin, D., Jerominek, H., and Campbell, M. C. W. (2005). A ferrofluidic deformable mirror for ophthalmology. *Progr. Biomed. Opt. Imaging – Proc. SPIE*, **5969**, 59691C1–4.

McNab, T. K., Fox, R. A., and Boyle, A. J. F. (1968). Some magnetic properties of magnetite (Fe_3O_4) microcrystals. *J. Appl. Phys.* **39**, 5703–5711.

Morgan, J. A. W., Winstanley, C., Pickup, R. W., and Saunders, J. R. (1991). Rapid immuno-capture of *Pseudomonas putida* cells from lake water by using bacterial flagella. *Appl. Environ. Microbiol.* **57**, 503–509.

Mosbach, K., and Schröder, U. (1979). Preparation and application of magnetic polymers for targeting of drugs. *FEBS Lett.* **102**, 112–116.

Mukhopadhyay, A., Ganguly, R., Sen, S., and Puri, I. K. (2005). Scaling analysis to characterize thermomagnetic convection. *Int. J. Heat Mass Transfer* **48**, 3485–3492.

Müller, H. W., and Engel, A. (1999). Dissipation in ferrofluids: Mesoscopic versus hydrodynamic theory. *Phys. Rev. E* **60**(6), 7001–7009.

Müller-Schulte, D., and Schmitz-Rode, T. (2006). Thermosensitive magnetic polymer particles as contactless controllable drug carriers. *J. Magn. Magn. Mater.* **302**, 267–271.

Odenbach, S. (2004). Recent progress in magnetic fluid research. *J. Phys. Condens. Matter* **16**, R1135–R1150.

Pai, V. M., Chen, C. -J., and Haik, Y. (1999). Microscopic flow visualization system for fluids in magnetic field. *J. Magn. Magn. Mater.* **194**, 262–266.

Pankhurst, Q. A., Connolly, J., Jones, S. K., and Dobson, J. (2003). Applications of magnetic nanoparticles in biomedicine. *J. Phys. D: Appl. Phys.* **36**, R167–R181.

Pekas, N., Granger, M., Tondra, M., Popple, A., and Porter, M. D. (2005). Magnetic particle diverter in an integrated microfluidic format. *J. Magn. Magn. Mater.* **293**, 584–588.

Probstein, R. F. (1994). *Physicochemical Hydrodynamics*. Wiley, Inc., New York.

Puri, I. K., Ganguly, R., and Sinha, A. (2006). Method and apparatus for magnetic mixing in micron size droplets. US provisional patent application filed, March 3.

Radbruch, A., Mechtold, B., Thiel, A., Miltényi, S., and Pfluger, E. (1994). High-gradient magnetic cell sorting. *Methods Cell Biol.* **42**, 387–403.

Rife, J. C., Miller, M. M., Sheehan, P. E., Tamanaha, C. R., Tondra, M., and Whitman, L. J. (2003). Design and performance of GMR sensors for the detection of magnetic microbeads in biosensors. *Sensors Actuators B* **107**, 209–218.

Roger, J., Pons, J. N., Massart, R., Halbreich, A., and Bacri, J. C. (1999). Some biomedical applications of ferrofluids. *Euro. Phys. J. Appl. Phys.* **5**(3), 321–325.

Rosensweig, R. E. (1985). *Ferrohydrodynamics*. Cambridge University Press, Cambridge.

Rotariu, O., Iacob, G., Strachan, N. J. C., and Chiriac, H. (2004). Simulating the embolization of blood vessels using magnetic microparticles and acupuncture needle in a magnetic field. *Biotechnol. Prog.* **20**, 299–305.

Rusetski, A. N., and Ruuge, E. K. (1990). Magnetic fluid as a possible drug carrier for thrombosis treatment. *J. Magn. Magn. Mater.* **85**, 299–302.

Ruuge, E. K., and Rusetski, A. N. (1993). Magnetic fluids as drug carriers: Targeted transport of drugs by a magnetic field. *J. Magn. Magn. Mater.* **122**, 335–339.

Schwab, L., Hildebrandt, U., and Stierstadt, K. (1983). Magnetic Bénard convection. *J. Magn. Magn. Mater.* **39**, 113–114.

Shestopalov, I., Tice, J. D., and Ismagilov, R. F. (2004). Multi-step synthesis of nanoparticles performed on millisecond time scale in a microfluidic droplet-based system. *Lab Chip* **4**, 316–321.

Shliomis, M. I., and Stepanov, V. I. (1993). Rotational viscosity of magnetic fluids – contribution of the Brownian and Néel relaxational processes. *J. Magn. Magn. Mater.* **122**, 196–199.

Sinha, A., Ganguly, R., and Puri, I. K. (2004). Magnetically assembled 3-d mesoscopic patterns using a suspension of superparamagnetic nanoparticles. *Proc. 3rd ASME Integrated Nano-systems – Design, Synth. Appl.* 89–90.

Sinha, A., Ganguly, R., and Puri, I. K. (2005). Immunomagnetic separation in microchannels – from MEMS to BioNEMS. ASME International Mechanical Engineering Congress, Orlando, FL, Paper No. IMECE2005-81569.

Snyder, S. M., Cader, T., and Finlayson, B. A. (2003). Finite element model of magnetoconvection of a ferrofluid. *J. Magn. Magn. Mater.* **262**, 269–279.

Sofonea, V., and Fröhlich, W. -G. (2001). Lattice Boltzmann model for magnetic fluid interfaces. *Euro. Physical J. B* **20**, 141–149.

Suzuki, H., and Ho, C. M. (2002). A magnetic force driven chaotic micro-mixer. *Proc. IEEE MEMS* 40–43.

Suzuki, H., Ho, C. -M., and Kasagi, N. (2004). A chaotic mixer for magnetic bead-based micro cell sorter. *J. MEMS* **13**, 779–790.

Tangthieng, C., Finlayson, B. A., Maulbetsch, J., and Cader, T. (1999). Finite element model of magnetoconvection of a ferrofluid. *J. Magn. Magn. Mater.* **201**, 252–255.

Tibbe, A. G., de Groot, B. G., Greve, J., Liberti, P. A., Dolan, G. J., and Terstappen, L. W. M. M. (1999). Optical tracking and detection of immunomagnetically selected and aligned cells. *Nat. Biotechnol.* **17**, 1210–1213.

Trivedi, P., Patel, R., Parekh, K., Upadhyay, R. V., and Mehta, R. V. (2004). Magneto-optical effects in temperature-sensitive ferrofluids. *Appl. Opt.* **43**, 3619–3622.

Ugelstad, J., Stenstad, P., Kilaas, L., Prestvik, W. S., Herje, R., Berge, A., and Hornes, E. (1993). Monodisperse magnetic polymer particles – new biochemical and biomedical. *Blood Purif.* **11**, 349–369.

van Ewijk, G. A., Vroege, G. J., and Phillipse, A. P. (2002). Susceptibility measurements on a fractionated aggregate-free ferrofluid. *J. Phys.: Condens. Mater.* **14**, 4915–4925.

Voltairas, P. A., Fotiades, D. I., and Michalis, L. K. (2002). Hydrodynamics of magnetic drug targeting. *J. Biomech.* **35**, 813–821.

Weilepp, J., and Brand, H. R. (1996). Competition between the Bénard-Marangoni and the Rosensweig instabilities in magnetic fluids. *J. Phys. II France* **6**, 419–441.

Wong, P. K., Chen, C. -Y., Wang, T. -H., and Ho, C. -M. (2004). Electrokinetic bioprocessor for concentrating cells and molecules. *Anal. Chem.* **76**, 6908–6914.

Wright, D. J., Chapman, P. A., and Siddons, C. A. (1994). Immunomagnetic separation as a sensitive method for isolating *E. coli* O157 from food samples. *Epidemiol. Infect.* **113**, 31–39.

Xuan, Y., Ye, M., and Li, Q. (2005). Mesoscale simulation of ferrofluid structure. *Int. J. Heat Mass Trans.* **48**, 2443–2451.

Yamaguchi, H., Kobori, I., and Uehata, Y. (1999b). Heat transfer in natural convection of magnetic fluids. *J. Thermophys. Heat Transfer* **13**, 501–507.

Yamaguchi, H., Kobori, I., Uehata, Y., and Shimada, K. (1999a). Natural convection of magnetic fluid in a rectangular box. *J. Magn. Magn. Mater.* **201**, 264–267.

Ye, P. D., Weiss, D., von Klitzing, K., and Eberl, K. (1995). Fabrication and characterization of micromagnet arrays on top of GaAs/AlGaAs heterostructures. *Appl. Phys. Lett.* **67**, 1441–1443.

Yellen, B., Friedman, G., and Feinerman, A. (2003). Printing superparamagnetic colloidal particle arrays on patterned magnetic film. *J. Appl. Phys.* **93**, 7331–7333.

Yellen, B. B., Zachary, G. F., Halverson, D. S., Fridman, G., Barbee, K. A., Chorny, M., Levy, R., and Friedman, G. (2005). Targeted drug delivery to magnetic implants for therapeutic applications. *J. Magn. Magn. Mater.* **293**, 647–654.

Yu, H. (1998). Use of an immunomagnetic separation-fluorescent immunoassay (IMS-FIA) for rapid and high throughput analysis of environmental water samples. *Anal. Chim. Acta* **376**, 77–81.

Zahn, M. (1979). *Electromagnetic Field Theory*. Wiley, Inc., New York.

This page intentionally left blank

Subject Index

An italic f (or t) following a page number indicates that the material referred to is in a figure caption (or table)

Axisymmetric flows, 32–38

Beaded electrospun nanofibers, 150

Bending electrospun jets, non-linear dynamics, 124–139

electrically driven bending instability, jet path calculated for, 126–129, 129–131

electrospun jets branching, theory, 138–139

elongation and drying of the jet, 133–135

envelope cone, 131–132

jet velocity, 131–133

longitudinal strain rate and molecular orientation, 136–137

multiple-jet electrospinning, 139–144

perturbations to bending instability, 127*f*

viscosity profile in the bending jet, 135–136

Bernoulli's equation, 236

Bifurcation theory and fluid flows, 1–40. *see also under* Fluid flows and their bifurcations

cusp bifurcation, 16

for fifth order normal form, 27*f*

for folded mapping of the physical parameters, 38*f*

for fourth order normal form, 26*f*

local bifurcation, 17

for normal form of order 4, 17*f*

for normal form of order 6, 29*f*

Biharmonic equation, 59

Biodegradable scaffolds, nanofibers in, 174

Biomedical, MEMS and BioMEMS applications

superparamagnetic nanoparticles for, 293–331. *see also under* Nanoparticles, superparamagnetic

Biosensors, nanofibers in, 181–184

Biot-Savart law of electromagnetism, 213

Birefringent jets, 99–103

of the as-spun fiber, 102

ultra-low-intensity birefringence, 102

Boundary layer concept, 236

Carbon nanotubes (CNTs), 46

Cathode Rays, 232

Cauchy-Stokes decomposition theorem, 212

Centers, 2

Chaplygin-Lamb dipole, 243

Chemical sensors, nanofibers in, 181–184

Codimension, 19

Co-electrospun nanofibers, 153

carbonization, 155

experimental set-up, 156

preparation, 153

Core-shell nano/meso fibers, 152

Coulomb's law, 108, 110

Critical points, 2

Cusp bifurcation, 16

Deborah number, 125

Degenerate center, 12

Dividing streamlines, 3

Drug delivery applications, of nanofibers, 172–179

electrospinning as encapsulation of drugs, 176

Earnshaw instability, 108

Elasticity theory, 59

Electrified jets, bending instability of, 107–109

Electrified liquid column

- aerodynamic versus electric driven bending, 122
- bending perturbations, growth rate and wavelength, 122–124

Electrified liquid jets, continuous quasi-one-dimensional equations of, 112–115

Electrospinning

- jets in, 143
- for luminescent nanofibers

 - fabrication, 180
 - multiple-jet, 139–144

- of nanofibers from polymer solutions and melts, 43–184. *see also under Nanofibers*
- polymer solutions in, electrically charged liquid jets, 73–145. *see also under Polymer solutions*
- for scaffold formation, 173*f*

Electrospun jets. *see also Bending electrospun jets*

- branching on, theory, 138–139
- dynamics, discretized three-dimensional equations of, 115–119
- nine-jet electrospinning process, 142

Electrospun polyaniline (VERSICON®) fibers, 180

Electrostatic spinning, 175

Envelope cone, 131–132

- shape of, 131–132

Enzyme-linked immunosorbent assay (ELISA), 325

Euler equations, 229, 241–242

Evaporation and solidification, 119–122

Ferrofluid aggregation, field-induced, 300–319

accumulation of, 313*f*

computational domain, 309–310, 310*f*

depletion phase of, 314*f*

ferrofluid accumulation, oscillation of, 317*f*

ferrofluid aggregate, erosion of, 315

ferrofluid dispersion mechanism, physical insight, 314

ferrofluid hydrodynamics, 300–303

ferrofluid structures produced on a flat substrate using a bar magnet, 306*f*

ferrofluid washaway, phases of, 315*f*

field-induced self-assembly and transport in forced flow, 307–319

hydrodynamic equations, 300

in MDT systems, 308

in steady and pulsatile flows, 311

Levi–Civita tensor, 302

magnetically saturated ferrofluid structures, dynamic response of, 305

magnetoviscous effect, 300

Maxwell's equations, 302

Rosenzweig instability, 303

self-assembly due to force interactions, 303–307

Stokesian migration, 301–302

thermomechanical ferrofluid applications, 319–322. *see also individual entry*

Young–Laplace's equation, 303

Ferrofluids

- controlled transport, 294
- dispersion and localization of, 313
- field-assisted aggregations of, 295
- magnetic fluids in microscale, advantages of using, 295
- and magnetic microspheres, practical significance, 294–299
- magnetization curves, 298*f*
- suspended nanoparticles in, 296*f*

Field-assisted self-assembly of superparamagnetic nanoparticles for Biomedical, MEMS and BioMEMS applications, 293–331.

see also under Nanoparticles,
superparamagnetic
Field-guided transport, 323–324
Flow Box Theorem, 7
Flow-induced molecular chain
orientation, in the electrospinning
jets, 98–99
Fluid flows and their bifurcations, 1–40.
see also under Bifurcation theory
2D flows, 39
3D flows, 39
around circular cylinder, numerical
simulations, 2f
axisymmetric flows and application
to vortex breakdown, 32–38
Bakker’s approach, 3
basic concepts, 4–9
bifurcation of flows away from
boundaries, 9–20
degenerate no-slip critical points, 24f
degenerate symmetric critical point,
30f
flow close to a no-slip wall, 20f
flow near a wall with mirror
symmetry, 27–31
flow near a wall, 20–27
heteroclinic streamlines, 18
near-identity quadratic
transformation, 10
non-degenerate no-slip critical points,
22f
for the normal form of order 5, 19f
normal form transformations, 3
no-slip critical points, 21–22
patterns, 1–40
qualitative insight in, 3
simple linear degeneracy, 9
structural stability and instability, 5
structurally unstable heteroclinic
connections, 26
symmetric flow, coordinate system
for, 30f
topology flow, 3
truncated normal form, analysis, 18
truncated normal forms, 12, 15
vortex breakdown of bubble type, 34
Fluid mechanics problem
qualitative, 2
quantitative, 2
Föppl problem, 225
Four mill roll, 6f
Giant magneto resistive (GMR), 330
Grashof number, 322
Green’s theorem in hydrodynamics, 198
Hamilton’s canonical form, 221
Helmholtz’s papers, on Vortex
dynamics 1858–1956, 210–220
Biot-Savart law of electromagnetism,
213
Cauchy-Stokes decomposition
theorem, 212
circular vortex-filaments, 215
classical textbooks and monographs
on fluid mechanics, 220
first law of Helmholtz, 212
on Lagrange-Cauchy velocity-
potential theorem, 212
*Ostwalds Klassiker der exakten
Wissenschaften* series, 217
parallel rectilinear vortices (or point
vortices), 214f
point vortex concept, 213
qualitative point of view of, 219
‘straight parallel vortex-filaments’,
213
vortex pair motion, 215f
vortex pairs, ‘leapfrogging’ by, 217f
vortex ring, self-induced forward
motion of, 216f
vorticity notion, 211
Heteroclinic streamlines, 18
Hill’s spherical vortex, 243
Hollow nanofibers, 45
Hyperboloidal solutions, 51–58
self-similarity assumption for, 58–61
Immunomagnetic separation (IMS),
325
Implicit function theorem, 13
Inverse function theorem, 10
Jacobian matrix, 8

Jet splaying/branching and garlands, 83–90

Kármán drag formula, 239

Kelvin body force (KBF), 301

Kelvin oval, 226

Kelvin's circulation theorem, 229

Kirchhoff vortex, 241

Lab-in-a-droplet (LID) concept, 328–329

Lagrange-Cauchy velocity-potential theorem, 212

Lamb dipole, 243

Langevin equation, 297, 299

Laplace equation, 53, 59, 72

Legendre functions, 53

Levi–Civita tensor, 302

Light-emitting diodes (LED), 44

Liquid alloy ion sources (LAIS), 67

Local bifurcation, 17

Localized induction approximation, 210

Longitudinal strain rate and molecular orientation, 136–137

Magnetic drug targeting (MDT), 294

Magnetic microspheres, 297–299

 dipole–dipole interaction potential for, 299*f*

Magnetic microspheres, bioMEMS and biomedical applications, 322–329

 field-guided transport, 323–324

 force dynamics in a viscous fluid, 324*f*

 immunomagnetic separation (IMS), 325

Mason number, 328

MEMS-based IMS sensor, 327*f*

 in micro-capillary flow, 326*f*

 micro mixers using self-assembled chains, 327–329

 micro total analytical systems, 325–327

 as 'mobile substrates', 323

Magnetic nanoparticles, 295–296

'Magnetostatic pressure', 319

Magnetoviscous effect, 300

Mason number, 328

Maxwell equations, 68, 103–104, 141, 302

MEMS (micro-electromechanical, 294–331

Micro mixers using self-assembled chains, 327–329

Miniversal, 19

'Mobile substrates', 294–295

Movement principle, 14

Multi-walled (MWCNT), 146–149

Nanofiber properties

 characterization methods and tools for, 156–172

 conducting, 179–181

 electric current in electrospun jets, measuring, 171*f*

 elongational viscosities, 167–168

 entire filament during stretching and self-thinning, 167

 extensional elongational flows, 167

 fluid stretching apparatus in, 165

 molecular chain alignment, 169

 morphological characterization, 156

 polymer nanofibers, electrospinning of, 143

 rheological characterization, 161

 solvents, characteristic properties, 164

 tensile stress and elastic and plastic properties, characterization, 157

 test fluids, characteristic properties, 163*t*

Nanofibers, from polymer solutions and melts, electrospinning of, 43–184

 thin compact fibers and hollow fibers, 45

 carbon nanotubes (CNTs), 46

 methods of producing nanofibers, 46

 Taylor cone and jetting from liquid droplets in, 47–73. *see also individual entry*

Nanofibers production

 beaded electrospun nanofibers, 150

 conductive and photosensitive nanofibers preparation, 146

 core-shell nano/meso fibers, 152

PEO based nanofibers, 154*f*
scientific and technological challenges in, 146–156

Nanofibers, development and applications, 172–184
air permeable nanofiber mats, 183
bulletproof vests incorporating nanofibers, 182
for drug delivery and wound dressing, 172–179
electrospinning as encapsulation of drugs, 176
electrospinning techniques for scaffold formation, 173*f*
electrospun KEVLAR® fibers, 182
mechanical properties, 178–179
porosity, 178
processing techniques, 173–176
in protective clothing, chemical and biosensors and smart fabrics, 181–184
for scaffolds in tissue engineering applications, 172–179
surface properties, 177–178

Nanoparticles, superparamagnetic, for biomedical, MEMS and BioMEMS applications, 293–331
ferrofluid aggregation, field-induced, 300–319. *see also individual entry*
ferrofluids and magnetic microspheres, practical significance, 294–299. *see also individual entry*
ferrofluids, 293, 296–697
Langevin equation, 297
magnetic microspheres, 297–299
magnetic nanoparticles, 295–296
'mobile substrates', 294
thermomechanical ferrofluid applications, 319–322. *see also individual entry*

Nanotubes, 45

Navier–Stokes equation, 4, 6, 39

Near-identity quadratic transformation, 10

NEMS (nano-electromechanical systems), 294–331

Newton's second law, 4, 117, 323
Newtonian fluid, 123
Nusselt number, 119, 320

Particle tracing technique, 92–95

Pathlines, 4

Pendant droplets, 47, 61
pendant droplet experiment, 63*f*
steady-state shapes of, 65

Perturbed four mill roll, 6*f*

Perturbed six mill roll, 6*f*

Piezoelectric polymer poly(vinylidene fluoride), 150

Point of attachment, 3

Point of separation, 3

Point vortex concept, 213

Point vortices, 220–227. *see also* Vortex pair
Föppl problem, 225
Hero's formula, 222
Kelvin oval, 226
Kutta-Joukovskii condition on flow, 225
nature of motion of, 223
Routh correction, 225
Synge's analysis, 223
theory of conformal mappings, 225

Poisson bracket, 221

Poly(D,L-lactide-co-glycolide) (PLGA) nanofibers, 177

Polycaprolactone (PCL) droplet, 69
measured and predicted shapes of, 69*f*

Polydimethylsiloxane (PDMS), 306

Polymer nanofibers, electrospinning of, 143

Polymer solutions in electrospinning, 73–145
bending electrospun jets, non-linear dynamics, 124–139. *see also individual entry*
birefringence of the electrospinning jets, 99–103
coiled and looped jets captured on a hard surface, 90–91
dimensionless groups and parameters employed, 76

electrical bending instability,
evolution, 80

electrically driven bending instability,
78f

electrified jets, bending instability of,
107–109

electrified liquid column, bending
perturbations of, 122–124. *see also*
individual entry

electrified liquid jets, continuous
quasi-one-dimensional equations
of, 112–115

electrospun jets dynamics, discretized
three-dimensional equations of,
115–119

evaporation and solidification,
119–122

experimental observations, 79–103

experimental set-up, 74–78

flow-induced molecular chain
orientation in the electrospinning
jets, 98–99

glass particle in a jet, positions of, 93/
jet paths, 79–83

jet splaying/branching and garlands,
83–90

jet velocity versus position along the
jet axis in different electric fields,
94f

jet velocity versus time in different
electric fields, *94f*

lateral jets from PCL solution, *87f*

localized approximation, 109–111

nine-jet electrospinning process, 142

particle tracing technique in
electrospinning, jet velocity,
92–95

PCL solution in acetone, 88

rectilinear electrified jet, viscoelastic
model, 103–107

secondary and tertiary cycles of
bending instabilities, 81

straight part of the jet, diameter of,
91–92

strain rate of the electrospinning jets,
95–98

symbols employed, 75

Polyvinylpyrrolidone (PVP), 181

Porous systems with narrow channels,
45

Prandtl equations, 50, 119

Protective clothing, nanofibers in,
181–184

Quasi-one-dimensional equations,
continuous, 112–115

Rankine vortex, 232

Rayleigh number, 320

Rayleigh–Bénard convection, 320

Rectilinear electrified jet, viscoelastic
model, 103–107

Reynolds number, 2, 119, 236, 317

Rosenweig instability, 303

Routh correction, 225

Saddle points, 2

Separatrices, 3

- unstable separatrices, 3
- stable separatrices, 2

Sessile droplets, 47, 61

- critical droplet shape observed for,
64f
- sessile drop experiment, *62f*
- steady-state shapes of, 65

Sherwood number, 119

Simple linear degeneracy, 9

Single-walled (SWCNT) carbon
nanotubes, 146–147

- elastic modulus of, 159

Singularity theory, 18

Six mill roll, *6f*

Smart fabrics, nanofibers in,
181–184

Smoke-box apparatus, for vortex rings,
234

Spider dragline silk, 158

Stokesian migration of
superparamagnetic nanoparticles,
301–302

Streaklines, 4

Streamlines, 4

Superconducting quantum interference
device (SQUID) sensors, 330

Taylor cone and jetting from liquid droplets in, 47–73. *see also* Pendant droplets; Sessile droplets
experimental results and comparison with theory, 61–68
non-self-similar solutions for hyperboloidal liquid bodies, 51–58.
see also under Hyperboloidal solutions
numerical analysis, 71
self-similar nature of the solution, 49–50
sessile and pendant droplets of polymer solutions, 47
static cone formation, critical potential for, 71
Taylor cone as a self-similar solution, 48–51
Taylor cone formation, dynamics of, 68
transient shapes and jet initiation, 68–73
Taylor's theorem, 21, 28
Tetrahydroperfluoroctyl acrylate (TAN), 177
Tetraisopropyl titanate (TPT), 181
Theory of conformal mappings, 225
Thermomechanical ferrofluid applications, 319–322
thermomagnetic convection in square enclosure, 321*f*
'Thomson and Tait', 228
Tissue engineering applications, of nanofibers, 172–179
Topological saddle, 12
Truncated normal form, 12
analysis, 18
UCM model, 141
Upper-convected Maxwell (UCM) model, 114
Versal, 18
von Kármán's theory, 236–238
Kármán drag formula, 239
Vortex atoms, 228–233
Euler's equation, 229
Kelvin's circulation theorem, 229
Maxwell's contribution, 232
Rankine vortex, 232
Tait's drawings, 231*f*
'Thomson and Tait', 228
vortex crystals, 232
Vortex breakdown, 32–38
Vortex dynamics 1858–1956, 197–245
1930's research papers, 204
case studies, 209–243
coherent vortex structures, 241–243.
see also Vortex structures, coherent
Green's theorem in hydrodynamics, 198
Helmholtz's contribution, 197–199
Helmholtz's papers, 210–220. *see also individual entry*
Hill's paper of 1893, 202
journals and periodicals on, list of, 205–209
localized induction approximation, 210
Pearson, Karl contribution, 200
point vortices, 220–227. *see also individual entry*
Truesdell's bibliography, 202
velocity potential, 198
vortex atoms, 228–233. *see also individual entry*
vortex generators, examples, 201
vortex motion, three 'laws' of, 197
vortex ring formation by injecting one fluid into another, 203*f*
vortex rings with plates of various shapes, 202*f*
vortex rings, 234–236. *see also individual entry*
vortex streets, 236–241. *see also individual entry*
Vortex methods, 220
Vortex pair
atmosphere traveling with, 227*f*
'leapfrogging' by, 217*f*
symmetric motion of, 225
Vortex rings, 234–236
generation and interaction of, 235

identical vortex rings, interaction of, 235
self-induced forward motion of, 216f
smoke-box apparatus, 234

Vortex streets, 236–241
Dolaptschiew’s papers, 241
in the co-moving frame based on the point vortex model, 240f
Kármán drag formula, 239
Kármán vortex street, 236
symmetric and a staggered vortex street downstream of a bluff body, 239f
von Kármán’s theory, 236–238
vortex wake formation downstream of a flat plate, 237

Vortex structures, coherent, 241–243

Chaplygin’s paper, 242
Chaplygin-Lamb dipole, 243
Hill’s spherical vortex, 243
Kirchhoff vortex, 241
Lamb dipole, 243
Rankine vortex, 241
Rankine’s model, 241
streamlines of, analytical determination by Chaplygin, 243f

Vorticity notion, 211

Wide-angle X-ray diffraction (WAXD), 148

Wound dressing applications, of nanofibers, 172–179

Young–Laplace’s equation, 303

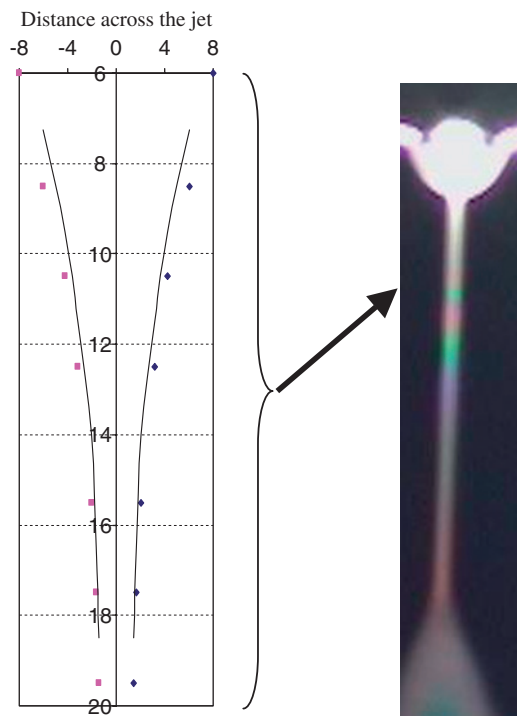


Plate 1. Diameter of the straight segment of a jet as a function of position along the jet. The graph shows the results of a series of measurements of the diffraction of a laser beam. The photograph shows the corresponding range of interference colors (Xu, 2003). (For black and white version see page 91).

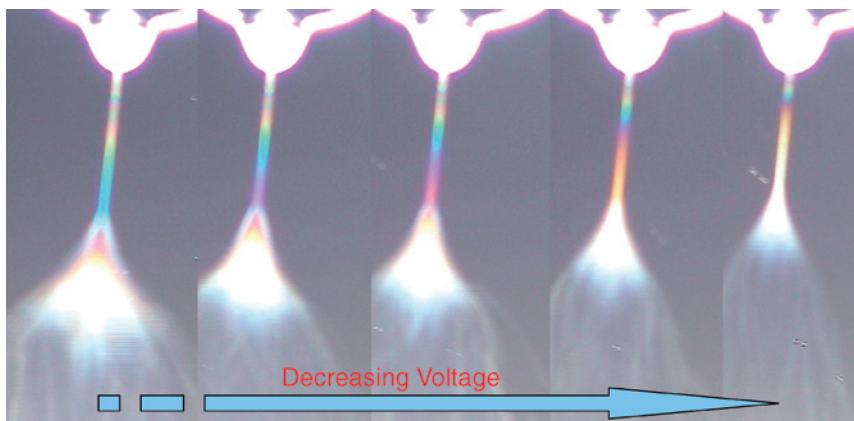


Plate 2. Interference colors provide live information on jet diameter and taper rate change during electrospinning. After Xu et al. (2003). (For black and white version see page 95).

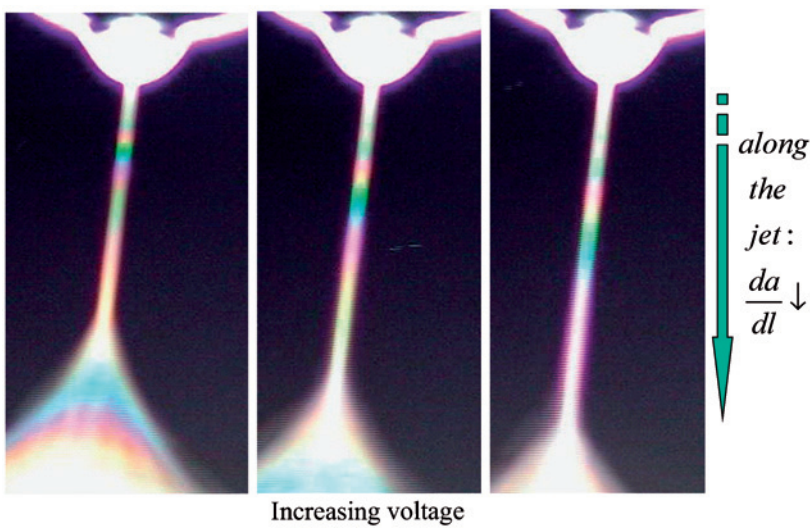


Plate 3. The trend of da/dx observed from the interference colors along the jet axis (Xu, 2003). (For black and white version see page 97).